



POLITECNICO DI TORINO
Repository ISTITUZIONALE

Super Insulating Materials for energy efficient buildings: thermal performance and experimental uncertainty

Original

Super Insulating Materials for energy efficient buildings: thermal performance and experimental uncertainty / Lorenzati, Alice. - (2018 Jul 10).

Availability:

This version is available at: 11583/2711530 since: 2018-07-30T11:18:42Z

Publisher:

Politecnico di Torino

Published

DOI:10.17632/v9r5pkwkyg.2

Terms of use:

Altro tipo di accesso

This article is made available under terms and conditions as specified in the corresponding bibliographic description in the repository

Publisher copyright

(Article begins on next page)



ScuDo

Scuola di Dottorato ~ Doctoral School
WHAT YOU ARE, TAKES YOU FAR

Doctoral Dissertation
Doctoral Program in Metrology (30th Cycle)

Super Insulating Materials for energy efficient buildings: thermal performance and experimental uncertainty

By

Alice Lorenzati

Supervisors:

Prof. Marco Perino
Prof. Vito Fericola

Doctoral Examination Committee:

Prof. Marco Dell'Isola, *Referee*, Università di Cassino
Prof. Andreas Holm, *Referee*, University of Applied Science Munich
Prof.ssa Valentina Serra, *Internal member*, Politecnico di Torino
Prof. Piercarlo Romagnoni, *External member*, Università IUAV di Venezia
Prof.ssa Arianna Astolfi, *Internal member*, Politecnico di Torino

Politecnico di Torino
2018

Declaration

I hereby declare that the contents and organisation of this dissertation constitute my own original work and does not compromise in any way the rights of third parties, including those relating to the security of personal data.

Alice Lorenzati

2018

Joint researches

Chapter 4 - § 4.1.3 Methodologies for the measurement of ψ -values: the proposed methodology was developed in a joint research activity with Arch. Stefano Fantucci

Chapter 4 - § 4.3.2 Energy analysis and thermal load simulation: the presented activities were performed in a joint research project with Arch. Stefano Fantucci (with the contribution of Ing. Stefania Garbaccio)

Chapter 6 - Theoretical standard-based measurement uncertainty analysis: the presented activities were performed in a joint research project with Dr.-Ing. Andreas Holm, Ing. Christoph Sprengard and Dr.-Ing. Sebastian Treml (FIW - Munich)

Chapter 8 - § 8.1 Effects of temperature and ageing on SIM thermal properties (HFM): the presented activities were performed in a joint research project with Arch. Stefano Fantucci

Chapter 9 - Potentialities of VIPs for the energy efficient retrofit of buildings: the presented activities were performed in a joint research project with Arch. Stefano Fantucci (with the contribution of Ing. Stefania Garbaccio)

Contributions of other authors

Chapter 7 - § 7.4 Thermal bridging effects uncertainty: the presented activities were performed with the contribution of M.sc Lukas Berger (FIW - Munich)

Contributions of the author

Chapter 4 - § 4.3.3.3 Validation of the numerical models: the in-situ experimental monitoring campaign and the validation of the simulation models were performed by Arch. Stefano Fantucci with the contributions of the author

Chapter 10 - § 10.2 Life expectancy: the evaluation of VIPs service life was performed by Arch. Stefano Fantucci with the contributions of the author

* This dissertation is presented in partial fulfilment of the requirements for a **Ph.D. degree** in the Graduate School of Politecnico di Torino (ScuDo).

To Paolo

Acknowledgement

I would like to acknowledge my scientific referees, Marco and Vito (my tutors), Alfonso, Valentina and Luigi, always present and sources of useful tips.

My special gratitude to all my colleagues for the wonderful relationship established over the years. A special thanks to Stefano, without whom this path would not even have begun.

My heartfelt thanks to Andreas Holm, Christoph Sprengard and all the FIW colleagues for the hospitality and the constructive cooperation.

Thanks to my family, and my friends (in particular Michi, Giulia, Fede F., Fede N. and Vero) for the laughs together and for having endured with patience my thousand commitments.

The last thanks to Marco, my partner in life, travel and unconditional presence: thank you for all your support and esteem.

Abstract

In a global energy-saving policy, Super Insulating Materials (SIMs) represent an effective solution, especially in a world almost saturated with old buildings for which energy refurbishments are needed. Given their extremely low thermal conductivity, they allow reaching an excellent insulation level, with reduced thicknesses. Anyway, they are recent materials or at least recent insulation solutions for the building sector. And as all the new technologies, they bring with them some critical issues to be solved. For example, what is the accuracy of their available thermal conductivity, what are the criteria for their optimal laboratory characterisation, what are their actual thermal performances in situ and how long is their durability and what is their practical convenience still remain open questions.

The aim of this research was to provide an answer to these questions, although sometimes in a preliminary way.

Therefore, the thermal properties of SIMs (and in particular of the Vacuum Insulation Panels, since, between the SIMs they are the most performing and the most critical solution) were explored at different levels, from the material/panel scale to the building scale.

SIMs are actually laboratory tested using traditional experimental apparatuses, such as the Heat Flow Meter (HFM) and the Guarded Hot Plate (GHP), and in accordance with as traditional standard, developed for the most common insulating material. Indeed, at the first stage of this research, the applicability of

the current methodologies was extensively verified, with an in-depth analysis of the obtainable measurement uncertainties. The uncertainty assessment was performed in three different ways, to analyse the various scenarios that may occur: a theoretical standard based uncertainty evaluation, and both the Type A and Type B experimental uncertainty assessment.

Once defined the best criteria for a proper evaluation of the SIMs thermal properties, they were experimentally characterised, considering the different parameters which could have some effects on their thermal behaviour (different thicknesses, average testing temperature, temperature difference, ageing conditions and so on).

In practical applications of the VIPs, they must be assembled one to each other: innovatively, both the HFM and GHP apparatuses were also used for the evaluation of the linear thermal transmittance of the thermal bridges that occur in case of VIPs assemblies. The investigation performed at the material/panel level were then repeated at the component scale, to evaluate the variability and the measurement uncertainty of the linear thermal transmittance.

The so defined thermal performances represented a reliable pool of input data for the dynamic hygrothermal simulations at the building scale. The goals were the evaluation of the energy efficiency of building insulated with SIMs and the prediction of the durability of these materials (considering different severities of the building envelope component boundary conditions).

The outputs of the numerical simulations were then coupled with an economic analysis, to evaluate the convenience of VIP insulation, in terms of discounted pay-back period.

Contents

Abstract	i
Contents.....	iii
List of Figures	vii
List of Tables.....	xix
Nomenclature	xxxix
1. Introduction	1
2. Super Insulating Materials - SIMs	5
2.1 Advanced Porous Materials - APMs	8
2.1.1 Fumed Silica - FS	9
2.1.2 Aerogel Based Products - ABPs	13
2.2 Vacuum Insulation Panels - VIPs	21
2.2.1 Properties	22
2.2.2 Building applications.....	28
3. Heat transfer in SIMs	39
3.1 Heat transfer mechanism	40
3.2 VIPs thermal performance parameters	44
4. Testing and simulation approaches	51
4.1 Steady-state measurement methods.....	52
4.1.1 Guarded Hot Plate - GHP	52
4.1.2 Heat Flow Meter - HFM.....	56
4.1.3 Methodologies for the measurement of ψ -values	59
4.2 Transient measurement methods	61
4.2.1 Hot wire/Hot strip.....	61
4.2.2 Hot disk	63

4.2.2 Laser flash	64
4.3 Numerical simulations	65
4.3.1 Bi-dimensional steady-state heat transfer.....	65
4.3.2 Energy analysis and thermal load simulation.....	71
4.3.3 Dynamic hygrothermal simulation	74
5. Measurement uncertainty analysis	85
5.1 Type A, type B and combined uncertainty	86
5.1.1 Combined uncertainty	93
5.1.2 Correlated quantities.....	93
5.2 Thermal conductivity.....	96
5.2.1 Heat Flow Meter	97
5.2.2 Guarded Hot Plate	99
5.3 Linear thermal transmittance	102
5.3.1 Heat Flow Meter.....	103
5.3.2 Guarded Hot Plate	105
6. Theoretical standard-based measurement uncertainty analysis	107
6.1 Heat Flow Meter approach	108
6.1.1 HFM sensitivity analysis	110
6.2 Guarded Hot Plate approach.....	117
6.2.1 GHP sensitivity analysis.....	119
7. Experimental assessment and validation of measurement uncertainty	123
7.1 Numerical bi-dimensional analysis of the edge effects	124
7.2 Repeatability issues in VIPs thermal conductivity measurements (HFM).....	125
7.2.1 ANOVA analysis.....	129
7.3 Thermal conductivity uncertainty (Type A).....	137
7.3.1 Heat Flow Meter - VIP	138
7.3.2 Guarded Hot Plate - Aerogel blanket	144

7.4 Thermal bridging effects uncertainty	147
7.4.1 Guarded Hot Plate	148
7.4.2 Heat Flow Meter	156
7.4.3 Comparison between GHP and HFM methods	160
8. Experimental investigation of the thermal behaviour of SIMs	165
8.1 Effects of temperature and ageing on SIM thermal properties (HFM)	166
8.1.1 Convective, radiative and conductive contributions in VIP and Fumed Silica core	173
8.1.2 Performance at the building component scale	176
8.2 VIPs Type B uncertainty variability (HFM)	180
8.3 Experimental campaign for VIPs thermal properties measurement (HFM)	181
8.3.1 Thermal conductivity	182
8.3.2 Linear thermal transmittance	191
9. Potentialities of VIPs for the energy efficient retrofit of buildings	195
9.1 The energy analysis	195
9.2 The thermo-economic analysis	197
9.2.1 Economic parameter	197
9.2.2 Results	201
10. Outlook: prediction of VIPs long-term performances and associated uncertainties	210
10.1 Building component simulation model	211
10.1.1 Brick wall in Torino	211
10.1.2 Pitched Roof – wood frame in Torino	219
10.2 Life expectancy	226
11. Conclusions	233
11.1 Theoretical standard-based measurement uncertainties	234
11.2 Experimental assessment of the measurement uncertainties	236

11.3 VIPs thermal behaviour	240
11.4 Potentialities and thermo-economic analysis of VIPs	245
11.5 Long-term VIPs thermal performances and service-life	247
11.6 Final remarks and outlooks.....	250
References	253
Appendix A HFM sensitivity analysis	271
Appendix B Thermal conductivity uncertainty - HFM.....	277
Appendix C Thermal conductivity uncertainty - GHP.....	327
Appendix D VIP centre of panel thermal characterisation - GHP	339
Appendix E Linear thermal transmittance uncertainty - GHP	347
Appendix F Linear thermal transmittance uncertainty - HFM.....	361

List of Figures

Figure 1: European final energy consumption in 2014 [5].....	2
Figure 2: European thermal insulation market in 2014 [16].....	5
Figure 3: Overview of various silica manufacturing processes [19]	8
Figure 4: Fumed silica powder [24].....	9
Figure 5: Fumed silica pressed board	10
Figure 6: Fumed silica manufacturing [30]	11
Figure 7: Fumed silica, coupled with calcium silicate panels [31].....	12
Figure 8: Fumed silica integrated brick [30]	13
Figure 9: Solid aerogel placed upon an aerogel blanket [45]	16
Figure 10: Several aerogel typologies, from transition metal oxide, including iron oxide (rust) aerogel (top), compared to silica aerogel (bottom) [35].....	17
Figure 11: a) Aerogel-based on resorcinol-formaldehyde polymer (left) and electrically-conductive carbon aerogel (right); b) another carbon aerogel [48]	17
Figure 12: Liquid-vapour critical point in a pressure/temperature phase diagram [55].....	19
Figure 13: a) Vacuum Insulation Panels; b) VIP structure.....	21
Figure 14: Thermal conductivity of different insulation materials as a function of the internal residual pressure [28]	23
Figure 15: Structure of a VIP with MF envelope	26
Figure 16: Thermal conductivity during time, considering several envelope typologies [63]	26
Figure 17: Thermal bridge at the panel level.....	31
Figure 18: Comparison between the linear thermal conductivity of an AF and MF envelope, varying the panel thickness [99]	31

Figure 19: Edge effects as a function of the panel size [101].....	32
Figure 20: Schemes of VIPs assemblies: a) air joint; b) structural joint [103].....	34
Figure 21: Influence of the air joint width (d) on the value of ψ . Experimental and numerical results for 10, 20, 30 mm thick panels [103].....	34
Figure 22: ψ versus R_{Joint} : experimental and numerical results [103]	35
Figure 23: Linear thermal transmittance for wood joints and polyurethane joint as a function of the variation of $R_i + R_e$ for three different types of wall (a, b, c) [65].....	36
Figure 24: Linear thermal transmittance for different materials joints as a function of the resistance of additional layers ($R_i + R_e$) [105].....	37
Figure 25: Sketch of the three heat transfer paths in nanostructured materials [108].....	40
Figure 26: VIPs thermal conductivity as a function of water content [78].....	43
Figure 27: Calculation scheme for the linear thermal transmittance of the thermal bridge, ψ , for a portion of the envelope component having a width of (l_x+l_z) and a depth of l_y . The thick black line represents the thermal bridge	47
Figure 28: Two specimens symmetrical GHP apparatus.....	53
Figure 29: Single specimen symmetrical GHP apparatus	54
Figure 30: Single specimen symmetrical HFM apparatus.....	56
Figure 31: HFM apparatus method for the determination of ψ -values	59
Figure 32: Different affected areas with exemplary thermocouples distribution [116].....	60
Figure 33: TLS method scheme [42].....	62
Figure 34: THB method scheme	63
Figure 35: TPS method scheme. a) Sensor; b) sensor positioning and generated heat flux; c) obtainable λ -values [129]	64
Figure 36: Laser flash method scheme [132].....	65
Figure 37: Model for 2D numerical analyses of HFM apparatus [29]	68
Figure 38: Model for 2D numerical analyses of GHP apparatus.....	68

Figure 39: Number of pixels for triangulations. a) HFM - 1; b) GHP - 1	69
Figure 40: HHD in different European cities [135].....	73
Figure 41: Simulation outputs. a) Example of yearly time profiles; b) example of cumulative frequency analysis [144]	77
Figure 42: Simulated brick wall structure.....	78
Figure 43: Simulated pitched roof structure	78
Figure 44: a) VIP in roof component; b) Roof insulation assembly; c) Roof sections (Configurations A and B).....	79
Figure 45: Comparison between measured and simulated results. $\lambda = f(\vartheta)$ (temperature dependent thermal conductivity). $\lambda_{(10^{\circ}\text{C})}$ (constant thermal conductivity measured at 10°C). RMSE values were calculated for the period 24/09/2016 – 08/10/2016	82
Figure 46: Temperature regression line at the interface 2-3 (interior side).....	82
Figure 47: Temperature regression line at the interface 3-4 (exterior side)	83
Figure 48: Graphical illustration of the standard uncertainty from repeated observations of an input quantity: a) normal PDF distribution; b) histogram [13].....	90
Figure 49: Graphical illustration of the rectangular distribution of standard uncertainty [13].....	91
Figure 50: Graphical illustration of the triangular distribution of standard uncertainty [13].....	92
Figure 51: Uncorrelation of the least-squares fitting	95
Figure 52: Uncertainty isolines ($u_c(\lambda)$ between 1.0 % and 3.0 %) for different values of $\lambda = 0.004$ to 0.016 W/mK, as a function of the temperature difference $\Delta\vartheta$ and the thickness of the specimen t , assuming the maximum uncertainty according to EN 1946-3:1999 [148], equipment B [150].....	114
Figure 53: Uncertainty isolines ($u_c(\lambda)$ between 1.0 % and 3.0 %) for different values of $\lambda = 0.004$ to 0.016 W/mK, as a function of the temperature difference $\Delta\vartheta$ and the thickness of the specimen t , equipment B. a) assuming the maximum uncertainty according to EN 1946-3:1999 [148]; b) increasing the heat flux error by a factor	

2; c) increasing the thickness error by a factor 2; d) multiplying the $\Delta\vartheta$ error by a factor 2 [150].....	116
Figure 54: Uncertainty isolines ($u_c(\lambda)$ between 1.0 % and 3.0 %) for different values of $\lambda = 0.004$ to 0.016 W/mK, as a function of the temperature difference $\Delta\vartheta$ and the thickness of the specimen t , assuming the maximum uncertainty according to EN 1946-2:1999 [148], equipment B [150].....	120
Figure 55: Uncertainty isolines ($u_c(\lambda)$ between 1.0 % and 3.0 %) for different values of $\lambda = 0.004$ to 0.016 W/mK, as a function of the temperature difference $\Delta\vartheta$ and the thickness of the specimen t , equipment B. a) assuming the maximum uncertainty according to EN 1946-2:1999 [149]; b) increasing the electrical power error by a factor 2; c) increasing the thickness error by a factor 2; d) multiplying the $\Delta\vartheta$ error by a factor 2 [150]	122
Figure 56: Output of the HFM numerical 2D analysis: 30 mm VIP, $\vartheta_{avg} = 52.5$ °C [29].....	124
Figure 57: Output of the GHP numerical 2D analysis: 30 mm VIP, $\vartheta_{avg} = 40$ °C	125
Figure 58: Plot of repeatability data	127
Figure 59: Dot plot of λ	127
Figure 60: Boxplot of λ , and λ normalised from the effects of Sample blocks....	132
Figure 61: Residuals analysis	136
Figure 62: Boxplot of λ , and λ normalised from the effects of Temperature blocks	137
Figure 63: Tested VIP samples. a) 10 and 30 mm thick; b) 20 mm thick	138
Figure 64: λ_{COP} -values assessed by means of HFM-1 apparatus. a) FS based VIP 10 mm thick, $\vartheta_{avg} = 23^\circ\text{C}$, $\Delta\vartheta = 30^\circ\text{C}$; b) FS based VIP 30 mm thick, $\vartheta_{avg} = 5^\circ\text{C}$, $\Delta\vartheta = 20^\circ\text{C}$	140
Figure 65: 10 mm thick VIP thermal conductivity, a) as a function of ϑ_{avg} and b) $\Delta\vartheta$	141
Figure 66: 20 mm thick VIP thermal conductivity, a) as a function of ϑ_{avg} and b) $\Delta\vartheta$	142

Figure 67: 30 mm thick VIP thermal conductivity, a) as a function of ϑ_{avg} and b) $\Delta\vartheta$	143
Figure 68: Tested aerogel blanket [41]	144
Figure 69: Aerogel thermal conductivity, a) as a function of ϑ_{avg} and b) $\Delta\vartheta$	146
Figure 70: Samples. a) VIP 10 and 30 mm thick; b) punctured VIP and VIP core material; c) XPS [29]	168
Figure 71: Centre of panel λ depending on the mean testing temperature a) aged VIPs after 32 months of storage; b) fresh VIPs [29]	170
Figure 72: λ depending on the mean testing temperature. a) punctured VIP and FS core; b) XPS [29]	170
Figure 73: Evolution of the measured thermal conductivity over ageing time for different average temperature (λ_{10} , λ_{25} , λ_{40}) [75]	172
Figure 74: Measured thermal conductivity of VIP ($\lambda(\vartheta_i)_{VIP}$) as a function of the cube of average absolute temperature ϑ_{avg} [K] [75]	174
Figure 75: Measured $\lambda(\vartheta_i)_{core}$ for the FS sample, and $\Delta\lambda(\vartheta_i)$ calculated as the difference between the $\lambda(\vartheta_i)_{core}$ and the $\lambda(\vartheta_0)_{core}$, as a function of the cube of average absolute temperature ϑ_{avg} [K] [75]	174
Figure 76: VIP average temperature. a) Configuration A (VIP above the XPS layer); b) Configuration B (VIP below the XPS layer) [75].....	176
Figure 77: VIP actual thermal conductivity (temperature dependent). a) Configuration A (VIP above the XPS layer); b) Configuration B (VIP below the XPS layer) [75]	177
Figure 78: Monthly heat gains (positive values) and heat losses (negative values) across the roof component [75]	178
Figure 79: Indoor surface temperature profile of 11 th August [75]	179
Figure 80: Thermal conductivity relative uncertainty, as a function of $\Delta\vartheta$	181
Figure 81: Extra XPS insulating mask for VIPs with dimension 300 x 600 mm	183
Figure 82: APM rigid board. a) sample; b) drying phase; c) plastic wrapping ...	183
Figure 83: VIP - 1 thermal conductivity at different average temperatures and ageing conditions (300 x 600 mm).....	185

Figure 84: VIP - 1 thermal conductivity at different average temperatures and ageing conditions (600 x 600 mm).....	185
Figure 85: VIP - 4 thermal conductivity at different average temperatures and ageing conditions (300 x 600 mm).....	187
Figure 86: VIP - 4 thermal conductivity at different average temperatures and ageing conditions (600 x 600 mm).....	187
Figure 87: VIP - 4 and VIP - 5 thermal conductivity at different average temperatures and ageing conditions (500 x 500 mm).....	189
Figure 88: APM - 2 thermal conductivity at different average temperatures and ageing conditions (600 x 600 mm).....	190
Figure 89: VIP - 1.12 + 1.13 assembly. Equivalent thermal conductivity and linear thermal transmittance at different average temperatures and ageing conditions	192
Figure 90: VIP - 1.12 + 1.14 assembly. Equivalent thermal conductivity and linear thermal transmittance at different average temperatures and ageing conditions	193
Figure 91: VIP - 4.15 + 4.16 assembly. Equivalent thermal conductivity and linear thermal transmittance at different average temperatures and ageing conditions	193
Figure 92: VIP - 4.17 + 4.18 assembly. Equivalent thermal conductivity and linear thermal transmittance at different average temperatures and ageing conditions	193
Figure 93: Example of the evaluation of BERV [138]	201
Figure 94: DPBP as a function of climatic zones. The grey area represents the VIP convenience [138].....	202
Figure 95: BERV as a function of the climatic zone [138]	203
Figure 96: DPBP according to the wall U -value _{im} of the different countries. The crosses show the BERVs [138].....	204
Figure 97: DPBP as a function of aspect ratios [138].....	205
Figure 98: BERV according to the different aspect ratios [138]	205
Figure 99: DPBP as a function of insulation thicknesses [138]	206

Figure 100: BERV according to the VIP thicknesses (10, 20 and 30 mm) [138].....	207
Figure 101: DPBP as a function of the heating systems [138]	208
Figure 102: BERV according to the heating systems [138]	209
Figure 103: Data-sheet of the analysed wall [93]	212
Figure 104: Torino - year 2004 outdoor weather conditions (graphical output from Wufi [®]) [93]	212
Figure 105: Torino - year 2004 a) solar radiation; b) driving rain and mean wind speed (graphical output from Wufi [®]) [93]	213
Figure 106: Temperatures yearly time profiles (1.W_D_m_20) [93]	214
Figure 107: Relative humidities yearly time profiles (1.W_D_m_20) [93]	214
Figure 108: Vapour pressure yearly time profiles (1.W_D_m_20) [93]	215
Figure 109: Temperature cumulative frequency (1.W_D_m_20) [93].....	215
Figure 110: Relative humidity cumulative frequency (1.W_D_m_20) [93]	215
Figure 111: Vapour pressure cumulative frequency (1.W_D_m_20) [93].....	216
Figure 112: Data-sheet of the analysed roof [93]	220
Figure 113: Temperatures yearly time profiles (2.S_D_m_20) [93]	221
Figure 114: Relative humidities yearly time profiles (2.S_D_m_20) [93].....	222
Figure 115: Vapour pressure yearly time profiles (2.S_D_m_20) [93].....	222
Figure 116: Temperature cumulative frequency (2.S_D_m_20) [93]	222
Figure 117: Relative humidity cumulative frequency (2.S_D_m_20) [93].....	223
Figure 118: Vapour pressure cumulative frequency (2.S_D_m_20) [93]	223
Figure 119: Procedure for estimating the VIPs service life [93]	227
Figure 120: Time evolution of λ_{core} as a function of the envelope typology (20 mm thick VIP, south bright roof, medium internal moisture load) ...	229
Figure 121: Time evolution of λ_{core} as a function of the panel thickness (10 and 20 mm thick VIP, south bright roof, medium internal moisture load, MF4 envelope)	229

Figure 122: VIP internal air pressure trend over time as a function of the envelope typology (20 mm thick VIP, south bright roof, medium internal moisture load)	230
Figure 123: VIP internal air pressure trend over time as a function of the panel thickness (10 and 20 mm thick VIP, south bright roof, medium internal moisture load, MF4 envelope).....	231
Figure 124: VIP internal water content trend over time as a function of the envelope typology (20 mm thick VIP, south bright roof, medium internal moisture load)	232
Figure 125: VIP internal water content trend over time as a function of the panel thickness (10 and 20 mm thick VIP, south bright roof, medium internal moisture load, MF4 envelope).....	232
Figure A. 1: HFM - Combined relative uncertainty as a function of thermal conductivity and temperature difference, equipment A, B and C according to EN 1946-3:1999 [148] (sample thickness of 10 mm) [150].....	273
Figure A. 2: HFM - Combined relative uncertainty as a function of thermal conductivity and temperature difference, equipment A, B and C according to EN 1946-3:1999 [148] (sample thickness of 20 mm) [150].....	274
Figure A. 3: HFM - Combined relative uncertainty as a function of thermal conductivity and temperature difference, equipment A, B and C according to EN 1946-3:1999 [148] (sample thickness of 40 mm) [150].....	275
Figure A. 4: HFM - Combined relative uncertainty as a function of thermal conductivity and temperature difference, equipment A, B and C according to EN 1946-3:1999 [148] (sample thickness of 80 mm) [150].....	276
Figure B. 1: λ_{COP} -values assessed by means of HFM-1 apparatus (Sample: FS based VIP 10 mm thick, $\vartheta_{avg} = 5^{\circ}\text{C}$, $\Delta\vartheta = 10^{\circ}\text{C}$).....	279

Figure B. 2: λ_{COP} -values assessed by means of HFM-1 apparatus (Sample: FS based VIP 10 mm thick, $\vartheta_{avg} = 5^{\circ}\text{C}$, $\Delta\vartheta = 20^{\circ}\text{C}$).....	280
Figure B. 3: λ_{COP} -values assessed by means of HFM-1 apparatus (Sample: FS based VIP 10 mm thick, $\vartheta_{avg} = 5^{\circ}\text{C}$, $\Delta\vartheta = 30^{\circ}\text{C}$).....	281
Figure B. 4: λ_{COP} -values assessed by means of HFM-1 apparatus (Sample: FS based VIP 10 mm thick, $\vartheta_{avg} = 5^{\circ}\text{C}$, $\Delta\vartheta = 40^{\circ}\text{C}$).....	282
Figure B. 5: λ_{COP} -values assessed by means of HFM-1 apparatus (Sample: FS based VIP 10 mm thick, $\vartheta_{avg} = 10^{\circ}\text{C}$, $\Delta\vartheta = 10^{\circ}\text{C}$).....	283
Figure B. 6: λ_{COP} -values assessed by means of HFM-1 apparatus (Sample: FS based VIP 10 mm thick, $\vartheta_{avg} = 10^{\circ}\text{C}$, $\Delta\vartheta = 20^{\circ}\text{C}$).....	284
Figure B. 7: λ_{COP} -values assessed by means of HFM-1 apparatus (Sample: FS based VIP 10 mm thick, $\vartheta_{avg} = 10^{\circ}\text{C}$, $\Delta\vartheta = 30^{\circ}\text{C}$).....	285
Figure B. 8: λ_{COP} -values assessed by means of HFM-1 apparatus (Sample: FS based VIP 10 mm thick, $\vartheta_{avg} = 10^{\circ}\text{C}$, $\Delta\vartheta = 40^{\circ}\text{C}$).....	286
Figure B. 9: λ_{COP} -values assessed by means of HFM-1 apparatus (Sample: FS based VIP 10 mm thick, $\vartheta_{avg} = 23^{\circ}\text{C}$, $\Delta\vartheta = 10^{\circ}\text{C}$).....	287
Figure B. 10: λ_{COP} -values assessed by means of HFM-1 apparatus (Sample: FS based VIP 10 mm thick, $\vartheta_{avg} = 23^{\circ}\text{C}$, $\Delta\vartheta = 20^{\circ}\text{C}$).....	288
Figure B. 11: λ_{COP} -values assessed by means of HFM-1 apparatus (Sample: FS based VIP 10 mm thick, $\vartheta_{avg} = 23^{\circ}\text{C}$, $\Delta\vartheta = 30^{\circ}\text{C}$).....	289
Figure B. 12: λ_{COP} -values assessed by means of HFM-1 apparatus (Sample: FS based VIP 10 mm thick, $\vartheta_{avg} = 23^{\circ}\text{C}$, $\Delta\vartheta = 40^{\circ}\text{C}$).....	290
Figure B. 13: λ_{COP} -values assessed by means of HFM-1 apparatus (Sample: FS based VIP 10 mm thick, $\vartheta_{avg} = 40^{\circ}\text{C}$, $\Delta\vartheta = 10^{\circ}\text{C}$).....	291
Figure B. 14: λ_{COP} -values assessed by means of HFM-1 apparatus (Sample: FS based VIP 10 mm thick, $\vartheta_{avg} = 40^{\circ}\text{C}$, $\Delta\vartheta = 20^{\circ}\text{C}$).....	292
Figure B. 15: λ_{COP} -values assessed by means of HFM-1 apparatus (Sample: FS based VIP 10 mm thick, $\vartheta_{avg} = 40^{\circ}\text{C}$, $\Delta\vartheta = 30^{\circ}\text{C}$).....	293
Figure B. 16: λ_{COP} -values assessed by means of HFM-1 apparatus (Sample: FS based VIP 10 mm thick, $\vartheta_{avg} = 40^{\circ}\text{C}$, $\Delta\vartheta = 40^{\circ}\text{C}$).....	294
Figure B. 17: λ_{COP} -values assessed by means of HFM-1 apparatus (Sample: FS based VIP 20 mm thick, $\vartheta_{avg} = 5^{\circ}\text{C}$, $\Delta\vartheta = 10^{\circ}\text{C}$).....	295

Figure B. 18: λ_{COP} -values assessed by means of HFM-1 apparatus (Sample: FS based VIP 20 mm thick, $\vartheta_{avg} = 5^{\circ}\text{C}$, $\Delta\vartheta = 20^{\circ}\text{C}$).....	296
Figure B. 19: λ_{COP} -values assessed by means of HM-1 apparatus (Sample: FS based VIP 20 mm thick, $\vartheta_{avg} = 5^{\circ}\text{C}$, $\Delta\vartheta = 30^{\circ}\text{C}$).....	297
Figure B. 20: λ_{COP} -values assessed by means of HFM-1 apparatus (Sample: FS based VIP 20 mm thick, $\vartheta_{avg} = 5^{\circ}\text{C}$, $\Delta\vartheta = 40^{\circ}\text{C}$).....	298
Figure B. 21: λ_{COP} -values assessed by means of HFM-1 apparatus (Sample: FS based VIP 20 mm thick, $\vartheta_{avg} = 10^{\circ}\text{C}$, $\Delta\vartheta = 10^{\circ}\text{C}$).....	299
Figure B. 22: λ_{COP} -values assessed by means of HFM-1 apparatus (Sample: FS based VIP 20 mm thick, $\vartheta_{avg} = 10^{\circ}\text{C}$, $\Delta\vartheta = 20^{\circ}\text{C}$).....	300
Figure B. 23: λ_{COP} -values assessed by means of HFM-1 apparatus (Sample: FS based VIP 20 mm thick, $\vartheta_{avg} = 10^{\circ}\text{C}$, $\Delta\vartheta = 30^{\circ}\text{C}$).....	301
Figure B. 24: λ_{COP} -values assessed by means of HFM-1 apparatus (Sample: FS based VIP 20 mm thick, $\vartheta_{avg} = 10^{\circ}\text{C}$, $\Delta\vartheta = 40^{\circ}\text{C}$).....	302
Figure B. 25: λ_{COP} -values assessed by means of HFM-1 apparatus (Sample: FS based VIP 20 mm thick, $\vartheta_{avg} = 23^{\circ}\text{C}$, $\Delta\vartheta = 10^{\circ}\text{C}$).....	303
Figure B. 26: λ_{COP} -values assessed by means of HFM-1 apparatus (Sample: FS based VIP 20 mm thick, $\vartheta_{avg} = 23^{\circ}\text{C}$, $\Delta\vartheta = 20^{\circ}\text{C}$).....	304
Figure B. 27: λ_{COP} -values assessed by means of HFM-1 apparatus (Sample: FS based VIP 20 mm thick, $\vartheta_{avg} = 23^{\circ}\text{C}$, $\Delta\vartheta = 30^{\circ}\text{C}$).....	305
Figure B. 28: λ_{COP} -values assessed by means of HFM-1 apparatus (Sample: FS based VIP 20 mm thick, $\vartheta_{avg} = 23^{\circ}\text{C}$, $\Delta\vartheta = 40^{\circ}\text{C}$).....	306
Figure B. 29: λ_{COP} -values assessed by means of HFM-1 apparatus (Sample: FS based VIP 20 mm thick, $\vartheta_{avg} = 40^{\circ}\text{C}$, $\Delta\vartheta = 10^{\circ}\text{C}$).....	307
Figure B. 30: λ_{COP} -values assessed by means of HFM-1 apparatus (Sample: FS based VIP 20 mm thick, $\vartheta_{avg} = 40^{\circ}\text{C}$, $\Delta\vartheta = 20^{\circ}\text{C}$).....	308
Figure B. 31: λ_{COP} -values assessed by means of HFM-1 apparatus (Sample: FS based VIP 20 mm thick, $\vartheta_{avg} = 40^{\circ}\text{C}$, $\Delta\vartheta = 30^{\circ}\text{C}$).....	309
Figure B. 32: λ_{COP} -values assessed by means of HFM-1 apparatus (Sample: FS based VIP 20 mm thick, $\vartheta_{avg} = 40^{\circ}\text{C}$, $\Delta\vartheta = 40^{\circ}\text{C}$).....	310
Figure B. 33: λ_{COP} -values assessed by means of HFM-1 apparatus (Sample: FS based VIP 30 mm thick, $\vartheta_{avg} = 5^{\circ}\text{C}$, $\Delta\vartheta = 10^{\circ}\text{C}$).....	311

Figure B. 34: λ_{COP} -values assessed by means of HFM-1 apparatus (Sample: FS based VIP 30 mm thick, $\vartheta_{avg} = 5^{\circ}\text{C}$, $\Delta\vartheta = 20^{\circ}\text{C}$).....	312
Figure B. 35: λ_{COP} -values assessed by means of HFM-1 apparatus (Sample: FS based VIP 30 mm thick, $\vartheta_{avg} = 5^{\circ}\text{C}$, $\Delta\vartheta = 30^{\circ}\text{C}$).....	313
Figure B. 36: λ_{COP} -values assessed by means of HFM-1 apparatus (Sample: FS based VIP 30 mm thick, $\vartheta_{avg} = 5^{\circ}\text{C}$, $\Delta\vartheta = 40^{\circ}\text{C}$).....	314
Figure B. 37: λ_{COP} -values assessed by means of HFM-1 apparatus (Sample: FS based VIP 30 mm thick, $\vartheta_{avg} = 10^{\circ}\text{C}$, $\Delta\vartheta = 10^{\circ}\text{C}$).....	315
Figure B. 38: λ_{COP} -values assessed by means of HFM-1 apparatus (Sample: FS based VIP 30 mm thick, $\vartheta_{avg} = 10^{\circ}\text{C}$, $\Delta\vartheta = 20^{\circ}\text{C}$).....	316
Figure B. 39: λ_{COP} -values assessed by means of HFM-1 apparatus (Sample: FS based VIP 30 mm thick, $\vartheta_{avg} = 10^{\circ}\text{C}$, $\Delta\vartheta = 30^{\circ}\text{C}$).....	317
Figure B. 40: λ_{COP} -values assessed by means of HFM-1 apparatus (Sample: FS based VIP 30 mm thick, $\vartheta_{avg} = 10^{\circ}\text{C}$, $\Delta\vartheta = 40^{\circ}\text{C}$).....	318
Figure B. 41: λ_{COP} -values assessed by means of HFM-1 apparatus (Sample: FS based VIP 30 mm thick, $\vartheta_{avg} = 23^{\circ}\text{C}$, $\Delta\vartheta = 10^{\circ}\text{C}$).....	319
Figure B. 42: λ_{COP} -values assessed by means of HFM-1 apparatus (Sample: FS based VIP 30 mm thick, $\vartheta_{avg} = 23^{\circ}\text{C}$, $\Delta\vartheta = 20^{\circ}\text{C}$).....	320
Figure B. 43: λ_{COP} -values assessed by means of HFM-1 apparatus (Sample: FS based VIP 30 mm thick, $\vartheta_{avg} = 23^{\circ}\text{C}$, $\Delta\vartheta = 30^{\circ}\text{C}$).....	321
Figure B. 44: λ_{COP} -values assessed by means of HFM-1 apparatus (Sample: FS based VIP 30 mm thick, $\vartheta_{avg} = 23^{\circ}\text{C}$, $\Delta\vartheta = 40^{\circ}\text{C}$).....	322
Figure B. 45: λ_{COP} -values assessed by means of HFM-1 apparatus (Sample: FS based VIP 30 mm thick, $\vartheta_{avg} = 40^{\circ}\text{C}$, $\Delta\vartheta = 10^{\circ}\text{C}$).....	323
Figure B. 46: λ_{COP} -values assessed by means of HFM-1 apparatus (Sample: FS based VIP 30 mm thick, $\vartheta_{avg} = 40^{\circ}\text{C}$, $\Delta\vartheta = 20^{\circ}\text{C}$).....	324
Figure B. 47: λ_{COP} -values assessed by means of HFM-1 apparatus (Sample: FS based VIP 30 mm thick, $\vartheta_{avg} = 40^{\circ}\text{C}$, $\Delta\vartheta = 30^{\circ}\text{C}$).....	325
Figure B. 48: λ_{COP} -values assessed by means of HFM-1 apparatus (Sample: FS based VIP 30 mm thick, $\vartheta_{avg} = 40^{\circ}\text{C}$, $\Delta\vartheta = 40^{\circ}\text{C}$).....	326

Figure C. 1: λ -values assessed by means of GHP-1 apparatus (Sample: Aerogel blanket 10 mm thick, $\vartheta_{avg} = 5^{\circ}\text{C}$, $\Delta\vartheta = 5^{\circ}\text{C}$)	329
Figure C. 2: λ -values assessed by means of GHP-1 apparatus (Sample: Aerogel blanket 10 mm thick, $\vartheta_{avg} = 5^{\circ}\text{C}$, $\Delta\vartheta = 10^{\circ}\text{C}$)	330
Figure C. 3: λ -values assessed by means of GHP-1 apparatus (Sample: Aerogel blanket 10 mm thick, $\vartheta_{avg} = 5^{\circ}\text{C}$, $\Delta\vartheta = 15^{\circ}\text{C}$)	331
Figure C. 4: λ -values assessed by means of GHP-1 apparatus (Sample: Aerogel blanket 10 mm thick, $\vartheta_{avg} = 10^{\circ}\text{C}$, $\Delta\vartheta = 5^{\circ}\text{C}$)	332
Figure C. 5: λ -values assessed by means of GHP-1 apparatus (Sample: Aerogel blanket 10 mm thick, $\vartheta_{avg} = 10^{\circ}\text{C}$, $\Delta\vartheta = 10^{\circ}\text{C}$)	333
Figure C. 6: λ -values assessed by means of GHP-1 apparatus (Sample: Aerogel blanket 10 mm thick, $\vartheta_{avg} = 10^{\circ}\text{C}$, $\Delta\vartheta = 15^{\circ}\text{C}$)	334
Figure C. 7: λ -values assessed by means of GHP-1 apparatus (Sample: Aerogel blanket 10 mm thick, $\vartheta_{avg} = 23^{\circ}\text{C}$, $\Delta\vartheta = 5^{\circ}\text{C}$)	335
Figure C. 8: λ -values assessed by means of GHP-1 apparatus (Sample: Aerogel blanket 10 mm thick, $\vartheta_{avg} = 23^{\circ}\text{C}$, $\Delta\vartheta = 10^{\circ}\text{C}$)	336
Figure C. 9: λ -values assessed by means of GHP-1 apparatus (Sample: Aerogel blanket 10 mm thick, $\vartheta_{avg} = 23^{\circ}\text{C}$, $\Delta\vartheta = 15^{\circ}\text{C}$)	337

List of Tables

Table 1: Classification of insulating materials	6
Table 2: Typical APMs properties [19]	9
Table 3: Typical Aerogels properties [42]	15
Table 4: Silica aerogel typical properties ([46],[47])	16
Table 5: Three different LCA analysis, comparing Glass wool, EPS and VIP [42]	27
Table 6: Politecnico di Torino apparatus: HFM - 1	66
Table 7: INRiM apparatus: GHP - 1	67
Table 8: Envelope thermal conductivities. Model measurements in [mm]. Data provided by the producer of the simulated VIPs [14]	70
Table 9: Different aspect ratios	72
Table 10: Simulation approach [144]	76
Table 11: Ranges of ϑ , RH and p_v values [144]	78
Table 12: Roof layers from inside to outside - Configuration A. (*from VIP datasheet)	80
Table 13: Measuring chains and uncorrelation assumption	96
Table 14: Adopted apparatuses, joints configurations and thermocouples positions	102
Table 15: Apparatuses geometrical properties and configuration	103
Table 16: HFM - Maximum probable relative errors $u(x_i)$ of equipment A, B and C [148]	108
Table 17: HFM - Overall size and limitations of specimen thickness and range of thermal conductivity of equipment A, B and C [148]	109
Table 18: HFM - Set of data for the calculation of the $u_c(\lambda_{HFM})$, equipment A, B and C	109

Table 19: HFM - Absolute errors for the calculation of the $u_c(\lambda_{HFM})$, equipment A, B and C [148]	110
Table 20: Combined uncertainty $u_c(\lambda)$ in % as a function of λ (equal to 0.002, 0.002, 0.008 and 0.020 W/mK), varying temperature difference $\Delta\vartheta$ and with constant thickness t , assuming the maximum uncertainty according to EN 1946-3:1999 [148]; equipment A	111
Table 21: Combined uncertainty $u_c(\lambda)$ in % as a function of λ (equal to 0.002, 0.002, 0.008 and 0.020 W/mK), varying temperature difference $\Delta\vartheta$ and with constant thickness t , assuming the maximum uncertainty according to EN 1946-3:1999 [148]; equipment B.....	112
Table 22: Combined uncertainty $u_c(\lambda)$ in % as a function of λ (equal to 0.002, 0.002, 0.008 and 0.020 W/mK), varying temperature difference $\Delta\vartheta$ and with constant thickness t , assuming the maximum uncertainty according to EN 1946-3:1999 [148]; equipment C.....	113
Table 23: GHP - Maximum probable relative errors $u(x_i)$ of equipment A, B and C [149].....	117
Table 24: GHP - Overall size and limitations of specimen thickness and range of thermal conductivity of equipment A, B and C [149]	118
Table 25: GHP - Set of data for the calculation of the $u_c(\lambda_{GHP})$, equipment A, B and C.....	118
Table 26: GHP - Absolute errors for the calculation of the $u_c(\lambda_{GHP})$, equipment A, B and C [149]	118
Table 27: Repeatability testing plan and the related thermal conductivity results	126
Table 28: Means and standard deviation calculation (λ and s are in $[10^{-4} \cdot \text{W/mK}]$).....	128
Table 29: Nested ANOVA results	131
Table 30: One-Way ANOVA results.....	135
Table 31: 10 mm thick VIP thermal conductivities and related Type A measurement uncertainties (HFM-1)	141
Table 32: 20 mm thick VIP thermal conductivities and related Type A measurement uncertainties (HFM-1)	142

Table 33: 30 mm thick VIP thermal conductivities and related Type A measurement uncertainties (HFM-1)	142
Table 34: $u_c(\lambda_{COP})$ sensitivity coefficient general trend increasing the $\Delta\vartheta$	144
Table 35: Aerogel thermal conductivities and related Type A measurement uncertainties (GHP-1)	146
Table 36: GHP-2 and GHP-3 warming analysis.....	150
Table 37: Summary of the dimensions of the useful areas of GHP-2 and GHP-3 apparatuses, with the related combined uncertainties.....	152
Table 38: VIP centre of panel thermal conductivities and related Type B measurement uncertainties (apparatus GHP-2 for FS based VIPs and GHP-3 for FG based VIPs)	152
Table 39: Summary of the dimensions of the useful areas of GHP-2 apparatus involved in the evaluation of $\Delta\vartheta_m$, with the related combined uncertainties	154
Table 40: VIP assemblies thermal properties and related Type B measurement uncertainties (apparatus GHP-2 for FS based VIPs and GHP-3 for FG based VIPs, Commutated joint)	155
Table 41: VIP assemblies thermal properties and related Type B measurement uncertainties (apparatus HFM-2, Commutated joint).....	158
Table 42: VIP assemblies thermal properties and related Type B measurement uncertainties (apparatus HFM-2, Offset joint).....	159
Table 43: VIP assemblies thermal properties and related Type B measurement uncertainties (apparatus HFM-2, Gasket strip joint)	159
Table 44: VIP assemblies thermal properties and related measurement uncertainties (comparison between GHP-2 and HFM-2, Commutated joint).....	161
Table 45: Characteristics of FS based VIPs declared by producer [29]	167
Table 46: VIPs experimentally assessed characteristics [29]	167
Table 47: Experimentally assessed characteristics of fresh VIPs [29]	168
Table 48: Thermal conductivity depending on average temperature, and measurement uncertainty of different insulating materials [29]	169

Table 49: Measured thermal conductivities at various test temperatures and ageing time [75]	172
Table 50: Thermal conductivity and relative uncertainty, as a function of $\Delta\vartheta$, for VIPs 10, 20 and 30 mm thick	180
Table 51: VIP - 1 thermal conductivity and relative uncertainty at different average temperatures and ageing conditions	184
Table 52: VIP - 4 thermal conductivity and relative uncertainty at different average temperatures and ageing conditions (first part)	185
Table 53: VIP - 4 (second part) and VIP - 5 thermal conductivity and relative uncertainty at different average temperatures and ageing conditions	188
Table 54: APM - 2 thermal conductivity and relative uncertainty at different average temperatures and ageing conditions	190
Table 55: VIP - 1 and VIP - 4 assemblies. Equivalent thermal conductivity with the relative uncertainty, and linear thermal transmittance at different average temperatures and ageing conditions.....	191
Table 56: Space heating energy demand, according to different climatic zones and aspect ratios [138]	196
Table 57: Insulation investment costs [138]	197
Table 58: Internal space savings [138]	199
Table 59: Calculation of the BERV according to the wall $U\text{-value}_{lim}$ of the different countries [138].....	204
Table 60: Summary of the different wall configurations [93]	213
Table 61: Wall: frequency distribution at the faces of a VIP 20 mm thick, considering a medium moisture load (1% of frequency corresponds to 3.65 days/year of exposure) [93]	218
Table 62: Wall: frequency distribution at the faces of a VIP 10 and 20 mm thick, considering a high moisture load (1% of frequency corresponds to 3.65 days/year of exposure) [93]	219
Table 63: Summary of the different roof configurations [93]	221

Table 64: Roof: frequency distribution at the faces of a VIP 20 mm thick, considering a medium moisture load (1% of frequency corresponds to 3.65 days/year of exposure) [93]	225
Table 65: Service life of the different roof configurations, considering a medium moisture load.....	228
Table B. 1: Type A $u_c(\lambda_{COP})$ assessment, by means of HFM-1 apparatus (Sample: FS based VIP 10 mm thick, $\vartheta_{avg} = 5^\circ\text{C}$, $\Delta\vartheta = 10^\circ\text{C}$)	279
Table B. 2: Type A $u_c(\lambda_{COP})$ sensitivity coefficients, by means of HFM-1 apparatus (Sample: FS based VIP 10 mm thick, $\vartheta_{avg} = 5^\circ\text{C}$, $\Delta\vartheta = 10^\circ\text{C}$).....	279
Table B. 3: Type A $u_c(\lambda_{COP})$ assessment, by means of HFM-1 apparatus (Sample: FS based VIP 10 mm thick, $\vartheta_{avg} = 5^\circ\text{C}$, $\Delta\vartheta = 20^\circ\text{C}$)	280
Table B. 4: Type A $u_c(\lambda_{COP})$ sensitivity coefficients, by means of HFM-1 apparatus (Sample: FS based VIP 10 mm thick, $\vartheta_{avg} = 5^\circ\text{C}$, $\Delta\vartheta = 20^\circ\text{C}$).....	280
Table B. 5: Type A $u_c(\lambda_{COP})$ assessment, by means of HFM-1 apparatus (Sample: FS based VIP 10 mm thick, $\vartheta_{avg} = 5^\circ\text{C}$, $\Delta\vartheta = 30^\circ\text{C}$)	281
Table B. 6: Type A $u_c(\lambda_{COP})$ sensitivity coefficients, by means of HFM-1 apparatus (Sample: FS based VIP 10 mm thick, $\vartheta_{avg} = 5^\circ\text{C}$, $\Delta\vartheta = 30^\circ\text{C}$).....	281
Table B. 7: Type A $u_c(\lambda_{COP})$ assessment, by means of HFM-1 apparatus (Sample: FS based VIP 10 mm thick, $\vartheta_{avg} = 5^\circ\text{C}$, $\Delta\vartheta = 40^\circ\text{C}$)	282
Table B. 8: Type A $u_c(\lambda_{COP})$ sensitivity coefficients, by means of HFM-1 apparatus (Sample: FS based VIP 10 mm thick, $\vartheta_{avg} = 5^\circ\text{C}$, $\Delta\vartheta = 40^\circ\text{C}$).....	282
Table B. 9: Type A $u_c(\lambda_{COP})$ assessment, by means of HFM-1 apparatus (Sample: FS based VIP 10 mm thick, $\vartheta_{avg} = 10^\circ\text{C}$, $\Delta\vartheta = 10^\circ\text{C}$)	283
Table B. 10: Type A $u_c(\lambda_{COP})$ sensitivity coefficients, by means of HFM-1 apparatus (Sample: FS based VIP 10 mm thick, $\vartheta_{avg} = 10^\circ\text{C}$, $\Delta\vartheta = 10^\circ\text{C}$).....	283
Table B. 11: Type A $u_c(\lambda_{COP})$ assessment, by means of HFM-1 apparatus (Sample: FS based VIP 10 mm thick, $\vartheta_{avg} = 10^\circ\text{C}$, $\Delta\vartheta = 20^\circ\text{C}$)	284

Table B. 12: Type A $u_c(\lambda_{COP})$ sensitivity coefficients, by means of HFM-1 apparatus (Sample: FS based VIP 10 mm thick, $\vartheta_{avg} = 10^\circ\text{C}$, $\Delta\vartheta = 20^\circ\text{C}$).....	284
Table B. 13: Type A $u_c(\lambda_{COP})$ assessment, by means of HFM-1 apparatus (Sample: FS based VIP 10 mm thick, $\vartheta_{avg} = 10^\circ\text{C}$, $\Delta\vartheta = 30^\circ\text{C}$)	285
Table B. 14: Type A $u_c(\lambda_{COP})$ sensitivity coefficients, by means of HFM-1 apparatus (Sample: FS based VIP 10 mm thick, $\vartheta_{avg} = 10^\circ\text{C}$, $\Delta\vartheta = 30^\circ\text{C}$).....	285
Table B. 15: Type A $u_c(\lambda_{COP})$ assessment, by means of HFM-1 apparatus (Sample: FS based VIP 10 mm thick, $\vartheta_{avg} = 10^\circ\text{C}$, $\Delta\vartheta = 40^\circ\text{C}$)	286
Table B. 16: Type A $u_c(\lambda_{COP})$ sensitivity coefficients, by means of HFM-1 apparatus (Sample: FS based VIP 10 mm thick, $\vartheta_{avg} = 10^\circ\text{C}$, $\Delta\vartheta = 40^\circ\text{C}$).....	286
Table B. 17: Type A $u_c(\lambda_{COP})$ assessment, by means of HFM-1 apparatus (Sample: FS based VIP 10 mm thick, $\vartheta_{avg} = 23^\circ\text{C}$, $\Delta\vartheta = 10^\circ\text{C}$)	287
Table B. 18: Type A $u_c(\lambda_{COP})$ sensitivity coefficients, by means of HFM-1 apparatus (Sample: FS based VIP 10 mm thick, $\vartheta_{avg} = 23^\circ\text{C}$, $\Delta\vartheta = 10^\circ\text{C}$).....	287
Table B. 19: Type A $u_c(\lambda_{COP})$ assessment, by means of HFM-1 apparatus (Sample: FS based VIP 10 mm thick, $\vartheta_{avg} = 23^\circ\text{C}$, $\Delta\vartheta = 20^\circ\text{C}$)	288
Table B. 20: Type A $u_c(\lambda_{COP})$ sensitivity coefficients, by means of HFM-1 apparatus (Sample: FS based VIP 10 mm thick, $\vartheta_{avg} = 23^\circ\text{C}$, $\Delta\vartheta = 20^\circ\text{C}$).....	288
Table B. 21: Type A $u_c(\lambda_{COP})$ assessment, by means of HFM-1 apparatus (Sample: FS based VIP 10 mm thick, $\vartheta_{avg} = 23^\circ\text{C}$, $\Delta\vartheta = 30^\circ\text{C}$)	289
Table B. 22: Type A $u_c(\lambda_{COP})$ sensitivity coefficients, by means of HFM-1 apparatus (Sample: FS based VIP 10 mm thick, $\vartheta_{avg} = 23^\circ\text{C}$, $\Delta\vartheta = 30^\circ\text{C}$).....	289
Table B. 23: Type A $u_c(\lambda_{COP})$ assessment, by means of HFM-1 apparatus (Sample: FS based VIP 10 mm thick, $\vartheta_{avg} = 23^\circ\text{C}$, $\Delta\vartheta = 40^\circ\text{C}$)	290
Table B. 24: Type A $u_c(\lambda_{COP})$ sensitivity coefficients, by means of HFM-1 apparatus (Sample: FS based VIP 10 mm thick, $\vartheta_{avg} = 23^\circ\text{C}$, $\Delta\vartheta = 40^\circ\text{C}$).....	290

Table B. 25: Type A $u_c(\lambda_{COP})$ assessment, by means of HFM-1 apparatus (Sample: FS based VIP 10 mm thick, $\vartheta_{avg} = 40^\circ\text{C}$, $\Delta\vartheta = 10^\circ\text{C}$)	291
Table B. 26: Type A $u_c(\lambda_{COP})$ sensitivity coefficients, by means of HFM-1 apparatus (Sample: FS based VIP 10 mm thick, $\vartheta_{avg} = 40^\circ\text{C}$, $\Delta\vartheta =$ 10°C)	291
Table B. 27: Type A $u_c(\lambda_{COP})$ assessment, by means of HFM-1 apparatus (Sample: FS based VIP 10 mm thick, $\vartheta_{avg} = 40^\circ\text{C}$, $\Delta\vartheta = 20^\circ\text{C}$)	292
Table B. 28: Type A $u_c(\lambda_{COP})$ sensitivity coefficients, by means of HFM-1 apparatus (Sample: FS based VIP 10 mm thick, $\vartheta_{avg} = 40^\circ\text{C}$, $\Delta\vartheta =$ 20°C)	292
Table B. 29: Type A $u_c(\lambda_{COP})$ assessment, by means of HFM-1 apparatus (Sample: FS based VIP 10 mm thick, $\vartheta_{avg} = 40^\circ\text{C}$, $\Delta\vartheta = 30^\circ\text{C}$)	293
Table B. 30: Type A $u_c(\lambda_{COP})$ sensitivity coefficients, by means of HFM-1 apparatus (Sample: FS based VIP 10 mm thick, $\vartheta_{avg} = 40^\circ\text{C}$, $\Delta\vartheta =$ 30°C)	293
Table B. 31: Type A $u_c(\lambda_{COP})$ assessment, by means of HFM-1 apparatus (Sample: FS based VIP 10 mm thick, $\vartheta_{avg} = 40^\circ\text{C}$, $\Delta\vartheta = 40^\circ\text{C}$)	294
Table B. 32: Type A $u_c(\lambda_{COP})$ sensitivity coefficients, by means of HFM-1 apparatus (Sample: FS based VIP 10 mm thick, $\vartheta_{avg} = 40^\circ\text{C}$, $\Delta\vartheta =$ 40°C)	294
Table B. 33: Type A $u_c(\lambda_{COP})$ assessment, by means of HFM-1 apparatus (Sample: FS based VIP 20 mm thick, $\vartheta_{avg} = 5^\circ\text{C}$, $\Delta\vartheta = 10^\circ\text{C}$)	295
Table B. 34: Type A $u_c(\lambda_{COP})$ sensitivity coefficients, by means of HFM-1 apparatus (Sample: FS based VIP 20 mm thick, $\vartheta_{avg} = 5^\circ\text{C}$, $\Delta\vartheta =$ 10°C)	295
Table B. 35: Type A $u_c(\lambda_{COP})$ assessment, by means of HFM-1 apparatus (Sample: FS based VIP 20 mm thick, $\vartheta_{avg} = 5^\circ\text{C}$, $\Delta\vartheta = 20^\circ\text{C}$)	296
Table B. 36: Type A $u_c(\lambda_{COP})$ sensitivity coefficients, by means of HFM-1 apparatus (Sample: FS based VIP 20 mm thick, $\vartheta_{avg} = 5^\circ\text{C}$, $\Delta\vartheta =$ 20°C)	296
Table B. 37: Type A $u_c(\lambda_{COP})$ assessment, by means of HFM-1 apparatus (Sample: FS based VIP 20 mm thick, $\vartheta_{avg} = 5^\circ\text{C}$, $\Delta\vartheta = 30^\circ\text{C}$)	297

Table B. 38: Type A $u_c(\lambda_{COP})$ sensitivity coefficients, by means of HFM-1 apparatus (Sample: FS based VIP 20 mm thick, $\vartheta_{avg} = 5^\circ\text{C}$, $\Delta\vartheta = 30^\circ\text{C}$).....	297
Table B. 39: Type A $u_c(\lambda_{COP})$ assessment, by means of HFM-1 apparatus (Sample: FS based VIP 20 mm thick, $\vartheta_{avg} = 5^\circ\text{C}$, $\Delta\vartheta = 40^\circ\text{C}$)	298
Table B. 40: Type A $u_c(\lambda_{COP})$ sensitivity coefficients, by means of HFM-1 apparatus (Sample: FS based VIP 20 mm thick, $\vartheta_{avg} = 5^\circ\text{C}$, $\Delta\vartheta = 40^\circ\text{C}$).....	298
Table B. 41: Type A $u_c(\lambda_{COP})$ assessment, by means of HFM-1 apparatus (Sample: FS based VIP 20 mm thick, $\vartheta_{avg} = 10^\circ\text{C}$, $\Delta\vartheta = 10^\circ\text{C}$)	299
Table B. 42: Type A $u_c(\lambda_{COP})$ sensitivity coefficients, by means of HFM-1 apparatus (Sample: FS based VIP 20 mm thick, $\vartheta_{avg} = 10^\circ\text{C}$, $\Delta\vartheta = 10^\circ\text{C}$).....	299
Table B. 43: Type A $u_c(\lambda_{COP})$ assessment, by means of HFM-1 apparatus (Sample: FS based VIP 20 mm thick, $\vartheta_{avg} = 10^\circ\text{C}$, $\Delta\vartheta = 20^\circ\text{C}$)	300
Table B. 44: Type A $u_c(\lambda_{COP})$ sensitivity coefficients, by means of HFM-1 apparatus (Sample: FS based VIP 20 mm thick, $\vartheta_{avg} = 10^\circ\text{C}$, $\Delta\vartheta = 20^\circ\text{C}$).....	300
Table B. 45: Type A $u_c(\lambda_{COP})$ assessment, by means of HFM-1 apparatus (Sample: FS based VIP 20 mm thick, $\vartheta_{avg} = 10^\circ\text{C}$, $\Delta\vartheta = 30^\circ\text{C}$)	301
Table B. 46: Type A $u_c(\lambda_{COP})$ sensitivity coefficients, by means of HFM-1 apparatus (Sample: FS based VIP 20 mm thick, $\vartheta_{avg} = 10^\circ\text{C}$, $\Delta\vartheta = 30^\circ\text{C}$).....	301
Table B. 47: Type A $u_c(\lambda_{COP})$ assessment, by means of HFM-1 apparatus (Sample: FS based VIP 20 mm thick, $\vartheta_{avg} = 10^\circ\text{C}$, $\Delta\vartheta = 40^\circ\text{C}$)	302
Table B. 48: Type A $u_c(\lambda_{COP})$ sensitivity coefficients, by means of HFM-1 apparatus (Sample: FS based VIP 20 mm thick, $\vartheta_{avg} = 10^\circ\text{C}$, $\Delta\vartheta = 40^\circ\text{C}$).....	302
Table B. 49: Type A $u_c(\lambda_{COP})$ assessment, by means of HFM-1 apparatus (Sample: FS based VIP 20 mm thick, $\vartheta_{avg} = 23^\circ\text{C}$, $\Delta\vartheta = 10^\circ\text{C}$)	303
Table B. 50: Type A $u_c(\lambda_{COP})$ sensitivity coefficients, by means of HFM-1 apparatus (Sample: FS based VIP 20 mm thick, $\vartheta_{avg} = 23^\circ\text{C}$, $\Delta\vartheta = 10^\circ\text{C}$).....	303

Table B. 51: Type A $u_c(\lambda_{COP})$ assessment, by means of HFM-1 apparatus (Sample: FS based VIP 20 mm thick, $\vartheta_{avg} = 23^\circ\text{C}$, $\Delta\vartheta = 20^\circ\text{C}$)	304
Table B. 52: Type A $u_c(\lambda_{COP})$ sensitivity coefficients, by means of HFM-1 apparatus (Sample: FS based VIP 20 mm thick, $\vartheta_{avg} = 23^\circ\text{C}$, $\Delta\vartheta =$ 20°C)	304
Table B. 53: Type A $u_c(\lambda_{COP})$ assessment, by means of HFM-1 apparatus (Sample: FS based VIP 20 mm thick, $\vartheta_{avg} = 23^\circ\text{C}$, $\Delta\vartheta = 30^\circ\text{C}$)	305
Table B. 54: Type A $u_c(\lambda_{COP})$ sensitivity coefficients, by means of HFM-1 apparatus (Sample: FS based VIP 20 mm thick, $\vartheta_{avg} = 23^\circ\text{C}$, $\Delta\vartheta =$ 30°C)	305
Table B. 55: Type A $u_c(\lambda_{COP})$ assessment, by means of HFM-1 apparatus (Sample: FS based VIP 20 mm thick, $\vartheta_{avg} = 23^\circ\text{C}$, $\Delta\vartheta = 40^\circ\text{C}$)	306
Table B. 56: Type A $u_c(\lambda_{COP})$ sensitivity coefficients, by means of HFM-1 apparatus (Sample: FS based VIP 20 mm thick, $\vartheta_{avg} = 23^\circ\text{C}$, $\Delta\vartheta =$ 40°C)	306
Table B. 57: Type A $u_c(\lambda_{COP})$ assessment, by means of HFM-1 apparatus (Sample: FS based VIP 20 mm thick, $\vartheta_{avg} = 40^\circ\text{C}$, $\Delta\vartheta = 10^\circ\text{C}$)	307
Table B. 58: Type A $u_c(\lambda_{COP})$ sensitivity coefficients, by means of HFM-1 apparatus (Sample: FS based VIP 20 mm thick, $\vartheta_{avg} = 40^\circ\text{C}$, $\Delta\vartheta =$ 10°C)	307
Table B. 59: Type A $u_c(\lambda_{COP})$ assessment, by means of HFM-1 apparatus (Sample: FS based VIP 20 mm thick, $\vartheta_{avg} = 40^\circ\text{C}$, $\Delta\vartheta = 20^\circ\text{C}$)	308
Table B. 60: Type A $u_c(\lambda_{COP})$ sensitivity coefficients, by means of HFM-1 apparatus (Sample: FS based VIP 20 mm thick, $\vartheta_{avg} = 40^\circ\text{C}$, $\Delta\vartheta =$ 20°C)	308
Table B. 61: Type A $u_c(\lambda_{COP})$ assessment, by means of HFM-1 apparatus (Sample: FS based VIP 20 mm thick, $\vartheta_{avg} = 40^\circ\text{C}$, $\Delta\vartheta = 30^\circ\text{C}$)	309
Table B. 62: Type A $u_c(\lambda_{COP})$ sensitivity coefficients, by means of HFM-1 apparatus (Sample: FS based VIP 20 mm thick, $\vartheta_{avg} = 40^\circ\text{C}$, $\Delta\vartheta =$ 30°C)	309
Table B. 63: Type A $u_c(\lambda_{COP})$ assessment, by means of HFM-1 apparatus (Sample: FS based VIP 20 mm thick, $\vartheta_{avg} = 40^\circ\text{C}$, $\Delta\vartheta = 40^\circ\text{C}$)	310

Table B. 64: Type A $u_c(\lambda_{COP})$ sensitivity coefficients, by means of HFM-1 apparatus (Sample: FS based VIP 20 mm thick, $\vartheta_{avg} = 40^\circ\text{C}$, $\Delta\vartheta = 40^\circ\text{C}$).....	310
Table B. 65: Type A $u_c(\lambda_{COP})$ assessment, by means of HFM-1 apparatus (Sample: FS based VIP 30 mm thick, $\vartheta_{avg} = 5^\circ\text{C}$, $\Delta\vartheta = 10^\circ\text{C}$)	311
Table B. 66: Type A $u_c(\lambda_{COP})$ sensitivity coefficients, by means of HFM-1 apparatus (Sample: FS based VIP 30 mm thick, $\vartheta_{avg} = 5^\circ\text{C}$, $\Delta\vartheta = 10^\circ\text{C}$).....	311
Table B. 67: Type A $u_c(\lambda_{COP})$ assessment, by means of HFM-1 apparatus (Sample: FS based VIP 30 mm thick, $\vartheta_{avg} = 5^\circ\text{C}$, $\Delta\vartheta = 20^\circ\text{C}$)	312
Table B. 68: Type A $u_c(\lambda_{COP})$ sensitivity coefficients, by means of HFM-1 apparatus (Sample: FS based VIP 30 mm thick, $\vartheta_{avg} = 5^\circ\text{C}$, $\Delta\vartheta = 20^\circ\text{C}$).....	312
Table B. 69: Type A $u_c(\lambda_{COP})$ assessment, by means of HFM-1 apparatus (Sample: FS based VIP 30 mm thick, $\vartheta_{avg} = 5^\circ\text{C}$, $\Delta\vartheta = 30^\circ\text{C}$)	313
Table B. 70: Type A $u_c(\lambda_{COP})$ sensitivity coefficients, by means of HFM-1 apparatus (Sample: FS based VIP 30 mm thick, $\vartheta_{avg} = 5^\circ\text{C}$, $\Delta\vartheta = 30^\circ\text{C}$).....	313
Table B. 71: Type A $u_c(\lambda_{COP})$ assessment, by means of HFM-1 apparatus (Sample: FS based VIP 30 mm thick, $\vartheta_{avg} = 5^\circ\text{C}$, $\Delta\vartheta = 40^\circ\text{C}$)	314
Table B. 72: Type A $u_c(\lambda_{COP})$ sensitivity coefficients, by means of HFM-1 apparatus (Sample: FS based VIP 30 mm thick, $\vartheta_{avg} = 5^\circ\text{C}$, $\Delta\vartheta = 40^\circ\text{C}$).....	314
Table B. 73: Type A $u_c(\lambda_{COP})$ assessment, by means of HFM-1 apparatus (Sample: FS based VIP 30 mm thick, $\vartheta_{avg} = 10^\circ\text{C}$, $\Delta\vartheta = 10^\circ\text{C}$)	315
Table B. 74: Type A $u_c(\lambda_{COP})$ sensitivity coefficients, by means of HFM-1 apparatus (Sample: FS based VIP 30 mm thick, $\vartheta_{avg} = 10^\circ\text{C}$, $\Delta\vartheta = 10^\circ\text{C}$).....	315
Table B. 75: Type A $u_c(\lambda_{COP})$ assessment, by means of HFM-1 apparatus (Sample: FS based VIP 30 mm thick, $\vartheta_{avg} = 10^\circ\text{C}$, $\Delta\vartheta = 20^\circ\text{C}$)	316
Table B. 76: Type A $u_c(\lambda_{COP})$ sensitivity coefficients, by means of HFM-1 apparatus (Sample: FS based VIP 30 mm thick, $\vartheta_{avg} = 10^\circ\text{C}$, $\Delta\vartheta = 20^\circ\text{C}$).....	316

Table B. 77: Type A $u_c(\lambda_{COP})$ assessment, by means of HFM-1 apparatus (Sample: FS based VIP 30 mm thick, $\vartheta_{avg} = 10^\circ\text{C}$, $\Delta\vartheta = 30^\circ\text{C}$)	317
Table B. 78: Type A $u_c(\lambda_{COP})$ sensitivity coefficients, by means of HFM-1 apparatus (Sample: FS based VIP 30 mm thick, $\vartheta_{avg} = 10^\circ\text{C}$, $\Delta\vartheta =$ 30°C)	317
Table B. 79: Type A $u_c(\lambda_{COP})$ assessment, by means of HFM-1 apparatus (Sample: FS based VIP 30 mm thick, $\vartheta_{avg} = 10^\circ\text{C}$, $\Delta\vartheta = 40^\circ\text{C}$)	318
Table B. 80: Type A $u_c(\lambda_{COP})$ sensitivity coefficients, by means of HFM-1 apparatus (Sample: FS based VIP 30 mm thick, $\vartheta_{avg} = 10^\circ\text{C}$, $\Delta\vartheta =$ 40°C)	318
Table B. 81: Type A $u_c(\lambda_{COP})$ assessment, by means of HFM-1 apparatus (Sample: FS based VIP 30 mm thick, $\vartheta_{avg} = 23^\circ\text{C}$, $\Delta\vartheta = 10^\circ\text{C}$)	319
Table B. 82: Type A $u_c(\lambda_{COP})$ sensitivity coefficients, by means of HFM-1 apparatus (Sample: FS based VIP 30 mm thick, $\vartheta_{avg} = 23^\circ\text{C}$, $\Delta\vartheta =$ 10°C)	319
Table B. 83: Type A $u_c(\lambda_{COP})$ assessment, by means of HFM-1 apparatus (Sample: FS based VIP 30 mm thick, $\vartheta_{avg} = 23^\circ\text{C}$, $\Delta\vartheta = 20^\circ\text{C}$)	320
Table B. 84: Type A $u_c(\lambda_{COP})$ sensitivity coefficients, by means of HFM-1 apparatus (Sample: FS based VIP 30 mm thick, $\vartheta_{avg} = 23^\circ\text{C}$, $\Delta\vartheta =$ 20°C)	320
Table B. 85: Type A $u_c(\lambda_{COP})$ assessment, by means of HFM-1 apparatus (Sample: FS based VIP 30 mm thick, $\vartheta_{avg} = 23^\circ\text{C}$, $\Delta\vartheta = 30^\circ\text{C}$)	321
Table B. 86: Type A $u_c(\lambda_{COP})$ sensitivity coefficients, by means of HFM-1 apparatus (Sample: FS based VIP 30 mm thick, $\vartheta_{avg} = 23^\circ\text{C}$, $\Delta\vartheta =$ 30°C)	321
Table B. 87: Type A $u_c(\lambda_{COP})$ assessment, by means of HFM-1 apparatus (Sample: FS based VIP 30 mm thick, $\vartheta_{avg} = 23^\circ\text{C}$, $\Delta\vartheta = 40^\circ\text{C}$)	322
Table B. 88: Type A $u_c(\lambda_{COP})$ sensitivity coefficients, by means of HFM-1 apparatus (Sample: FS based VIP 30 mm thick, $\vartheta_{avg} = 23^\circ\text{C}$, $\Delta\vartheta =$ 40°C)	322
Table B. 89: Type A $u_c(\lambda_{COP})$ assessment, by means of HFM-1 apparatus (Sample: FS based VIP 30 mm thick, $\vartheta_{avg} = 40^\circ\text{C}$, $\Delta\vartheta = 10^\circ\text{C}$)	323

Table B. 90: Type A $u_c(\lambda_{COP})$ sensitivity coefficients, by means of HFM-1 apparatus (Sample: FS based VIP 30 mm thick, $\vartheta_{avg} = 40^\circ\text{C}$, $\Delta\vartheta = 10^\circ\text{C}$).....	323
Table B. 91: Type A $u_c(\lambda_{COP})$ assessment, by means of HFM-1 apparatus (Sample: FS based VIP 30 mm thick, $\vartheta_{avg} = 40^\circ\text{C}$, $\Delta\vartheta = 20^\circ\text{C}$)	324
Table B. 92: Type A $u_c(\lambda_{COP})$ sensitivity coefficients, by means of HFM-1 apparatus (Sample: FS based VIP 30 mm thick, $\vartheta_{avg} = 40^\circ\text{C}$, $\Delta\vartheta = 20^\circ\text{C}$).....	324
Table B. 93: Type A $u_c(\lambda_{COP})$ assessment, by means of HFM-1 apparatus (Sample: FS based VIP 30 mm thick, $\vartheta_{avg} = 40^\circ\text{C}$, $\Delta\vartheta = 30^\circ\text{C}$)	325
Table B. 94: Type A $u_c(\lambda_{COP})$ sensitivity coefficients, by means of HFM-1 apparatus (Sample: FS based VIP 30 mm thick, $\vartheta_{avg} = 40^\circ\text{C}$, $\Delta\vartheta = 30^\circ\text{C}$).....	325
Table B. 95: Type A $u_c(\lambda_{COP})$ assessment, by means of HFM-1 apparatus (Sample: FS based VIP 30 mm thick, $\vartheta_{avg} = 40^\circ\text{C}$, $\Delta\vartheta = 40^\circ\text{C}$)	326
Table B. 96: Type A $u_c(\lambda_{COP})$ sensitivity coefficients, by means of HFM-1 apparatus (Sample: FS based VIP 30 mm thick, $\vartheta_{avg} = 40^\circ\text{C}$, $\Delta\vartheta = 40^\circ\text{C}$).....	326
Table C. 1: Type A $u_c(\lambda)$ assessment, by means of GHP-1 apparatus (Sample: Aerogel blanket 10 mm thick, $\vartheta_{avg} = 5^\circ\text{C}$, $\Delta\vartheta = 5^\circ\text{C}$).....	329
Table C. 2: Type A $u_c(\lambda)$ sensitivity coefficients, by means of GHP-1 apparatus (Sample: Aerogel blanket 10 mm thick, $\vartheta_{avg} = 5^\circ\text{C}$, $\Delta\vartheta = 5^\circ\text{C}$).....	329
Table C. 3: Type A $u_c(\lambda)$ assessment, by means of GHP-1 apparatus (Sample: Aerogel blanket 10 mm thick, $\vartheta_{avg} = 5^\circ\text{C}$, $\Delta\vartheta = 10^\circ\text{C}$).....	330
Table C. 4: Type A $u_c(\lambda)$ sensitivity coefficients, by means of GHP-1 apparatus (Sample: Aerogel blanket 10 mm thick, $\vartheta_{avg} = 5^\circ\text{C}$, $\Delta\vartheta = 10^\circ\text{C}$).....	330
Table C. 5: Type A $u_c(\lambda)$ assessment, by means of GHP-1 apparatus (Sample: Aerogel blanket 10 mm thick, $\vartheta_{avg} = 5^\circ\text{C}$, $\Delta\vartheta = 15^\circ\text{C}$).....	331

Table C. 6: Type A $u_c(\lambda)$ sensitivity coefficients, by means of GHP-1 apparatus (Sample: Aerogel blanket 10 mm thick, $\vartheta_{avg} = 5^\circ\text{C}$, $\Delta\vartheta = 15^\circ\text{C}$).....	331
Table C. 7: Type A $u_c(\lambda)$ assessment, by means of GHP-1 apparatus (Sample: Aerogel blanket 10 mm thick, $\vartheta_{avg} = 10^\circ\text{C}$, $\Delta\vartheta = 5^\circ\text{C}$).....	332
Table C. 8: Type A $u_c(\lambda)$ sensitivity coefficients, by means of GHP-1 apparatus (Sample: Aerogel blanket 10 mm thick, $\vartheta_{avg} = 10^\circ\text{C}$, $\Delta\vartheta = 5^\circ\text{C}$).....	332
Table C. 9: Type A $u_c(\lambda)$ assessment, by means of GHP-1 apparatus (Sample: Aerogel blanket 10 mm thick, $\vartheta_{avg} = 10^\circ\text{C}$, $\Delta\vartheta = 10^\circ\text{C}$).....	333
Table C. 10: Type A $u_c(\lambda)$ sensitivity coefficients, by means of GHP-1 apparatus (Sample: Aerogel blanket 10 mm thick, $\vartheta_{avg} = 10^\circ\text{C}$, $\Delta\vartheta = 10^\circ\text{C}$).....	333
Table C. 11: Type A $u_c(\lambda)$ assessment, by means of GHP-1 apparatus (Sample: Aerogel blanket 10 mm thick, $\vartheta_{avg} = 10^\circ\text{C}$, $\Delta\vartheta = 15^\circ\text{C}$).....	334
Table C. 12: Type A $u_c(\lambda)$ sensitivity coefficients, by means of GHP-1 apparatus (Sample: Aerogel blanket 10 mm thick, $\vartheta_{avg} = 10^\circ\text{C}$, $\Delta\vartheta = 15^\circ\text{C}$).....	334
Table C. 13: Type A $u_c(\lambda)$ assessment, by means of GHP-1 apparatus (Sample: Aerogel blanket 10 mm thick, $\vartheta_{avg} = 23^\circ\text{C}$, $\Delta\vartheta = 5^\circ\text{C}$).....	335
Table C. 14: Type A $u_c(\lambda)$ sensitivity coefficients, by means of GHP-1 apparatus (Sample: Aerogel blanket 10 mm thick, $\vartheta_{avg} = 23^\circ\text{C}$, $\Delta\vartheta = 5^\circ\text{C}$).....	335
Table C. 15: Type A $u_c(\lambda)$ assessment, by means of GHP-1 apparatus (Sample: Aerogel blanket 10 mm thick, $\vartheta_{avg} = 23^\circ\text{C}$, $\Delta\vartheta = 10^\circ\text{C}$).....	336
Table C. 16: Type A $u_c(\lambda)$ sensitivity coefficients, by means of GHP-1 apparatus (Sample: Aerogel blanket 10 mm thick, $\vartheta_{avg} = 23^\circ\text{C}$, $\Delta\vartheta = 10^\circ\text{C}$).....	336
Table C. 17: Type A $u_c(\lambda)$ assessment, by means of GHP-1 apparatus (Sample: Aerogel blanket 10 mm thick, $\vartheta_{avg} = 23^\circ\text{C}$, $\Delta\vartheta = 15^\circ\text{C}$).....	337
Table C. 18: Type A $u_c(\lambda)$ sensitivity coefficients, by means of GHP-1 apparatus (Sample: Aerogel blanket 10 mm thick, $\vartheta_{avg} = 23^\circ\text{C}$, $\Delta\vartheta = 15^\circ\text{C}$).....	337

Table D. 1: Uncertainty assessment of FS based VIP ($t = 20$ mm, $\vartheta_{avg} = 10^\circ\text{C}$).....	341
Table D. 2: Sensitivity coefficients and uncertainty contributions of FS based VIP	341
Table D. 3: Uncertainty assessment of FS based VIP ($t = 40$ mm, $\vartheta_{avg} = 10^\circ\text{C}$).....	342
Table D. 4: Sensitivity coefficients and uncertainty contributions of FS based VIP	342
Table D. 5: Uncertainty assessment of FG based VIP ($t = 20$ mm, $\vartheta_{avg} = 10^\circ\text{C}$).....	343
Table D. 6: Sensitivity coefficients and uncertainty contributions of FG based VIP	343
Table D. 7: Uncertainty assessment of FG based VIP ($t = 20$ mm, $\vartheta_{avg} = 23^\circ\text{C}$).....	344
Table D. 8: Sensitivity coefficients and uncertainty contributions of FG based VIP	344
Table D. 9: Uncertainty assessment of FG based VIP ($t = 30$ mm, $\vartheta_{avg} = 10^\circ\text{C}$).....	345
Table D. 10: Sensitivity coefficients and uncertainty contributions of FG based VIP	345
Table D. 11: Uncertainty assessment of FG based VIP ($t = 30$ mm, $\vartheta_{avg} = 23^\circ\text{C}$).....	346
Table D. 12: Sensitivity coefficients and uncertainty contributions of FG based VIP	346
Table E. 1: λ_{eq} - Uncertainty assessment of FS based VIPs, Commutated joint ($t = 20$ mm, $\vartheta_{avg} = 10^\circ\text{C}$).....	349
Table E. 2: λ_{eq} - Sensitivity coefficients and uncertainty contributions of FS based VIPs, Commutated joint ($t = 20$ mm, $\vartheta_{avg} = 10^\circ\text{C}$).....	349
Table E. 3: ψ - Uncertainty assessment of FS based VIPs, Commutated joint ...	350

Table E. 4: $u(\psi)$ - Sensitivity coefficients and uncertainty contributions of FS based VIPs, Commutated joint ($t = 20$ mm, $\vartheta_{avg} = 10^\circ\text{C}$)	350
Table E. 5: λ_{eq} - Uncertainty assessment of FS based VIPs, Commutated joint	351
Table E. 6: $u(\lambda_{eq})$ - Sensitivity coefficients and uncertainty contributions of FS based VIPs, Commutated joint ($t = 40$ mm, $\vartheta_{avg} = 10^\circ\text{C}$)	351
Table E. 7: ψ - Uncertainty assessment of FS based VIPs, Commutated joint ...	352
Table E. 8: $u(\psi)$ - Sensitivity coefficients and uncertainty contributions of FS based VIPs, Commutated joint ($t = 40$ mm, $\vartheta_{avg} = 10^\circ\text{C}$)	352
Table E. 9: λ_{eq} - Uncertainty assessment of FG based VIPs, Commutated joint	353
Table E. 10: λ_{eq} - Sensitivity coefficients and uncertainty contributions of FG based VIPs, Commutated joint ($t = 20$ mm, $\vartheta_{avg} = 10^\circ\text{C}$).....	353
Table E. 11: ψ - Uncertainty assessment of FG based VIPs, Commutated joint	354
Table E. 12: $u(\psi)$ - Sensitivity coefficients and uncertainty contributions of FG based VIPs, Commutated joint ($t = 20$ mm, $\vartheta_{avg} = 10^\circ\text{C}$).....	354
Table E. 13: λ_{eq} - Uncertainty assessment of FG based VIPs, Commutated joint	355
Table E. 14: λ_{eq} - Sensitivity coefficients and uncertainty contributions of FG based VIPs, Commutated joint ($t = 20$ mm, $\vartheta_{avg} = 23^\circ\text{C}$).....	355
Table E. 15: ψ - Uncertainty assessment of FG based VIPs, Commutated joint	356
Table E. 16: $u(\psi)$ - Sensitivity coefficients and uncertainty contributions of FG based VIPs, Commutated joint ($t = 20$ mm, $\vartheta_{avg} = 23^\circ\text{C}$).....	356
Table E. 17: λ_{eq} - Uncertainty assessment of FG based VIPs, Commutated joint	357
Table E. 18: $u(\lambda_{eq})$ - Sensitivity coefficients and uncertainty contributions of FG based VIPs, Commutated joint ($t = 30$ mm, $\vartheta_{avg} = 10^\circ\text{C}$).....	357
Table E. 19: ψ - Uncertainty assessment of FG based VIPs, Commutated joint	358

Table E. 20: $u(\psi)$ - Sensitivity coefficients and uncertainty contributions of FG based VIPs, Commutated joint ($t = 30$ mm, $\vartheta_{avg} = 10^\circ\text{C}$).....	358
Table E. 21: λ_{eq} - Uncertainty assessment of FG based VIPs, Commutated joint	359
Table E. 22: $u(\lambda_{eq})$ - Sensitivity coefficients and uncertainty contributions of FG based VIPs, Commutated joint ($t = 30$ mm, $\vartheta_{avg} = 23^\circ\text{C}$).....	359
Table E. 23: ψ - Uncertainty assessment of FG based VIPs, Commutated joint	360
Table E. 24: $u(\psi)$ - Sensitivity coefficients and uncertainty contributions of FG based VIPs, Commutated joint ($t = 30$ mm, $\vartheta_{avg} = 23^\circ\text{C}$).....	360
Table F. 1: λ_{eq} - Uncertainty assessment of FS based VIPs, Commutated joint	363
Table F. 2: λ_{eq} - Sensitivity coefficients and uncertainty contributions of FS based VIPs, Commutated joint ($t = 20$ mm, $\vartheta_{avg} = 10^\circ\text{C}$).....	364
Table F. 3: ψ - Uncertainty assessment of FS based VIPs, Commutated joint ...	365
Table F. 4: $u(\psi)$ - Sensitivity coefficients and uncertainty contributions of FS based VIPs, Commutated joint ($t = 20$ mm, $\vartheta_{avg} = 10^\circ\text{C}$)	365
Table F. 5: λ_{eq}, ψ - Uncertainty assessment of FS based VIPs, Commutated joint	366
Table F. 6: λ_{eq} - Uncertainty assessment of FS based VIPs, Offset joint.....	367
Table F. 7: λ_{eq} - Sensitivity coefficients and uncertainty contributions of FS based VIPs, Offset joint ($t = 20$ mm, $\vartheta_{avg} = 10^\circ\text{C}$).....	368
Table F. 8: ψ - Uncertainty assessment of FS based VIPs, Offset joint.....	369
Table F. 9: $u(\psi)$ - Sensitivity coefficients and uncertainty contributions of FS based VIPs, Offset joint ($t = 20$ mm, $\vartheta_{avg} = 10^\circ\text{C}$)	369
Table F. 10: λ_{eq}, ψ - Uncertainty assessment of FS based VIPs, Offset joint.....	370
Table F. 11: λ_{eq} - Uncertainty assessment of FS based VIPs, Gasket strip joint	371
Table F. 12: λ_{eq} - Sensitivity coefficients and uncertainty contributions of FS based VIPs, Gasket strip joint ($t = 20$ mm, $\vartheta_{avg} = 10^\circ\text{C}$)	372

Table F. 13: ψ - Uncertainty assessment of FS based VIPs, Gasket strip joint...	373
Table F. 14: $u(\psi)$ - Sensitivity coefficients and uncertainty contributions of FS based VIPs, Gasket strip joint ($t = 20$ mm, $\vartheta_{avg} = 10^\circ\text{C}$).....	373
Table F. 15: λ_{eq} , ψ - Uncertainty assessment of FS based VIPs, Gasket strip joint	374
Table F. 16: λ_{eq} - Uncertainty assessment of FS based VIPs, Commutated joint	375
Table F. 17: λ_{eq} - Sensitivity coefficients and uncertainty contributions of FS based VIPs, Commutated joint ($t = 40$ mm, $\vartheta_{avg} = 10^\circ\text{C}$).....	376
Table F. 18: ψ - Uncertainty assessment of FS based VIPs, Commutated joint	377
Table F. 19: $u(\psi)$ - Sensitivity coefficients and uncertainty contributions of FS based VIPs, Commutated joint ($t = 40$ mm, $\vartheta_{avg} = 10^\circ\text{C}$)	377
Table F. 20: λ_{eq} , ψ - Uncertainty assessment of FS based VIPs, Commutated joint	378
Table F. 21: λ_{eq} - Uncertainty assessment of FS based VIPs, Offset joint.....	379
Table F. 22: λ_{eq} - Sensitivity coefficients and uncertainty contributions of FS based VIPs, Offset joint ($t = 40$ mm, $\vartheta_{avg} = 10^\circ\text{C}$).....	380
Table F. 23: ψ - Uncertainty assessment of FS based VIPs, Offset joint.....	381
Table F. 24: $u(\psi)$ - Sensitivity coefficients and uncertainty contributions of FS based VIPs, Offset joint ($t = 40$ mm, $\vartheta_{avg} = 10^\circ\text{C}$)	381
Table F. 25: λ_{eq} , ψ - Uncertainty assessment of FS based VIPs, Offset joint.....	382
Table F. 26: λ_{eq} - Uncertainty assessment of FS based VIPs, Gasket strip joint	383
Table F. 27: λ_{eq} - Sensitivity coefficients and uncertainty contributions of FS based VIPs, Gasket strip joint ($t = 40$ mm, $\vartheta_{avg} = 10^\circ\text{C}$)	384
Table F. 28: ψ - Uncertainty assessment of FS based VIPs, Gasket strip joint...	385
Table F. 29: $u(\psi)$ - Sensitivity coefficients and uncertainty contributions of FS based VIPs, Gasket strip joint ($t = 40$ mm, $\vartheta_{avg} = 10^\circ\text{C}$).....	385
Table F. 30: λ_{eq} , ψ - Uncertainty assessment of FS based VIPs, Gasket strip joint	386

Table F. 31: λ_{eq} - Uncertainty assessment of FG based VIPs, Commutated joint	387
Table F. 32: λ_{eq} - Sensitivity coefficients and uncertainty contributions of FG based VIPs, Commutated joint ($t = 20$ mm, $\vartheta_{avg} = 10^\circ\text{C}$).....	388
Table F. 33: ψ - Uncertainty assessment of FG based VIPs, Commutated joint	389
Table F. 34: $u(\psi)$ - Sensitivity coefficients and uncertainty contributions of FG based VIPs, Commutated joint ($t = 20$ mm, $\vartheta_{avg} = 10^\circ\text{C}$).....	389
Table F. 35: λ_{eq} , ψ - Uncertainty assessment of FG based VIPs, Commutated joint	390
Table F. 36: λ_{eq} - Uncertainty assessment of FG based VIPs, Commutated joint	391
Table F. 37: λ_{eq} - Sensitivity coefficients and uncertainty contributions of FG based VIPs, Commutated joint ($t = 20$ mm, $\vartheta_{avg} = 23^\circ\text{C}$).....	392
Table F. 38: ψ - Uncertainty assessment of FG based VIPs, Commutated joint	393
Table F. 39: $u(\psi)$ - Sensitivity coefficients and uncertainty contributions of FG based VIPs, Commutated joint ($t = 20$ mm, $\vartheta_{avg} = 23^\circ\text{C}$).....	393
Table F. 40: λ_{eq} , ψ - Uncertainty assessment of FG based VIPs, Commutated joint	394
Table F. 41: λ_{eq} - Uncertainty assessment of FG based VIPs, Gasket strip joint	395
Table F. 42: λ_{eq} - Sensitivity coefficients and uncertainty contributions of FG based VIPs, Gasket strip joint ($t = 20$ mm, $\vartheta_{avg} = 10^\circ\text{C}$)	396
Table F. 43: ψ - Uncertainty assessment of FG based VIPs, Gasket strip joint	397
Table F. 44: $u(\psi)$ - Sensitivity coefficients and uncertainty contributions of FG based VIPs, Gasket strip joint ($t = 20$ mm, $\vartheta_{avg} = 10^\circ\text{C}$)	397
Table F. 45: λ_{eq} , ψ - Uncertainty assessment of FG based VIPs, Gasket strip joint	398
Table F. 46: λ_{eq} - Uncertainty assessment of FG based VIPs, Gasket strip joint	399

Table F. 47: λ_{eq} - Sensitivity coefficients and uncertainty contributions of FG based VIPs, Gasket strip joint ($t = 20$ mm, $\vartheta_{avg} = 23^{\circ}\text{C}$)	400
Table F. 48: ψ - Uncertainty assessment of FG based VIPs, Gasket strip joint	401
Table F. 49: $u(\psi)$ - Sensitivity coefficients and uncertainty contributions of FG based VIPs, Gasket strip joint ($t = 20$ mm, $\vartheta_{avg} = 23^{\circ}\text{C}$)	401
Table F. 50: λ_{eq} , ψ - Uncertainty assessment of FG based VIPs, Gasket strip joint	402
Table F. 51: λ_{eq} - Uncertainty assessment of FG based VIPs, Commutated joint	403
Table F. 52: λ_{eq} - Sensitivity coefficients and uncertainty contributions of FG based VIPs, Commutated joint ($t = 30$ mm, $\vartheta_{avg} = 10^{\circ}\text{C}$).....	404
Table F. 53: ψ - Uncertainty assessment of FG based VIPs, Commutated joint	405
Table F. 54: $u(\psi)$ - Sensitivity coefficients and uncertainty contributions of FG based VIPs, Commutated joint ($t = 30$ mm, $\vartheta_{avg} = 10^{\circ}\text{C}$).....	405
Table F. 55: λ_{eq} , ψ - Uncertainty assessment of FG based VIPs, Commutated joint	406
Table F. 56: λ_{eq} - Uncertainty assessment of FG based VIPs, Commutated joint	407
Table F. 57: λ_{eq} - Sensitivity coefficients and uncertainty contributions of FG based VIPs, Commutated joint ($t = 30$ mm, $\vartheta_{avg} = 23^{\circ}\text{C}$).....	408
Table F. 58: ψ - Uncertainty assessment of FG based VIPs, Commutated joint	409
Table F. 59: $u(\psi)$ - Sensitivity coefficients and uncertainty contributions of FG based VIPs, Commutated joint ($t = 30$ mm, $\vartheta_{avg} = 23^{\circ}\text{C}$).....	409
Table F. 60: λ_{eq} , ψ - Uncertainty assessment of FG based VIPs, Commutated joint	410
Table F. 61: λ_{eq} - Uncertainty assessment of FG based VIPs, Gasket strip joint	411
Table F. 62: λ_{eq} - Sensitivity coefficients and uncertainty contributions of FG based VIPs, Gasket strip joint ($t = 30$ mm, $\vartheta_{avg} = 10^{\circ}\text{C}$)	412

Table F. 63: ψ - Uncertainty assessment of FG based VIPs, Gasket strip joint	413
Table F. 64: $u(\psi)$ - Sensitivity coefficients and uncertainty contributions of FG based VIPs, Gasket strip joint ($t = 30$ mm, $\vartheta_{avg} = 10^\circ\text{C}$)	413
Table F. 65: λ_{eq} , ψ - Uncertainty assessment of FG based VIPs, Gasket strip joint	414
Table F. 66: λ_{eq} - Uncertainty assessment of FG based VIPs, Gasket strip joint	415
Table F. 67: λ_{eq} - Sensitivity coefficients and uncertainty contributions of FG based VIPs, Gasket strip joint ($t = 30$ mm, $\vartheta_{avg} = 23^\circ\text{C}$)	416
Table F. 68: ψ - Uncertainty assessment of FG based VIPs, Gasket strip joint	417
Table F. 69: $u(\psi)$ - Sensitivity coefficients and uncertainty contributions of FG based VIPs, Gasket strip joint ($t = 30$ mm, $\vartheta_{avg} = 23^\circ\text{C}$)	417
Table F. 70: λ_{eq} , ψ - Uncertainty assessment of FG based VIPs, Gasket strip joint	418

Nomenclature

Roman Symbols

A	area	m^2
a	wind coefficient	Ws/m^3K
A_m	measuring area	m^2
C_j	gap correction	-
d	air joint width	m
e	Euler constant	-
E	emittance	-
E_{del}	delivered energy	kWh
E_{rd}	energy room demand	kWh
f_{cal}	HFM calibration factor	$W/m^2\mu V$
h	surface heat transfer coefficient	W/m^2K
I	electric current	A
k_B	Boltzmann constant	J/K
Kn	Knudsen number	-
l	length	m
$L^{2D(x,z)}$	bidimensional coupling effect	W/mK
l_{mean}	mean free path of air molecules	m
n	number of data	
\emptyset	diameter	m

p	pressure	Pa
P	semi-perimeter	m
$p(x)$	Probability Density Function	
p_v	partial water vapour pressure	Pa
Q	electric signal from the transducer	V
R	thermal resistance	m^2K/W
r	correlation coefficient	
R^2	coefficient of determination	-
R_{el}	electric resistance	Ω
RH	relative humidity	-
S/V	aspect ratio	1/m
s_i	estimated standard deviations	
s_i^2	estimated variances	
t	thickness	m
U	electric signal	V
u_c	combined standard uncertainty	
u_i	standard uncertainty	
U -value	thermal transmittance	$[W/m^2K]$
v	velocity	m/s
ΔQ_{losses}	heat losses	Wh/m^2

Greek Symbols

α	solar absorption coefficient	-
δ	characteristic size	m
$\Delta\vartheta$	temperature difference	°C or K
$\Delta\lambda_E$	edge heat loss	-
$\Delta\lambda_g$	maximum allowable calibrating drift	-
$\Delta\lambda_K$	calibration accuracy of the specimen	-
$\Delta\lambda_L$	maximum permissible non-linearity of the calibration	-
$\Delta\lambda_O$	imperfect contact	-
$\Delta\lambda_O$	imperfect contact	-
$\Delta\lambda_{R,E}$	imbalance and edge heat loss	-
$\Delta\lambda_S$	asymmetrical conditions	-
ϑ	temperature	°C
λ	thermal conductivity	W/mK
μ	best estimate	
ρ	density	kg/m ³
σ	Stefan-Boltzmann constant	W/m ² K ⁴
τ	time	h
ν	number of degrees of freedom	-
Φ	measured heat flux	W
φ	specific heat flux	W/m ²
ψ	linear thermal transmittance of the thermal bridge	W/mK

Subscripts

<i>avg</i>	average
<i>c</i>	convective
<i>cal</i>	calibration
<i>COP</i>	centre of panel
<i>core</i>	core material
<i>cpl</i>	coupling
<i>e</i>	external
<i>eff</i>	effective
<i>el</i>	electric
<i>eq</i>	equivalent
<i>exp</i>	experimental
<i>g</i>	gaseous
<i>i</i>	internal
<i>J</i>	VIP assembly joint
<i>J</i>	joint
<i>lim</i>	limit
<i>lim,sl</i>	limit for service life
<i>m</i>	mean
<i>MAX</i>	maximum
<i>num</i>	numerical
<i>r</i>	radiative
<i>s</i>	solid

<i>SA</i>	slightly affected
<i>se</i>	superficial external
<i>si</i>	superficial internal
<i>SP</i>	gap space
<i>sur</i>	surface
<i>VIP</i>	Vacuum Insulation Panel
ψ	thermal bridge

Acronyms / Abbreviations

<i>1D</i>	Monodimensional
<i>2D</i>	Bidimensional
<i>ABP</i>	Aerogel Based Product
<i>AF</i>	Aluminium Foil
<i>ANOVA</i>	Analysis of Variance
<i>APM</i>	Advanced Porous Material
<i>BERV</i>	Break-Even Rental Value
<i>COP</i>	Centre Of Panel
<i>CV</i>	variation coefficient
<i>DPBP</i>	Discounted Pay Back Period
<i>EPS</i>	Expanded Polystyrene
<i>FEM</i>	Finite Element Method
<i>FS</i>	Fumed Silica
<i>GF</i>	Fibre Glass

<i>GHP</i>	Guarded Hot Plate
<i>HDD</i>	heating degree days
<i>HFM</i>	Heat Flux Meter
<i>LCA</i>	Life Cycle Assessment
<i>MDF</i>	Medium Density Fibreboard
<i>MF</i>	Multilayer Foil
<i>PCF</i>	Present Cash Flow
<i>PDF</i>	Probability Density Function
<i>PE</i>	Polyethylene
<i>PET</i>	Polyethylene Terephthalate
<i>RMSE</i>	Root Mean Square Error
<i>SIM</i>	Super Insulating Material
<i>THB</i>	Transient Hot Bridge
<i>TLS</i>	Transient Line Source
<i>TPS</i>	Transient Plane Source
<i>VIP</i>	Vacuum Insulation Panel
<i>XPS</i>	Extruded Polystyrene
<i>1D</i>	Monodimensional
<i>2D</i>	Bidimensional

Chapter 1

Introduction

The topic of the energy efficiency has become increasingly important during recent years. In particular buildings. After the 20-20-20 policy [1], the EU countries have set more ambitious targets for 2030 [2], in order to build a more sustainable energy system, achieving the EU long-term 2050 roadmaps for the greenhouse gas reductions [3]. These targets can be summarised in three main points: the decrease of the greenhouse gas emission of 40% (up to 80-95% in 2050) compared to the values obtained in 1990, the increase of the use of renewable energy sources higher than 27%, and at least 27% increase in energy efficiency.

In particular buildings for civil uses account for around 40% [4] of the final energy consumptions, and the potential of energy saving in this sector has been evaluated to be similar to the energy consumption in the transport sector (~ 33%) [5] (**Figure 1**). The first way to achieve this point is to minimise the energy needs of the new buildings, by means of, for example, Zero Energy Buildings or Nearly Zero Energy Buildings (ZEB and NZEB respectively). They are defined in the Energy Performance of Buildings Directive (EPBD) recast in 2010 [6] (buildings with very high energy performances and nearly zero or very low amount of energy needs, that must be mainly covered by renewable sources), and promoted in the International Energy Agency Annex 52 in 2014 [7].

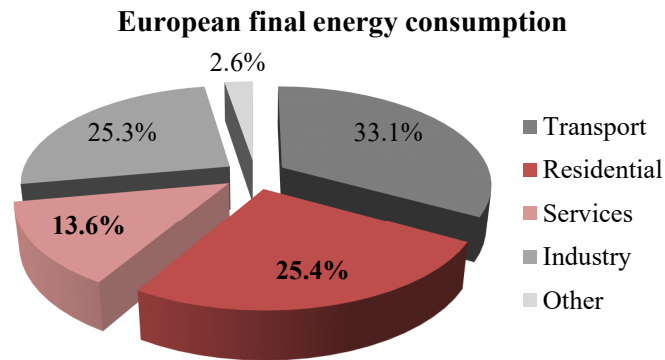


Figure 1: European final energy consumption in 2014 [5]

However, in the countries affiliated to the Organisation for Economic Co-operation and Development (OECD), the building stock until 2050 should be principally composed by already existing buildings (75 - 90%), which will influence the energy consumption of about 80% [8], and which were mainly built before 1990 (around 75%) and therefore before any energy regulations [9]. For this reason, the building refurbishment and renovation is a crucial point for the achievement of the expected energy demand reduction. In particular, the OECD highlighted that, 20% to 60% of all buildings energy uses depends on the quality of the building envelope (design and construction) [8], and several studies demonstrated that the more efficient way to shrink the energy demand of both new and existing buildings, is to reduce the building envelope heat losses, by improving the insulating solutions [10], [11] using efficient insulating materials with reliable thermal performance values.

At present, the European market, as well as the European technical standards, are characterised by the domination of “traditional” insulating materials. However, a further point of interest is the development of Super Insulating Materials (SIM), such as Vacuum Insulation Panels (VIP) and Advanced Porous Materials (APM). Due to their very low thermal conductivity (that ranges from 0.015/0.020 W/mK to 0.0015/0.0050 W/mK in case of VIP, so up to a magnitude smaller than conventional insulating materials), they allow to achieve excellent thermal performances with thin thicknesses, but need accurate measurement of heat-flux, temperatures, electrical power and thickness of the specimens in order to reduce measurement uncertainty

Actually, the thermal properties of insulating materials are assessed using several experimental apparatus, such as Heat Flow Meter (HFM) and Guarded

Hot Plate (GHP). The existing devices, as well as the current standards, were developed for the experimental assessment of the so defined traditional insulating materials for building applications. But in case of SIMs, their low thermal conductivity often lies over the applicability range of the apparatus, which are forced to work beyond their limit. For this reason, the accuracies of existing device could often be inadequate, or not in line with the standards uncertainty maximum values (2% for GHP and 3% in case of HFM [12]).

Therefore, in the first part of the research, the applicability of the current standards and measurement devices to SIMs evaluation was verified. This investigation was also performed in the framework of an International Energy Agency project, named Annex 65: Long-Term Performance of Super-Insulating Materials in Building Components and Systems. In a second stage, the weak points of usual approaches were analysed, in order to support the development of new or revised methods and/or standards. In this context, one of the most crucial point on the laboratory assessment of each material, is the evaluation of the uncertainty of the measured properties, in accordance with the GUM [13]. The uncertainty analysis represents the key point of this research, and for this reason, it was deeply investigated under different points of view, considering both the Type A and Type B evaluations (based respectively on a statistical approach or other scientific and relevant information available). The approach represents a complete novelty compared to the correlated literature. Currently, the thermal properties of SIMs are declared neglecting the measurement uncertainty values, but, (and especially in case of SIMs), this assumption could lead to completely unreliable results (as demonstrated in the following sections).

The reduction of measurement uncertainty for Super Insulating Materials could lead to a higher level of confidence among customers and potential users for the new materials. The enhancement of measurement procedures and boundary conditions to get more reliable values of thermal performance of SIMs could represent a basis for energy demand calculations on the building envelope and HVAC systems and a fair declaration of performance, leading to equal chances for manufacturers of SIMs on the market. Furthermore, once defined the thermal conductivity variability due to the measurement uncertainty, it will be possible to identify the small changes of the performance over time resulting from ageing of these materials due to physical or chemical deterioration, and consequently more accurate simulations and calculations of the thermal performance of constructions containing SIMs can be carried out, resulting in higher reliability due to smaller security add-ons and fewer construction damages.

Moreover, for the first time, the HFM apparatus was also used for the evaluation of the linear thermal transmittance of the thermal bridges that occur in case of VIPs assemblies. Starting from the master thesis researches, the proposed methodologies for the measurements of the thermal bridging effects were further deepened and developed [14], and then systematically spread within the usual practice of the scientific community. The procedure was indeed experimentally optimised and then was used to validate numerical model (the numerical simulation of thermal bridges is not a topic of this research because the related investigations represent a fundamental background of the current research activities [14]). Numerical simulations are essential for the assessment of thermal bringing effects, since they depend on several boundary conditions (the type of the joint between the panels e its thermal conductivity and geometry, adjunctive layers and so on) and it is obviously impossible to test all the possible configurations. The numerical simulations were also used to verify the reliability of the experimental measurements, checking the absence of lateral heat losses.

Once validated the models at the component scale, some dynamic hygrothermal simulations at the building scale were performed. The goals were the evaluation of the energy efficiency of building insulated with SIMs and the prediction of the durability of these materials (after an in-situ experimental monitoring validation).

The knowledge gained in this research represents the fundamental basis for a submitted EMPIR (European Metrology Programme for Innovation and Research) Euramet Normative project, aimed to provide a contribution to standardisation within CEN and ISO (CEN TC 88 WG11, CEN TC 89 and ISO TC 163 SC3, and SC1), and enhance the experience of the European Institutes involved in the determination of the performance of SIMs. This can be achieved in three different time scale. It could be used as a basis for the development of a new measurement standard that could complement the existing standards (Long and Mid Term realisation). For a faster adoption, the results of the work could be implemented in the VIP product standard. In addition to that, it could be published as a TR (technical report) by CEN to define the procedure for CE-Marking of these new products (Short Term realisation).

Chapter 2

Super Insulating Materials - SIMs

The improvement of the insulation of the building envelope (floors, walls, roofs and so on) represents one of the most effective solutions for the reduction of the final energy consumption related to the building sector, for both new and already existing buildings.

Nowadays, many different materials are used to this purpose, and they can be classified into traditional and innovative insulating materials, accounting their chemical composition, physical structure and thermal properties (**Table 1**) [15]. Between them, the European market is dominated by the traditional solutions.

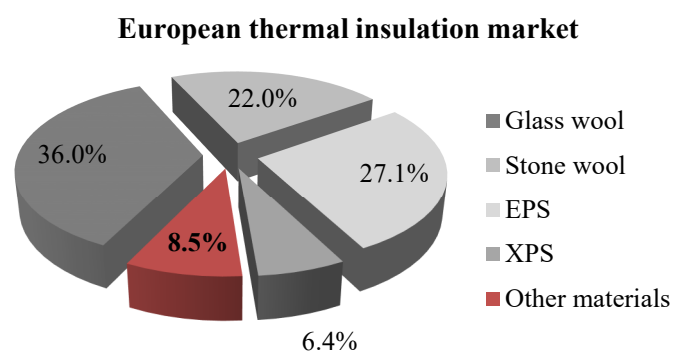


Figure 2: European thermal insulation market in 2014 [16]

Inorganic fibrous materials (glass wool and stone wool) reached the 58% of the thermal insulation market in 2014, and foamy organic materials (expanded and extruded polystyrene) the 33%, as shown in **Figure 2** [16]. However, some

alternative natural insulating elements (for example sheep and cotton wool) and innovative ones are increasing their diffusion. In particular, the last group would be a more energy efficient alternative to conventional insulating materials, due to its lower thermal conductivity.

Table 1: Classification of insulating materials

		Materials	Thermal conductivity [W/mK]
Traditional	Inorganic	Cellular glass	0.040 - 0.080
		Glass wool	0.030 - 0.040
		Rock wool	0.040
	Organic	Expanded polystyrene - EPS	0.030 - 0.040
		Extruded polystyrene - XPS	0.030 - 0.032
		Polyurethane - PUR	0.020 - 0.030
		Expanded clay	0.090
		Sheep wool	0.040
		Wadding	0.040
		Cellulose	0.040 - 0.050
		Cork	0.040 - 0.050
		Coconut fibre	0.050
	Composite	Gypsum foam	0.045
Fibre wood		0.040 – 0.060	
Innovative	Vacuum Insulation Panel - VIP	0.0015 - 0.007	
	Gas Filled Panel - GFP	0.008 - 0.010	
	Advanced Porous Material - APM	≈ 0.020	
	Aerogel Based Products - ABP	0.013 - 0.017	
Transient	Phase Change Material - PCM	-	

The main characteristic of insulating materials is their thermal conductivity (λ measured in [W/mK]), which is defined as “*the rate of heat flow through a unit thickness of material over a unit area, with a unit difference in temperature*” [17], [18].

The heat transfer due to a temperature gradient can be split into three different contributions:

- conduction between particles of solid, liquid and gaseous phases;
- convection due to the movement of the molecules in fluids;
- radiation (infrared heat transfer) in the form of electromagnetic waves or particles through space.

Reducing these contributions, the overall thermal conductivity will be reduced as well. Usually, the insulating materials are highly porous, since gasses have smaller thermal conduction than solid and liquid substances (moreover, the gas conductivity is the higher contribution to the heat transfer phenomena). By the optimisation of air-filled materials, it's possible to balance the radiative heat transfer and the solid conduction. To reduce the remaining gaseous thermal conductivity, it is possible to act in three main different ways:

- the filling of the pores with heavy gasses (e.g., argon and CO₂) that have lower thermal conductivity than air (e.g., blowing agent in case of foam insulation or Gas-Filled Panels);
- reducing the pores dimension, in order to impede the gas conduction by means of the several collisions between gas and solid particles (nanoporous materials or Advanced Porous Materials – APM, such as aerogel and fumed silica);
- evacuating the insulating material (this is the case of Vacuum Insulation Panels – VIPs).

The so obtained materials can be defined as Super Insulating Materials (SIMs), that can generally be classified as:

- Advanced Porous Materials - APM (between whom the Aerogel Based Products - ABP are accounted);
- Vacuum Insulation Panels - VIPs.

SIMs are characterised by a very low thermal conductivity (0.0015 W/mK (VIP) < λ < 0.0200 W/mK (APM)), five to ten times lower than insulating materials traditionally used in the building sector ($\lambda \sim 0.0300 - 0.0400$ W/mK).

In the following sections, the mentioned SIMs will be in detail presented.

2.1 Advanced Porous Materials - APMs

Advanced Porous Materials for super insulation are composed of materials with a nano-open porous structure and a higher porosity compared to the most common insulating materials (around 97% instead of 90 – 94%). The solid matter consists of connected particles and pores (size of about 20 nm).

APMs can be classified into two main categories:

- Fumed Silica - FS, made by synthetic amorphous silica packed boards obtained from hydrophobised pyrogenic (fumed) silicon dioxide;
- Aerogel Based Products - APM, which are lightweight solids or granular material obtained by sol-gel processing, where the air replaces the liquid component of the gel (they can be found on the market as monoliths, granules, and fibre reinforced sheet that can be bonded or packed between other elements).

Most of them are based on synthetic amorphous silica, but obtained through different manufacturing processes (as shown in **Figure 3**).

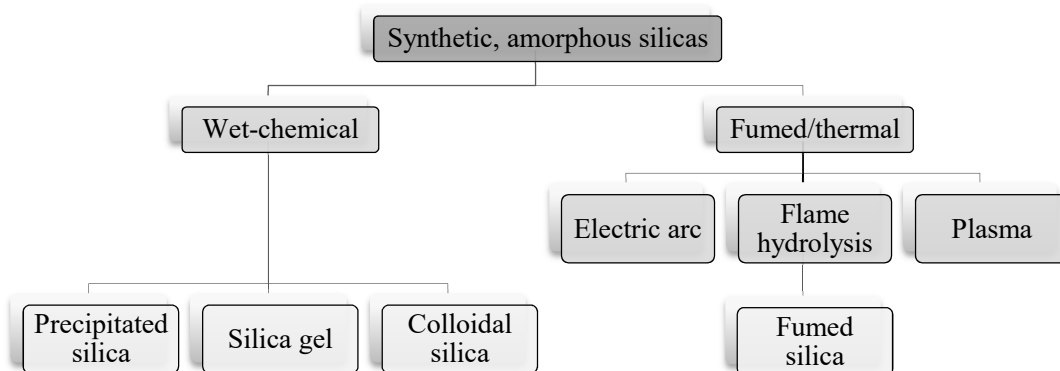


Figure 3: Overview of various silica manufacturing processes [19]

As already mentioned in the previous section, the small size of the pores provides to APM a very low thermal conductivity, which dimly depends on the variation of temperature. For this reason, APM may be excellent thermal insulators in case of high temperature applications, especially when they include infrared opacifier to reduce the IR radiative heat transfer.

The main typical properties of APM are summarised in **Table 2**.

Table 2: Typical APMs properties [19]

Property	Unit	Material			
		Fumed silica	Precipitated silica	Silica gel	Aerogels
Specific surface area	$[m^2/g]$	50 - 500	30 - 800	250 - 1000	250 - 400
Mean primary particle size	$[nm]$	5 - 50	5 - 100	3 - 20	3 - 20
Aggregate or agglomerate size	$[mm]$	dependent on dispersion conditions	1 - 40	1 - 20	1 - 15
Tamped density	$[g/l]$	50 - 250	50 - 500	500 - 1000	50 - 125
Loss on drying	$[%]$	≤ 3	3 - 7	3 - 6	3 - 5
Pore diameter	$[nm]$	Non-porous	≥ 30	2 - 20	≥ 25

The first applications of APM as building insulation date back to 2003 [20], and some examples and detailed analyses can be found in [21] and [22].

2.1.1 Fumed Silica - FS

Fumed silica (FS) was first developed in Germany in 1942 by Degussa AG (currently Evonik Industries), and it is composed by particles of amorphous silica (silicon dioxide - SiO_2), agglomerated into tertiary particles.

FS looks like a very thin powder, with an extremely high surface area and low bulk density (**Figure 4**). When it is used as a thickener or reinforcing filler, it increases the viscosity of the mixture, because of its three-dimensional structure [23]. For this reason, FS is one of the most common thickening and anticaking (or free-flow) agents in powder and can be used as viscosity regulator in silicone elastomers, paints and coatings.



Figure 4: Fumed silica powder [24]

2.1.1.1 Properties

The primary particles of FS (non-porous) have a dimension of 5 to 50 nm, with a surface area of 50 to 600 m²/g and a consequent density of about 160 - 190 kg/m³, however, they typically don't exist as isolated particles. These particles, by means of covalent bonding, form indivisible units, the aggregates, with external dimensions usually above 100 nm. The so obtained aggregates are fused together with no apparent physical boundaries among them (amorphous state) [25].

“Fumed Silica (FS) has his largest pore size of ~ 300 nm that is in the same order of magnitude of the mean free path of the air molecule at ambient temperature and pressure. For this reason, the gas conduction between the pores is drastically reduced even at atmospheric pressure [26],[27]. Moreover, since opacifier (silicon carbide powder, or titanium dioxide) contribute to reducing the radiative heat transfer, a total thermal conductivity in the range 0.019 - 0.020 W/mK can be reached (lower than the conductivity of dry air ~ 0.025 W/mK)[28]”¹.

For these reasons, FS can be used as insulating material itself (in the way of composite material with some fibre-reinforcement, see **Figure 5**) or as the core material of Vacuum Insulation Panels (VIPs).



Figure 5: Fumed silica pressed board

The excellent insulation properties and the high temperature resistance of silica-based materials make them especially suitable for insulating applications in higher temperature ranges.

Because of its thinness, FS can be easily inhaled: in the production phase, the highest exposure has been obtained during packaging and loading operations (mean value peaks of 3 mg/m³ inhalable dust and 1 mg/m³ respirable dust).

¹ Text from the author's paper: "The effect of temperature on thermal performance of fumed silica based Vacuum Insulation Panels for buildings" [29].

Anyway, FS is not listed as a carcinogen neither as toxic hazardous material for the environment. During its life cycle, the quantity of synthetic amorphous silica released into the atmosphere is negligible, if compared to the natural presence of silica [25].

2.1.1.2 Production

Fumed silica is manufactured from flame pyrolysis of silicon tetrachloride (SiCl_4) or quartz sand, vaporised in an electric arc at a temperature higher than $1500\text{ }^\circ\text{C}$.

During this process, SiCl_4 changes his aggregation status into the gaseous phase, and then reacts spontaneously in an oxyhydrogen flame with the intermediately formed water, providing the final silicon dioxide (**Figure 6**):

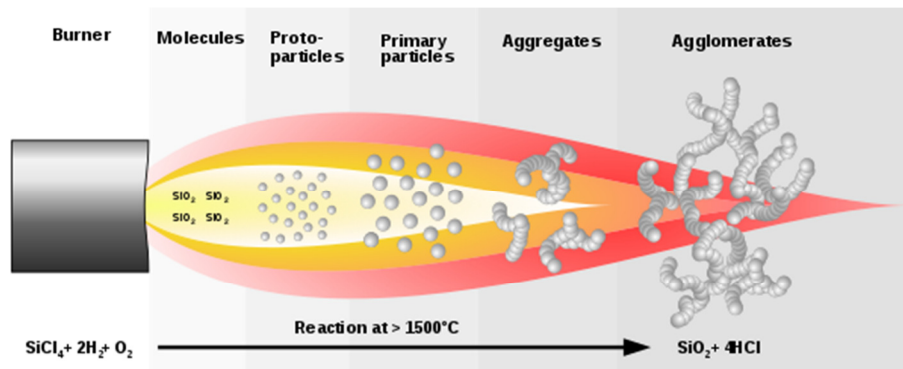
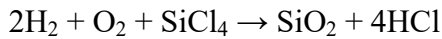
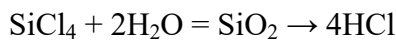
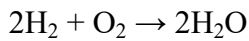


Figure 6: Fumed silica manufacturing [30]

The described reactions are extremely exothermic: the released heat is eliminated in a cooling line, while the only by-product is gaseous HCl (which can be easily separated from the fumed silica solid matter).

The so obtained hydrophilic SiO_2 is then converted into the hydrophobic silica by a silane (SiH_4) fluid-bed reactor.

2.1.1.3 Applications

This kind of material can find several applications in the building sector: insulation of façades, roofs and also fire protection. Some examples can be found in the reference projects of Evonik 0, most of them are building refurbishment, where the space saving represents a fundamental issue.

A historical farmhouse (Germany, 1867) was renovated in 2012, adding interior insulation to façades and roof. Before the intervention, the structure of the building was a 50-cm-thick, uninsulated brick wall. The renovation project consisted of a purely mineral, open-pored interior insulation with a thickness of 8 cm. The insulating layer was composed of a hydrophobic FS core material (thermal conductivity of 0.019 W/mK), embedded in a capillary-active layer of calcium silicate (**Figure 7**).



Figure 7: Fumed silica, coupled with calcium silicate panels [31]

In case of internal insulation, the worst criticism is the endogenous production of damp and condensation: capillary active insulating systems allow the moisture transfer from inside to outside and therefore represent a practical solution to this problem. The obtained overall mean thermal conductivity of the panel was lower than 0.030 W/mK. This project was developed with the Institute of Building Climatology at Dresden University, to analyse the active interaction of the products at a hygrothermal level. The observed advantages of this solution are due to the fact that it is extremely space saving (because of the FS insulating performances), permeable, capillary-active, mold-inhibiting, non-water-soluble, resistant to pests, dimensionally stable, and therefore self-supporting.

In 2015 an office and administration building (4200 m³) in Switzerland (1965), was subject to a façade insulating renovation (windows included). The proposed solution for the opaque building envelope consists of a 72 mm FS + VIP insulation layer. For the façade, the planned energy consumptions reduction was about 143201 kWh/a with CO₂ savings of 28.9 t CO₂/a.

Another example of FS composite material was applied during the building of a new residential house in Germany (2017). In this case, the nonflammable silica was used to optimise brickwork and construction elements such as ceiling edge blocks and U-blocks (**Figure 8**).

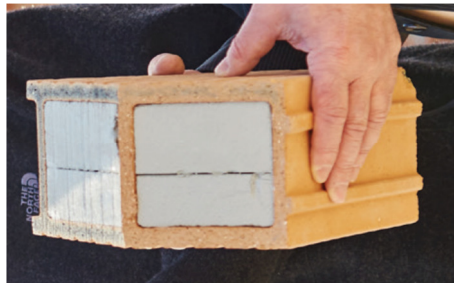


Figure 8: Fumed silica integrated brick [30]

2.1.2 Aerogel Based Products - ABPs

One of the most common definitions of the aerogel is the one proposed by Leventis et al. (2010): “*Aerogel is an open non-fluid colloidal network or polymer network that is expanded throughout its whole volume by a gas, and is formed by the removal of all swelling agents from a gel without substantial volume reduction or network compaction*” [32]. In other words, the aerogel is a gel composed of a solid phase and a gaseous dispersed phase (not liquid).

The first aerogel was produced in 1931 by Steven Kistler [33], exchanging the liquid phase with gas, avoiding the collapse of the structure. To this aim, it's essential to prevent the compresence of water and vapour during the drying of the sample (fluid evaporation), in order to minimise the surface tensions which cause the fracture of the sample. This is possible drying the material at extremely high temperatures and pressures (the so named “supercritical conditions” of the fluid), as explained from now on.

The most common, and first produced, aerogel is based on silica gels, Kistler's later work involved aerogels based on alumina, metal (for example chromo and tin) dioxide, carbon and organic matter.

2.1.2.1 Properties

Aerogel is a solid, rigid and friable material. This means that with intense pressure on its surface, the structure will break down. Despite that, it can support weighty loads, because of its dendritic microstructure, composed of spherical particles (average dimension of about 2 - 5 nm) fused together into clusters. The so obtained structure is highly porous in the three dimensions: the average size (usually < 100 nm) [34] and density of the pores can be defined during the manufacturing process. Anyway, almost the whole space is occupied by air or other gasses (95-99% in volume, with a maximum of 99.98% volume [35]) and consequently, this material is almost weightless (silica aerogel is only three times heavier than air). Aerogels can have different classes of porosity, but most of them have an extremely low density (from 0.0011 to 0.5 g/cm³ approximatively), but usually have densities of at least 0.020 g/cm³, that means about 15 times heavier than air ([36],[37]).

Because of their high content in gas, since gas is a very poor conductor, aerogels are excellent conductive insulators. Moreover, they are an excellent convective insulator (the air cannot circulate into the lattice) but poor radiative insulator (infrared radiations are free to cross the material).

Aerogels are hydrophilic materials: they must be chemically hydrophobised because the contact with water can demolish the aerogel structure (as an effect of the pores surface tension [38]). For this reason, aerogel is often used evacuated, to have an envelope which avoids water inclusion (moreover the vacuum improve the insulating performances furthermore [33]).

The slight and opaline colouring is due to the Rayleigh scattering of the visible light shorter wavelengths in the nanoporous structure.

The main typical properties of Aerogels are summarised in **Table 3**.

Commercial silica aerogels have an embodied energy of 53.9 MJ/kg and an emitted CO₂ of 4.3 kg_{CO2}/kg, excluding the CO₂ during the production phase. These values are higher compared to conventional insulating materials which lie respectively between 16.6 to 38.8 MJ/kg and 1.1 to 1.4 kg_{CO2}/kg [39]. The aerogel embodied energy is so high because it takes into account both the energy of the raw materials used for the synthesis of the aerogel and the energy used during processing and production. In [40] was demonstrated that emissions decrease exponentially with the increase in thickness of the insulating material.

Table 3: Typical Aerogels properties [42]

Materials	Thermal conductivity (20°C) [W/mK]	Water vapour permeability [-]	Hydrophobicity (contact angle) [°]	Fire classification [-]	Density [kg/m ³]
Synthetic amorphous silica boards	0.016 - 0.020		≤ 160°	A - B	
aerogel					
Granular silica aerogels	0.014 - 0.020	5 - 10		B - C	50 - 250
Silica aerogel composite	0.015 - 0.020		140° - 160°	A - F	
Organic aerogel Products	0.009 - 0.040			C - F	

Since aerogel has extremely thin particles, the inhalation of dust may cause temporary irritation of the mucous membranes and upper respiratory tract and the contact with skin and eye may cause dryness and temporary irritation. Anyway, none of its components is toxic or carcinogen [41].

2.1.2.2 Typologies

As already mentioned, aerogels can be obtained starting from different materials. From now on, the most common are described:

- **Silica**

Silica aerogel is the most studied and used kind of aerogel, and it is obtained from silicon dioxide (SiO₂). The strong point of this material is due to its solid material properties: the structural silicon dioxide chains are cross-linked, obtaining a lot of air-filled pores. As already mentioned, the dimension of these pores is minimal: pure aerogel pores diameter ranges between 1 and 100 nm [43], but in general, the average size in case of silica aerogels lies in the range 5 - 70 nm, depending on the purity and the production process [44]. This means that the filling air represents the 85 to 99.9% of the overall aerogel volume. The overall density of aerogel used for building insulation is around 70 - 150 kg/m³. Nevertheless, it's characterised by a high compression resistance (up to 300'000 Pa), while the tensile strength is meagre (therefore the material is extremely fragile) [33]. Usually, the weak tensile strength is solved by incorporating the

solid aerogel (powder) in a fibrous matrix, obtaining aerogel blankets (Figure 9).



Figure 9: Solid aerogel placed upon an aerogel blanket [45]

Silica aerogel extremely low thermal conductivity at atmospheric pressure is commonly equal to about 0.020 W/mK, but it can decrease down to 0.004 W/mK if evacuated [33].

The main characteristics of silica aerogel are summarised in Table 4 ([46],[47])

Table 4: Silica aerogel typical properties ([46],[47])

Property	Value	Property	Value
Density	$[kg/m^3]$ 3 - 350 (typical 100)	Primary particle diameter	$[nm]$ 2 - 5
Pore diameter	$[nm]$ 1 - 100 (average 20)	Surface area	$[m^2/g]$ 600 - 1000
Porosity	$[%]$ 85 - 99.9 (typical 95)	Thermal conductivity	$[W/mK]$ 0.015 - 0.020

- **Metal oxides**

The so obtained aerogels are usually used as chemical catalysts, especially when "doped" with another metal (e.g., Nickel + alumina aerogel), or to produce other materials.

Metal oxide aerogel differs from silica primarily for their variety of colour (which depends on the starting metal).

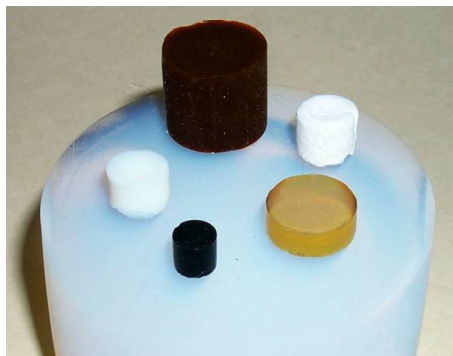


Figure 10: Several aerogel typologies, from transition metal oxide, including iron oxide (rust) aerogel (top), compared to silica aerogel (bottom) [35]

- **Carbon and Organic**

Carbon aerogels are characterised by very high porosity (over 50% and average pore diameter lower than 100 nm), with a resulting surface area between 400 - 1000 m²/g. The manufacturing process is similar to the one followed for the composite paper: carbon fibres making a non-woven paper, then impregnated with resorcinol-formaldehyde aerogel and in the end exposed to final pyrolysis (**Figure 11**).

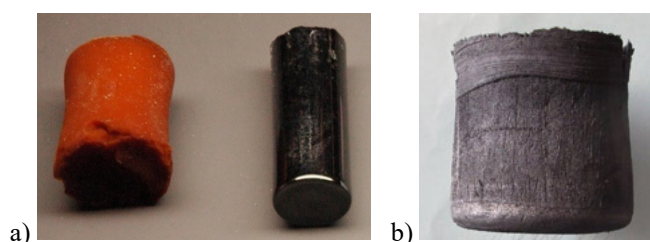


Figure 11: a) Aerogel-based on resorcinol-formaldehyde polymer (left) and electrically-conductive carbon aerogel (right); b) another carbon aerogel [48]

Carbon aerogels may be electrically conductive, depending on their density, and they can be used to create supercapacitors, considering their extremely high surface area. Moreover, in the infrared spectrum, carbon aerogels reflect only 0.3% of the radiation, and for this reason, they are useful for solar energy collectors [35].

Moreover, aerogel can also be based on different organic polymers: from the agar alga, it is possible to obtain SEAgel (Safe Emulsion Agar gel), while a flexible aerogel can also be produced with vegetal cellulose [49].

2.1.2.3 Aerogel synthesis

Silica aerogel is the first created and the most common typology of aerogel. Its synthesis consists of three different phases: gel preparation, ageing and drying. The process starts by mixing liquid alcohol, ethanol, with a precursor $\text{Si}(\text{OR})_4$ (silicon alkoxide, such as tetramethoxysilane - TMOS, tetraethoxysilane - TEOS and polyethoxydisiloxane - PEDS) which leads to the formation of silica gel. The silica solution is indeed combined with a catalyst (acid or basis), to accelerate the process, and through a hydrolysis reaction particles of silicon dioxide gel are obtained. Primary catalysts are useful to get transparent aerogels and to minimise the shrinkage and avoid pore collapse during the drying phase [33]. When a sol reaches the gel point, it doesn't mean that the reactions of the silicon alkoxide are complete. The reactions continue because the silica backbone of the gel still contains a significant number of unreacted alkoxide groups. It is fundamental to give enough to the reactions, so as to strengthen the silica connections. This can be achieved by controlling the pH and water content of the covering solution, and ageing the gel undisturbed in this solution for up to two days [50]. The ageing method and duration strongly affects the microstructure of the aerogel (porosity, surface area, pore size, volume shrinkage and optical transmittance), as investigated in [51], [52] and [53]. Moreover, the more is the length of the ageing period, the stronger and stiffer the aerogel [54].

At this point, all the water is still inside the pores, and it must be removed before proceeding with the drying process, drenching the aerogel in a bath of ethanol or heptane.

The drying can take place in two ways: at ambient pressure or in supercritical conditions. In the first case, the evaporation of the liquid takes place at ambient pressure, and the porous structure is subject to capillary tensions which cannot be avoided, and that could destroy the fragile gel network. This alternative is the cheaper solution, but the obtained material (named xerogel) is characterised by low porosity and a lot of shrinkage post-drying. Differently, in the second method, the temperature and pressure are increased to force the liquid into a supercritical fluid. A critical state is the endpoint of a phase equilibrium curve, and in this particular case, is the end point of the pressure-temperature curve between the liquid phase and vapour (**Figure 12**). Over this point, phase boundaries vanish, and a liquid and its vapour can coexist.

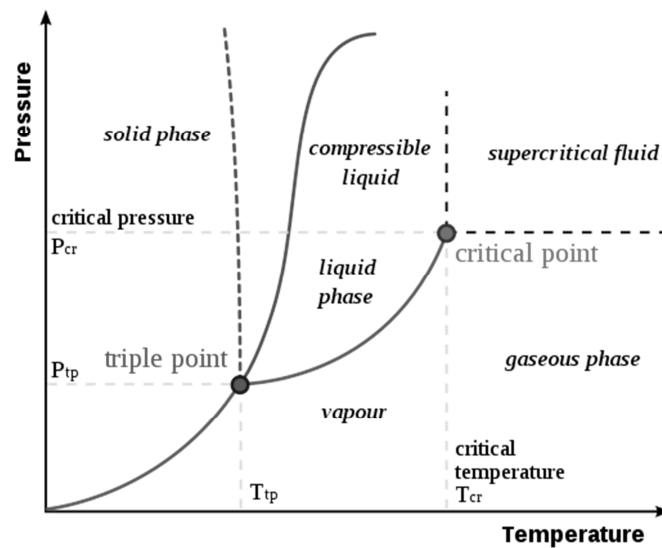


Figure 12: Liquid-vapour critical point in a pressure/temperature phase diagram [55]

In this way, the supercritical fluid immediately reaches the gaseous phase, removing the liquid inside the aerogel (without any damage to the aerogel structure) [33],[56].

A similar procedure is followed for the production of the other described aerogel typologies.

2.1.2.4 Building applications

Silica aerogel finds several applications in the building sector, for the insulation of both transparent and opaque building envelope components.

Generally, transparent buildings surfaces are responsible for more than 45% of the total energy dispersions of the building envelope [39]. The silica aerogel strongly absorbs the infrared radiation and thanks to its structure is translucent. Consequently, it can diffuse very well the light while having excellent thermal properties. Indeed it turns out to be a valid alternative to single or double chamber glazed surfaces for the thermal insulation. In this type of application, aerogel can be used in two ways: granular aerogel or monolithic aerogel. The monolithic aerogel has better thermal properties (thermal conductivity of 0.013 W/mK) than the granular one (0.020 W/mK) [39], but the most commonly used one is the second one because the mechanical resistance of the monolithic aerogel panels is very low.

A recent study [57] evaluated the energy performance of a multi-storey office located in Dhahran, Saudi Arabia. The used glass with aerogel was composed by granular aerogel enclosed in a core of 16 mm, separated from the outer glass by a gas layer of 12 mm; the 5 mm outer glass has undergone low-emissive treatments. This solution contributed to saving 14% of the annual energy consumption, in comparison to a traditional double glass window.

In cold climates (Norway), the energy saving could be 21% of the annual energy consumption, with a 58% reduction of the heat losses [39].

The differences between triple glass with argon (thermal transmittance U -value = 0.79 W/m²K), double glass with monolithic aerogel (U -value = 0.65 W/m²K) and granular aerogel (U -value = 0.44 W/m²K) were investigated by Lolli and Anderson [58]. Aerogel-insulated windows allow an energy saving of about 45% for space heating and 13% for the building energy use (the results are similar for both monolithic and granular aerogel).

Opaque building envelopes can be insulated from the outside, the inside, or eventually in the air cavity. Aerogel requires thicknesses remarkably lower than traditional insulating materials, and for this reason, this material is particularly suitable when the available space is limited (internal and cavity insulation). In [46] was demonstrated that an aerogel layer of 20 mm contributes reducing the wall thickness by 50% compared to polyurethane and 70% compared to rock wool.

At Politecnico di Milano four different interior insulation solutions were examined (south-exposed façade) [59]. The four configurations were: A.1 = base of natural perlite with a hydrophobic layer in the middle (55 mm); B.1 = recycled expanded glass panel with a multilayer of silica aerogel and polyester (30 mm); B.2 = a single flexible layer of silica aerogels (7 mm); A.2 = hydrophobic layer of expanded natural perlite to fill the air gap (330 mm). The observed U -value reductions were: 44.3% for the case A.1, 39.4% for the case B.1, 24.1% for the case B.2 and 89.2% for the case A.2.

Granular aerogel can also be used to improve the thermal properties of plasters (aerogel-based plasters). For example, in [60], this solution was adopted for the energy refurbishment of a building (built in 1950), obtaining a plaster with a thermal conductivity of 0.029 W/mK, and a consequent reduction of the wall thermal transmittance of about 35%.

A further application of aerogel is in the form of reinforced aerogel blankets for pipe insulation [33], and Thermal Energy Storage (*TES*) insulation [61]. The advantages are correlated to the obtainable lower thickness of the insulation, and consequent smaller dimensions of pipes (beneficial for both transport and installation) or bigger volume storage. In both cases the heat losses are radial, and therefore the thickness is of large importance. If the insulation thickness is too high, the consequently increased dispersing surface compensates the insulating effects. Halving the thermal conductivity, less than half insulation thickness for the same design losses is required [62].

2.2 Vacuum Insulation Panels - VIPs

Vacuum Insulation Panels (VIPs) represent one of the future boundaries in the field of thermal insulation. This technology usually consists of a multi-layer hermetic envelope surrounding a porous core from which the air and gases present have been evacuated (**Figure 13**). This structure makes the VIPs one of the best insulation solutions in terms of heat transmission, able to reach thermal conductivity that can vary over the lifetime of the panel from 0.0015 to 0.0080 W/mK, offering, at the same thickness, a resistance about 8 to 10 times more thermal than a conventional insulating material [63].

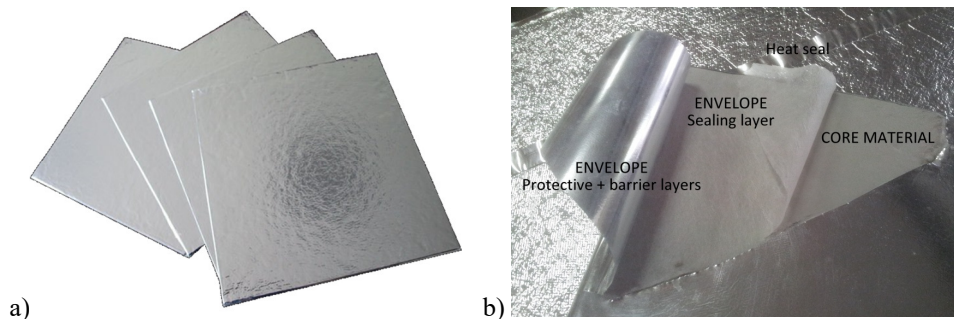


Figure 13: a) Vacuum Insulation Panels; b) VIP structure

The first VIP was manufactured in 1930 by a German patent, using a porous core material coated with rubber. Approximately 20 years later, a second patent was presented in the United States, which provided for the use of glass wool as the core material, sealed with steel sheet. In 1963 the first panel with a core of a nanostructured material was produced. In the following years, the development of VIPs continues with experiments on different types of material for the core and the envelope, in order to reduce the thermal conductivity, the thickness of the panel and to improve the permeability of the protective envelope. Many nanostructured materials usable as the core of the panel were already available in 1930,

such as aerogel; however, over the course of time, numerous studies have led to the development of alternative materials [64].

In recent years, the interest of research on VIPs has increased, with studies aimed at analysing in particular thermal conductivity ([65],[66]), the permeability of gases through the envelope and the creation of vacuum ([67],[68]); analytical optimization models have been formulated and various materials for the production of vacuum panels have been tested, leading to applications in the construction sector, which is still growing [63]. These panels are successfully integrated into buildings only if careful planning is made, regarding durability, lack of flexibility, brittleness and thermal bridges between the boards. It is necessary to take into account their short life in relation to the average times of a building, and the significant decrease in performance over time. Not to be underestimated is also the cost of production, very high, which amounted on average about 168 €/m² ([69],[28]): therefore “*much effort has been done in the last few years in studying novel and low cost core materials (e.g. expanded cork and cellulosic-crystal, as described in [70],[71],[72],[73] and [74])*”².

2.2.1 Properties

The main components of a VIP panel are the inner core, some getter/desiccant and opacifier additives, and the protective sealing envelope. There are many types of materials and configurations of these essential elements that generate panels with different properties and characteristics.

2.2.1.1 Core material

The choice of the core material is fundamental to minimise the thermal conductivity of the VIP. To optimise the performance of the panels, the core must meet specific requirements listed below [63]:

- the pore diameter of the core material must have nanometric size (for materials with larger pores, a much lower internal pressure is required to achieve the same thermal conductivity [28], as shown in **Figure 14**);
- the structure of the pores inside the material must be 100% open so that all the gas inside the panel can flow from one pore to another without hindrance and be easily evacuated;

² Text from the author’s paper: “Actual thermal performances of Vacuum Insulation Panels for buildings” [75].

- the core material must resist compression: the usual VIP internal pressure range is initially between 20 and 300 Pa [28], while the external panel pressure is about 101325 Pa (atmospheric pressure);
- the material must be impermeable to infrared radiation, in order to reduce the radiative heat transfer.

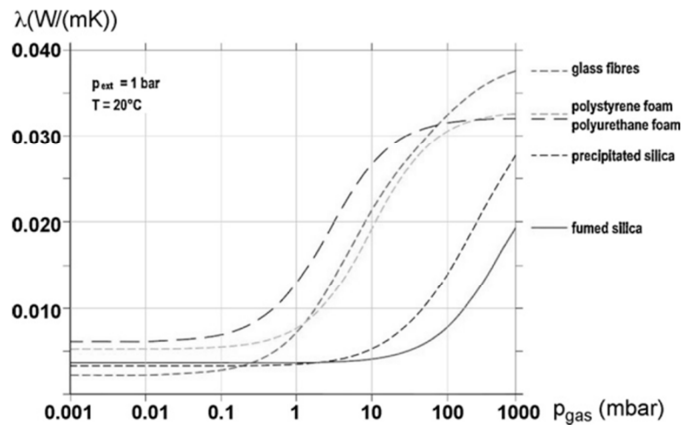


Figure 14: Thermal conductivity of different insulation materials as a function of the internal residual pressure [28]

Several materials have been studied as VIP core material, and some of them are analysed from now on ([63],[69],[28],[76]).

- **Polyurethane foam - PU**
This was the first VIP core material. It meets the criteria of mechanical strength and open porous structure; however, the size of the pores is quite big (millimetric scale), so that this material requires a low degree of vacuum to obtain a typical VIP thermal conductivity, e.g. 0.004 W/mK. The internal pressure must remain below 1 mbar, beyond which the conductivity increases considerably. However, these pressures cannot be reached with the currently available envelopes.
- **Glass Fibre - GF**
Fibreglass cores have similar problems to PUR foam panels. In fact, given the relatively large pore size, ranging from 1 to 12 μm , the internal pressure must be very low: at about 0.1 mbar the thermal conductivity reaches the value of 0.0015 W/mK. The base material is relatively inexpensive, and the life expectancy for a GF VIP is around 15 years [77]: too low for building applications (the lifetime of buildings is assumed to be 50 years).

- **Aerogel**

Aerogel is a nanoporous material with a pore size of about 20 nm. Subjected to a pressure of 50 mbar, and with the addition of carbon black to suppress the radiative transfer, the aerogel reaches very low thermal conductivity (about 0.004 W/mK), while at ambient pressure the thermal conductivity rises to around 0,013 W/mK [33].

- **Fumed Silica - FS**

The small size of pores (maximum dimension ~ 300 nm) combined with the effect of the opacifiers inside the core (silicon carbide powder, or titanium dioxide), makes it possible to reach core thermal conductivity in the order of 0.019 - 0.020 W/mK ([26],[27],[28]), with a good compression resistance. *“Once the core is evacuated, the VIP is characterised by a value of the equivalent thermal conductivity around 0.004 W/mK. Due to the small pore size, a gas pressure below 10 mbar is in general sufficient to strongly reduce the gaseous conductivity contribution, while in case of other core materials (foams and fibres) a pressure value below 0.2 mbar is needed [26]. Fumed Silica (FS) based VIP are particularly suitable for building applications, because of several advantages compared to VIP made with other kind of cores [78]. Among these advantages are worthy of mention: the relatively long service life expectancy, (since the component is less sensitive to the increase of the internal pressure) and the relatively low thermal conductivity in case of complete loss of vacuum (equal to about 0.020 W/mK). For all these reasons, FS based VIPs were in-depth investigated in the scientific literature, under different perspectives. In particular, the heat transfer mechanism was described in [27],[26],[79],[80],[81]. The dependence of thermal conductivity on the internal gas pressure was analysed in [82], while the variation of thermal conductivity over time for different VIP envelope typologies was investigated in [83]. Usually, manufacturers declare a thermal conductivity lower than 0.005 W/mK for FS based VIPs, which is a typical value at a pressure of 10 mbar [63].”*³

³ Text from the author’s paper: “Actual thermal performances of Vacuum Insulation Panels for buildings” [75].

2.2.1.2 Getters/desiccants and opacifiers

The conductive heat transfer inside VIPs is closely linked to the low gas pressure inside the panel. Vapours and gases that permeate through the envelope contribute to the increase of the internal pressure of the VIP, with the consequent lower effectiveness of insulation. To counteract this drawback, desiccants and adsorbents are added to the core [28],[63]. They are chemical components which absorb residual gases and water vapour after vacuum process, or which subsequently permeate, in order to maintain a constant thermal conductivity. Desiccants are made of materials with high hygroscopic properties to trap moisture (CaO, BaO) [84]. The adsorbents, on the other hand, are materials with a high degree of porosity: a large surface exposed to the permeated gases, which are attracted and captured, maintaining the internal pressure low.

The opacifiers are added to the core of the panel to reduce the radiative heat losses [78].

2.2.1.3 Envelope

The primary purpose of the envelope is to contain the core material and provide a hermetic seal against air and steam, to maintain a certain degree of vacuum inside the panel. Depending on the materials and the structure of the envelope, the lateral heat flux dispersions due to the presence of thermal bridges (edges of the panel) will also vary. There are several studies in the literature about the reduction of these effects [85]. Considerable attention must be paid to envelope heat sealing process, to minimise infiltrations through these edges [86].

The envelope is composed of three main layers: the sealing layer (more internal), a barrier layer and an outer protective layer. The main typologies of envelope are:

- **Aluminum Foil - AF**

The outer protective layer is composed by a polyethylene terephthalate (PET) laminate, a central aluminium sheet (with a thickness of about 5-10 μm) constitutes the barrier layer, and as an inner sealing layer is made of polyethylene (PE). The use of aluminium as a barrier layer considerably reduces the permeation through the envelope, increasing the service life of the panel. However, the thickness of the metal foil contributes to the increase in the thermal bridging effects, given the high thermal conductivity of aluminium [87]. This type of envelope is no longer used.

- **Multilayer Foil - MF**

MF envelope is a glued multilayer film solution, which consists of several outer protective layers in PET, alternated with as many layers of aluminium (thickness of 20 - 100 nm each), and an inner sealing layer in PE [76] (**Figure 15**). The number of PET + Al layers provides the name of the envelope structure.

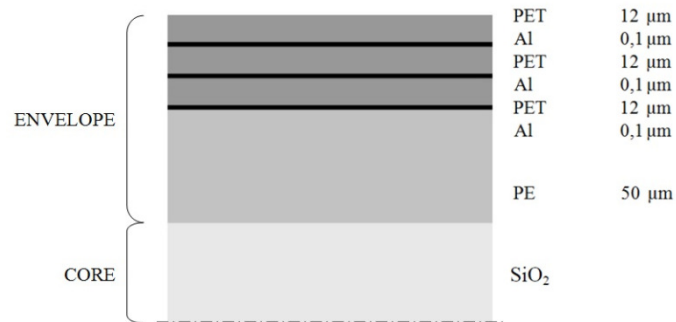


Figure 15: Structure of a VIP with MF envelope

Nowadays, the MF solution is the most widely used for civil applications [63]. However, reducing the total thickness of the metal layer leads to significantly faster moisture and air permeation through the envelope [68], which causes more rapid ageing of the panel (**Figure 16**).

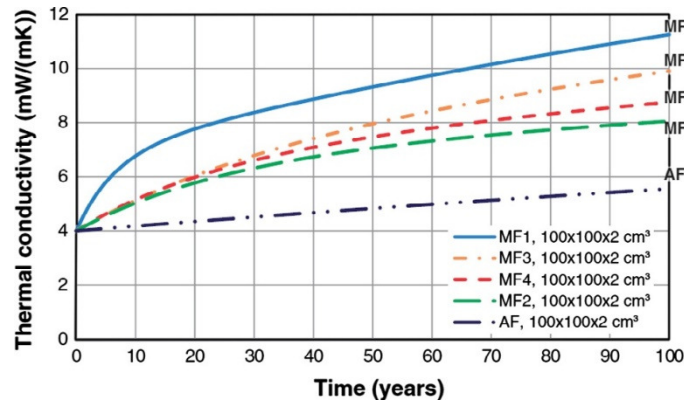


Figure 16: Thermal conductivity during time, considering several envelope typologies [63]

2.2.1.4 Environmental impact

The environmental impact of VIPs must be assessed according to EN 15978:2011 [88]. It defines the calculation method to evaluate the environmental performance of a building, basing on the life cycle analysis, divided into four phases: used raw materials, building construction, use and disposal at the end of the life cycle. Only through a Life Cycle Assessment (LCA) study is it possible to obtain information on the effective range of impacts in the various phases. This methodology is internationally standardised according to ISO 14040:2006 [89].

In [90] three different LCA methods were used to investigate the environmental impact of FS VIPs with a multilayer envelope. The vacuum panel was compared to glass wool and expanded polystyrene (EPS) used in 1 m² of wall with a transmittance value of 0.15 W/m²K, considering 40 years of time. The three methods are:

- **Embodied energy:** this method measures the grey energy which is the sum of the amount of energy used for the production and the processing of the material;
- **UPB97:** or Environmental Impact Point method, which allows the comparison of materials considering the use of resources, the production of radioactive waste, the need for landfill and the quantity of emissions in the air, water and soil;
- **Eco99:** (Ecoindicator 99) it is used to calculate the impact caused by the production of these materials on human health, the effects on the ecosystem and the depletion of resources.

Table 5: Three different LCA analysis, comparing Glass wool, EPS and VIP [42]

Method		Glass wool		EPS		VIP
Embodied energy	<i>[MJ/m²]</i>	455	46% _{of VIP}	890	89% _{of VIP}	99
UBP97	<i>[UBP97/m²]</i>	21646	50% _{of VIP}	35767	83% _{of VIP}	43245
Eco99	<i>[milli-points/m²]</i>	1254	52% _{of VIP}	3402	142% _{of VIP}	2393

The results of LCA calculations are shown in **Table 5**. VIPs cause a higher environmental impact than glass wool and EPS considering the grey energy and the UBP97 method. The Eco99 analysis instead shows how they have a lower environmental impact than EPS, 42% higher than the VIPs, while the glass wool is only half of the VIPs. The high value of EPS is due to the use of non-renewable fossil-based materials. The analyses showed that 90% of the energy used in the

production of VIPs is caused by the core material, while only 4% of the production is used for the protective films. Therefore, it's possible to assume that, with alternative core materials or a more efficient core material production process (regarding the primary energy used), the environmental impact of VIPs can be reduced by 45% [64].

2.2.2 Building applications

During the past few years, VIPs have been extensively studied under several aspects (thermal conductivity, air and humidity permeation, thermal bridges, ageing and durability, quality, control and integration in the construction of buildings) from both the experimental point of view and through the realisation of analytical simulation models. Recently, economic analyses have also been carried out for the evaluation of the convenience of using the highly expensive VIPs: in case of new high-performance buildings or energy refurbishment in areas with a high market value of the living space per square meter, a reduced wall thickness can significantly entail the surface savings and therefore a higher value of the building [91],[92]. Given the interesting results obtained by researchers, several building applications of these materials can be found [93]:

- door and window insulation (limited available space);
- glazed façade (limited available space);
- façade in new buildings (high performances or high surface value);
- floor insulation (high performances or limited available space);
- façade interior retrofit (high value of the floor surface);
- façade exterior renovation (limited available space);
- structural façade sandwich panels;
- attic hatches and stairs (limited available space);
- roof and terrace insulation (limited available space);
- saunas and pipes (with some problems related to the high humidity and temperatures, which cause an increase of VIP thermal conductivity, see § 8.1 *Effects of temperature and ageing on SIM thermal properties (HFM)*).

Beyond the economic aspect, the central criticisms related to the use of VIPs are due to their actual durability and the correct evaluation of the existing thermal bridging effects.

2.2.2.1 Durability and Service life

The durability, or service life, is the time during which the VIP has thermal conductivity below a defined limit required to maintain the designed thermal efficiency of isolation. Instead, ageing of the product is defined as the set of all irreversible changes that affect the VIP over time [67].

During their use, VIPs are stressed both chemically and physically (oxygen, water, acidity, basicity, air pressure, vapour pressure, temperature, and even UV and IR radiation).

In laboratory investigations, VIPs can be subjected to two principal ageing mechanisms. The accelerated ageing occurs typically with temperatures higher than 50 °C and/or with relative humidity higher than 70%. The failure of the technology is indeed due to the deterioration of the protective barrier (delamination, corrosion of the aluminium or hydrolysis of the polymers), which is no longer able to play its role. The second mechanism is a slower and more regular ageing of the VIP, due to the permeation of atmospheric gases inside, without particular deterioration of the external barrier; this involves a double effect, causing an increase in the internal pressure and consequently in the thermal conduction [67]. Some measurements on envelope permeability have shown that it decreases exponentially with the increase in thickness of aluminium, but it slightly changes if the number of layers is increased while maintaining the same thickness of the single film. In other words, the accumulation of several layers is not useful to improve the performance against the humidity of the VIP barrier [68].

The reasons for the in situ deterioration may instead be the most disparate. For example, the degradation of the barrier layer is closely correlated with the presence of chlorine in the elements with which the VIP comes into contact (necessary but not sufficient to promote the degradation process) [68]. Or, the southern exposure, subjected to intense solar radiation, is often the cause of a sudden increase in internal pressure that leads the panels to collapse: the formation of condensation inside a building and the thermal excursions between day and night create solicitations on the structure of the materials. The damage to the panels could also be due to the possible presence of defects on the sides of the panel, where they are sealed.

The main components that should be taken into account to evaluate the life expectancy are four: the characteristics of the core material, the characteristics of

the envelope material, the external conditions to which they are subjected (temperature, humidity, etc.) and the thickness of the panels. Any method for the evaluation of the life cycle or the thermal conductivity over time cannot be considered reliable the relationships between these four factors are not taken into consideration [67].

2.2.2.2 Thermal bridging effects

One of the significant challenges in the application of VIP panels in the building sector is to minimise the impact of thermal bridges: “*the greater the material insulating power, the greater the impact on the overall performance of the thermal bridging effect*”⁴. To reduce this problem, it is necessary to know what are the causes that lead to a considerable increase of the overall thermal conductivity [84]. A thermal bridge is defined as the limited local area of the building envelope characterised by a greater thermal flux density than the adjacent building elements. “*The overall effect of thermal bridges in VIP can be evaluated by means of the so-called linear thermal transmittance of the thermal bridge ψ [W/mK] [96]*”⁵. This parameter can be evaluated according to EN ISO10211-1:2017 [97], as will be explained in 3.2 VIPs thermal performance parameters. The linear thermal transmittance indicates the heat flow dispersed through the thermal bridge for each meter of length and a unit temperature difference between the two sides of the panel; this value depends on the thickness and thermal conductivity of the VIP, on the thickness and thermal conductivity of the barrier film and the layout of the envelope.

Thermal bridging effects can be analysed at three different levels/scales ([66],[98]):

- **Material scale:** every single panel;
- **Component scale:** VIP panels coupled together using frames (structural joint) or spacers (air joints);
- **Building scale:** considering the effects due to the whole façade.

At the material level, thermal bridging effects depend mainly on four parameters: the thickness and layout of the envelope, its thermal conductivity (and

⁴ Text from the author’s paper: “The effect of different materials joint in Vacuum Insulation Panels” [95].

⁵ Text from the author’s paper: “Experimental and numerical investigation of thermal bridging effects of jointed Vacuum Insulation Panels” [103].

therefore the chosen configuration), the thermal conductivity of the core and the total thickness of the VIP panel [65],[66] (Figure 17).

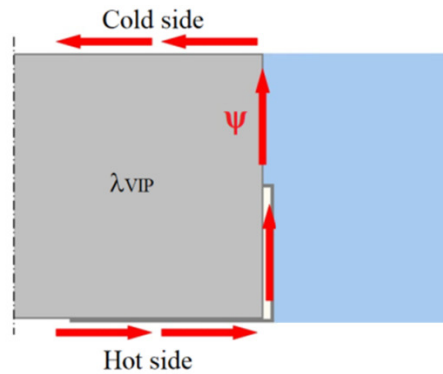


Figure 17: Thermal bridge at the panel level

The thermal losses are located on the edges of the VIPs and the layout of the envelope (AF or MF), has a strong influence (Figure 18). Over the last few years, great efforts have been made to reduce the thickness of the aluminium layers by improving sputtering techniques (physical deposition technique of thin films on a surface), by suitably treating the PET surfaces before the metallization. The result is an improvement in permeation resistance but without an increase in thickness of the barrier layers [99].

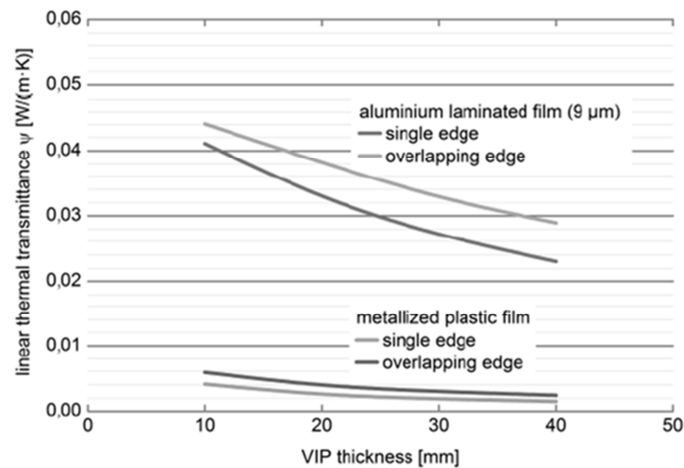


Figure 18: Comparison between the linear thermal conductivity of an AF and MF envelope, varying the panel thickness [99]

Because of the non-homogeneity of the VIP materials (and therefore of the different thermal conductivity), the total effective thermal conductivity value of a VIP (λ_{eff}) is higher than the ideal conductivity in the centre of the panel (λ_{COP}). The magnitude of this increase is also influenced by the thermal properties of the layers of the materials adjacent to the panel.

The effective thermal conductivity of a VIP is equal to the conductivity of a homogeneous material with equivalent thermal behaviour [100], and can be calculated by adding to the λ_{COP} the ψ -value of the thermal bridge, weighted with the specific geometry under analysis (see § 3.2 *VIPs thermal performance parameters*).

The effect of the thermal bridge is strictly correlated to the dimension of the panel: since it depends on the total edge length, heat losses will be more significant for smaller panels. **Figure 19** shows the edge effect as a function of the panel size: it is therefore recommended to use larger VIPs, within limits dictated by construction and vacuum conservation technologies. Furthermore, the energy lost at the edge of the panels is slightly more significant for thinner panels than for thicker panels ([65],[98],[99],[101]).

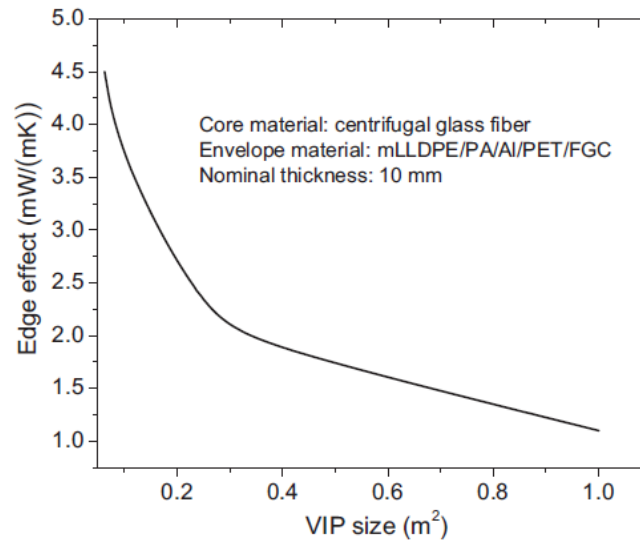


Figure 19: Edge effects as a function of the panel size [101]

Moving to a larger scale than the one of the single panel (component scale), focusing on the constructions realised with the VIPs, it must be taken into account that VIPs require many precautions during their installation. “*In case of vertical*

*component insulation, is necessary to provide a mounting and support systems to the structure for VIPs. This can be made with laths and battens in different materials (like MDF and XPS), with metal and plastic rail system, or with plaster and adhesives. For roofs, floors and horizontal surface panels are instead put close each other without additional structural support: so only air joint have to be considered.”*⁶ In this way, a “cobweb” of distributed linear thermal bridges occurs.

The overall thermal transmittance of the wall depends not only on the laboratory assessed λ_{COP} , but also on the effect of the thermal bridge caused by the structure with which they are assembled [65]. Moreover, the linear thermal transmittance does not depend only on the thickness and the material of the barrier layer, but on a series of other constructive factors, such as [99]:

- the material used in the joints between two panels;
- cover layers on the panel sides, widely used to produce "sandwich" elements for easy use on construction sites (e.g., wood, plastic, metal);
- components for mounting and fixing (e.g., glue, screws, mechanical fasteners, etc.);
- application of a double layer of insulation [102].

Each added material has its own value of conductivity significantly higher than the panel, causing a thermal discontinuity.

Indeed, between adjacent panels, there is always a certain distance given either by the thickness of the frame or by an air gap due to the non-perfect adhesion of two adjacent panels. It is, therefore, possible to identify two factors that influence the value of linear thermal transmittance of the wall: air joints and structural joints (**Figure 20** a) and b) respectively). In [103] the author proposed an experimental method (subsequently verified through comparison with the data reported in the literature and numerically validated) for the measurements of the thermal bridging effects.

The analysis shows the influence of the thickness of the air joint on the value of the linear thermal transmittance; this depends on both the effective distance between the panels and the thickness of the single panel.

⁶ Text from the author’s paper: “The effect of different materials joint in Vacuum Insulation Panels” [95].

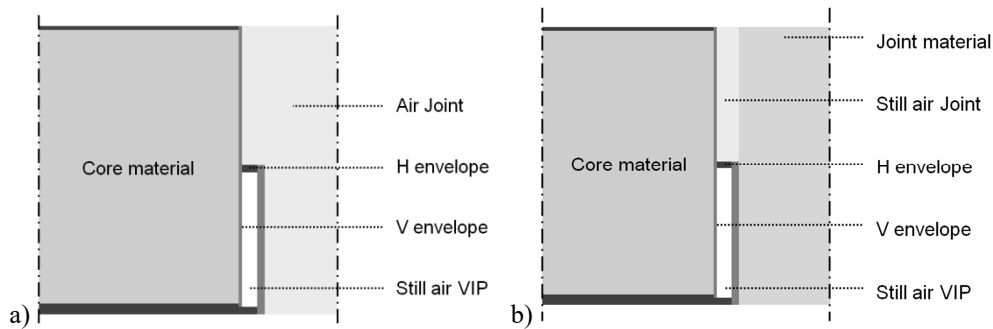


Figure 20: Schemes of VIPs assemblies: a) air joint; b) structural joint [103]

In **Figure 21** it can be seen that the greater the space between the panels, the greater the effect of the thermal bridge will be. “Some hypotheses can be made to explain why the results related to the 20 mm thick panel are in better agreement than those for other panel thicknesses. First, the width of the air joint used for the calculation is a constant value that is equal to the average value (measured along the entire panel edge) of the local widths of the real sample. Two identical configurations, with the same average joint width, but significant local differences of the air gaps between the panels, do not necessarily behave in the same way when tested in the lab (although they do provide the same results when simulated numerically). This is primarily due to convection and radiation, which are highly non-linear phenomena. Moreover, the measurement of the width of the air is characterised by a consistent uncertainty (due to the photographic survey method) and, again, this factor can determine a discrepancy between predicted and measured quantities.

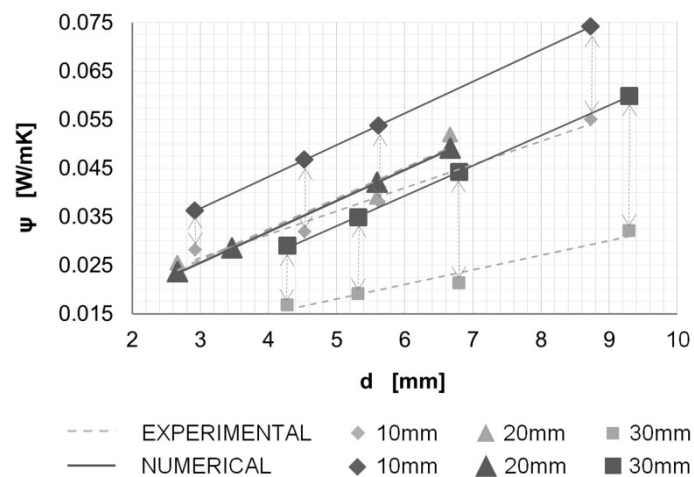


Figure 21: Influence of the air joint width (d) on the value of ψ . Experimental and numerical results for 10, 20, 30 mm thick panels [103]

The thermal bridge caused by structural joints is mainly characterised by the thermal resistance of the joint, R_{Joint} . [...] Both the experimental and the numerical results are distributed along similar curves that have a power law shape (Figure 22). The measured and numerical values of the linear thermal transmittance are in a good agreement with each other, although the prediction accuracy is better when the thermal resistance of the joint is higher (e.g., joint made with another insulating material, like XPS or ABP). [...] The numerical model can be considered reliable for cases in which $R_{Joint} > 0.100$ (m^2K/W), and can consistently be applied to estimate the thermal bridge effect of structural joints in typical building applications (the data shown in Figure 21 and Figure 22 cannot be used directly for practical applications, since they do not include the effects of the internal and external surface heat transfer coefficients)⁷.

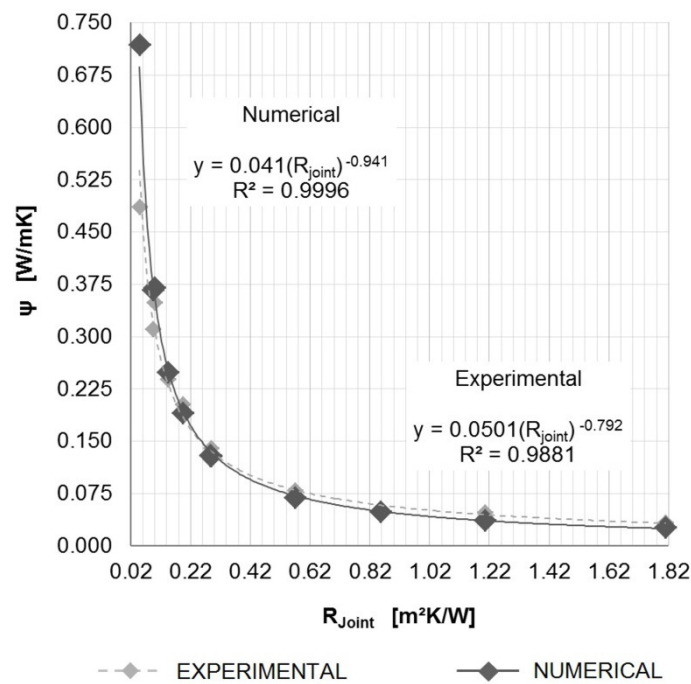


Figure 22: ψ versus R_{Joint} : experimental and numerical results [103]

Considering an even higher scale, at the building level, it is necessary to investigate not only the type of joint material to be used but also the building envelope material and structure (additional internal thermal resistances - R_i and

⁷ Text from the author's paper: "Experimental and numerical investigation of thermal bridging effects of jointed Vacuum Insulation Panels" [103].

external - R_e). The lower the conductivity of the envelope (higher R_i and R_e), the less the total effect of the thermal bridges between the VIPs [65] (**Figure 23**).

The most common materials used as a structural joint are: EPS - Expanded Polystyrene, XPS - Extruded Polystyrene and MDF - Medium Density Fibreboard. Moreover, some studies have analysed the effects resulting from the use of a non-conventional material for joints, namely the aerogel – ABP (**Figure 24**). The use of ABP has considerably reduced the effect of thermal bridges on the thermal transmittance of the whole façade ([103],[104],[105]).

The coupling of SIMs both as insulating and joint materials leads to excellent energy performance; however, their use could affect the economic balance of the building. In [104] “*a double analysis (economical and thermal) was carried out on a typological façade model, in order to compare the results of different assembling materials (Aerogel, EPS and MDF). As expected the cost increasing due to coupling VIPs and Aerogel assemblies is almost negligible providing, on the contrary, a great increasing of SIMs assembly insulating performances. This trend is due to the higher cost and quantity of VIPs in comparison to other structural material used as joints. For all these reasons, SIMs coupling could be a solution to optimise VIPs performances, and might be the right direction for the optimisation and deployment of these technologies*”⁸.

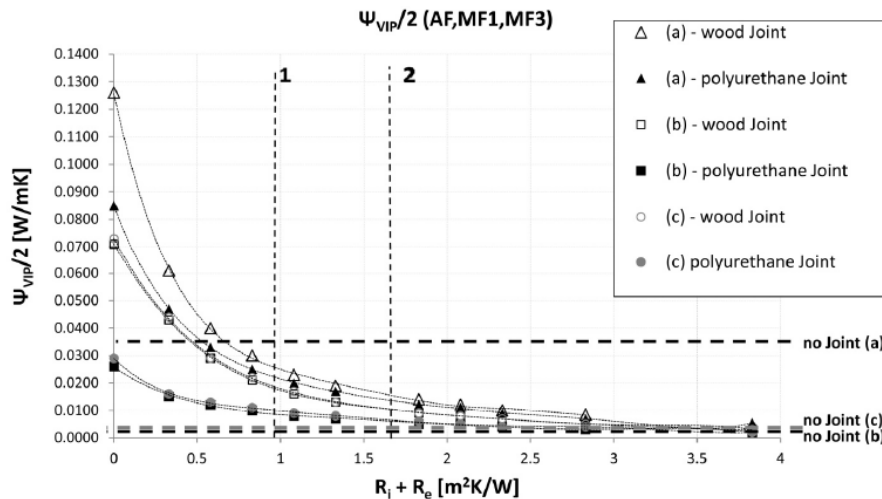


Figure 23: Linear thermal transmittance for wood joints and polyurethane joint as a function of the variation of $R_i + R_e$ for three different types of wall (a, b, c) [65]

⁸ Text from the author’s paper: “Coupling VIPs and ABPs: assessment of overall thermal performance in building wall insulation” [104].

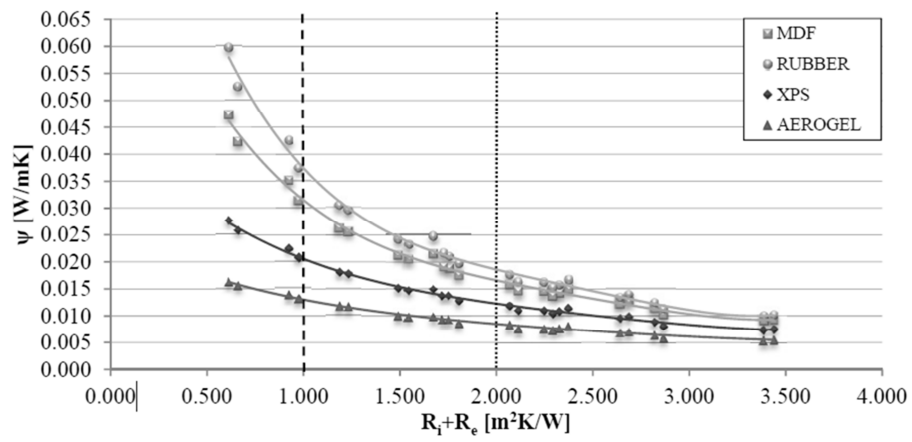


Figure 24: Linear thermal transmittance for different materials joints as a function of the resistance of additional layers ($R_i + R_e$) [105]

Chapter 3

Heat transfer in SIMs

The fundamental mechanisms through which the heat transfer occurs in nanoporous materials (SIMs) are in principle the same as for any other porous insulating material: conduction heat transfer in a solid matrix, gaseous heat transfer, and radiation heat transfer. In addition to these, there is another term called coupling effect, which is a second order effect between the other heat transfer terms, and it represents the interaction between solid and gas phase. It is relevant for powder and fibre materials, but it is negligible for the most theoretical study of VIPs thermal performance.

The most representative characteristic of an insulating material is its thermal conductivity λ [W/mK], which define the property of the material to conduct the heat.

Moreover, in the previous chapter, was highlighted that in case of VIPs, the thermal bridging effects must be taken into account, through their linear thermal transmittance ψ . Consequently, it is essential to discern between the thermal conductivity at the VIP centre of panel (λ_{COP}), the effective thermal conductivity (λ_{eff}), which takes into account the thermal bridging effects at the panel level, and also a new quantity, the equivalent thermal conductivity (λ_{eq}), which takes into account the thermal bridging effects at the component and building level (where other materials are involved, both as joint material between the VIPs and as building envelope structural material).

3.1 Heat transfer mechanism

In case of porous materials, “the heat transfer mechanism is generally described by the Eq. (1) as the sum of the contribution of the solid thermal conductivity (λ_s), the radiative thermal conductivity (λ_r), the gaseous thermal conductivity (λ_g), and a coupling thermal conductivity which takes into account the interactions between gas and solid particles of the core material (λ_{cpl}) ([28],[78],[106],[107])”⁹:

$$\lambda = \lambda_s + \lambda_r + \lambda_g + (\lambda_{cpl}) \quad (1)$$

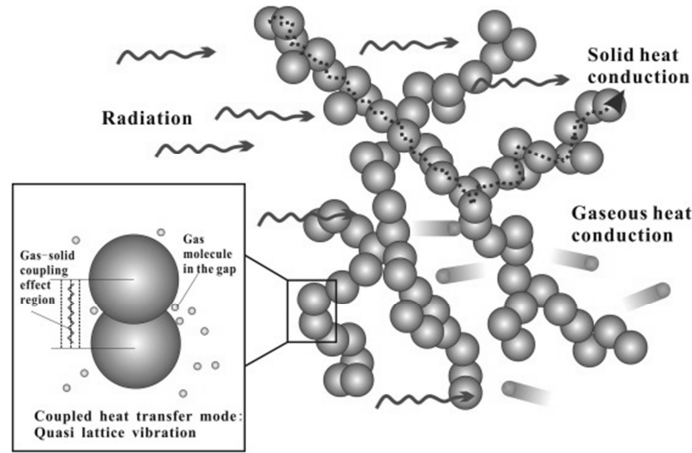


Figure 25: Sketch of the three heat transfer paths in nanostructured materials [108]

λ_{cpl} can be neglected in case of foams with non-broken structure, while it can assume significant values at elevated gas pressures (e.g., 0.020 - 0.030 W/mK for hard grains powders see [109]). Increasing the pressure, if the contact resistance between the grains is thermally shorted by the gas molecules, the coupling term is no more negligible.

The gas pressure (p_g) has a strong influence also on the gaseous conduction λ_g , as explained in [110], which depends also on the Knudsen number.

In particular, the Knudsen number can be evaluated by the following equation [28]:

$$K_n = \frac{l_{mean}}{\delta_{pores}} = \frac{1}{\delta_{pores}} \cdot \frac{k_B \cdot \vartheta}{\sqrt{2} \cdot \pi \cdot \phi_g^2 \cdot p_g} \quad (2)$$

⁹ Text from the author’s paper: “Actual thermal performances of Vacuum Insulation Panels for buildings” [75].

Where: δ_{pores} is the characteristic size of pores [m];

l_{mean} is the mean free path of air molecules [m], that can be expressed as a function of the following parameters:

$k_B = 1.38064852 (79) \cdot 10^{-23}$ J/K is the Boltzmann constant;

ϑ is the temperature [K];

\varnothing_g is the average diameter of the gas particles [m];

p_g is the gas pressure [Pa].

Depending on the value of Kn , it is possible to identify three different heat flow regimes:

- $Kn < 0.01$ - viscous flow: the overall molecules flow is dominated by impacts between the molecules, while the collisions with the walls of the vessel or the pipeline play a secondary role (the typical situation at atmospheric pressure or in low vacuum regimes);
- $0.01 < Kn < 1$ - transition regime;
- $Kn \geq 1$ - molecular regime: the mean free path is larger than the characteristic dimension s of the system; the gas flow is dominated by the impacts of the molecules with the walls and the impacts between the molecules themselves are negligible (this regime typically begins to occur for pressures below 1 Pa, depending on the dimensions of the material pores).

For nano-porous materials ($\delta_{pores} \approx 200$ nm), if the gas pressure is reduced below 10 mbar, the gaseous conductivity can be considered negligible ($Kn \geq 1$) [42], while, considering materials with $\delta_{pores} \approx 20$ nm, an evacuation to about 0.1 mbar is required, in order to suppress gaseous conduction, since the gaseous conductivity is fully developed at 1 bar: this is the case of most common VIPs. Indeed, the gaseous heat transfer depends not only on the internal pressure but also on the size of the pore diameters: with a smaller diameter, the gas molecules will collide with the pores surface without exchanging energy. Decreasing the size pore diameters and increasing the pressure for fumed silica, it is possible to reach low gaseous thermal conductivity at atmospheric pressure (as shown in **Figure 14**, § 2.2.1.1 Core material).

The solid conductivity λ_s is the lowest term in Eq. (1): the finer structured the material (SIMs are nano-structured), the more the resulting thermal resistance is. λ_s is proportional to the density (ρ [kg/m³]) of the material:

$$\lambda_s \propto \rho^\beta \quad (3)$$

Where $\beta \approx 1$ for foams, and $\alpha \approx 1.5 - 2$ for nanostructured materials [111].

The solid thermal conductivity also depends on the external pressure, but, since most materials show a hysteresis behaviour with an increase of the solid conduction with the rise of external pressure load, a quantitative description of this phenomena is difficult [42].

The radiative heat transfer λ_r can be evaluated as a function of index of refraction for low-density materials, the extinction coefficient of the insulating material and an average temperature (ϑ_r^3 [K³]) between the surfaces temperatures (ϑ_1 and ϑ_2) of the insulating material, evaluated through the following Eq. (4) [112]:

$$\vartheta_r^3 = \frac{(\vartheta_1 + \vartheta_2) \cdot (\vartheta_1^2 + \vartheta_2^2)}{4} \quad (4)$$

To reduce the radiative thermal transport, absorbing and scattering particles (opacifiers, such as SiC) must be added into the insulating material. These additives cause an increase in the extinction coefficient, reducing the λ_r value.

Therefore, as explained in detail in [42], for a dried, evacuated and opacified silica board (FS VIP), the expected (and most typical) thermal conductivity value (λ) can be assumed to be around 0.004 W/mK, composed by $\lambda_s = 0.003$ W/mK, $\lambda_r = 0.003$ W/mK and $\lambda_g = \lambda_{cpl} \approx 0$ W/mK.

All the different λ contributions are temperature dependent and typically increases with temperature. Anyway, all of them have a distinct correlation with temperature.

For the solid heat transfer within the typical temperature range of building applications, the temperature increase is usually linear but weakly pronounced, and therefore it is often neglected.

$$\lambda_s(\vartheta) \propto \vartheta \approx constant \quad (5)$$

The radiative thermal conduction λ_r varies with the third power of ϑ_r (Stefan-Boltzmann-law):

$$\lambda_r(\vartheta) \propto \vartheta_r^3 \quad (6)$$

The total heat transfer in traditional building insulating materials is dominated by λ_g . Consequently, also its temperature dependence is governed by the effects of the temperature on the gaseous thermal conduction. Contrariwise, in case of nanoporous materials, λ_g is reduced by enhanced collisions of the gas particles with the pores structural elements. The mean free path of gas molecules typically increases linearly with absolute temperature. Moreover, the thermal conductivity of a free still gas (λ_{g0}), without convection, usually varies with the square root of the absolute temperature [42]. Therefore:

$$\lambda_g(\vartheta) \propto \sqrt{\vartheta} \text{ and } 1/\vartheta \quad (7)$$

For APMs the temperature increase of the total thermal conductivity is lower than conventional insulating materials, while for VIPs the increase in temperature is typically dominated by the rise of λ_r , but also the gaseous contribution has a significant impact (as will be explained in § 8.1.1 *Convective, radiative and conductive contributions in VIP and Fumed Silica core*) ([29],[75],[79],[113]). This phenomenon depends on the residual internal pressure and residual vapour content inside the core (**Figure 26**).

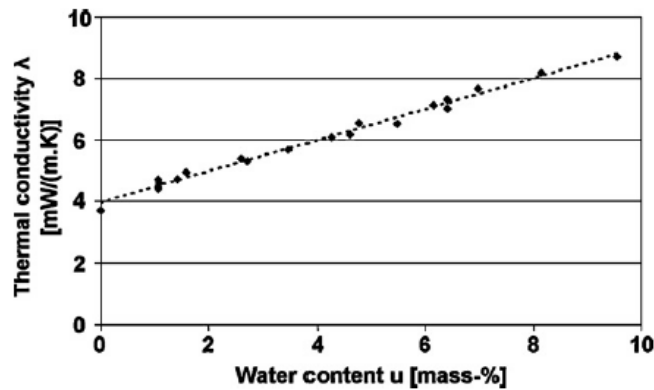


Figure 26: VIPs thermal conductivity as a function of water content [78]

An increase of the temperature in bound volume also determines an increase of the internal pressure [114], as well as of the partial vapour saturation pressure $p_{vs}(\vartheta)$, and hence of the gaseous thermal conductivity.

3.2 VIPs thermal performance parameters

The thermal conductivity λ [W/mK] is the most important and significant characteristic to evaluate the insulating performance of any materials, but it is not the only relevant parameter. The effective heat flow which crosses the insulating material also depends on the thickness of the insulator, and therefore on its thermal resistance R [m²K/W].

Traditional insulating materials and APMs can be easily characterised through their λ -value, but in case of VIPs, the thermal bridging effects must be taken into account. Thermal bridging effects are evaluated by the linear thermal transmittance ψ [W/mK], which affects the overall thermal conductivity of a VIP or a VIPs assembly. It is, therefore, necessary to differentiate between the centre of panel thermal conductivity (λ_{COP}), and the effective (λ_{eff}) or equivalent (λ_{eq}) thermal conductivity, in case of thermal bridges at the panel scale or component/building scale respectively (as already explained, both the λ_{eff} and the λ_{eq} take into account the thermal bridging effects, considered distributed over the entire panel surface).

At the building scale, the overall façade thermal properties also depend on the stratigraphy of the building envelope, which means on the adjunctive internal and external thermal resistances of all the other building materials ($R_i + R_e$), reducing the effects of the VIPs thermal bridges. Finally, the overall façade thermal performance can be expressed by the thermal transmittance U [W/m²K].

- **Thermal conductivity - λ**

“The general measuring method is based on the one-dimensional Fourier-Biot law:

$$\lambda_{COP} = \frac{\varphi \cdot t}{\Delta\vartheta} = \frac{\varphi \cdot t}{(\vartheta_h - \vartheta_c)} \quad (8)$$

Where: λ_{COP} is the sample thermal conductivity [W/mK];

φ is the measured specific heat flux through the sample [W/m²];

$\Delta\vartheta$ is the temperature difference between the hot and cold plates [K];

t is the measured sample thickness [m]¹⁰.

- **Thermal resistance - *R***

The thermal resistance is the resistance of a particular material or system to the heat flow through its boundaries. It depends on the geometry and thermal properties of the element, such as thermal conductivity. It is based on an analogy with the Ohm's law:

$$U = I \cdot R_{el} \quad (9)$$

Where U [V] is the electric signal related to a current I [A], proportional to the electric resistance R_{el} [Ω].

For mono-dimensional and steady-state heat transfer mechanisms, the heat flow is proportional to a temperature difference (as already noticeable from Eq. (8)):

$$\Phi = \lambda \cdot A \cdot \frac{\Delta\vartheta}{t} \quad (10)$$

Where: Φ is the measured heat flux through the sample [W];

λ is the sample thermal conductivity [W/mK];

$\Delta\vartheta$ is the temperature difference between the hot and cold plates [K];

t is the measured sample thickness [m].

Creating an analogy between electrical current and heat, and voltage and temperature difference, it is possible to write the heat flow equation in a form similar to Ohm's law:

$$\Delta\vartheta = \Phi \cdot R \quad (11)$$

And therefore R can be defined as:

$$R = \frac{t}{\lambda \cdot A} \quad (12)$$

¹⁰ Text from the author's paper: "The effect of temperature on thermal performance of fumed silica based Vacuum Insulation Panels for buildings" [29].

The thermal resistance will increase for a small cross-sectional area of heat flow (A) or a big thickness (t), as well as the electrical resistance [115]. In case of a multi-layered structure, the total thermal resistance can be easily obtained by the sum of the R -value of each layer (EN ISO 6946:2017 [116]).

- **Thermal transmittance - U -value**

The thermal transmittance [$\text{W}/\text{m}^2\text{K}$] describes the insulation capacity of a structure: to improve the insulation, the thermal transmittance must be reduced. It takes into account all the losses due to thermal radiation, thermal convection and thermal conduction. The U -value of a structure depends on the thermal resistance (R) of each layer in the structure (thermal conduction), and on heat transfer resistance on the surface of a structure (radiative and convective contributions from the building construction to the air and vice versa), named R_{si} and R_{se} for internal and external surfaces respectively [116].

If all the involved heat transfer resistances are known, the U -value of the structure can be calculated as:

$$U = \frac{1}{R_{si} + \sum_{i=1}^n R_i + R_{se}} \quad (13)$$

- **Thermal bridging effects - ψ , λ_{eff} , λ_{eq}**

“The overall effect of the thermal bridges in multi-layered walls making use of VIP is relevant and can be evaluated as yet by means of the so-called linear thermal transmittance of the thermal bridge, ψ . This parameter can be assessed accordingly to EN ISO 10211-1:2007 [97], as also shown in [117]:

$$\psi_y = L^{2D(x,z)} - U_{x,y} \cdot l_x - U_{y,z} \cdot l_z \quad (14)$$

Where symbols in Eq. (14) refer to the calculation scheme of **Figure 27**.

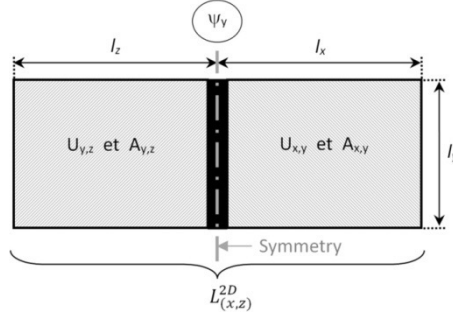


Figure 27: Calculation scheme for the linear thermal transmittance of the thermal bridge, ψ , for a portion of the envelope component having a width of (l_x+l_z) and a depth of l_y . The thick black line represents the thermal bridge

Being $L^{2D(x,z)}$ the so-called “2D coupling coefficient” [W/mK]:

$$L^{2D(x,z)} = \frac{1}{l_y} \frac{\Phi_{2D}}{\Delta\vartheta} \quad (15)$$

Φ_{2D} is the overall heat flux [W] that actually crosses the considered portion of the envelope component (having a length l_x+l_z and a depth l_y) and accounts for both:

- the heat flux through the zones where the panels show an undisturbed behaviour;
- the heat flux through the thermal bridge and those areas of the panels where the temperature field is influenced by the thermal bridge itself.

Due to the 3D distortion of the temperature field, induced by the joints between the panels, the actual heat flux, Φ_{2D} , will be higher than the one that would cross the same component should it be made of homogeneous VIP panels alone, Φ_{1D} . This last quantity could be evaluated by the well-known equation:

$$\Phi_{1D} = (U_{x,y} \cdot A_{x,y} + U_{y,z} \cdot A_{y,z}) \cdot (\vartheta_h - \vartheta_c) \quad (16)$$

The difference $\Delta\Phi$, between Φ_{2D} and Φ_{1D} , is the so-called “extra-flux”, that is the additional heat transmission caused by the linear thermal bridge.

Hence, Eq. (14) can be rewritten as:

$$\psi_y = \frac{1}{l_y} \left(\frac{\Phi_{2D}}{\Delta\vartheta} - U_{x,y} \cdot A_{x,y} - U_{y,z} \cdot A_{y,z} \right) \quad (17)$$

It is worth noting that the value of the linear thermal bridge calculated using Eq. (14) or (17) depends on the geometrical configuration adopted for its estimate. Consequently, designers and engineers must carefully take into account how this quantity was assessed, in order to correctly apply it when developing the calculations.

[...] The geometrical configuration of **Figure 27** is the typical one, suggested by the Appendix C of EN ISO 10211-1:2007 Standard [97]. However, different choices can be done. For example, another geometrical configuration that is sometimes used for assessing the ψ parameter (see e.g. [118] and [99]) considers the symmetry plane sketched in **Figure 27** and, consequently, focuses just on one half of the building element (e.g., just the portion of area $A_{x,y}$ shown in **Figure 27** is considered). In this case, the resulting value of ψ (let's call it ψ') will be one half of that provided by Eq. (17). In fact, assuming a symmetrical configuration (that is $A_{x,y} = A_{y,z} = A$ and $U_{x,y} = U_{y,z} = U$) and applying Eq. (17) to the scheme of **Figure 27**, it results:

$$\psi_y = \frac{1}{l_y} \left(\frac{\Phi_{2D}}{\Delta\vartheta} - 2 \cdot U \cdot A \right) \quad (18)$$

Instead, if only the right-hand side of the envelope component is considered (e.g. only the part of area $A_{x,y}$), one obtains:

$$\psi'_y = \frac{1}{l_y} \left(\frac{\Phi_{2D}/2}{\Delta\vartheta} - U \cdot A \right) \quad (19)$$

Thus it holds:

$$\psi'_y = \frac{\psi_y}{2} \quad (20)$$

In this research, the linear thermal transmittance, ψ_y , was determined by means of Eq. (18), both as far as the numerical simulations and the experimental tests were concerned.

Specifically, the methodology adopted for the assessment of ψ was as follow:

- a suitable cross length of the sample (e.g., l_x and l_z values) was chosen such to include the entire region in which the heat flux departs from the one-dimensional condition (e.g., undisturbed flux), accordingly to the guidelines of EN ISO 14683:2008 [119];

- the heat flux Φ_{1D} was determined starting from the knowledge of the centre of panel thermal conductivity (λ_{COP}) of the VIP boards. In fact, at steady state, it holds:

$$|\Phi_{1D}| = U \cdot A \cdot (\vartheta_h - \vartheta_c) = \frac{\lambda_{COP}}{t} \cdot A \cdot (\vartheta_{sur,h} - \vartheta_{sur,c}) \quad (21)$$

For the assessment of the ψ -value, the VIP surface temperatures, $\vartheta_{sur,h}$ and $\vartheta_{sur,c}$ were used. Therefore, the final equation adopted for the calculation was:¹¹

$$\psi_y = \frac{1}{l_y} \left(\frac{\Phi_{2D}}{\Delta\vartheta_{sur}} - 2 \cdot \frac{\lambda_{COP}}{t} \cdot A \right) \quad (22)$$

The effective thermal conductivity of a VIP (λ_{eff}) can be calculated by adding to the centre of panel thermal conductivity the linear thermal transmittance of the thermal bridge at the edge of the panel, referring to the geometry under analysis:

$$\lambda_{eff} = \lambda_{COP} + \psi_{edge} \cdot t \cdot \frac{P}{A} \quad (23)$$

Where: ψ_{edge} is the linear thermal transmittance of the thermal bridge at the edge of the panel [W/mK];

P is the panel semi-perimeter [m];

A is the panel area [m²].

Similarly, it is possible to calculate the equivalent thermal conductivity (λ_{eq}) of VIPs assemblies or VIPs insulated building components, which is defined as [14]:

$$\lambda_{eq} = \frac{\Phi_{2D} \cdot t}{A \cdot \Delta\vartheta_{sur}} \quad (24)$$

¹¹ Text from the author's paper: "Experimental and numerical investigation of thermal bridging effects of jointed Vacuum Insulation Panels" [103].

λ_{eq} can also be evaluated through Eq. (23): what changes are the value of ψ , which is estimated by using the following equation (in accordance with EN ISO 14683:2007 [119]):

$$\psi = \frac{\Phi - \frac{1}{R_{tot}} \cdot P \cdot \Delta\vartheta_{sur}}{\Delta\vartheta_{sur}} \quad (25)$$

Where R_{tot} is the sum of all the thermal resistances involved in the building component [105]:

$$R_{tot} = R_i + R_e + \frac{t}{\lambda_{eff}} \quad (26)$$

The applicability of the effective and equivalent thermal conductivity is less general than the ψ parameter. In fact, with the same VIP core and joint materials, the value of λ_{eff} and λ_{eq} depends on the geometrical configuration of the assembly and the shape of the VIP panels (number and length of the thermal bridges).

Chapter 4

Testing and simulation approaches

Thermal conductivity is the most important and significant quantity for the characterisation of thermal insulating materials. It may be measured by two different experimental approaches: steady-state methods (most common) and transient methods.

Steady-state methods (Guarded Hot Plate - GHP and Heat Flux Meter - HFM) are also useful for the assessment of the thermal bridging effects in case of VIPs, through the evaluation of their ψ -values. Moreover, thermal bridges require numerical simulations to take into account all the possible configurations and boundary conditions (the type of the joint between the panels e its thermal conductivity and geometry, adjunctive layers and so on). Therefore the ψ measuring procedure was experimentally optimised and then used to validate numerical simulation models. The numerical simulations were also used to verify the reliability of the experimental measurements, checking the absence of lateral heat losses.

Once characterised the SIMs at the material and component level, it's fundamental to evaluate the energy efficiency of building insulated with SIMs, and predict the durability of this kind of materials. These aims can be achieved using dynamic hygrothermal simulations (validated with the data obtained from in-situ experimental monitoring).

4.1 Steady-state measurement methods

Steady-state methods are the primary and still most precise measurement methods. The thermal properties of the materials are measured when the thermal equilibrium of the specimen is achieved (which means that the temperatures of all the sample points are constant and stationary during the time). When the specimen has reached a steady-state condition, the Fourier's law is used to calculate the thermal conductivity and to simplify the calculation it is considered only as a one-dimensional problem.

The steady-state methods are Guarded Hot Plate (GHP) and Heat Flux Meter (HFM).

The experimental section of the present research was performed using several GHP and HFM apparatuses (with different characteristics). From now on, the general operating principle of these devices is presented, while the details of the involved apparatuses will be summarised at the beginning of each experimental chapter (so as to improve the legibility of the document).

4.1.1 Guarded Hot Plate - GHP

Guarded Hot Plate is a conventional method to determine the transfer properties of non-metals such as glass, ceramics, polymers and insulating materials. Thereby the heat transfers through radiation, conduction (solid and gas phase) and convection are considered. Since only the measurements of length, temperature and electrical power are required, it is an absolute or primary method to measure the thermal properties in according to ISO 8302:1991 [18].

This method is quite versatile: it may be used to measure the thermal characteristic of a wide variety of material, in a wide range of environmental condition and the test may be carried out with both vertical and horizontal specimens. Samples must be in the form of uniform slabs having flat parallel faced, and the apparatus measures a unidirectional uniform heat flow-rate density at steady-state conditions (as if the sample was an infinite slab bounded by two flat parallel isothermal surfaces).

The GHP apparatus can be configured in two different ways (see **Figure 28** and **Figure 29** respectively):

- two specimens symmetrical device, with a central heating plate and two cold plates, which usually takes into account the gravity effects on the heat

flow (convective part) averaging the values of upward and downward heat flow [120];

- single specimen symmetrical apparatus, with one heating plate and one cold plate.

The heating unit (composed by a heater and metal surface plates) consists of a separate metering section, where the unidirectional uniform and constant density of heat flow-rate can be established, surrounded by a guard section, to which it is separated by a narrow gap. The cooling units may consist of a continuous flat assembly, but it is better to have them with a similar configuration to the heating unit. The heating unit is sandwiched between two specimens (two specimens apparatus) (**Figure 28**), or between a single specimen and an insulated guard plate in the single-specimen device (**Figure 29**). The two-specimen configuration offers the possibility to control more the heat losses from the heating unit due to the symmetry in the arrangement of the samples. In this type of setup, solid materials are tested because for the other materials the heating unit shall be placed above the specimen to avoid the convection. [120].

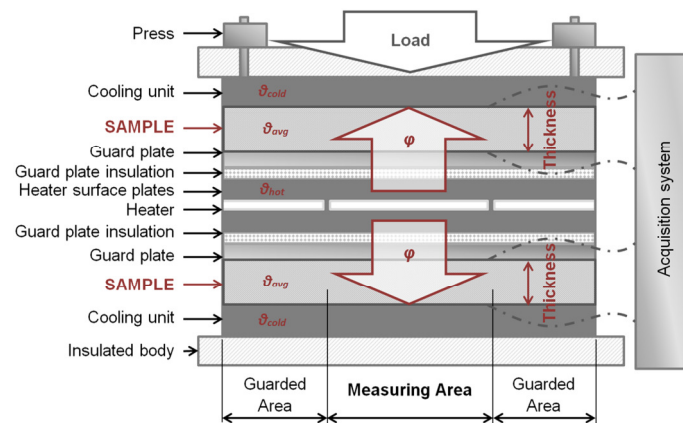


Figure 28: Two specimens symmetrical GHP apparatus

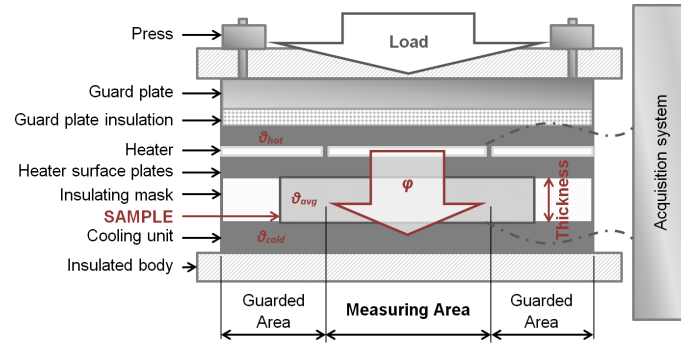


Figure 29: Single specimen symmetrical GHP apparatus

GHP method requires the achievement of the steady-state condition, but this is not easy to get it, because of the lateral heat losses due to the fact that the samples have finite dimensions and different temperature from the external environment. This condition could be achieved after several hours or even days, depending on the size and thermal properties of the specimen. However, GHP apparatus is realised in a way to reduce as much as possible these losses. The heating unit is made up by a metering section and a guard ring separated by a narrow gap. The metering area consists of a central heater placed between two heater surface plates. The guarded ring is composed of one or more guard heaters enclosed by guard plates. The gap (not bigger than 5% of the measuring area) divides the metering area from the guarded ring, and its primary function is to reduce lateral heat flow within the apparatus. The guarded ring has the aim to establish a unidirectional and uniform heat flow through the test specimen: therefore its temperature is automatically set equal to the one of the metering area to reduce heat losses from the sample and to achieve a unidirectional heat flow. The cooling unit must have the same surface dimensions of the heating unit (metering area + guard ring). It is constructed of metal plates having a constant temperature lower than the one of the heating unit. In addition, the apparatus is surrounded by thermal insulation to reduce the heat losses [18],[120].

When the thermal equilibrium in the metering area is established (steady state), the heat flow rate Φ [W] (equal to the power generated by the hot plate) can be calculated from the measured voltage U [V] and current I [A]:

$$\Phi = U \cdot I \quad (27)$$

The temperature difference across the specimens, $\Delta\vartheta$, is measured by thermocouples inside the plates, or fixed at the surfaces of the metal plates and/or to the surface of the samples, where possible.

The thermal resistance R is indeed calculated from the knowledge of Φ , A_m (metering area) and $\Delta\vartheta$:

$$R = \frac{\vartheta_1 - \vartheta_2}{\Phi} A_m \quad (28)$$

Where the metering area is calculated from the area of the guarded hot plate (A) and the gap area (A_g):

$$A_m = A + \frac{A_g}{2} \quad (29)$$

The mean thermal conductivity of the sample(s) is calculated from the thermal resistance as follows:

$$\lambda = \frac{t}{R} = \frac{\Phi \cdot t}{2 \cdot A_m \cdot (\vartheta_{hot} - \vartheta_{cold})} \quad (30)$$

In case of single specimen apparatus, the coefficient 2 in the denominator has to be deleted, because the whole heating power of the heating unit crosses the specimen.

Normal mean temperatures range for buildings is between 0°C and 50°C, but the GHP method can also be used for the whole insulating materials working temperature range (e.g., from -180°C to +900°C). For higher temperatures, other measurement methods are available. The temperature difference values in which it may operate are many: from a minimum of 10 to 20 K, according to ISO 8302:1991 [18], to a maximum that depends on the capacity of the instrument to provide the power required to maintain constant the temperatures.

GHP method is described in detail in the following standard: ISO 8302:1991 [18], EN 12667:2001 [12] and EN 12664:2002 [121].

4.1.2 Heat Flow Meter - HFM

The Heat Flow Meter method defines the steady-state and transient heat transfer through flat slab specimens and the calculation of its thermal properties (resistance and conductivity). The method defines the global heat transfer through the specimen and does not allow to evaluate the contribution of solid and gas phase thermal conduction, radiation and convection.

The Heat Flow Meter (HFM) apparatus is mainly based on digital thickness measurements, responsive temperature control (thermocouples) and heat flow transducers electrical power measurements. Thermocouples and heat flux transducers are usually integrated inside the plates, but can also be used as external devices. The primary purpose of the experimental method is the evaluation of the thermal properties (thermal conductivity or resistance) for the tested materials, through the measurement of heat flow density. This heat flow density is measured using one or two heat flow meter(s) placed against the specimen(s). The HFM is composed of a heating unit, one or two heat flow meters, one or two specimens and a cooling unit (**Figure 30**).

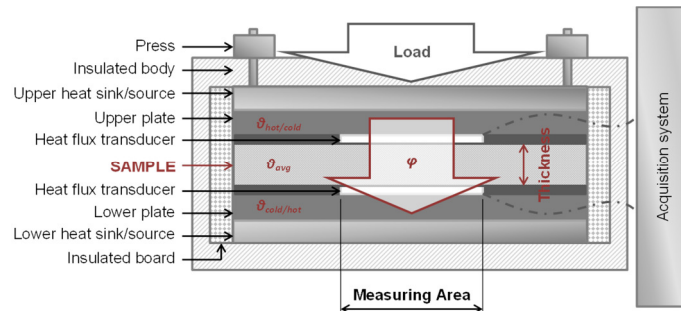


Figure 30: Single specimen symmetrical HFM apparatus

Samples must have flat parallel faces, to be inserted between two plates in the test stack. The plates may be positioned automatically in contact with the specimen (always exerting the same pressure on the sample faces), or to a user-defined thickness. Plates are set with different temperatures, generating a heat flux through the specimen proportional to its thermal resistance. For low-density materials, such as mineral wool, the upper plate is the heating unit and the lower is the cooling unit to avoid the natural convection which would alter the measurement of the thermal properties.

The heat flux transducer provides a reliable representative measurement of the total heat flow, integrating it over the entire measuring area of the plates (the area

where sensors are placed). A significant amount of thermocouples are used for the control of the temperature of the heating and cooling plates. The edge heat losses shall be controlled using edge insulation and/or a guard area [17],[122].

Several apparatus configurations are available: single-specimen configuration (with single or double heat flow meter configuration) and two-specimen configuration. In case of specimens characterised by high thermal resistance, the single specimen configuration is adequate. Otherwise, for low-resistance materials, the two-specimens' configuration is the best-suited solution [17]. For this reason, in case of SIMs, the most common configuration is the single specimen (symmetrical or not). The following procedure is specific for single-specimen configuration [123]: for the other cases see ISO 8302:1991 [17], EN 12667:2001 [12] and EN 12664:2002 [121].

The general measuring method is based on the one-dimensional Fourier-Biot law, shown in Eq. (8). The temperature field in the sample should be considered uniform within all the sample's volume. This is due to the following reasons:

- the apparatus plates are isothermal (uniform one-dimensional temperature field);
- the size of the plates much larger than the thickness of the sample.

HFM apparatus must be calibrated through the test of reference certified sample materials (standard) with reliable known values of thermal conductivity λ_{cal} [W/mK], before measurements of materials with unknown thermal properties (differently from GHP, this is an indirect, secondary or relative method).

The specific heat flux φ [W/m²] is proportional to the electric signal from the transducer Q [μ V]:

$$\varphi = \frac{\lambda_{cal}(\vartheta_{cal}) \cdot \Delta\vartheta_{cal}}{t_{cal}} = f_{cal}(\vartheta_{cal}) \cdot Q \quad (31)$$

The physical properties of the transducer change with temperature, for this reason, a calibration standard is always necessary for the calibration of the instrument and get the temperature dependent calibration factors $f_{cal}(\vartheta)$ [W/m² μ V]. The calibration factors should be referred to the transducers actual temperatures (each sensor has its own temperature, and so separate sets of the calibration factors are measured).

The calibration factors $f_{cal}(\vartheta)$ represent a characteristic of the device. They are used for the evaluation of the thermal conductivity during the test run:

$$\lambda_{test} = \frac{f_{cal}(\vartheta_{test}) \cdot Q \cdot t_{test}}{\Delta\vartheta_{test}} = \frac{\varphi \cdot t_{test}}{\Delta\vartheta_{test}} \quad (32)$$

Because of each plate has its temperature, the calibration factors should be calculated for plate's actual temperature: the result of thermal conductivity test is obtained by averaging two thermal conductivity values.

The calibration may be carried out in two ways: through the GHP when the heat flux plates are new, or with a certified reference material, whose thermal conductivity value and uncertainty are provided. The second procedure can also be followed to check if the equipment is performing correctly. To this purpose, it is necessary to use reference materials having similar heat properties and thickness as the materials to evaluate. Moreover, the conditions under which the test is carried out, such as the orientation and the heat flow direction, shall be similar too.

Before determining the results, the two heat flow meter signals have to reach equilibrium (experimental check demonstrated that equilibrium is reached faster in case of the mean value of two heat flow meter measures than in case of their individual values). When stable conditions are achieved, the specific heat flow over the centre measurement area, A_m [m²] is measured.

The thermal resistance of the panels is then determined as (according to EN 12667:2001 [12]):

$$R_{test} = \frac{\Delta\vartheta_{test}}{\varphi_{test}} \cdot A_m = \frac{\Delta\vartheta_{test}}{f_{cal}(\vartheta_{test}) \cdot Q} \quad (33)$$

Some specimens are characterised by different thermal conductivity values if measured in a direction parallel to the surfaces or normal to the surfaces (anisotropic samples). In these cases (e.g., glass-fibre VIP), when the ratio between the two measurable thermal conductivity values is larger than two, the ISO 8302:1991 [17] standard must be consulted [42].

The HFM method is more rapid than the GHP since the time required to reach the steady-state condition is lower. At the same time, however, the reliability of the results depends on the calibration and its uncertainty. So this method is less accurate than the GHP.

4.1.3 Methodologies for the measurement of ψ -values

An innovative procedure for the experimental assessment of the thermal bridging effects, which occurs in case of VIPs assemblies, was developed at Politecnico di Torino during this research.

It is based on the use of the commercial measurement apparatus (GHP and HFM), without any adjunctive external device or thermocouples [14]. This method represents a practical way to determine the thermal bridging effects. In this way the actual overall heat flux through two adjoining VIP panels with a thermal bridge in between is measured, and the related equivalent thermal conductivity λ_{eq} [W/mK] and thermal bridge linear thermal transmittance ψ [W/mK] can be evaluated (as already introduced in § 3.2 *VIPs thermal performance parameters*).

The linear thermal transmittance ψ can be assessed accordingly to EN ISO 10211-1:2007 [97], considering the extra-flux ($\Delta\Phi$ [W]) caused by the linear thermal bridge (Figure 31).

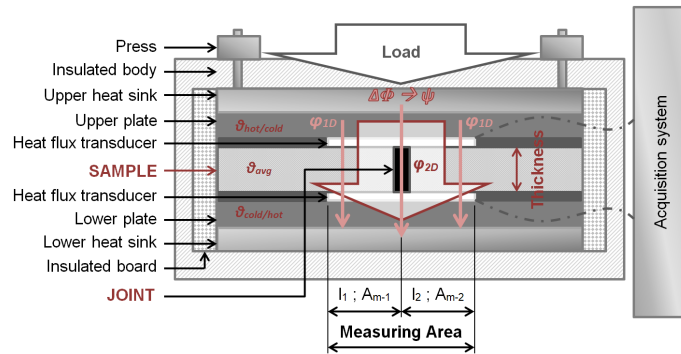


Figure 31: HFM apparatus method for the determination of ψ -values

Because of the joints between the panels distorts the temperature field, the measured heat flux (Φ_{2D}) will be higher than the one that would cross a single VIP panel alone (Φ_{1D}):

$$\Delta\Phi = \Phi_{2D} - \Phi_{1D} \quad (34)$$

The heat flux Φ_{1D} is determined starting from the knowledge of the centre of panel thermal conductivity (λ_{COP}) of the VIP specimens, see Eq. (21).

$$\Phi_{1D} = \frac{\lambda_{COP}}{t} \cdot A_m \cdot (\vartheta_{sur,h} - \vartheta_{sur,c}) \quad (21)$$

The calculation of the thermal bridge linear thermal transmittance can be performed through Eq.(22):

$$\psi = \frac{1}{l_\psi} \left(\frac{\Phi_{2D}}{\Delta\vartheta_{sur}} - 2 \cdot \frac{\lambda_{COP}}{t} \cdot A_{m-1;2} \right) \quad (22)$$

Moreover, the equivalent thermal conductivity of the assembly, λ_{eq} , is defined by Eq. (24):

$$\lambda_{eq} = \frac{\Phi_{2D} \cdot t}{A_m \cdot \Delta\vartheta_{sur}} \quad (24)$$

A different approach was proposed in [114], based on the use of several thermocouples fixed on the assembly sample surfaces, mapping its different surfaces temperatures.

The most critical phase of this procedure is the definition of several areas over the sample surfaces that are thermally affected in different ways by the increased heat flux through the joint (**Figure 32**). The temperature distribution in the three areas defined in **Figure 32** is measured with thermocouples. The number of the thermocouples is not determined, but it is recommendable to use at least two thermocouples for the joint as well as for the slightly affected area and three thermocouples for the COP area (**Figure 32**), for both the cold and the hot side of the sample. All the measured temperature differences are averaged and area weighted, as required for the calculation of the equivalent thermal conductivity. The equivalent thermal conductivity is then calculated using the area weighted temperature difference, $\Delta\vartheta_m$, and then it is possible to obtain the value of the linear thermal transmittance ψ (through the already known equations).

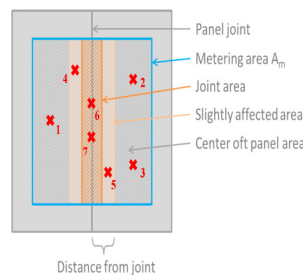


Figure 32: Different affected areas with exemplary thermocouples distribution [116]

4.2 Transient measurement methods

The transient methods measure the thermal properties of the materials through the response signal to a pulse required to increase the temperature of the specimen.

Such kind of methods is characterised by the short time required to measure the sample thermal properties. Measurements that typically need one or several hours with the steady-state procedure are reduced to a few minutes: the surveys are performed during the heating process. The specimen, in a thermal equilibrium condition, is heated with a thermal impulse. This temperature increase during the time is used to calculate the thermal conductivity of the material. Among transient methods, the most common are: hot wire, hot strip and hot disk (similar principle) and laser flash.

4.2.1 Hot wire/Hot strip

The hot wire (or Transient Line Source - TLS) is a transient technique which allows the determination of the thermal conductivity for opaque, homogeneous and isotropic materials and loose-fill materials. The method considers all the three heat transfer mechanisms (radiation, conduction and convection).

This method allows to measure the thermal conductivity in a brief time, and it is composed of two main sections:

- the probe, made of heating needle and thermocouple, and placed between two identical samples, or wholly immersed in case of loose-fill materials (**Figure 33**);
- the control unit, divided in a programmable power supply which can generate electrical power for the heating needle (lead wire) and analyses the temperature increases, and a computer for the control of the power supply.

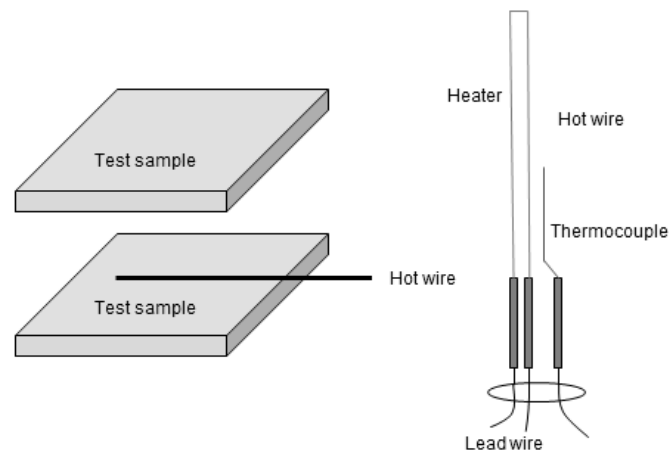


Figure 33: TLS method scheme [42]

The heating cycle starts when the temperature variation is less than $\pm 3\%$. After a period of generally 120 seconds, the heating electrical power supply stops. During this period the temperature is measured every 1 to 5 seconds. At the end of the test, the thermal conductivity is automatically calculated by the control unit, from the slope of the linear temperature profile as a function of time, obtained from the measurement. This method provides the direct determination of the thermal conductivity, so no calibrations are required. Furthermore, it is a simple method which allows the measurement of thin material size, a short exposure of the specimen to a high temperature and a good measurement accuracy. On the other hand, it required specimens with identical size, structure and density and a low contact resistance between the sample and the heating wire [124],[125].

TLS method is described in detail in the following standard: ASTM C1113:2013 [125], ISO 8894-1:2010 [126] and EN 993-15:2005 [127].

The hot strip (or Transient Hot Bridge - THB) method is an enhancement of the transient hot strip method and is based on the theory of transient temperature increase over a flat surface that is also used as a heat source. A combined heat source and a temperature sensor, in the shape of a very thin strip, is embedded between two pieces of the sample material as shown in **Figure 34**.

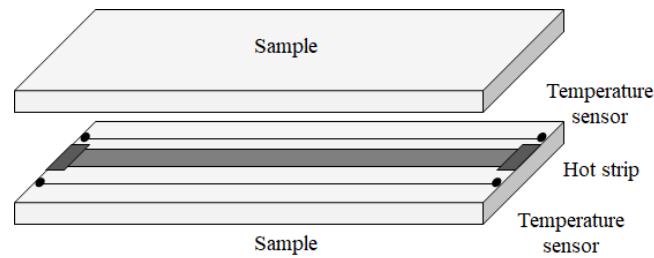


Figure 34: THB method scheme

A constant current is supplied to the metal strip, obtaining a continuous heat flow during the experiment, while the strip also serves as a resistance thermometer. The temperature increase during time represents the tested sample thermal transport properties. The measurement usually requires a time of 1 min and generally less than 10 min (influenced by the thermal properties of samples). The procedure to evaluate the sample thermal conductivity is similar to the TPS method.

THB method is described in detail in EN 993-15:2005 [127].

4.2.2 Hot disk

The hot disk or Transient Plane Source (TPS) method is a modified version of the transient hot strip method and allows the calculation of thermal conductivity and thermal diffusivity. The sensor (**Figure 35 a**) is made of a very thin (10 μm thick) double metal spiral (usually nickel) insert between two protective layers of supporting polyamide materials of 25 μm thick (typically Kapton or Mica). During measurements, it is placed between two identical samples (**Figure 35 b**), and acts both as a heat source for increasing the temperature of the sample and as a “resistance thermometer” for recording the time-dependent temperature increase [42].

The heating current is generated in the coil, which is assumed to consist of number concentric circles (assumed to be located in an infinitely large sample), crossing the spiral. The electrical current generates a dynamic temperature field within the sample whose increase is measured as a function of the time. The temperature rise can be related to the thermal transport properties of the surrounding materials. The rate of change in the registered voltage corresponds to the resistance variation of the metal spiral when the electric power is held constant. The thermal conductivity is calculated through a process of iteration

from the comparison of the temperature versus the time response in the sensor. The advantage of this method is that it allows a measurement of the thermal properties in a short amount of time, but it is necessary to reduce the resistance between the sample surface and the sensor [124],[128]. The short time interval makes it possible to neglect the end effects of the finite size of the metal strip and the temperature distribution around and in the coil is identical to that of an infinitely long plane heat source.

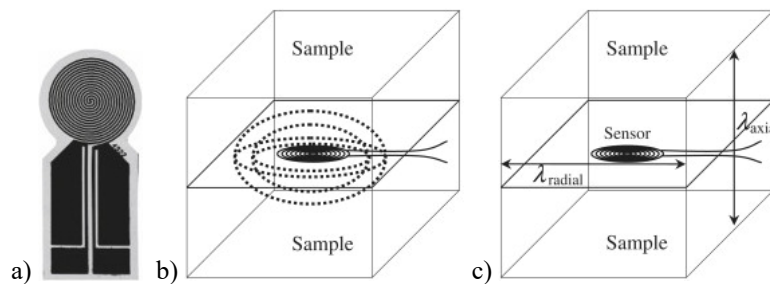


Figure 35: TPS method scheme. a) Sensor; b) sensor positioning and generated heat flux; c) obtainable λ -values [129]

Hot disk method is described in detail in the standard ISO 22007-2:2015 [128].

4.2.2 Laser flash

The laser flash method allows measuring several thermal properties. A short laser pulse is sent to one side of the specimen, and it increases the temperature of the other side (**Figure 36**). The rise of the temperature is evaluated through non-contact infrared radiation measurement. The time required by the test depends on the material but generally is very short. The thermal conductivity is calculated as a function of the thermal diffusivity, the specific heat capacity and the density of the material [124],[130].

Laser flash method is described in detail in the following standard: ASTM E1461 [130], DIN EN 821-1:1995 [131] (for ceramic materials).

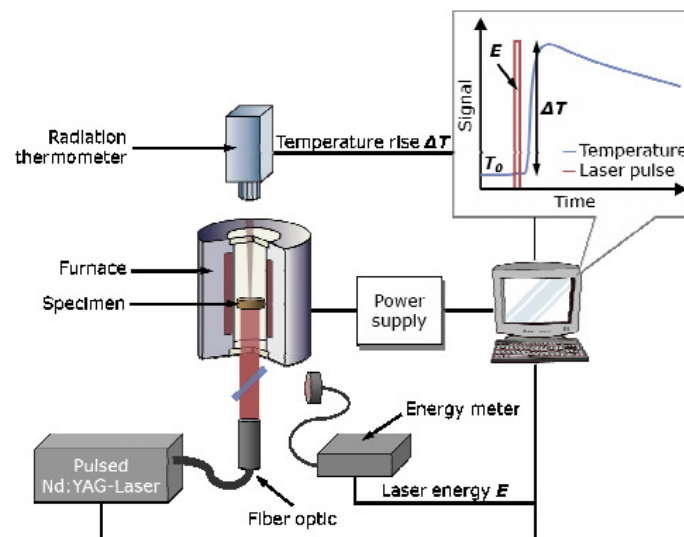


Figure 36: Laser flash method scheme [132]

4.3 Numerical simulations

Numerical simulations are extremely useful for the investigation of the actual thermal performances of materials or building components/systems. Indeed they can be performed at a different scale (from the single material to an entire building or district), depending on the final aim of the simulation.

In this context, two different levels of simulation were performed, in three different ways. First of all, the reliability of the measurement apparatuses (GHP and HFM) was verified using a bi-dimensional energy balance simulation. After that, some energy analysis, thermal load simulations and dynamic hygrothermal simulations were performed at the building scale, to evaluate the actual benefits of SIMs (in particular VIPs) on the overall thermal performance of buildings. These investigations also allow estimating the durability/service life of the insulating materials.

4.3.1 Bi-dimensional steady-state heat transfer


“A significant criticism in the measurement of centre of panel thermal conductivity by means of GHP and HFM is represented by potential heat losses through the edges of the specimens. For this reason, the apparatus plates consist of a central metering area (A_m), into which the thermocouples and the other sensors are distributed, surrounded by an outer heated metal plate (guard ring in case of GHP, or guarded apparatuses) that reduces the lateral heat losses. Indeed,

the apparatus can be equipped with a hermetic closure and insulation in order to prevent interactions with the external laboratory environment.

Some numerical analyses were carried out to verify whether the specimen surfaces were characterised by a constant temperature distribution in correspondence of the apparatus metering area. This kind of analysis became necessary because the experimental measurements of SIMs thermal conductivity are usually performed with an average temperature of the plates much higher than the temperature of the surrounding environment (laboratory). The objective was to determine whether, the lateral heat losses (and, in case of VIPs, the thermal bridging effects, due to the relatively high thermal conductivity of envelope) can be considered negligible in the metering area”¹².


The investigation was performed on the apparatuses owned by Politecnico di Torino and INRiM (characteristics summarised in the following **Table 6** and **Table 7**). Due to a lack of technical information related to the actual configuration of the GHP guard ring, the modelling was simplified by assuming a single surface temperature for each plate (equal to the one of the measurement area).

Table 6: Politecnico di Torino apparatus: HFM - 1

Politecnico di Torino	
HFM - 1	
TA Instrument	
Lasercomp FOX 600	
	
Max. Sample Thickness	203 mm (8")
Sample Size	610 x 610 mm (24" x 24")
Temperature Range	- 10 °C to 65 °C
Absolute Thermal Conductivity Accuracy	± 1%
Reproducibility	± 0.5%
Thermal Conductivity Range	0.005 to 0.35 W/mK With External Thermocouple Kit: 0.001 to 2.5 W/m K
Heat Flux Transducers Area	254 x 254 mm (10" x 10")

¹² Text from the author's paper: "The effect of temperature on thermal performance of fumed silica based Vacuum Insulation Panels for buildings" [29].

Table 7: INRiM apparatus: GHP - 1

INRiM	
GHP - 1	
Lambda-Meßtechnik λ-Meter EP 500	
Max. Sample Thickness	10 to 120 mm
Sample Size	500 x 500 mm (min. 150 x 150 mm)
Temperature Range / Difference	10 °C to 40 °C / 5 °C to 15 °C
1° Range - Thermal conductivity	0.005 to 0.180 W/m K
Thermal resistance	0.25 to 5 m ² K/W
2° Range - Thermal conductivity	0.180 to 2 W/mK
Thermal resistance	0.03 to 0.25 m ² K/W
Absolute rate for errors	< 1.5 % (1° Range and t < 90 mm) < 2.5 % (2° Range and t > 90 mm)
Measuring area	150 x 150 mm

The numerical model was developed through the Physibel BISCO software, which is a “*thermal analysis program for steady state heat transfer in two-dimensional objects consisting of different materials and submitted to different boundary conditions*” [133]. Half apparatus was modelled (symmetric configuration), considering a thermal conductivity for the outer insulation guard ring of 0.05 W/mK.

The surfaces temperatures of plates (Dirichlet boundary conditions) were imposed equal to the hottest and coldest values of average temperature considered in the experimental campaigns ($\vartheta_{avg} = 2.5^{\circ}\text{C}$ and 52.5°C with $\Delta\vartheta = 25^{\circ}\text{C}$ in case of HFM, $\vartheta_{avg} = 10^{\circ}\text{C}$ and 40°C with $\Delta\vartheta = 15^{\circ}\text{C}$ in case of GHP). This assumption was possible considering that the contact resistance of the plates is extremely lower compared to the thermal resistance of SIMs, and therefore, its effect on the plates temperature variation can be assumed negligible. Differently, for the laboratory environment, the air temperature and the internal surface heat transfer coefficient h_i were required (Robin type boundary conditions). The internal air temperature was assumed equal to 20°C , while h_i was approximated to $7.69 \text{ W/m}^2\text{K}$ (as a reference value for buildings).

Moreover, two different VIP thicknesses were simulated (10 mm and 30 mm).

The software requires a bitmap input model, that defines the analysed geometry and in which the physical properties of each material and/or boundary condition are associated to a different colour. The model is then subdivided in triangulations, where the system nodes are located in the triangles vertices. The number of pixels for each triangulation is defined by the user, as a function of the element thickness: a thinner element requires a igher number of triangulations, that is a lower number of pixels each.

Figure 37 and **Figure 38** show the models adopted for the numerical simulation of HFM and GHP respectively.

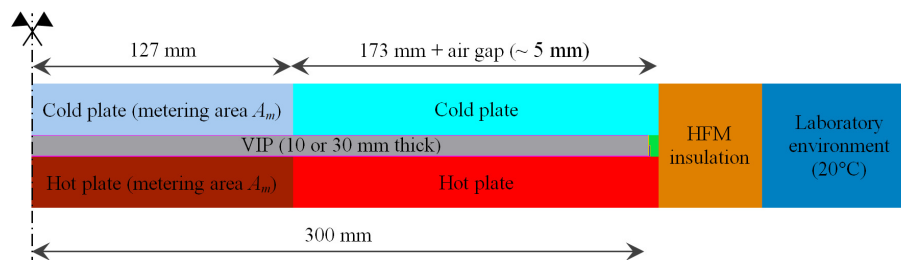


Figure 37: Model for 2D numerical analyses of HFM apparatus [29]

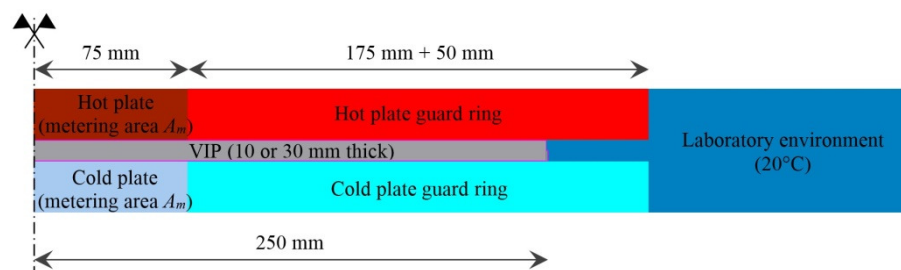


Figure 38: Model for 2D numerical analyses of GHP apparatus

*“A preliminary grid dependency analysis was performed in order to provide grid independent results (the heat flux divergence of the whole numerical model was lower than 0.1%, according to the guidelines given in EN ISO 10211:2017 [97])”*¹³. The analysis started from the default value of 10 pixels for each triangulation, and then the pixels numbers was reduced to the vlues shown in **Figure 39**.

¹³ Text from the author’s paper: “Experimental and numerical investigation of thermal bridging effects of jointed Vacuum Insulation Panels” [103].

	Width [pix.]	Width [m]	Height [pix.]	Height [m]	Area [pix.]	Zones	Triang. [pix.]
	1	0.0002	1	0.0002			
	1857	0.4300	260	0.0602			10.00
	549	0.1271	108	0.0250	59292	1	
	549	0.1271	107	0.0248	58743	1	
	217	0.0502	260	0.0602	56420	1	2.00
	5	0.0012	44	0.0102	109	2	1.00
	20	0.0046	45	0.0104	828	1	1.00
	2	0.0005	21	0.0049	42	1	1.00
	324	0.0750	260	0.0602	84240	1	
	1294	0.2996	42	0.0097	54348	1	5.00
	767	0.1776	107	0.0248	82069	1	
	1299	0.3008	45	0.0104	3893	3	1.00
a)	767	0.1776	108	0.0250	82836	1	

	Width [pix.]	Width [m]	Height [pix.]	Height [m]	Area [pix.]	Zones	Triang. [pix.]
	1	0.0002	1	0.0002			
	1883	0.4300	264	0.0603			10.00
	329	0.0751	109	0.0249	35861	1	
	329	0.0751	109	0.0249	35861	1	
	2	0.0005	21	0.0048	42	1	1.00
	788	0.1799	264	0.0603	160412	1	
	1094	0.2498	42	0.0096	45948	1	5.00
	984	0.2247	109	0.0249	107256	1	
	1099	0.2510	46	0.0105	4476	1	1.00
b)	984	0.2247	109	0.0249	107256	1	

Figure 39: Number of pixels for triangulations. a) HFM - 1; b) GHP - 1

“The actual multilayer structure of the VIP envelope was simplified into a single “equivalent” homogeneous layer (this approach was already used in [118]). The thermal conductivity of this equivalent homogeneous layer was evaluated in a different way, depending on whether it was crossed by a heat flux perpendicular (\perp) or parallel (\parallel) to the surface”¹⁴:

$$\lambda_{\perp} = \frac{t_{tot}}{\sum t_i / \lambda_i} \quad (35)$$

$$\lambda_{\parallel} = \frac{\sum t_i \cdot \lambda_i}{t_{tot}} \quad (36)$$

Where: t_{tot} is the VIP envelope total thickness [m];

t_i is the single layer thickness [m];

λ_i is the single layer thermal conductivity [W/mK].

¹⁴ Text from the author’s paper: “Experimental and numerical investigation of thermal bridging effects of jointed Vacuum Insulation Panels” [103].

Table 8: Envelope thermal conductivities. Model measurements in [mm]. Data provided by the producer of the simulated VIPs [14]

Panel section dimensions and stratigraphy	Envelope layers	t [μm]	λ [W/mK]
	PET	12	0.19
	Al	0.1	160
	PET	12	0.19
	Al	0.1	160
	PET	12	0.19
	Al	0.1	160
	PE	12	0.19
	Al	0.1	160
	PE	50	0.33
		λ_{\perp}	
	$\lambda_{//}$		0.827

The thermal conductivity of the still air inside the VIP envelop folding and inside the closed device was evaluated like horizontal gap with ascending thermal flux, in accordance with UNI EN ISO 6946:2017 [116]. The radiation and convection heat transfer across an air cavity is approximately proportional to the temperature difference between the bounding surfaces and the cavity surfaces temperatures depends on the air cavities thermal resistance. For this reason, an iterative calculation is operated to find the temperature's repartition on the cavity surfaces, and after that, the thermal resistance was calculated using the following equation:

$$R_g = \frac{1}{h_a + h_r} \quad (37)$$

Where: R_g is the thermal resistance of the airspace [$\text{m}^2\text{K/W}$];

h_a is the conduction/convection coefficient [$\text{W/m}^2\text{K}$];

h_r is the radiative coefficient [$\text{W/m}^2\text{K}$].

The h_a -value is calculated with the Table B.1 and B.2 of the same European Standard, while h_r is given by Eq. (38):

$$h_r = E \cdot h_{r0} = \frac{1}{\frac{1}{\varepsilon_1} + \frac{1}{\varepsilon_2} - 1} \cdot h_{r0} \quad (38)$$

Where: E is the intersurface emittance [-];

$\varepsilon_1, \varepsilon_2$ are the hemispherical emissivities of the surfaces bounding the airspace (equals to 0.04 for aluminium foil) [-];

$h_{r,0}$ is the radiative coefficient for a black body [$\text{W}/\text{m}^2\text{K}$].

If the small airspace has a width less than 10 times its thickness, h_r is also given by:

$$h_r = \frac{h_{r0}}{\frac{1}{\varepsilon_1} + \frac{1}{\varepsilon_2} - 2 + \frac{2}{1 + \sqrt{1 + \frac{d^2}{b^2}} - \frac{d}{b}}} \quad (39)$$

Where: d is the thickness of the airspace [m];

b is the width of the airspace [m].

4.3.2 Energy analysis and thermal load simulation

“The evaluation of building energy performances was carried out through a dynamic energy analysis and thermal load simulation. It is the most appropriate procedure to estimate the envelope performances, because it considers in detail the contributions of walls thermal inertia, outside temperature variability, solar radiation, natural ventilation and users’ management.

EnergyPlus™ 2.0 was used as Building Energy Software 0. The thermal properties of the wall materials and the boundary conditions were defined in details, while the heating system was set out as an ideal system. Hence, the heating system was not modelled, and that it was able to satisfy anyhow/anyway the set point temperatures.

In this study, it was important to select a reliable building reference model, and to carefully determine the reliability of the energy simulations outputs. For this reason, simulations were carried out in accordance with the standard EN ISO 15256:2007 [135].

The Test room 1 of [135] was chosen as the reference room for this study. The test room is a typical office room and its internal size is: length = 3.6 m; depth = 5.5 m; height = 2.8 m. The window is facing West. The internal gains are 20 W/m^2 during the weekdays, and the ventilation rate is equal to 1 air change per hour. The setpoint temperature for heating was set to 20 °C while the cooling

temperature was 26 °C. In order to adapt the test room to the aim of the study and to make it most representative of a real (typical) office space, a cavity wall was chosen as external wall, and the window area was reduced from 7 to 3.6 m².

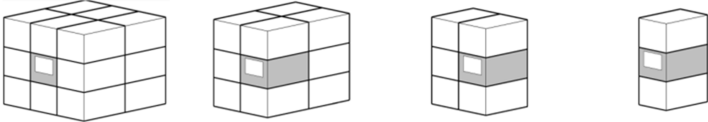
The accuracies of the heating annual energy need results were checked through a comparison between the reference values given by the standard [135] and the EnergyPlus™ outputs. The performed tests assured that the outputs were reliable. The difference between the value of the energy demand for the space heating given by [135] and the EnergyPlus™ output was less than 4%.

After this validation of the model, the energy simulation of all the cases was carried out. These various configurations resulted from the combination of the shape, the aspect ratio, the heating system, and the climate conditions of the building, as described in the next sections.

- **Reference building and aspect ratio**

As mentioned in Section 2, once the reference room (the “module”) was chosen, the reference buildings were created by combining in various ways this module, as graphically sketched in **Table 9**. The aspect ratio (S/V) of the building was then obtained by the proportional correlation between the external surface area (S) of the building and its heated volume (V). Four different aspect ratios (0.12, 0.37, 0.53, 0.75) were analysed by varying the number of adiabatic walls in the office model (**Table 9**).

Table 9: Different aspect ratios

Number of adiabatic walls	[-]				
		3	2	1	0
S	[m ²]	8.06	27.21	40.48	61.25
V	[m ³]	69.00	73.78	77.02	82.00
S/V	[1/m]	0.12	0.37	0,53	0,75

- **Climatic zone**

In order to have a picture of the influence of the climate conditions on the final results of the economic analysis, three European cities were considered. They were selected based on the Heating Degree Days (HDD)

provided by the International Weather for Energy Calculations (IWEC) [136]. Tampere and Palermo are, respectively, the coldest and the warmest European cities, while London represents the average value of the HDD of the other European locations (**Figure 40**).

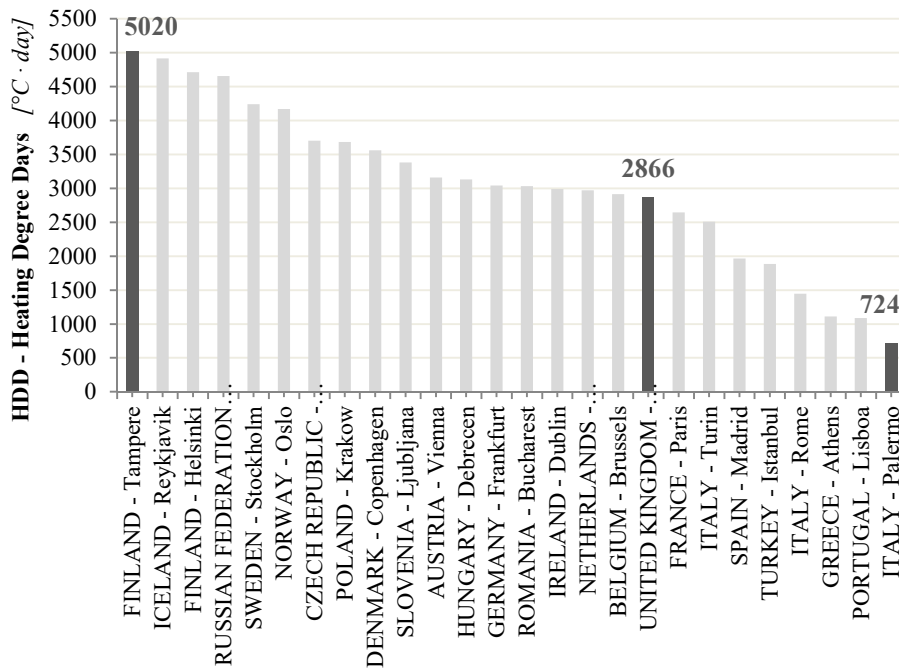


Figure 40: HDD in different European cities [135]

- **Heating systems**

The energy retrofit is usually done on existing buildings with old heating systems. However, it is unreasonable to invest a lot of money for a well-performing internal wall insulation without also improving the heating system, especially if its efficiency is lower than the minimum enforced by laws (see, e.g. [137] for Italy). For this reason, a natural gas condensing boiler (30 kW of power) and a geothermal heat pump were selected for the simulations, respectively as a low and a high efficiency heating system.

The efficiency of the gas condensing boiler was set equal to 79.4% (which is the minimum value established by the Italian law [137]), while the

average value of the coefficient of performance (COP) for a geothermal heat pump was assumed equal to 4.”¹⁵.

- **Insulating materials**

The purpose of the investigation was to compare VIP and traditional insulating materials. The expanded polystyrene (EPS, $\lambda = 0.04$ W/mK) was selected because it is nowadays one of the most commonly used types of insulation [16]. About VIPs, fumed silica panels with an MF4 envelope and thicknesses of 10, 20 and 30 mm were considered. The equivalent thermal conductivity of the VIPs insulated cavity wall was calculated through Eq. (25), in accordance with [105], considering two different VIPs assembling joints (2 mm air joint and XPS structural joint). Based on these considerations, the equivalent EPS thicknesses were calculated to achieve the same cavity wall thermal transmittance obtained by using VIPs.

4.3.3 Dynamic hygrothermal simulation

The thermal performances of VIPs, as well as their service life, strictly depends on the effective boundary working conditions (high temperatures and relative humidities). Numerical dynamic hygrothermal simulations are indeed useful, on one hand, to identify potential critical hygrothermal operating conditions of VIPs, depending on the building envelope configurations, and on the other hand to investigate the effects of the VIP thermal conductivity variation on the overall thermal behaviour of a building envelope component (as also demonstrated in [139]).

The evaluation of the actual VIPs working conditions required the analysis of a comprehensive set of VIP based building envelope configurations (brick wall and pitched roof), considering different exposures, weather and indoor climatic conditions. As results, the yearly profiles of temperature, relative humidity and partial water vapour pressure at the VIP surfaces were obtained. The numerical simulations were performed using WUFI[®] Pro software [140].

A similar approach was followed to investigate the influence of the temperature on the thermal behaviour of a VIPs insulated pitched roof (which can be subjected to higher temperature variation respect to a vertical wall).

¹⁵ Text from the author's paper: "Thermo-economic analysis of building energy retrofits by using VIP - Vacuum Insulation Panels" [138].

In particular, the roof model was experimentally validated, by an in-situ monitoring campaign.

4.3.3.1 Actual VIPs operating conditions

“The VIPs service life may be limited by water vapour as well as gas permeation. The extent of their occurrence is strictly dependent on the severity of temperature and humidity at which VIPs are exposed during their operation. In the context of IEA EBC Annex 65 activities, a common simulation based procedure was introduced to identify potential critical hygrothermal working conditions for VIPs when they are used in different building components. A methodological framework was developed to estimate the yearly profiles of temperature and relative humidity at the boundaries of VIPs considering different indoor and external conditions and envelope configurations. This procedure provided general data suggesting guidelines for the correct design of VIP based building components considering their actual working conditions.

The yearly profiles of temperature, relative humidity and partial water vapour pressure at the VIP surfaces were obtained for different weather and indoor climatic conditions. The methodological framework at the base of the procedure is presented. [...]

The main aims of the research activity were:

- *highlight critical building applications/configurations of VIPs due to severe boundary conditions;*
- *identify potential solutions to mitigate the working conditions and to protect the VIPs;*
- *provide general guidelines for the correct design of VIPs based building components;*
- *contribute to the definition of laboratory “accelerated ageing test“, considering various component configurations and climatic conditions.*

The proposed methodology is based on the following steps:

- *selection of typical building VIP based components representative of the building technologies for various countries (only centre of wall configurations were considered, without accounting – at this stage – the influence of thermal bridges: further investigations will be needed to address the thermal bridges);*

- *selection of boundary conditions for the analyses (external and indoor conditions);*
- *assessment of the yearly profiles of: temperature (ϑ), relative humidity (RH), and partial water vapour pressure (p_v), at the VIPs surfaces (by means of numerical simulations);*
- *results analysis, in order to identify critical conditions at the VIP layer surfaces”¹⁶.*

Between the ten collected configurations, two were proposed by Politecnico di Torino: a brick wall and a pitched roof.

Temperature and relative humidity of the indoor space were defined according to different technical standards (EN 15026:2007 [141], ASHRAE 160:2016 [142], ISO 13788:2012 [143]), while for the outdoor weather conditions the data (temperature, relative humidity, direct, diffuse and global solar radiation, rainfall) were extracted from WUFI[®] Pro database (Turin - year 2004).

“Numerical analyses were performed by means of 1D and 2D dynamic heat and moisture simulation tools [140]. **Table 10** summarises the criteria used for the simulations. To minimise the computational efforts, a series of simplifying assumptions were adopted:

- *VIP panels were modelled as an equivalent homogeneous layer, simplifying the actual structure (envelope and core material);*
- *1D and 2D heat and moisture transport phenomena were considered;*
- *the thermal conductivity of VIP layer was assumed equal to the centre of panel thermal conductivity λ_{COP} ;*
- *the water vapour permeability of the VIP layer was considered infinite.*

Table 10: Simulation approach [144]

Time interval	Simulation period	Selected results
≤ 60 min	Many years (until ϑ and RH equilibrium is reached)	Last year of simulation

¹⁶ Text from the author’s paper: “A methodological framework for the analysis of the service life of VIPs based envelope components in buildings” [144].

Simulations were performed for various design alternatives varying those parameters that mostly affect the severity of the operating conditions:

- location;
- orientation/exposure;
- external finishing colour (bright, medium and dark, with a solar absorption coefficient α of 0.3, 0.6 and 0.9 respectively);
- indoor moisture load (low, medium and high);
- presence of vapour barrier;
- VIPs thickness.

[...] For each selected design alternative and for each component, two different set of data related to ϑ , RH and p_v were considered (Figure 41): i) time profiles, ii) cumulative frequency distributions.

The cumulative frequency distributions of each variable were divided into four ranges, from (I) to (IV): the first range represents the less severe operating conditions, while the fourth the worst (Table 11).

The results of the simulations, for all the design alternatives, were organised in summary tables, containing the peak values of ϑ , RH and p_v on each side of the VIP panel, and the percentage of time for which, during the year, the VIPs are exposed to a specific class of severity”¹⁷.

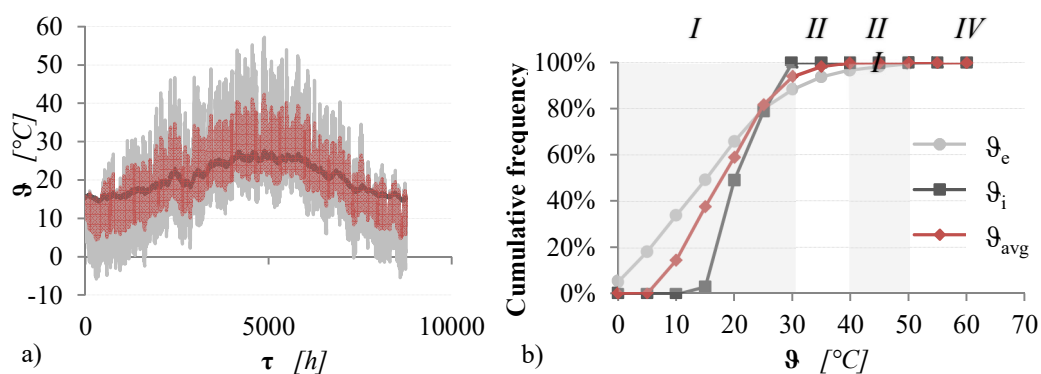


Figure 41: Simulation outputs. a) Example of yearly time profiles; b) example of cumulative frequency analysis [144]

¹⁷ Text from the author’s paper: “A methodological framework for the analysis of the service life of VIPs based envelope components in buildings” [144].

Table 11: Ranges of ϑ , RH and p_v values [144]

Range	ϑ [°C]	RH [%]	p_v [hPa]
I	$\vartheta \leq 30$	$RH \leq 50$	$p_v \leq 21.2$
II	$30 < \vartheta < 40$	$50 < RH < 60$	$21.2 < p_v < 44.4$
III	$40 < \vartheta < 50$	$60 < RH < 70$	$44.3 < p_v < 86.3$
IV	$\vartheta \geq 50$	$RH \geq 70$	$p_v > 86.3$

The two analysed configurations are represented in **Figure 42** and **Figure 43**, and will be described in details in § 10.1 *Building component simulation model*.

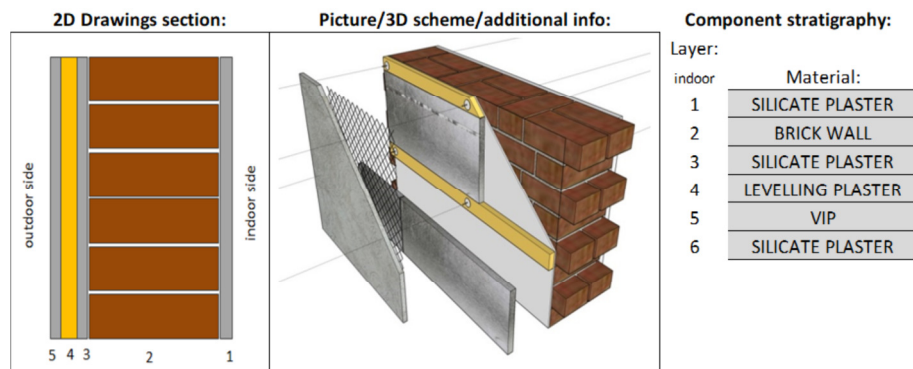


Figure 42: Simulated brick wall structure

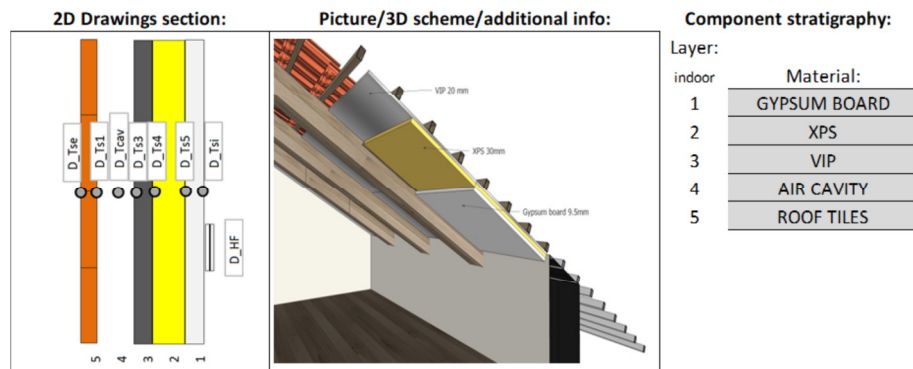


Figure 43: Simulated pitched roof structure

In this document, only the results of the most representative and/or critical design alternative for each case study will be presented (e.g., darker surface, medium moisture load, and so on).

4.3.3.2 Effects of temperature on VIPs at the building component scale

“The variability of its centre of panel (COP) thermal conductivity with the working temperatures influences the overall energy performance of the building envelope component. To study the impact of the variation of the λ_{COP} , due to the working temperature at the building component scale, the thermal behaviour of a roof implementing a VIP layer was analysed. A pitched roof was selected as case study considering that potentially it can be subjected to higher temperature variation respect to a vertical wall and hence the effect on the variation on the thermal conductivity should be more relevant.

The selected component analysed is a timber frame pitched roof. [...] The roof is located in San Francesco al Campo (Torino – Italy), and it is characterised by south - south - west orientation and 28° slope (Figure 44 a) and b)).

Simulations were carried out on two different design alternatives (Figure 44 c)). The monitored one (Configuration A) is composed, from inside to outside, by 1) a gypsum board layer, 2) an extruded polystyrene XPS layer, 3) Vacuum Insulation Panel, 4) a slightly ventilated air layer and 5) roof clay tiles. In the second one (Configuration B) the position of the VIP and the XPS layers are reversed, to analyse the influence of the VIP layer position.

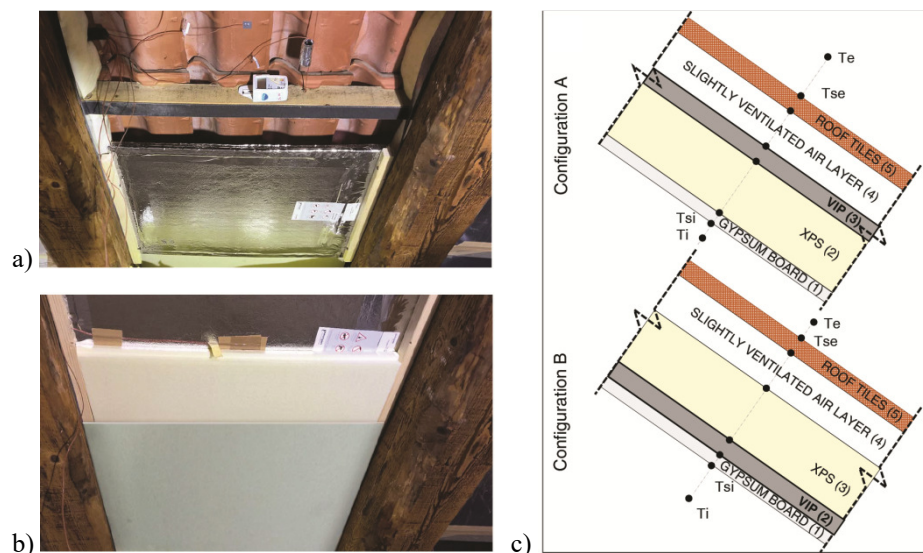


Figure 44: a) VIP in roof component; b) Roof insulation assembly; c) Roof sections (Configurations A and B)

Thermal and physical properties are resumed in Table 12.

Table 12: Roof layers from inside to outside - Configuration A. (*from VIP datasheet)

Layer	Material	t [mm]	ρ [kg/m ³]	λ [W/mK]	c [J/kgK]	α [-]
1	Gypsum board	9.5	800	0.200	1000	-
2	XPS	30	32	0.036	1500	-
3	VIP	10	200	0.005*	800	-
4	Air layer	100	1.2	-	1020	-
5	Roof tiles	30	1700	0.700	840	0.55

The data collected during the experimental campaign (where a VIP stored 32 months in laboratory conditions was installed) were used to validate the simulation model.

The roof was modelled as a simplified 1D multilayer roof structure, and the effect of thermal bridges and 2D heat transfer phenomena were neglected, as well as the water vapour transport phenomena.

The indoor climate conditions defined in EN 15026:2007 [141] were assumed for the analysis:

- *heating season (15th October - 15th April): $\vartheta = 20^\circ\text{C}$;*
- *cooling season (15th April - 15th October): $\vartheta = 25^\circ\text{C}$.*

For the outdoor climate, the Torino weather data implemented in WUFI[®] database (Turin - year 2004) were again used.

Simulations were performed with a time-step of 15 min, while for the spatial discretisation the option “fine grid” was used.

The internal surface heat transfer coefficient (h_i) was assumed equal to 5.88 W/m²K, according to EN ISO 6946:2017 [116], while a wind dependent heat transfer coefficient for the outside layer (h_e) was considered according to Eq. (40):

$$h_e = (h_c + h_r) + (a \cdot v) \quad (40)$$

Where: $h_c = 4.5 \text{ W/m}^2\text{K}$ is the convective heat transfer coefficient;

$h_r = 6.5 \text{ W/m}^2\text{K}$ is the radiative heat transfer coefficient;

$a = 1.6 \text{ Ws/m}^3\text{K}$ (for windward conditions) and $0.33 \text{ Ws/m}^3\text{K}$ (for leeward conditions) is the wind coefficient;

v is the wind velocity [m/s]¹⁸.

4.3.3.3 Validation of the numerical models

The numerical model analysed in the previous chapter “was validated by the comparison with the measured temperatures at the boundaries of the VIP (fifteen days of measurements). **Figure 45** shows the measured and the simulated temperatures at the interface 2-3 (between the VIP and the XPS board, see **Table 12**), together with the corresponding Root Mean Square Error - RMSE (between the VIP and the XPS board), evaluated through Eq. (41).

$$RMSE = \sqrt{\frac{\sum_{\tau=1}^n (\vartheta_{exp} - \vartheta_{num})^2}{n}} \quad (41)$$

Where: ϑ_{exp} is the experimentally monitored temperature [°C];

ϑ_{num} is the numerically simulated temperature [°C].

*To improve the readability of **Figure 45** only three days of comparison are presented. However, the values of RMSE are related to the whole period of measurements. Moreover, as can be seen in **Figure 45** the model which takes into account the temperature dependence of the thermal conductivity makes it possible to better fit the measured data*¹⁹.

The *RMSE* is the standard deviation of the residuals. Residuals are a measure of prediction error in case of regression and define the distance between the regression line and the data points. Indeed, the *RMSE* measures the spread of these residuals. **Figure 46** and **Figure 47** represent the regression lines between the measured and simulated temperatures, at the interface 2-3 (interior side) and 3-4 (exterior side) respectively.

¹⁸ Text from the author’s paper: “Actual thermal performances of Vacuum Insulation Panels for buildings” [75].

¹⁹ Text from the author’s paper: “Actual thermal performances of Vacuum Insulation Panels for buildings” [75].

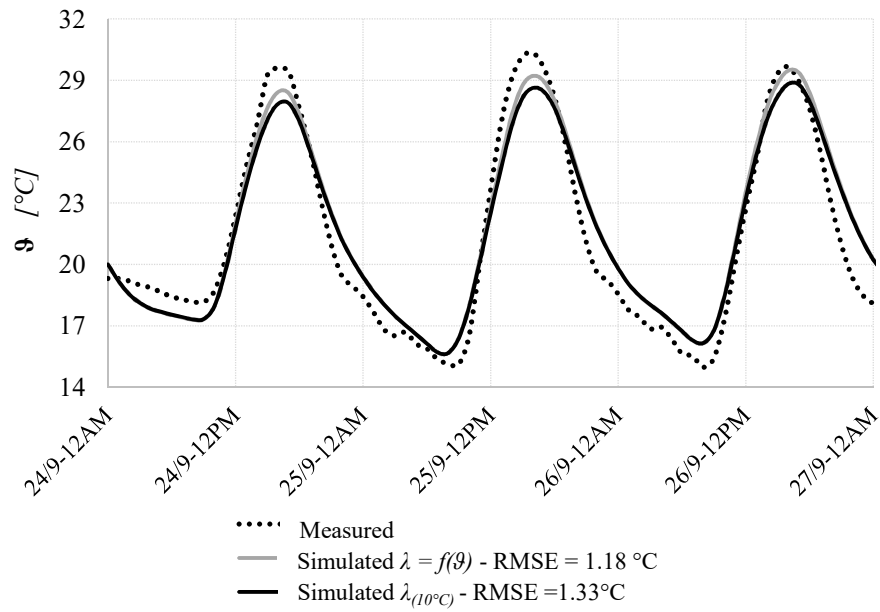


Figure 45: Comparison between measured and simulated results. $\lambda = f(\theta)$ (temperature dependent thermal conductivity). $\lambda_{(10^\circ\text{C})}$ (constant thermal conductivity measured at 10°C). RMSE values were calculated for the period 24/09/2016 – 08/10/2016

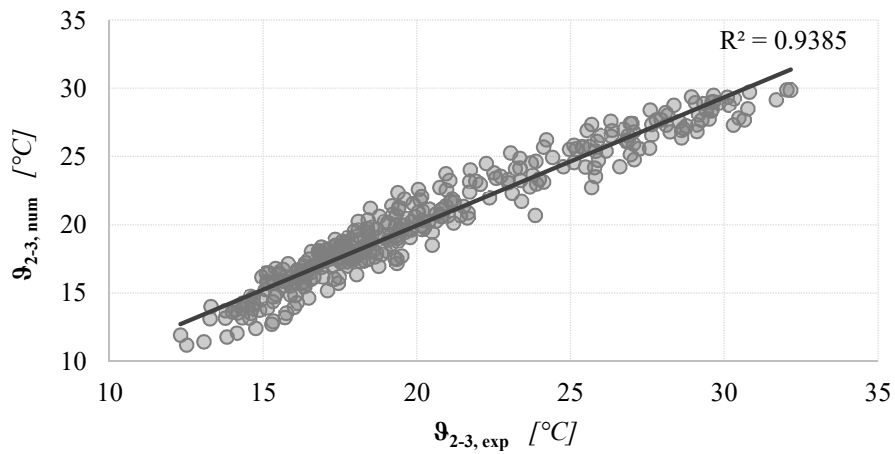


Figure 46: Temperature regression line at the interface 2-3 (interior side)

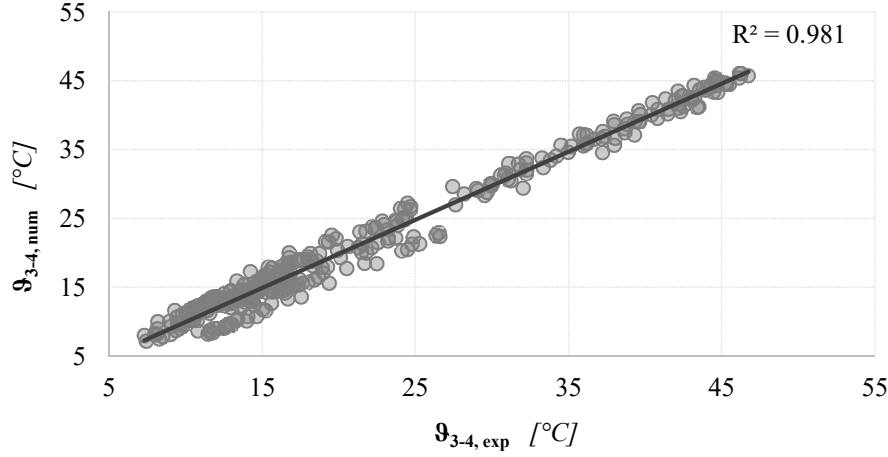


Figure 47: Temperature regression line at the interface 3-4 (exterior side)

The coefficient of determination (R^2) shown in the previous figures, is the proportion of the variance in the dependent variable that is predictable from the independent variable. In other words, it defines how well a model explains and predicts future outcomes (distance between the data and the fitted regression line). It lies between 0 and 1 (perfect fitting). Both internal and external VIP surface temperatures present an R^2 -value next to 1, which means a good agreement between the numerical model and the monitored roof.

Moreover, to evaluate the accuracy of the model, the variation coefficient (CV) of the $RMSE$ was calculated for both the VIP interfaces (the lower the CV , the smaller the predicted value residuals):

$$CV(RMSE) = \frac{RMSE}{\xi} \cdot 100 \quad (42)$$

Where: ξ is the difference between the highest and the lowest experimental values of the interface temperature [$^{\circ}C$].

In the specific case, the $CV(RMSE)$ was found out to be equal to 4,0% for the VIP exterior surface temperature, and to 5,9% for the interior surface.

Both R^2 and $CV(RMSE)$ are characterised by a higher value for the interior interface of the VIP: this may be due to the fact that the analytical results are more influenced by the internal surface heat transfer coefficient (h_i), assumed constant during the simulations (while h_e was supposed to be variable, depending on the wind velocity).

Chapter 5

Measurement uncertainty analysis

All measurements are subject to uncertainty, to a lack of exact information about the performed measurement. The uncertainty depends on several factors, such as the tested specimen, the resolution of the apparatuses, the operator skills, the environmental conditions, the simplified assumptions of the method and procedure and so on. Because of this, the measured value is always an estimate of the measurand. For this reason, every result should be expressed with two essential components:

- a numerical value (a single measurement or the mean value of a series of measures), expressed in SI units, which represent the best estimate of the measurand;
- the uncertainty associated with this estimated value (for example the variability or dispersion of a series of similar measurements expressed as a standard uncertainty/standard deviation, or combined standard uncertainty (see the following chapters)).

The primary definition of uncertainty can be found in the International Vocabulary of Metrology – VIM (“*non-negative parameter characterising the dispersion of the quantity values being attributed to a measurand, based on the information used*”) [145].

General rules to evaluate and express measurement uncertainty are provided by the “Evaluation of Measurement Data - Guide to the Expression of Uncertainty in Measurement” (usually referred to as the GUM) [13].

The SIMs thermal properties are assessed using several experimental apparatus, in particular, Heat Flow Meter (HFM) and Guarded Hot Plate (GHP). The existing device, as well as the related current standards, were developed for the experimental assessment of the so defined traditional insulating materials for building applications. But in case of SIMs, their low thermal conductivity often lies over the applicability range of the apparatus, which are forced to work beyond their limit. For this reason, the accuracies of existing device could often be inadequate, or not in line with the standards uncertainty maximum values (2% for GHP and 3% in case of HFM [12]). Therefore, the primary core of this research was to verify the applicability of the current standards and measurement devices to SIMs evaluation, together with the assessment of the actual obtainable experimental uncertainty. Between SIMs, only VIPs were considered for these analyses, because they are characterised by the lowest thermal conductivity values.

The uncertainty analysis was indeed the key point of this research, and for this reason, it was deeply investigated under different points of view, considering both the Type A and Type B evaluations (based respectively on a statistical approach or other scientific and relevant information available).

First of all, a theoretical analysis of HFM measurement uncertainty, based on current standards, was performed (to check the applicability of the HFM standards in case of VIPs). After that a complete analysis for the assessment and validation of measurement uncertainty based on experimental data was developed: the investigation was focused on the comprehensive thermal performances of VIPs (thermal conductivities - λ_{COP} and λ_{eq} , and linear thermal transmittance ψ), evaluated by means of both GHP and HFM apparatuses.

5.1 Type A, type B and combined uncertainty

The GUM [13] defines two different categories of uncertainty: Type A (statistical analysis of series of observations) and Type B (use of no-statistical available information, such as previous measurement data, experience with or general knowledge of the behaviour and properties of relevant materials and instruments, manufacturer's specifications, data provided in calibration and other certificates, uncertainties assigned to reference data taken from handbooks). Type A and Type B uncertainty evaluations give substantially the same information, and they can be applied considering both random and systematic errors (where an error is the difference between one measured quantity value and a reference quantity value [145]).

Both Type A and Type B uncertainties are composed by the standard uncertainty value (equivalent to standard deviations) and the number of degrees of freedom (ν [-]). The degrees of freedom define the number of parameters of the system that may vary independently. This concept is closely linked to the process of fitting population values (parameters) to a sample of several observations, and to the reliability of the uncertainties associated with this fitting process. The general way to obtain the number of degrees of freedom is the difference between the number of measurements affected by errors and the number of fitted parameters. The associated uncertainty of each measurement is obtained combining Type A and Type B components, which is, in general, the root-sum-square of Type A and Type B standard uncertainties. It is important to highlight that the once the measurement results are obtained, the related combined standard uncertainty is always a Type B uncertainty, even if it is composed of Type A components.

It is very common to find the combined standard uncertainty multiplied by a factor required to indicate the confidence level in the measurement result (the so-called coverage factor), obtaining the expanded uncertainty. Unless differently stated, it is possible to assume that a normal distribution was used to assess the uncertainty. Usually, the level of confidence is 95% (or 95.4%), obtained with a coverage factor equal to 1.96 (or 2). The so obtained expanded uncertainty is indeed the double of the standard uncertainty. If a higher level of confidence is required, the coverage factor must be naturally higher (for example, to a confidence level of 99%, the factor is approximately 2.6 must be used).

The GUM [13] provides the clear guidelines for evaluating and combining Type A and Type B standard uncertainties, that can be summarised in the following points [146]:

- Type A components are characterised by an estimate of their variances (s_i^2) or estimated standard deviations (s_i) and the related ν -value. A standard deviation (s_i) is numerically identical to a standard uncertainty (u_i). Covariances should be given when correlated quantities are involved.
- Type B components are characterised by uncertainty quantities (u_i), which can represent the approximation of the standard deviations. The squared uncertainty (u_i^2) may be treated as variances or squared standard uncertainties, and the uncertainties themselves (u_i) like standard deviations

or standard uncertainties. Covariances should be given when correlated quantities are involved.

- The combined standard uncertainty should be obtained by the root-sum-squaring the Type A and Type B standard uncertainties. The combined standard uncertainty is statistically equivalent to a standard deviation.
- If the expanded uncertainty is required, the adopted multiplying coverage factor must always be declared.

Type A uncertainty is experimentally determined, through a set of measurements: in this way the uncertainty is calculated with information that comes directly from the experiment. The measures are repeated n -times, while each influencing parameter is controlled. The uncertainty is indeed obtained from a Probability Density Function (PDF or $p(x)$ [147]) derived from an observed frequency distribution: u_i is expressed by the standard deviations of a statistical distribution.

When it is not possible to take repeated observations of the measurand, the Type B uncertainty must be evaluated. In this case, the uncertainty is obtained through the pool of the available information on the possible variability of the value x_i . In other words, it is derived from an assumed probability density function based on the degree of belief that an event will occur (also called subjective probability).

The Probability Density Function defines the probability distribution of a continuous random variable as opposed to a discrete random. It allows calculating the probability that the variable has value in a specified interval. The PDF definition requires that the relation in Eq. (43) is satisfied [13]:

$$\int p(x) dx = 1 \quad (43)$$

The standard uncertainty is indeed equal to the standard deviation of the PDF of the observed phenomenon:

$$u(x) = \sigma = \sqrt{\sigma^2} = \sqrt{\int (x - \mu_x)^2 p(x) dx} \quad (44)$$

PDFs can often be simplified in some more general distributions, as follow.

NORMAL DISTRIBUTION [13]

In most cases, the best estimate of a set of measures is given by the mean or average \bar{x} of the n observations:

$$\bar{x} = \frac{1}{n} \sum_{i=1}^n x_i \quad (45)$$

The experimental standard deviation is obtained as the positive square root of the experimental variance:

$$s(x_i) = \sqrt{\frac{1}{n-1} \sum_{j=1}^n (x_j - \bar{x})^2} \quad (46)$$

Since the mean value represents the best estimate of the measurand, the best estimate of the standard deviation of the mean is:

$$s(\bar{x}) = \sqrt{\frac{1}{n(n-1)} \sum_{j=1}^n (x_j - \bar{x})^2} \quad (47)$$

The experimental variance of the mean $s^2(\bar{x})$ and the experimental standard deviation of the mean $s(\bar{x})$ define how well \bar{x} estimates the expectation of x (μ_x), and therefore they may be used as a measure of the uncertainty of \bar{x}

So the uncertainty is equal to the standard deviation of the mean value:

$$u(x) = s(\bar{x}) \quad (48)$$

For n independent observations x_i obtained in the same condition, the uncertainty can be calculated by:

$$u(x) = s(\bar{x}) = \frac{s(x_i)}{\sqrt{n}} \quad (49)$$

The experimental standard deviation (measurement uncertainty) is reduced by a factor equal to the square root of the performed measurements number. This means that an increase of the number of measurements causes a decrease of the error, with a higher accuracy of the result, but only in case of independent variables.

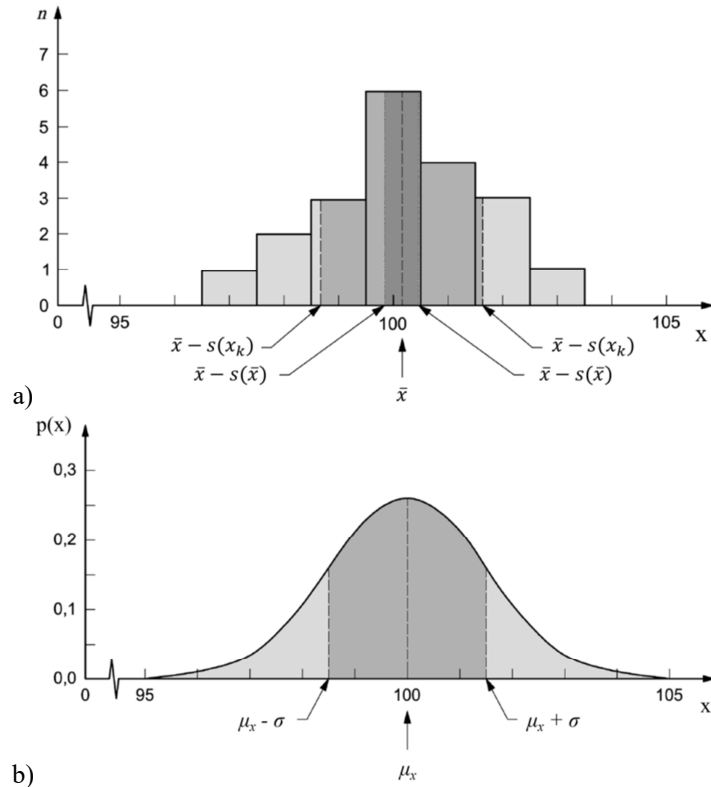


Figure 48: Graphical illustration of the standard uncertainty from repeated observations of an input quantity: a) normal PDF distribution; b) histogram [13]

Figure 48 shows how to estimate the value of an input quantity X_i and its uncertainty, starting from the probability distribution of X_i obtained from repeated measurements (it is also the unknown distribution of the possible measured values of X_i). In **Figure 48** a) the histogram of n° repeated observation (x_k) of X_i is reported. To obtain the histogram, all the observations must be grouped into intervals with a defined constant width. The histogram is not required for the statistical data analysis. Anyway it is useful to better estimate the probability distribution of the observations. In this case, the unknown *PDF* of the input quantity X_i can be simplified in a normal distribution.

Its PDF is defined as:

$$p(x) = \frac{1}{\sigma \cdot \sqrt{2\pi}} \cdot e^{\left[-\frac{1}{2} \left(\frac{x - \mu_x}{\sigma}\right)^2\right]} \quad (50)$$

RECTANGULAR DISTRIBUTION [13]

Rectangular (or uniform) distribution is an example of a priori distribution (Figure 49). It occurs when little information is available about the input quantity X_i . In this case it is only possible to suppose that X_i is described by a symmetric, rectangular a priori probability distribution, with defined upper bound a_+ and lower bound a_- : if the values of X_i are not known within the range, it is possible to assume that it is equally probable for X_i to fall everywhere in the range.

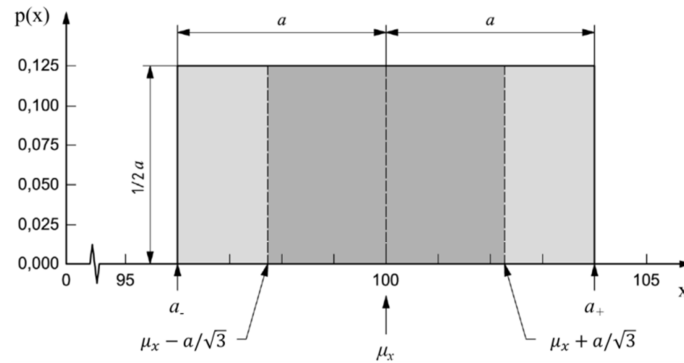


Figure 49: Graphical illustration of the rectangular distribution of standard uncertainty [13]

The probability density function of X_i is then:

$$\begin{cases} p(x) = \frac{1}{2 \cdot a} & a_- \leq X_i \leq a_+ \\ p(x) = 0 & \text{otherwise} \end{cases} \quad (51)$$

The best estimate is indeed the mean between the two bounds:

$$\mu_x = \frac{a_+ - a_-}{2} \quad (52)$$

The variance for rectangular distribution is given by Eq. (53):

$$u^2(x_i) = \frac{(a_+ - a_-)^2}{12} = \frac{1}{3} a^2 \quad (53)$$

If the difference between a_+ and a_- is $2a$ (symmetrical PDF, where a is the semi-range), the uncertainty is:

$$u(x_i) = \frac{a}{\sqrt{3}} \quad (54)$$

TRIANGULAR DISTRIBUTION [13]

Triangular symmetric distribution is another example of a priori probability distribution (Figure 50).

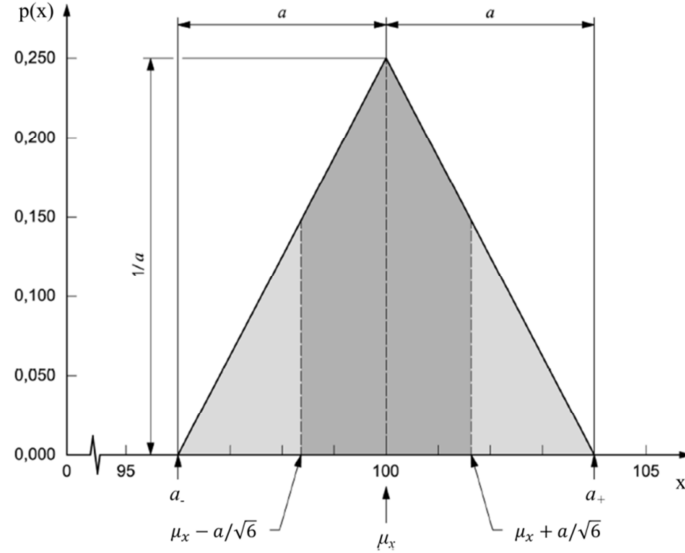


Figure 50: Graphical illustration of the triangular distribution of standard uncertainty [13]

In this case, the available information about X_i is less limited than in the case of rectangular distribution, considering the same defined upper bound a_+ , lower bound a_- and half-width a . The triangular *PDF* is defined as:

$$\begin{cases} p(x) = \frac{(a_+ - x_i)}{a^2} & \frac{a_+ + a_-}{2} \leq X_i \leq a_+ \\ p(x) = \frac{(x_i - a_-)}{a^2} & \frac{a_+ + a_-}{2} \leq X_i \leq a_- \\ p(x) = 0 & \text{otherwise} \end{cases} \quad (55)$$

The best estimate is again the mean between the two bounds, defined by Eq. (52), while the uncertainty is defined as:

$$u(x_i) = \frac{a}{\sqrt{6}} \quad (56)$$

5.1.1 Combined uncertainty

The measurand Y is usually not directly measured, but is expressed as a function of other measured parameters:

$$Y = f(X_1; X_2; X_3; \dots; X_N) \quad (57)$$

In this case, the uncertainties of the various parameters will propagate through the function f to an uncertainty in Y . When these quantities are uncorrelated (see the following § 5.1.2 *Correlated quantities* for further details), the uncertainty of y (estimate of the measurand Y) is calculated through the combined standard uncertainty - $u_c(y)$. It is obtained combining the uncertainty contributions of each input quantity [13]:

$$u_c(y) = \sqrt{\sum_{i=1}^N \left(\frac{\partial f}{\partial x_i}\right)^2 \cdot u(x_i)^2} \quad (58)$$

Where: f is the mathematical relation, which linked N parameters to determine Y ;

$u(x_i)$ is the Type A or Type B standard uncertainty of every parameter;

$\frac{\partial f}{\partial x_i}$ is the sensitivity coefficient of the input quantity x_i , and describes the variation of the output y when the input values x_i changes;

$\left(\frac{\partial f}{\partial x_i}\right)^2 \cdot u(x_i)^2$ is the uncertainty contribution and considers the influence of the uncertainty of each input quantity x_i on the output uncertainty $u_c(y)$.

5.1.2 Correlated quantities

The above-described procedure is valid when the input variables have no relationship between themselves (uncorrelated variables). Otherwise, it's possible to have some situations where a relationship may exist between two or more of the input variables.

When the input quantities are correlated, the correct expression for the combined uncertainty $u^2(y)$ is [13]:

$$\begin{aligned}
u_c(y) &= \sqrt{\sum_{i=1}^N \sum_{j=1}^N \frac{\partial f}{\partial x_i} \cdot \frac{\partial f}{\partial x_j} \cdot u(x_i, x_j)} = \\
&= \sqrt{\sum_{i=1}^N \left(\frac{\partial f}{\partial x_i}\right)^2 \cdot u(x_i)^2 + 2 \cdot \sum_{i=1}^{N-1} \sum_{j=i+1}^N \frac{\partial f}{\partial x_i} \cdot \frac{\partial f}{\partial x_j} \cdot u(x_i, x_j)} = \\
&= \sqrt{\sum_{i=1}^N \left(\frac{\partial f}{\partial x_i}\right)^2 \cdot u(x_i)^2 + 2 \cdot \sum_{i=1}^{N-1} \sum_{j=i+1}^N \frac{\partial f}{\partial x_i} \cdot \frac{\partial f}{\partial x_j} \cdot u(x_i) \cdot u(x_j) \cdot r(x_i, x_j)}
\end{aligned} \tag{59}$$

Where $u(x_i, x_j) = u(x_j, x_i)$ is the estimated covariance associated with x_i and x_j , and $r(x_i, x_j) = r(x_j, x_i)$ is the correlation coefficient which defines the degree of correlation between x_i and x_j [13]:

$$r(x_i, x_j) = \frac{u(x_i, x_j)}{u(x_i) \cdot u(x_j)} \tag{60}$$

The correlation coefficient lies between -1 and 1 and is equal to 0 if the variables are independent.

Correlated variables are observable for example, as in this specific research, when the measurements are performed and repeated with the same experimental apparatuses. Anyway, it is possible to eliminate this correlation if all the single measurement outputs are averaged before the calculation of the final result (in this case, the thermal conductivity). This principle can be derived from the example H.3 of the GUM [13] (calibration of a thermometer, least-squares fitting).

In case of n measurements, Eq. (60) can be re-written as:

$$r(x_i, x_j) = \frac{\sum_{k=1}^n \delta_k}{\sqrt{n \cdot \sum_{k=1}^n \delta_k^2}} \tag{61}$$

Where δ_k is the deviation between x_k and x_0 :

$$\delta_k = x_k - x_0 \tag{62}$$

For each point distribution with the same mean value of x and y , there is a bundle of lines which cross the mean value, and which is described by the regression line and the confidence interval. The regression line is characterised by

the slope and the intercept with the Y-axis. Moving the barycentre of the distribution in the middle point (and therefore, the axes origin), the value of the intercept becomes equal to zero, while the trend of the regression line remains the same (see **Figure 51**).

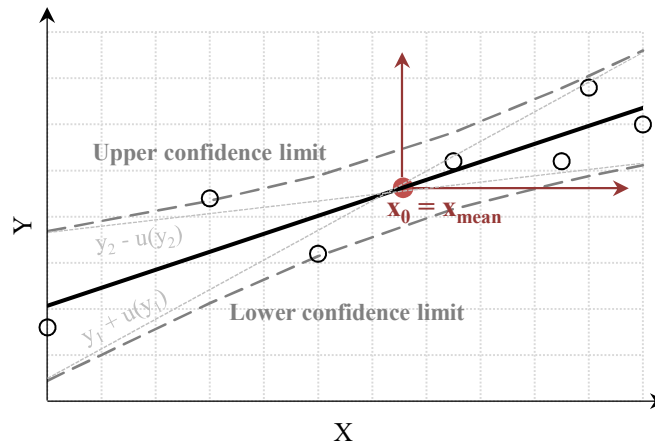


Figure 51: Uncorrelation of the least-squares fitting

Indeed, if x_0 is chosen as the mean of the several x_k :

$$\sum_{k=1}^n \delta_k = \sum_{k=1}^n (x_k - x_0) = 0 \quad (63)$$

because the sum of the deviations from the mean is zero.

The straight line that describes each pair of points $(x_i - x_{\text{mean}})$ and $(y_i - y_{\text{mean}})$, no longer having the intercept term, also loses the correlation between intercept and slope (because the new origin of the axes coincides with the meanpoint). This implies that the input variables becomes uncorrelated:

$$r(x_i, x_j) = 0$$

As described in the following chapters, five different measuring devices were used for the thermal characterisation of SIMs. Two of them (GHP-1 and HFM-1) were commercial apparatuses made by different manufacturers, while the other three were produced directly at the FIW Institute.

Table 13 summarises all the available informations about the apparatuses measuring chains, considered for the evaluation of the possible correlations between the measurement outputs.

Table 13: Measuring chains and uncorrelation assumption

		Measuring chain	Correlation	Devices correlation
INRiM	GHP - 1	<ul style="list-style-type: none"> Acquisition with different channels; Mean value of the outputs 	Uncorrelated	Uncorrelated
PoliTo	HFM - 1	<ul style="list-style-type: none"> One single output, one single measuring chain, mean value of the outputs 	Uncorrelated	
FIW	GHP - 2	<ul style="list-style-type: none"> Acquisition with different channels; Mean value of the outputs; 	Uncorrelated	Assumed uncorrelated
	GHP - 3	<ul style="list-style-type: none"> No information about sensors calibration 	Uncorrelated	
	HFM - 2		Uncorrelated	

For these reasons, all the following uncertainty budget assessments were performed considering uncorrelated input variables, since each measured signal was averaged used.

5.2 Thermal conductivity

The thermal conductivity of a material is the expected result of the experimental evaluation of the materials thermal properties. Therefore is essential to define the reliability of this result, especially in case of high performing insulating materials.

To this purpose, an extensive experimental campaign was performed, using the already described devices GHP - 1 and HFM - 1 (§ 4.3.1 *Bi-dimensional steady-state heat transfer*), allowing a Type A uncertainty analysis. Since the specifications and applicability ranges of the two devices were different, two different sample typologies were tested: VIPs for the HFM apparatus, and an aerogel blanket for the GHP device.

The experimental setup for the HFM measurements was composed by:

- three different VIP sample thicknesses: 10, 20 and 30 mm;
- four different average temperature of the sample: 5, 10, 23 and 40°C;
- four distinct temperature differences between the plates: 10, 20, 30 and 40°C.

The experimental setup for the GHP measurements was instead as follows:

- one single aerogel sample thicknesses: 10 mm;
- three different average temperature of the sample: 5, 10 and 23°C;
- three different temperature differences between the plates: 5, 10 and 15°C.

Anyway, for the other performed measurements, aimed at the evaluation of the thermal performances of SIMs, the Type B uncertainty was evaluated (through the data provided by the material producers).

5.2.1 Heat Flow Meter

The assessment of the thermal conductivity with the HFM method was already discussed in § 4.1.2 *Heat Flow Meter - HFM*. To facilitate the reading, Eq. (32) is hereinafter re-written:

$$\lambda_{HFM} = \frac{f_{cal}(\vartheta) \cdot Q \cdot t}{\Delta\vartheta} = \frac{\varphi \cdot t}{\Delta\vartheta} \quad (32)$$

Since each plate has its own temperature, the calibration factors should be calculated for each plate's actual temperature, obtaining two different values of thermal conductivity: the final thermal conductivity test is the average of these two values.

For different exemplary types of equipment, the standard EN 1946-3:1999 [148] contains maximum probable errors for each of the parameters. Moreover, to consider also the influence of the apparatus geometrical aspects and general quality on the measurement uncertainty, the standard proposes two additional uncertainty contributions:

- $\Delta\lambda_E$ edge heat loss [-];
- $\Delta\lambda_O$ imperfect contact [-].

These parameters can be included in the formula of thermal conductivity by adding them as factors of 1.0 and with a defined relative error in the calculation.

In the same way, the specific heat flux (φ) is affected by the calibration factor ($f_{cal}(\vartheta)$) and the measured electrical signal (Q). It is possible to consider the following errors, directly for the evaluation of the specific heat flux uncertainty:

- $\Delta\lambda_K$ calibration accuracy of the specimen [-];
- $\Delta\lambda_L$ maximum permissible non-linearity of the calibration [-];

- $\Delta\lambda_g$ maximum allowable calibrating drift [-].

These parameters can be included in the formula of the specific heat flux by adding them as factors of 1.0 and with a defined relative error in the calculation.

Therefore the equation of the thermal conductivity is extended:

$$\lambda_{HFM} = \frac{(\varphi \cdot \Delta\lambda_K \cdot \Delta\lambda_L \cdot \Delta\lambda_g) \cdot t}{\Delta\vartheta} \cdot \Delta\lambda_E \cdot \Delta\lambda_O \quad (64)$$

The thermal conductivity uncertainty is calculated through the combined standard uncertainty, applied to Eq. (64):

$$u_c(\lambda_{HFM}) = \sqrt{\left(\frac{\partial\lambda_{HFM}}{\partial\varphi} \cdot u(\varphi)\right)^2 + \left(\frac{\partial\lambda_{HFM}}{\partial t} \cdot u(t)\right)^2 + \left(\frac{\partial\lambda_{HFM}}{\partial\Delta\vartheta} \cdot u(\Delta\vartheta)\right)^2 + \left(\frac{\partial\lambda_{HFM}}{\partial\Delta\lambda_E} \cdot u(\Delta\lambda_E)\right)^2 + \left(\frac{\partial\lambda_{HFM}}{\partial\Delta\lambda_O} \cdot u(\Delta\lambda_O)\right)^2} \quad (65)$$

The heat flux, in turn, depends on three other factors, so its uncertainty is given by:

$$u_c(\varphi) = \sqrt{\left(\frac{\partial\varphi}{\partial\Delta\lambda_K} \cdot u(\Delta\lambda_K)\right)^2 + \left(\frac{\partial\varphi}{\partial\Delta\lambda_L} \cdot u(\Delta\lambda_L)\right)^2 + \left(\frac{\partial\varphi}{\partial\Delta\lambda_g} \cdot u(\Delta\lambda_g)\right)^2} \quad (66)$$

If also the electric signals from the transducer Q [μV] and the calibration factors $f_{cal}(\vartheta)$ [$\text{W}/\text{m}^2\mu\text{V}$] are measurable and available, $\Delta\lambda_K$, $\Delta\lambda_L$, and $\Delta\lambda_g$ are not required and Eq. (64) can be simplified in :

$$\lambda_{HFM} = \frac{f_{cal}(\vartheta) \cdot Q \cdot t}{\Delta\vartheta} \cdot \Delta\lambda_E \cdot \Delta\lambda_O \quad (67)$$

And consequently the uncertainty $u_c(\lambda_{HFM})$ can be calculated through:

$$u_c(\lambda_{HFM}) = \sqrt{\left(\frac{\partial\lambda_{HFM}}{\partial t} \cdot u(t)\right)^2 + \left(\frac{\partial\lambda_{HFM}}{\partial f_{cal}(\vartheta)} \cdot u(f_{cal}(\vartheta))\right)^2 + \left(\frac{\partial\lambda_{HFM}}{\partial Q} \cdot u(Q)\right)^2 + \left(\frac{\partial\lambda_{HFM}}{\partial\Delta\vartheta} \cdot u(\Delta\vartheta)\right)^2 + \left(\frac{\partial\lambda_{HFM}}{\partial\Delta\lambda_E} \cdot u(\Delta\lambda_E)\right)^2 + \left(\frac{\partial\lambda_{HFM}}{\partial\Delta\lambda_O} \cdot u(\Delta\lambda_O)\right)^2} \quad (68)$$

All the different sensitivity coefficients (partial derivatives) are:

$$\begin{aligned} \frac{\partial \lambda_{HFM}}{\partial \varphi} &= \frac{t}{\Delta \vartheta} \\ \frac{\partial \lambda_{HFM}}{\partial t} &= \frac{\varphi}{\Delta \vartheta} = \frac{f_{cal}(\vartheta) \cdot Q}{\Delta \vartheta} \\ \frac{\partial \lambda_{HFM}}{\partial \Delta \vartheta} &= \frac{\varphi \cdot t}{\Delta \vartheta^2} = \frac{f_{cal}(\vartheta) \cdot Q \cdot t}{\Delta \vartheta^2} \\ \frac{\partial \lambda_{HFM}}{\partial f_{cal}(\vartheta)} &= \frac{Q \cdot t}{\Delta \vartheta} \\ \frac{\partial \lambda_{HFM}}{\partial Q} &= \frac{f_{cal}(\vartheta) \cdot t}{\Delta \vartheta} \\ \frac{\partial \varphi}{\partial \Delta \lambda_K} &= \frac{\partial \varphi}{\partial \Delta \lambda_L} = \frac{\partial \varphi}{\partial \Delta \lambda_g} = \varphi \\ \frac{\partial \lambda_{HFM}}{\partial \Delta \lambda_E} &= \frac{\partial \lambda_{HFM}}{\partial \Delta \lambda_O} = \lambda_{HFM} \end{aligned}$$

5.2.2 Guarded Hot Plate

A similar procedure was performed in case of GHP measurements.

In this case, the thermal conductivity value is given by Eq. (30), as explained in § 4.1.1 *Guarded Hot Plate - GHP*, hereinafter re-written (double specimen apparatus):

$$\lambda_{GHP} = \frac{\Phi \cdot t}{2 \cdot A_m \cdot \Delta \vartheta} \quad (30)$$

For different exemplary types of equipment, the standard EN 1946-2:1999 [149] provides maximum probable errors for each of the parameters. Again, the main difference between the various experimental devices is the size of the metering area: 150² mm² (equipment A), 250² mm² (equipment B) and 500² mm² (equipment C). Moreover, to consider also the influence of the apparatus geometrical aspects and general quality on the measurement uncertainty, the standard proposes three additional uncertainty contributions:

- $\Delta \lambda_{R,E}$ imbalance and edge heat loss [-];
- $\Delta \lambda_O$ imperfect contact [-];
- $\Delta \lambda_S$ asymmetrical conditions [-].

These parameters can be included in the formula of thermal conductivity by adding them as factors of 1.0 and with a defined relative error in the calculation.

Considering also these parameters, the thermal conductivity equation is then extended:

$$\lambda_{GHP} = \frac{\Phi \cdot t}{2 \cdot A_m \cdot \Delta\vartheta} \cdot \Delta\lambda_{R,E} \cdot \Delta\lambda_O \cdot \Delta\lambda_S \quad (69)$$

The thermal conductivity uncertainty is calculated through the combined standard uncertainty, applied to Eq. (69):

$$u_c(\lambda_{GHP}) = \sqrt{\left(\frac{\partial\lambda_{GHP}}{\partial\Phi} \cdot u(\Phi) \right)^2 + \left(\frac{\partial\lambda_{GHP}}{\partial t} \cdot u(t) \right)^2 + \left(\frac{\partial\lambda_{GHP}}{\partial A_m} \cdot u(A_m) \right)^2 + \left(\frac{\partial\lambda_{GHP}}{\partial\Delta\vartheta} \cdot u(\Delta\vartheta) \right)^2 + \left(\frac{\partial\lambda_{GHP}}{\partial\Delta\lambda_{R,E}} \cdot u(\Delta\lambda_{R,E}) \right)^2 + \left(\frac{\partial\lambda_{GHP}}{\partial\Delta\lambda_O} \cdot u(\Delta\lambda_O) \right)^2 + \left(\frac{\partial\lambda_{GHP}}{\partial\Delta\lambda_S} \cdot u(\Delta\lambda_S) \right)^2} \quad (70)$$

A more detailed procedure can be followed if the measurement outputs also provide the values of voltage U [V] and current I [A], and the geometrical characteristics of the measuring plate are available (providing the gap correction factor C_j [-], defined by Eq. (71))

$$C_j = 1 + \frac{1}{2} \cdot \frac{A_{SP}}{A_m} \cdot \frac{\lambda_{SP}}{\lambda_m} \quad (71)$$

Where: A_{SP} is the gap surface [m²];

λ_{SP} is the thermal conductivity of the gap [W/mK];

A_m is the surface of the metering area [m²];

λ_m is the thermal conductivity of the metering area [W/mK].

Usually $\lambda_{SP} = \lambda_m$ and therefore this member is equal to 1.

In this case, the equation for the λ_{GHP} calculation becomes:

$$\lambda_{GHP} = \frac{U \cdot I \cdot t}{2 \cdot A_m \cdot \Delta\vartheta \cdot C_j} \cdot \Delta\lambda_{R,E} \cdot \Delta\lambda_O \cdot \Delta\lambda_S \quad (72)$$

Consequently the uncertainty $u_c(\lambda_{GHP})$ can be calculated through:

$$u_c(\lambda_{GHP}) = \sqrt{\left(\frac{\partial\lambda_{GHP}}{\partial U} \cdot u(U)\right)^2 + \left(\frac{\partial\lambda_{GHP}}{\partial I} \cdot u(I)\right)^2 + \left(\frac{\partial\lambda_{GHP}}{\partial t} \cdot u(t)\right)^2 + \left(\frac{\partial\lambda_{GHP}}{\partial A_m} \cdot u(A_m)\right)^2 + \left(\frac{\partial\lambda_{GHP}}{\partial \Delta\vartheta} \cdot u(\Delta\vartheta)\right)^2 + \left(\frac{\partial\lambda_{GHP}}{\partial C_j} \cdot u(C_j)\right)^2 + \left(\frac{\partial\lambda_{GHP}}{\partial \Delta\lambda_{R,E}} \cdot u(\Delta\lambda_{R,E})\right)^2 + \left(\frac{\partial\lambda_{GHP}}{\partial \Delta\lambda_O} \cdot u(\Delta\lambda_O)\right)^2 + \left(\frac{\partial\lambda_{GHP}}{\partial \Delta\lambda_S} \cdot u(\Delta\lambda_S)\right)^2} \quad (73)$$

All the different sensitivity coefficients (partial derivatives) are:

$$\begin{aligned} \frac{\partial\lambda_{GHP}}{\partial\Phi} &= \frac{t}{2 \cdot A_m \cdot \Delta\vartheta} \\ \frac{\partial\lambda_{GHP}}{\partial t} &= \frac{\Phi}{2 \cdot A_m \cdot \Delta\vartheta} = \frac{U \cdot I}{2 \cdot A_m \cdot \Delta\vartheta \cdot C_j} \\ \frac{\partial\lambda_{GHP}}{\partial A_m} &= -\frac{1}{A_m^2} \cdot \frac{\Phi \cdot t}{2 \cdot \Delta\vartheta} = -\frac{1}{A_m^2} \cdot \frac{U \cdot I \cdot t}{2 \cdot \Delta\vartheta \cdot C_j} \\ \frac{\partial\lambda_{GHP}}{\partial \Delta\vartheta} &= -\frac{1}{\Delta\vartheta^2} \cdot \frac{\Phi \cdot t}{2 \cdot A_m} = -\frac{1}{\Delta\vartheta^2} \cdot \frac{U \cdot I \cdot t}{2 \cdot A_m \cdot C_j} \\ \frac{\partial\lambda_{GHP}}{\partial U} &= \frac{I \cdot t}{2 \cdot A_m \cdot \Delta\vartheta \cdot C_j} \\ \frac{\partial\lambda_{GHP}}{\partial I} &= \frac{U \cdot t}{2 \cdot A_m \cdot \Delta\vartheta \cdot C_j} \\ \frac{\partial\lambda_{GHP}}{\partial C_j} &= -\frac{1}{C_j^2} \cdot \frac{U \cdot I \cdot t}{2 \cdot A_m \cdot \Delta\vartheta} \\ \frac{\partial\lambda_{GHP}}{\partial \Delta\lambda_{R,E}} &= \frac{\partial\lambda_{GHP}}{\partial \Delta\lambda_O} = \frac{\partial\lambda_{GHP}}{\partial \Delta\lambda_S} = \lambda_{GHP} \end{aligned}$$

5.3 Linear thermal transmittance

Thermal bridging effects are, as already announced, one of the most critical aspects regarding the application of VIPs. It's not only essential to quantify their entity (through the evaluation of the linear thermal transmittance ψ) but also to define the reliability of the measurement procedure, and consequently its uncertainty.

An experimental campaign was performed, on two kind of VIPs (Fumed Silica core – FS, and Fiber Glass core – FG), with different thicknesses (20 and 40 mm in case of FS VIPs, or 20 and 30 mm for FG VIPs), by means of three different apparatuses (two double symmetrical GHPs and one double symmetrical HFM), see **Table 14**. The aim was to measure the COP thermal conductivity, the equivalent thermal conductivity of two joined panels and the correspondent linear thermal transmittance of the joint. **Table 14** also shows the several VIPs joints tested, and the thermocouples position for each experimental device. This investigation was performed during the internship at FIW - Forschungsinstitut für Wärmeschutz e.V. (München), so the measurements were carried out using their apparatuses and measuring procedures.


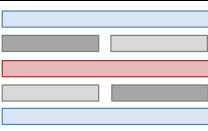
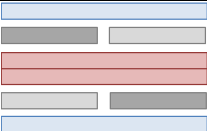
Table 14: Adopted apparatuses, joints configurations and thermocouples positions

VIP typology	λ_{COP} [W/mK]	ψ [W/mK]		
		GHP - 2	GHP - 2	HFM - 2
FS	Joint configurations	<i>Commutated</i>		<i>Commutated</i>
				<i>Offset</i>
				<i>Gasket strip</i>
FG	GHP - 3	GHP - 2	HFM - 2	
Joint configurations	<i>Commutated</i>		<i>Commutated</i>	
			<i>Gasket strip</i>	
Thermocouples position				
COP: centre of panel area		COP SA J SA COP	COP SA J SA COP	
SA: slightly affected area				
J: joint area				

The main difference between the two GHP apparatuses is the dimension of the plates and consequently of the measuring surfaces: **Table 15** provides the equipments useful dimensions and configurations.

The investigation was performed at an average temperature of the specimen equal to 10 °C in case of FS based VIPs, and in case of FG based VIPs equal to 10 and 23 °C. The temperature difference between the plates was continuously kept around 15 °C. The uncertainty analyses were type B for GHP measurements, and both Type B and Type A for HFM. Since all the apparatuses were double specimens and symmetrical, the following described procedure was repeated twice and then averaged (the uncertainty of the average was then evaluated through the combined uncertainty method).

Table 15: Apparatuses geometrical properties and configuration

			GHP - 2	GHP - 3	HFM - 2
Plate	l_1	$[m]$	0.8000	0.4000	0.8000
	l_2	$[m]$	0.8000	0.4000	0.8000
	A	$[m^2]$	0.6400	0.1600	0.6400
Measuring area	a_m	$[m]$	0.4983	0.2002	0.5008
	b_m	$[m]$	0.4983	0.2002	0.5008
	A_m	$[m^2]$	0.2483	0.0401	0.2508
Measuring area + gap	a_{SP+m}	$[m]$	0.5011	0.2161	-
	b_{SP+m}	$[m]$	0.5011	0.2161	-
	A_{SP+m}	$[m^2]$	0.2511	0.0467	-
Gap	A_{SP}	$[m^2]$	0.0028	0.0066	-
Apparatus configuration					

5.3.1 Heat Flow Meter

In case of HFM measurements, the uncertainty of ψ was assessed with both Type A and Type B criteria. The HFM apparatus was symmetrical double specimens, but only the cold sides were considered, because of a calibration problem on the warm plates.

The evaluation of the linear thermal transmittance was already discussed in § 3.2 VIPs thermal performance parameters. Eq. (22) can be re-written as:

$$\psi = \frac{A_m}{t \cdot l_\psi} \cdot (\lambda_{eq} - \lambda_{COP}) \quad (74)$$

The COP measurements were always performed using the GHP-3 or GHP-4 apparatus (Eq. (72)), while the λ_{eq} can be evaluated through Eq. (67). Since the average thickness (t_m) of the specimens for both GHP and HFM apparatuses (it was externally measured using a digital calliper), the extended equation of ψ_{HFM} was considered:

$$\psi_{HFM} = \frac{A_m}{t_m \cdot l_\psi} \cdot \left(\left[\frac{t_m \cdot f_{cal}(\vartheta) \cdot Q}{\Delta \vartheta_m} \cdot \Delta \lambda_E \cdot \Delta \lambda_O \right]_{eq_HFM} - \left[\frac{U \cdot I \cdot t_m}{2 \cdot A_m \cdot \Delta \vartheta_m \cdot C_j} \cdot \Delta \lambda_{R,E} \cdot \Delta \lambda_O \cdot \Delta \lambda_S \right]_{COP_avg} \right) \quad (75)$$

Since the values of λ_{COP} were assessed by means of a double specimen GHP, the obtained results are an average of two samples (λ_{COP_avg}).

The combined standard uncertainty was indeed evaluated through the square root of:

$$\begin{aligned} u_c^2(\psi_{HFM}) = & \left(\frac{\partial \psi_{HFM}}{\partial A_{m_HFM}} \cdot u(A_{m_HFM}) \right)^2 + \left(\frac{\partial \psi_{HFM}}{\partial t_m} \cdot u(t_m) \right)^2 + \left(\frac{\partial \psi_{HFM}}{\partial l_\psi} \cdot \right. \\ & u(l_\psi) \left. \right)^2 + \left[\left(\frac{\partial \psi_{HFM}}{\partial f_{cal}(\vartheta)} \cdot u(f_{cal}(\vartheta)) \right)^2 + \left(\frac{\partial \psi_{HFM}}{\partial Q} \cdot u(Q) \right)^2 + \left(\frac{\partial \psi_{HFM}}{\partial \Delta \vartheta_m} \cdot \right. \right. \\ & u(\Delta \vartheta_m) \left. \right)^2 + \left(\frac{\partial \psi_{HFM}}{\partial \Delta \lambda_E} \cdot u(\Delta \lambda_E) \right)^2 + \left(\frac{\partial \psi_{HFM}}{\partial \Delta \lambda_O} \cdot u(\Delta \lambda_O) \right)^2 \left. \right]_{eq} + \left[\left(\frac{\partial \psi_{HFM}}{\partial U} \cdot \right. \right. \\ & u(U) \left. \right)^2 + \left(\frac{\partial \psi_{HFM}}{\partial I} \cdot u(I) \right)^2 + \\ & + \left(\frac{\partial \psi_{HFM}}{\partial A_m} \cdot u(A_m) \right)^2 + \left(\frac{\partial \psi_{HFM}}{\partial \Delta \vartheta_m} \cdot u(\Delta \vartheta_m) \right)^2 + \left(\frac{\partial \psi_{HFM}}{\partial C_j} \cdot u(C_j) \right)^2 + \left(\frac{\partial \psi_{HFM}}{\partial \Delta \lambda_{R,E}} \cdot \right. \\ & u(\Delta \lambda_{R,E}) \left. \right)^2 + \left(\frac{\partial \psi_{HFM}}{\partial \Delta \lambda_O} \cdot u(\Delta \lambda_O) \right)^2 + \left(\frac{\partial \psi_{HFM}}{\partial \Delta \lambda_S} \cdot u(\Delta \lambda_S) \right)^2 \left. \right]_{COP} \quad (76) \end{aligned}$$

5.3.2 Guarded Hot Plate

In case of GHP measurements, the ψ uncertainty was assessed with only Type B criteria. The GHP apparatuses were both symmetrical double specimens. Therefore both λ_{COP} and λ_{eq} can be evaluated through Eq. (72).

The linear thermal transmittance was indeed obtained by the extension Eq. (74):

$$\psi_{GHP} = \frac{A_m}{t_m \cdot l_\psi} \cdot \left(\left[\frac{U \cdot I \cdot t_m}{2 \cdot A_m \cdot \Delta \vartheta_m \cdot C_j} \cdot \Delta \lambda_{R,E} \cdot \Delta \lambda_O \cdot \Delta \lambda_S \right]_{eq_GHP} - \left[\frac{U \cdot I \cdot t_m}{2 \cdot A_m \cdot \Delta \vartheta_m \cdot C_j} \cdot \Delta \lambda_{R,E} \cdot \Delta \lambda_O \cdot \Delta \lambda_S \right]_{COP_avg} \right) \quad (77)$$

The linear thermal transmittance uncertainty was then calculated through the combined standard uncertainty, applied to Eq. (77).

$$\begin{aligned} u_c^2(\psi_{GHP}) = & \left(\frac{\partial \psi_{GHP}}{\partial t_m} \cdot u(t_m) \right)^2 + \left(\frac{\partial \psi_{GHP}}{\partial l_\psi} \cdot u(l_\psi) \right)^2 + \left[\left(\frac{\partial \psi_{GHP}}{\partial U} \cdot u(U) \right)^2 + \right. \\ & + \left(\frac{\partial \psi_{GHP}}{\partial I} \cdot u(I) \right)^2 + \left(\frac{\partial \psi_{GHP}}{\partial A_m} \cdot u(A_m) \right)^2 + \left(\frac{\partial \psi_{GHP}}{\partial \Delta \vartheta_m} \cdot u(\Delta \vartheta_m) \right)^2 + \left(\frac{\partial \psi_{GHP}}{\partial C_j} \cdot \right. \\ & \left. u(C_j) \right)^2 + \left(\frac{\partial \psi_{GHP}}{\partial \Delta \lambda_{R,E}} \cdot u(\Delta \lambda_{R,E}) \right)^2 + \left(\frac{\partial \psi_{GHP}}{\partial \Delta \lambda_O} \cdot u(\Delta \lambda_O) \right)^2 + \left(\frac{\partial \psi_{GHP}}{\partial \Delta \lambda_S} \cdot \right. \\ & \left. u(\Delta \lambda_S) \right)^2 \Big]_{eq} + \left[\left(\frac{\partial \psi_{GHP}}{\partial U} \cdot u(U) \right)^2 + \left(\frac{\partial \psi_{GHP}}{\partial I} \cdot u(I) \right)^2 + \left(\frac{\partial \psi_{GHP}}{\partial A_m} \cdot u(A_m) \right)^2 + \right. \\ & + \left(\frac{\partial \psi_{GHP}}{\partial \Delta \vartheta_m} \cdot u(\Delta \vartheta_m) \right)^2 + \left(\frac{\partial \psi_{GHP}}{\partial C_j} \cdot u(C_j) \right)^2 + \left(\frac{\partial \psi_{GHP}}{\partial \Delta \lambda_{R,E}} \cdot u(\Delta \lambda_{R,E}) \right)^2 + \left(\frac{\partial \psi_{GHP}}{\partial \Delta \lambda_O} \cdot \right. \\ & \left. u(\Delta \lambda_O) \right)^2 + \left. \left(\frac{\partial \psi_{GHP}}{\partial \Delta \lambda_S} \cdot u(\Delta \lambda_S) \right)^2 \right]_{COP} \quad (78) \end{aligned}$$

The previous equation is useful in case of FS VIP, for which the apparatus used for the assessment of the COP thermal behaviour and the linear thermal transmittance is the same. In case of FG VIP, Eq. (78) can be simplified by directly using the value of λ_{COP} and its previously evaluated uncertainty:

$$\begin{aligned} u_c^2(\psi_{GHP}) = & \left(\frac{\partial \psi_{GHP}}{\partial t_m} \cdot u(t_m) \right)^2 + \left(\frac{\partial \psi_{GHP}}{\partial l_\psi} \cdot u(l_\psi) \right)^2 + \left[\left(\frac{\partial \psi_{GHP}}{\partial U} \cdot u(U) \right)^2 + \right. \\ & + \left(\frac{\partial \psi_{GHP}}{\partial I} \cdot u(I) \right)^2 + \left(\frac{\partial \psi_{GHP}}{\partial A_m} \cdot u(A_m) \right)^2 + \left(\frac{\partial \psi_{GHP}}{\partial \Delta \vartheta_m} \cdot u(\Delta \vartheta_m) \right)^2 + \left(\frac{\partial \psi_{GHP}}{\partial C_j} \cdot \right. \end{aligned} \quad (79)$$

$$\begin{aligned}
 & u(C_j)^2 + \left(\frac{\partial \psi_{GHP}}{\partial \Delta \lambda_{R,E}} \cdot u(\Delta \lambda_{R,E}) \right)^2 + \left(\frac{\partial \psi_{GHP}}{\partial \Delta \lambda_O} \cdot u(\Delta \lambda_O) \right)^2 + \left(\frac{\partial \psi_{GHP}}{\partial \Delta \lambda_S} \cdot \right. \\
 & \quad \left. u(\Delta \lambda_S) \right)^2 \Big]_{eq} + \left(\frac{\partial \psi_{GHP}}{\partial \lambda_{COP}} \cdot u(\lambda_{COP}) \right)^2
 \end{aligned}$$

Chapter 6

Theoretical standard-based measurement uncertainty analysis

Experimental uncertainty always refers to a specific measurement gauge and will vary from lab to lab. But in case of Type B uncertainty evaluation this difference can be neglected, if the same information is used for the uncertainty assessment (e.g. declarations of the measuring apparatus producer, data provided by standards, and so on)

Currently, there are several standards related to the thermal conductivity measurements, containing the information required for a Type B uncertainty assessment (such as maximum probable relative errors and apparatus limitations). To achieve general conclusions about the applicability of these standards for the characterisation of SIMs, a theoretical study was performed in case of HFM apparatus, considering standard reference uncertainties obtained from EN 1946-3:1999 [148]. This standard contains technical criteria about minimum requirements on measurement uncertainty for the experimental assessment of thermal conductivities, in accordance with EN 12667:2001 [12] and EN 12664:2001 [121].

In this way, a theoretical and standard-based analysis of SIMs measurement uncertainty was obtained.

A similar investigation was performed by FIW - Forschungsinstitut für Wärmeschutz e.V. (München) on the GHP approach, with few secondary

contributions from the author. For this reason, only the main results of this investigation will be presented, so as to provide some general and comprehensive conclusions to the standard-based theoretical uncertainty analysis.

The approach and results are part of the IEA EBC Annex 65 project [150].

The performed sensitivity analyses assume uncertainties for the measurands according to the standards EN 1946-3:1999 [148] and EN 1946-2:1999 [149]. Therefore the recommendations and conclusions are based on theoretical assumptions and may be strongly affected, in practical applications, by the variation of the equipment specific uncertainties, and the adoption of conventional methods of lab-handling.

6.1 Heat Flow Meter approach

To check if the thermal properties of SIMs can be adequately evaluated by means of the HFM, a sensitivity analysis was performed, in accordance with the standard EN 1946-3:1999 [148]. This standard identifies three different types of equipment, among which the main difference is the size of the metering area: 150^2 mm² (equipment A), 200^2 mm² (equipment B) and 300^2 mm² (equipment C).

For each equipment typology, the standard EN 1946-3:1999 [148] provides the maximum probable relative errors (**Table 16**).

Table 16: HFM - Maximum probable relative errors $u(x_i)$ of equipment A, B and C [148]

Relative errors	Abbr.	Unit	A	B	C
Edge heat loss	$u(\lambda_E)$	[%]	0.5	0.5	0.5
Imperfect contact	$u(\lambda_O)$	[%]	0.5	0.5	0.5
Specimen thickness	$u(t)$	[%]	0.5	0.5	0.5
Temperature difference	$u(\Delta\theta)$	[%]	1.0	1.0	1.0
Calibration accuracy of the specimen	$u(\Delta\lambda_K)$	[%]	1.5	1.5	1.5
Maximum permissible non-linearity of the calibration	$u(\Delta\lambda_L)$	[%]	1.0	1.0	1.0
Maximum permissible calibrating drift	$u(\Delta\lambda_q)$	[%]	1.0	1.0	1.0

Limitations to the measurable thickness and thermal conductivity are specified. The minimum and maximum specimen thicknesses are connected to the gap width between the guard ring and the metering area, and it will influence especially the errors referred to the edge heat loss, the thickness determination and the electrical power.

Table 17: HFM - Overall size and limitations of specimen thickness and range of thermal conductivity of equipment A, B and C [148]

Equipment specifications	Abbr.	Unit	A	B	C
Overall apparatus size	A_{tot}	$[mm^2]$	300 ²	500 ²	600 ²
Metering section width	A_m	$[mm^2]$	150 ²	200 ²	300 ²
Min. specimen thickness	t_{min}	$[mm]$	15	25	30
Max. specimen thickness	t_{max}	$[mm]$	50	140	100
Min. thermal conductivity	$\lambda_{\text{HFM-min}}$	$[W/mK]$	0.015	0.015	0.015
Max. thermal conductivity	$\lambda_{\text{HFM-max}}$	$[W/mK]$	0.4	0.4	0.4
Minimum temperature difference through the specimen	$\Delta\vartheta_{\text{min}}$	$[K]$	300	500	600

Commercially available measurement equipment for determination of thermal conductivity typically will meet the values in the standard (EN 1946-3:1999 [148] in the HFM specific case). Considering a constant error for one parameter, the relative error of this parameter will increase with the decrease of the observed values. For the measuring of SIMs, much lower values of thermal conductivity are likely to occur, going down to less than 0.002 W/mK (Fibre Glass VIP). Therefore it is questionable how the combined uncertainty of thermal conductivity $u_c(\lambda_{\text{HFM}})$ will develop, decreasing the thermal conductivity and varying the thickness of the specimen.

The absolute errors of all necessary parameters were quantified by applying the maximum relative errors according to the standard on a defined set of data. Since the relative errors are maximum relative errors, the set of data must be composed of the minimum thickness and the minimum thermal conductivity, according to the specifications in equipment A, B and C, in order to obtain the absolute minimum error.

Table 18: HFM - Set of data for the calculation of the $u_c(\lambda_{\text{HFM}})$, equipment A, B and C

Set of data	Abbr.	Unit	A	B	C
Min. thermal conductivity	$\lambda_{\text{HFM-min}}$	$[W/mK]$	0.015	0.015	0.015
Heat flux	φ	$[W/m^2]$	3.0	1.1	1.5
Min. specimen thickness	t_{min}	$[m]$	0.015	0.025	0.03
Temperature difference	$\Delta\vartheta$	$[K]$	10	10	10

The absolute errors necessary for the subsequent combined uncertainty evaluation (Table 19) were obtained applying the maximum probable relative errors (Table 16) to the defined set of data (Table 18), and were kept constant for all the sensitivity analysis.

Table 19: HFM - Absolute errors for the calculation of the $u_c(\lambda_{HFM})$, equipment A, B and C [148]

Absolute errors for calculation	Abbr.	Unit	A	B	C
Edge heat loss	$u(\Delta\lambda_E)$	$[W/mK]$	0.000075	0.000075	0.000075
Imperfect contact	$u(\Delta\lambda_O)$	$[W/mK]$	0.000075	0.000075	0.000075
Specimen thickness	$u(t)$	$[m]$	0.000075	0.000125	0.00015
Temperature difference	$u(\Delta\theta)$	$[K]$	0.1	0.1	0.1
Calibration accuracy of the specimen	$u(\Delta\lambda_K)$	$[W/m^2]$	0.045	0.016	0.023
Maximum permissible non-linearity of the calibration	$u(\Delta\lambda_L)$	$[W/m^2]$	0.03	0.01	0.02
Maximum permissible calibrating drift	$u(\Delta\lambda_q)$	$[W/m^2]$	0.03	0.01	0.02

6.1.1 HFM sensitivity analysis

As explained before, the relative uncertainty of thermal conductivity is influenced by the uncertainty of the involved measurand and the differential quotients, as well as by the level of thermal conductivity. Reducing the value of the measurand, the uncertainty and the relative errors will increase.

In order to check if the thermal properties of SIMs can be properly evaluated by means of the HFM, a sensitivity analysis was performed. Equipment A, B and C, proposed by EN 1946-3:1999 [148] were analysed, considering several values of thermal conductivity, representing the ones of FG based VIP (0.002 W/mK), FS core VIP (0.004 W/mK), aged VIP (0.008 W/mK) and APM (0.016 W/mK - 0.020 W/mK). 0.02 W/mK also represents a common maximum limit of SIMs thermal conductivity: for this reason, no higher values were taken into account. More detailed results of this investigation are presented in Appendix A.

6.1.1.1 Effects of thickness and temperature difference on the combined uncertainty

The heat flux through the specimens during an HFM test is sensibly lower in case of SIMs if compared to traditional insulating materials: the lower is the heat flux, the highest must be the sensitivity of the adopted Heat Flux Meter. The temperature difference between the HFM plates during the tests and the sample thickness (which defines its thermal resistance) are the two main factors that influenced the heat flux through the sample.

For this reason a sensitivity analysis was performed, in order to evaluate the effects on the combined measurement uncertainty $u_c(\lambda)$, varying four different specimen thicknesses (0.01, 0.02, 0.04 and 0.08 m) and four distinct temperature

differences (5, 10, 15 and 20 K or °C), considering the same sample thermal conductivity range mentioned before (between 0.002 and 0.02 W/m K).

The most relevant results of this investigation are summarised in **Table 20**, **Table 21** and **Table 22**, referred to the equipment A, B and C respectively (while the related graphs are reported in Appendix A).

Table 20: Combined uncertainty $u_c(\lambda)$ in % as a function of λ (equal to 0.002, 0.002, 0.008 and 0.020 W/mK), varying temperature difference $\Delta\vartheta$ and with constant thickness t , assuming the maximum uncertainty according to EN 1946-3:1999 [148]; equipment A

Thickness [m]	λ [W/mK]	$\Delta\vartheta$ [°C]			
		5	10	15	20
0.01	0.002	6.58	3.41	2.40	1.92
	0.004	3.82	2.11	1.60	1.38
	0.008	2.73	1.63	1.33	1.21
	0.016	2.38	1.49	1.25	1.16
	0.020	2.33	1.47	1.24	1.16
0.02	0.002	12.56	6.32	4.25	3.23
	0.004	6.55	3.35	2.31	1.81
	0.008	3.77	2.01	1.47	1.22
	0.016	2.65	1.50	1.16	1.02
	0.020	2.48	1.42	1.12	0.99
0.04	0.002	24.83	12.43	8.31	6.25
	0.004	12.55	6.31	4.24	3.22
	0.008	6.54	3.33	2.29	1.78
	0.016	3.75	1.98	1.43	1.18
	0.020	3.26	1.75	1.29	1.08
0.08	0.002	49.52	24.77	16.52	12.40
	0.004	24.83	12.43	8.30	6.25
	0.008	12.55	6.31	4.24	3.21
	0.016	6.54	3.33	2.28	1.77
	0.020	5.38	2.76	1.92	1.51

From this table, the general trend of uncertainties is. They increase with the increase of the thickness, and the decreasing of both temperature difference and thermal conductivity. Moreover, it's possible to define for each panel thickness the minimum testing temperature difference, to reach a defined uncertainty value. The EN 12667:2001 standard [12] defines equal to 3 % the expected value of HFM uncertainty (while for the GHP apparatus this value is 2 %). The light grey highlighted values in the table define the minimum temperature difference (between those analysed) that guarantees $u_c(\lambda) < 3$ %, while the dark grey values

correspond to the minimum $\Delta\vartheta$ to obtain $u_c(\lambda) < 2\%$ (to have the same reliability of GHP method). For example, a 20 mm thick FS based VIP ($\lambda = 0.004$ W/mK) needs a $\Delta\vartheta_{min} = 15$ °C to obtain a $u_c(\lambda) < 3\%$, and a $\Delta\vartheta_{min} = 20$ °C to obtain a $u_c(\lambda) < 2\%$. On the contrary, an FG VIP ($\lambda = 0.002$ W/mK) with the same thickness needs a $\Delta\vartheta_{min} = 20$ °C for both 3% and 2% of uncertainty.

As already mentioned, the same analysis was also performed on equipment B (Table 21).

Table 21: Combined uncertainty $u_c(\lambda)$ in % as a function of λ (equal to 0.002, 0.002, 0.008 and 0.020 W/mK), varying temperature difference $\Delta\vartheta$ and with constant thickness t , assuming the maximum uncertainty according to EN 1946-3:1999 [148]; equipment B

Thickness [m]	λ [W/mK]	$\Delta\vartheta$ [K]			
		5	10	15	20
0.01	0.002	3.35	2.09	1.75	1.62
	0.004	2.71	1.84	1.63	1.55
	0.008	2.53	1.77	1.59	1.53
	0.016	2.48	1.76	1.59	1.52
	0.020	2.47	1.75	1.59	1.52
0.02	0.002	5.05	2.65	1.90	1.56
	0.004	3.17	1.78	1.38	1.21
	0.008	2.49	1.49	1.22	1.10
	0.016	2.28	1.40	1.17	1.08
	0.020	2.26	1.39	1.17	1.07
0.04	0.002	9.32	4.71	3.19	2.45
	0.004	5.02	2.60	1.82	1.46
	0.008	3.12	1.70	1.27	1.08
	0.016	2.43	1.39	1.09	0.96
	0.020	2.33	1.34	1.06	0.95
0.08	0.002	18.27	9.15	6.13	4.62
	0.004	9.32	4.70	3.18	2.43
	0.008	5.01	2.58	1.80	1.44
	0.016	3.11	1.68	1.24	1.05
	0.020	2.80	1.53	1.16	0.99

In this case, a 20 mm thick FS based VIP needs a $\Delta\vartheta_{min} = 10$ °C to obtain a $u_c(\lambda)$ lower than 3% (and also 2%), while an FG based VIP with the same thickness needs a $\Delta\vartheta_{min} = 10$ °C for 3% of uncertainty and $\Delta\vartheta_{min} = 15$ °C for 2%.

For equipment C, the same FS based VIP needs a $\Delta\vartheta_{min} = 10$ °C or 15 °C to obtain a $u_c(\lambda)$ lower than 3 % and 2 % respectively, while the same VIP but with FG core needs a $\Delta\vartheta_{min} = 15$ °C for 3% of uncertainty and $\Delta\vartheta_{min} = 20$ °C for 2%.

Table 22: Combined uncertainty $u_c(\lambda)$ in % as a function of λ (equal to 0.002, 0.002, 0.008 and 0.020 W/mK), varying temperature difference $\Delta\vartheta$ and with constant thickness t , assuming the maximum uncertainty according to EN 1946-3:1999 [148]; equipment C

Thickness [m]	λ [W/mK]	$\Delta\vartheta$ [K]			
		5	10	15	20
0.01	0.002	4.04	2.48	2.06	1.90
	0.004	3.02	2.09	1.86	1.77
	0.008	2.71	1.97	1.81	1.74
	0.016	2.63	1.95	1.79	1.73
	0.020	2.62	1.94	1.79	1.73
0.02	0.002	6.58	3.41	2.40	1.92
	0.004	3.82	2.11	1.60	1.38
	0.008	2.73	1.63	1.33	1.21
	0.016	2.38	1.49	1.25	1.16
	0.020	2.33	1.47	1.24	1.16
0.04	0.002	12.56	6.32	4.25	3.23
	0.004	6.55	3.35	2.31	1.81
	0.008	3.77	2.01	1.47	1.22
	0.016	2.65	1.50	1.16	1.02
	0.020	2.48	1.42	1.12	0.99
0.08	0.002	24.83	12.43	8.31	6.25
	0.004	12.55	6.31	4.24	3.22
	0.008	6.54	3.33	2.29	1.78
	0.016	3.75	1.98	1.43	1.18
	0.020	3.26	1.75	1.29	1.08

In case of HFM, the different equipment used strongly influences the obtainable uncertainty level: single-specimen symmetrical configuration, with higher maximum available thickness, represents the best solution.

After that, it's possible to observe that the measurement uncertainties of lower thermal conductivities are more influenced by the applied temperature difference. Increasing the thermal conductivity, the $u_c(\lambda)$ tends to similar values for each ΔT considered (except for $\Delta\vartheta = 5$ K, which is always characterised by higher uncertainty values, especially for thinner samples). Moreover, the thermal conductivity measurement uncertainty is often higher than the expected value proposed by the standard EN 12667:2001, equal to 3 % (Table 20).

Another way to show the combined effects of sample thickness and temperature difference on the uncertainty level is through the isolines curves, for each analysed thermal conductivity. As an example, only the results about apparatus B are shown (**Figure 52**), since this configuration is the most common between A, B and C. The thickness and temperature according to the definitions in EN 1946-3:1999 [148] for equipment B are shown by the greyed box (actually the maximum thickness is equal to 140 mm, but it was limited to 40 mm, because after this value all the isolines were parallel straight lines).

The spread between the curves is quite wide, but with temperature differences smaller than 10 K the distance between the isolines becomes smaller, and the same happens for a specimen thickness lower than 10 mm. The curves referred to uncertainty $u_c(\lambda) = 1\%$ are obtainable only in case of thermal conductivity higher than 0.008 W/mK, $\Delta\vartheta > 20$ K, and thickness higher than 0.02 m. The minimum observable $u_c(\lambda)$, in case of samples with λ equal to 0.004 W/mK and 0.002 W/mK, is equal to 1.5 %, with $\Delta\vartheta > 10$ K and $\Delta\vartheta \approx 20$ K respectively.

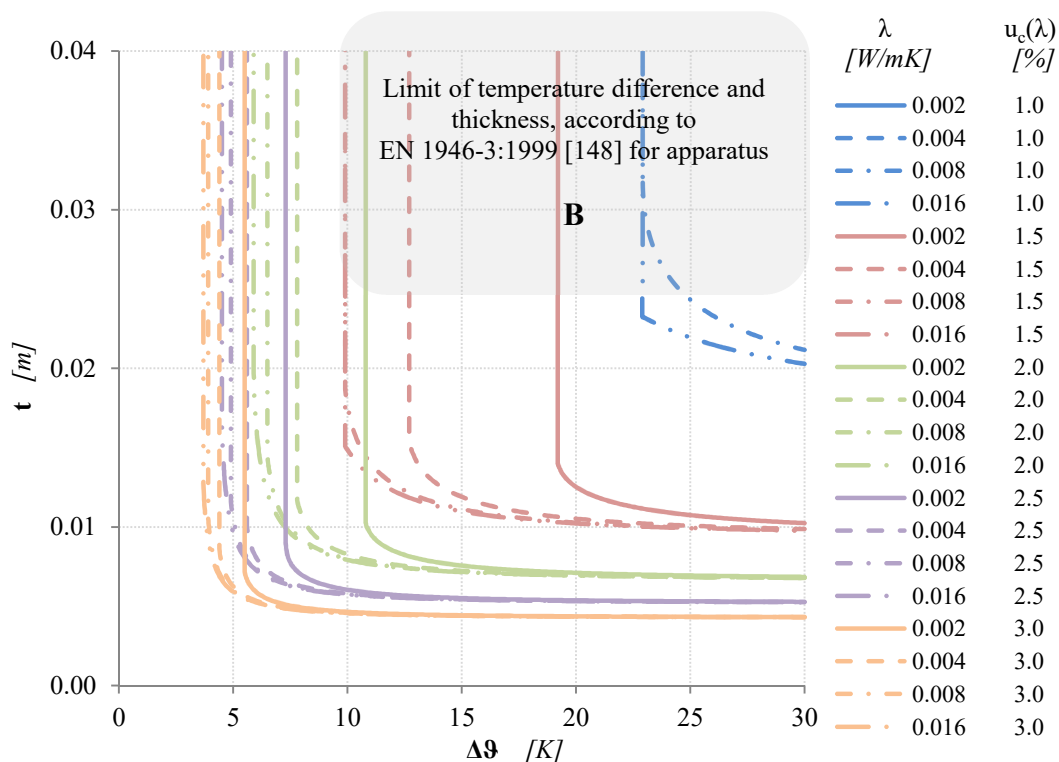


Figure 52: Uncertainty isolines ($u_c(\lambda)$) between 1.0 % and 3.0 % for different values of $\lambda = 0.004$ to 0.016 W/mK, as a function of the temperature difference $\Delta\vartheta$ and the thickness of the specimen t , assuming the maximum uncertainty according to EN 1946-3:1999 [148], equipment B [150]

Generally, considering a fixed thickness, high variations in temperature difference are necessary for their uncertainty reduction (especially for the lowest thermal conductivities and desired uncertainty value). Otherwise, for a defined value of $\Delta\vartheta$, a smaller variation in thickness is required for the uncertainty improvement. As mentioned before, thicker panels have higher values of uncertainty, especially for very low thermal conductivities (substantial reduction of the heat flux through the sample because of its high thermal resistance).

6.1.1.2 Sensitivity analysis of selected parameters

To identify the more influencing parameters involved in the measurement uncertainty budget, a sensitivity analysis was carried out. In case of HFM measurements, the quantities that have to be considered are: the temperature difference, the sample thickness and the heat flux through the specimens. For these parameters, variable errors were assumed. This investigation provides the variation of the $u_c(\lambda)$ as a function of the singles uncertainty contributions. Moreover, if one of the sensors uncertainties is not declared, this analysis clarifies how much this unknown could affect the final combined uncertainty.

In case of commercial measurement devices, the setpoint temperatures and consequently the temperature difference are usually the unique parameter that can be changed by users. This kind of survey allows estimating if the temperatures variation is enough to compensate the other parameters uncertainty increasing.

Figure 53 compares the modifications of $u_c(\lambda)$ isolines if one of the parameters heat flux (**Figure 53 b**)), thickness (**Figure 53 c**)) or temperature difference (**Figure 53 d**)) are increasing by a factor of two, compared to the $u_c(\lambda)$ obtained with the absolute uncertainties for all the parameters according to EN 1946-3:1999 [148] (**Figure 53 a**)).

As observable from **Figure 53 b**), the effects of a doubled value of heat flux uncertainty causes a right shifting and a broader spread of all the curves, compared to the standard case (**Figure 53 a**)), depending on the thermal conductivity and of the expected combined uncertainty. For instance, FG VIP could reach minimum values of uncertainty equal to 1.5% (in the considered range of $\Delta\vartheta < 30$ K) with a testing temperature difference higher than around 23 K (instead of approximately 14 K required in the standard case). Otherwise, for lower uncertainty expectancy or thermal conductivities higher than 0.002 W/mK, is possible to compensate the increase of the heat flux uncertainty by the rise of $\Delta\vartheta$.

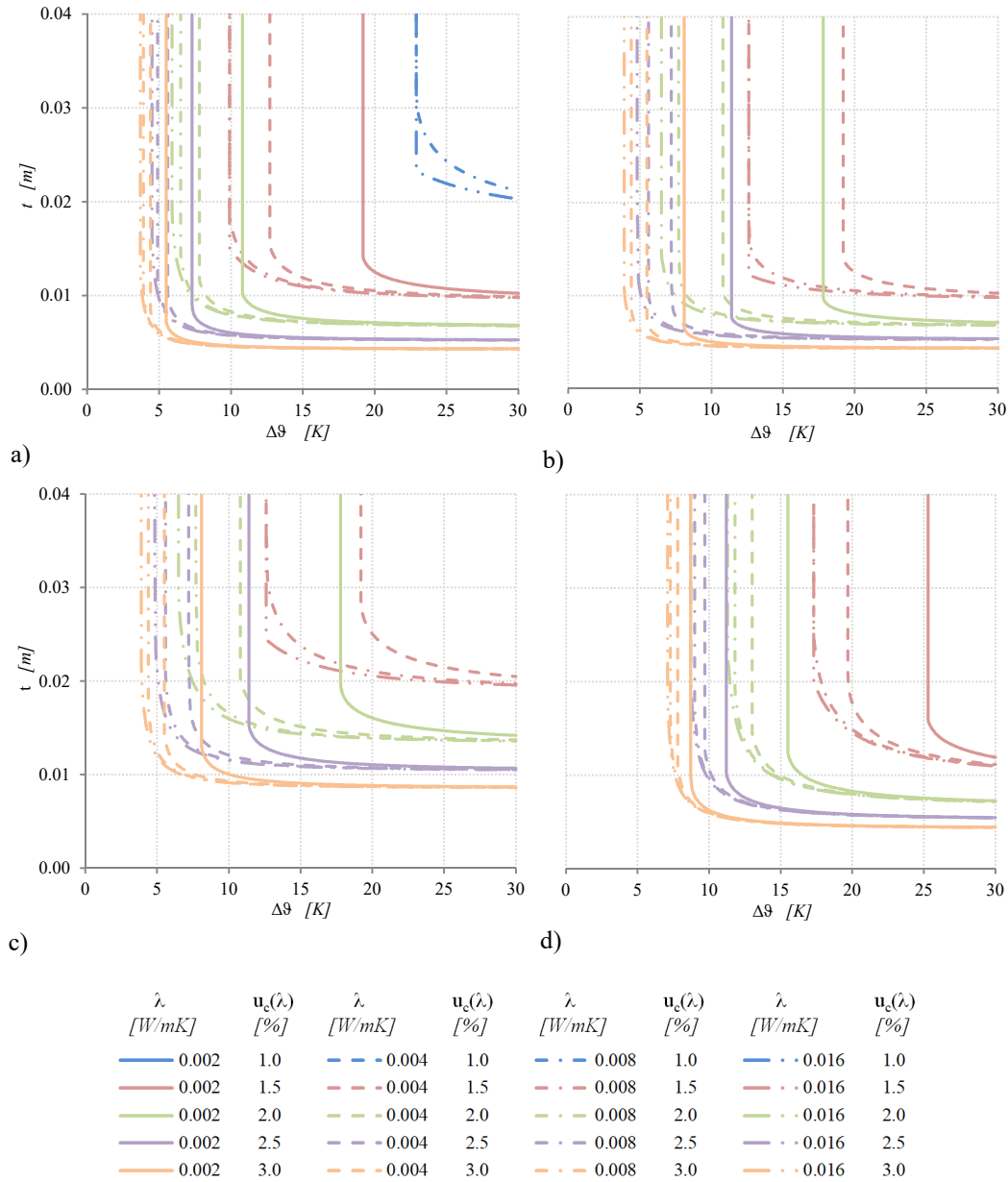


Figure 53: Uncertainty isolines ($u_c(\lambda)$ between 1.0 % and 3.0 %) for different values of $\lambda = 0.004$ to 0.016 W/mK, as a function of the temperature difference $\Delta\theta$ and the thickness of the specimen t , equipment B. a) assuming the maximum uncertainty according to EN 1946-3:1999 [148]; b) increasing the heat flux error by a factor 2; c) increasing the thickness error by a factor 2; d) multiplying the $\Delta\theta$ error by a factor 2 [150]

The increasing of the thickness determination uncertainty (**Figure 53 c)**) has the same effects of the heat flux increased uncertainty (right shifting and a more significant spread), but it also moves the isolines upwards. This effect is hard to

compensate with an increased temperature difference. For any values of $\Delta\vartheta$, 10 mm thick specimens could reach uncertainty values not lower than 3%, while $u_c(\lambda) = 1.5\%$ is available only for thicknesses higher than 20 mm (for each considered thermal conductivity).

The HFM method is less sensitive to a variation of temperature measurement uncertainty. Indeed, the doubling of the $\Delta\vartheta$ uncertainty causes a shorter right shifting of the curves if compared with the previous situations. The same $u_c(\lambda)$ level is still possible by merely increasing the temperature difference of around 5 - 7 K (except for $u_c(\lambda) = 1\%$, for which $\Delta\vartheta > 30$ K are required).

6.2 Guarded Hot Plate approach

As already mentioned, the same investigation was performed, mainly by the FIW institute, for the GHP apparatuses.

The maximum probable relative errors for each apparatus configuration, provided by the standard EN 1946-2:1999 [149], are summarised in **Table 23**:

Table 23: GHP - Maximum probable relative errors $u(x_i)$ of equipment A, B and C [149]

Relative errors	Abbr.	Unit	A	B	C
Imbalance and edge heat loss	$u(\Delta\lambda_{R,E})$	[%]	0.5	0.5	0.5
Imperfect contact	$u(\Delta\lambda_O)$	[%]	0.5	0.5	0.5
Non symmetrical condition	$u(\Delta\lambda_S)$	[%]	0.1	0.1	0.1
Electrical power	$u(\Phi)$	[%]	0.1	0.1	0.1
Specimen thickness	$u(t)$	[%]	0.5	0.5	0.5
Metering section	$u(A_m)$	[%]	0.37	0.34	0.26
Temperature difference	$u(\Delta\vartheta)$	[%]	1.0	1.0	1.0

To avoid the increasing of the total combined uncertainty, some limitations to the thickness and thermal conductivity ranges are specified (**Table 24**). The minimum and maximum thickness is connected to the gap width between the metering area and the guard ring and will influence especially the errors due to the edge heat loss, the thickness determination and the electrical power.

Table 24: GHP - Overall size and limitations of specimen thickness and range of thermal conductivity of equipment A, B and C [149]

Equipment specifications	Abbr.	Unit	A	B	C
Overall size	A_{tot}	$[mm^2]$	300^2	500^2	800^2
Metering section	A_m	$[mm^2]$	150^2	250^2	500^2
Min. gap width	$w_{g-\text{min}}$	$[mm]$	2	3	4
Min. specimen thickness	t_{min}	$[mm]$	20	30	40
Max. specimen thickness	t_{max}	$[mm]$	45	75	100
Min. therm. Conductivity	$\lambda_{\text{GHP-min}}$	$[W/mK]$	0.015	0.015	0.015
Max. therm. Conductivity	$\lambda_{\text{GHP-max}}$	$[W/mK]$	1.5	1.5	1.5

To investigate how the combined uncertainty of thermal conductivity $u_c(\lambda_{\text{GHP}})$ will develop, decreasing the thermal conductivity and varying the thickness of the specimen, the absolute errors were obtained by applying the maximum relative errors according to the standard [149] to a defined set of data. Since the relative errors are maximum relative errors, the set of data must be composed by the minimum thickness and the minimum thermal conductivity, according to the specifications in equipment A, B and C (Table 25). Applying the maximum probable relative errors (Table 23) to the defined set of data (Table 25), it is possible to obtain the absolute errors necessary for the subsequent combined uncertainty evaluation (Table 26).

Table 25: GHP - Set of data for the calculation of the $u_c(\lambda_{\text{GHP}})$, equipment A, B and C

Set of data	Abbr.	Unit	A	B	C
Min. thermal conductivity	$\lambda_{\text{GHP-min}}$	$[W/mK]$	0.015	0.015	0.015
Electrical power	Φ	$[W]$	0.15	0.25	0.75
Min. specimen thickness	t_{min}	$[m]$	0.02	0.03	0.04
Metering section	A_m	$[m^2]$	0.0225	0.0625	0.25
Temperature difference	$\Delta\theta$	$[K]$	10	10	10

Table 26: GHP - Absolute errors for the calculation of the $u_c(\lambda_{\text{GHP}})$, equipment A, B and C [149]

Absolute errors for calculation	Abbr.	Unit	A	B	C
Imbalance and edge heat loss	$u(\Delta\lambda_{\text{R,E}})$	$[W/mK]$	0.000075	0.000075	0.000075
Imperfect contact	$u(\Delta\lambda_{\text{O}})$	$[W/mK]$	0.000075	0.000075	0.000075
Non symmetrical condition	$u(\Delta\lambda_{\text{S}})$	$[W/mK]$	0.000015	0.000015	0.000015
Electrical power	$u(\Phi)$	$[W]$	0.00015	0.00025	0.00075
Specimen thickness	$u(t)$	$[m]$	0.0001	0.00015	0.0002
Metering section	$u(A_m)$	$[m^2]$	0.00008325	0.0002125	0.00065
Temperature difference	$u(\Delta\theta)$	$[K]$	0.10	0.10	0.10

6.2.1 GHP sensitivity analysis

The three types of equipment A, B and C, proposed by EN 1946-2:1999 [149] were analysed, considering the same thermal conductivity values of the HFM case: FG based VIP (0.002 W/mK), FS core VIP (0.004 W/mK), aged VIP (0.008 W/mK) and APM (0.016 W/mK - 0.020 W/mK). 0.02 W/m K also represents a common maximum limit of SIMs thermal conductivity: for this reason, no higher values were taken into account.

Only the main outputs of this investigation will be from now on presented.

6.2.1.1 *Effects of thickness and temperature difference on the combined uncertainty*

In case of GHP, the relative uncertainty for a defined temperature difference was found out to be not significantly affected by the decreasing values of thermal conductivity from 0.020 – 0.002 W/mK.

As a general trend, a big difference between the combined uncertainty values obtained with a $\Delta\vartheta$ equal to 5 and 10 K was observed for all the analysed configurations. A reduction of the temperatures causes a proportional decrease of the electrical power, and therefore the error of both parameters increases. Increasing the temperature difference to e.g. 15 K offers some potentials to significantly reduce the combined uncertainty $u_c(\lambda)$.

Another noticeable effect was the general increase of $u_c(\lambda)$ varying the equipment, from A to C. This behaviour seems surprising, as a larger measurement area leads to an increased electrical heating power, with consequent less relative uncertainty and also less uncertainty for the determination of the measurement area. Both these effects would decrease the relative uncertainty for the thermal conductivity, but they are overcompensated by the increase of the absolute uncertainty for the thickness determination. Indeed, the thickness absolute uncertainty of equipment A to C varies from $u(t) = 0.1$ mm for equipment A to $u(t) = 0.2$ mm for equipment C. This is plausible, as the variation of thickness gets higher for an increased metering area.

Moreover, increasing thickness of the specimen, the values of the relative uncertainty decreases for all the apparatus. This effect is especially pronounced for equipment B and C with bigger metering areas and can be mainly explained considering the improvement of the thickness determination relative uncertainty. With increased thickness, the thermal resistance gets higher and therefore,

especially for the smaller apparatus, the relative uncertainty for the electrical power determination dramatically increases. In case of specimen thickness equal to 40 mm the relative uncertainty is not affected down to 0.004 W/mK for equipment B. For specimen thickness up to 80 mm, a type C apparatus is recommendable (larger measuring area), to avoid influences on $u_c(\lambda)$, even for very low values of thermal conductivity.

Figure 54 shows the isolines for GHP equipment B, which summarises the observations above. The range of thickness and temperature according to the definitions in EN 1946-2:1999 [149] are shown in the greyed box. With temperature differences smaller than 10 K the distance between the isolines becomes smaller, and the same happens for a specimen thickness lower than 15 mm.

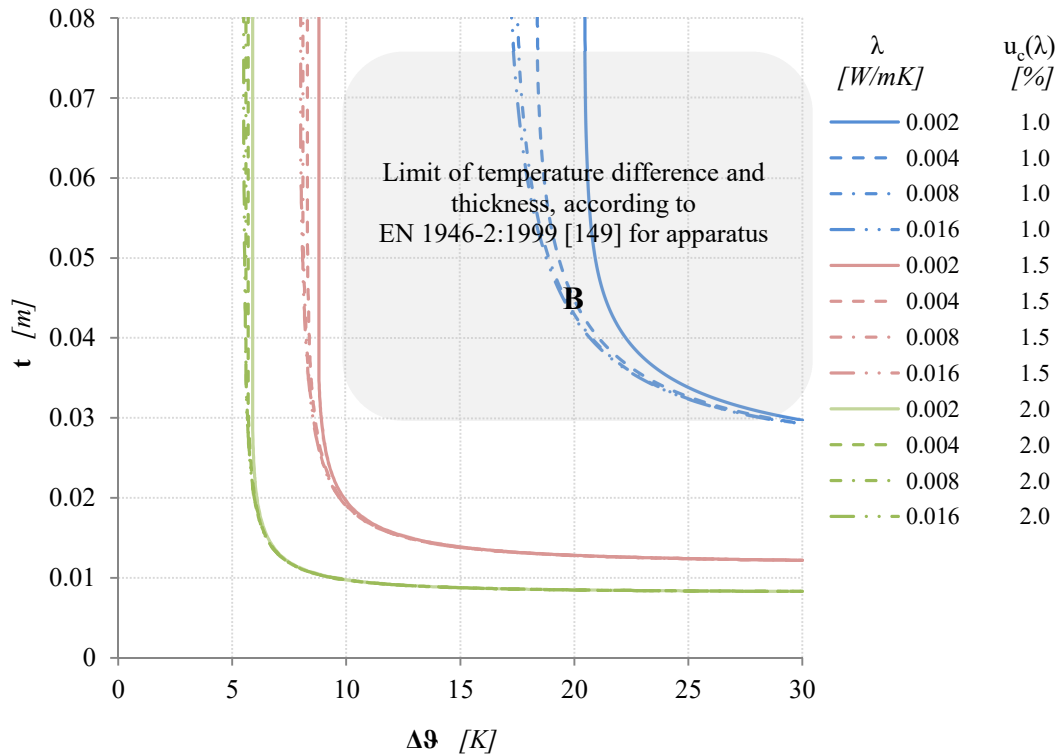


Figure 54: Uncertainty isolines ($u_c(\lambda)$) between 1.0 % and 3.0 % for different values of $\lambda = 0.004$ to 0.016 W/mK, as a function of the temperature difference $\Delta\theta$ and the thickness of the specimen t , assuming the maximum uncertainty according to EN 1946-2:1999 [149], equipment B [150]

6.2.1.2 Sensitivity analysis of selected parameters

Figure 55 shows the variation of $u_c(\lambda)$ isolines, if one parameter between the electrical power (**Figure 55 b**)), thickness (**Figure 55 c**)) or temperature difference (**Figure 55 d**)) are multiplied by a factor of two, compared to the relative uncertainty obtained assuming the absolute uncertainties for all parameters provided by EN 1946-2:1999 [149] (**Figure 55 a**)). The effects are discussed separately in detail.

With a doubled uncertainty for the electrical power determination (**Figure 55 b**)), the isolines have a wider spread, compared to the standard case. Especially in case of low thermal conductivity, this will lead to an increase in the combined relative uncertainty. However, the isolines are not shifted dramatically: the effect can be compensated quite easily by an increased temperature difference. An increasing of the thickness error (**Figure 55 c**)) also causes an inevitable spreading of the isolines, but coupled with an upwards shifting. Especially for low specimen thicknesses, it is hard to compensate this phenomenon by an increased temperature difference. In the end, the increase of the temperature difference uncertainty (**Figure 55 d**)) cannot be compensated increasing the temperature difference in a reasonable temperature range.

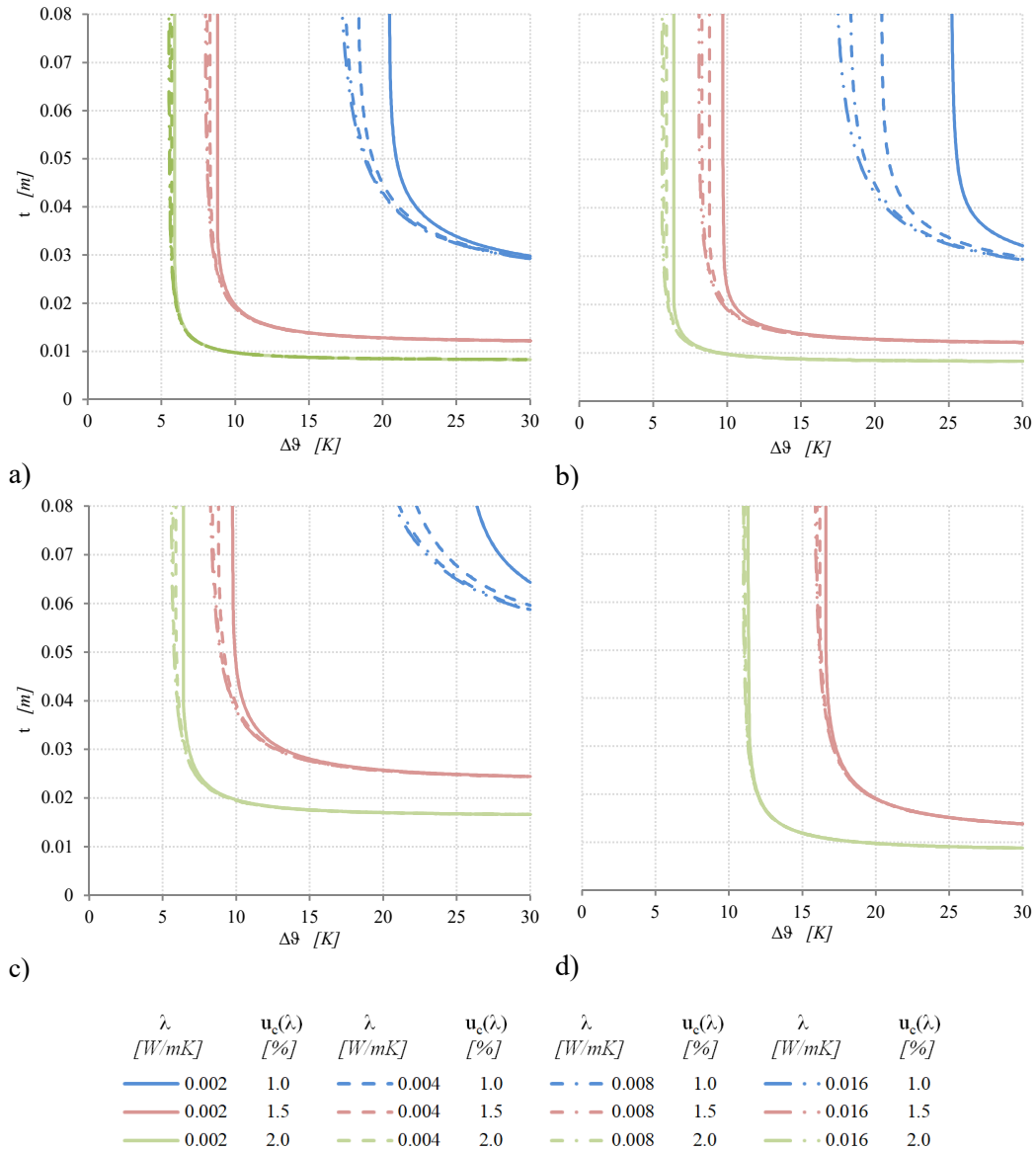


Figure 55: Uncertainty isolines ($u_c(\lambda)$ between 1.0 % and 3.0 %) for different values of $\lambda = 0.004$ to 0.016 W/mK, as a function of the temperature difference $\Delta\theta$ and the thickness of the specimen t , equipment B. a) assuming the maximum uncertainty according to EN 1946-2:1999 [149]; b) increasing the electrical power error by a factor 2; c) increasing the thickness error by a factor 2; d) multiplying the $\Delta\theta$ error by a factor 2 [150]

Chapter 7

Experimental assessment and validation of measurement uncertainty

In this chapter, the experimental evaluation of the measurement uncertainty is presented. Differently, from the previous section, the results here obtained provides indications about how the real laboratory life can be accurate.

Two preliminary investigations were performed, to verify the adequacy of the available experimental devices (numerical bi-dimensional analysis of the edge effects) and the repeatability of the measurements in case of VIPs.

After that, two experimental campaigns were performed. The first one had the aim to assess the Type A uncertainty of the measured VIP λ_{COP} (by mean of the HFM-1 apparatus) and of the measured aerogel blanket λ (GHP-1 apparatus). The objective of the second one was instead the assessment of $u_c(\psi)$ and $u_c(\lambda_{eq})$, both Type A and B when possible (using the devices GHP-2, GHP-3 and HFM-2, available at FIW). Both these investigations were never performed before. In particular, if the one related to the $u_c(\lambda)$ has a more theoretical interest, the one about the thermal bridges uncertainty provides useful practical information.

7.1 Numerical bi-dimensional analysis of the edge effects

The first step for a proper experimental assessment of SIMs thermal performances is to verify the capability of the available measuring devices.

In fact, measurements can be affected by lateral heat losses from the device during the tests. Numerical 2D simulations of the used experimental apparatuses were performed, in order to assess the effects of these dispersions on the measurement results, as explained in § 4.3.1 *Bi-dimensional steady-state heat transfer*.

“The results of the most relevant HFM numerical simulation (worst condition: 30 mm VIP and $\vartheta_{avg} = 52.5^\circ\text{C}$) are reported in **Figure 56**. As it can be seen, the temperature profile is influenced by the thermal bridging effect and lateral heat losses only for around the firsts 5 cm from the edge of the sample. This result demonstrated that in this case the metering area of the HFM was not affected by any kind of impact, and hence the measurement of the centre of panel thermal conductivity can be correctly evaluated²⁰ .

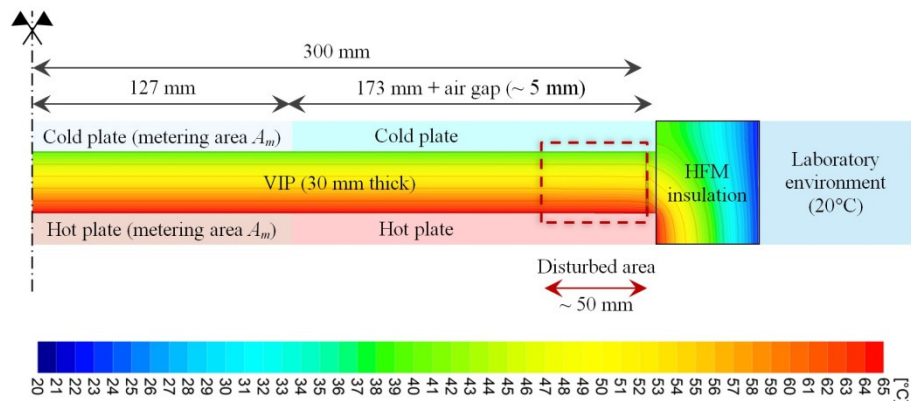


Figure 56: Output of the HFM numerical 2D analysis: 30 mm VIP, $\vartheta_{avg} = 52.5^\circ\text{C}$ [29]

²⁰ Text from the author’s paper: “The effect of temperature on thermal performance of fumed silica based Vacuum Insulation Panels for buildings” [29].

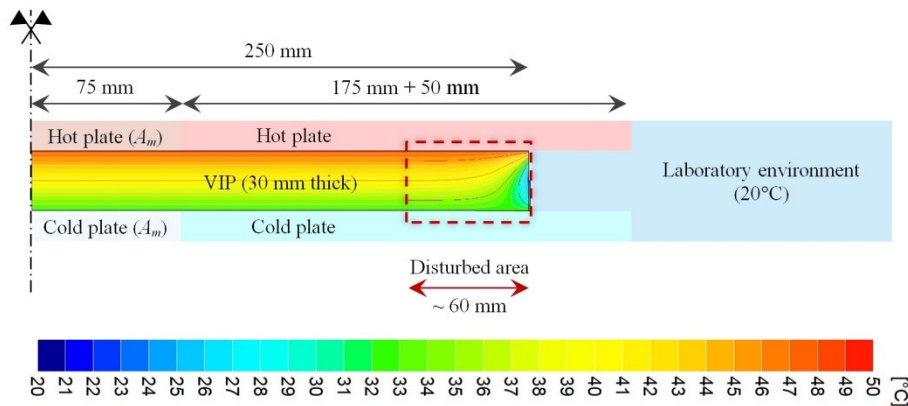


Figure 57: Output of the GHP numerical 2D analysis: 30 mm VIP, $\vartheta_{avg} = 40\text{ }^{\circ}\text{C}$

A similar result was obtained in case of GHP simulations, with a slightly larger affected area of about 60 mm, as shown in **Figure 57** (again only the worst condition is presented: 30 mm VIP and $\vartheta_{avg} = 40\text{ }^{\circ}\text{C}$).

Therefore, since the measuring area of both HFM and GHP is far from the disturbed area, both the devices can be used for the SIMs experimental characterisation.

7.2 Repeatability issues in VIPs thermal conductivity measurements (HFM)

Verifying the repeatability of laboratory measurements is a fundamental aspect for the proper conduction of the future tests.

Repeatability is defined as the variability of the measurements results obtained in the following conditions: the same location, the same measurement equipment and procedure, the same testing conditions, the same operator and repetition over a short period of time. It is also known as the measurement device inherent precision.

In this context, to evaluate the short-term and medium-term repeatability of VIP thermal conductivity measurements, a total of 81 λ tests were performed (with the HFM-1) on three different samples at three set point temperatures, with a temperature difference between the HFM plates of 20 $^{\circ}\text{C}$. The tests were repeated three times a week (short-term repeatability) and then repeated for three weeks (medium-term repeatability).

The three VIP samples were expected to behave significantly different from each other:

- Sample 1 is an aged sample from manufacturer A;
- Sample 2 is an aged sample from manufacturer B;
- Sample 3 is a new sample from manufacturer B.

For this reason, a randomised block design (with repetition) was chosen. **Table 27** and **Figure 58** show the testing plan and the measured thermal conductivities.

Table 27: Repeatability testing plan and the related thermal conductivity results

ϑ_{avg} [°C]	Week	Sample 1 [W/mK]	Sample 2 [W/mK]	Sample 3 [W/mK]	
20	1	0.00454	0.00373	0.00321	
		0.00455	0.00373	0.00321	
		0.00455	0.00374	0.00322	
	2	2	0.00456	0.00370	0.00321
			0.00456	0.00370	0.00320
			0.00456	0.00371	0.00321
		3	0.00456	0.00374	0.00328
			0.00457	0.00375	0.00324
			0.00458	0.00375	0.00322
	35	1	0.00486	0.00396	0.00338
			0.00486	0.00396	0.00339
			0.00486	0.00396	0.00338
2		2	0.00489	0.00394	0.00337
			0.00489	0.00394	0.00337
			0.00488	0.00394	0.00337
		3	0.00478	0.00396	0.00341
			0.00479	0.00397	0.00341
			0.00479	0.00396	0.00339
50		1	0.00528	0.00426	0.00366
			0.00526	0.00426	0.00362
			0.00526	0.00426	0.00363
	2	2	0.00531	0.00426	0.00360
			0.00531	0.00425	0.00360
			0.00531	0.00425	0.00360
		3	0.00528	0.00427	0.00365
			0.00528	0.00427	0.00364
			0.00528	0.00426	0.00363

From a first analysis of the results, it is possible to observe that the three samples are composed of different core materials: Sample 1 (with higher thermal conductivity) is probably made of Fumed Silica core, while Samples 2 and 3 could be Fibre Glass panels.

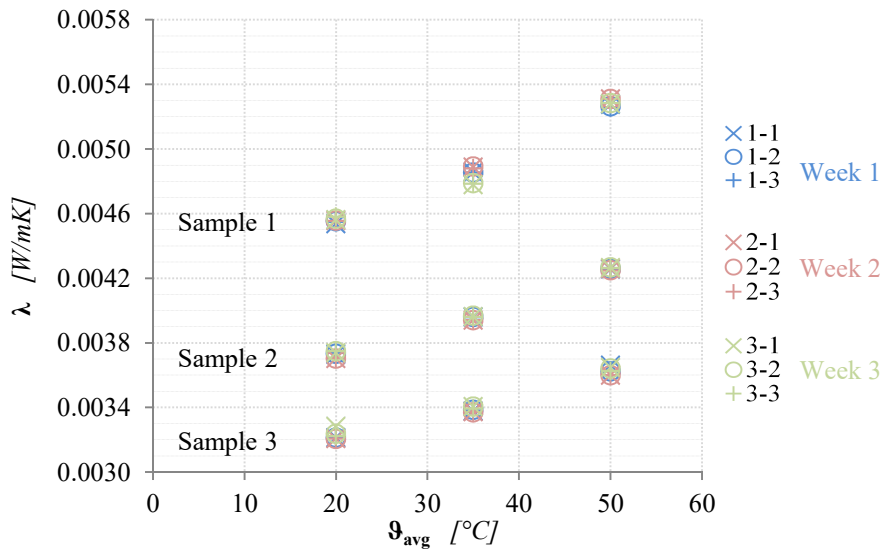


Figure 58: Plot of repeatability data

The dot plot of λ (Figure 59) provides a qualitative indication of the short and medium term repeatability, comparing the sample data distributions:

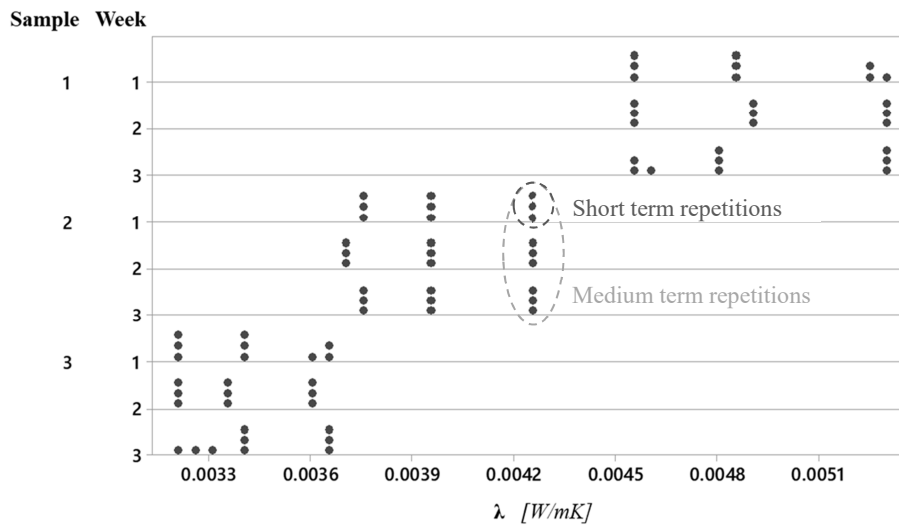


Figure 59: Dot plot of λ

Short term repetition appears to be generally very good, whereas more variation can be observed for medium-term repetitions.

Table 28: Means and standard deviation calculation (λ and s are in [10^{-4} ·W/mK])

		$\vartheta_{\text{avg}} [^{\circ}\text{C}]$			$\vartheta_{\text{avg}} [^{\circ}\text{C}]$				
		20	35	50	20	35	50		
<i>Sample 1</i>		45	49	53	\bar{y}	45.47	48.60	52.67	Short term
		46	49	53	s	0.06	0.00	0.12	
		46	49	53	s [%]	0.13%	0.00%	0.22%	
		46	49	53	\bar{y}	45.60	48.87	53.10	
		46	49	53	s	0.00	0.06	0.00	
		46	49	53	s [%]	0.00%	0.12%	0.00%	
		46	48	53	\bar{y}	45.70	47.87	52.80	Medium term
		46	48	53	s	0.10	0.06	0.00	
		46	48	53	s [%]	0.22%	0.12%	0.00%	
					\bar{y}	45.59	48.44	52.86	
					s	0.12	0.45	0.20	
					s [%]	0.26%	0.93%	0.38%	
<i>Sample 2</i>		37	40	43	\bar{y}	37.33	39.60	42.60	Short term
		37	40	43	s	0.06	0.00	0.00	
		37	40	43	s [%]	0.15%	0.00%	0.00%	
		37	39	43	\bar{y}	37.03	39.40	42.53	
		37	39	43	s	0.06	0.00	0.06	
		37	39	43	s [%]	0.16%	0.00%	0.14%	
		37	40	43	\bar{y}	37.47	39.63	42.67	Medium term
		38	40	43	s	0.06	0.06	0.06	
		38	40	43	s [%]	0.15%	0.15%	0.14%	
					\bar{y}	37.28	39.54	42.60	
					s	0.20	0.11	0.07	
					s [%]	0.53%	0.29%	0.17%	
<i>Sample 3</i>		32	34	37	\bar{y}	32.13	33.83	36.37	Short term
		32	34	36	s	0.06	0.06	0.21	
		32	34	36	s [%]	0.18%	0.17%	0.57%	
		32	34	36	\bar{y}	32.07	33.70	36.00	
		32	34	36	s	0.06	0.00	0.00	
		32	34	36	s [%]	0.18%	0.00%	0.00%	
		33	34	37	\bar{y}	32.47	34.03	36.40	Medium term
		32	34	36	s	0.31	0.12	0.10	
		32	34	36	s [%]	0.94%	0.34%	0.27%	
					\bar{y}	32.22	33.86	36.26	
					s	0.24	0.16	0.22	
					s [%]	0.76%	0.47%	0.62%	
		$0 \leq s < 0.1$	$0.1 \leq s < 0.2$	$0.2 \leq s < 0.3$	$0.3 \leq s < 0.4$	$s \geq 0.4$			

Means and standard deviations were evaluated for both short-term tests (three groups of data for each week) and for medium-term analyses (9 data for each sample). The results are shown in **Table 28**. In case of short-term variability, extremely good results were found for sample 2, while the highest variability was observed for sample 3 during week 3 (but a measurement problem occurred during the first two measurement cycles). The highest medium-term variability was found for sample 1 at 35 °C, although a very low variability was found for the short-term tests.

7.2.1 ANOVA analysis

The analysis of variance (ANOVA) was performed to assess the importance of one or more factors by comparing the response variable means at the different factor groups (in this specific case, the groups are temperature and sample). It evaluates the "variation" among and between two or more groups, and it represents a way to define if survey or experiment results are significant. Indeed, ANOVA is based on the evaluation of two mutually exclusive statements about two or more population means: the null hypothesis (the group means are all equal) and the alternative hypothesis (not all group means are equal). If the averages are different the comparison between such averages is appropriate.

Two different typologies of ANOVA were carried out: the Nested ANOVA and the One-Way ANOVA, both of them using the Minitab[®] software 0.

The Nested ANOVA must be used when at least one group is subdivided by several subgroups (several temperatures or samples) and defines whether factors (necessarily random) in the model affect the response variable. The quantities involved in this analysis and reported in **Table 29** are the following 0:

- **DF**

The total Degrees of Freedom (*DF*) represents the information amount in the data, and it is used to assess the value of population parameters which are unknown. The *DF* is obtained from the number of observations in the sample minus 1. The *DF* of a term is an indicator of how much information the term uses. The more is the population of the sample, the more is the available information about the population, and the higher is the total *DF*.

- **SS**

Sequential Sums of Squares defines the variation for the different model components, due to various sources (the first two rows in **Table 29**). The residual error row (second to the last row) shows the variation not explained by any of the other sources, while the Total row (the last one) indicates the total amount of difference among all the values. The sequential Sum of Squares for a term is the portion of the variation explained by every single term. The Total Sum of Squares is the sum of the Term *SS* and the Error *SS* and indicates the total variation in the data. This value is used to calculate the *P*-value (described below) for a term.
- **MS**

Sequential Mean Squares (also called *MSE* or s^2) measure the variation due to a single term or model and is computed by dividing a sum-of-squares value by the corresponding degrees of freedom. The *MS* depends on the order the terms are inserted in the model. In other words, the *MS* is the variance around the fitted values. Also this value can be used to calculate the *P*-value (described below) for a term.
- **F-value**

The *F*-value is used to determine if the term and the response are associated. This value can be used to calculate the *P*-value. A high *F*-value means that the term or model is significant.
- **P-value**

The *P*-value measures the probability against the null hypothesis (no association between terms and responses). The lower the *P*-value, the stronger the evidence against the null hypothesis. This value defines the statistical significance of the association between the response and each term in the model when compared to the significance level considered to assess the null hypothesis. Commonly, the significance level (α) is assumed equal to 0.05: this means a 5% risk to conclude that an association exists even if there is no real association. If the *P*-value $\leq \alpha$ the association between the response variable and the term is statistically significant, while if the *P*-value $> \alpha$ the association is not statistically significant. In this second case, the model must be refitted without the not significant term. Since all factors in a fully nested ANOVA model are random, a statistically significant factor contributes to the variation in the response.

- **Var Comp**

Variance components assess the amount of variation in the response that can be attributed to each random term. The higher the value, the more the contribution to the response variability.

- **% of Total (Variance)**

The % of Total defines the percentage of the total variance that is due to each random term in the model. It is calculated as the ratio between the variance for each source and the total variation.

- **StDev**

It is the standard deviation for each random term, which is equal to the square root of the variance for that source. The standard deviation has the same units of measurement as the response variable.

Table 29: Nested ANOVA results

Variance for λ - versus Sample and ϑ_{avg}					
Source	DF	SS	MS	F	P
Sample	2	30.3165	15.1582	20.5	0.002
ϑ_{avg}	6	4.4374	0.7396	1483	0.000
Error	72	0.0359	0.0005	-	-
Total	80	34.7897	-	-	-

Variance components			
Source	Var Comp.	% of Total	StDev
Sample	0.534	86.60	0.73
ϑ_{avg}	0.082	13.32	0.29
Error	0.000	0.08	0.02
Total	0.617	-	0.79

As expected, high significance of both sample and temperature was obtained.

To remove the effect of samples (that can be assumed as blocks), results were normalised concerning the global average, by adding the deviation of each value from the average of its block:

$$x_{i,norm} = \bar{x}_{tot} + (x_i - \bar{x}_{block}) \quad (80)$$

The effects of the normalisation can be observed in **Figure 60**, which represents the boxplot of λ . A boxplot is a graphical summary of the distribution

of a sample that shows its shape, central tendency, variability and outliers. It is composed by an upper whisker (representing the upper 25% of the distribution, outliers excluded), the interquartile range box (with the middle 50% of the data) and a lower whisker (representing the lower 25% of the distribution, outliers excluded) 0.

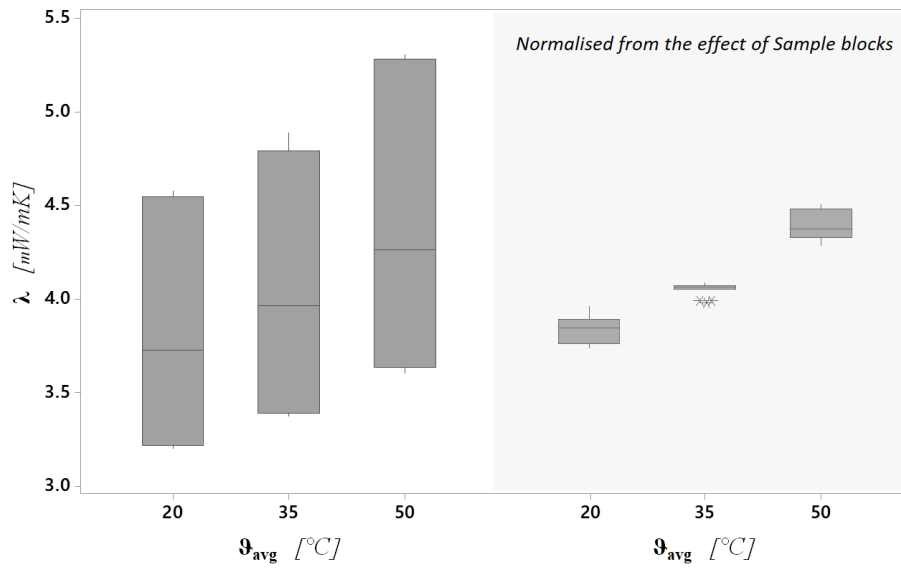


Figure 60: Boxplot of λ , and λ normalised from the effects of Sample blocks

If no values were treated as outliers, the variability would be quite homogeneous among temperatures: the variability is indeed temperature independent.

After that, a normalised One-Way ANOVA analysis was performed (Table 30). The One-Way ANOVA 0 is a method that allows the comparison of the means of two or more samples when there are one categorical factor and continuous response. It can be used to determine if the means of two or more groups are different, or to obtain a range of values for this differences between each pair of groups. Some of the outputs of the One-Way ANOVA are similar to the one of the Nested ANOVA, the others are hereinafter explained 0:

- **Adj P-value**

The adjusted P -value define which pairs within a comparisons family are significantly different.

- **S-value**

S is the standard deviation of how far the data values are from the fitted values, and therefore it defines how well the model describes the response (the lower S -value, the better is the model). S has the same measurement unit of the response.
- **R-sq**

R -sq (R^2) defines the variation percentage explained by the model and provides an indication of how well the model fits the data. The higher the value of R^2 , the better the model is and the more variation explained by the model. R^2 always increases increasing the sample. Even if the model has a high R^2 , it is essential to check the residual plots to verify the meeting between the model and the model assumptions.
- **R-sq (adj)**

Adjusted R^2 has the same characteristics of R^2 , but it is adjusted considering the number of predictors in the model related to the number of observations. R -sq (*adj*) is calculated as 1 minus the ratio between the Mean Square Error (MSE) and the Mean Square total (MS Total). R -sq (*adj*) must be used when models with different numbers of predictors are compared.
- **R-sq (pred)**

Predicted R^2 is calculated removing each observation from the data set, estimating the regression equation, defining in this way how well the model predicts the removed observation. R -sq (*pred*) must be used to determine how well the response of new observations are predicted by the model. The larger is the R -sq (*pred*) value, the better is the prediction. When the R -sq (*pred*) is substantially lower than R^2 , the model could be over-fit. It means that there are some not important effects in the population, even if they may appear important between the sample data. In this way, the model may not be useful for population predictions. Predicted R^2 can also be better than Adjusted R^2 for the comparison of models because the observations used for the calculation are not included in the model calculation.

- **N**
N is the sample size, which represents, for each group, the total number of observations. Usually, a larger sample provides a tighter confidence interval.
- **Confidence Interval for group means (95% CI)**
This Confidence Interval (*CI*) defines the interval which probably contains the true mean of the population (with a defined percentage of probability). Since samples are taken randomly, two samples from the same population unlikely have the same confidence interval. The *CI* is composed of two parts: the point estimate and the margin of error. The point estimate is calculated from the sample data, and the *CI* is centred around this value. The margin of error measures the width of the *CI* and is defined by the sample variability, the sample size, and the confidence level. The upper limit of the *CI* is obtained adding the error margin to the estimated point, while for the lower limit the error margin is subtracted from the estimated point. The Confidence Interval can be used to assess, for each group, the estimate of the population mean. For example, with a 95% *CI*, the probability that the *CI* contains the group mean is the 95%. If the interval is too wide to be useful, the sample size should be increased. *CI*s are calculated using the following described pooled standard deviation.
- **Pooled StDev**
The pooled standard deviation is the standard deviation of all data points around their group mean, and not around the total mean. Groups with more data strongly affect the overall estimate of the Pooled StDev. As for the standard deviation, the higher the value of the pooled standard deviation, the higher the spread in the data, the wider the confidence interval, and the lower the statistical power.

Table 30: One-Way ANOVA results

Variance for λ corrected Sample - versus ϑ_{avg}							
Source	DF	Seq SS	Contribution	Adj SS	Adj MS	Adj F	Adj P
ϑ_{avg}	2	4.1929	93.73%	4.1929	2.09643	583	0.000
Error	78	0.2804	6.27%	0.2804	0.00360	-	-
Total	80	4.4733	100%	-	-	-	-
Model summary							
S	R-sq	R-sq(adj)		PRESS	R-sq(pred)		
0.060	93.73%	93.57%		0.302397	93.24%		
Means							
T	N	Mean	StDev		95% CI		
20	27	3.836	0.065		(3.810; 3.862)		
35	27	4.061	0.030		(4.049; 4.073)		
50	27	4.390	0.076		(4.360; 4.420)		
Pooled StDev = 0.060							

As already mentioned, it is crucial to check also the residuals. In this case, the residuals are represented by four different graphs (see **Figure 61**):

- **Normal probability plot**

It shows the residuals versus their expected value. If the points are approximatively along a straight line (as the analysed case, **Figure 61**), the residuals are normally distributed. The few points lying away from the line and fare from the other points means that the distribution has outliers. Since the residuals follow the normal distribution, the confidence interval and the P-value can be considered accurate.

- **Histogram**

The Histogram of the residuals represents their distribution for all the observations. It is useful to define if the data are skewed (a long tail in one direction) or include outliers (a bar far from the other bars). A histogram is most significant if the data points are more than 20, otherwise each bar does not contain enough data points to reliably individuate skewness or outliers. Since the layout of the histogram depends on the data grouping rule, the histogram must not be used to assess the normality of the residuals: use a normal probability plot.

- **Residuals versus fit**

This graph represents the residuals (ordinate axis) versus the fitted values (abscissa axis). It is useful to verify if the residuals are randomly distributed and are characterised by constant variance. If so, the points must be spread randomly on both sides of the 0, in the same range and without any point distant from the others. In the specific case (**Figure 61**), a non-constant variance can be observable (the points related to 35°C are spread in a smaller range than for the other two temperatures, as also shown in **Table 30**, StDev cell), but no outliers are obtained (all the points are contained in the same range)

- **Residuals versus order**

It represents the residuals in the order of the data collection. This graph allows verifying if the residuals are independent each other. Independent residuals are characterised by no trends or patterns (randomly distributed points, as observed in **Figure 61**)

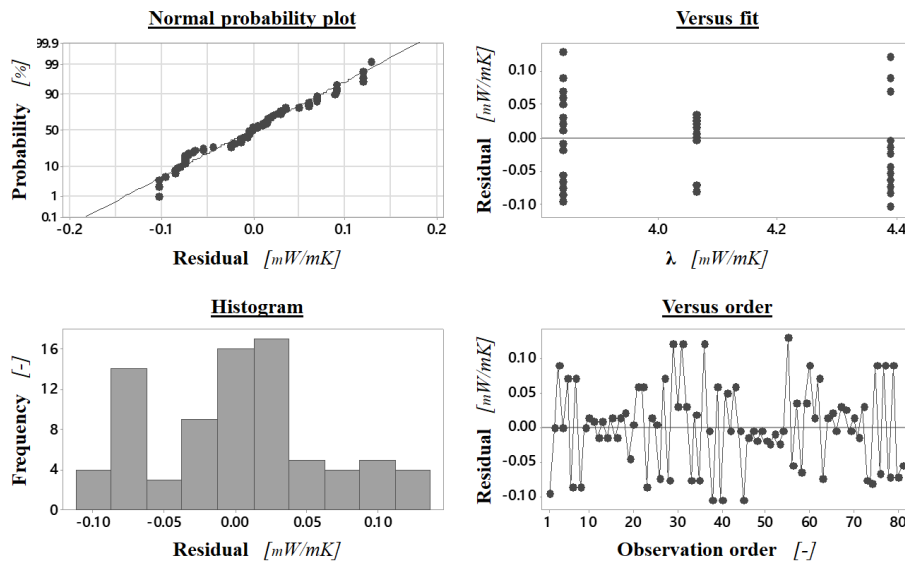


Figure 61: Residuals analysis

A similar investigation was performed to remove the effect of temperatures, assumed as blocks (in this case only the boxplot of λ is presented, see **Figure 62**).

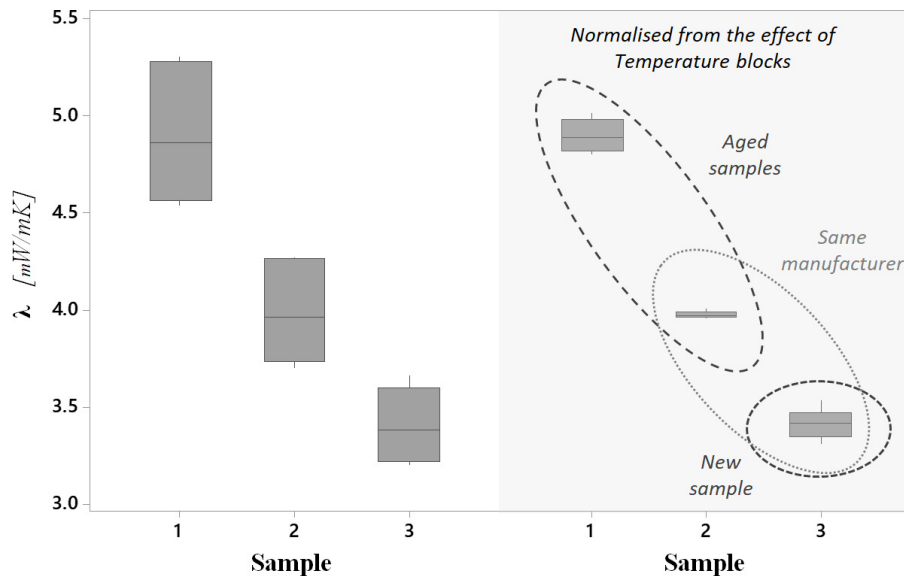


Figure 62: Boxplot of λ , and λ normalised from the effects of Temperature blocks

To conclude, the short-term repeatability was found to be generally extremely accurate, with a relative standard deviation almost always lower than 0.3%. Repeating the tests along allowed to observe a higher variability, but in any case, the repeatability could be considered good, with a relative standard deviation lower than 1%. The lowest variability was obtained for Sample 2, and in general, the variability was largely found to be both temperature and ageing independent.

7.3 Thermal conductivity uncertainty (Type A)

The repeatability of measurement is a fundamental issue for the proper evaluation of the Type A measurement uncertainty (based on repeated observations). This kind of uncertainty evaluation represents the most detailed analysis, related to the single laboratory where the measurements are performed. In fact, it depends on the set-up of the experiment, the adopted apparatus and the environmental conditions. Therefore, it is not recommended to use the so obtained results for direct comparisons with different measurement campaigns. On the contrary, this approach is essential for the certification/declaration of the thermal properties of the tested materials, and for the evaluation of the reliability, accuracy and precision degree of the lab.

To this aim, two experimental campaigns were performed at Politecnico di Torino and INRiM, in order to assess the capability of the two available thermal conductivity measuring devices (HFM-1 and GHP-1 respectively), in case of SIMs characterisation. The two experimental set-ups were different, to consider

the applicability range of each apparatus (summarised in **Table 6** and **Table 7**, § 4.3.1 *Bi-dimensional steady-state heat transfer*). Both of them consisted in repeating 8 times the measurements carried out at different average temperatures (ϑ_{avg}) and temperature differences between the plates ($\Delta\vartheta$) on a SIM sample (VIP in case of HFM-1 and aerogel blanket in the case of GHP-1). The detailed configurations and results will be presented in the following sections.

7.3.1 Heat Flow Meter - VIP

A Type A uncertainty budget for different VIP samples tested by means of the HFM-1 apparatus (**Table 6**) was assessed, considering several boundary conditions.

The three measured samples were FS based VIPs, with dimensions 600 x 600 mm and thickness equal to 10, 20 and 30 mm (**Figure 63**).

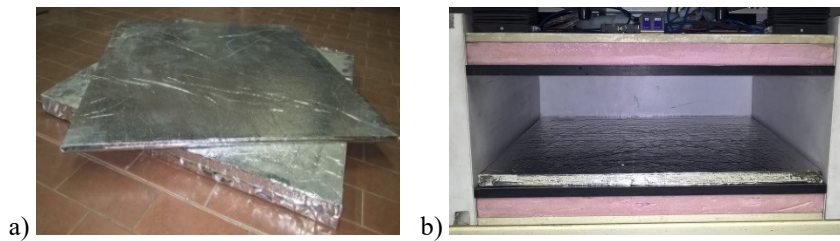


Figure 63: Tested VIP samples. a) 10 and 30 mm thick; b) 20 mm thick

Measurements were repeated 8 times for each sample considering the following four average testing temperatures and temperature differences, randomly alternated:

- $\vartheta_{avg} = 5, 10, 23$ and 40°C ;
- $\Delta\vartheta = 10, 20, 30$ and 40°C .

For each test, the last 10 output data for each signal were analysed for the $u_c(\lambda_{COP})$ evaluation (with a total amount of 80 data). The only exception is represented by the thickness reading, which was repeated three or four times according to the experimental campaign. The investigated signals were:

- the sample thickness (t [mm]);
- the calibration factors of the two plates ($f_{cal}(\vartheta)$ upper and lower [$\text{W}/\text{m}^2\mu\text{V}$]);
- the set-point temperatures of the two plates (ϑ upper and lower [$^{\circ}\text{C}$]);

- the electric signal measured in the two measuring areas of the plates (Q upper and lower [μV]);
- the specific heat flux through the sample measured in the two measuring areas of the plates (φ upper and lower [W/m^2]).

The results were then statistically analysed to define to identify the most representative Probability Density Function (PDF) distributions and to define in the most appropriate way the measurement uncertainty of each output signal. Three different situations may occur regarding the considered PDF, depending on the investigated output variable:

- $t \rightarrow$ UNIFORM or TRIANGULAR distribution
since the thicknesses measurement was repeated only three or four times, the data amount was not enough to consider a more accurate normal distribution;
- $\vartheta \rightarrow$ UNIFORM or TRIANGULAR distribution
even if the temperatures (of both upper and lower plate) were measured 80 times for each test configuration, they always lie between two or (rarely) three values;
- Q and $\varphi \rightarrow$ NORMAL distribution
the number of measurements and their variability made it possible to assume a normal PDF. In particular, since the data were often spread in an asymmetric way from the mean, the median and the skew factor (see Eq. (81)) were also determined.

$$SKEW = \frac{1}{n} \cdot \sum \left(\frac{x_i - \bar{x}}{s(\bar{x})} \right)^3 \quad (81)$$

Differently, from the other quantities, the uncertainty of both the calibration factors was evaluated on the basis of the declaration provided by the HFM producer ($u(f_{cal}(\vartheta)) = 2\%$).

Once defined the measurement uncertainty of each parameter involved in the calculation of the COP thermal conductivity (indirect measurement), the related combined uncertainty $u_c(\lambda_{COP})$ was assessed, in accordance with § 5.2.1 *Heat Flow Meter* (neglecting the effects of $\Delta\lambda_E$, $\Delta\lambda_O$, $\Delta\lambda_K$, $\Delta\lambda_L$ and $\Delta\lambda_g$, since all the uncertainty contributions were obtained from a Type A analysis).

As an introductory comment to the results, a particular trend observed in the measures should be highlighted. In case of 10 mm thickness, the COP thermal conductivity values are always (for all the investigated average temperatures and temperature differences) more or less randomly spread around the mean values (**Figure 64 a**) provides an example). On the contrary, for thickness equal to 20 or 30 mm the λ_{COP} values have ascending or descending trends generally tending to stabilise around the mean (e.g., **Figure 64 b**), except in the case of $\Delta\vartheta = 40^\circ\text{C}$ (in which a situation similar to the case of 10 mm thickness occurs). This behaviour may be attributed to the HFM-1 control system, and therefore it can not be corrected.

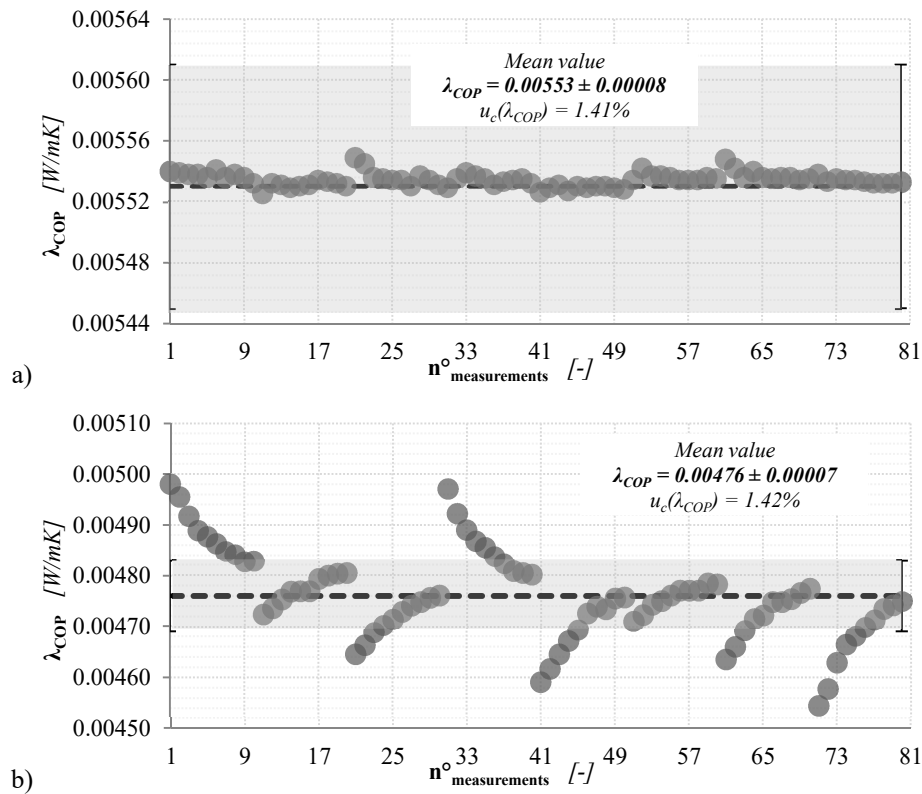


Figure 64: λ_{COP} -values assessed by means of HFM-1 apparatus. a) FS based VIP 10 mm thick, $\vartheta_{\text{avg}} = 23^\circ\text{C}$, $\Delta\vartheta = 30^\circ\text{C}$; b) FS based VIP 30 mm thick, $\vartheta_{\text{avg}} = 5^\circ\text{C}$, $\Delta\vartheta = 20^\circ\text{C}$

In the graphs, the dashed lines identify the λ_{COP} mean value calculated starting from the means of all the directly measured output signals, while the grey band represents the combined uncertainty $u_c(\lambda_{COP})$.

The detailed results are reported in Appendix B, while summaries of the main results are shown below (from Table 31 to Table 33 and from Figure 65 to Figure 67)

Table 31: 10 mm thick VIP thermal conductivities and related Type A measurement uncertainties (HFM-1)

		5				10				
ϑ_{avg}	$[\text{°C}]$	10	20	30	40	10	20	30	40	
t = 10 mm	λ_{COP}	$[\text{mW/mK}]$	5.09	5.09	5.09	5.08	5.17	5.17	5.17	5.17
	$u_c(\lambda_{COP})$	$[\text{mW/mK}]$	0.07	0.07	0.07	0.07	0.07	0.07	0.07	0.07
		$[\%]$	1.38	1.38	1.38	1.38	1.35	1.35	1.35	1.35
		23				40				
ϑ_{avg}	$[\text{°C}]$	10	20	30	40	10	20	30	40	
t = 10 mm	λ_{COP}	$[\text{mW/mK}]$	5.55	5.54	5.53	5.52	6.37	6.34	6.30	6.25
	$u_c(\lambda_{COP})$	$[\text{mW/mK}]$	0.08	0.08	0.08	0.08	0.09	0.09	0.09	0.09
		$[\%]$	1.44	1.44	1.45	1.45	1.41	1.42	1.43	1.44

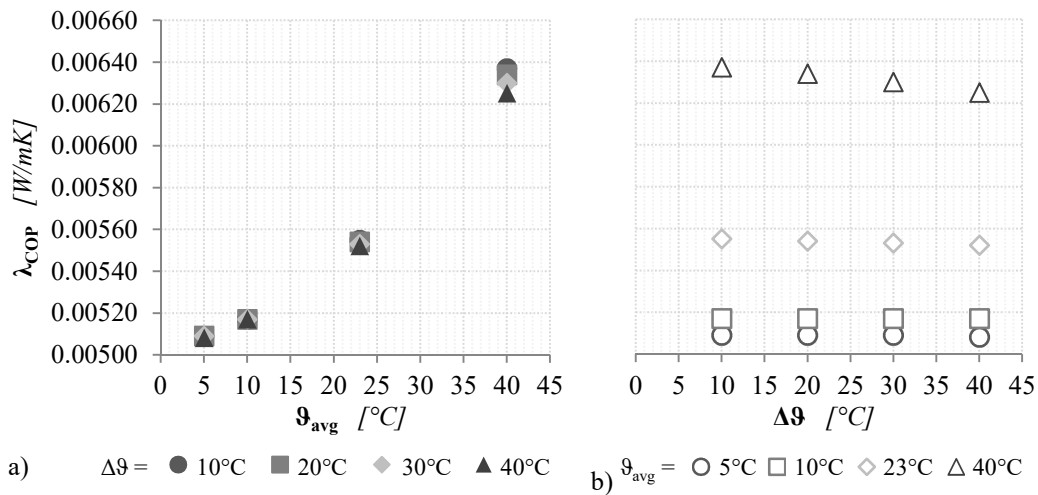
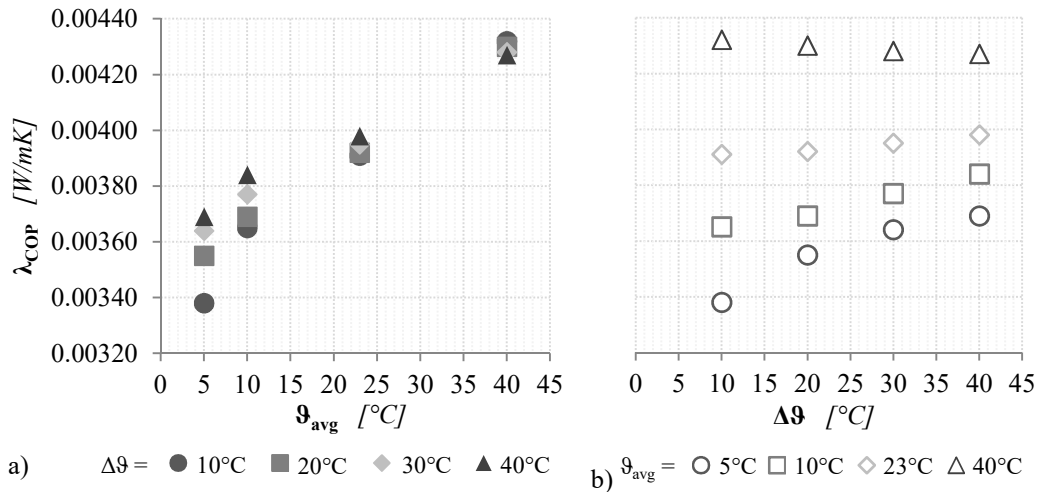


Figure 65: 10 mm thick VIP thermal conductivity, a) as a function of ϑ_{avg} and b) $\Delta\vartheta$

Table 32: 20 mm thick VIP thermal conductivities and related Type A measurement uncertainties (HFM-1)

ϑ_{avg} [$^{\circ}\text{C}$]		5				10			
$\Delta\vartheta$ [$^{\circ}\text{C}$]		10	20	30	40	10	20	30	40
$t = 20$ mm	λ_{COP} [mW/mK]	3.38	3.55	3.64	3.69	3.65	3.69	3.77	3.84
	$u_c(\lambda_{\text{COP}})$ [%]	0.05	0.05	0.05	0.05	0.05	0.05	0.05	0.05
ϑ_{avg} [$^{\circ}\text{C}$]		23				40			
$\Delta\vartheta$ [$^{\circ}\text{C}$]		10	20	30	40	10	20	30	40
	λ_{COP} [mW/mK]	3.91	3.92	3.95	3.98	4.32	4.30	4.28	4.27
	$u_c(\lambda_{\text{COP}})$ [%]	0.06	0.06	0.06	0.06	0.06	0.06	0.06	0.06

Figure 66: 20 mm thick VIP thermal conductivity, a) as a function of ϑ_{avg} and b) $\Delta\vartheta$ **Table 33:** 30 mm thick VIP thermal conductivities and related Type A measurement uncertainties (HFM-1)

ϑ_{avg} [$^{\circ}\text{C}$]		5				10			
$\Delta\vartheta$ [$^{\circ}\text{C}$]		10	20	30	40	10	20	30	40
$t = 30$ mm	λ_{COP} [mW/mK]	4.66	4.76	4.81	4.92	4.78	4.84	4.91	4.98
	$u_c(\lambda_{\text{COP}})$ [%]	0.07	0.07	0.07	0.07	0.07	0.07	0.07	0.07
ϑ_{avg} [$^{\circ}\text{C}$]		23				40			
$\Delta\vartheta$ [$^{\circ}\text{C}$]		10	20	30	40	10	20	30	40
	λ_{COP} [mW/mK]	5.17	5.19	5.23	5.24	6.02	5.98	5.98	5.94
	$u_c(\lambda_{\text{COP}})$ [%]	0.07	0.07	0.07	0.07	0.09	0.09	0.08	0.08

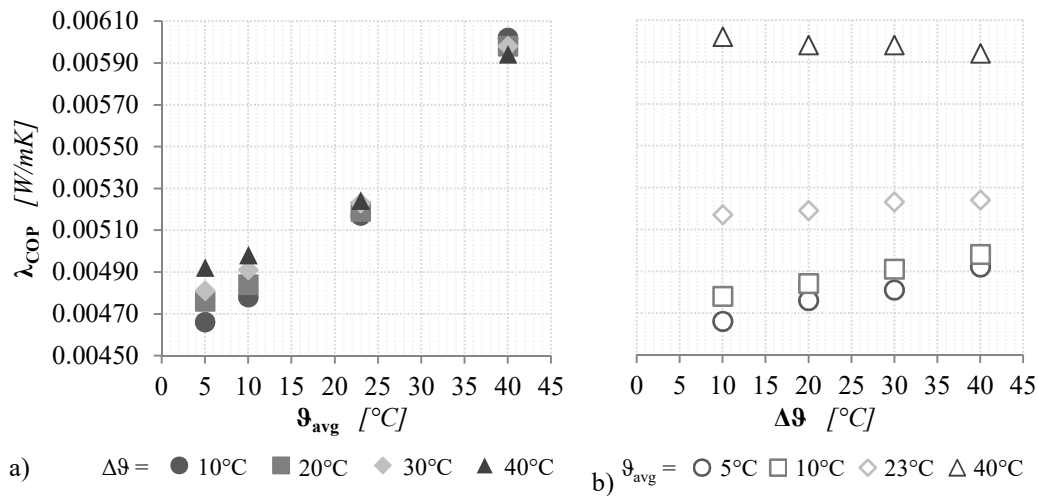


Figure 67: 30 mm thick VIP thermal conductivity, a) as a function of ϑ_{avg} and b) $\Delta\vartheta$

Considering all the investigated samples, the correlation between the λ_{COP} values and the average testing temperature is clearly shown.

Moreover, even if the effects of $\Delta\vartheta$ on the variability of the measurement uncertainty seems to be lost, from **Figure 65 b)**, **Figure 66 b)** and **Figure 67 b)** it is possible to observe how the temperature difference affects the COP thermal conductivity. Increasing the value of $\Delta\vartheta$, the λ_{COP} increases or decreases, depending on the average testing temperature. This behaviour can be explained considering the variation of the various uncertainty sensitivity coefficients (values in Appendix B). In the figures, two different data trends were observed, depending on the ϑ_{avg} : ascendant (or rarely stationary) for $\vartheta_{avg} = 5, 10$ and 23°C , descendant in case of $\vartheta_{avg} = 40^\circ\text{C}$. It was observed that these trends reflect the variation of the sensitivity coefficient $\partial\lambda_{COP}/\partial f_{cal}$ with the temperature (as it is possible to see in **Table 34**), as they represent by far the most influencing factors.

Consequently, with higher temperature differences between the measuring plates, the λ_{COP} temperature dependency becomes weaker, reducing the difference between the thermal conductivity measured values at different average temperatures.

Table 34: $u_c(\lambda_{COP})$ sensitivity coefficient general trend increasing the $\Delta\theta$

$\vartheta_{avg} = 5, 10 \text{ and } 23^\circ\text{C}$				$\vartheta_{avg} = 40^\circ\text{C}$			
$\partial\lambda_{COP}/\partial t$	$\partial\lambda_{COP}/\partial f_{cal}$	$\partial\lambda_{COP}/\partial Q$	$\partial\lambda_{COP}/\partial\Delta\theta$	$\partial\lambda_{COP}/\partial t$	$\partial\lambda_{COP}/\partial f_{cal}$	$\partial\lambda_{COP}/\partial Q$	$\partial\lambda_{COP}/\partial\Delta\theta$
\approx	\uparrow	\downarrow	\downarrow	\approx	\downarrow	\downarrow	\downarrow

As a last comment, it is noteworthy that the VIP with lower $u_c(\lambda_{COP})$ is the 20mm thick, which is a pristine panel (while the other two are about three years aged). The probably lower internal air and moisture content and the better homogeneity of the material contribute to the reduction of the variability of the measurements, and consequently of the related uncertainty.

7.3.2 Guarded Hot Plate - Aerogel blanket

The Type A uncertainty budget, related to the GHP-1 apparatus (**Table 7**) was assessed with different conditions compared to the case of HFM-1, because of some critical limitations of the Guarded Hot Plates apparatus.

From preliminary investigations, it was observed that GHP-1 cannot be used for the thermal characterisation of VIPs: therefore an aerogel blanket 10 mm thick was chosen as SIM testing sample (**Figure 68**).

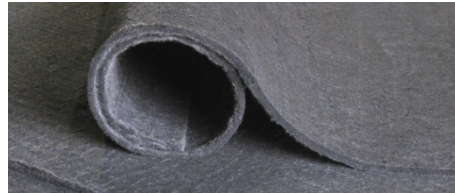


Figure 68: Tested aerogel blanket [41]

Measurements were repeated again eight times (seven times in the case of $\vartheta_{avg} = 23^\circ\text{C}$) considering the following temperature criteria (both upper and lower limit were fixed considering the temperature applicability ranges of the apparatus):

- $\vartheta_{avg} = 5, 10 \text{ and } 23^\circ\text{C}$;
- $\Delta\theta = 5, 10 \text{ and } 15^\circ\text{C}$.

Since the apparatus software is quite blinded and provides only the final results, the data collection was performed with an external multimeter. In this way all the desired measurements were available: in order to make an analysis as similar as possible to the previous one (HFM-1), the last 10 output data for each

signal were analysed for the $u_c(\lambda)$ evaluation (with a total amount of 80 data). The only exception is represented by the thickness reading, which was repeated eight times, one for each experimental test. The investigated signals were:

- the sample thickness (t [mm]);
- the set-point temperatures of the two plates (ϑ hot and cold [$^{\circ}\text{C}$]);
- the electric signal measured in the measuring area (U [mV]);
- the electric current measured in the measuring area (I [A]).

The results were then statistically analysed to define to define the most appropriate Probability Density Function (PDF) distributions and measurement uncertainty of each output signal.

Two different situations were considered about the PDF, depending on the investigated output variable:

- $t \rightarrow$ UNIFORM distribution
even if the eight repetitions of the thickness measurements were considered enough for a normal PDF, they always lie between two values, and therefore a uniform distribution should be more appropriate;
- ϑ , U and I and \rightarrow NORMAL distribution
the number of measurements and their variability made it possible to assume a normal PDF. In particular, since the data were often spread in an asymmetric way from the mean, the median and the skew factor (see Eq. (81)) were also determined.

Moreover also the measuring area A_m and its measurement uncertainty are required. The A_m has dimensions equal to 0.150 ± 0.001 m x 0.150 ± 0.001 m, which means $A_m = 0.0225 \pm 0.0006$ m, supposing a triangular PDF.

Once defined the measurement uncertainty of each parameter involved in the calculation of the COP thermal conductivity (indirect measurement), the related combined uncertainty $u_c(\lambda)$ was assessed, in accordance with ξ

5.2.2 *Guarded Hot Plate* (neglecting the effects of $\Delta\lambda_{R,E}$, $\Delta\lambda_O$, $\Delta\lambda_S$, since all the uncertainty contributions were obtained from a Type A analysis, and the unknown C_j value).

The laboratory internal climate condition was set to a temperature of 20°C with the 50% of RH.

The detailed results are reported in Appendix C, while a summary of the main results is shown below (Table 35 and Figure 69):

Table 35: Aerogel thermal conductivities and related Type A measurement uncertainties (GHP-1)

ϑ_{avg}	$[\text{°C}]$	5			10			23		
$\Delta\vartheta$	$[\text{°C}]$	5	10	15	5	10	15	5	10	15
λ	$[\text{mW/mK}]$	17.2	16.8	17.8	17.6	17.2	18.0	17.9	17.5	18.3
$u_c(\lambda)$	$[\text{mW/mK}]$	0.2	0.2	0.2	0.2	0.2	0.3	0.2	0.2	0.3
	$[\%]$	1.16	1.19	1.12	1.14	1.16	1.67	1.12	1.14	1.64

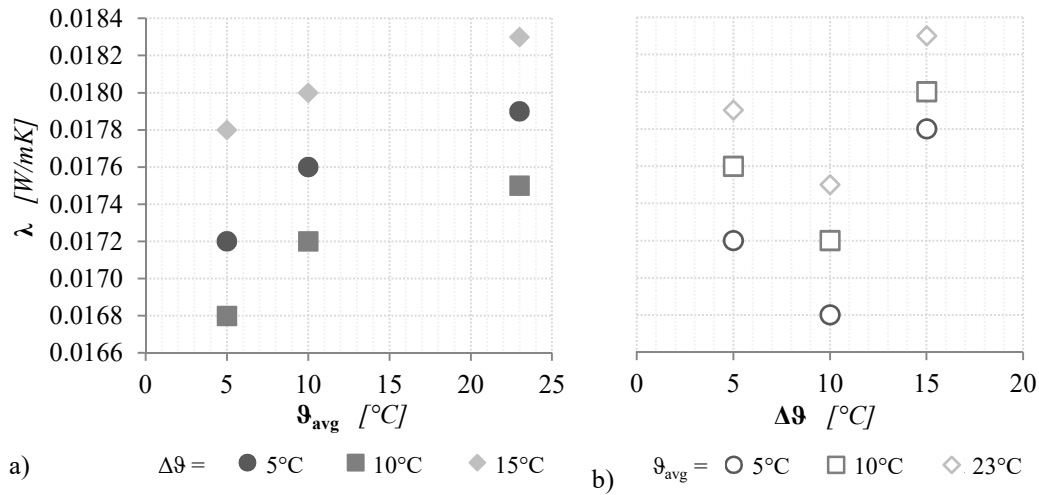


Figure 69: Aerogel thermal conductivity, a) as a function of ϑ_{avg} and b) $\Delta\vartheta$

The results confirm the temperature dependency of the thermal conductivity for all the considered temperature differences (λ increases with the increase of the ϑ_{avg}). But λ -values also depend on the temperature differences $\Delta\vartheta$: with higher temperature differences between the measuring plates, the heat flux through the sample will increase, and therefore the measurement uncertainty should be reduced. Consequently, increasing the $\Delta\vartheta$, the thermal conductivity values should stabilise, but this does not happen in practice: when $\Delta\vartheta = 10\text{°C}$ the lowest thermal conductivity is always observed, for all the analysed average testing temperatures.

Moreover, with $\vartheta_{avg} = 23\text{°C}$, the values of $u_c(\lambda)$ are considerably reduced (about one order of magnitude lower): this phenomenon is probably due to a greater stability of the apparatus electrical signals at higher temperatures.

In the end, it is once again possible to mark that in the case of a Type A uncertainty assessment, the statistical analysis of repeated measurements generally compensates the effect of the $\Delta\theta$ on the final uncertainty value.

7.4 Thermal bridging effects uncertainty

Thermal bridging effects are one of the most critical issues related to VIPs, as already discussed. In fact, they strongly affect the overall performances of a VIP assembly, depending on several factors (first of all the type and the quality of the joint between the panels). Another critical aspect to be solved is the experimental assessment of the thermal bridge thermal parameters (λ_{eq} and ψ): the most common measurement procedures were explained in § 3.2 *VIPs thermal performance parameters* and § 4.1.3 *Methodologies for the measurement of ψ - values*, but how these methods are reliable (in term of measurement uncertainty) was until now unknown.

To remedy this lack, an experimental campaign was performed in collaboration with FIW - Forschungsinstitut für Wärmeschutz e.V. (München). as described in § 5.3 *Linear thermal transmittance*. Four different VIP samples were tested (10 and 40 mm thick FS based VIPs, and 20 and 30 mm thick FG based VIPs) at different temperatures (10°C for FS based VIPs, and 10 and 23°C for FG based VIPs) with a temperature difference between the plates of around 15°C and assembled with different joint typologies and layout (commutated, offset and gasket strip joint). All the details of the experimental set-up are described in **Table 14**, while the specification of the adopted apparatuses (GHP-2, GHP-3 and HFM-2) are reported in **Table 15**.

First of all, the λ_{COP} of each sample was assessed by means of GHP-2, and the related $u_c(\lambda_{COP})$ was evaluated through Eq. (73). After that, the linear thermal transmittance of the coupled VIPs was measured with GHP-2, GHP-3 and/or HFM-2 depending on the joint configuration and consequently assembly dimensions. The values of $u_c(\psi)$ were then estimated by Eq. (78) in case of GHP FS based VIPs measurements (same apparatus for the measurement of λ_{COP} and ψ), Eq. (79) for GHP FG based VIPs measurements (different apparatus for λ_{COP} and ψ) and Eq. (76) in case of HFM measurements.

The uncertainty analyses were Type B for GHP measurements, and both Type B and Type A for HFM.

In the following sections, a summary of the main results is reported (measured thermal performance, related measurement uncertainty value and the sensitivity

coefficients of the most influencing factors), while the detailed reports are in Appendic D, Appendix E and Appendix F.

7.4.1 Guarded Hot Plate

Two different GHP apparatuses were used for the characterization of the VIPs centre of panel thermal performances (GHP-2 and GHP-e for panels with FS core and FG core respectively), while for the assessment of the assemblies thermal properties was used only the GHP-2. The dimensions of both the apparatuses made it possible to measure only the VIPs assemblies with commutated joint.

The principle of the measurement for the two devices, as well as of their uncertainty determination, is the same except for the temperatures evaluation (which is different due to the different position of the thermocouples, as hereinafter explained).

The COP thermal characterisation is essential for the subsequent assessment of the assemblies thermal performances.

In the following sections, the detailed procedure for the uncertainty evaluation is reported, firstly for what concerns the λ_{COP} value, and then related to λ_{eq} and ψ . Since all the apparatuses were double specimens and symmetrical, the described procedure was repeated twice and then averaged (the uncertainty of the average was then evaluated through the combined uncertainty method).

7.4.1.1 VIP centre of panel thermal characterisation

The COP thermal conductivity measured by means of GHP apparatuses is defined by Eq. (72), which is shown below to improve the ease of reading:

$$\lambda_{GHP} = \frac{U \cdot I \cdot t}{2 \cdot A_m \cdot \Delta\vartheta \cdot C_j} \cdot \Delta\lambda_{R,E} \cdot \Delta\lambda_O \cdot \Delta\lambda_S \quad (72)$$

The following list shows all the involved quantities and the procedure followed to assess their uncertainty:

- **Measuring area - A_m [m²]**

$$u_c(A_m) = \sqrt{\left(\frac{u(l_1)}{l_1}\right)^2 + \left(\frac{u(l_2)}{l_2}\right)^2} \cdot A_m \quad (82)$$

Where the uncertainty of each side $u(l_i)$ is defined supposing a triangular PDF:

$$u(l_i) = \frac{\text{Instrument scale resolution}}{\sqrt{12}} = \frac{0.001}{\sqrt{12}} = 0.003 \text{ m} \quad (83)$$

This approach was used for all the other area and length uncertainties (see the following points).

- **Specimens mean thickness - t_m [m]**

The thickness of the various samples was always manually measured with a callipers, repeating the measurements in several points. In this case, the uncertainty of each thickness data was assumed to be $u(t_i) = 0.00002 \text{ m}$ (considering the resolution of the callipers), while the values of $u_c(t_m)$ were defined through the standard deviation. Sometimes, directly the mean value of the several thickness readings was available, and in this case the $u(t_i)$ was evaluated through:

$$u(t_i) = \frac{\text{Mean digits}}{\sqrt{12}} = \frac{0.001}{\sqrt{12}} = 0.003 \text{ m} \quad (84)$$

These thickness uncertainties were assessed for each side of the apparatuses and then combined together to define the uncertainty of the mean $u_c(t_m)$.

- **Electric signal - U [V];**

The uncertainty of the electric signal was defined as a function of the measured voltage range (in accordance with the apparatus datasheet):

Range 0.1 V	$u(U) = 0.0050\% \cdot U + 0.0040\% \cdot \text{Range}(= 0.1)$	
1 V	$u(U) = 0.0040\% \cdot U + 0.0007\% \cdot \text{Range}(= 1)$	(85)
10 V	$u(U) = 0.0035\% \cdot U + 0.0005\% \cdot \text{Range}(= 10)$	

- **Electric current - I [A];**

The electric current is obtained from the ratio between the electric signal U and the electric resistance R [Ω]:

$$I = \frac{U}{R} = \frac{U \pm u(U) \pm u(U_{\text{Ripple residual}})}{R \pm u_c(R)} = \frac{U \pm u_c^*(U)}{R \pm u_c(R)} \quad (86)$$

where $U_{Ripple\ residual}$ is the residual fraction of an alternating (AC) voltage on the DC voltage after the rectification (incomplete suppression of the alternating waveform), and its $u(U_{Ripple\ residual})$ is equal to 0.025 V (provided by datasheet). Consequently:

$$u_c^*(U) = \sqrt{u(U)^2 + u(U_{Ripple\ residual})^2} \quad (87)$$

In the datasheet are also reported the value of R ($R_{basic\ value} = 0.1\ \Omega$) and the criteria for the evaluation of $u_c(R)$:

$$\begin{aligned} R = R_{basic\ value} \quad \pm u(R_{Tolerance}) = 0.1\% &= 0.0001\ \Omega \\ \pm u(R_{Stability}) = 0.01\% &= 0.00001\ \Omega \\ \pm u(R_{Long\ term\ stability}) = 50\ ppm &= 0.00005\ \Omega \\ \pm u_c(R_{Warming}) = 1\ ppm/K &= 0.00003\ \Omega \end{aligned} \quad (88)$$

The evaluation of $u_c(R_{Warming})$ requires a further analysis of the temperature limits that can be reached in the apparatus resistor and in the laboratory ambient. The values of this warming analysis are reported in the following table:

Table 36: GHP-2 and GHP-3 warming analysis

<i>Warming analysis</i>			<i>Correlations</i>	
<i>I</i>	Max temperature coeff.	[ppm]	1	= [ppm] in $u_c(R_{Warming})$
<i>II</i>	Max limit from the datasheet	[A]	3	Input
<i>III</i>	Max limit from the datasheet	[W]	3	Input
<i>IV</i>	Max resistor self-heating (3 A)	[W]	0.9	= $II^2 \cdot R_{basic\ value}$
<i>V</i>	Max ambient temperature	[°C]	70	Input
<i>VI</i>	Max resistor internal temperature	[°C]	155	Input
<i>VII</i>	Max heating resistor	[K]	85	= $IV - V$
<i>VIII</i>	Max heating resistor (3 A)	[K]	25.5	= $(IV/III) \cdot VII$
<i>IX</i>	Room temperature	[°C]	25	Input
<i>X</i>	Max fluctuation room temperature	[K]	5	Input
<i>XI</i>	Max temperature difference	[K]	30.5	= $X + VIII$
$u_c(R_{Warming})$		[ppm/K]	0.00003	= $XI \cdot I^{-6}$

Finally, it is possible to evaluate the $u_c(R)$ and then the $u_c(I)$:

$$u_c(R) = \sqrt{u(R_{Tolerance})^2 + u(R_{Stability})^2 + u(R_{Long\ term\ stab.})^2 + u(R_{Warming})^2} \quad (89)$$

$$u_c(I) = \sqrt{\left(\frac{u_c^*(U)}{U}\right)^2 + \left(\frac{u_c(R)}{R}\right)^2} \cdot I \quad (90)$$

- **Mean temperature difference - $\Delta\vartheta_m$ [$^{\circ}\text{C}$];**

In case of λ_{COP} measurements, five thermocouples were placed on both the warm side and the cold side of the VIP, in correspondence with the measuring area (Table 14). The several obtained temperature values were averaged for both sides ($\vartheta_{m,hot}$ and $\vartheta_{m,cold}$) then the mean temperature difference was evaluated ($\Delta\vartheta_m$). The uncertainty of each thermocouple was equal to $u(\vartheta_i) = 0.25$ $^{\circ}\text{C}$ (from datasheet), the values of $u_c(\vartheta_{m,i})$ were defined through their standard deviations, and the $u_c(\Delta\vartheta_m)$ was then evaluated with:

$$u_c(\Delta\vartheta_m) = \sqrt{u_c(\vartheta_{m,hot})^2 + u_c(\vartheta_{m,cold})^2} \quad (91)$$

- **Gap correction factor - C_j [-]**

The gap correction factor can be evaluated with Eq. (71), neglecting the plate and guarded ring thermal conductivity contributions (they are composed of the same material). The value of $u_c(C_j)$ can be defined as:

$$u_c(C_j) = \frac{1}{2} \cdot \sqrt{\left(\frac{u_c(A_{SP})}{A_{SP}}\right)^2 + \left(\frac{u_c(A_m)}{A_m}\right)^2} \cdot C_j \quad (92)$$

The uncertainty of A_{SP} (area of the gap between the measuring area and the guarded ring) was evaluated in the same way explained for $u_c(A_m)$.

- **Additional uncertainty contributions - $\Delta\lambda_{R,E}$, $\Delta\lambda_O$, $\Delta\lambda_S$ [-]**

The standard EN 1946-2:1999 [149] provides the maximum probable error for each one of this three unitary quantities, depending on the assessed value of λ_{COP} :

$$u(\lambda_{R,E}) = (\lambda_O) = 0.5\% \cdot \lambda_{COP} \quad (93)$$

$$u(\lambda_S) = 0.1\% \cdot \lambda_{COP} \quad (94)$$

The considerations stated so far are valid for both the GHP-2 and the GHP-3: the only difference between the two devices is the size, and consequently the surface of the measurement area and the gap surface: **Table 37** provides a summary of these dimensions coupled with the combined uncertainties.

Table 37: Summary of the dimensions of the useful areas of GHP-2 and GHP-3 apparatuses, with the related combined uncertainties

		Dimensions	GHP - 2	GHP - 3
Plate	l_1	$[m]$	0.8000	0.4000
	l_2	$[m]$	0.8000	0.4000
	A	$[m^2]$	0.6400	0.1600
	$u_c(A)$	$[m^2]$	0.0003	0.0002
Measuring area	a_m	$[m]$	0.4983	0.2002
	b_m	$[m]$	0.4983	0.2002
	A_m	$[m^2]$	0.2483	0.0401
	$u_c(A_m)$	$[m^2]$	0.0002	0.0001
Gap	A_{SP}	$[m^2]$	0.0028	0.0066
	$u_c(A_{SP})$	$[m^2]$	0.0003	0.0001

Once defined the quantities and the uncertainties of all the described contributions, it is possible to evaluate the $u_c(\lambda_{COP})$ through Eq. (73).

In **Table 38** the results related to the λ_{COP} are shown (thermal conductivity values, combined uncertainty and main influencing factors on $u_c(\lambda_{COP})$).

Table 38: VIP centre of panel thermal conductivities and related Type B measurement uncertainties (apparatus GHP-2 for FS based VIPs and GHP-3 for FG based VIPs)

VIP core	t $[mm]$	ϑ_{avg} $[^\circ C]$	λ_{COP} $[W/mK]$	$u_c(\lambda_{COP})$ $[W/mK]$	$u_c(\lambda_{COP})$ $[%]$	Main influence factors	
FS	20	10	0.00406	0.00007	1.72	t_m	52.70%
						A_m	27.08%
						I	15.51%
	40	10	0.00428	0.00006	1.40	A_m	33.81%
						t_m	33.59%
						I	26.57%
FG	20	10	0.00212	0.00002	0.95	t_m	48.40%
						A_m	26.27%
						I	20.65%
	30	23	0.00230	0.00002	0.87	t_m	49.67%
						A_m	26.96%
						I	18.63%
30	10	0.00216	0.00003	1.39	t_m	37.91%	
					A_m	29.07%	
					I	27.75%	
30	23	0.00235	0.00003	1.28	t_m	39.71%	
					A_m	30.46%	
						I	24.42%

The obtained $u_c(\lambda_{COP})$ are in line with the uncertainty limit defined by the standard EN 1946-2:1999 [149], equal to 2%. In addition, the FG panels are on average characterised by a lower uncertainty than the FS based VIPs. This is due to the fact that in case of VIPs with FG core, almost all the uncertainties contributions are lower (see Appendix D). In particular, in case of GF based VIPs, the uncertainty of the measuring area is about one half, the thickness is measured in height different points (while for FS core, they were repeated only four times or directly the thickness mean value was provided), and the uncertainty of $\Delta\vartheta_m$ is lower, due to a lower variability of the measurements.

Since t_m and A_m are the parameters defined with less precision, they represent the most influencing factors on the overall $u_c(\lambda_{COP})$ (t_m is particularly significant in the case of thin panels). Also the electric current I strongly affects the COP thermal conductivity uncertainty (the evaluation of $u_c(I)$ required a lot of assumptions and data from the device's datasheet).

7.4.1.2 Equivalent thermal conductivity and linear thermal transmittance

In case of VIPs assemblies (thermal bridging effects), the combined measurement uncertainty of the various λ_{eq} values was evaluated in exactly the same way of λ_{COP} . The only exception is the evaluation method of $\Delta\vartheta_m$ and $u_c(\Delta\vartheta_m)$. As mentioned in § 4.1.3 Methodologies for the measurement of ψ - values, several thermocouples fixed on the assembly sample surfaces, mapping its different surfaces temperatures (approach proposed in [114]), in three different areas thermally affected in different ways by the increased heat flux through the joint (

Figure 32). These three areas are the COP area (A_{COP}), the slightly affected area (A_{SA}) and the joint area (A_J), whose dimensions and combined uncertainties are shown in **Table 39**. To evaluate the $\Delta\vartheta_m$ all the measured temperature differences were area weighted (Eq. (95)), and then averaged between the two sides of the apparatus.

$$\Delta\vartheta_{m_i} = \frac{\Delta\vartheta_{COP} \cdot A_{COP} + \Delta\vartheta_{SA} \cdot A_{SA} + \Delta\vartheta_J \cdot A_J}{A_{COP} + A_{SA} + A_J} \quad (95)$$

Each $\Delta\vartheta_i$ and $u_c(\Delta\vartheta_i)$ was defined as the mean of each temperature reading ($u(\vartheta_i) = 0.25^\circ\text{C}$), and then the $u_c(\Delta\vartheta_{m_i})$ was evaluated.

Table 39: Summary of the dimensions of the useful areas of GHP-2 apparatus involved in the evaluation of $\Delta\vartheta_m$, with the related combined uncertainties

	Dimensions		GHP - 2		Dimensions		GHP - 2
FG - COP Area	a_{COP}	[m]	0.5000	FS - COP Area	a_{COP}	[m]	0.5000
	b_{COP}	[m]	0.3400		b_{COP}	[m]	0.4720
	A_{COP}	[m ²]	0.1700		A_{COP}	[m ²]	0.2360
	$\mathbf{u}(\mathbf{A}_{COP})$	[m ²]	0.0002		$\mathbf{u}(\mathbf{A}_{COP})$	[m ²]	0.0002
FG - SA Area	a_{SA}	[m]	0.5000	FS - SA Area	a_{SA}	[m]	0.5000
	b_{SA}	[m]	0.1200		b_{SA}	[m]	0.0120
	A_{SA}	[m ²]	0.0600		A_{SA}	[m ²]	0.0060
	$\mathbf{u}(\mathbf{A}_{SA})$	[m ²]	0.0001		$\mathbf{u}(\mathbf{A}_{SA})$	[m ²]	0.0001
FG - J Area	a_J	[m]	0.5000	FS - J Area	a_J	[m]	0.5000
	b_J	[m]	0.0400		b_J	[m]	0.0040
	A_J	[m ²]	0.0200		A_J	[m ²]	0.0020
	$\mathbf{u}(\mathbf{A}_J)$	[m ²]	0.0001		$\mathbf{u}(\mathbf{A}_J)$	[m ²]	0.0001

Anyway, when thermal bridging effects occur, the most significant and representative thermal property is the linear thermal transmittance ψ , defined by Eq. (74). In case of FS based VIPs, since the COP and the assembly measurements were both performed by means of GHP-2, the ψ equation can be rewritten as Eq. (77), which shown below:

$$\psi_{GHP} = \frac{A_m}{t_m \cdot l_\psi} \cdot \left(\left[\frac{U \cdot I \cdot t_m}{2 \cdot A_m \cdot \Delta\vartheta_m \cdot C_j} \cdot \Delta\lambda_{R,E} \cdot \Delta\lambda_O \cdot \Delta\lambda_S \right]_{eq_GHP} - \left[\frac{U \cdot I \cdot t_m}{2 \cdot A_m \cdot \Delta\vartheta_m \cdot C_j} \cdot \Delta\lambda_{R,E} \cdot \Delta\lambda_O \cdot \Delta\lambda_S \right]_{COP_avg} \right) \quad (77)$$

Differently, for VIPs with FG core, the values of λ_{COP} were measured using the GHP-3 apparatus, while the thermal bridging effects in their assemblies were evaluated with the GHP-2. Therefore Eq. (77) can be simplified:

$$\psi_{GHP} = \frac{A_m}{t_m \cdot l_\psi} \cdot \left(\left[\frac{U \cdot I \cdot t_m}{2 \cdot A_m \cdot \Delta\vartheta_m \cdot C_j} \cdot \Delta\lambda_{R,E} \cdot \Delta\lambda_O \cdot \Delta\lambda_S \right]_{eq_GHP} - \lambda_{COP_avg} \right) \quad (96)$$

The ψ uncertainty evaluation was at this point performed by applying the Eq. (78) and (79) for FS and FG based VIPs assemblies respectively.

Between all the assembly configurations presented in **Table 14**, the only one measured by means of the GHP-2 apparatus was the Commutated joint (no measurements with the GHP-3 were in this stage performed).

Table 40 shows the main results related to the λ_{eq} and ψ evaluation: thermal conductivity values, combined uncertainty and main influencing factors on $u_c(\lambda_{eq})$ and $u_c(\psi)$, while the detailed results are reported in Appendix E.

Even if a direct comparison between the results is not possible (the assemblies although similar are all different one from the other), from a first glance it is clear that FG VIPs are extremely more sensitive to the effects of thermal bridges (as they are more performing) than FS VIPs. The λ_{COP} values were about 9% lower than λ_{eq} in case of FS based panels, while for VIPs with FG core this reduction is around 70%. Consequently, also the ψ values are higher, and they strongly depend also on the sample thickness (the thinner is the sample, the higher is the ψ).

Table 40: VIP assemblies thermal properties and related Type B measurement uncertainties (apparatus GHP-2 for FS based VIPs and GHP-3 for FG based VIPs, Commutated joint)

VIP core	t [mm]	ϑ_{avg} [°C]	λ_{eq} [W/mK]	$u_c(\lambda_{eq})$ [W/mK]	$u_c(\lambda_{eq})$ [%]	Main influence factors	ψ [W/mK]	$u_c(\psi)$ [W/mK]	$u_c(\psi)$ [%]	Main influence factors
FS	20	10	0.00444	0.00008	1.80	t_m 76.98%	0.009	0.002	22.22	$t_{m,eq}$ 24.76%
						I 10.08%				$t_{m,COP}$ 24.70%
						A_m 6.37%				I_{eq} 21.99%
	40	10	0.00471	0.00008	1.70	t_m 52.93%	0.005	0.001	20.00	I_{eq} 34.95%
						I 21.04%				$t_{m,COP}$ 14.48%
						A_m 9.66%				$t_{m,eq}$ 14.43%
FG	20	10	0.00715	0.00010	1.40	t_m 77.09%	0.115	0.002	1.74	$t_{m,COP}$ 25.27%
						I 9.15%				$t_{m,eq}$ 25.16%
						A_m 6.78%				$A_{m,COP}$ 13.72%
	23	0.00735	0.00008	1.09	t_m 78.19%	0.115	0.002	1.74	$t_{m,COP}$ 26.30%	
					A_m 6.88%				$t_{m,eq}$ 26.19%	
					I 7.91%				$A_{m,COP}$ 14.28%	
30	10	0.00761	0.00010	1.31	t_m 69.67%	0.090	0.002	2.22	$t_{m,eq}$ 20.09%	
					I 13.04%				$t_{m,COP}$ 19.81%	
					A_m 8.50%				$A_{m,COP}$ 15.19%	
23	0.00794	0.00008	1.00	t_m 71.17%	0.092	0.001	1.09	$t_{m,eq}$ 21.26%		
				I 11.24%				$t_{m,COP}$ 20.96%		
				A_m 8.69%				$A_{m,COP}$ 16.08%		

The absolute uncertainties are for both the core materials between 0.00008 and 0.00010 W/mK in case of $u_c(\lambda_{eq})$, and between 0.001 and 0.002 W/mK considering the $u_c(\psi)$. Anyway, in terms of relative uncertainty, the situation completely changes, in particular for $u_c(\psi)$. In case of FS based VIPs, the 0.001 - 0.002 W/mK equates to more than 20% of relative uncertainty, against about the

2% observed for the FG VIPs. This is due to the lower extra heat flux which crosses the joint in the case of FS VIPs assemblies (which also depends on the assembly thickness), and consequently the lower difference between λ_{COP} and λ_{eq} . The thicker is the assembly, the lower is the difference between λ_{COP} and λ_{eq} and the higher is the influence of the measured electric current on the overall $u_c(\lambda_{eq})$.

The strong correlation with the thickness is also pointed out by the uncertainties main influencing factors, which are, in general, the thicknesses of both the single panels and the VIPs assemblies. After them, also the Am and I are extremely important, as just explained.

Moreover, higher temperatures contribute to a slight reduction of the combined uncertainties of both λ_{eq} and ψ .

7.4.2 Heat Flow Meter

The complete analysis of the three different assembly typologies (Commutated, Offset and Gasket strip) was performed by means of the HFM-3 apparatus, considering both the FS and the FG based VIPs.

To evaluate the ψ value of each sample configuration, the so measured λ_{eq} were compared with the COP values previously defined by means of GHP-2 or GHP-3 (no COP tests were performed with the HFM-2 device).

Differently from the GHP investigations, in case of HFM measurements, a multimeter report was available for each test, including all the recorded signals. Therefore, a Type A uncertainty evaluation was also performed, analysing around one hundred data for each signal. The related results are compared to the other two (Type B evaluation by means of GHP and HFM) in § 7.4.3 *Comparison between GHP and HFM methods*.

7.4.2.1 Equivalent thermal conductivity and linear thermal transmittance

The assemblies equivalent thermal conductivity was evaluated with Eq. (67):

$$\lambda_{HFM} = \frac{f_{cal}(\vartheta) \cdot Q \cdot t}{\Delta\vartheta} \cdot \Delta\lambda_E \cdot \Delta\lambda_O \quad (67)$$

The followed procedure for the assessment of the assemblies mean thickness was already described in the previous chapters, while for the assessment of the other involved quantities is hereinafter presented:

- **Calibration factor - $f_{cal}(\vartheta)$ [W/m²mV]**
The value of the calibration factor is a characteristic of each measuring plate and depends on its own temperature. To this aim, each plate temperature was measured with two thermocouples, each of which provided about 100 data. The uncertainty of the two measured temperatures was obtained from their standard deviation, and then the values were averaged, to find the mean plate temperature (ϑ_p). Once defined the ϑ_p of the four plates of the HFM-2 device, the values of the four $f_{cal}(\vartheta)$ and $u_c(f_{cal}(\vartheta))$ were derived from the calibration file of the apparatus, available at the FIW institute.
- **Mean temperature difference - $\Delta\vartheta_m$ [°C];**
The criteria for the evaluation of $\Delta\vartheta_m$ and $u_c(\Delta\vartheta_m)$ were the same presented in § 7.4.1.2 *Equivalent thermal conductivity and linear thermal transmittance*, but with six thermocouples, instead of five, placed in a slightly different position. In case of Type B uncertainty evaluation, the uncertainty of each thermocouple was assumed equal to 0.25°C, while in case of Type A approach, the measurements standard deviation was considered for the evaluation of the temperature uncertainty.
- **Electric signal from the transducer - Q [mV]**
Each one of the four plates of the HFM-3 device was equipped with a heat flux sensor, which, at the end of the measurements, provides again about 100 values of the measured electric signal, whose uncertainty was obtained from the standard deviation. The four values were then averaged, and the related combined uncertainty was evaluated as the uncertainty of the mean.
- **Additional uncertainty contributions - $\Delta\lambda_E, \Delta\lambda_O$ [-]**
The standard EN 1946-3:1999 [148] provides the maximum probable error for each one of this three unitary quantities, depending on the assessed value of λ_{eq} :

$$u(\lambda_E) = 0.1\% \cdot \lambda_{eq} \quad (97)$$

$$u(\lambda_O) = 0.5\% \cdot \lambda_{eq} \quad (98)$$

Once defined the value and the uncertainty of all the involved parameters, the $u_c(\lambda_{eq})$ was assessed through Eq. (68).

The linear thermal transmittance in case of HFM-2 measurements and the related combined experimental uncertainty were evaluated with Eq. (75) and (76) respectively.

$$\psi_{HFM} = \frac{A_m}{t_m \cdot l_\psi} \cdot \left(\left[\frac{t_m \cdot f_{cal}(\vartheta) \cdot Q}{\Delta\vartheta_m} \cdot \Delta\lambda_E \cdot \Delta\lambda_O \right]_{eq_HFM} - \left[\frac{U \cdot I \cdot t_m}{2 \cdot A_m \cdot \Delta\vartheta_m \cdot C_j} \cdot \Delta\lambda_{R,E} \cdot \Delta\lambda_O \cdot \Delta\lambda_S \right]_{COP_avg} \right) \quad (75)$$

The detailed results of these analyses are shown in Appendix F, while hereinafter some summary tables are presented (one for each joint configuration).

Table 41: VIP assemblies thermal properties and related Type B measurement uncertainties (apparatus HFM-2, Commutated joint)

VIP core	t [mm]	ϑ_{avg} [°C]	λ_{eq} [W/mK]	$u_c(\lambda_{eq})$ [W/mK]	$u_c(\lambda_{eq})$ [%]	Main influence factors	ψ [W/mK]	$u_c(\psi)$ [W/mK]	$u_c(\psi)$ [%]	Main influence factors
FS	20	10	0.0043	0.0001	2.32	t_m 91.53%	0.006	0.003	50.00	$t_{m,COP}$ 33.43%
						Q_m 4.25%				$t_{m,eq}$ 33.15%
	40	10	0.0045	0.0001	2.22	t_m 79.55%	0.003	0.002	66.67	$A_{m,COP}$ 17.18%
						Q_m 13.30%				$t_{m,COP}$ 23.70%
FG	20	10	0.0061	0.0002	3.28	t_m 92.03%	0.092	0.003	3.26	$t_{m,COP}$ 29.09%
		Q_m 3.52%	$t_{m,eq}$ 29.06%							
	23	0.0062	0.0002	3.22	t_m 92.27%	0.091	0.003	3.30	$t_{m,COP}$ 15.79%	
					Q_m 3.26%				$t_{m,eq}$ 29.83%	
	30	10	0.0069	0.0002	2.90	t_m 88.81%	0.079	0.003	3.80	$t_{m,COP}$ 23.81%
						Q_m 5.65%				$t_{m,eq}$ 23.81%
23	0.0070	0.0002	2.86	t_m 88.81%	0.078	0.003	3.85	$t_{m,COP}$ 17.88%		
				Q_m 5.25%				$t_{m,eq}$ 24.85%		
										$A_{m,COP}$ 18.67%

As expected, the obtained uncertainties (Table 41) are sensibly worse compared to the GHP measurements. Considering the absolute $u_c(\lambda_{eq})$ values, they are approximatively an order of magnitude higher than for the GHP results, while the relative uncertainties are about the double.

Even worse for what concerns the linear thermal transmittance. Though the rising of the relative $u_c(\psi)$ in case of FG based VIPs is analogous to the one observed for the $u_c(\lambda_{eq})$, in case of FS core, the $u_c(\psi)$ goes up to 50% and about 67% for assemblies with thickness equal to 20mm and 40 mm respectively.

Indeed, the strong correlation with the thickness is again observed, and also in terms of the uncertainties most influencing factors.

Moreover, the increasing of the average testing temperatures contributes to a slight reduction of the combined uncertainties of the λ_{eq} but not of the ψ .

The tests on the Offset joints revealed exactly the same performances as the Commutated joint (Table 42), except for the evaluation of the ψ of the 40 mm thick assembly, for which a relative uncertainty of 100% was obtained.

Table 42: VIP assemblies thermal properties and related Type B measurement uncertainties (apparatus HFM-2, Offset joint)

VIP core	t [mm]	ϑ_{avg} [°C]	λ_{eq} [W/mK]	$u_c(\lambda_{eq})$ [W/mK]	$u_c(\lambda_{eq})$ [%]	Main influence factors	ψ [W/mK]	$u_c(\psi)$ [W/mK]	$u_c(\psi)$ [%]	Main influence factors
FS	20	10	0.0043	0.0001	2.32	t_m 91.51%	0.006	0.003	50.00	$t_{m,COP}$ 34.43%
						Q_m 4.27%				$t_{m,eq}$ 33.15%
	40	10	0.0045	0.0001	2.22	t_m 79.45%	0.002	0.002	100.00	$A_{m,COP}$ 17.18%
						Q_m 13.41%				$t_{m,COP}$ 23.71%

Table 43: VIP assemblies thermal properties and related Type B measurement uncertainties (apparatus HFM-2, Gasket strip joint)

VIP core	t [mm]	ϑ_{avg} [°C]	λ_{eq} [W/mK]	$u_c(\lambda_{eq})$ [W/mK]	$u_c(\lambda_{eq})$ [%]	Main influence factors	ψ [W/mK]	$u_c(\psi)$ [W/mK]	$u_c(\psi)$ [%]	Main influence factors
FS	20	10	0.0045	0.0001	2.22	t_m 91.65%	0.010	0.004	40.00	$t_{m,COP}$ 33.39%
						Q_m 4.13%				$t_{m,eq}$ 33.11%
	40	10	0.0047	0.0001	2.13	t_m 79.90%	0.005	0.002	40.00	$A_{m,COP}$ 17.16%
						Q_m 12.92%				$t_{m,COP}$ 23.66%
FG	20	10	0.0070	0.0002	2.86	t_m 92.48%	0.113	0.004	3.54	$t_{m,COP}$ 33.43%
					Q_m 3.05%	$t_{m,eq}$ 33.15%				
	23	0.0072	0.0002	2.78	t_m 92.62%	0.116	0.004	3.45	$t_{m,COP}$ 28.65%	
					Q_m 2.89%				$t_{m,eq}$ 28.62%	
	30	10	0.0101	0.0003	2.97	t_m 89.93%	0.129	0.004	3.10	$A_{m,COP}$ 15.55%
						Q_m 3.95%				$t_{m,eq}$ 22.45%
	23	0.0085	0.0003	3.53	t_m 89.32%	0.103	0.003	2.91	$t_{m,eq}$ 23.05%	
				Q_m 4.60%	$t_{m,COP}$ 22.59%				$A_{m,COP}$ 17.61%	

Commenting the results related to the Gasket strip joint (Table 43), it can be observed how the λ_{eq} values slightly increase (although the Gasket strip joint is made of porous and compressible material, this could cause a greater width of the joint itself and therefore a greater extra thermal flow through the thermal bridge). As a consequence, since the absolute uncertainty values are in line with those of the Commutated joints, in case of Gasket strip joints the relative uncertainties are reduced (in particular for the assemblies of FS based VIPs).

Moreover, the uncertainties increase for thicker FG based samples or for thinner FS based assemblies, and for lower average testing temperatures.

Also in this case the thicknesses are confirmed as the most influential parameters on the overall uncertainties.

7.4.3 Comparison between GHP and HFM methods

The direct comparison between the results obtained with a GHP analysis and an HFM analysis is useful to clarify the precision and the accuracy of the two methods. Moreover, the values obtained from the HFM Type A uncertainty analysis provide an idea of how much the measurement uncertainty can be reduced if numerous outputs data are recorded from the acquisition system (about one hundred in this specific case).

The results related to two different core materials and the different thickness are presented, but the Commutated joint configuration is the only one discussed (the other configurations were not tested with the GHP devices).

First of all, it is of fundamental importance to underline how the measurements carried out with the HFM-3 always give results lower of those obtained with the GHP-2. For this reason, it is absolutely possible to assume that it would have given smaller values also for the COP measurements. In this way, the differences between COP and assemblies measurements would have been significantly higher, thus indicating a greater extra heat flux with a consequent reduction of the $u_c(\psi)$ values.

The confirmation of this assumption is that, when there are limited differences between the GHP and the HFM λ_{eq} (therefore more sensitive to a potential λ_{COP} measurement difference between the GHP and the HFM), both the value of $u_c(\psi)$ and $\Delta\psi_{GHP-HFM}$ is extremely high (this is the case of FS based VIPs). Otherwise, when the difference between the GHP and the HFM λ_{eq} increases (VIPs assemblies with FG core), the $u_c(\psi)$ and $\Delta\psi_{GHP-HFM}$ are considerably reduced.

Table 44: VIP assemblies thermal properties and related measurement uncertainties (comparison between GHP-2 and HFM-2, Commutated joint)

<i>FS based VIP (20 mm; $\vartheta_{avg} = 10^\circ\text{C}$)</i>							
	λ_{COP}	$\lambda_{\text{eq_GHP}}$	$\lambda_{\text{eq_HFM}}$	$\lambda_{\text{eq_HFM(A)}}$	Ψ_{GHP}	Ψ_{HFM}	$\Psi_{\text{HFM(A)}}$
	[W/mK]	[W/mK]	[W/mK]	[W/mK]	[W/mK]	[W/mK]	[W/mK]
$u(x_i)$	0.00406	0.00444	0.0043	0.00432	0.009	0.006	0.006
	0.00007	0.00008	0.0001	0.00006	0.002	0.003	0.002
	1.72%	1.80%	2.32%	1.39%	22.22%	50.00%	33.33%
$\Delta\lambda_{\text{GHP-HFM}}$		0.00014					
		-3.2%					
$\Delta\Psi_{\text{GHP-HFM}}$					0.003		
					-33.3%		
<i>FS based VIP (40 mm; $\vartheta_{avg} = 10^\circ\text{C}$)</i>							
	λ_{COP}	$\lambda_{\text{eq_GHP}}$	$\lambda_{\text{eq_HFM}}$	$\lambda_{\text{eq_HFM(A)}}$	Ψ_{GHP}	Ψ_{HFM}	$\Psi_{\text{HFM(A)}}$
	[W/mK]	[W/mK]	[W/mK]	[W/mK]	[W/mK]	[W/mK]	[W/mK]
$u(x_i)$	0.00428	0.00471	0.0045	0.00450	0.005	0.003	0.003
	0.00006	0.00008	0.0001	0.00006	0.001	0.002	0.001
	1.40%	1.70%	2.22%	1.33%	18.58%	66.11%	33.33%
$\Delta\lambda_{\text{GHP-HFM}}$		0.00021					
		-4.6%					
$\Delta\Psi_{\text{GHP-HFM}}$					0.002		
					-40.0%		
<i>FG based VIP ($t = 20$ mm; $\vartheta_{avg} = 10^\circ\text{C}$)</i>							
	λ_{COP}	$\lambda_{\text{eq_GHP}}$	$\lambda_{\text{eq_HFM}}$	$\lambda_{\text{eq_HFM(A)}}$	Ψ_{GHP}	Ψ_{HFM}	$\Psi_{\text{HFM(A)}}$
	[W/mK]	[W/mK]	[W/mK]	[W/mK]	[W/mK]	[W/mK]	[W/mK]
$u(x_i)$	0.00212	0.00715	0.0061	0.00610	0.115	0.092	0.092
	0.00002	0.00010	0.0002	0.00007	0.002	0.003	0.001
	0.95%	1.40%	3.28%	1.15%	1.74%	3.26%	1.09%
$\Delta\lambda_{\text{GHP-HFM}}$		0.00105					
		-14.7%					
$\Delta\Psi_{\text{GHP-HFM}}$					0.023		
					-20.0%		

<i>FG based VIP (20 mm; $\vartheta_{avg} = 23^{\circ}\text{C}$)</i>							
	λ_{COP}	$\lambda_{\text{eq_GHP}}$	$\lambda_{\text{eq_HFM}}$	$\lambda_{\text{eq_HFM(A)}}$	Ψ_{GHP}	Ψ_{HFM}	$\Psi_{\text{HFM(A)}}$
	[W/mK]	[W/mK]	[W/mK]	[W/mK]	[W/mK]	[W/mK]	[W/mK]
$u(x_i)$	0.00230	0.00735	0.0062	0.00623	0.115	0.091	0.091
	0.00002	0.00008	0.0002	0.00007	0.002	0.003	0.001
	0.87%	1.09%	3.22%	1.12%	1.74%	3.30%	1.10%
$\Delta\lambda_{\text{GHP-HFM}}$		0.00115					
		-15.6%					
$\Delta\Psi_{\text{GHP-HFM}}$					0.024		
					-20.9%		
<i>FG based VIP ($t = 30$ mm; $\vartheta_{avg} = 10^{\circ}\text{C}$)</i>							
	λ_{COP}	$\lambda_{\text{eq_GHP}}$	$\lambda_{\text{eq_HFM}}$	$\lambda_{\text{eq_HFM(A)}}$	Ψ_{GHP}	Ψ_{HFM}	$\Psi_{\text{HFM(A)}}$
	[W/mK]	[W/mK]	[W/mK]	[W/mK]	[W/mK]	[W/mK]	[W/mK]
$u(x_i)$	0.00216	0.00761	0.0069	0.00692	0.090	0.079	0.0791
	0.00003	0.00010	0.0002	0.00007	0.002	0.003	0.0010
	1.39%	1.31%	2.90%	1.01%	2.22%	3.80%	1.26%
$\Delta\lambda_{\text{GHP-HFM}}$		0.00071					
		-9.3%					
$\Delta\Psi_{\text{GHP-HFM}}$					0.011		
					-12.2%		
<i>FG based VIP (30 mm; $\vartheta_{avg} = 23^{\circ}\text{C}$)</i>							
	λ_{COP}	$\lambda_{\text{eq_GHP}}$	$\lambda_{\text{eq_HFM}}$	$\lambda_{\text{eq_HFM(A)}}$	Ψ_{GHP}	Ψ_{HFM}	$\Psi_{\text{HFM(A)}}$
	[W/mK]	[W/mK]	[W/mK]	[W/mK]	[W/mK]	[W/mK]	[W/mK]
$u(x_i)$	0.00235	0.00794	0.0070	0.00704	0.092	0.078	0.078
	0.00003	0.00008	0.0002	0.00008	0.001	0.003	0.001
	1.20%	1.00%	2.86%	1.14%	1.09%	3.85%	1.28%
$\Delta\lambda_{\text{GHP-HFM}}$		0.00094					
		-11.8%					
$\Delta\Psi_{\text{GHP-HFM}}$					0.014		
					-15.2%		

Regarding the HFM Type A uncertainty evaluation, in this specific case (statistical analysis of about one hundred data for each measured signal), it allows to obtain both $u_c(\lambda_{eq})$ and $u_c(\psi)$ values perfectly comparable to those obtained with the GHP method (except for the $u_c(\psi)$ of FS based VIPs assemblies, in which, however, the uncertainty is greatly reduced, approximately halved).

As a last comment, significant differences emerge from the analysis of the two different methods. These differences can be mainly assigned to the inconsistency of measurement data (the measurements weren't designed for the uncertainty evaluation, so the data collection was not properly performed), while

the uncertainty balance model was defined with a good accuracy level. Anyway, the purpose of the research was to propose the uncertainty evaluation method, highlighting the strong variability depending on the quality of the measurement campaign.

Chapter 8

Experimental investigation of the thermal behaviour of SIMs

Once defined the uncertainty level achievable in case of SIMs measurement (by means of GHP and HFM apparatuses), several experimental campaigns were performed, to characterise the thermal properties of such materials.

Firstly, the temperature dependency of the VIP thermal conductivity was analysed, trying to identify the different contributes of the gaseous (+ coupling), solid and radiative heat transfer mechanisms on the overall variability of the VIP λ_{COP} . This analysis was performed considering different ageing conditions of the samples.

After that, an interlaboratory comparison was carried out (in the context of the project IEA EBC Annex 65: Long-Term Performance of Super-Insulating Materials in Building Components and Systems) [150]. The aim of the comparison was again to verify the variability of the thermal performances of VIPs, VIP assemblies and APMs, as a function of the average testing temperature and the ageing condition. Where possible, the measurements were performed using the HFM-1 apparatus. (Initially, a comparison between HFM-1 and GHP-1 was pursued, but it was found out that GHP-1 wasn't adequate for most of the VIPs measurements, because of its severe applicability range limits).

In these investigations, the Type B uncertainty of the thermal conductivities was often evaluated. In laboratories, for the sake of time, the measurements for

the thermal characterisation of insulating material are usually performed once or repeated no more than two/three times. This makes impossible to define the Type A uncertainty, and the so obtained results are affected by a higher uncertainty level, which is a Type B uncertainty. It is precisely this value (Type B uncertainty) that must be considered as characterising the measure, that must be taken into account to evaluate the compliance with the standards or not.

8.1 Effects of temperature and ageing on SIM thermal properties (HFM)

The real performance of VIPs when they are applied to buildings can be influenced by several issues, such as the boundary conditions (e.g. temperature) and ageing conditions (if they are new/fresh/pristine panels or not).

Therefore, the aim of this section “*is to investigate through experimental measurements the relationship between the average temperature and centre of panel thermal conductivity of fumed silica VIPs, considering the typical range of temperatures in building applications. In order to carry out a comprehensive analysis, two specimens of fumed silica based VIPs characterised by two different thicknesses (10 and 30 mm) were analysed. The samples centre of panel thermal conductivity was measured in two different stages: when they were fresh (as delivered by the producer), and after they were stored in a laboratory for 32 months at a temperature ranging between 18 and 30°C. Also non-evacuated insulating materials were measured (punctured VIP, fumed silica pressed board and extruded polystyrene - XPS), in order to compare their thermal behaviour with that one of the VIPs. [...] Each sample was measured (by means of HFM-1 apparatus) at different average temperatures ϑ_{avg} (mean temperature between hot and cold plates of the HFM) ranging between 2.5°C and 52.5°C, maintaining the same temperature difference between the plates. The temperature difference $\Delta\vartheta$ was kept equal to 20°C for fresh VIPs and to 25°C for aged VIPs and all the other samples (non-evacuated insulating materials). The Type B uncertainty analyses were carried out in accordance with the GUM [13] considering composite uncertainty that takes into account the measured factors which influence the experimental evaluation of centre of panel thermal conductivity λ_{COP} .*

In Table 45 the main characteristics of the VIP samples analysed in this study are reported, as declared by the producer.

Table 45: Characteristics of FS based VIPs declared by producer [29]

Dimensions		Composition			Properties (provided by the producer)		
Area [mm]	t [mm]	SiO ₂ [%]	SiC [%]	Other [%]	ρ_p [kg/m ³]	$\lambda_{COP - (22.5^\circ C)_p}$ [W/mK]	P _p [mbar]
600 x 600	10	80	15	5	150 - 300	≤ 0.005	≤ 0.5
	30						

The thermal conductivity of fresh VIPs considering a mean temperature of 22.5°C (the same temperature condition of manufacturer declaration) was first measured by means of the HFM. In order to obtain a complete comparison with the manufacturer data, the densities were also estimated by weighting the samples. **Table 46** shows the assessed characteristics of the VIPs. The measured thermal conductivities are in good agreement with the values declared by the producer ($\lambda_{COP - (22.5^\circ C)_p} \leq 0.005$ W/mK). The small difference that occurs between the λ -values lies within the measurement uncertainty (around 2.1% in case of 10 mm VIP thickness and 2.5% in case of 30 mm VIP thickness). The declared density was also confirmed, in both cases its value lied in the range between 150 and 300 kg/m³. These results demonstrate that the adopted experimental procedure is robust and reliable.

Table 46: VIPs experimentally assessed characteristics [29]

Dimensions		Properties (experimental)			
Area [mm]	t [mm]	ρ_{VIP} [kg/m ³]	ρ_{core} [kg/m ³]	$\lambda_{COP - (22.5^\circ C)}$ [W/mK]	P [mbar]
600 x 600	10	~ 200	~ 170	0.0051 ± 0.0001	≤ 0.5
	30	~ 190	~ 180	0.0050 ± 0.0001	

To investigate the influence that the vacuum degree inside the panel has on the correlation between the thermal conductivity and the average temperature, experimental tests were also conducted on non-evacuated insulating materials. In particular, the following specimens were analysed (**Figure 70**):

- Punctured VIP, dimension 600 x 500 x 25 (thickness) mm, density ~ 214 kg/m³, to evaluate the effects of a complete loss of vacuum) on the behaviour of the panels thermal conductivity at different temperatures;
- Fumed Silica pressed board (VIP core material), dimension 600 x 500 x 25 (thickness) mm, density ~ 198 kg/m³, to verify whether the high conductivity VIP envelope can be an influent factor on the VIPs thermal conductivity behaviour;

- Extruded polystyrene (XPS), dimension 600 x 600 x 20 (thickness) mm, density $\sim 30 \text{ kg/m}^3$, to have a reference trend (λ - ϑ characteristic curve) for a traditional macro-porous insulating material.

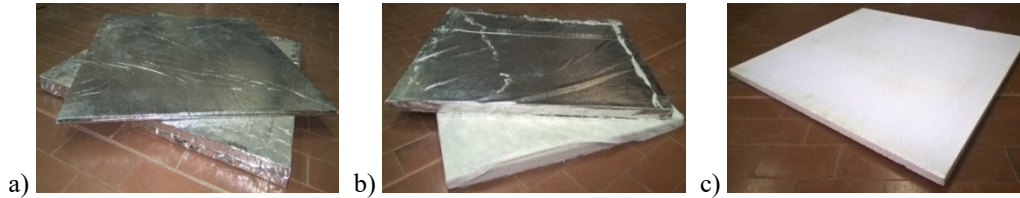


Figure 70: Samples. a) VIP 10 and 30 mm thick; b) punctured VIP and VIP core material; c) XPS [29]

The experimental tests were carried out in two separate stages with different boundary conditions. In the first stage, experimental measurements were performed on two fresh VIPs characterised by the two different thicknesses (10 and 30 mm). Three different values of average temperature ϑ_{avg} (mean temperature of cold and hot plates) were analysed considering a fixed temperature difference between the plates of 20°C. Results of the experiments related to the variation of thermal conductivity as a function of average temperature are summarised in **Table 47** together with the estimated experimental uncertainties.

Table 47: Experimentally assessed characteristics of fresh VIPs [29]

	10 mm VIP - Fresh		30 mm VIP - Fresh	
	λ [W/mK]	$u(\lambda)$ [%]	λ [W/mK]	$u(\lambda)$ [%]
ϑ_{avg} [°C]				
10	0.0048	2.2	0.0046	2.7
25	0.0052	2.1	0.0051	2.6
40	0.0058	2.1	0.0059	2.4
$\Delta\lambda_{(\text{max-min})}$ [W/mK]	0.0010		0.0013	
$\Delta\lambda_{(\text{max-min})}$ [%]	20.4%		28.7%	

In the second stage, experimental tests considering a wide range of average temperatures were carried out on the same panels after that they were stored in the laboratory for 32 months. Moreover, the same kind of analysis was conducted on a punctured VIP, Fumed Silica pressed board (namely VIP core material) and an XPS board (**Table 48**). The thermal conductivity values were evaluated at the centre of panel, and hence no thermal bridging or edge effects were taken into account in the measurements.

Table 48: Thermal conductivity depending on average temperature, and measurement uncertainty of different insulating materials [29]

	10 mm VIP		30 mm VIP		Punctured VIP		FS core		XPS	
ϑ_{avg} [°C]	λ_{COP} [W/mK]	$u(\lambda_{\text{COP}})$ [%]	λ_{COP} [W/mK]	$u(\lambda_{\text{COP}})$ [%]	λ_{COP} [W/mK]	$u(\lambda_{\text{COP}})$ [%]	λ_{COP} [W/mK]	$u(\lambda_{\text{COP}})$ [%]	λ_{COP} [W/mK]	$u(\lambda_{\text{COP}})$ [%]
2.5	0.0050	2.1	0.0047	2.4	0.0213	2.0	0.0211	2.0	0.0307	2.0
12.5	0.0052	2.1	0.0050	2.4	0.0215	2.0	0.0212	2.0	0.0317	2.0
22.5	0.0054	2.1	0.0052	2.3	0.0216	2.0	0.0213	2.0	0.0327	2.0
32.5	0.0058	2.0	0.0056	2.3	0.0218	2.0	0.0214	2.0	0.0337	2.0
42.5	0.0063	2.0	0.0061	2.2	0.0221	2.0	0.0216	2.0	0.0348	2.0
52.5	0.0070	2.0	0.0069	2.2	0.0224	2.0	0.0219	2.0	0.0361	2.0
$\Delta\lambda_{(\text{max-min})}$ [W/mK]	0.0020		0.0022		0.0010		0.0009		0.0054	
[%]	40.4%		45.8%		4.8%		4.1%		17%	

Analysing **Table 47** and **Table 48**, it can be observed that the thermal conductivity strictly depends on the average temperature both for fresh and aged VIPs. Considering the range of average temperature from 10 to 40°C the thermal conductivity of fresh VIPs increases of about 20% (10 mm thickness) and 29% (30 mm thickness). With the same difference of average temperatures (30°C) the centre of panel thermal conductivity of aged VIPs increases of about 16% and 17/18% for 10 mm and 30 mm thickness respectively (~ 0.002 W/mK). Moreover, from 2.5°C to 52.5°C, the thermal conductivity of aged VIP worsened of about 40% and 46% for 10 mm and 30 mm VIP thick, respectively (Fig. 4(a) and (b)). Moreover, it is possible to observe that, in comparison to fresh samples, the ageing effect caused an average increase of thermal conductivity of 5% and 4%, respectively for 10 mm and 30 mm thick.

Considering the measurement uncertainty, results pointed out that a temperature difference between the plates of 25°C provides more reliable data than $\Delta\vartheta = 20^\circ\text{C}$. This is due to the higher heat flux that crosses the specimen in the case of higher temperature gradient [113].

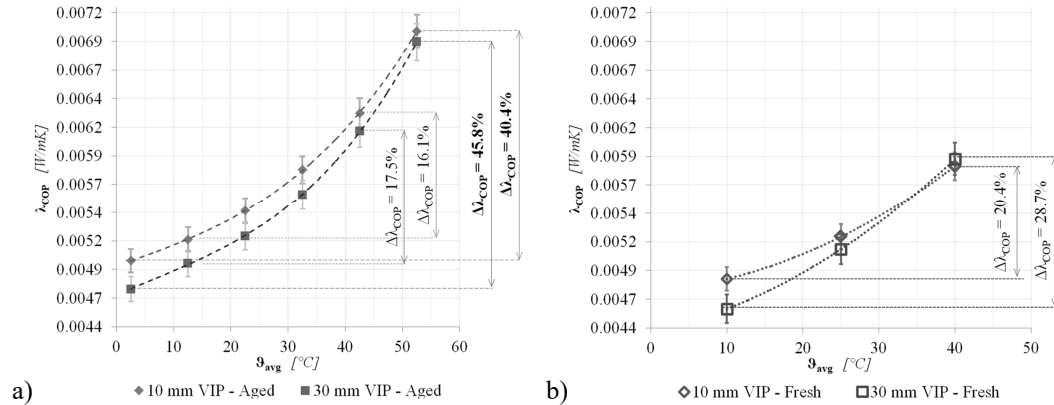


Figure 71: Centre of panel λ depending on the mean testing temperature a) aged VIPs after 32 months of storage; b) fresh VIPs [29]

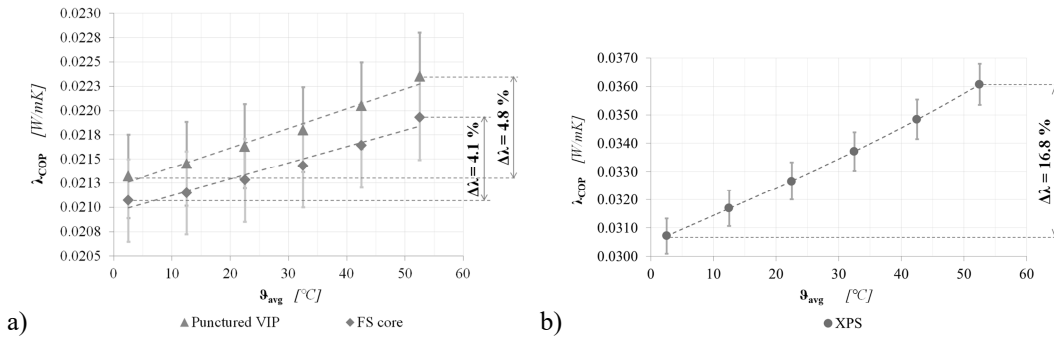


Figure 72: λ depending on the mean testing temperature. a) punctured VIP and FS core; b) XPS [29]

The punctured VIP and the fumed silica core material were instead characterised by an approximated linear trend and a lower variation of thermal conductivity with the increase of average temperature (Figure 72 a). The increase in thermal conductivity was equal to about 0.001 W/mK for both punctured VIP and Fumed Silica core material. The wide variation of VIPs centre of panel thermal conductivity, measured with different average temperatures, is related to the weights of the different heat transfer contributions presented in Eq. (32). Firstly, the radiative heat transfer contribution λ_r could increase considering that it is a function of the cube of the mean temperature. Secondly, the increase in average temperature could influence the internal pressure of fumed silica-based VIPs. In the critical pressure range, the centre of panel thermal conductivity may increase, influenced by the gaseous thermal conductivity λ_g which cannot be considered completely suppressed at high temperatures. Moreover, a further increment of the internal pressure could be due to the effect of high temperature

on the eventual residual water content inside the VIP. Instead, in case of punctured VIP and FS core, the thermal conductivity increase is not sensibly influenced by the variation of gaseous thermal conductivity, considering the constant internal pressure. This could explain the difference experimentally observed between the increment of VIP thermal conductivity (~ 0.002 W/mK) and the increment in punctured VIP and FS core (~ 0.001 W/mK) in the same range of temperatures.

From **Figure 72 a)** it is also possible to observe that the thermal conductivity of the punctured VIP was always slightly higher than that of the FS core material. This difference is about 0.004 W/mK, and it could be due to the more conductive VIP envelope. However, the effects of VIP envelope on heat losses can be considered negligible. In **Figure 72 b)** the variation of the centre of panel thermal conductivity as a function of the average temperature is also shown for a traditional insulating material, i.e. extruded polystyrene (XPS). In this case, similarly to the case of non-evacuated VIP (with or without the envelope), a linear trend was observed, but with a more marked variation of thermal conductivity (about 17%) in the same range of average temperature ($2.5^{\circ}\text{C} - 52.5^{\circ}\text{C}$). This variation could be due to the radiative effect, also considering the absence of opacifier. Moreover, the large dimension of XPS pores could increase the effect of the average temperature on the gaseous thermal conductivity²¹.

The effects of ageing (coupled with the temperature dependency) were deeply investigated in [75], on the same 10 mm thick panel, after 0, 20, 32 and 40 months of storage in the laboratory. The measured “thermal conductivities are summarised in **Table 49** and shown in **Figure 73** for three different average test temperatures (10 , 25 and 40°C), with the corresponding thermal conductivities denoted as λ_{10} , λ_{25} , and λ_{40} .

Results show a fast growth of the thermal conductivity during the first 20 months, while a slower increment was observed between the 20th and the 40th months. This phenomenon can be explained analysing the effect of the mechanisms of the air and water vapour permeation across the laminated envelope. In particular, in the first period (0 - 20 months) the magnitude of the gas and vapour transport is driven by high pressure difference determining a fast increase of the internal pressure of the VIP. In the second period between the 20th

²¹ Text from the author’s paper: “The effect of temperature on thermal performance of fumed silica based Vacuum Insulation Panels for buildings” [29].

and the 40th months, the pressure gradient becomes lower, explaining the less variation of the thermal conductivity.

The above-mentioned behaviour of the thermal conductivity is clearly observable for the measurement at 10°C and 25°C, while at 40°C a less evident variation of the slope in the evolution of λ over time occurs. This fact can be explained considering that at high testing temperature the internal pressure is higher, even in pristine VIPs. The internal pressure in the 40 months aged VIP is higher at 40°C than at 10°C [152], and as a consequence, the λ_g is higher²².

Table 49: Measured thermal conductivities at various test temperatures and ageing time [75]

ϑ_{avg} [°C]	Ageing period						
	0 (pristine)	20 (months)		32 (months)		40 (months)	
	λ [mW/mK]	λ [mW/mK]	$\Delta\lambda_{\text{aged-prist.}}$ [mW/mK]	λ [mW/mK]	$\Delta\lambda_{\text{aged-prist.}}$ [mW/mK]	λ [mW/mK]	$\Delta\lambda_{\text{aged-prist.}}$ [mW/mK]
10	4.83	5.12	0.29	5.17	0.34	5.20	0.37
25	5.20	5.49	0.30	5.50	0.39	5.55	0.43
40	5.81	6.14	0.32	6.29	0.48	6.38	0.57

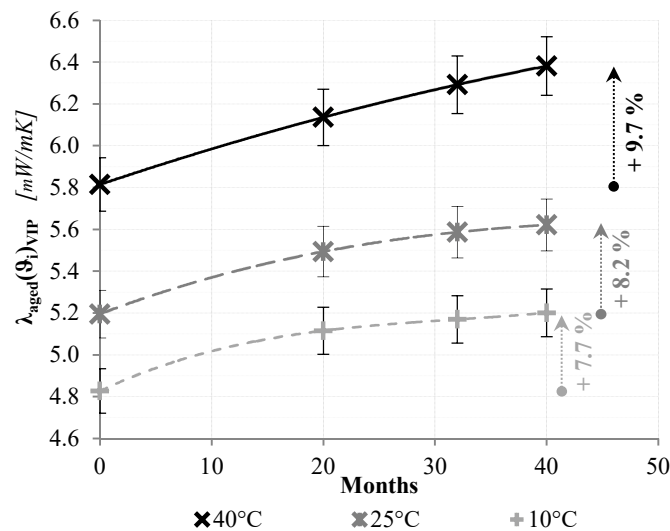


Figure 73: Evolution of the measured thermal conductivity over ageing time for different average temperature (λ_{10} , λ_{25} , λ_{40}) [75]

²² Text from the author's paper: "The effect of temperature on thermal performance of fumed silica based Vacuum Insulation Panels for buildings" [29].

8.1.1 Convective, radiative and conductive contributions in VIP and Fumed Silica core

In case of FS based VIPs, the gaseous thermal conductivity (λ_g) is generally assumed to be negligible, because of their microporous structure (as already discussed in § 3.1 *Heat transfer mechanism*). The level of λ_g contribution depends on the operating temperature, but at atmospheric pressure and at the building typical temperatures variation, the effects are minimal ([78];[81]).

“The assumption mentioned in § 3.1 Heat transfer mechanism about the heat transfer contributions, allows analysing the increment of thermal conductivity focusing the attention on the variation of radiative and gaseous contributions due to the increase of temperature. The variation of the thermal conductivity ($\Delta\lambda(\vartheta_i)$) at the temperature i (ϑ_i) in VIP and in fumed silica core, compared to thermal conductivity obtained at the lowest measured temperature (ϑ_0), was analysed:

$$\Delta\lambda(\vartheta_i) = \lambda(\vartheta_i) - \lambda(\vartheta_0) \quad (99)$$

Where: $\lambda(\vartheta_i)$ is the thermal conductivity measured at the temperature i , while $\lambda(\vartheta_0)$ correspond to the thermal conductivity measured at the lowest testing temperature (-7.5°C)”²³.

Thermal conductivity measurements were performed on the same 10 mm thick VIP sample and FS pressed board already analysed (**Figure 70 a**) and **b**) respectively), considering ten different testing average temperatures at ambient pressure.

*“Results highlight a 53% of increase (~ 2.6 mW/mK) of the VIP thermal conductivity (from ~ 4.9 to ~ 7.5 mW/mK) in the range of temperature between -7.5°C and 55.5°C (**Figure 74**); in the same range of temperatures the increase of thermal conductivity for the FS core (**Figure 75**) is considerably lower (around 1.7 mW/mK). Considering that the radiative contribution λ_r is linearly dependent by the third power of the absolute temperature, the VIP and FS core thermal conductivity were plotted against ϑ^3 [K] in **Figure 74** and **Figure 75** respectively.*

²³ Text from the author’s paper: “Actual thermal performances of Vacuum Insulation Panels for buildings” [75].

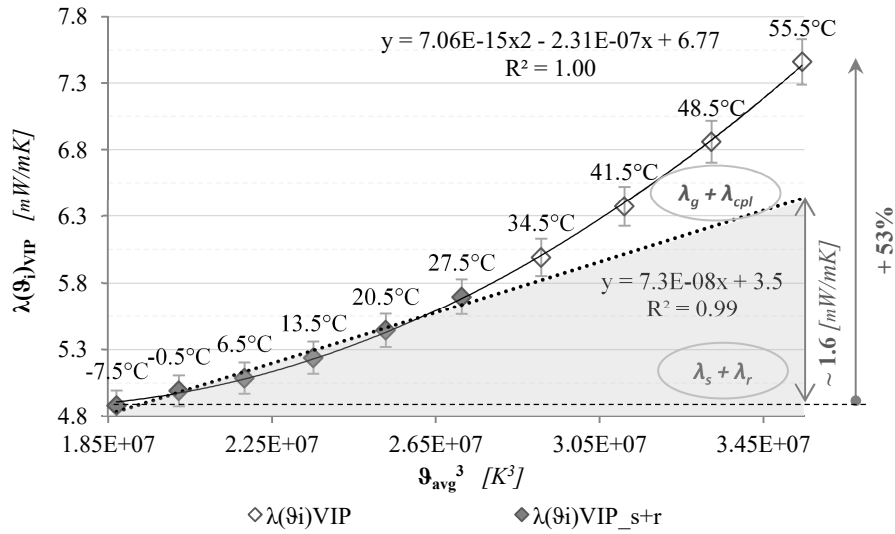


Figure 74: Measured thermal conductivity of VIP ($\lambda(\theta_i)_{VIP}$) as a function of the cube of average absolute temperature θ_{avg} [K] [75]

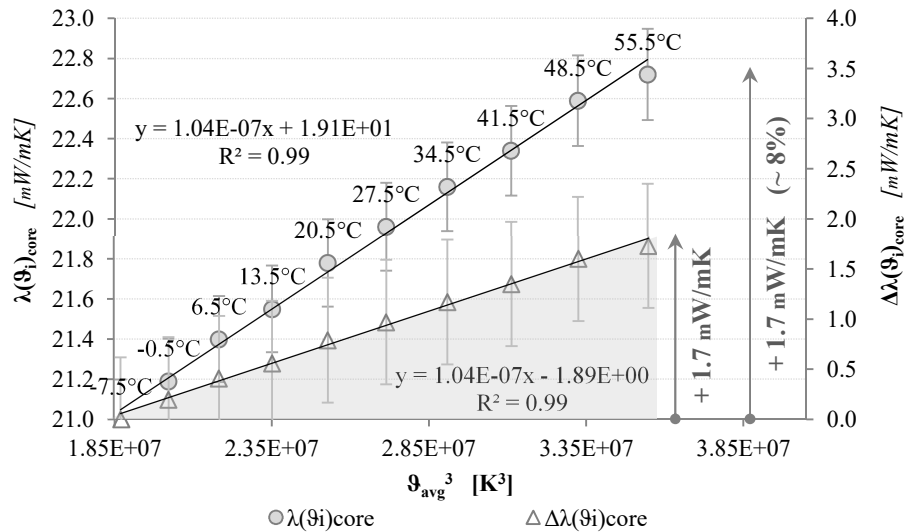


Figure 75: Measured $\lambda(\theta_i)_{core}$ for the FS sample, and $\Delta\lambda(\theta_i)$ calculated as the difference between the $\lambda(\theta_i)_{core}$ and the $\lambda(\theta_0)_{core}$, as a function of the cube of average absolute temperature θ_{avg} [K] [75]

The difference of thermal conductivity between the two samples (VIP and FS board) for each testing temperature $\Delta\lambda(\theta_i)$ can be attributed to the increase of the gaseous and the coupling contribution ($\lambda_g + \lambda_{cpl}$) which are relevant in the VIP (variation of the internal pressure) and negligible in the FS core (atmospheric pressure).

Nevertheless, it is important to remark that a separate analysis of the λ_g , λ_r , λ_c , λ_{cpl} contribution on the overall thermal conductivity is characterised by a certain degree of uncertainty, because it is impossible to completely suppress the influence of three factors while analysing the effect of the fourth one. The presented analysis has the only scope to qualitatively analyse the phenomena that are responsible for the increment of the thermal conductivity with the temperature.

As it is possible to observe in **Figure 74**, in the range between -7.5 and 27.5 °C a linear increment of the thermal conductivity as a function of the average temperature is observed. This means that in the analysed range of temperatures the λ_r is dominant and the gaseous conduction λ_g can be considered negligible. Moreover, as proposed in [152], the solid thermal conductivity can be estimated as the intercept of this regression line on the y-axis where the gaseous contribution can be neglected.

The increment of thermal conductivity from -7.5 to 55.5 °C explained by the dotted line in **Figure 74** (~ 1.6 mW/mK) is in agreement with the one measured in the FS board and represented in **Figure 75** (~ 1.7 mW/mK).

Considering that the contribution of $\lambda_g + \lambda_{cpl}$ to the variation of thermal conductivity in the FS board is negligible, it can be inferred that the increment of thermal conductivity related to the dotted line in **Figure 74** for a VIP is mainly due to the increment of $\lambda_s + \lambda_r$. When the temperature is higher than 27.5 °C a significant change of the slope occurs in **Figure 74** demonstrating that for high temperature the contribution of $\lambda_g + \lambda_{cpl}$ becomes more significant. This change of the slope (from linear to quadratic) can be related to the internal pressure of VIP that overcomes the critical pressure due to the temperature increment ($5 < p < 10$ mbar in fumed silica core ([82];[152]) for which the gaseous contribution can be considered suppressed.

By plotting the linear regression line of the measured points between -7.5 °C and 27.5 °C (dotted line in **Figure 74**), it is possible to highlight the contribution of the $\lambda_g + \lambda_{cpl}$ terms (that is the difference between the $\lambda(\vartheta)$ continuous line and the dotted line).

This representation allows to qualitatively isolate the gaseous and the coupling contribution from the solid and the radiative contributions. The results confirm that the increment of the gaseous contribution in the range of

temperatures in which the VIP could be exposed in building applications and in the plant and storage systems insulation, determines a non-negligible reduction of the performance, that should be carefully accounted during the design phase”²⁴.

8.1.2 Performance at the building component scale

The impact of a VIP temperature-dependent thermal conductivity on the overall thermal behaviour of a building envelope component was investigated through a transient heat transfer simulation, performed using a validated model (as described in § 4.3.3 *Dynamic hygrothermal simulation*). The followed procedure and the analysed model were already explained in § 4.3.3.2 *Effects of temperature on VIPs at the building component scale* (see **Figure 44** and **Table 12** for further details).

“For a typical year, the frequency distribution of thermal conductivities for the two configurations of the roof were analysed.

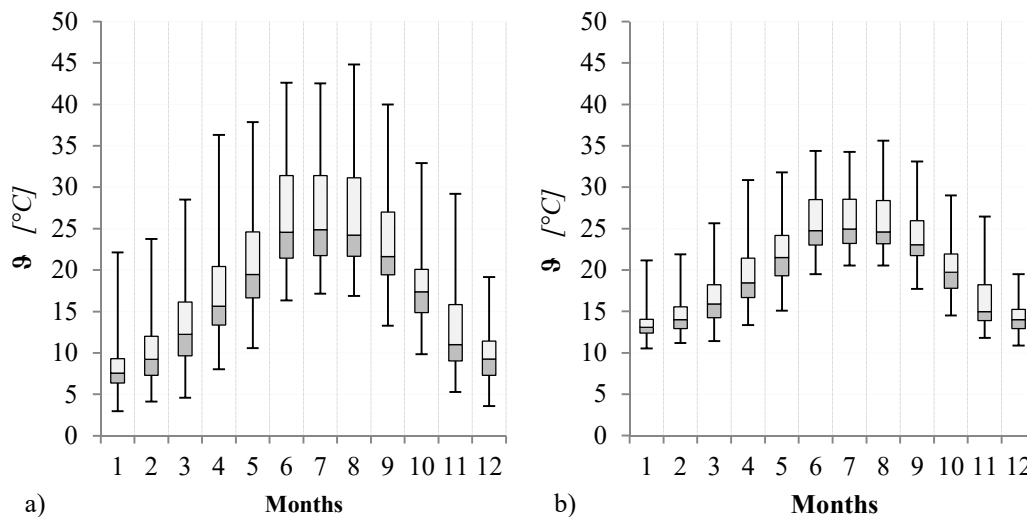


Figure 76: VIP average temperature. a) Configuration A (VIP above the XPS layer); b) Configuration B (VIP below the XPS layer) [75]

Figure 76 a) and b) show for each month the box plot of the average temperatures reached by the VIP, while the correspondent VIP thermal conductivity values are shown in **Figure 77 a) and b)**.

²⁴ Text from the author’s paper: “Actual thermal performances of Vacuum Insulation Panels for buildings” [75].

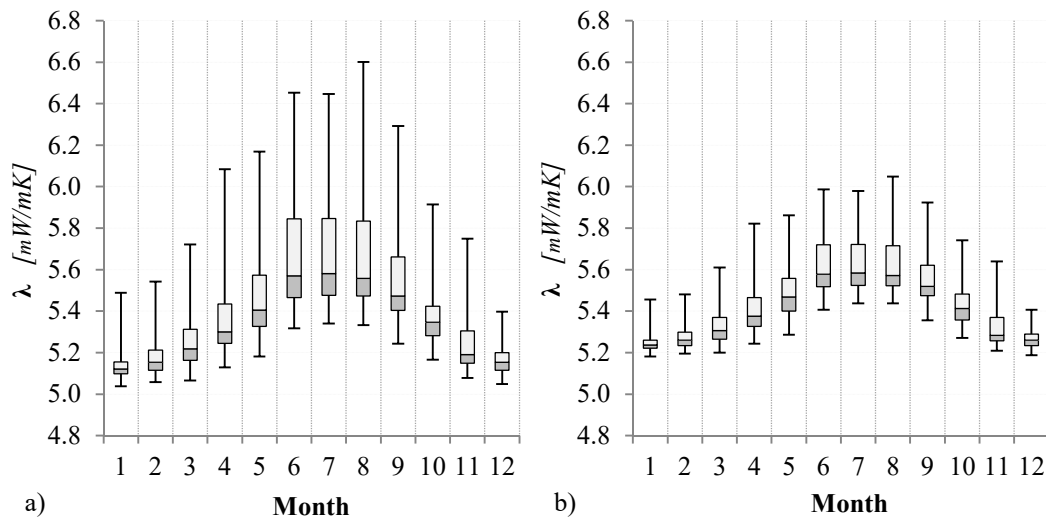


Figure 77: VIP actual thermal conductivity (temperature dependent). a) Configuration A (VIP above the XPS layer); b) Configuration B (VIP below the XPS layer) [75]

As it is possible to see:

- *For the configuration A, during summer (June – August) for the 25% of the time, the VIP reaches temperatures higher than 32°C , with peak values of $\sim 45^{\circ}\text{C}$, while in the configuration B (VIP below the XPS layer) the maximum temperature is $\sim 36^{\circ}\text{C}$;*
- *The variation of thermal conductivity switching from the summer hottest peak to the winter coldest peak can span from ~ 5.00 to 6.60 mW/mK with a variation of $\sim 32\%$ for configuration A. For the configuration B, the thermal conductivity changes from 5.20 and 6.05 mW/mK , with an increase of the peak temperature of $\sim 9\%$ respect to configuration A.*

*The monthly energy gains and losses across the roof component (config. A) were assessed considering a temperature-dependent thermal conductivity and a constant thermal conductivity respectively. Comparing the results of these two calculations (see **Figure 78**) it emerged that:*

- *In winter if one assumes a constant thermal conductivity for the energy calculation, the heat losses are slightly underestimated. Nevertheless, the maximum difference between the heat losses assessed considering a constant thermal conductivity and those obtained considering a value*

dependent on the temperature (ΔQ_{losses}) is $\sim 3\%$ and can be considered negligible;

- In summer an underestimation of the heat gains occurs, with a maximum difference of $\sim 15\%$ in July and August.

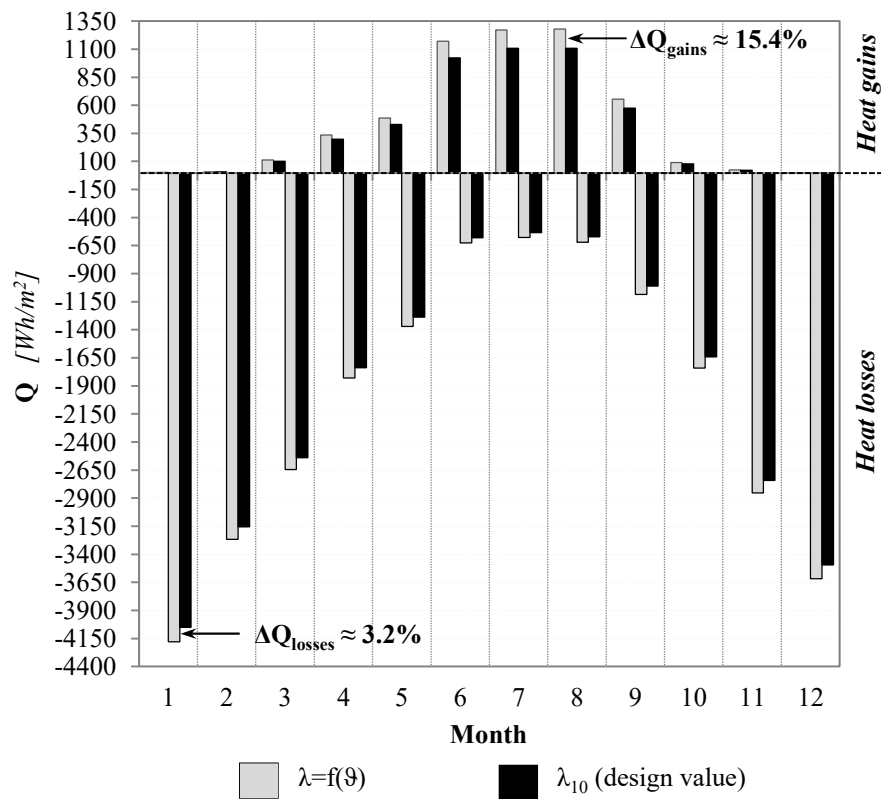


Figure 78: Monthly heat gains (positive values) and heat losses (negative values) across the roof component [75]

The proper evaluation of the ceiling peak temperature has a direct impact on the indoor comfort condition. In fact, the ceiling temperature in attic space is crucial for the determination of the mean radiant temperature of the room and hence of the operative temperature. Figure 79 shows the effect of the different values of the VIPs thermal conductivity on the interior surface temperature (ceiling) during the 11th August, which represents the hottest day of the year. It is possible to see that considering a constant value of thermal conductivity (λ_{10}), the peak ceiling temperature is underestimated of ~ 0.32 °C compared to the case with a $\lambda = f(\theta)$, while during the night and in the coldest hours, the results are in

good agreement with the ones calculated with the temperature-dependent thermal conductivity.

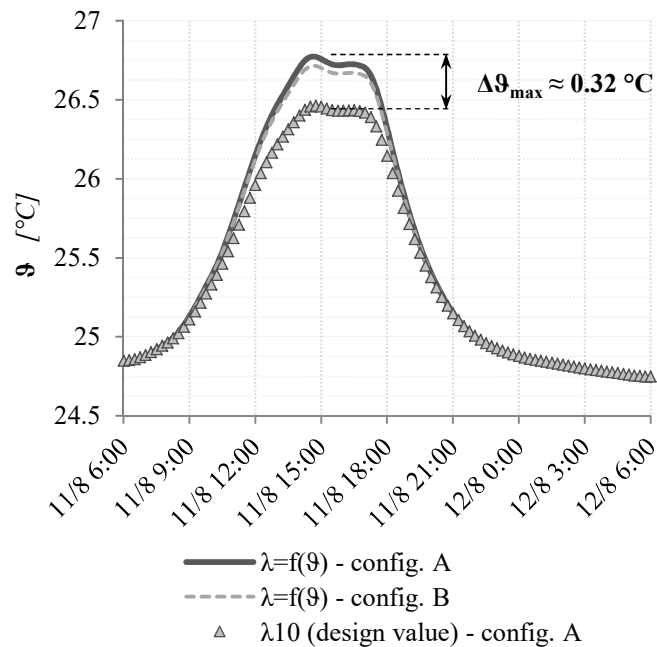


Figure 79: Indoor surface temperature profile of 11th August [75]

The difference in the ceiling temperature peak calculation is marginal, but this value is strictly dependent on the assumed indoor surface heat transfer coefficient. This value could be sharply different from the assumed $h_i = 5.88 \text{ W/m}^2\text{K}$ (EN ISO 6946:2017 [116]), especially in a transient condition. The lower the h_i , the higher the indoor surface temperature and even the difference between the two simulation methods”²⁵.

²⁵ Text from the author’s paper: “Actual thermal performances of Vacuum Insulation Panels for buildings” [75].

8.2 VIPs Type B uncertainty variability (HFM)

In § 6.1.1 *HFM sensitivity analysis*, the importance of a proper selection of the $\Delta\vartheta$ between the plates of the HFM apparatuses, for the reduction of the thermal conductivity theoretical standard-based measurement uncertainty, was highlighted.

Therefore, an experimental campaign was carried out with the purpose of evaluating the influence of the $\Delta\vartheta$ on a Type B uncertainty evaluation (HFM-1 apparatus). Fourteen tests were performed, with a constant average temperature (equal to 30°C), and different $\Delta\vartheta$ values, on three VIP samples 10, 20 and 30 mm thick. Results are summarised in **Table 56** and **Figure 80**.

EN 12667:2002 [12] provides indications about the acceptable temperature values and reference accuracy of HFM method, for high thermal resistant materials. The recommended limit for temperature difference across the specimen is 10°C, while the expected heat flux meter method accuracy is $\pm 3\%$.

Table 50: Thermal conductivity and relative uncertainty, as a function of $\Delta\vartheta$, for VIPs 10, 20 and 30 mm thick

t	$\Delta\vartheta$									
	10		12		14		16		18	
[mm]	λ_{10} [W/mK]	$u_c(\lambda_{10})$ [%]	λ_{12} [W/mK]	$u_c(\lambda_{12})$ [%]	λ_{14} [W/mK]	$u_c(\lambda_{14})$ [%]	λ_{16} [W/mK]	$u_c(\lambda_{16})$ [%]	λ_{18} [W/mK]	$u_c(\lambda_{18})$ [%]
10	0.0057	2.9	0.0057	2.6	0.0057	2.5	0.0057	2.4	0.0057	2.3
20	0.0051	2.3	0.0051	2.2	0.0051	2.2	0.0051	2.2	0.0051	2.1
30	0.0054	3.5	0.0054	3.1	0.0054	2.9	0.0054	2.7	0.0054	2.6
t	$\Delta\vartheta$									
	20		24		30		34		36	
[mm]	λ_{20} [W/mK]	$u_c(\lambda_{20})$ [%]	λ_{24} [W/mK]	$u_c(\lambda_{24})$ [%]	λ_{30} [W/mK]	$u_c(\lambda_{30})$ [%]	λ_{34} [W/mK]	$u_c(\lambda_{34})$ [%]	λ_{36} [W/mK]	$u_c(\lambda_{36})$ [%]
10	0.0057	2.3	0.0057	2.2	0.0057	2.1	0.0057	2.1	0.0057	2.1
20	0.0051	2.1	0.0051	2.1	0.0051	2.1	0.0051	2.1	0.0051	2.1
30	0.0054	2.5	0.0054	2.4	0.0054	2.2	0.0054	2.2	0.0054	2.2

On the basis of the experimental analysis performed, the $\pm 3\%$ uncertainty limit was respected, with a temperature difference equal to 10°C, for 10 and 20 mm thick VIPs, but not for 30 mm. In this last case, the $\Delta\vartheta$ must be higher than 13°C. Therefore, a modification of the measurement procedure described by the European standard is recommendable.

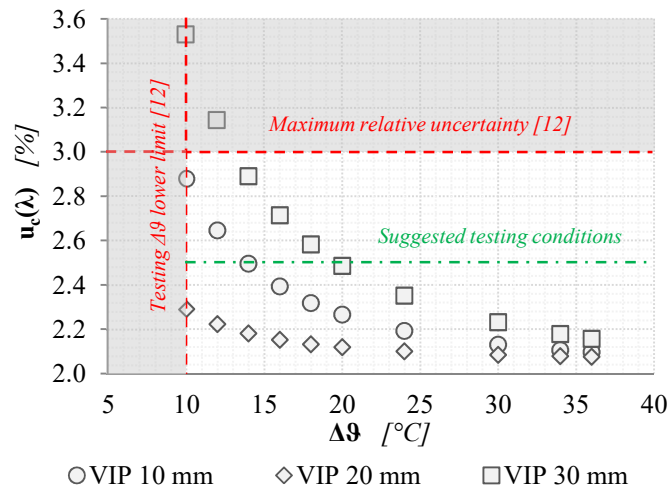


Figure 80: Thermal conductivity relative uncertainty, as a function of $\Delta\theta$

Moreover, to increment the reliability of the results and the comparability with the GHP measurements (for which the uncertainty limit provided by [12] is 2%) is suggested to perform measurements with $\Delta\theta$ values higher than 20°C, reaching uncertainties lower than 2.5% in most of the cases.

8.3 Experimental campaign for VIPs thermal properties measurement (HFM)

The experimental campaign presented in the following sections is a part of a more extensive interlaboratory comparison, performed in the framework of the IEA EBC Annex 65 activities, sub-task 2 [150].

Different kinds of VIP and APM, provided by several manufacturers, were assigned to several laboratories between the participant countries: each sample typology was tested by at least two institutes. Producer and technical data of each sample were covered by industrial secrecy since the declared purpose of the study was merely to discuss about methods.

The investigated characteristics were the centre of panel thermal conductivities of both VIPs and APMs, and the ψ -values for VIPs assemblies. Measurements were required at the average temperatures of 10 and 23°C, but, to better characterise the variability of the thermal conductivity, measurements were also performed at 7 and 40°C. In accordance with the previous chapter, the temperature difference between the plates was kept equal to 20°C. Even the ageing effects were investigated: samples were tested pristine and after 30 and 90

days of storage at 50°C and 70 % RH (accelerated ageing). Measurements were performed using the HFM-1 apparatus.

The measurement criteria (e.g., $\Delta\theta$, width and material for the joint in VIPs assemblies, drying process and so on), were not declared, except for the average testing temperature and the ageing conditions. Moreover, for logistical reasons, each sample was tested by only one laboratory. Though the various samples were taken from the same production batch, the direct comparison between the results obtained in all the different laboratories wasn't straightforward. In fact, a significant influence on the spread of the measurement results can be ascribed to the variability of the properties among the various samples of the same production batch.

Hereinafter, the results obtained by Politecnico di Torino will be presented.

8.3.1 Thermal conductivity

Thermal conductivity measurements were performed on different family of samples:

- VIP - 1: dimensions 300 x 600 x 20mm and 600 x 600 x 20mm;
- VIP - 4: dimensions 300 x 600 x 20mm, 600 x 600 x 20mm and 500 x 500 x 20mm;
- VIP - 5: dimensions 500 x 500 x 20mm;
- APM - 2: dimensions 600 x 600 x 30mm.

To avoid lateral heat losses during measurement, samples with dimensions 300 x 600 mm were tested adding an extra XPS insulating mask all around the edges of the panels (**Figure 81**).

All samples were weighed before the measurement, to define the density and weight variation due to the ageing process. Moreover, APMs were dried before the Fresh analysis (**Figure 82 b**), but not before the aged tests: otherwise all the effects of the adsorbed water would have disappeared (the higher water content is one of the reasons of the specimens weight increment).

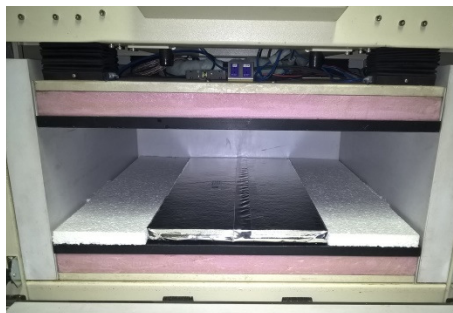


Figure 81: Extra XPS insulating mask for VIPs with dimension 300 x 600 mm

The APM rigid boards were wrapped in plastic bags to avoid water vapour adsorption during the measurement (**Figure 82 c**).

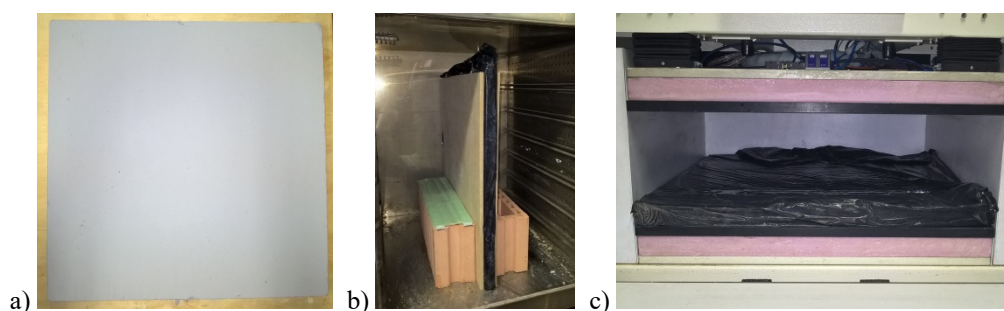


Figure 82: APM rigid board. a) sample; b) drying phase; c) plastic wrapping

The investigation results are reported from **Table 51** to **Table 53** and represented from **Figure 83** to **Figure 87** for what concerns VIPs, and in **Table 54** and **Figure 88** for APMs (in figures, the same colour defines the same sample).

The composition of samples was unknown, but analysing the results, it is possible to make some assumption. VIPs - 1 are characterised by a mean thermal conductivity of about 0.005 W/mK, which means that they can be assumed as FS based VIPs. VIPs - 4 are marked by slightly lower λ_{COP} values (with a maximum pristine thermal conductivity equal to 0.0041 W/mK): this range of value is again typical of VIPs with FS core, with a greater internal vacuum degree. The last family of analysed VIPs is VIP - 5, which is characterised by better thermal properties, with pristine thermal conductivities < 0.0020 W/mK: therefore they are probably composed by FG.

Table 51: VIP - 1 thermal conductivity and relative uncertainty at different average temperatures and ageing conditions

Sample	Ageing conditions	Weight [g]	Density [kg/m^3]	$\vartheta_{\text{avg}} [^{\circ}\text{C}]$							
				7	10	23	40	$\lambda_{7^{\circ}\text{C}}$ [W/mK]	$u_c(\lambda)$ [%]	$\lambda_{10^{\circ}\text{C}}$ [W/mK]	$u_c(\lambda)$ [%]
1.12 600 x 300 mm t = 20 mm	Fresh	765	194	0.0045	2.4	0.0045	2.4	0.0047	2.4	0.0052	2.3
	30 days	765	195	-	-	0.0047	2.4	0.0049	2.3	0.0053	2.3
	$\Delta_{\text{fresh-30}}$ [%]	0.0%	0.5%	-	-	3.5%	-	4.5%	-	2.7%	-
	90 days	766	197	0.0049	2.3	0.0049	2.3	0.0052	2.3	0.0058	2.2
	$\Delta_{\text{fresh-90}}$ [%]	0.2%	1.6%	8.9%	-	9.3%	-	11.7%	-	13.2%	-
	Δ_{30-90} [%]	0.2%	1.1%	-	-	5.6%	-	6.9%	-	10.2%	-
1.13 600 x 300 mm t = 20 mm	Fresh	834	210	0.0048	2.4	0.0048	2.4	0.0050	2.3	0.0053	2.3
	30 days	835	211	-	-	0.0049	2.3	0.0052	2.3	0.0055	2.3
	$\Delta_{\text{fresh-30}}$ [%]	0.1%	0.5%	-	-	2.5%	-	3.4%	-	5.0%	-
	90 days	835	213	0.0051	2.3	0.0052	2.3	0.0055	2.3	0.0060	2.2
	$\Delta_{\text{fresh-90}}$ [%]	0.1%	1.2%	7.1%	-	7.5%	-	9.4%	-	13.7%	-
	Δ_{30-90} [%]	0.0%	0.7%	-	-	4.9%	-	5.8%	-	8.3%	-
1.14 600 x 300 mm t = 20 mm	Fresh	805	211	0.0046	2.4	0.0047	2.4	0.0048	2.3	0.0051	2.3
	30 days	805	202	-	-	0.0048	2.4	0.0051	2.3	0.0054	2.3
	$\Delta_{\text{fresh-30}}$ [%]	0.0%	-4.3%	-	-	3.9%	-	4.8%	-	6.3%	-
	90 days	806	205	0.0050	2.3	0.0050	2.3	0.0053	2.3	0.0059	2.2
	$\Delta_{\text{fresh-90}}$ [%]	0.1%	-3.0%	8.1%	-	8.5%	-	10.7%	-	15.9%	-
	Δ_{30-90} [%]	0.1%	1.3%	-	-	4.5%	-	5.7%	-	9.0%	-
1.25 600 x 600 mm t = 20 mm	Fresh	1515	195	0.0045	2.4	0.0045	2.4	0.0047	2.3	0.0050	2.3
	30 days	1516	197	0.0045	2.4	0.0046	2.4	0.0048	2.3	0.0051	2.3
	$\Delta_{\text{fresh-30}}$ [%]	0.1%	1.0%	1.1%	-	1.3%	-	2.1%	-	3.8%	-
	90 days	1518	198	0.0048	2.3	0.0049	2.3	0.0051	2.3	0.0056	2.2
	$\Delta_{\text{fresh-90}}$ [%]	0.2%	1.5%	7.1%	-	7.5%	-	9.3%	-	13.6%	-
	Δ_{30-90} [%]	0.1%	0.5%	5.9%	-	6.1%	-	7.0%	-	9.4%	-
1.26 600 x 600 mm t = 20 mm	Fresh	1526	190	0.0043	2.4	0.0043	2.4	0.0045	2.3	0.0048	2.3
	30 days	1526	192	0.0043	2.5	0.0043	2.4	0.0046	2.4	0.0050	2.3
	$\Delta_{\text{fresh-30}}$ [%]	0.0%	1.1%	0.5%	-	0.9%	-	2.5%	-	4.4%	-
	90 days	1527	194	0.0046	2.4	0.0046	2.4	0.0049	2.3	0.0054	2.3
	$\Delta_{\text{fresh-90}}$ [%]	0.1%	1.8%	7.3%	-	7.6%	-	9.2%	-	13.2%	-
	Δ_{30-90} [%]	0.1%	0.8%	6.8%	-	6.6%	-	6.5%	-	8.4%	-

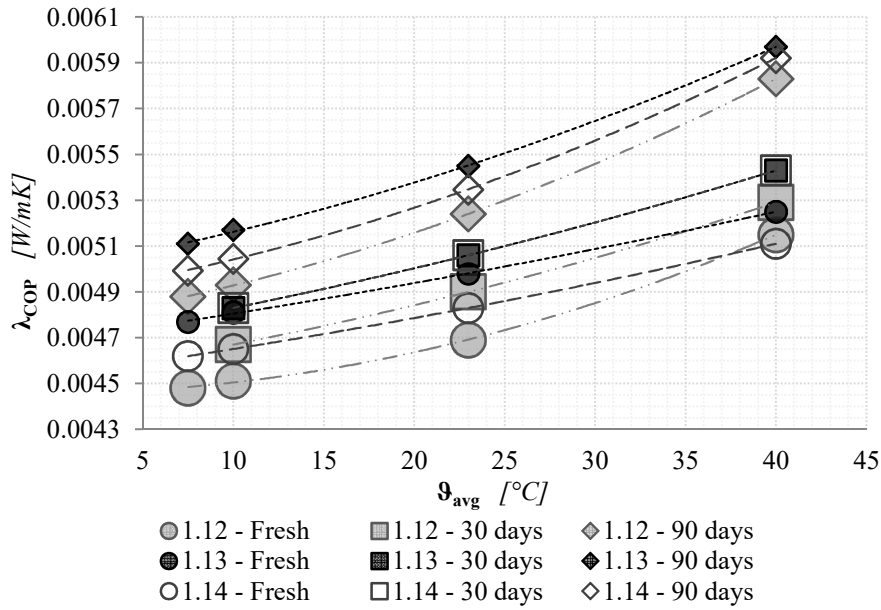


Figure 83: VIP - 1 thermal conductivity at different average temperatures and ageing conditions (300 x 600 mm)

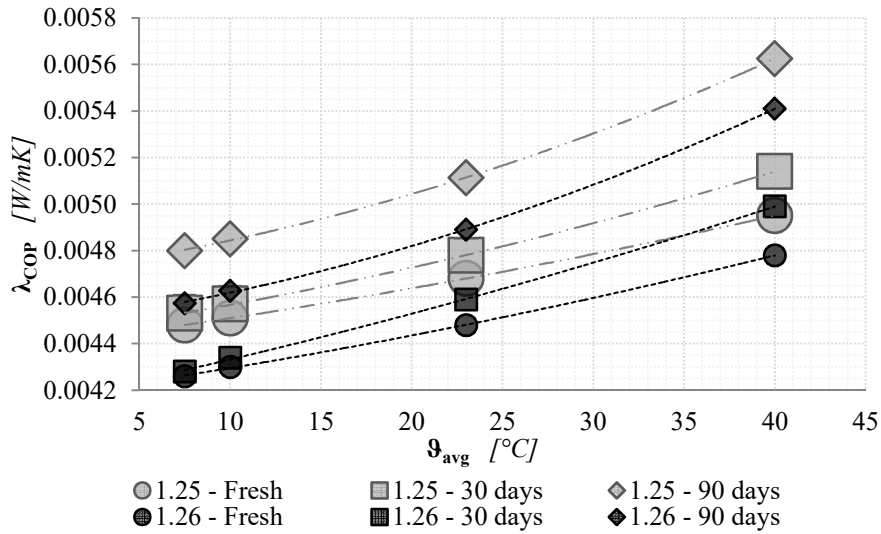


Figure 84: VIP - 1 thermal conductivity at different average temperatures and ageing conditions (600 x 600 mm)

Table 52: VIP - 4 thermal conductivity and relative uncertainty at different average temperatures and ageing conditions (first part)

Sample	Ageing conditions	$\vartheta_{\text{avg}} [^{\circ}\text{C}]$									
		Weight Density		7		10		23		40	
		[g]	[kg/m ³]	$\lambda_{7^{\circ}\text{C}}$	$u_c(\lambda)$	$\lambda_{10^{\circ}\text{C}}$	$u_c(\lambda)$	$\lambda_{23^{\circ}\text{C}}$	$u_c(\lambda)$	$\lambda_{40^{\circ}\text{C}}$	$u_c(\lambda)$
4.15	Fresh	773	198	0.0037	2.6	0.0037	2.6	0.0038	2.5	0.0041	2.4
	30 days	774	199	-	-	0.0039	2.5	0.0040	2.5	0.0043	2.4
	$\Delta_{\text{fresh-30}} [\%]$	0.1%	0.5%	-	-	6.5%	-	6.1%	-	5.7%	-
	90 days	777	200	0.0043	2.4	0.0042	2.4	0.0044	2.4	0.0049	2.3
	$\Delta_{\text{fresh-90}} [\%]$	0.5%	1.0%	17.9%	-	14.5%	-	16.9%	-	19.6%	-
	$\Delta_{30-90} [\%]$	0.3%	0.5%	-	-	7.5%	-	10.2%	-	13.2%	-
4.16	Fresh	756	193	0.0037	2.5	0.0037	2.5	0.0039	2.5	0.0041	2.4
	30 days	777	200	0.0040	2.5	0.0040	2.5	0.0041	2.4	0.0045	2.4
	$\Delta_{\text{fresh-30}} [\%]$	2.8%	3.6%	7.5%	-	6.7%	-	7.5%	-	9.8%	-
	90 days	780	201	0.0044	2.4	0.0044	2.4	0.0047	2.3	0.0053	2.3
	$\Delta_{\text{fresh-90}} [\%]$	3.2%	4.2%	18.9%	-	19.1%	-	22.3%	-	29.1%	-
	$\Delta_{30-90} [\%]$	0.4%	0.6%	10.6%	-	11.6%	-	13.7%	-	17.6%	-
4.17	Fresh	732	188	0.0037	2.6	0.0037	2.6	0.0038	2.5	0.0040	2.4
	30 days	734	190	-	-	0.0039	2.5	0.0040	2.4	0.0043	2.4
	$\Delta_{\text{fresh-30}} [\%]$	0.3%	1.1%	-	-	5.9%	-	5.8%	-	7.7%	-
	90 days	736	191	0.0044	2.4	0.0043	2.4	0.0045	2.4	0.0049	2.3
	$\Delta_{\text{fresh-90}} [\%]$	0.6%	1.6%	17.6%	-	16.1%	-	18.0%	-	22.9%	-
	$\Delta_{30-90} [\%]$	0.3%	0.5%	-	-	9.6%	-	11.5%	-	14.1%	-
4.18	Fresh	721	187	0.0036	2.6	0.0036	2.6	0.0037	2.5	0.0039	2.5
	30 days	722	188	-	-	0.0039	2.5	0.0040	2.5	0.0043	2.4
	$\Delta_{\text{fresh-30}} [\%]$	0.1%	0.5%	-	-	8.4%	-	7.6%	-	9.7%	-
	90 days	725	189	0.0044	2.4	0.0043	2.4	0.0045	2.4	0.0050	2.3
	$\Delta_{\text{fresh-90}} [\%]$	0.5%	1.1%	22.3%	-	19.5%	-	21.4%	-	27.1%	-
	$\Delta_{30-90} [\%]$	0.4%	0.5%	-	-	10.3%	-	12.9%	-	15.8%	-
4.20	Fresh	1491	195	0.0035	2.6	0.0035	2.6	0.0036	2.5	0.0039	2.5
	30 days	1491	196	0.0036	2.6	0.0036	2.6	0.0038	2.5	0.0040	2.4
	$\Delta_{\text{fresh-30}} [\%]$	0.0%	0.5%	2.6%	-	2.3%	-	3.3%	-	4.5%	-
	90 days	1493	196	0.0038	2.5	0.0038	2.5	0.0040	2.5	0.0043	2.4
	$\Delta_{\text{fresh-90}} [\%]$	0.1%	0.6%	8.2%	-	8.4%	-	9.1%	-	10.9%	-
	$\Delta_{30-90} [\%]$	0.1%	0.1%	5.5%	-	6.0%	-	5.6%	-	6.1%	-

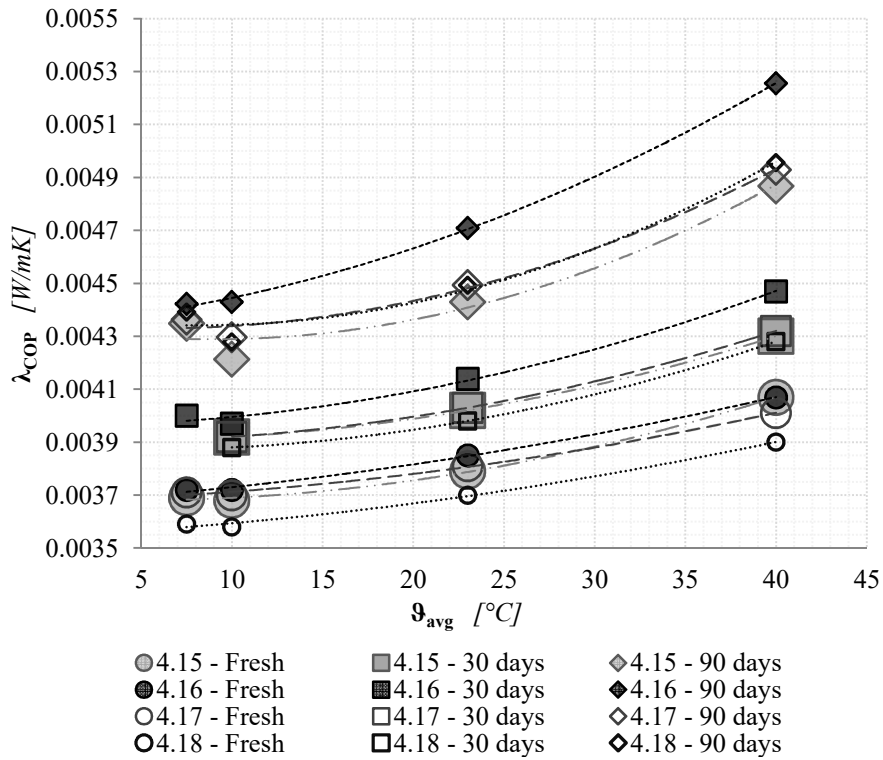


Figure 85: VIP - 4 thermal conductivity at different average temperatures and ageing conditions (300 x 600 mm)

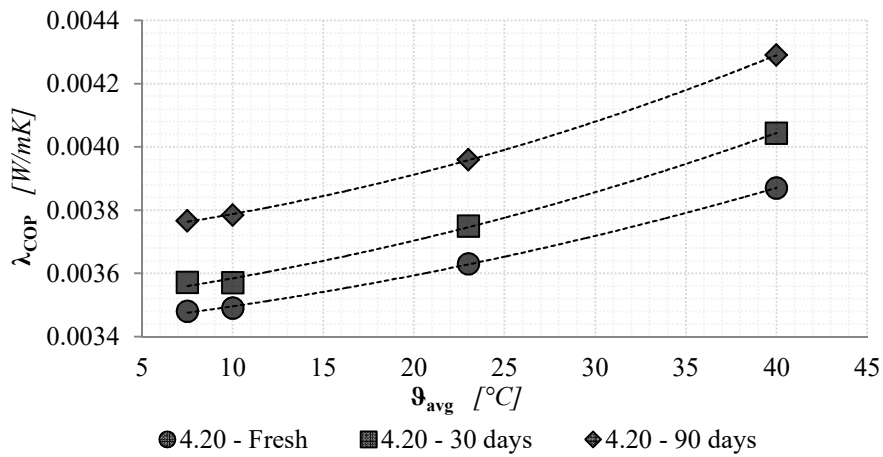


Figure 86: VIP - 4 thermal conductivity at different average temperatures and ageing conditions (600 x 600 mm)

The combined uncertainty of the thermal conductivity was found to be almost always lower than 2.5% (in accordance with the choice of the temperature difference between the plates $\Delta\theta = 20^\circ\text{C}$, as highlighted in the previous chapter).

Increasing the average testing temperature ϑ_{avg} , the VIPs thermal conductivity increases, whilst the measurement uncertainty decreases (higher heat flux through the sample). The ageing condition has a similar effect on both the thermal conductivity and the measurement uncertainty: the longer the ageing, the higher the thermal conductivity and the lower the measurement uncertainty. In particular, the ageing effects are stronger in case of higher testing temperature. The consequences of the different ageing steps are almost proportional to the number of the days of critical storage. The worsening scale of the thermal insulation properties is due for around 1/3 (between 3 and 10%, depending on the sample) to the first 30 days of ageing, while the other 2/3 (from 10 to 30%) occur after 60 more days.

Table 53: VIP - 4 (second part) and VIP - 5 thermal conductivity and relative uncertainty at different average temperatures and ageing conditions

Sample	Ageing conditions	Weight	Density	$\vartheta_{avg} [^{\circ}C]$							
				7	10	23	40				
		[g]	[kg/m ³]	$\lambda_{7^{\circ}C}$	$u_c(\lambda)$	$\lambda_{10^{\circ}C}$	$u_c(\lambda)$	$\lambda_{23^{\circ}C}$	$u_c(\lambda)$	$\lambda_{40^{\circ}C}$	$u_c(\lambda)$
				[W/mK]	[%]	[W/mK]	[%]	[W/mK]	[%]	[W/mK]	[%]
4.14 500 x 500 mm t = 20 mm	Fresh	999	194	0.0031	2.7	0.0031	2.7	0.0033	2.6	0.0034	2.5
	30 days	-	-	0.0033	2.6	0.0033	2.6	0.0035	2.5	0.0037	2.5
	$\Delta_{fresh-30}$ [%]	-	-	5.7%	-	6.1%	-	6.2%	-	8.3%	-
4.24 500 x 500 mm t = 20 mm	Fresh	1017	196	0.0033	2.6	0.0033	2.6	0.0034	2.6	0.0036	2.5
	30 days	-	-	-	-	-	-	-	-	-	-
	$\Delta_{fresh-30}$ [%]	-	-	-	-	-	-	-	-	-	-
5.21 500 x 500 mm t = 20 mm	Fresh	1408	269	0.0015	4.3	0.0015	4.3	0.0017	3.9	0.0018	3.7
	30 days	-	-	0.0021	3.3	0.0022	3.3	0.0023	3.1	0.0026	2.9
	$\Delta_{fresh-30}$ [%]	-	-	42.4%	-	46.0%	-	40.7%	-	43.1%	-
5.22 500 x 500 mm t = 20 mm	Fresh	1396	267	0.0016	4.2	0.0016	4.1	0.0017	3.9	0.0019	3.5
	30 days	-	-	0.0022	3.2	0.0023	3.2	0.0024	3.1	0.0026	2.9
	$\Delta_{fresh-30}$ [%]	-	-	42.0%	-	41.8%	-	42.2%	-	40.7%	-

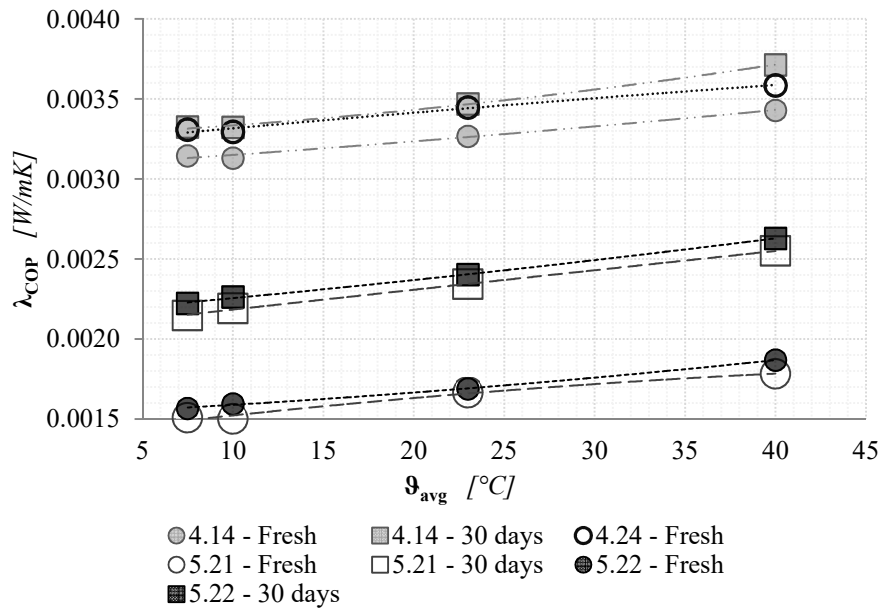


Figure 87: VIP - 4 and VIP - 5 thermal conductivity at different average temperatures and ageing conditions (500 x 500 mm)

VIPs - 4 with dimensions of 500 x 500 mm have a similar behaviour of the already analysed samples belonging to the same family, considering both the obtained uncertainties (slightly higher than 2.5%) and the ageing effects.

Finally, VIPs - 5 resulted in being the best performing samples. Therefore the measurement uncertainties are always higher than 3%, which is the uncertainty limit defined by the current standard EN 12667:2001 [12]. Since FG based VIPs are becoming more widespread on the market, it is demonstrated that a revision of the standards (and measuring instruments) is required, so as to consider these very efficient materials and leading the measurements on the edge of the experimental apparatuses own applicability.

In case of highly performing materials, the ageing has very significant consequences. After 30 days of ageing, the lambda values are almost doubled (always > 40%), but, due to the wide measurement uncertainty, the correlation between ageing and the average testing temperature is no more observable. Again, the longer is the ageing period, the lower the combined measurement uncertainty (especially for VIPs - 5).

Table 54: APM - 2 thermal conductivity and relative uncertainty at different average temperatures and ageing conditions

Sample	Ageing conditions	Weight [g]	$\vartheta_{\text{avg}} [^{\circ}\text{C}]$											
			2.5		10		23		32.5		42.5		52.5	
			$\lambda_{2.5^{\circ}\text{C}}$ [W/mK]	$u_c(\lambda)$ [%]	$\lambda_{10^{\circ}\text{C}}$ [W/mK]	$u_c(\lambda)$ [%]	$\lambda_{23^{\circ}\text{C}}$ [W/mK]	$u_c(\lambda)$ [%]	$\lambda_{32.5^{\circ}\text{C}}$ [W/mK]	$u_c(\lambda)$ [%]	$\lambda_{42.5^{\circ}\text{C}}$ [W/mK]	$u_c(\lambda)$ [%]	$\lambda_{52.5^{\circ}\text{C}}$ [W/mK]	$u_c(\lambda)$ [%]
APM 2.12 600 x 600 mm t = 30 mm	Fresh	1866	0.0185	2.0	0.0186	2.1	0.0188	2.1	0.0189	2.1	0.0191	2.1	0.0193	2.0
	30 dd	1882	-	-	0.0187	2.1	0.0189	2.1	-	-	-	-	-	-
	$\Delta_{\text{fresh-30}}$ [%]	0.9%	-	-	0.7%	-	0.7%	-	-	-	-	-	-	-
	90 dd	1885	-	-	0.0189	2.1	0.0192	2.1	-	-	-	-	-	-
	$\Delta_{\text{fresh-90}}$ [%]	1.0%	-	-	2.1%	-	2.2%	-	-	-	-	-	-	-
	Δ_{30-90} [%]	0.2%	-	-	1.4%	-	1.5%	-	-	-	-	-	-	-
APM 2.13 600 x 600 mm t = 30 mm	Fresh	1832	0.0192	2.0	0.0193	2.1	0.0194	2.1	0.0196	2.1	0.0198	2.1	0.0200	2.0
	30 dd	1844	-	-	0.0186	2.1	0.0190	2.1	-	-	-	-	-	-
	$\Delta_{\text{fresh-30}}$ [%]	0.7%	-	-	-3.5%	-	-2.4%	-	-	-	-	-	-	-
	90 dd	1850	-	-	0.0189	2.1	0.0191	2.1	-	-	-	-	-	-
	$\Delta_{\text{fresh-90}}$ [%]	1.0%	-	-	-1.9%	-	-1.6%	-	-	-	-	-	-	-
	Δ_{30-90} [%]	0.3%	-	-	1.7%	-	0.7%	-	-	-	-	-	-	-

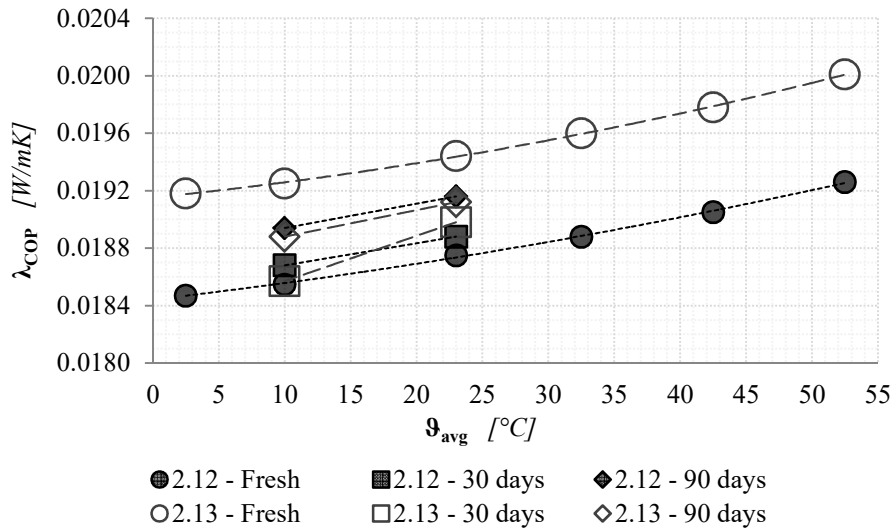


Figure 88: APM - 2 thermal conductivity at different average temperatures and ageing conditions (600 x 600 mm)

The APM samples were presumably FS pressed boards. As expected they are less influenced by the ageing procedure: the thermal conductivity increments can be due to the internal water content, but they lie more or less in the measurement uncertainty range.

8.3.2 Linear thermal transmittance

Samples with dimension 300 x 600 mm were than coupled to form VIPs assemblies. Since no indications about the joining procedure e technology, the panels were sealed together with an adhesive tape, without any structural joint material (panels pressed as close as possible to each other).

These assemblies were tested at the same average temperatures, but only in two ageing steps, Fresh and after 90 days of storage. The results of the investigation are summarised in **Table 55** and represented from **Figure 89** to **Figure 92**.

Table 55: VIP - 1 and VIP - 4 assemblies. Equivalent thermal conductivity with the relative uncertainty, and linear thermal transmittance at different average temperatures and ageing conditions

Sample	Ageing conditions	$\vartheta_{avg} [^{\circ}C]$												
		7			10			23			40			
		$\lambda_{7^{\circ}C}$ [W/mK]	$u_c(\lambda)$ [%]	$\psi_{7^{\circ}C}$ [W/mK]	$\lambda_{10^{\circ}C}$ [W/mK]	$u_c(\lambda)$ [%]	$\psi_{10^{\circ}C}$ [W/mK]	$\lambda_{23^{\circ}C}$ [W/mK]	$u_c(\lambda)$ [%]	$\psi_{23^{\circ}C}$ [W/mK]	$\lambda_{40^{\circ}C}$ [W/mK]	$u_c(\lambda)$ [%]	$\psi_{40^{\circ}C}$ [W/mK]	
1.12 +	1.14	Fresh	0.0056	2.3	0.0136	0.0057	2.3	0.0137	0.0059	2.2	0.0140	0.0062	2.2	0.0145
		90 dd	0.0061	2.1	0.0144	0.0062	2.1	0.0147	0.0065	2.0	0.0154	0.0072	1.9	0.0164
1.12 +	1.13	Fresh	0.0057	2.3	0.0141	0.0058	2.3	0.0143	0.0060	2.2	0.0146	0.0063	2.2	0.0153
		90 dd	0.0060	2.1	0.0188	0.0061	2.1	0.0192	0.0064	2.1	0.0211	0.0070	2.0	0.0252
4.15 +	4.16	Fresh	0.0047	2.4	0.0122	0.0047	2.4	0.0121	0.0048	2.3	0.0122	0.0050	2.3	0.0126
		90 dd	0.0052	2.1	0.0080	0.0052	2.1	0.0077	0.0055	2.0	0.0091	0.0060	1.9	0.0122
4.17 +	4.18	Fresh	0.0046	2.4	0.0118	0.0046	2.4	0.0119	0.0047	2.3	0.0121	0.0050	2.3	0.0128
		90 dd	0.0052	2.1	0.0079	0.0051	2.1	0.0071	0.0054	2.0	0.0082	0.0059	1.9	0.0114

First of all, it is worth mentioning that a direct comparison between the two ageing steps is not allowed because the results refer to different assemblies (even if made with the same VIPs). In fact, after the Fresh measurements, the assemblies were dismantled to measure the VIPs λ_{COP} after 30 days of storage. This is why the assemblies thermal performances can be remarkably different, and even be better after the ageing. This behaviour is due to the fact that the additional heat flux through the VIP assembly joint is strongly influenced by the quality of assembling and the width of the gap in between the panels.

Anyway, the obtained measurement uncertainty of the equivalent thermal conductivity is, on average, significantly below the 2.5%: λ_{eq} is always higher

than λ_{COP} (as well as the heat flux through the sample), and therefore the $u_c(\lambda_{eq})$ is lower.

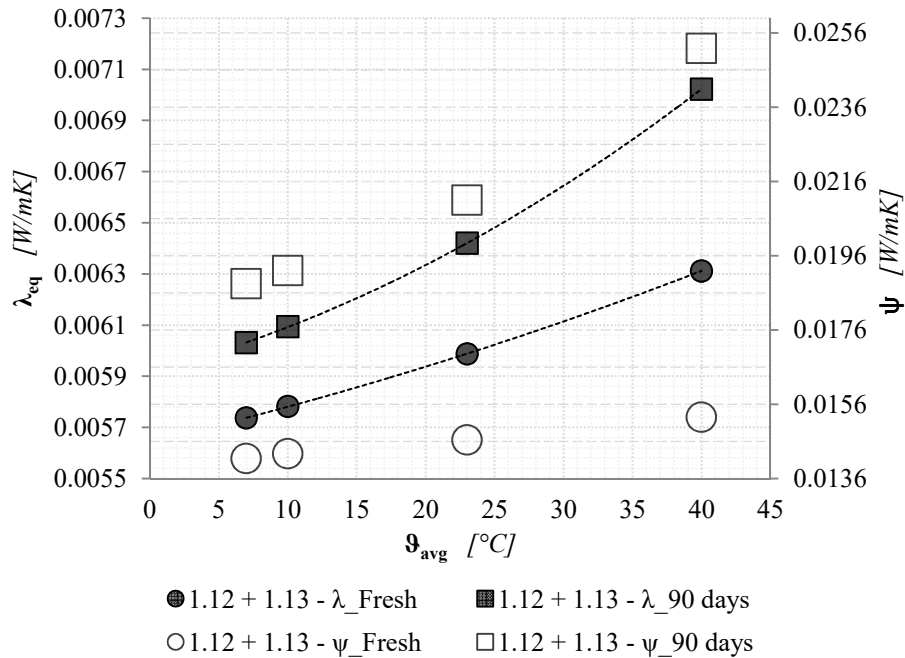


Figure 89: VIP - 1.12 + 1.13 assembly. Equivalent thermal conductivity and linear thermal transmittance at different average temperatures and ageing conditions

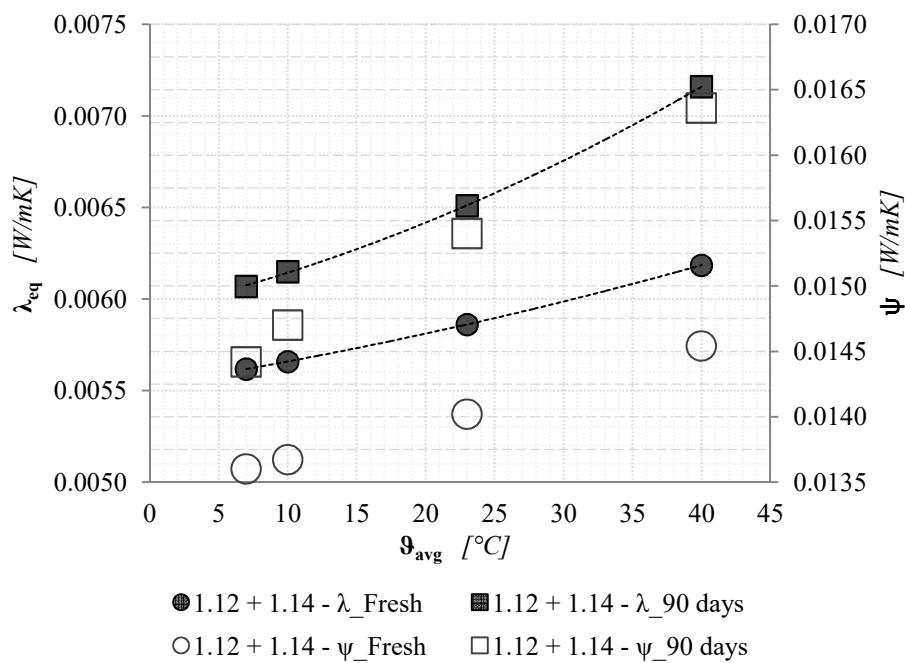


Figure 90: VIP - 1.12 + 1.14 assembly. Equivalent thermal conductivity and linear thermal transmittance at different average temperatures and ageing conditions

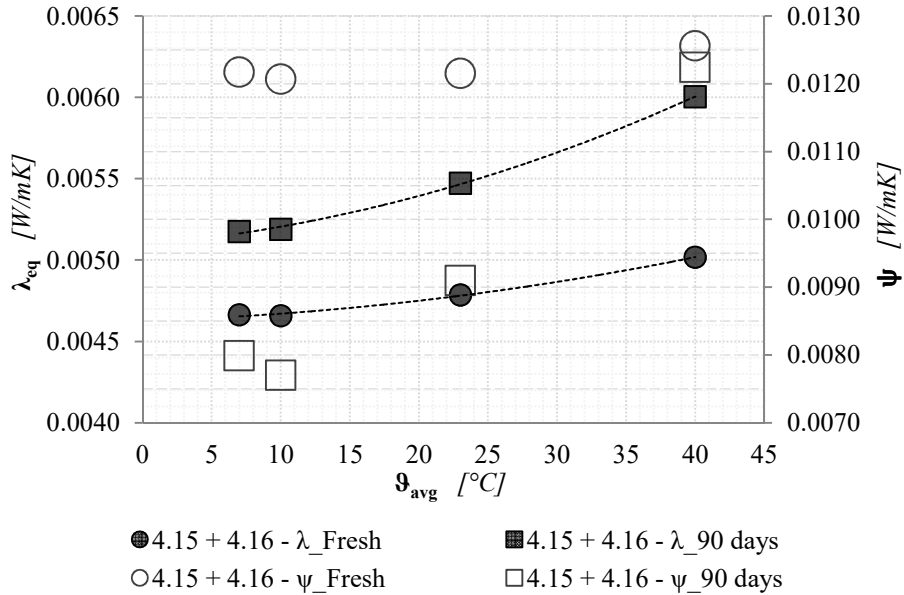


Figure 91: VIP - 4.15 + 4.16 assembly. Equivalent thermal conductivity and linear thermal transmittance at different average temperatures and ageing conditions

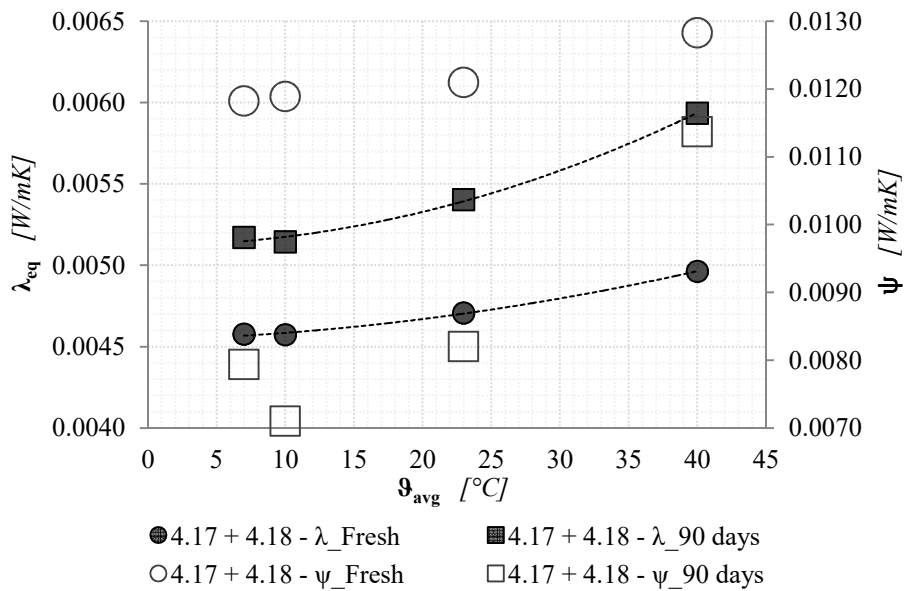


Figure 92: VIP - 4.17 + 4.18 assembly. Equivalent thermal conductivity and linear thermal transmittance at different average temperatures and ageing conditions

As it is possible to see, both the values of λ_{eq} and ψ increase with the increase of the average testing temperature. In fact, the ψ -value reflects the difference between the centre of panel undisturbed case and the disturbed case with a joint in between two assembled VIPs.

Chapter 9

Potentialities of VIPs for the energy efficient retrofit of buildings

The evaluation of the potentialities of VIPs for building retrofitting purposes is connected to the energy saving and the economic aspects. For this reason, the energy analyses and thermal load simulations presented in § 4.3.2 *Energy analysis and thermal load simulation* were coupled with an economic study, in order to evaluate whether VIPs can be more convenient than traditional insulating materials as building internal wall insulation.

9.1 The energy analysis

The estimate of the energy demand for space heating is essential to define the energy saving due to the insulation strategy. The energy saving is a crucial input data for the following thermo-economic analysis, aimed at the assessment of the potentialities of VIPs in buildings.

The energy demand analysis for space heating was assessed for all the cases presented in § 4.3.2 *Energy analysis and thermal load simulation*, before and after the energy retrofit with VIPs (2 mm air joints) and EPS, and performed using the EnergyPlus SW. Results are shown in **Table 56**.

Table 56: Space heating energy demand, according to different climatic zones and aspect ratios [138]

Energy demand for space heating								
t_{VIP}	t_{EPS}	S/V	Climatic zone	Before retrofit	Retrofit with VIP (air joint - 2mm) or EPS	Energy saving		
[m]	[m]	[1/m]		[kWh·year]	[kWh·year]	[kWh·year]		
0.01	0.09	0.12	Tampere	1505	937	568		
			London	590	299	291		
			Palermo	16	0	16		
		0.37	Tampere	3519	1477	2042		
			London	1783	592	1191		
			Palermo	313	26	287		
		0.53	Tampere	4798	1820	2978		
			London	2568	790	1778		
			Palermo	541	69	472		
		0.75	Tampere	6648	2371	6646		
			London	3727	1122	2605		
			Palermo	894	156	738		
		0.02	0.17	0.12	Tampere	1505	860	645
					London	590	260	330
					Palermo	16	0	16
				0.37	Tampere	3519	1185	2334
					London	1783	436	1347
					Palermo	313	5	308
				0.53	Tampere	4798	1407	3391
					London	2568	558	2010
					Palermo	541	23	518
				0.75	Tampere	6648	1730	4918
					London	3727	747	2980
					Palermo	894	64	830
0.03	0.22			0.12	Tampere	1505	838	667
					London	590	250	340
					Palermo	16	0	16
		0.37	Tampere	3519	1091	2428		
			London	1783	387	1396		
			Palermo	313	1	312		
		0.53	Tampere	4798	1268	3530		
			London	2568	484	2084		
			Palermo	541	12	529		
		0.75	Tampere	6648	1526	5122		
			London	3727	632	3095		
			Palermo	894	40	854		

9.2 The thermo-economic analysis

9.2.1 Economic parameter

The economic analysis was developed evaluating the Discounted Pay Back Period (DPBP) and the Break-Even Rental Value (BERV). These two quantities will be better defined and discussed in the next sections.

The calculation of the DPBP and the BERV requires the following information:

- the investment cost of the insulation retrofit (with both VIPs or EPS),
- the saved operative costs (due to the lower space heating demand),
- the extra-profit obtainable from the more usable space obtained when VIPs are used instead of traditional insulating solutions.

In the following sections, all the involved quantities and parameters will be described in detail.

9.2.1.1 Investment cost and savings in the operative costs

The cost of the investment was assessed through a price analysis, according to the current Italian regulation [154]. The data-cost of the selected insulating materials (VIPs and EPS) were obtained from two random manufacturing companies ([155];[156]). VIP panels were assumed to have an average size of about 1000 x 1000 mm. The additional materials (e.g., adhesive and screws) required for the insulators installation were estimated at approximately 10 €/m² for both VIPs and EPS, on the basis of market investigations. For the installation cost, double time for the VIPs installation compared to the one for EPS was supposed (more caution is needed for VIP, to avoid puncturing of the panels and to install them properly). The investment costs are summarised in see **Table 57**.

Table 57: Insulation investment costs [138]

Item	Investment costs	
	VIP [€/m ²]	EPS [€/m ²]
Insulating material	205	21
Additional material for laying	10	10
Manpower	40	20
TOTAL	255	51

9.2.1.2 Estimate of the profit due to the space saving

The operative costs savings were assessed through the following procedure.

“Firstly, the energy demand for space heating was assessed for the existing building by means of a dynamic energy simulation (using the EnergyPlus SW). The same simulation was then repeated for the retrofitted building (using either the VIP or the EPS as insulating material). The difference between these two heating demands provided the energy saving obtainable by means of the retrofit. This energy is the so-called room demand, E_{rd} (e.g. the total heat that has to be delivered to the room air for keeping the desired set-point temperature). Nevertheless, in order to convert such information into a cost saving, the so-called “delivered energy” has to be preliminarily assessed, E_{del} (the delivered energy is the one that the consumer receives at her/his “gate”). The relation between these two quantities is given by the efficiency of the heat generator:

$$E_{del} = \frac{E_{rd}}{\eta} \quad (100)$$

As discussed in § 4.3.2 Energy analysis and thermal load simulation, two alternatives were considered: a natural gas condensing boiler ($\eta = 79.4\%$) and a geothermal heat pump ($COP = 4.0$).

Finally, the operative costs were assessed by multiplying the delivered energy by the market price of the used energy vector, that is, natural gas or electricity.

For the prices quantification the Eurostat database for the year 2014 was used [157]:

- natural gas price: 0.056 €/kWh;
- electric energy price: 0.141 €/kWh.

These investment costs were assumed to be the same for all the considered locations.

The profit related to the internal space saving due to the VIP application instead of the EPS is rarely (if never) considered, but it is a crucial issue for the economic assessment (Table 58).

Table 58: Internal space savings [138]

t	Space saving							
	S/V = 0.12		S/V = 0.37		S/V = 0.53		S/V = 0.75	
[mm]	[%]	[m ²]	[%]	[m ²]	[%]	[m ²]	[%]	[m ²]
10	1.5%	0.29	4.2%	0.84	5.1%	1.00	7.2%	1.42
20	2.7%	0.54	7.3%	1.45	9.3%	1.84	13.1%	2.60
30	3.4%	0.68	9.0%	1.79	11.7%	2.31	16.4%	3.25

Indeed, if the space saving provided by VIP insulation is not taken into account, the traditional insulating materials would be generally more convenient than VIP. On the contrary, if the space saving due to a thin VIP insulating layer is considered, the Discounted Pay-Back Period (DPBP) of VIP could be shorter than the one of EPS.

If the real estate value of the square meters saved using the VIP insulation would be adopted, a difficulty would arise. In fact, in this case, the profit due to the VIP application would occur only when and if the sale of the building would eventually take place. For this reason, the rental value was considered, instead of the real estate value. The rent rate is a monthly occurrence, and it allows to quickly evaluate the profit due to the internal space saving for each year.

The range of the considered rental values starts from a very low annual value of 50 €/m² per year and rises up to 800 €/m² per year. It is worth mentioning that these values reflect the actual rental rates of office spaces in Europe. In [158] is shown that the rental values in the central business district can be quite expensive: e.g. the most expensive office market in the world is London, with a monthly rental value of office spaces higher than 1400 €/m² in the West End²⁶.

9.2.1.3 The Discounted Pay-Back Period (DPBP)

“The comparison between VIP and traditional insulating materials (i.e. EPS) was carried out by the Discounted Pay-Back Period (DPBP):

$$DPBP = (y - 1) + |B^{(y-1)}| \cdot D^{-y} \quad (101)$$

Where: y is the year in which the cumulative present value of cash flows exceed the initial investment cost;

²⁶ Text from the author’s paper: “Thermo-economic analysis of building energy retrofits by using VIP - Vacuum Insulation Panels” [138].

B is the cumulative present value of the cash flows from the initial investment cost at the end of the year before y;

D is the current value of net cash flow in year y.

Accordingly, the annual net cash flows had to be discounted to the Present Cash Flow (PCF) value by Eq. (102):

$$PCF = \text{actual cash flow} \cdot (1 + i)^{-n} \quad (102)$$

Where: i is the discount rate;

n are the years to which the cash inflow relates.

The discount rate used for the analysis was chosen equal to 0.88%, corresponding to the average European 10-year Government Benchmark bond (2.28%) [159] corrected by excluding the expected inflation rate in Europe (1.4%) [160].

The data considered in the DPBP calculation were:

- *the investment cost to buy and install the internal wall insulation;*
- *the annual rental profit considering the space saving by VIP application instead of traditional insulation;*
- *the yearly operating cost saving due to the energy savings (e.g., the difference between pre and post-retrofit energy consumption cost).*

In detail, the investment cost was accounted in the year zero, then for each year, the annual profits were subtracted. The rental profit and the operating cost saving were taken into account as yearly profits in the DPBP calculation for VIP, while only the operating cost saving is considered as annual profit in the EPS DPBP calculation. The yearly net value of both rental benefits and operating cost savings were assumed constant. The hypothesis of constant values was considered acceptable because it was impossible to make accurate forecasts about the long-term perspectives of the real estate market and of the energy price (anyway, the energy price was the same both for VIPs and EPS)²⁷.

²⁷ Text from the author's paper: "Thermo-economic analysis of building energy retrofits by using VIP - Vacuum Insulation Panels" [138].

9.2.1.4 The Break-Even Rental Value (BERV)

“An essential parameter for the comparison between VIP and EPS is the Break-Even Rental Value (BERV). It represents the break-even point between the DPBP calculated for VIP and the one calculated for EPS. It is, thus, the limit value of the rental rate above which VIP is more convenient than EPS.

Figure 93 shows, as an example, the DPBP values versus the rental rate for two retrofit actions, one using VIPs (continuous blue curve), the other using EPS (dashed orange line). This figure shows how BERV can be graphically found. Its value is represented by the point of intersection between the two curves (the big point in **Figure 93**)²⁷.

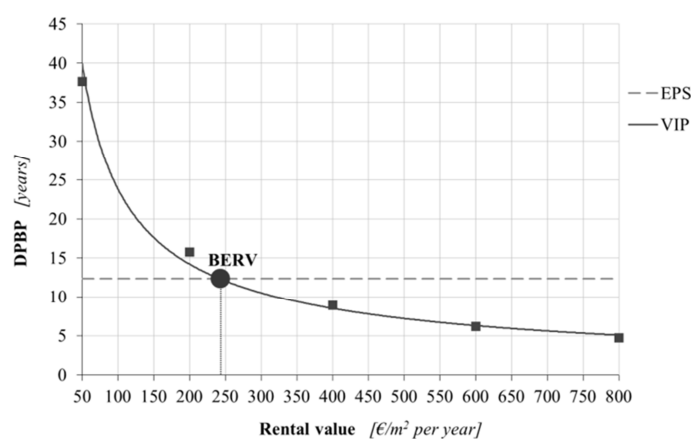


Figure 93: Example of the evaluation of BERV [138]

9.2.2 Results

The thermo-economic analysis results will be presented in the following sections, assessing the influence of the several considered parameters (climatic zone, aspect ratio, thermal insulation level, type of the heating system).

9.2.2.1 Influence of the climate conditions

“The analysis of the influence of the climate conditions was done keeping constant the insulation level ($U = 0.192 \text{ W/m}^2\text{K}$, $t_{VIP} = 20 \text{ mm}$), the aspect ratio (0.53) and the heating system (gas boiler).

As shown in **Figure 94**, the DPBP is shorter in coldest countries with a high heating degree days (HDD) and increases with the decreasing of HDD. The VIP trend lines represent different behaviours. The trend for the rental value of 50

€/m^2 is exponential, then becomes approximately linearly for rental values higher than 200 €/m^2 per year. On the other hand, the EPS trend line (dashed line) has an exponential trend. This is because, in case of EPS, the energy saving represents the only profit and this lost is negligible compared to investment cost, especially in the warmer locations (e.g., Palermo).

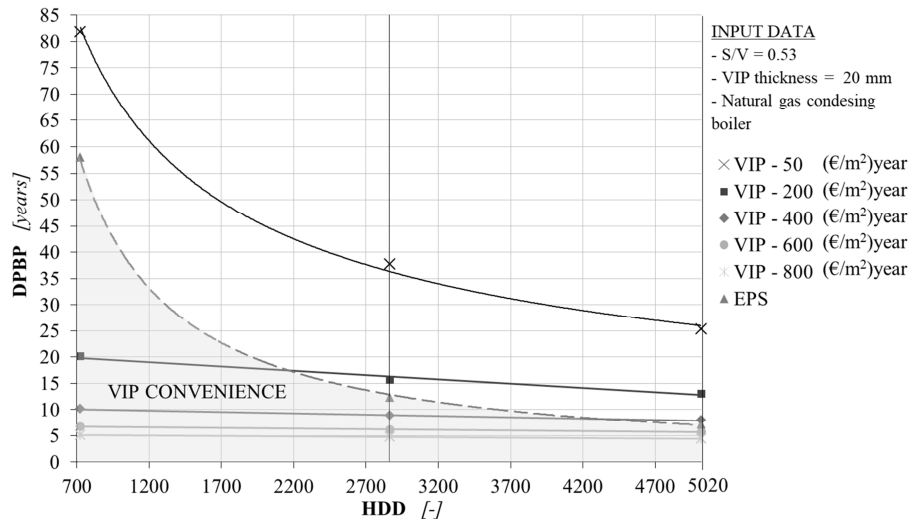


Figure 94: DPBP as a function of climatic zones. The grey area represents the VIP convenience [138]

The linearity of the DPBP curves for very high rental rate and their almost non-dependency by the HDD is obviously due to the fact that in such cases the profit comes almost only by the rental rate and the influence of the cost saved for the operational energy (that is a function of the HDD) is negligible.

It is worth mentioning that the BERV increases as the climate conditions become more severe (e.g., when the HDDs are higher). This appears to be a strange result, but in reality is the consequence of coupling economic and energy effects.

As it is possible to see in **Figure 95**, the Break-Even Rental Value is higher in Tampere than in Palermo. This unexpected trend is due to the different length of the time needed to reach the balance between the DPBP of VIPs and EPS. In Palermo such period is very long (i.e., almost 50 years), so even a low rental profit, but repeated for many many years, makes the VIP more convenient. In Tampere, by contrast, the DPBP of the EPS is short (i.e., 7 years) and the rental

profit per month has to be high, otherwise the gap cannot be recovered within a short period of time.

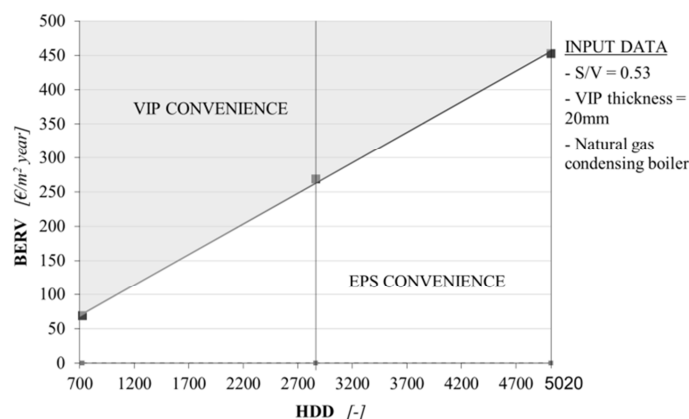


Figure 95: BERV as a function of the climatic zone [138]

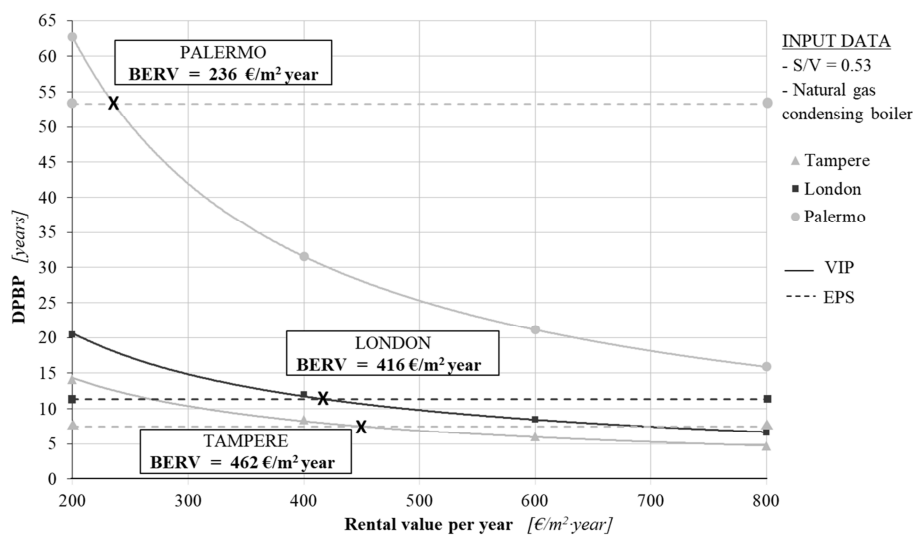
Results shown in Figure 94 and Figure 95 are useful to understand trends and behaviours, but they are affected by an inherent limitation. All this data, in fact, refer to a case in which the U-value of the retrofitted wall is the same, regardless of the climate condition. Such comparison, however, is not coherent with the real world of constructions, whose, usually, the insulation level of walls is strongly related to the local climate conditions. Therefore, in order to leave a picture of what would happen in real cases applications, a further investigation was done.

Firstly, the thickness of insulation needed to respect the limit U-value (U_{lim}) for Finland, United Kingdom and Italy was calculated, respectively for VIP and EPS (Table 59). Then, the BERV was again calculated. It resulted that the BERV in Tampere (462 €/m² per year) is still higher than the one in London (416 €/m² per year), but the two values are now closer (Figure 96). On the contrary, Palermo has a break-even rental value much smaller (Figure 96 - 236 €/m² per year), because the insulation level required in Palermo is lower than the one provided by 10 mm VIP and the EPS Pay-Back Period is too long (i.e., 53 years). This means that the retrofit strategy of insulating the wall is not convenient in itself in such climate zone. However, if an internal wall insulation would be necessary to respect the limit U-value, the VIPs were generally more convenient than EPS”²⁸.

²⁸ Text from the author’s paper: “Thermo-economic analysis of building energy retrofits by using VIP - Vacuum Insulation Panels” [138].

Table 59: Calculation of the BERV according to the wall $U\text{-value}_{lim}$ of the different countries [138]

	$U\text{-value}_{lim}$ [W/m^2K]	VIP thickness		EPS thickness		BERV [$€/m^2$ per year]
		Calculated	Market	Calculated	Market	
		[mm]		[mm]		
Tampere	0.17	26	30	197	200	462
London	0.30	10	10	96	100	416
Palermo	0.48	5	10	46	50	236

Figure 96: DPBP according to the wall $U\text{-value}_{lim}$ of the different countries. The crosses show the BERVs [138]

9.2.2.2 Influence of the aspect ratio

“In order to investigate the influence of the aspect ratio, the case characterised by a thickness of the VIP layer equal to 20 mm (the equivalent thickness of the EPS was of about 170 mm) and the condensing boiler as heat generator was chosen. As it is possible to see in **Figure 97** and **Figure 98** the aspect ratio (S/V) of the building does not play a significant role in the economic return of the energy retrofit. The trend of the DPBP versus the aspect ratio is somewhat parabolic for low rental rates and becomes almost linear and constant when the rental rate is higher than 200 €/m². Again this is due to the fact that for higher rental costs most of the revenues derive from the space saving (that is independent by the S/V parameter) while the revenues of the energy saving during the operation of the building are negligible (**Figure 97**).

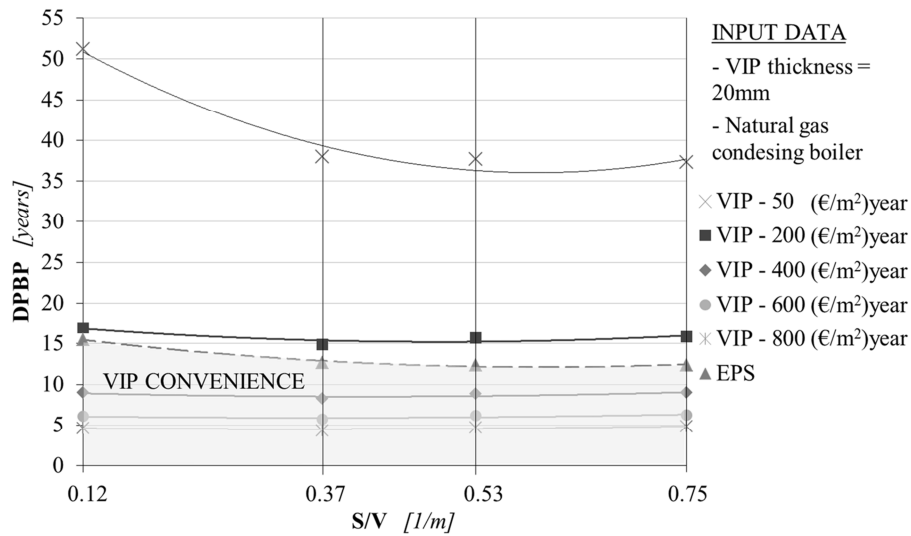


Figure 97: DPBP as a function of aspect ratios [138]

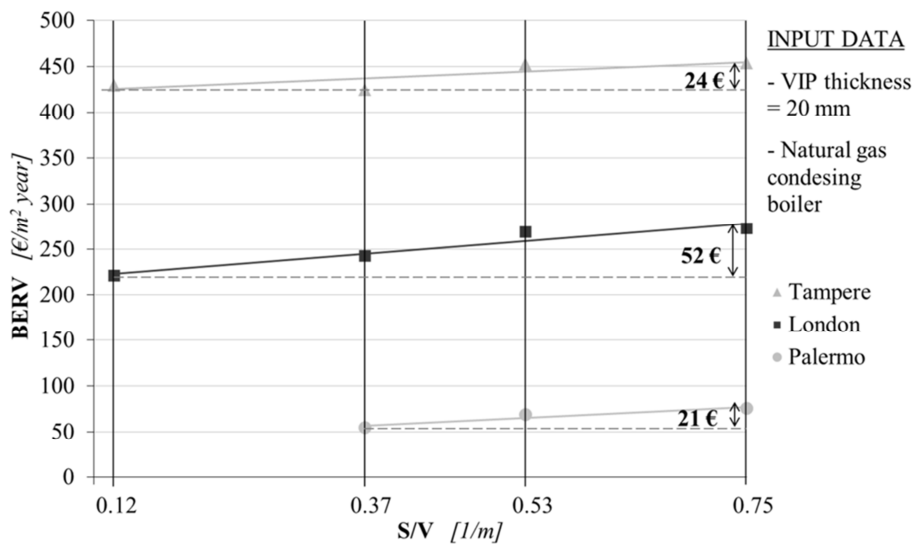


Figure 98: BERV according to the different aspect ratios [138]

Accordingly, the BERV (Figure 98) slightly increases with the increase of the aspect ratio, even if the variation is not so significant and is similar for the three reference climatic conditions. What makes the difference is the climatic context (passing from Palermo to Tampere the BERV switches from around 50 €/m² to

4400 €/m²; for both these cities, passing from $S/V = 0.37$ 1/m to $S/V = 0.75$ 1/m means increasing the DPBP of about 20 – 25 €/m²)”²⁹.

9.2.2.3 Influence of the insulation thickness

“The influence of the thickness of the insulating material on the DPBP and BERV was analysed for the case characterised by an S/V ratio of 0.53 1/m and the condensing boiler as a heat generator. **Figure 99** shows the trend of DPBP versus the insulation thickness for various values of the rental cost. As far as the VIP system is concerned, and for rental rates around 200 €/m², the DPBP curves decrease slightly from the thickness of 10 mm to 20 mm and then remain basically constant up to 30 mm. Such behaviour depends on the fact that there is a greater advantage in using the VIP when the internal space saving is maximised (e.g. for lower thicknesses of the VIP panels). At all events, when the rental rates are exceeding approximately 400 €/m² the variation of the DPBP with the VIP thickness becomes negligible.

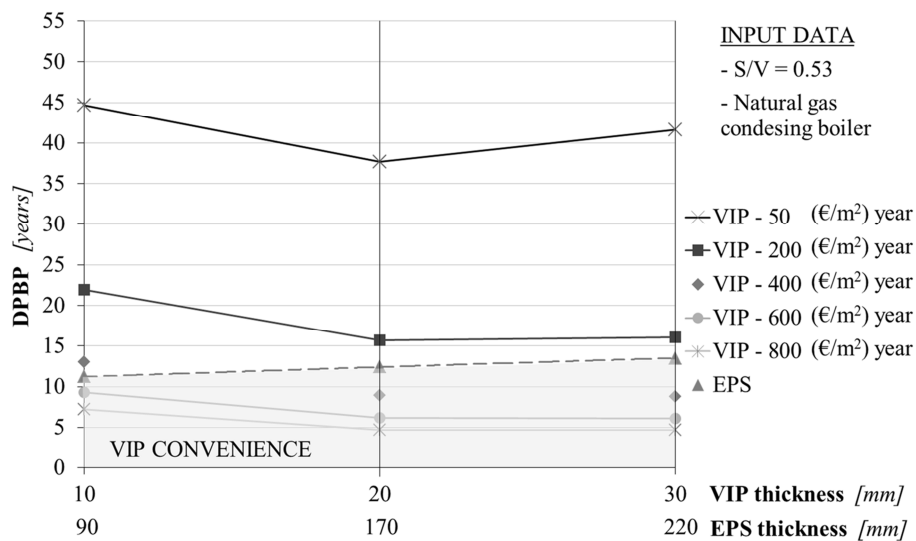


Figure 99: DPBP as a function of insulation thicknesses [138]

²⁹ Text from the author’s paper: “Thermo-economic analysis of building energy retrofits by using VIP - Vacuum Insulation Panels” [138].

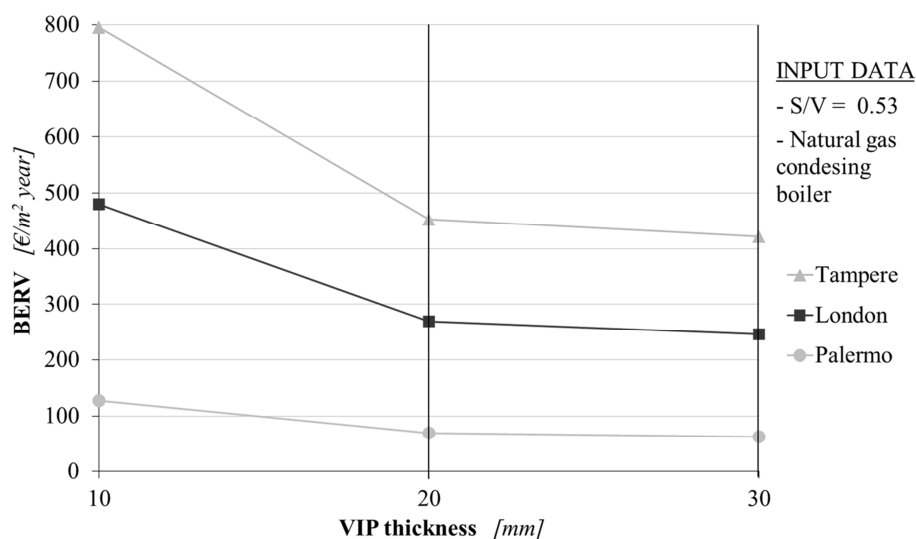


Figure 100: BERV according to the VIP thicknesses (10, 20 and 30 mm) [138]

Instead, for low rental rates (e.g. 50 €/m²) there seems to be a cost-optimal thickness of the VIP above and below which the DPBP rises (being such thickness around 20 mm).

On the contrary, when the EPS is considered, the DPBP versus the thickness follows an opposite trend. It increases linearly with the increase of the EPS thickness (**Figure 99**).

These two contrasting behaviours result in a BERV that decreases with the increase of the VIP thickness, as it is possible to see in **Figure 100**, where the BERV is plotted versus the VIP thickness for the three considered reference cities (assumed as representative of the three characteristics climatic conditions). This means that lower rental costs are sufficient to match the EPS Pay Back Period when the VIP thickness is equal or higher than 20 mm. The variation of the BERV with the VIP thickness is significant for colder climate conditions (e.g. from about 800 €/m² to 400 €/m² for Tampere) and is marginal for warmer locations ((e.g. from about 120 €/m² to 80 €/m² for Palermo).

Nevertheless, it is worth mentioning that in real life the decision about the required thickness of the insulating layer, besides the economic issues, is also

(and mainly) driven by the thermal performance that is to be achieved by standards and laws”³⁰.

9.2.2.4 Influence of the heating system efficiency

“Figure 101 shows the trend of the DPBP versus the HDD for various rental costs and for the two considered heat generators, i.e. the gas condensing boiler (solid lines) and the geothermal heat pump (dashed lines).

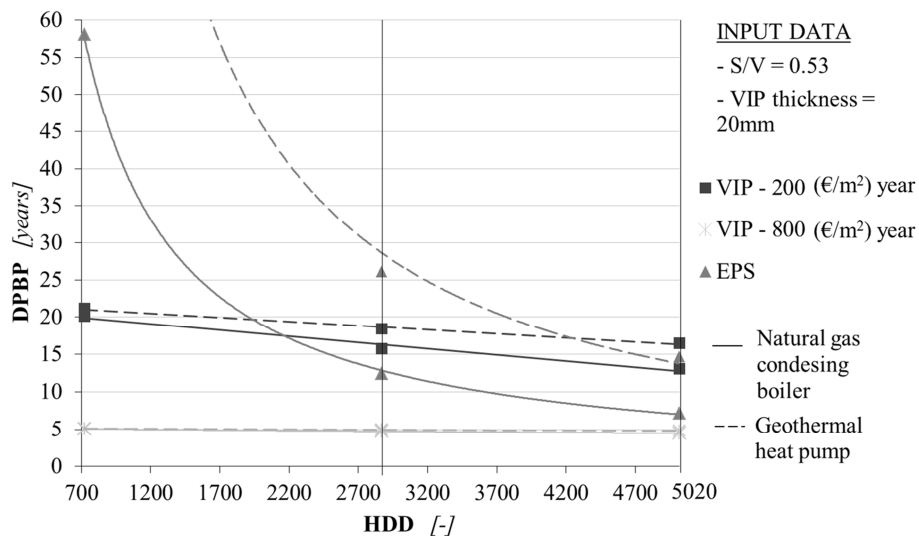


Figure 101: DPBP as a function of the heating systems [138]

Calculations have been done keeping constant the S/V ratio (equal to 0.53 1/m) and the thickness of the VIP/EPS layers (20 mm for the VIP, while the equivalent thickness of the EPS was of about 170 mm).

As expected, a well-performing heating system, like the geothermal heat pump, makes the DPBP worst. Clearly, this is due to the fact that an improvement of the performance of the energy conversion system reduces the economic advantages derived from the saved room demand (that is, the same decrease of the E_{rd} , which is obtained with the energy retrofit, results in a smaller variation of E_{del} when the efficiency η is higher). Indeed, the thermal insulation retrofit is generally less valuable when high efficient mechanical systems are used.

³⁰ Text from the author’s paper: “Thermo-economic analysis of building energy retrofits by using VIP - Vacuum Insulation Panels” [138].

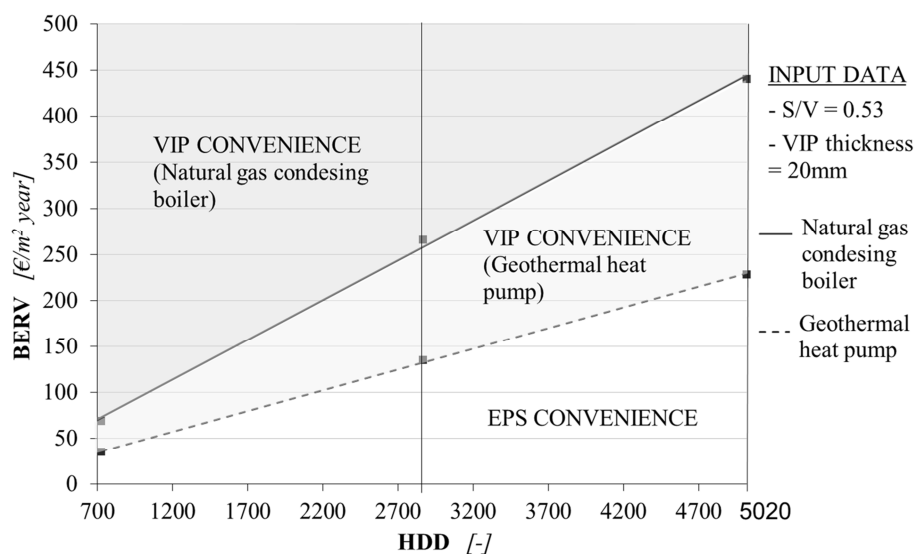


Figure 102: BERV according to the heating systems [138]

It is, however, interesting to notice that if an energy retrofit must be done anyway (for example in order to comply with mandatory regulations) then the VIP solution results to be economically more convenient than the EPS if it is coupled with a better performing heat generator (that is, with the geothermal heat pump instead of the gas condensing boiler) (Figure 102). The DPBP is longer when a geothermal heat pump is instead of a condensing boiler, both for VIP and EPS, but the BERV is better for the former material (i.e. a lower rental cost is needed for the VIP to match the EPS PayBack Period at equal HDD - dashed line in Figure 102)³¹.

³¹ Text from the author's paper: "Thermo-economic analysis of building energy retrofits by using VIP - Vacuum Insulation Panels" [138].

Chapter 10

Outlooks: prediction of VIPs long-term performances and associated uncertainties

The research activity described in the previous chapters allowed to identify suitable testing procedure able to reliably assess the thermal performances of SIMs, as well the critical issues that can be met during measurements. In the previous chapters, a detailed analysis was performed to investigate all the factors which influence SIMs thermal properties and their experimental uncertainties, providing some guidelines for improving the reliability of the results. But what about the SIMs in situ actual thermal behaviour? As already mentioned in § 4.3 *Numerical simulations* numerical simulations can be very useful for this analysis, and they can be performed at different scales (from the single material to an entire building or district). Moreover, since SIMs (and especially VIPs) are a recent technology for building insulation, these investigations are also useful for the assessment of their durability/service life of the insulating materials. In fact, up to now, there are few SIMs long-term applications on buildings to experimentally determine these aspects appropriately. How reliable are the simulation results however is still unknown, and it represents an interesting issue to be solved in future researches.

In the following sections, the results of the dynamic hygrothermal simulation presented in § 4.3 *Numerical simulations* are reported, to define the actual VIPs operating conditions in case of the two described building envelope configurations

(a brick wall structure and a pitched roof structure), and provide an estimation of the VIPs service life in roof applications. Investigations were performed considering only VIPs (and not other SIMs) because their thermal properties are more influenced by temperature, humidity and ageing than the other materials.

These investigations were proposed and developed in the context of the IEA EBC Annex 65 project, sub-task 3 [93] (ten building envelope configurations in four different countries, Italy, France, Germany and Sweden, characterised by different climatic conditions were analysed).

10.1 Building component simulation model

The numerical simulations of the brick wall structure and the pitched roof structure were performed using WUFI[®] Pro software [140], in accordance with the criteria and the design alternatives described in § 4.3 *Numerical simulations*. For each considered design alternative of each component, two different results related to ϑ , RH and p_v were obtained: the time profiles and the cumulative frequency distributions.

The cumulative frequency distributions were subdivided into four ranges, from (I) to (IV) representing the increasing of the VIP operating condition severity. The limit between the intervals (III) and (IV) was assumed to be equal to the thermohygro-metric conditions to which the samples were subjected during accelerated aging tests (see § 8.3 *Experimental campaign for VIPs thermal properties measurement (HFM)* and IEA EBC Annex 65 sub-task 2 [150]): $\vartheta = 50^\circ\text{C}$ and $RH = 70\%$.

Hereinafter, only the most representative and/or critical design alternative for each case study will be discussed.

10.1.1 Brick wall in Torino

The brick wall configuration is representative of a typical Italian wall refurbishment (building time before 1945, which corresponds to about 30 % of the overall residential buildings). Technical details about this configuration are reported in **Figure 103**.

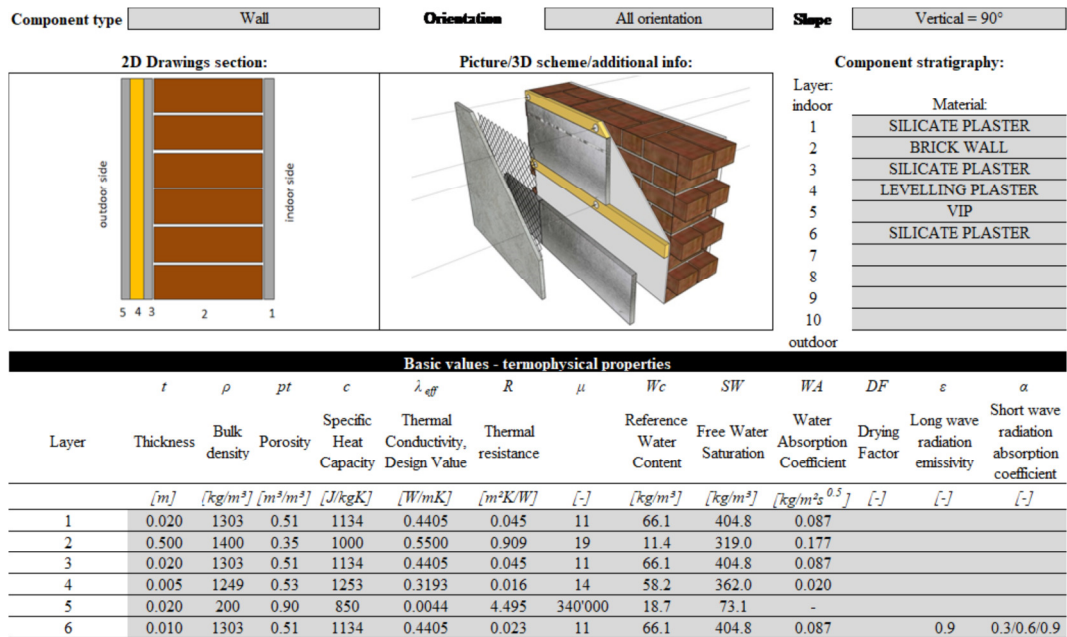


Figure 103: Data-sheet of the analysed wall [93]

The outdoor weather conditions of Torino (year 2004) were obtained directly from the Wufi® 6.0 database (Figure 104 and Figure 105), while the indoor climate conditions were provided by the standard EN 15026:2007 [141]:

- heating season (15th October - 15th April): $\vartheta = 20^{\circ}\text{C}$;
- cooling season (15th April - 15th October): $\vartheta = 25^{\circ}\text{C}$.

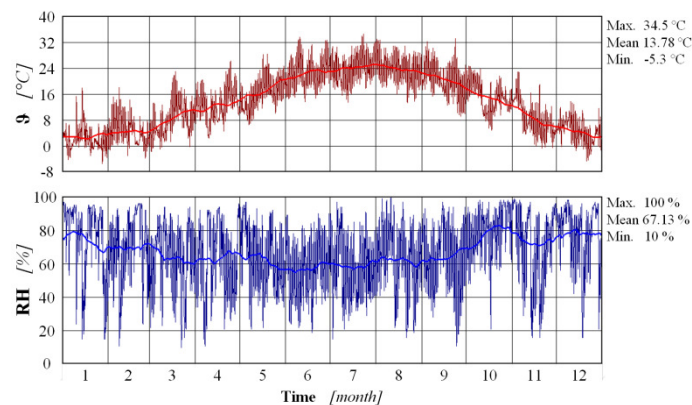


Figure 104: Torino - year 2004 outdoor weather conditions (graphical output from Wufi®) [93]

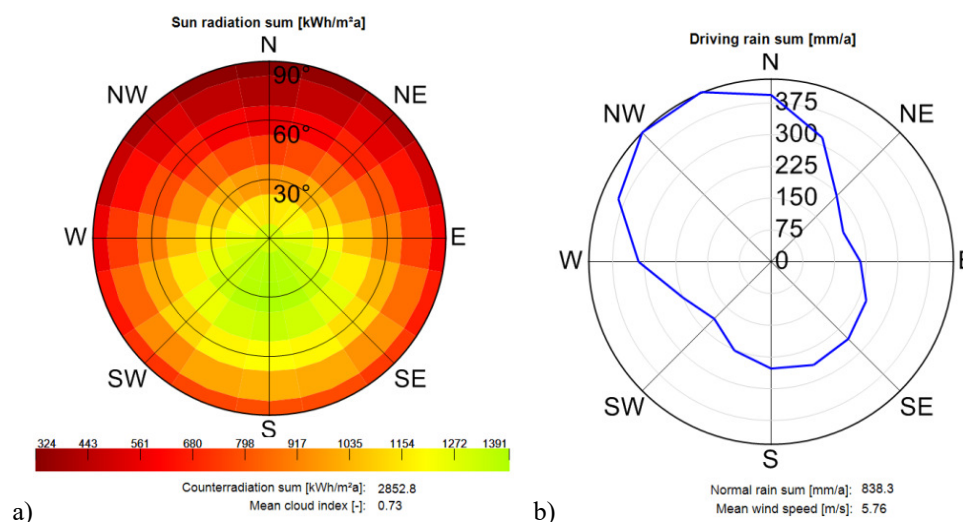


Figure 105: Torino - year 2004 a) solar radiation; b) driving rain and mean wind speed (graphical output from Wufi[®]) [93]

As already mentioned, the simulations were performed considering all the possible combination of different design alternatives: two VIP thicknesses (10 and 20 mm), four orientations (north, south, east and west), two moisture loads (medium and high) and three external finishing colours (bright, medium and dark finishing, corresponding to a solar absorption coefficient α equal to 0.3, 0.6 and 0.9 respectively). **Table 60** provides the list of all the analysed wall configurations.

Table 60: Summary of the different wall configurations [93]

Name	Orientation	Solar absorption coefficient - α	Moisture load	t
1. N_B_m_20		Bright		
1. N_M_m_20	NORTH	Medium		
1. N_D_m_20		Dark		
1. E_B_m_20		Bright		
1. E_M_m_20	EAST	Medium		
1. E_D_m_20		Dark		
1. S_B_m_20		Bright	medium ($\leq 60\%$)	20 mm
1. S_M_m_20	SOUTH	Medium		
1. S_D_m_20		Dark		
1. W_B_m_20		Bright		
1. W_M_m_20	WEST	Medium		
1. W_D_m_20		Dark		
1. W_D_h_10	WEST	Dark	high (> 60%)	10 mm
1. W_D_h_20				20 mm

For the sake of brevity, only the results related to the worst design alternative combinations are discussed in detail: west exposed dark vertical façade, with medium internal moisture load, and VIP thickness equal to 20 mm (1.W_D_m_20).

The time profiles during a year of the temperature ϑ , the relative humidity UR and the water vapour pressure p_v are represented in Figure 106, Figure 107 and **Figure 108** respectively. Each figure plots the results of the external (e) and the internal VIP side (i), and the average value (avg).

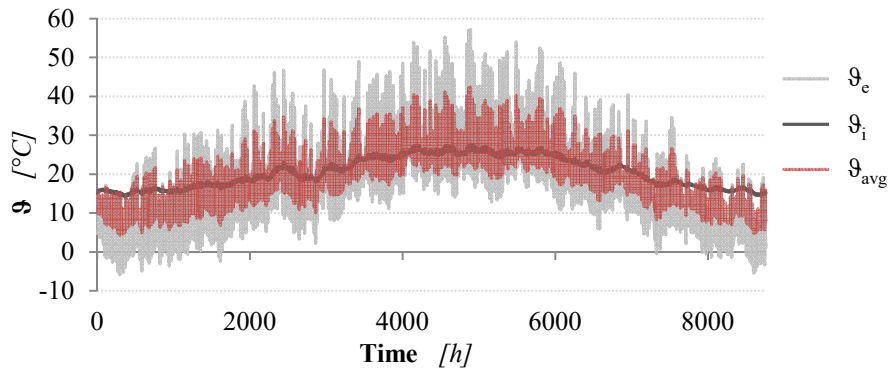


Figure 106: Temperatures yearly time profiles (1.W_D_m_20) [93]

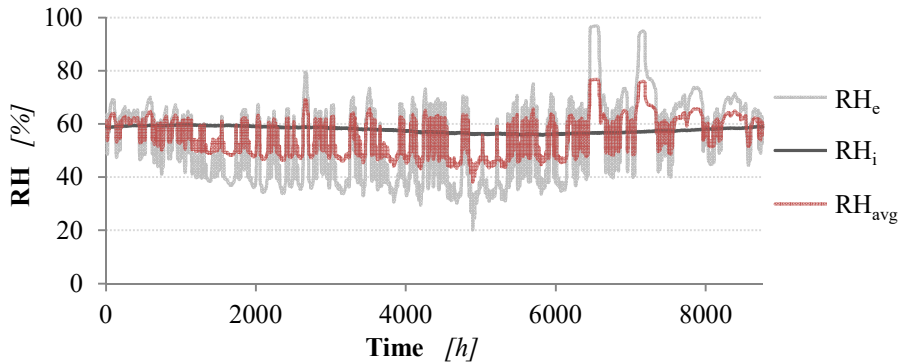


Figure 107: Relative humidities yearly time profiles (1.W_D_m_20) [93]

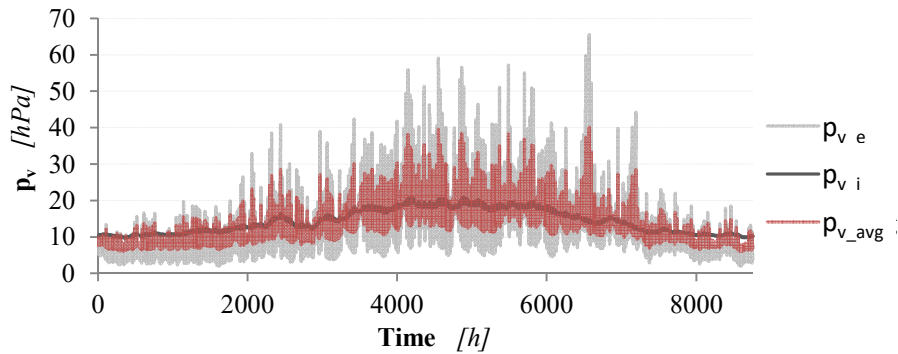


Figure 108: Vapour pressure yearly time profiles (1.W_D_m_20) [93]

Moreover, the cumulative frequency distributions of the same quantities (ϑ , UR and p_v) are shown in **Figure 109**, **Figure 110** and **Figure 111**, respectively.

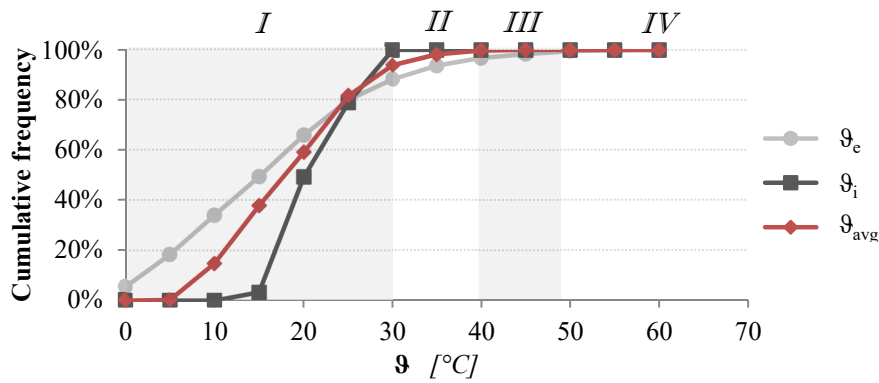


Figure 109: Temperature cumulative frequency (1.W_D_m_20) [93]

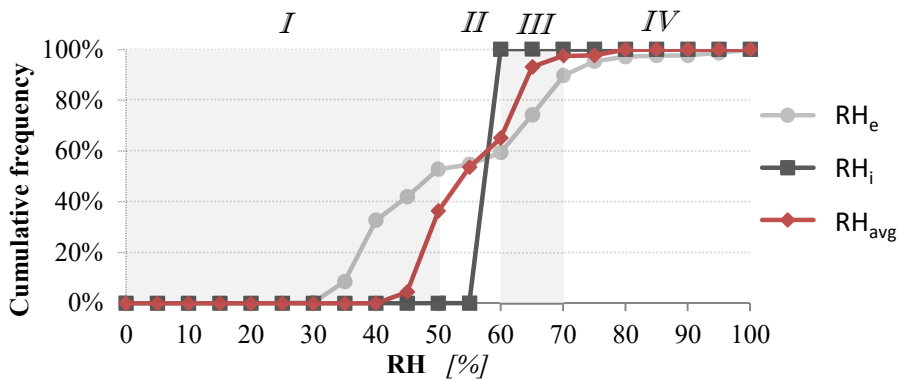


Figure 110: Relative humidity cumulative frequency (1.W_D_m_20) [93]

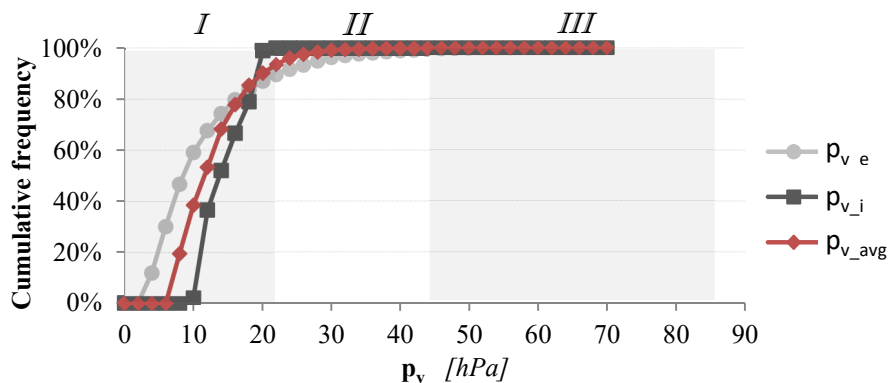


Figure 111: Vapour pressure cumulative frequency (1.W_D_m_20) [93]

The overall results related to all the design alternatives combinations are summarised in **Table 61** (medium moisture load, 20 mm VIP) and **Table 62** (high moisture load, 10 and 20 mm VIP). The table shows, for the specific range of temperature, relative humidity and water vapour pressure, the frequency distribution values. Cells are coloured in a gradient greyscale to highlight the highest values among the different design alternatives.

The results will be discussed separately for temperature, relative humidity and vapour pressure.

In case of medium moisture load (20 mm VIP), all the wall design alternatives lie between the temperature ranges (I) and (II). Range (III) is reached by few design alternatives:

- S_D_m_20 (south exposure and dark surface finishing) on the VIP external surface, where the temperature is from 40°C and 50°C for about 2.6% of the time (≈ 9.5 days/year, $\vartheta_{MAX} = 49.4^\circ\text{C}$);
- W_D_m_20 (west exposure and dark surface finishing) on the VIP external surface, where the range (III) was reached for about 2.8% of the time (around 10 days). For this design alternative also the range (IV) is reached, even for a very short percentage of time (about 0.4% ≈ 1.5 days, $\vartheta_{MAX} = 57.2^\circ\text{C}$).

The RH reaches range (III) for almost all the design alternatives, many of whom also reach the range (IV), with the highest frequencies in case of bright and medium finishing colours:

- S_B_m_20 (south exposure and bright surface finishing) on the VIP external surface, cumulative frequency $\approx 22.5\%$ of the time (about 82 days);
- E_B_m_20 (east exposure and bright surface finishing) on the VIP external surface, cumulative frequency $\approx 22.8\%$ (about 83 days);
- N_M_m_20 (north exposure and medium surface finishing) on the VIP external surface, cumulative frequency $\approx 23.8\%$ (about 87 days);
- W_B_m_20 (west exposure and bright surface finishing) on the VIP external surface, cumulative frequency $\approx 25.2\%$ (about 92 days, with $RH_{MAX} = 97.0\%$);
- N_B_m_20 (north exposure and bright surface finishing) on the VIP external surface, cumulative frequency $\approx 30.7\%$ (about 112 days, with $RH_{MAX} = 97.8\%$).
- W_D_m_20 (west exposure and dark surface finishing) on the VIP external surface, reaches the range (IV) in the 10.4% of the time (about 38 days, with $RH_{MAX} = 96.7\%$).

In case of vapour pressure ranges, few design alternatives reach range (III). These are the same design alternatives that lie in the temperature ranges (III) and (IV). In particular, the cases with vapour pressure between 44.3 hPa and 86 hPa are:

- S_D_m_20 (south exposure and dark surface finishing) on the VIP external surface, cumulative frequency around 0.3% ≈ 1 day ($p_{v\ MAX} = 67.8$ hPa);
- E_D_m_20 (east exposure and dark surface finishing) on the VIP external surface, cumulative frequency around 0.4% ≈ 1.5 days ($p_{v\ MAX} = 64.1$ hPa);
- W_D_m_20 (west exposure and dark surface finishing) on the VIP external surface, cumulative frequency around 0.6% ≈ 2 days ($p_{v\ MAX} = 65.5$ hPa).

Table 61: Wall: frequency distribution at the faces of a VIP 20 mm thick, considering a medium moisture load (1% of frequency corresponds to 3.65 days/year of exposure) [93]

Configuration	Orientation	Solar adsorption coefficient	Side	Temperature ranges					Relative Humidity Ranges				Vapour Pressure Ranges				
				I (≤ 30 °C)	II (30-40 °C)	III (40-50 °C)	IV (> 50 °C)	MAX	I (≤ 50 %)	II (50-60 %)	III (60-70 %)	IV (> 70 %)	MAX	I ($\leq 21,2$ hPa)	II (21,2-44,3 hPa)	III (44,3-86 hPa)	MAX
				[%]	[%]	[%]	[%]	[°C]	[%]	[%]	[%]	[%]	[%]	[%]	[%]	[%]	[hPa]
1.N_B_m_20	0.3	avg.	100.0	0.0	0.0	0.0	30.1	0.2	21.6	70.5	7.6	79.4	95.5	4.5	0.0	30.3	
		ext.	98.1	1.9	0.0	0.0	35.1	15.6	7.1	46.7	30.7	97.8	91.6	8.4	0.0	42.6	
		int.	100.0	0.0	0.0	0.0	25.5	0.0	25.3	74.7	0.0	61.9	100.0	0.0	0.0	19.8	
1.N_M_m_20	North	0.6	avg.	99.6	0.4	0.0	0.0	31.4	2.3	29.6	62.3	5.8	78.7	95.1	4.9	0.0	33.9
			ext.	95.9	4.1	0.0	0.0	37.3	24.2	7.1	44.9	23.8	97.2	90.9	9.0	0.1	49.6
			int.	100.0	0.0	0.0	0.0	25.9	0.0	44.7	55.3	0.0	61.4	100.0	0.0	0.0	19.9
1.N_D_m_20	0.9	avg.	98.2	1.8	0.0	0.0	32.7	9.1	33.4	53.2	4.2	78.0	94.4	5.6	0.0	37.8	
		ext.	92.7	7.3	0.0	0.0	39.5	32.9	7.7	40.7	18.7	96.6	90.1	9.8	0.1	57.4	
		int.	100.0	0.0	0.0	0.0	26.3	0.0	61.8	38.2	0.0	60.8	100.0	0.0	0.0	20.0	
1.E_B_m_20	0.3	avg.	99.9	0.1	0.0	0.0	30.3	1.1	29.0	67.9	1.9	78.4	95.7	4.3	0.0	30.1	
		ext.	97.2	2.8	0.0	0.0	35.3	21.9	8.1	47.2	22.8	96.2	92.4	7.6	0.0	42.1	
		int.	100.0	0.0	0.0	0.0	25.7	0.0	39.9	60.1	0.0	61.6	100.0	0.0	0.0	19.8	
1.E_M_m_20	East	0.6	avg.	98.0	2.0	0.0	0.0	34.5	13.0	33.7	51.7	1.5	77.7	94.9	5.1	0.0	34.1
			ext.	92.9	6.9	0.2	0.0	43.2	36.4	7.8	41.5	14.4	96.1	91.7	8.2	0.1	50.2
			int.	100.0	0.0	0.0	0.0	26.3	0.0	65.0	35.0	0.0	60.7	100.0	0.0	0.0	20.0
1.E_D_m_20	0.9	avg.	94.7	5.3	0.0	0.0	39.1	31.2	32.0	35.8	1.1	76.9	93.6	6.4	0.0	41.0	
		ext.	88.3	10.1	1.6	0.0	51.5	49.7	7.2	34.5	8.6	95.7	90.3	9.3	0.4	64.1	
		int.	100.0	0.0	0.0	0.0	27.0	0.0	100.0	0.0	0.0	59.9	100.0	0.0	0.0	20.3	
1.S_B_m_20	0.3	avg.	99.6	0.4	0.0	0.0	31.5	2.0	32.6	59.1	6.2	78.0	96.1	3.9	0.0	30.0	
		ext.	96.7	3.3	0.0	0.0	37.7	25.6	8.7	43.2	22.5	96.9	92.0	8.0	0.0	41.5	
		int.	100.0	0.0	0.0	0.0	25.7	0.0	43.8	56.2	0.0	61.3	100.0	0.0	0.0	19.6	
1.S_M_m_20	South	0.6	avg.	97.4	2.6	0.0	0.0	34.4	23.7	35.5	37.4	3.4	77.2	94.5	5.5	0.0	33.3
			ext.	91.9	7.8	0.3	0.0	43.2	48.6	6.8	29.7	14.9	96.8	89.9	10.0	0.1	50.7
			int.	100.0	0.0	0.0	0.0	26.3	0.0	89.6	10.4	0.0	60.3	100.0	0.0	0.0	19.7
1.S_D_m_20	0.9	avg.	93.9	6.1	0.0	0.0	38.0	54.6	22.2	21.0	2.1	76.4	92.6	7.4	0.0	41.5	
		ext.	85.8	11.7	2.6	0.0	49.4	67.1	4.6	19.3	9.0	96.6	87.5	12.2	0.3	67.8	
		int.	100.0	0.0	0.0	0.0	27.0	0.0	100.0	0.0	0.0	59.0	100.0	0.0	0.0	19.9	
1.W_B_m_20	0.3	avg.	99.1	0.9	0.0	0.0	32.7	2.4	27.2	64.2	6.2	78.2	95.8	4.2	0.0	31.1	
		ext.	96.2	3.8	0.0	0.0	40.0	22.5	7.1	45.2	25.2	97.0	91.6	8.4	0.0	43.4	
		int.	100.0	0.0	0.0	0.0	26.0	0.0	40.9	59.1	0.0	61.5	100.0	0.0	0.0	20.0	
1.W_M_m_20	West	0.6	avg.	96.7	3.3	0.0	0.0	37.4	17.0	31.2	47.1	4.6	77.5	93.9	6.1	0.0	33.2
			ext.	92.1	6.7	1.2	0.0	48.1	38.5	7.6	37.8	16.2	96.9	89.7	10.2	0.1	47.9
			int.	100.0	0.0	0.0	0.0	26.9	0.0	69.8	30.2	0.0	60.7	100.0	0.0	0.0	20.3
1.W_D_m_20	0.9	avg.	93.8	6.0	0.1	0.0	42.4	36.3	28.7	32.4	2.6	76.8	92.4	7.6	0.0	40.1	
		ext.	88.3	8.5	2.8	0.4	57.2	52.7	6.7	30.2	10.4	96.9	88.6	10.8	0.6	65.5	
		int.	100.0	0.0	0.0	0.0	27.7	0.0	100.0	0.0	0.0	59.7	100.0	0.0	0.0	20.9	

In case of medium moisture load and considering all the three analysed parameters (temperature, relative humidity and vapour pressure), the worst configuration was found to be the 1.W_D_m_20. Consequently, for this configuration also the simulation results obtained with high moisture loads are shown (Table 62).

Table 62: Wall: frequency distribution at the faces of a VIP 10 and 20 mm thick, considering a high moisture load (1% of frequency corresponds to 3.65 days/year of exposure) [93]

Configuration	Orientation	Solar adsorption coefficient	Side	Temperature ranges					Relative Humidity Ranges				Vapour Pressure Ranges				
				I (≤ 30 °C)	II (30÷40 °C)	III (40÷50 °C)	IV (> 50 °C)	MAX	I (≤ 50 %)	II (50÷60 %)	III (60÷70 %)	IV (> 70 %)	MAX	I ($\leq 21,2$ hPa)	II (21,2÷44,3 hPa)	III (44,3÷86 hPa)	MAX
				[%]	[%]	[%]	[%]	[°C]	[%]	[%]	[%]	[%]	[%]	[%]	[%]	[%]	[hPa]
1.W_D_h_20	West	0.9	avg.	93.8	6.0	0.1	0.0	42.4	3.4	50.3	39.3	7.0	82.0	89.3	10.7	0.0	41.5
			ext.	88.3	8.5	2.8	0.4	57.2	52.7	6.7	30.2	10.4	96.9	88.6	10.8	0.6	65.5
			int.	100.0	0.0	0.0	0.0	27.8	0.0	0.0	100.0	0.0	68.5	77.5	22.5	0.0	25.0
1.W_D_h_10	West	0.9	avg.	93.5	6.2	0.3	0.0	43.2	0.6	51.2	38.1	10.1	83.1	88.2	11.8	0.0	42.6
			ext.	88.4	8.5	2.6	0.4	56.6	53.0	6.9	30.1	10.0	96.8	88.7	10.8	0.5	64.5
			int.	100.0	0.0	0.0	0.0	30.0	0.0	0.0	43.5	56.5	71.1	73.9	26.1	0.0	29.1

The effect was a global increase in relative humidity, especially on the internal surface (7.0 % of time, equal to about 25.5 days in range (IV), instead of 22 days) and in the middle of the VIP (100 % of time in range (III), instead of never), with relative humidity peaks of 82 % and 68.5 % respectively. The vapour pressure is characterised by a similar trend, in particular on the internal side of VIP, where the range (II) was reached in 22.5 % of the time (about 82 days) with an increase of the peak value from 20.9 hPa to 25.0 hPa.

10.1.2 Pitched Roof – wood frame in Torino

The second analysed configuration was a pitched roof (wood framed with clay tiles), always located in Torino. This building component represents an Italian traditional roof structure. The supposed energy retrofit was obtained by using both VIPs and XPS panels placed on the indoor side of the attic, covered by an internal gypsum board finishing layer (Figure 112).

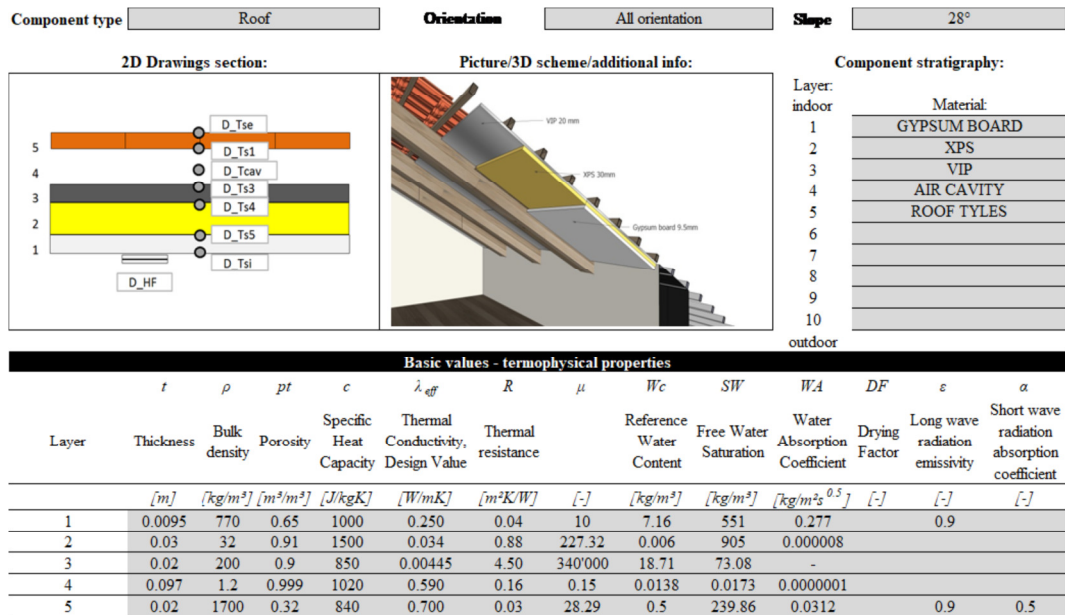


Figure 112: Data-sheet of the analysed roof [93]

The outdoor and indoor climate conditions are the same assumed for the simulations of the roof.

Simulation were performed on different roof design alternatives, considering the same parameters already presented for the wall case (four orientations and three different external finishing colour), a medium moisture load and a VIPs thickness of 20 mm. The resulting combinations are summarised in **Table 63**.

Again, only the results related to the worst design alternative combinations are discussed in detail: south dark pitched roof, with medium internal moisture load, and VIP thickness equal to 20 mm (2. S_D_m_20).

Table 63: Summary of the different roof configurations [93]

Name	Orientation	Solar absorption coefficient - α	Moisture load	t
2. N_B_m_20	NORTH	Bright	medium ($\leq 60\%$)	20 mm
2. N_M_m_20		Medium		
2. N_D_m_20		Dark		
2. E_B_m_20	EAST	Bright		
2. E_M_m_20		Medium		
2. E_D_m_20		Dark		
2. S_B_m_20	SOUTH	Bright		
2. S_M_m_20		Medium		
2. S_D_m_20		Dark		
2. W_B_m_20	WEST	Bright		
2. W_M_m_20		Medium		
2. W_D_m_20		Dark		

The time profiles of the temperature ϑ , relative humidity RH and water vapour pressure p_v are plotted from **Figure 113** to **Figure 115**, while their cumulative frequency distributions are shown in **Figure 116**, **Figure 117** and **Figure 118**, respectively.

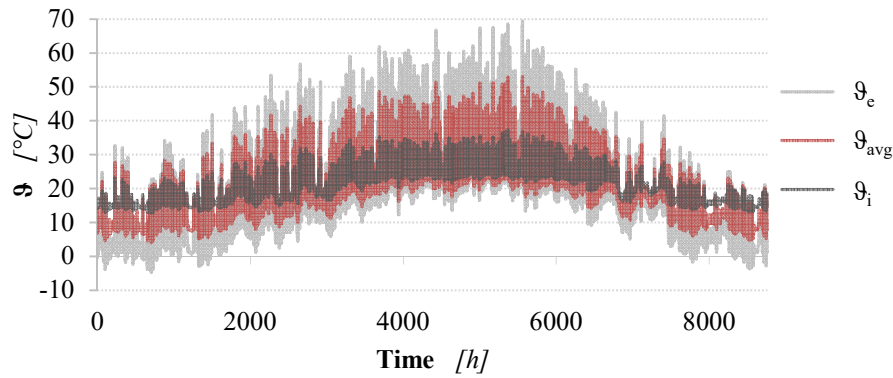


Figure 113: Temperatures yearly time profiles (2.S_D_m_20) [93]

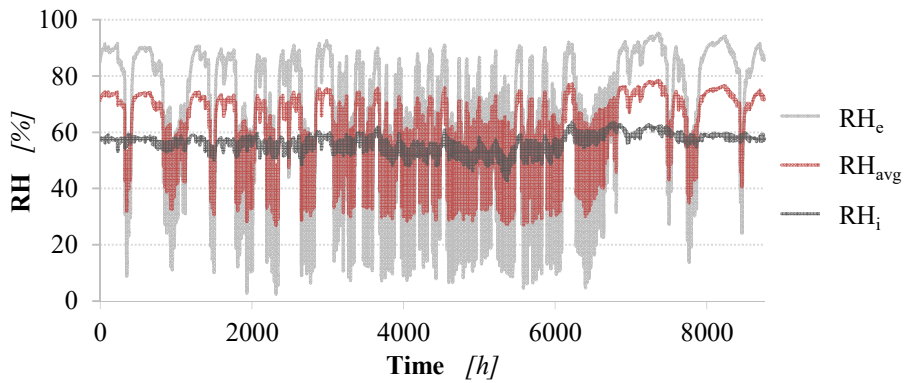


Figure 114: Relative humidities yearly time profiles (2.S_D_m_20) [93]

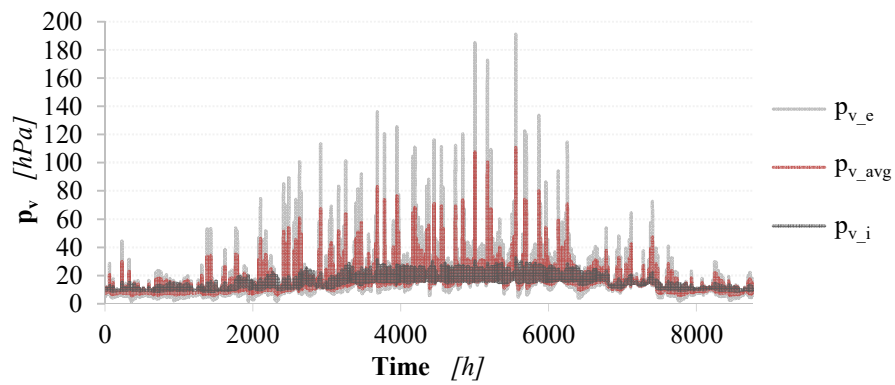


Figure 115: Vapour pressure yearly time profiles (2.S_D_m_20) [93]

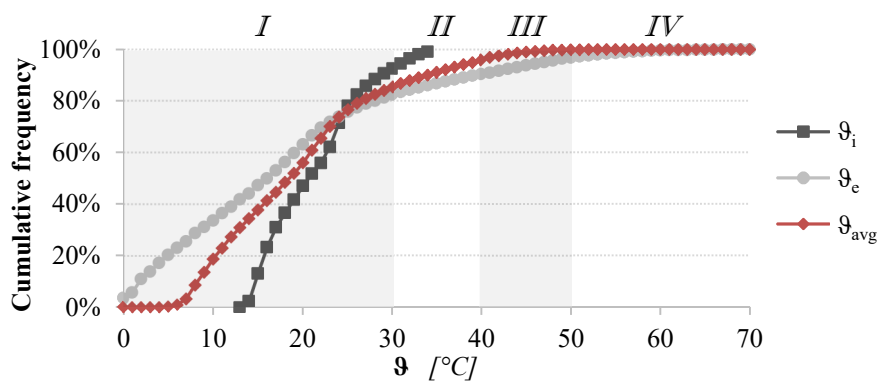


Figure 116: Temperature cumulative frequency (2.S_D_m_20) [93]

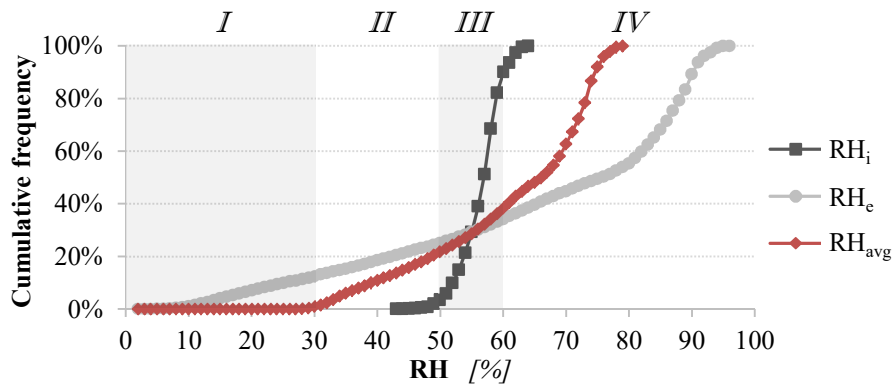


Figure 117: Relative humidity cumulative frequency (2.S_D_m_20) [93]

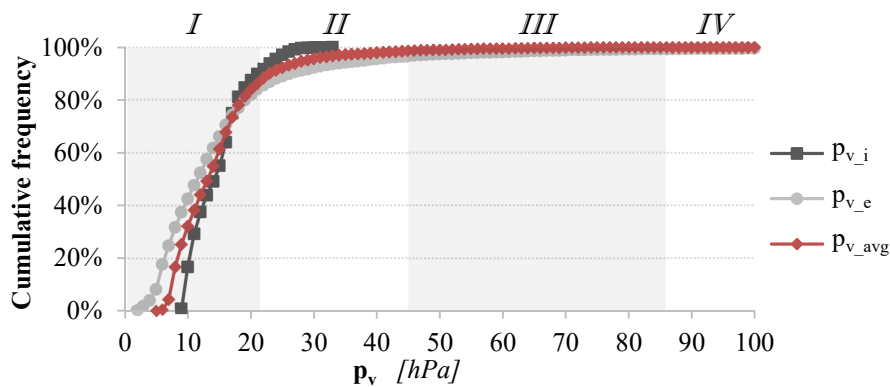


Figure 118: Vapour pressure cumulative frequency (2.S_D_m_20) [93]

The results related to the overall design alternatives are summarised in **Table 64**.

As it is possible to observe from **Table 64**, more than half of the design alternatives lies in the temperature ranges (*I*) and (*II*). The field (*III*) is reached by about the 45% of them while range (*IV*) by more than 30%, in particular:

- 2. W_D_m_20 (west exposure and dark surface finishing) on the VIP external surface, where range (*IV*) was reached for about 2.0% of the time (≈ 7 days/year, $\vartheta_{MAX} = 62.6^\circ\text{C}$);
- 2. E_D_m_20 (east exposure and dark surface finishing) on the VIP external surface, where temperatures higher than 50°C were observed for about 3.0% of the time (≈ 11 days, $\vartheta_{MAX} = 65.0^\circ\text{C}$);

- 2. S_D_m_20 (south exposure and dark surface finishing) on the VIP external surface, where the temperatures were within range (IV) for about the 3.2% of the time (≈ 12 days, $\vartheta_{MAX} = 69.2^\circ\text{C}$).

The analysis of the relative humidity shows that almost all the configurations lie in range (III), and the 67% of them very often reach range (IV). As for the wall configuration, the cases with bright and medium finishing colours are the most critical:

- 2. N_M_m_20 (north exposure and medium surface finishing) on the VIP external surface, frequency $\approx 71.1\%$ of time, corresponding to about 259 days ($RH_{MAX} = 95.6\%$);
- 2. S_B_m_20 (south exposure and bright surface finishing) on the VIP external surface, frequency $\approx 76.8\%$ corresponding to about 280 days ($RH_{MAX} = 95.7\%$);
- 2. E_B_m_20 (east exposure and bright surface finishing) on the VIP external surface, frequency $\approx 77.9\%$ corresponding to about 284 days ($RH_{MAX} = 95.7\%$);
- 2. W_B_m_20 (west exposure and bright surface finishing) on the VIP external surface, frequency $\approx 80.9\%$ corresponding to about 295 days ($RH_{MAX} = 95.7\%$);
- 2. N_B_m_20 (north exposure and bright surface finishing) on the VIP external surface, frequency $\approx 83.3\%$ corresponding to about 304 days ($RH_{MAX} = 95.8\%$).

Few design alternatives reach the vapour pressure range (IV). These are the same design alternatives that lie in the temperature range (IV). In particular, the cases with vapour pressure higher than 86 hPa are:

- 2. E_D_m_20 (east exposure and dark surface finishing) on the VIP external surface, frequency $\approx 0.3\%$ equal to about 1 day ($p_{v\ MAX} = 151.7$ hPa);
- 2. W_D_m_20 (west exposure and dark surface finishing) on the VIP external surface, frequency $\approx 0.3\%$ equal to about 1 day ($p_{v\ MAX} = 151.8$ hPa);
- 2. S_D_m_20 (south exposure and dark surface finishing) on the VIP external surface, frequency $\approx 0.3\%$ equal to about 1 day ($p_{v\ MAX} = 191.0$ hPa).

Table 64: Roof: frequency distribution at the faces of a VIP 20 mm thick, considering a medium moisture load (1% of frequency corresponds to 3.65 days/year of exposure) [93]

Configuration	Orientation	Solar adsorption coefficient	Side	Temperature ranges					Relative Humidity Ranges				Vapour Pressure Ranges					
				I (≤ 30 °C)	II (30-40 °C)	III (40-50 °C)	IV (> 50 °C)	MAX	I (≤ 50 %)	II (50-60 %)	III (60-70 %)	IV (> 70 %)	MAX	I ($\leq 21,2$ hPa)	II (21,2-44,3 hPa)	III (44,3-86 hPa)	IV (≥ 86 hPa)	MAX
				[%]	[%]	[%]	[%]	[°C]	[%]	[%]	[%]	[%]	[%]	[%]	[%]	[%]	[%]	[%]
2.N_B_m_20	0.3	ext.	97.0	3.0	0.0	0.0	36.2	6.0	4.7	6.0	83.3	95.8	85.5	14.3	0.2	0.0	49.4	
		int.	100.0	0.0	0.0	0.0	28.2	0.0	10.4	89.6	0.0	67.7	98.0	2.0	0.0	0.0	22.3	
		avg.	98.5	1.5	0.0	0.0	32.2	3.0	7.5	47.8	41.7	81.7	89.7	10.3	0.0	0.0	35.6	
2.N_M_m_20	North	0.6	ext.	89.6	8.6	1.8	0.0	45.7	13.4	6.4	9.0	71.1	95.6	85.0	13.2	1.7	0.0	78.4
			int.	99.4	0.6	0.0	0.0	30.9	0.0	42.7	57.3	0.0	66.3	93.5	6.5	0.0	0.0	25.2
			avg.	94.5	4.6	0.9	0.0	38.3	6.7	24.6	33.2	35.6	81.0	88.9	10.9	0.3	0.0	51.8
2.N_D_m_20	0.9	ext.	85.0	8.4	5.5	1.2	55.7	18.9	7.3	9.9	63.9	95.4	84.7	12.6	2.4	0.2	113.0	
		int.	94.8	5.2	0.0	0.0	34.1	1.5	68.9	29.6	0.0	64.7	91.4	8.6	0.0	0.0	27.9	
		avg.	89.9	6.8	2.7	0.6	44.9	10.2	38.1	19.8	32.0	80.1	87.7	11.3	1.0	0.0	69.4	
2.E_B_m_20	0.3	ext.	95.5	4.5	0.0	0.0	37.6	8.3	5.4	8.4	77.9	95.7	85.3	14.2	0.4	0.0	55.5	
		int.	100.0	0.0	0.0	0.0	28.7	0.0	18.2	81.8	0.0	66.5	97.2	2.8	0.0	0.0	22.8	
		avg.	97.7	2.3	0.0	0.0	33.1	4.1	11.8	45.1	39.0	81.1	89.3	10.7	0.0	0.0	39.0	
2.E_M_m_20	East	0.6	ext.	88.5	8.1	3.3	0.1	51.3	16.1	7.8	9.3	66.8	95.6	85.0	12.7	2.2	0.1	99.9
			int.	98.1	1.9	0.0	0.0	32.6	0.0	60.3	39.7	0.0	65.3	92.9	7.1	0.0	0.0	26.5
			avg.	93.3	5.0	1.7	0.0	41.9	8.1	34.0	24.5	33.4	80.4	88.5	10.8	0.6	0.0	62.4
2.E_D_m_20	0.9	ext.	83.7	8.0	5.3	3.0	65.0	22.9	8.6	9.9	58.6	95.4	84.9	11.8	2.6	0.3	151.7	
		int.	93.4	6.6	0.0	0.0	36.7	3.1	81.6	15.3	0.0	64.2	90.8	9.2	0.0	0.0	30.0	
		avg.	88.5	7.3	2.6	1.5	50.8	13.0	45.1	12.6	29.3	79.8	87.5	11.2	1.3	0.0	90.0	
2.S_B_m_20	0.3	ext.	94.7	5.3	0.0	0.0	40.3	9.0	5.4	8.8	76.8	95.7	85.5	14.1	0.4	0.0	54.6	
		int.	100.0	0.0	0.0	0.0	29.3	0.0	22.4	77.6	0.0	66.5	96.1	3.9	0.0	0.0	22.9	
		avg.	97.4	2.6	0.0	0.0	34.8	4.5	13.9	43.2	38.4	81.1	89.5	10.5	0.0	0.0	38.6	
2.S_M_m_20	South	0.6	ext.	87.2	8.8	3.8	0.2	54.9	17.3	8.3	10.5	63.9	95.4	84.4	13.1	2.4	0.0	116.7
			int.	97.8	2.2	0.0	0.0	33.4	0.1	70.8	29.1	0.0	64.7	92.2	7.8	0.0	0.0	27.3
			avg.	92.5	5.5	1.9	0.1	44.2	8.7	39.6	19.8	31.9	80.1	87.9	11.3	0.7	0.0	72.0
2.S_D_m_20	0.9	ext.	82.4	8.0	6.4	3.2	69.2	25.1	9.1	10.6	55.3	95.2	84.2	12.2	2.8	0.3	191.0	
		int.	92.6	7.4	0.0	0.0	37.3	3.5	86.6	9.9	0.0	63.6	90.1	9.9	0.0	0.0	32.7	
		avg.	87.5	7.7	3.2	1.6	53.2	14.3	47.8	10.2	27.6	79.4	86.7	11.8	1.4	0.0	110.6	
2.W_B_m_20	0.3	ext.	95.3	4.7	0.0	0.0	39.1	6.9	4.5	7.7	80.9	95.7	85.4	14.1	0.5	0.0	54.4	
		int.	100.0	0.0	0.0	0.0	29.0	0.0	14.7	85.3	0.0	67.0	96.6	3.4	0.0	0.0	23.1	
		avg.	97.7	2.3	0.0	0.0	34.1	3.5	9.6	46.5	40.4	81.4	89.5	10.5	0.0	0.0	38.5	
2.W_M_m_20	West	0.6	ext.	88.7	8.3	3.0	0.0	50.9	14.4	7.1	9.5	69.1	95.5	84.7	13.1	2.2	0.0	85.5
			int.	98.6	1.4	0.0	0.0	32.5	0.0	56.9	43.1	0.0	64.9	92.8	7.2	0.0	0.0	25.6
			avg.	93.6	4.8	1.5	0.0	41.7	7.2	32.0	26.3	34.5	80.2	88.3	11.3	0.4	0.0	55.3
2.W_D_m_20	0.9	ext.	83.8	8.2	5.9	2.0	62.6	21.3	8.6	10.6	59.4	95.3	84.3	12.5	2.7	0.3	151.8	
		int.	93.8	6.2	0.0	0.0	35.8	2.2	81.7	16.1	0.0	64.0	90.6	9.4	0.0	0.0	29.1	
		avg.	88.8	7.2	2.9	1.0	49.2	11.8	45.1	13.4	29.7	79.6	87.3	11.3	1.3	0.0	90.4	

10.2 Life expectancy

The time profiles of ϑ , RH and p_v obtained in the previous sections provide an indication about the severity of the VIPs working conditions during their use: for this reason, they represent a basis for the evaluation of the expected service life of the analysed product.

The service life is defined as the time required by a VIP thermal conductivity to rise over a predefined limit ($\lambda_{lim,sl}$), which no longer ensures the design insulating level. Usually, the VIP typical value of $\lambda_{lim,sl}$ is assumed to be equal to 0.008 W/mK [161]. Air and water vapour permeation through the VIP envelope is the most effective ageing phenomena that causes the decreasing of the panel core thermal conductivity (λ_{core}), as clearly described in [42], [82] and [162]. Therefore, the VIP service life can be estimated considering this two degradation processes.

Nowadays there are several methods for the service life evaluation (as explained in [67]). In this research, the following example of service life calculation was performed applying a generally accepted method [82] which considers both the moisture impact and the dry air impact. Therefore, an estimate of the expected service life (τ_i) of the roof configuration (investigated in the previous section) was obtained, adopting the dynamic model proposed and described in [163]. **Figure 119** schematically shows the followed procedure.

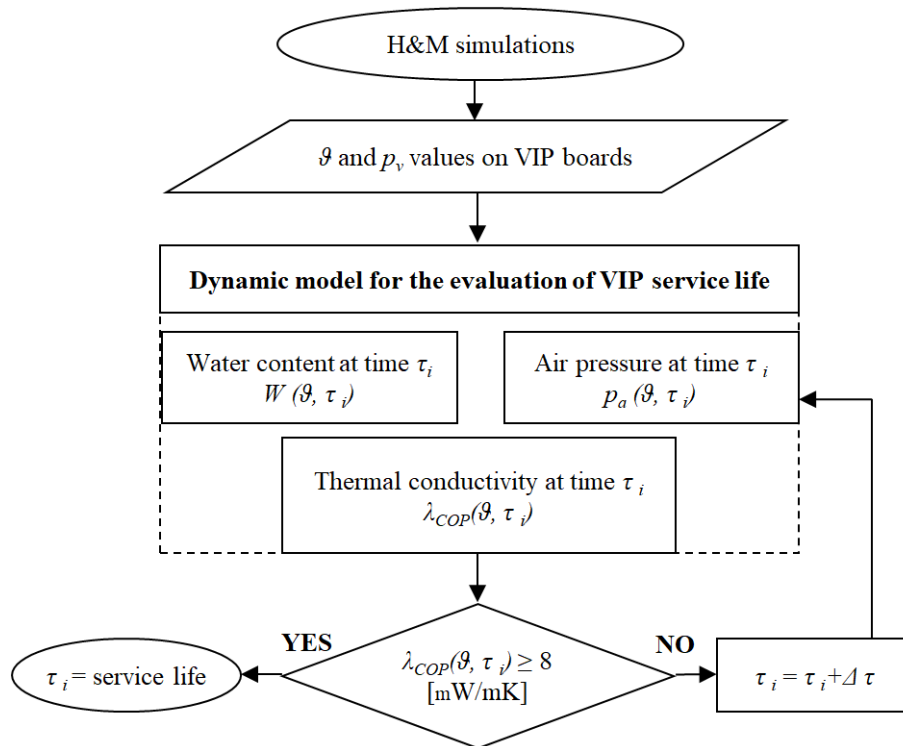


Figure 119: Procedure for estimating the VIPs service life [93]

The calculation of the expected VIP service life was performed considering all the previously analysed roof configurations (medium and high moisture load). Detailed results about the worst configurations regarding air and water permeation inside the VIP are then presented. The analysis was carried out considering a VIP panel having a size of 500 x 600 mm (assuming density = 200 kg/m³ and porosity = 90%), and the calculations were repeated for two different thicknesses (20 mm and 10 mm). Moreover, four VIP envelope structures (MF1, MF2, MF3 and MF4), were considered, which differ in the surface Air Transmission Rate (ATR) and Water Transmission Rate (WTR).

Table 65 provides the overall results of the service life analyses (medium moisture load). As it is possible to see, in case of MF1 and MF3 envelopes the service life of VIPs is very low (always lower than 14 and 21 years, respectively). On the contrary, the service life of VIPs with MF2 or MF4 reach about 40 years. In general, the optimal solution foresees the VIPs inserted within a south inclined roof having tiles with a shortwave absorption coefficient equal to 0.9.

Table 65: Service life of the different roof configurations, considering a medium moisture load

Name	Orientation	α	$t_{VIP} = 20 \text{ mm}$				$t_{VIP} = 10 \text{ mm}$
			MF1 [years]	MF2 [years]	MF3 [years]	MF4 [years]	MF4 [years]
2. N_B_m_		0.3	12.9	38.9	20.4	40.7	20.3
2. N_M_m_	NORTH	0.6	13.1	38.9	20.2	41.2	20.5
2. N_D_m_		0.9	13.2	39.0	20.0	42.0	21.1
2. E_B_m_		0.3	13.0	38.9	20.4	40.8	20.2
2. E_M_m_	EAST	0.6	13.1	38.8	20.1	41.3	20.6
2. E_D_m_		0.9	13.3	39.0	19.9	42.1	21.3
2. S_B_m_		0.3	13.0	39.0	20.4	40.9	20.3
2. S_M_m_	SOUTH	0.6	13.1	38.8	20.0	41.3	20.7
2. S_D_m_		0.9	13.3	39.0	19.9	42.5	21.4
2. W_B_m_		0.3	12.9	38.9	20.4	40.7	20.2
2. W_M_m_	WEST	0.6	13.1	38.8	20.1	41.2	20.6
2. W_D_m_		0.9	13.2	39.0	19.9	42.1	21.2

From the performed simulations, it could be observed that as the temperature increases (higher α values), there is a decrease in the RH and an increase in the vapour pressure at the edges of the panel. In this case, the durability is improved, due to the lower air and water permeation rates through the panel envelope. Therefore, for what concerns the temperature values, the worst roof condition was the south exposition with $\alpha = 0.3$.

The service life of 10 mm thick panels was determined considering only the MF4 envelope, both because this is the type with a wider diffusion on the market and because they allow a greater durability of the panel. Results show that the service life is reduced by about half, compared to the 20 mm thickness: this leads to not recommend the use of such small thicknesses in building applications.

In **Figure 120** the results of time evolutions of VIP core thermal conductivity are plotted for different metallised envelope films (20 mm thick VIP, south bright roof, medium internal moisture load). **Figure 121** shows the comparison between the evolution of the λ_{core} over the time in case of 10 and 20 mm tick VIP (MF4 envelope configuration).

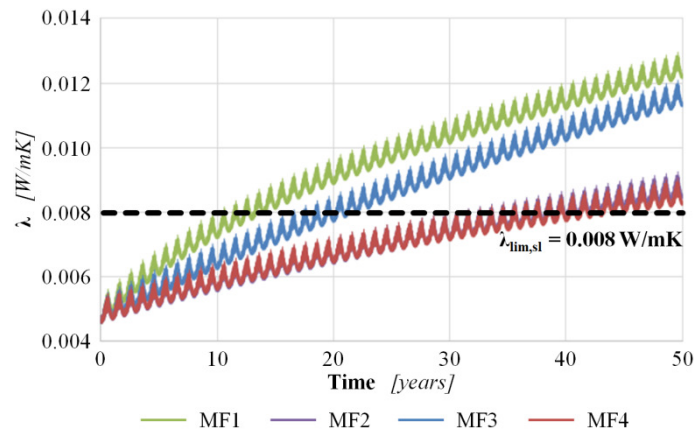


Figure 120: Time evolution of λ_{core} as a function of the envelope typology (20 mm thick VIP, south bright roof, medium internal moisture load)

The “zig-zag” trend of the VIP core thermal conductivity is due to the variability of the VIP internal water content, air pressure and average temperature: each year during summer the thermal conductivity is higher than in winter season.

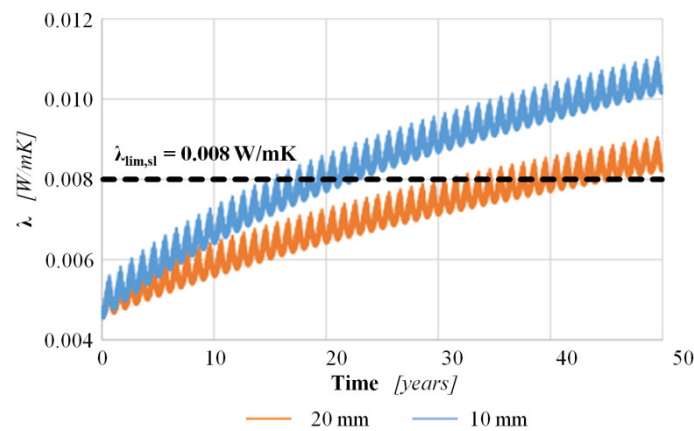


Figure 121: Time evolution of λ_{core} as a function of the panel thickness (10 and 20 mm thick VIP, south bright roof, medium internal moisture load, MF4 envelope)

From **Figure 121** it is possible to observe that, after 50 years, the two core thermal conductivities differ for about 0.002 W/mK.

The results obtained so far refer to the case of an environment with a medium internal moisture load. The same simulations were performed considering a high moisture load, but only in the case of the north-oriented roof. The service life was found to be equal to 37.5, 37.8 and 38.6 years, for bright, medium and dark

finishing colours respectively. These values do not differ significantly from those obtained in the case of medium internal moisture load: a high amount of indoor humidity has no significant effect on the deterioration of the VIP. However, in the case of a high interior relative humidity, problems of interstitial condensation could occur, which would damage the materials composing the structure.

Since the main causes of VIPs ageing are the air and water permeation through the VIPs envelope, which leads to a reduction in the vacuum degree, it is interesting to plot the evolution of the air pressure and the water content inside the panel over time (see **Figure 122** and **Figure 123** for the air pressure, and **Figure 124** and **Figure 125** for the water content, south-oriented roof, $\alpha = 0.3$ and medium moisture load).

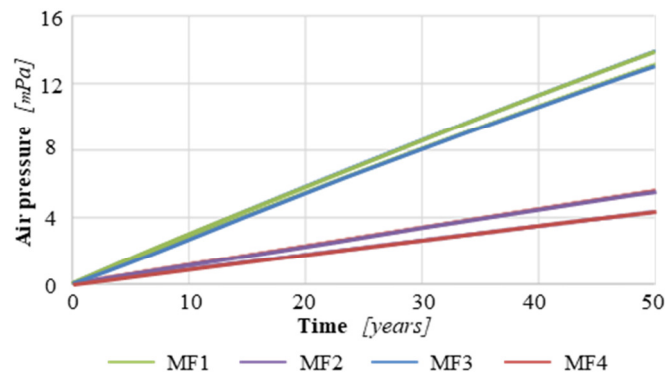


Figure 122: VIP internal air pressure trend over time as a function of the envelope typology (20 mm thick VIP, south bright roof, medium internal moisture load)

The increase in air pressure over time is undoubtedly the cause that leads to a reduction in the thermal properties of the material, especially in the case of MF1 and MF3 envelopes. In fact, the air pressure inside these panels exceeds 12000 Pa within 50 years of use. Vice versa, in the case of an MF4 envelope, this parameter does not reach 5000 Pascal at the same time. In general, the panels with MF2 and MF4 envelopes have very similar behaviours in term of internal air pressure evolution during the time (**Figure 122**).

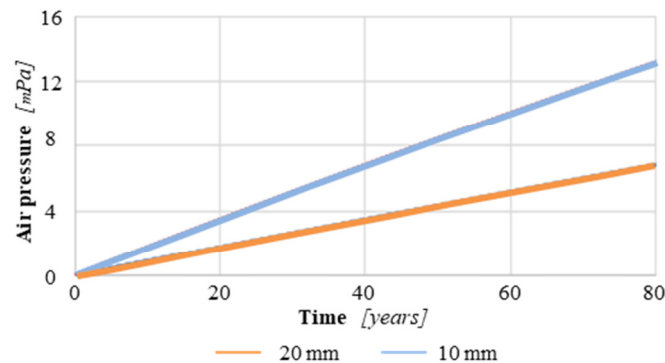


Figure 123: VIP internal air pressure trend over time as a function of the panel thickness (10 and 20 mm thick VIP, south bright roof, medium internal moisture load, MF4 envelope)

Comparing panels with a thickness of 20 and 10 mm, it is possible to notice how, over time, the different trends of the residual air pressure inside the panels lead to a considerable difference in the service life. In fact, the air pressure inside the VIP 10 mm thick is about double compared to a thickness of 20 mm, while its durability turns out to be almost half. After about 40 years, the air pressure inside a 20 mm VIP is about 3500 Pa, twice as much in the case of half-thickness VIP. (Figure 123).

The content of water inside a VIP affects its durability because it causes a variation in its thermal conductivity. When it is placed inside a building component (pristine panel), the percentage of water content is almost zero. It increases as water vapour permeability through the panel and the vapour pressure registered in the VIP interfaces increase. Figure 124 shows the water content trend during the VIP service life (north-oriented roof, $\alpha = 0.3$ and different types of envelopes).

From Figure 124 it can be observed that the MF4 envelope is not the most performing envelope structure in the case of water vapour permeation. In fact, it shows the highest rate of water content inside the panel (slightly exceeding the 4% after 50 years), with the exception of the MF1 envelope typology, whose panel reaches a percentage of water content close to 5% after the same time. In general, the MF2 envelope has the lowest water vapour permeability.

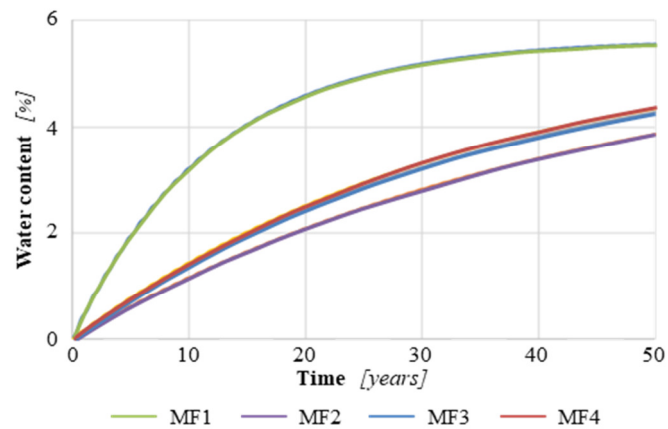


Figure 124: VIP internal water content trend over time as a function of the envelope typology (20 mm thick VIP, south bright roof, medium internal moisture load)

Reducing the thickness of the VIP from 20 mm to 10 mm, an increase in the water content inside the panel was observed during its service life. **Figure 125** shows that, after 20 years, a 10 mm thick panel has a water content of 4%, a value that a 20 mm VIP only reaches after 40 years.

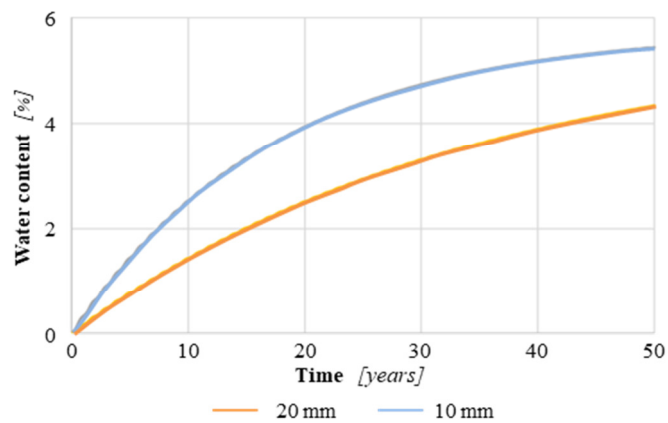


Figure 125: VIP internal water content trend over time as a function of the panel thickness (10 and 20 mm thick VIP, south bright roof, medium internal moisture load, MF4 envelope)

Chapter 11

Conclusions

The aim of the present research was a comprehensive characterization of Super Insulating Materials for building applications, from the material/panel scale (laboratory assessment of their thermal properties) to the building scale (dynamic hygrothermal simulations). Particular attention was focused on the Vacuum Insulation Panels, as the more critical material among the SIMs.

The current experimental apparatus for the evaluation of the thermal properties of insulating materials (in particular the analysed Heat Flow Meter (HFM) and Guarded Hot Plate (GHP) devices) were developed for the characterization of the so defined traditional insulating materials (with thermal conductivity values up to an order of magnitude higher than SIMs). Therefore, the first investigated aspect was the applicability of the current standards and measurement devices to SIMs. This was achieved through two different approaches: a theoretical standard based uncertainty analysis and the experimental assessment and validation of the measurement uncertainty. The experimental uncertainty assessment was also performed on the VIPs assemblies, measured by means of the HFM and GHP apparatuses.

After that, an in-depth analysis of the thermal properties of SIMs was carried out, to define the short term and long term (in case of VIPs) thermal behaviour of SIMs and VIPs insulated building components, consequently estimating the potentialities of VIPs (also economic) and their service life.

11.1 Theoretical standard-based measurement uncertainties

The current standards related to the thermal conductivity measurements, contains the information required for a Type B uncertainty assessment (such as maximum probable relative errors and apparatus limitations).

To achieve general conclusions about the applicability of these standards for the characterisation of SIMs, a theoretical study was performed in case of HFM apparatus (EN 1946-3:1999 [148]), considering a thermal conductivity range of the sample from 0.020 W/mK (Advanced Porous Materials) down to 0.002 W/mK (Fibre Glass based VIPs). A similar investigation was performed by the FIW institute on the GHP approach (EN 1946-2:1999 [149]), with few contributions from the author. Anyway, the main conclusions related to the GHP measurement are essential to provide a comparison of the HFM results (the GHP is an absolute method, and therefore more accurate).

The applicability of the current standard related to the of GHP method was verified and demonstrate, but with some general conclusive recommendations [150]:

- the combined relative uncertainty is inversely proportional to the temperature difference, and therefore a $\Delta\vartheta_{min} > 10$ K is required (as a recommendation the $\Delta\vartheta$ value should be increased to 15 K);
- the metering area of the apparatus should be chosen in function of the thickness of the sample: the lower the thickness, the smaller the apparatus metering area. This is explained by the increase of relative uncertainty in case of small thickness and large metering areas. The following recommendations can be suggested:
 - for thicknesses $t < 20$ mm \rightarrow metering area of around 150^2 mm²;
 - for thicknesses $20 < t < 40$ mm \rightarrow metering area of around 250^2 mm²;
 - for thicknesses $t > 40$ mm \rightarrow metering area of around 500^2 mm²;
- the GHP method allows achieving a theoretical combined relative standard uncertainty of the thermal conductivity equal to about 1.0 – 1.7 % when the right equipment is used.

On the contrary, the standards related to the HFM approach were found to have some critical aspects, that would require a revision of the reported criteria. The following general recommendations can be concluded:

- the thermal conductivity measurement uncertainty is often higher than the expected value proposed by the standard EN 12667:2001 [12], that is equal to 3%;
- the higher the temperature difference is, the lower the combined relative uncertainty is. For this reason, a minimum temperature difference of 15 K is required, in order to obtain $u_c(\lambda) < 3\%$ for all the three apparatuses proposed by the standard. As a recommendation the temperature difference should be increased to 20 K, to reach the same uncertainty limit for GHP equal to 2%;
- the higher the thickness of the specimen, the lower the combined uncertainty. Therefore, single-specimen symmetrical configuration, with higher maximum available thickness are suggested;
- the different typology of equipment used, strongly influence the obtainable uncertainty level: single-specimen symmetrical configuration, with higher maximum available thickness represent the best solution;
- using the HFM method, for theoretical reasons a combined relative standard uncertainty of thermal conductivity lower than 2.0% can be achieved when the right equipment is used, except for thick specimens (more than 40 mm) with thermal conductivity lower than 0.004 W/mK: in this case, a $\Delta\vartheta_{min} > 20$ K is required.

Moreover, it's important to highlight that the so defined uncertainties are represented by theoretical values (obtained considering the minimum uncertainty of the heat flux measurement). During real measurements, the combined uncertainty values could be higher, and therefore higher temperature differences could be required.

11.2 Experimental assessment of the measurement uncertainties

The experimental evaluation of the SIMs measurement uncertainty was the key point of this research. The assessment of a Type A measurement uncertainty is essential for the definition of the reliability, accuracy and precision degree of the laboratory (even if not recommended for a direct comparison with different measurement campaigns). The thermal conductivity is the most important property of all the insulating materials, but in case of VIPs, when they are coupled together, the overall performances of a VIP assembly is strongly affected by the thermal bridging effects. These effects can be evaluated by means of the GHP and HFM methods, but how the so obtained results are reliable (in term of measurement uncertainty) was until now unknown.

To define the obtainable measurement uncertainties when SIMs are tested by means of GHP and HFM devices, three different experimental campaigns were performed, under different boundary conditions (average testing temperatures):

- HFM-1 Type A uncertainty investigation on VIPs (λ_{COP});
- GHP-1 Type A uncertainty investigation on one aerogel blanket (λ);
- GHP-2 and 3 + HFM-2 Type B uncertainty investigation on VIPs assemblies (λ_{eq} , ψ), performed in collaboration with the FIW institute.

In the case of HFM-1 Type A uncertainty investigation on VIPs, the correlation between the λ_{COP} values and the average testing temperature was further demonstrated. The obtained uncertainty values lie between 0.00005 W/mK (sample 20 mm thick) and 0.00009 W/mK (for the other thicknesses, 10 and 30 mm), which corresponds to a range of relative uncertainty between 1.4 and 1.5% (significantly lower than the limit value proposed by the standard EN 12667:2001 [12], equal to 3%).

Indeed, the panel with lower $u_c(\lambda_{COP})$ was the 20mm thick, which was the only pristine panel. The reduced variability of the measurement results, and consequently of the related uncertainty was probably due to the lower internal air and moisture content and the better homogeneity of the material.

With Type A analysis, the effects of $\Delta\theta$ on the variability of the measurement uncertainty seems to be lost. Anyway, it was observed that the temperature difference affects the COP thermal conductivity: increasing the value of $\Delta\theta$, the λ_{COP} increases or decreases, depending on the average testing temperature, and on the variation of the sensitivity coefficient $\partial\lambda_{COP}/\partial f_{cal}$ with the temperature (they

represent by far the most influencing factors). As a consequence, with higher temperature differences between the measuring plates, the λ_{COP} temperature dependency became weaker, reducing the difference between the measurements at different average temperatures.

Also the Type A uncertainty budget, related to the GHP-1 apparatus confirms the temperature dependency of the aerogel thermal conductivity for all the considered temperature differences (λ increases with the increase of the ϑ_{avg}). But λ -values were found to be also correlated to the temperature differences $\Delta\vartheta$: with higher temperature differences between the measuring plates, the heat flux through the sample will increase, and therefore the measurement uncertainty should be reduced. Consequently, increasing the $\Delta\vartheta$, the thermal conductivity values should stabilise. But in practice exactly the opposite happened. The assessed absolute uncertainties were always equal to 0.2 W/mK ($\approx 1.20\%$ of relative uncertainty), except in the case of the maximum value of $\Delta\vartheta$ ($= 15^\circ\text{C}$). In this case, the uncertainties had the value of 0.3 W/mK $\approx 1.70\%$. Consequently, it is once again possible to mark that in the case of a Type A uncertainty assessment, the statistical analysis of repeated measurements generally compensates the effect of the $\Delta\vartheta$ variation on the final uncertainty value.

For the uncertainty analysis of the thermal bridging effects, a Type B evaluation was performed. The VIP centre of panel performances were assessed by means of the GHP-2 and GHP-3 apparatuses, while the several λ_{eq} and ψ were evaluated with both GHP-2 and HFM-2.

The so obtained $u_c(\lambda_{COP})$ were in line with the uncertainty limit defined by the standard EN 12667:2001 [12], equal to 2%. Moreover, the FG panels were generally characterised by a lower uncertainty than the FS based VIPs. This can be explained because in case of VIPs with FG core, almost all the uncertainties contributions were lower (the uncertainty of the measuring area was about one half, the thickness was measured in height different points instead of four, , and the uncertainty of $\Delta\vartheta_m$ was lower).

Since they represent the most influencing factors on the overall $u_c(\lambda_{COP})$ were t_m and A_m because they were defined with less precision (t_m is particularly significant in the case of thin panels). Also the electric current I strongly affects the COP thermal conductivity uncertainty (the evaluation of $u_c(I)$ required a lot of assumptions and data from the device's datasheet).

After the COP measurements, the assembly with Commutated joint (panels joined without any joint material and sealed with an adhesive tape) was characterised. Even if a direct comparison between the results is not possible (the assemblies although similar are all different one from the other), it was clear that FG VIPs are extremely more sensitive to the effects of thermal bridges (as they are more performing) than FS VIPs. The λ_{COP} values were about 9% lower than λ_{eq} in case of FS based panels, while for VIPs with FG core this reduction was around 70%. Consequently, also the ψ values were higher, and they strongly depend also on the sample thickness (the thinner is the sample, the higher is the ψ).

The absolute uncertainties were for both the core materials between 0.00008 and 0.00010 W/mK in case of $u_c(\lambda_{eq})$, and between 0.001 and 0.002 W/mK considering the $u_c(\psi)$. But considering the relative uncertainty, the situation completely changed, in particular for $u_c(\psi)$. In case of FS based VIPs, the absolute uncertainty value equates to more than 20% of relative uncertainty, with about the 2% observed for the FG VIPs. This is due to the lower extra heat flux through the joint in the case of FS VIPs assemblies (which also depends on the assembly thickness), and consequently the lower difference between λ_{COP} and λ_{eq} . The thicker is the assembly, the lower is the difference between λ_{COP} and λ_{eq} and the higher is the influence of the measured electric current on the overall $u_c(\lambda_{eq})$.

The strong correlation with the thickness was also pointed out by the uncertainties main influencing factors, which were, almost always, the thicknesses of both the single panel and the VIPs assemblies.

Moreover, the combined uncertainties of both λ_{eq} and ψ were slightly reduced with higher average temperatures.

The HFM-3 apparatus was then used to perform the complete analysis of the three different assembly typologies (Commutated, Offset and Gasket strip), considering both the FS and the FG based VIPs.

As expected, the obtained uncertainties were sensibly worse than the values obtained with GHP measurements: . Considering the absolute $u_c(\lambda_{eq})$ values, the HFM values were approximatively an order of magnitude higher than for the GHP results, while the relative uncertainties were about the double.

The results related to the ψ evaluation were even worse. Even if the rising of the relative $u_c(\psi)$ in case of FG based VIPs was similar to the one observed for the

$u_c(\lambda_{eq})$, in case of FS core the $u_c(\psi)$ went up to 50% and about 67% for assemblies with thickness equal to 20mm and 40 mm respectively. Indeed, the strong correlation with the thickness was again observed, and also in terms of the uncertainties most influencing factors.

Also in this case, the increasing of the average testing temperatures contributes to a slight reduction of the combined uncertainties of the λ_{eq} (but not of the ψ).

The tests on the Offset joints revealed almost the same performances as the Commutated joint, while for the Gasket strip joint the λ_{eq} values slightly increased. As a consequence, since the absolute uncertainty values were in line with those of the Commutated joints, in case of Gasket strip joints the relative uncertainties were reduced (in particular for the assemblies of FS based VIPs).

Moreover, the uncertainties increased for thicker FG based samples or for thinner FS based assemblies, and for lower average testing temperatures, and also in this case the thicknesses were confirmed as the most influential parameters on the overall uncertainties.

The direct comparison between the GHP and the HFM results could clarify the precision and the accuracy of the two methods (only the Commutated joint was measured with both the apparatuses).

First of all, it is essential to underline how the measurements carried out with the HFM-3 always gave results lower of those obtained with the GHP-2. For this reason, it is absolutely possible to assume that it would have provided smaller values also for the COP measurements. In this way, the differences between COP and assemblies measurements would have been significantly higher, thus indicating a greater extra heat flux with a consequent reduction of the $u_c(\psi)$ values. The confirmation of this assumption is that, when there were limited differences between the GHP and the HFM λ_{eq} (when the potential λ_{COP} measurement difference between the GHP and the HFM could have had stronger effects), both the value of $u_c(\psi)$ and $\Delta\psi_{GHP-HFM}$ were extremely high (FS based VIPs). Otherwise, when the difference between the GHP and the HFM λ_{eq} increased (VIPs assemblies with FG core), the $u_c(\psi)$ and $\Delta\psi_{GHP-HFM}$ were considerably reduced.

11.3 VIPs thermal behaviour

The contribution of each heat transfer mechanism (conduction, convection and radiation) inside VIPs is very different from all the other insulating materials, and therefore, also their reaction to the variation of external boundary conditions was found to be very different. VIPs thermal behaviour strongly depends on several aspects, the core material, the internal vacuum degree, the ageing conditions, and the external temperature and moisture loads. Moreover, when two samples are coupled together, also the typology and quality of the joint affect the overall thermal performances.

A first experimental analysis (by means of the HFM-1 apparatus) was performed to define the influence of the boundary temperatures on the centre of panel thermal conductivity.

The temperature difference between the two plates of the apparatus was kept equal to 20°C, in accordance with the results obtained in the Type B uncertainty investigation. The standard EN 12667:2002 [12] provides indications about the acceptable temperature values and reference accuracy of HFM method, for high thermal resistant materials. The defined expected accuracy is $\pm 3\%$, with a recommended limit for temperature difference across the specimen equal to 10°C. Anyway was observed that with $\Delta\theta = 10^\circ\text{C}$, the $\pm 3\%$ uncertainty limit was respected for FS based VIPs 10 and 20 mm thick VIPs, but not for 30 mm (and presumably not even for VIPs with FG core). Therefore, an implementation of the measurement procedure described by the European standard is recommendable. Moreover, was observed that with $\Delta\theta$ values higher than 20°C the measurement uncertainties were lower than 2.5% in most of the cases (improving the reliability of the results and the comparability with the GHP measurements (for which the uncertainty limit provided by [12] is 2%).

Indeed, *“two specimens of fumed silica-based VIPs characterised by two different thicknesses were analysed. The performance of the samples was measured when they were fresh (as delivered by the producer) and after they were stored in a laboratory for 32 months. The experimental analyses showed that thermal conductivity can increase up to 45% when the average temperature ranges from 2 to 50°C. Considering this behaviour, the manufacturers should provide different values of thermal performance of VIPs for different average temperatures. In this way, a more realistic performance, which takes into account the real temperature conditions at which the panels could work, are obtained.*

A comparison with a punctured VIP (with a complete loss of vacuum), and fumed silica pressed board (VIP core material), was carried out to investigate the influence of the internal vacuum degree. A quasi-linear trend between thermal conductivity and temperature was found with a very limited variation of thermal conductivity as a function of temperature (4 - 5%).

Moreover, the same experiment was also conducted for a traditional insulating material (extruded polystyrene). In this case trend similar to the case of non-evacuated VIP was observed, but with a more marked variation of thermal conductivity (about 17%), due to the different internal structure.

The wide increment of VIPs centre of panel thermal conductivity can be associated to the variation of the relative weights of the different heat transfer contributions with the average temperature³².

The causes of the variation of the thermal conductivity were further investigated in order to have a comprehensive understanding of this physical phenomenon (considering that in case of FS based VIPs, the gaseous thermal conductivity (λ_g) is generally assumed to be negligible at the atmospheric pressure and at the building typical temperature ranges).

Further measurements were indeed performed on the same 10 mm thick VIP sample, and FS pressed board already analysed, considering ten different testing average temperatures at ambient pressure and again different ageing conditions. *“Moreover, in order to understand the implications in terms of loss of performances, further analyses were performed using numerical model at the building component level for a roof.*

The laboratory analyses were carried out measuring the variation of the thermal conductivity due to: i) working temperature and ii) ageing stage. Results demonstrate that:

- *A significant variation of the thermal conductivity in the first 20 months was observed (~6% of increment for all the testing temperatures).*

³² Text from the author's paper: “The effect of temperature on thermal performance of fumed silica based Vacuum Insulation Panels for buildings” [29].

- *The variation of thermal conductivity (due to the temperature) measured on a sample with 32 months of ageing was of about 53%, passing from an average testing temperature of -7.5°C to 55°C.*
- *The contribution of the gaseous conduction (λ_g) cannot be considered completely suppressed. In fact, the study demonstrates that with a temperature higher than about 25°C, a significant increment of the thermal conductivity is observable.*
- *After 40 months the increase in thermal conductivity ranges between 8% (λ_{10}) and 10% (λ_{40}) respect to the λ pristine value, underlining that the influence of temperature on the thermal conductivity is more significant for aged VIP.*

The analyses at building component level were carried out through numerical simulations on a case study representing a possible retrofit intervention of a pitched roof using a VIP layer. The variation of thermal conductivity with the temperature was accounted (data measured in the lab were used as inputs):

- *The range of working temperatures in case of pitched roof are quite severe (between 3°C during winter and 45°C during summer) and may negatively influence both the performances of the VIP and its useful service life.*
- *In summer, if the variation of λ with the temperature is not taken into account, a non-negligible underestimation of both λ -values and heat gains occurs (up to 27% and 15% respectively).*
- *The effect of temperature on the λ -value can be considered negligible during the winter season in Torino. However, this difference can be higher in a colder climate.*

Therefore, the importance of properly considering the variation of the thermal conductivity of the VIP with the temperature was proved, especially when severe boundary conditions occur. Besides a detrimental influence on the λ -value, these severe boundary conditions may also leave significant impacts on the service life of the panel. Therefore, effective solutions to mitigate the exposure of the VIP are needed, for example adopting additional insulating layers on the side characterised by the higher temperature variations. As demonstrated, the configuration B (in which the VIP panel is more protected) determines an

increment of the performance of ~ 9% during the summer peak, also presenting a significant positive impact on the VIP durability”³³.

The strong correlation between the thermal performances and both the average testing temperature ϑ_{avg} and the ageing conditions was also confirmed by the experimental campaign performed in the framework of the of the IEA EBC Annex 65 activities, sub-task 2 [150]. Different typologies of VIPs (single panel and assemblies, whose internal compositions were unknown) and one APM were tested at four different average temperatures and three ageing conditions. The measurement criteria (e.g., $\Delta\vartheta$, width and material for the joint in VIPs assemblies, drying process and so on), were not declared, except for the average testing temperature and the ageing conditions. Moreover, for logistical reasons, each sample was tested by only one laboratory. The temperature difference between the plates was again chosen equal to 20°C, obtaining a Type B combined uncertainty of the thermal conductivities almost always lower than 2.5%.

Increasing the average testing temperature ϑ_{avg} , the VIPs thermal conductivity increases, and therefore the measurement uncertainty decreases (higher heat flux through the sample). The ageing condition had a similar effect on both the thermal conductivity and the measurement uncertainty.

One typology of VIPs was probably made by an FG core: in fact, the measurement uncertainties was always higher than 3%, which is the uncertainty limit defined by the current standard EN 12667:2001 [12]. Since FG based VIPs are becoming more widespread on the market, it again pointed out that a revision of the standards (and measuring instruments) is required, so as to consider these very efficient materials and leading the measurements on the edge of the experimental apparatuses own applicability.

In case of highly performing materials, the ageing was found to have very significant consequences. After 30 days of ageing (accelerated ageing under severe hygrothermal conditions), the lambda values were almost doubled (always > 40%), but, due to the wide measurement uncertainty, the correlation between ageing and the average testing temperature was no more observable. The longer is the ageing period, the lower the combined measurement uncertainty.

³³ Text from the author’s paper: “Actual thermal performances of Vacuum Insulation Panels for buildings” [75].

The APM samples were, as expected, less influenced by the ageing procedure: the thermal conductivity increments can be due to the internal water content, but they lied more or less in the measurement uncertainty range.

Some of the samples were then coupled to form VIPs assemblies. Again, no indication about the joining procedure e technology was provided, the panels were simply sealed together with an adhesive tape trying to press the panels as close as possible to each other.

A direct comparison between the assemblies was not allowed because it is impossible to have two perfectly identical assembly (even if made with the same VIPs). This is why the assemblies thermal performances can be remarkably different (the additional heat flux through the VIP assembly joint is strongly influenced by the quality of assembling and the width of the gap in between the panels). Anyway, the obtained measurement uncertainty of the equivalent thermal conductivity was, on average, significantly below the 2.5%: λ_{eq} is always higher than λ_{COP} (as well as the heat flux through the sample), and therefore the $u_c(\lambda_{eq})$ is lower.

Both the values of λ_{eq} and ψ increased with the increase of the average testing temperature. In fact, the ψ -value reflects the difference between the centre of panel undisturbed case and the disturbed case with a joint in between two assembled VIPs.

As a general conclusion and recommendation ,in case of comparative tests, if not possible to perform a real round robin test (all the laboratories measure the same samples), is at least essential to preliminarily define all the testing criteria and boundary conditions.

11.4 Potentialities and thermo-economic analysis of VIPs

Vacuum Insulation Panels represent one of the most promising Super Insulating Materials on the market today. Nevertheless the high cost (which is, on the average, five times higher than EPS, including installation) is their main drawback. Therefore, a common opinion is that VIPs are less convenient, from the economic point of view, than traditional insulating materials for the energy retrofits of buildings. Anyway, in some circumstances, taking into account all the relevant factors, VIP can become economically preferable than other insulating solutions.

“This, in particular, is the case of internal wall insulation. Although many designers and engineers claim that outdoor wall insulation is the best and only choice for the energy retrofit of existing buildings (and indeed there are a number of advantages from the Building Physics point of view in choosing such solution), there is however a number of situations in which internal insulation is the only feasible intervention. Examples are: listed buildings, retrofit done just on part of a façade and constraints on to the outdoor side of the building that make the logistic of the construction site critical (e.g. densely built or congested city centres).

The main advantage of using VIPs for the internal wall insulation is represented by the possibility of saving a considerable surface of the internal space, thanks to the thinner thickness. Such advantage translates into a larger usable floor area and hence on the possibility for the building owner to obtain a higher revenue due to the space rent or the building sale. Nevertheless, this economic plus is never (or seldom) considered when the thermo-economic analysis is done and two retrofit scenarios, one using VIPs and the other using common (and less expensive, but more “bulky”) insulation materials, are compared.

In this research, a procedure was proposed to take into account the economic advantage derived from the space saving. Since the increase of the real estate value requires a number of arbitrary assumptions (the revenue related to this factor is virtual/potential and becomes real only if and when the building is sold) it has been decided to base the method on the additional rental profit.

The Discounted pay Back Period (DPBP) and the Break-Even Rental Value (BERV) were chosen as the metrics for the analysis.

It resulted that VIPs can be more convenient than conventional insulating materials (in this study the EPS was considered) depending on: the climatic zone,

the insulation thickness and the efficiency of the heating system. The influence of these three factors on the final economic result is significant; on the contrary, the aspect ratio of the building [...] did not reveal to play a relevant role on the economic convenience.

The DPBP is, as expected, shorter in the coldest locations with high HDD, for both the VIP and the EPS. However, for the VIP the dependency of the DPBP on the climate conditions becomes less important as much as the rental values increase (and becomes negligible when the rental rate exceeds, approximately, 300 €/m²). This is clearly due to the fact that the operative cost reduction related to the energy savings becomes less important than the rental profit.

Finally, it is worth mentioning that for those locations characterized by lower values of the HDD (warm climates) the analysis here shown assumes an interest only in terms of research, while it has not a practical relevance and application. This because the insulation level that is reached even using the thinnest of the VIP greatly overcomes the mandatory requirements for the thermal resistance of walls set by the standards (at least the ones applied in Italia).

The BERV decreases with increasing the panel thickness (and the influence of the VIP thickness on the BERV is higher in the cold climatic zones. Fig. 9b), while the DPBP of the VIP (Fig. 9a) is almost independent by the thickness for rental rates above 300 – 400 €/m² and decreases with increasing the rental cost.

Only for low rental rates (e.g. around 50 €/m²) a cost optimal thicknesses of the VIP insulation appears, being the optimal equal to about 20 mm.

Obviously, a better performing heating system makes the VIP and EPS Pay Back Period worsening. This indeed depends on the fact that an internal wall insulation retrofit becomes less effective, from the economic point of view, when the energy converters are well performing and/or the energy cost is low. Nevertheless, if an internal wall insulation is anyhow required, for example because of mandatory prescriptions, the rental values for which VIPs becomes convenient in comparison to EPS are lower (e.g. lower BERV) for a more efficient heating system (Fig. 10b). [...]

Based on the previous analysis, the rental values above which VIP can become more convenient than traditional insulating materials are fairly high and in general higher than 200 €/m² per year. To comply with the mandatory wall U-

value limits set on by the different European countries, the BERV has to be between 400 and 500 €/m² per year.

In conclusion, nowadays VIPs are already a cost-effective alternative to traditional insulating materials (for indoor insulation) in the business district of big cities or in areas where the real estate values are high. However, the total built volume that belongs to these zones is quite small and, therefore, apart from the economic advantages, the global impact in terms of depletion of energy sources is limited.

If a widespread application of VIP is wished for and their mass application to the energy retrofit of a consistent quota of the existing buildings is hoped, then the future priority of the producers has to be that of reducing the costs of production. Only in this way the VIPs can become an effective measure to improve the global energy sustainability of the building stock”³⁴.

11.5 Long-term VIPs thermal performances and service-life

Super Insulating Materials (in particular Vacuum Insulation Panels) have to face a series of issues during both the design and the operation phases, that may influence their actual thermal behaviour. The study highlights that some physical phenomena (such as the influence of temperature on the thermal conductivity and the decay of performance over time as a function of the boundary conditions severity) should be carefully evaluated during the design phase in order to avoid unexpected reduced actual thermal performances.

The performed simulations on a cavity wall and a pitched roof exposed to the various severity of the boundary conditions (temperature and relative humidity) makes it possible to assert a series of final considerations:

- The hygric stress is generally higher when the VIP is placed in between tight layers with high vapour diffusion, especially when the moisture loads penetrate the building envelope (depending on the driving rain or air convection). In this case, the re-drying phase is slower and the mean relative humidity around the VIP increases.

³⁴ Text from the author’s paper: “Thermo-economic analysis of building energy retrofits by using VIP - Vacuum Insulation Panels” [138].

- Generally, for the same climatic conditions, roof applications reached higher maximum values of temperature compared to walls (except for solar exposed dark finished walls).
- In case of VIPs as internal insulation, usually, they not affected by severe temperatures. However, depending on the orientation and the surface solar absorbance, relatively higher annual average temperatures in comparison to external insulation applications may be reached.
- The influence of the indoor moisture load is relevant for both internal and external VIPs wall application if no vapour barrier is present.

Some recommendation to provide general guidelines to mitigate the severity of the VIP operating conditions are summarised in the following list:

- The adoption of ventilated air layer could dramatically reduce the severity of the VIP operating conditions when they are used as external wall insulation in solar exposed façade. Alternatively, light finishing colours are warmly encouraged to reduce the surface temperature.
- The VIP covering with thin traditional insulation layer is always suggested.
- Some effective solutions to mitigate the severe exposure for roof applications are the use of light colour (cool roof), performant water proof membrane, ventilated airspace and gravel covering layer (flat roof).
- When a wall is subjected to high driving rain, the adoption of a ventilated façade working as rain-screen to prevent the water absorption is preferable.

The above list simply contains guidelines for the early design stage: heat and moisture simulation are always recommended to prevent the VIPs exposure to severe hygrothermal conditions and to guarantee their long service life.

About the service life analysis, was observed that the less severe boundary conditions are represented by the south exposed roof with a dark covering tiles (which reaches the highest values of water vapour pressure and temperature, with temperature peaks on the external side of about 70°C). For this particular configuration, the estimated VIP service life was of about 43 years.

This result is due to the fact that an increase in temperature, directly related to an increase in water vapour pressure, produces a greater evaporation of the water settled above the VIP envelope. In fact, as the air and water vapour permeability increase, the thermal conductivity of the VIP increases and consequently its service life decreases. In general, as the external solar absorption coefficient increases, the service life of the panel also increases (despite an increase in the pressure, which, in this case, is less incisive in the decay of thermal performance of the panel respect to the increase of the water vapour).

The relative humidity, on the other hand, has a marked influence: in the case of north-exposed roof with light-coloured tiles presents, where the highest values of relative humidity on the external VIP surface are reached (in the 83% of time the relative humidity is over the 70%), the VIP has the lowest service life, equal to 40 years.

Moreover, it was observed that the type of VIP envelope significantly affects the performance of the panels and consequently their service life:

- envelopes MF1 and MF3 are not recommended for building purpose, as the VIP thermal conductivity reaches the limit value of 0.008 W/mK within 20 years;
- envelope MF4 is, in general, the typology that provides longer durability (about 42 years, against the \approx 38 years obtainable with the envelope).

Moreover, the most influent parameters on the VIP durability was found to be its thickness. In fact, when the thickness is reduced by half also the life expectancy of the panel is halved.

The service life tends to decrease also if the VIP is exposed to a high moisture load. In fact, even if this parameter does not change the VIP surface temperatures, the relative humidity on the internal interface considerably increases. Furthermore, this phenomenon could lead to the formation of interstitial condensation inside the building component. Indeed, the installation of VIPs in environments with humidity, such as bathrooms or kitchens, must be carefully designed, as the deterioration of the material is much faster than in other rooms characterised by lower moisture loads.

Thanks to this study, it was demonstrated that the installation of VIP in severe environments should be properly designed. The analysis highlighted a number of useful guidelines for the proper application of these materials in walls and, in

particular, in roofs. However, this type of investigation should be performed on a more significant group of case studies (even larger than the one analysed in the context of the IEA EBC Annex 65 project, sub-task 3 [93]), so that it should be possible to draw up a series of warnings for the correct design of VIPs insulations, useful for increasing the building applications.

11.6 Final remarks and outlooks

This thesis represents an extensive research on the characterisation criticism of Super Insulating Materials. The survey goes from the detailed evaluation of every single parameter involved in the analysis of laboratory measurement uncertainty, to the calculation of the energy needs of VIPs insulated buildings, through the assessment of the VIPs economic convenience. The scale of the research, the uncertainty evaluation topic and the overall approach on the thermal bridging effects represent the significance and the novelty of these results.

The reduction of measurement uncertainty for Super Insulating Materials it is very important since it could generate a higher level of confidence among customers and potential users. The enhancement of measurement procedures and boundary conditions to get more reliable values of thermal performance of SIMs could be an important basis for the energy demand calculations on the building envelope and HVAC systems and a fair declaration of performance, leading to equal chances for manufacturers of SIMs on the market. Moreover, a widening of the SIMs market would lead to a cost reduction, with a consequent increment of SIMs economic convenience.

If the thermal conductivity variability due to the measurement uncertainty is well defined, it will be possible to identify the small changes of the performance over time due to the ageing deterioration, obtaining more accurate simulations and calculations of the thermal performance of SIMs insulated buildings.

Moreover, the knowledge gained from this research is the starting point of a submitted EMPIR Euramet Normative project, with the aim of providing a contribution to standardisation within CEN and ISO (CEN TC 88 WG11, CEN TC 89 and ISO TC 163 SC3, and SC1), and enhancing the experience of the European Institutes involved in the determination of the performance of SIMs. These goals can be achieved in three different time scale. Initially, the results of the work could be implemented in the VIP product standard, and a TR (technical report) could be published by CEN to define the procedure for CE-Marking of these new products (Short Term realisation). While, for the Long and Mid Term

realisation, the results could be used as a basis for the development of a new measurement standard complementing the existing standards.

The results obtained in this research fulfil the complete characterisation of the actual thermal performances of SIMs at the material/panel level, as well the critical issues that can be met during measurements. A detailed analysis was performed to investigate all the factors which influence SIMs thermal properties and their experimental uncertainties, providing some guidelines for improving the reliability of the results. But what about the SIMs in situ actual thermal behaviour? Numerical simulations can be very useful for this purpose, and they can be performed at a different scale (from the single material to an entire building or district). Moreover, since SIMs (and especially VIPs) are a recent technology for building insulation, these investigations are also useful for the assessment of their durability/service life of the insulating materials: there are few SIMs long-term applications on buildings to experimentally determine these aspects appropriately. What is the actual behaviour in situ of SIMs and how reliable are the simulation predictions, however, is still unknown, and it represents an interesting issue to be solved in future researches.

References

- [1] European Commission, Europe 2020 (2010). A European strategy for smart, sustainable and inclusive growth.
url: <https://ec.europa.eu/energy/en/topics/energy-strategy-and-energy-union/2030-energy-strategy/>
- [2] European Commission (2014). A policy framework for climate and energy in the period from 2020 to 2030.
url: <https://ec.europa.eu/energy/en/topics/energy-strategy-and-energy-union/2030-energy-strategy/>
- [3] European Commission (2011). Energy Roadmap 2050.
url: <https://ec.europa.eu/energy/en/topics/energy-strategy-and-energy-union/2050-energy-strategy/>
- [4] Eurostat, Final energy consumption by sector (2015).
url: <http://ec.europa.eu/eurostat/web/main/home>
- [5] World Business Council For Sustainable Development (2009). Transforming the Market: Energy Efficiency in Buildings.
url: <http://www.wbcsd.org/Projects/Energy-Efficiency-in-Buildings/Resources/Transforming-the-Market-Energy-Efficiency-in-Buildings>
- [6] EU Directive 2010/31/EU (2010). Directive 2010/31/EU of the European Parliament and of the Council of 19 May 2010 on the energy performance of buildings.
url: <http://eur-lex.europa.eu/legal-content/EN/TXT/?uri=CELEX:32010L0031>
- [7] IEA EBC Annex 52 (2014). Towards Net Zero Energy Solar Buildings, a joint project with IEA Solar Heating and Cooling (Task 40).
url: <http://www.ieaebc.org/projects/completed-projects/ebc-annex-52/> and <http://task40.ieashc.org/about>
- [8] IEA (2013). Technology Roadmap - Energy efficient building envelopes.
url: <https://www.iea.org/publications/freepublications/publication/TechnologyRoadmapEnergyEfficientBuildingEnvelopes.pdf>
- [9] Buildings Performance Institute Europe - BPIE (2014). EU Buildings Database.
url: <https://ec.europa.eu/energy/en/eu-buildings-database>

- [10] Verbeeck, G.; Hens, H. (2005). Energy savings in retrofitted dwellings: economically viable? *Energy and Buildings*, 37(7): 747-754.
doi: <https://doi.org/10.1016/j.enbuild.2004.10.003>
- [11] Enkvist, P.A.; Nauc ler, T.; Rosander, J. (2007). A cost curve for greenhouse gas reduction. *McKinsey Quarterly*.
url: <https://www.mckinsey.com/business-functions/sustainability-and-resource-productivity/our-insights/a-cost-curve-for-greenhouse-gas-reduction>
- [12] EN ISO 12667:2001. Thermal performance of building materials and products. Determination of thermal resistance using guarded hot plate and heat flow meter methods. Products of high and medium thermal resistance.
- [13] BIPM - Bureau International des Poids et Mesures (2008). JCGM 100:2008. Evaluation of measurement data — Guide to the expression of uncertainty in measurement (GUM).
url: <https://www.bipm.org/en/publications/guides/>
(last access: 07/02/2017).
- [14] Lorenzati, A.; Fantucci, S.; Capozzoli, A.; Perino, M. (2016). Experimental and numerical investigation of thermal bridging effects of jointed Vacuum Insulation Panels. *Energy and Buildings*, 111: 164-175.
doi: <https://doi.org/10.1016/j.enbuild.2015.11.026>
- [15] Schiavoni, S.; D'Alessandro, F.; Bianchi, F.; Asdrubali, F. (2016). Insulation materials for the building sector: A review and comparative analysis. *Renewable and Sustainable Energy Reviews*, 62: 988-1011.
doi: <http://dx.doi.org/10.1016/j.rser.2016.05.045>
- [16] IAL Consultants (2015). The European market for thermal insulation products. *Press release*.
url: <http://www.ialconsultants.com/what%E2%80%99s-new/press-releases>
- [17] ISO 8301:1991. Thermal insulation - Determination of steady-state thermal resistance and related properties - Guarded hot plate apparatus.
- [18] ISO 8302:1991. Thermal insulation - Determination of steady-state thermal resistance and related properties - Heat flow meter apparatus.
- [19] AEROSILR - Fumed Silica. Technical Overview. *Evonik industries*.
url: <http://www.aerosil.com/product/aerosil/en/products/pages/default.aspx>
- [20] Koebel, M.; Rigacci, A.; Achard, P. (2012). Aerogel-based thermal superinsulation: An overview. *Journal of Sol-Gel Science and Technology*, 63(3): 315-339.
doi: <https://doi.org/10.1007/s10971-012-2792-9>

- [21] Ebert, H.P. (2013). High-Performance Insulation Materials. In: Torgal, F.P.; Mistretta, M.; Kaklauskas, A.; Granqvist, C.G.; Cabeza, L.F. (2013). Nearly zero energy building refurbishment. A multidisciplinary approach. *Springer-Verlag London*, Vol. 1, pages 457-481.
doi: <https://doi.org/10.1007/978-1-4471-5523-2>
- [22] Casini, M. (2016). Smart Buildings, Advanced Materials and Nanotechnology to improve Energy Efficiency and Environmental Performance. *Woodhead publishing*.
ISBN-13: 978-0081009727
- [23] Flörke, O.W.; Graetsch, H.A.; Brunk, F.; Benda, L.; Paschen, S.; Bergna, H.E.; Roberts, W.O.; Welsh, W.A.; Libanati, C.; Ettliger, M.; Kerner, D.; Maier, M.; Meon, W.; Schmoll, R.; Gies, H.; Schiffmann, D. (2008). Silica. Ullmann's Encyclopedia of Industrial Chemistry. *Wiley-VCH Verlag*.
doi: https://doi.org/10.1002/14356007.a23_583.pub3
- [24] Pyrogenic silica
url: https://www.wacker.com/cms/en/products/product_groups/hdk.jsp
(last access: 07/02/2017).
- [25] Association of Synthetic Amorphous Silica Producers - ASASP. (2012) Factsheet: Synthetic Amorphous Silica (SAS). *cefic*.
url: http://www.asasp.eu/images/Publications/Nano_-_SAS_factsheet_-_201209.pdf
- [26] Caps, R.; Heinemann, U.; Ehrmantraut, M.; Fricke, J. (2001) Evacuated insulation panels filled with pyrogenic silica powders: Properties and applications. *High Temperatures - High Pressures*, 33: 151-156.
doi: <https://doi.org/10.1068/htwu70>
- [27] Caps, R.; Fricke, J. (2000) Thermal conductivity of opacified powder filler materials for vacuum insulations. *International Journal of Thermophysics*, 21(4): 445-452.
doi: <https://doi.org/10.1023/A:1006691731253>
- [28] Baetens, R.; Jelle, B.P.; Thue, J.V.; Tenpierik, M.J.; Grynning, S.; Uvsløkk, S.; Gustavsen, A. (2010) Vacuum insulation panels for building applications: A review and beyond. *Energy and Buildings*, 43(4): 147-172.
doi: <https://doi.org/10.1016/j.enbuild.2009.09.005>
- [29] Lorenzati, A.; Fantucci, S.; Capozzoli, A.; Perino, M. (2017) The Effect of Temperature on Thermal Performance of Fumed Silica Based Vacuum Insulation Panels for Buildings. *Energy Procedia*, 111: 490-499.
doi: <https://doi.org/10.1016/j.egypro.2017.03.211>

- [30] Fumed silica
url: https://en.wikipedia.org/wiki/Fumed_silica
(last access: 07/02/2017).
- [31] EVONIK Calostat
url: <http://www.calostat.com/product/calostat/en/reference-projects/>
(last access: 07/02/2017).
- [32] Leventis, N.S.A.; Chandrasekaran, N.; Sotiriou-Leventis, C. (2010). Click Synthesis of Monolithic Silicon Carbide Aerogels from Polyacrylonitrile-Crosslinked 3D Silica Networks. *Chemistry of Materials*, 22(9): 2790-2803.
doi: <https://doi.org/10.1021/cm903662a>
- [33] Baetens, R.; Jelle, B.P.; Gustavsen, A. (2011) Aerogel insulation for building applications: A state-of-the-art review. *Energy and Buildings*, 43(4): 761-769.
doi: <https://doi.org/10.1016/j.enbuild.2010.12.012>
- [34] Aerogel
url: <https://it.wikipedia.org/wiki/Aerogel>
(last access: 07/02/2017).
- [35] Aerogel
url: <http://www.aerogel.org/?p=3>
(last access: 07/02/2017).
- [36] Husing, N.; Schubert, U. (1998) Aerogels – airy materials: chemistry, structure, and properties. *Angewandte Chem International Edition*, 37(1-2): 22–45.
doi: [https://doi.org/10.1002/\(SICI\)1521-3773\(19980202\)37:1/2<22::AID-ANIE22>3.0.CO;2-I](https://doi.org/10.1002/(SICI)1521-3773(19980202)37:1/2<22::AID-ANIE22>3.0.CO;2-I)
- [37] Gaponik, N.; Hermann, A.K.; Eychmuller, A. (2012) Colloidal Nanocrystal-Based Gels and Aerogels: Material Aspects and Application Perspectives. *Journal of Physical Chemistry Letters*, 3(1): 8–17.
doi: <https://doi.org/10.1021/jz201357r>
- [38] Jensen, K.I.; Schultz, J.M.; Kristiansen, F.H. (2004) Development of windows based on highly insulating aerogel glazings. *Journal of Non-Crystalline Solids*, 350: 351–357.
doi: <https://doi.org/10.1016/j.jnoncrysol.2004.06.047>
- [39] Gao, T.; Ihara, T.; Grynning, S.; Jelle, B.P.; Gunnarshaug Lien, A. (2016) Perspective of aerogel glazings in energy efficient buildings. *Building and Environment*, 95: 405-413.
doi: <https://doi.org/10.1016/j.buildenv.2015.10.001>

- [40] Cuce, E.; Cuce, P.M.; Wood, C.J.; Riffat, S.B. (2014) Optimizing insulation thickness and analysing environmental impacts of aerogel-based thermal superinsulation in buildings. *Energy and Buildings*, 77: 28-39.
doi: <https://doi.org/10.1016/j.enbuild.2014.03.034>
- [41] Aspen aerogel safety data sheet.
url: https://www.aerogel.com/resources/common/userfiles/file/SDS-AIS/Spaceloft_SDS.pdf
- [42] Heinemann, U. (2018) International Energy Agency, IEA EBC Annex 65: Long-Term Performance of Super-Insulating Materials in Building Components and Systems. Subtask 1: State of the Art on Materials & Components – Case Studies. *IEA Energy Technology Network*.
Under revision.
- [43] Zeng, S.Q.; Hunt, A.J.; Cao, W.; Greif, R. (1994) Pore Size Distribution and Apparent Thermal Conductivity of Silica Aerogel. *Journal of Heat Transfer*, 116(3): 756–759.
doi: <https://doi.org/10.1115/1.2910933>
- [44] Van Bommel, M.J.; Den Engelsens, C.W.; Van Miltenburg, J.C. (1997) A thermoporometry study of fumed silica/aerogel composites. *Journal of Porous Materials*, 4(3): 143–150.
doi: <https://doi.org/10.1023/A:1009636915203>
- [45] Aeropan aerogel
url: <http://www.aeropan.it/en/home-gb/>
(last access: 07/02/2017).
- [46] Cuce, E.; Cuce, P.M.; Wood, C.J.; Riffat, S.B. (2014) Toward aerogel based thermal super insulation in buildings: A comprehensive review. *Renewable and Sustainable Energy Reviews*, 34: 273–299.
doi: <http://dx.doi.org/10.1016/j.rser.2014.03.017>
- [47] Riffat, S.B.; Qiu, G. (2013) A review of state-of-the-art aerogel applications in buildings. *International Journal of Low-Carbon Technologies*, 8(1): 1-6.
doi: <https://doi.org/10.1093/ijlct/cts001>
- [48] Carbon aerogel
url: <http://supersciencebydiva.blogspot.it/2013/05/carbon-aerogel-lightest-material.html>
(last access: 07/02/2017).
- [49] Kobayashi, Y.; Saito, T.; Isogai, A. (2014). Aerogels with 3D Ordered Nanofiber Skeletons of Liquid-Crystalline Nanocellulose Derivatives as Tough and Transparent Insulators. *Angewandte Chemie International Edition*, 53(39): 10394-10397.

- doi: <https://doi.org/10.1002/anie.201405123>
- [50] Aegerter, M.A.; Leventis, N.; Koebel, M.M. (2011) *Aerogels Handbook*. Springer-Verlag New York.
doi: <https://doi.org/10.1007/978-1-4419-7589-8>
- [51] Rao, A.P., G.M. Pajonk, and A.V. Rao. (2005) Effect of preparation conditions on the physical and hydrophobic properties of two step processed ambient pressure dried silica aerogels. *Journal of Materials Science*, 40(13): 3481-3489.
doi: <https://doi.org/10.1007/s10853-005-2853-3>
- [52] Bhagat, S.D.; Rao, A.V. (2006) Surface chemical modification of TEOS based silica aerogels synthesized by two step (acid-base) sol-gel process. *Applied Surface Science*, 252(12): 4289-4297.
doi: <https://doi.org/10.1016/j.apsusc.2005.07.006>
- [53] Mahadik, D.B.; Rao, A.V.; Kumar, R.; Ingale, S.V.; Wagh, P.B.; Gupta, S.C. (2012) Reduction of processing time by mechanical shaking of the ambient pressure dried TEOS based silica aerogel granules. *Journal of Porous Materials*, 19(1): 87-94.
doi: <https://doi.org/10.1007/s10934-011-9451-3>
- [54] Sachithanadam, M.; Joshi, S.C. (2016) *Silica Aerogel Composites. Novel Fabrication Methods*. Springer Singapore.
doi: <https://doi.org/10.1007/978-981-10-0440-7>
- [55] Critical point
url: [https://en.wikipedia.org/wiki/Critical_point_\(thermodynamics\)](https://en.wikipedia.org/wiki/Critical_point_(thermodynamics))
(last access: 07/02/2017).
- [56] Dorcheh, S.; Abbasi, M. (2008). Silica Aerogel; Synthesis, Properties, and Characterization. *Journal of Materials Processing Technology*, 199(1-3): 10-26.
doi: <https://doi.org/10.1016/j.jmatprotec.2007.10.060>
- [57] Mujeebu, M.A.; Ashraf, N.; Alsuwayigh, A. (2016) Energy performance and economic viability of nano aerogel glazing and nano vacuum insulation panel in multi-story office building. *Energy*, 113: 949-956.
doi: <https://doi.org/10.1016/j.energy.2016.07.136>
- [58] Lolli, N.; Andresen, I. (2016) Aerogel vs. argon insulation in windows: A greenhouse gas emissions analysis. *Building and Environment*, 101: 64-76.
doi: <https://doi.org/10.1016/j.buildenv.2016.03.001>

- [59] Galliano, R.; Ghazi Wakili, K.; Stahl, T.; Binder, B.; Daniotti, B. (2016) Performance evaluation of aerogel-based and perlite-based prototyped insulations for internal thermal retrofitting: HMT model validation by monitoring at demo scale. *Energy and Buildings*, 126: 275-286.
doi: <https://doi.org/10.1016/j.enbuild.2016.05.021>
- [60] Ghazi Wakili, K.; Stahl, T.; Heiduck, E.; Schuss, M.; Vonbank, R.; Pont, U.; Sustr, C.; Wolosiuk, D.; Mahdavi, A. (2015) High performance aerogel containing plaster for historic buildings with structured facades. *Energy Procedia*, 78: 949-954.
doi: <https://doi.org/10.1016/j.egypro.2015.11.027>
- [61] Fantucci, S.; Lorenzati, A.; Kazas, G.; Levchenko, D.; Serale, G. (2015) Thermal Energy Storage with Super Insulating Materials: A Parametrical Analysis. *Energy Procedia*, 78: 441-446.
doi: <https://doi.org/10.1016/j.egypro.2015.11.691>
- [62] Berge, A.; Johansson, P. (2012). Literature Review of High Performance Thermal Insulation. *Chalmers University of Technology*.
url: http://publications.lib.chalmers.se/records/fulltext/local_159807.pdf
- [63] Kalnæs, S.E.; Jelle, B.P. (2014). Vacuum insulation panel products: A state-of-the-art review and future research pathways. *Applied Energy*, 116: 355-375.
doi: <https://doi.org/10.1016/j.apenergy.2013.11.032>
- [64] Johansson, P. (2012) Vacuum Insulation Panels in Buildings. Literature review. *Chalmers University of Technology*.
url: <http://publications.lib.chalmers.se/records/fulltext/155961.pdf>
- [65] Capozzoli, A.; Fantucci, S.; Favoino, F.; Perino, M. (2015). Vacuum Insulation Panels: Analysis of the Thermal Performance of Both Single Panel and Multilayer Boards. *Energies*, 8(4): 2528-2547.
doi: <https://doi.org/10.3390/en8042528>
- [66] Quénard, D.; Sallée, H. (2005). From VIP's to Building Façades : Three Levels of Thermal Bridges. *Proceedings of 7th International Vacuum Insulation Symposium*, pages 113-120.
- [67] Yrieix, B.; Morel, B.; Pons, E. (2014) VIP service life assessment: Interactions between barrier laminates and core material, and significance of silica core ageing. *Energy and Buildings*, 85: 617-630.
doi: <https://doi.org/10.1016/j.enbuild.2014.07.035>

- [68] Garnier, G.; Marouani, S.; Yrieix, B.; Pompeo, P.; Chauvois, M.; Flandin, L.; Brechet, Y. (2009) Interest and durability of multilayers: from model films to complex films. *Polymers for Advanced Technologies*, 22(6): 847-856.
doi: <https://doi.org/10.1002/pat.1587>
- [69] Alotaibi, S.S.; Riffat, S. (2013) Vacuum insulated panels for sustainable buildings: a review of research and applications. *International Journal of Energy Research*, 38(1): 1-19.
doi: <https://doi.org/10.1002/er.3101>
- [70] Zhuang, J.; Ghaffar, S.H.; Fan, M.; Corker, J. (2017) Restructure of expanded cork with fumed silica as novel core materials for vacuum insulation panels. *Composites Part B*, 127: 215-221.
doi: <https://doi.org/10.1016/j.compositesb.2017.06.019>
- [71] Chang, B.; Zhong, L.; Akinc, M. (2016) Low cost composites for vacuum insulation core material. *Vacuum*, 131: 120-126.
doi: <https://doi.org/10.1016/j.vacuum.2016.05.027>
- [72] Liang, Y.; Wu, H.; Huang, G.; Yang, J.; Wang, H. (2017) Thermal performance and service life of vacuum insulation panels with aerogel composite cores. *Energy and Buildings*, 154: 606–617.
doi: <http://dx.doi.org/10.1016/j.enbuild.2017.08.085>
- [73] Tetlow, D.; De Simon, L.; Liew, S.Y.; Hewakandamby, B.; Mack, D.; Thielemans, W.; Riffat, S. (2017) Cellulosic-crystals as a fumed-silica substitute in vacuum insulated panel technology used in building construction and retrofit applications. *Energy and Buildings*, 156: 187-196.
doi: <http://dx.doi.org/10.1016/j.enbuild.2017.08.058>
- [74] Gangåssæter, H.F.; Jelle, B.P.; Mofid, S.A.; Gao, T. (2017) Air-Filled Nanopore Based High-Performance Thermal Insulation Materials. *Energy Procedia*, 132: 231-236.
doi: <https://doi.org/10.1016/j.egypro.2017.09.760>
- [75] Fantucci, S.; Lorenzati, A.; Capozzoli, A.; Perino, M. (2018). Actual thermal performances of Vacuum Insulation Panels for buildings. *Energy and Buildings*.
In press.
- [76] Alam, M.; Singh, H.; Limbachiya, M.C. (2011) Vacuum insulation panels (VIPs) for building construction industry - a review of the contemporary developments and future directions. *Apply Energy*, 88(11): 3592-602.
doi: <https://doi.org/10.1016/j.apenergy.2011.04.040>

- [77] Di, X.; Gao, Y.; Bao, C.; Hu, Y.; Xie, Z. (2013) Optimization of glass fibre based core materials for vacuum insulation panels with laminated aluminium foils as envelopes. *Vacuum*, 97: 55-9.
doi: <https://doi.org/10.1016/j.vacuum.2013.04.005>
- [78] Bouquerel, M.; Duforestel, T.; Baillis, D.; Rusaouen, G. (2012) Heat transfer modeling in vacuum insulation panels containing nanoporous Silicas - A review. *Energy and Buildings*, 54: 320-336.
doi: <https://doi.org/10.1016/j.enbuild.2012.07.034>
- [79] Quénard, D.; Sallée, H. (2005) Micro-nano porous materials for high performance thermal insulation. *Proceedings of 2nd International Symposium on Nanotechnology in Construction*.
- [80] Schwab H., Heinemann U., Beck A., Ebert H.P., Fricke J. (2005) Prediction of service life for vacuum insulation panels with fumed silica kernel and foil cover. *Journal of Thermal Envelope and Building Science*, 28(4): 357-374.
doi: <https://doi.org/10.1177/1097196305051894>
- [81] Heinemann, U. (2008) Influence of water on the total heat transfer in ‘evacuated’ insulations. *International Journal of Thermophysics*, 29(2): 735-749.
doi: <https://doi.org/10.1007/s10765-007-0361-1>
- [82] Simmler, H.; Brunner, S. (2005) Vacuum insulation panels for building applications basic properties, ageing mechanisms and service life. *Energy and Buildings*, 37(11): 1122-1131.
doi: <https://doi.org/10.1016/j.enbuild.2005.06.015>
- [83] Wegger, E.; Jelle, B.P.; Sveipe, E.; Grynning, S.; Gustavsen, A.; Baetens, R.; Thue, J.V. (2011) Ageing effects on thermal properties and service life of vacuum insulation panels. *Journal of Building Physics*, 35(2): 128-167.
doi: <https://doi.org/10.1177/1744259111398635>
- [84] Heinemann, U. (2013) Vacuum Insulation Panels - Potentials, Challenges and Applications. *Proceedings of 11th International Vacuum Insulation Symposium*, pages 1-2.
- [85] Ghazi Wakili, K.; Nussbaumer, T.; Bundi, R. (2005) Thermal performance of VIP assemblies in building constructions. *Proceedings of 7th International Vacuum Insulation Symposium*, pages 131-138.
- [86] Brunner, S.; Stahl, T.; Ghazi Wakili, K. (2012) An example of deteriorated vacuum insulation panels in a building façade. *Energy and Buildings*, 54: 278-282.
doi: <https://doi.org/10.1016/j.enbuild.2012.07.027>

- [87] Bouquerel, M.; Duforestel, T.; Baillis, D.; Rusaouen, G. (2012) Mass transfer modeling in gas barrier envelopes for vacuum insulation panels: a review. *Energy and Buildings*, 55: 903-920.
doi: <https://doi.org/10.1016/j.enbuild.2012.09.004>
- [88] EN 15978:2011. Sustainability of construction works. Assessment of environmental performance of buildings. Calculation method.
- [89] ISO 14040:2006. Environmental Management - Life Cycle Assessment - Principles and Framework.
- [90] Schonhardt, U.; Binz, A.; Wohler, M.; Dott, R. (2003). Ökobilanz eines Vakuum-Isolations-Paneels (VIP). *Proceedings of Bundesamtes für Energie*.
- [91] Jelle, B.P. (2011). Traditional, state-of-the-art and future thermal building insulation materials and solutions - Properties, requirements and possibilities. *Energy and Buildings*, 43(10): 2549-2563.
doi: <https://doi.org/10.1016/j.enbuild.2011.05.015>
- [92] Alam, M.; Singh, H.; Suresh, S.; Redpath, D.A.G. (2017). Energy and economic analysis of Vacuum Insulation Panels (VIPs) used in non-domestic buildings. *Applied Energy*, 188: 1-8.
doi: <https://doi.org/10.1016/j.apenergy.2016.11.115>
- [93] Adl-Zarrabi, B.; Johansson, P.; Gudmundsson, K. (2018) International Energy Agency, IEA EBC Annex 65: Long-Term Performance of Super-Insulating Materials in Building Components and Systems. Subtask 3: Practical Applications - Retrofitting at the Building Scale - Field scale. *IEA Energy Technology Network*.
Under revision.
- [94] Johansson, P.; Adl-Zarrabi, B.; Berge, A. (2015) Evaluation of long-term performance of VIPs. *Energy Procedia*, 78: 388-393.
doi: <https://doi.org/10.1016/j.egypro.2015.11.680>
- [95] Lorenzati, A.; Fantucci, S.; Capozzoli, A.; Perino, M. (2014). The Effect of Different Materials Joint in Vacuum Insulation Panels. *Energy Procedia*, 62: 374-381.
doi: <https://doi.org/10.1016/j.egypro.2014.12.399>
- [96] Capozzoli, A.; Gorrino, A.; Corrado, V. (2013) A building thermal bridges sensitivity analysis. *Applied Energy*, 107: 229-243.
doi: <https://doi.org/10.1016/j.apenergy.2013.02.045>
- [97] EN ISO10211-1:2017. Thermal bridges in building construction - Heat flows and surface temperatures - Detailed calculations.

- [98] Boafo, F.E.; Ahn, J.G.; Kim, J.T.; Kim, J.H. (2005) Computing thermal bridge of VIP in building retrofits using DesignBuilder. *Energy Procedia*, 78: 400-405.
doi: <https://doi.org/10.1016/j.egypro.2015.11.683>
- [99] Sprengard, C.; Holm, A.H. (2014). Numerical examination of thermal bridging effects at the edges of vacuum-insulation-panels (VIP) in various constructions. *Energy and Buildings*, 85: 638-643.
doi: <https://doi.org/10.1016/j.enbuild.2014.03.027>
- [100] Heineman, U.; Schwab, H.; Simmler, H.; Brunner, S.; Ghazi Wakili, K.; Bundi, R.; Kumaran, K.; Mukhopadhyaya, P.; Quénard, D.; Sallée, H.; Noller, K.; Kücükpinar-Niarchos, E.; Stramm, C.; Tenpierik, M.J.; Cauberg, J.J.M.; Binz, A.; Steinke, G.; Moosmann, A.; Erb, M. (2005) International Energy Agency, IEA ECBCS Annex 39: High Performance Thermal Insulation Systems (HiPTI). Subtask B: Vacuum Insulation in the Building Sector. Systems and Applications. *IEA Energy Technology Network*.
doi: http://www.iea-ebc.org/Data/publications/EBC_Annex_39_Report_Subtask-B.pdf
- [101] Boafo, F.E.; Chen, Z.; Li, C.; Li, B.; Xu, T. (2014). Structure of vacuum insulation panel in building system. *Energy and Buildings*, 85: 644-653.
doi: <https://doi.org/10.1016/j.enbuild.2014.06.055>
- [102] Ghazi Wakili, K.; Stahl, T.; Brunner, S. (2011). Effective thermal conductivity of a staggered double layer of vacuum insulation panels. *Energy and Buildings*, 43(6): 1241-1246.
doi: <https://doi.org/10.1016/j.enbuild.2011.01.004>
- [103] Lorenzati, A.; Fantucci, S.; Capozzoli, A.; Perino, M. (2016). Experimental and numerical investigation of thermal bridging effects of jointed Vacuum Insulation Panels. *Energy and Buildings*, 111: 164-175.
doi: <https://doi.org/10.1016/j.enbuild.2015.11.026>
- [104] Lorenzati, A.; Fantucci, S.; Capozzoli, A.; Perino, M. (2015). Coupling VIPs and ABPs: assessment of overall thermal performance in building wall insulation. *Energy Procedia*, 78: 2760-2765.
doi: <https://doi.org/10.1016/j.egypro.2015.11.620>
- [105] Isaia, F.; Fantucci, S.; Capozzoli, A.; Perino, M. (2017). Thermal bridges in vacuum insulation panels at building scale. *Engineering Sustainability*, 170(1): 47-60.
doi: <https://doi.org/10.1680/jensu.15.00057>

- [106] Alam, M.; Singh, H.; Brunner, S.; Naziris, C. (2014). Experimental characterisation and evaluation of the thermo-physical properties of expanded perlite - Fumed silica composite for effective vacuum insulation panel (VIP) core. *Energy and Buildings*, 69: 442-450.
doi: <https://doi.org/10.1016/j.enbuild.2013.11.027>
- [107] Singh, H.; Geisler, M.; Menzel, F. (2015). Experimental investigations into thermal transport phenomena in vacuum insulation panels (VIPs) using fumed silica cores. *Energy and Buildings*, 107: 76-83.
doi: <https://doi.org/10.1016/j.enbuild.2015.08.004>
- [108] Qu, Z.G.; Fu, Y.D.; Liu, Y.; Zhou, L. (2018). Approach for predicting effective thermal conductivity of aerogel materials through a modified lattice Boltzmann method. *Applied Thermal Engineering*, 132: 730-739.
doi: <https://doi.org/10.1016/j.applthermaleng.2018.01.013>
- [109] Fricke, J.; Schwab, H.; Heinemann, U. (2006). Vacuum insulation panels - Exciting thermal properties and most challenging applications. *International Journal of Thermophysics*, 27(4): 1123-1139.
doi: <https://doi.org/10.1007/s10765-006-0106-6>
- [110] Kaganer, M.G. (1969). Thermal Insulation in Cryogenic Engineering. *IPST Press*.
ISBN-13: 978-0706506075
- [111] Yu, C.H.; Fu, Q.J.; Tsang, S.C.E. (2010). Materials for Energy Efficiency and Thermal Comfort in Buildings. 13 - Aerogel materials for insulation in buildings. *Woodhead Publishing Series in Energy*, pages 319-344.
doi: <https://doi.org/10.1533/9781845699277.2.319>
- [112] Fricke, J. (1993). Materials research for the optimization of thermal insulations. *High Temperatures - High Pressures*, 25(4): 379-390.
- [113] Lorenzati, A.; Fantucci, S.; Capozzoli, A.; Perino, M. (2015). VIPs Thermal Conductivity Measurement: Test Methods, Limits and Uncertainty. *Energy Procedia*, 78: 418-423.
doi: <http://dx.doi.org/10.1016/j.egypro.2015.11.686>
- [114] Sprengard, C.; Treml, S.; Engelhardt, M.; Simon, H.; Kagerer, F. (2017). Vakuum-Isolations-Paneele (VIP) in der Bauanwendung: vom Dämmstoff zum Dämmsystem. Verarbeitung, Befestigung, Dauerhaftigkeit. *Fraunhofer IRB Verlag*.
ISBN-13: 978-3738800234

- [115] Infineon Technologies AG (2000). Special Subject Book. Thermal Resistance. Theory and Practice. *Infineon Technologies AG*.
url: <https://www.infineon.com/dgdl/smdpact.pdf?fileId=db3a304330f6860601311905ea1d4599>
- [116] EN ISO 6946:2017. Building components and building elements - Thermal resistance and thermal transmittance - Calculation methods.
- [117] Capozzoli, A.; Gorrino, A.; Corrado, V. (2013). A building thermal bridges sensitivity analysis. *Applied Energy*, 107: 229-243.
doi: <https://doi.org/10.1016/j.apenergy.2013.02.045>
- [118] Ghazi Wakili, K.; Bundi, R.; Binder, B. (2004). Effective thermal conductivity of vacuum insulation panels. *Building Research & Information*, 32(4): 293-299.
doi: <https://doi.org/10.1080/0961321042000189644>
- [119] EN ISO 14683:2007. Thermal bridges in building construction - Linear thermal transmittance - Simplified methods and default values.
- [120] ASTM C 177:2010. Standard Test Method for Steady-State Heat Flux Measurements and Thermal Transmission Properties by Means of the Guarded-Hot-Plate Apparatus.
- [121] EN 12664:2001. Thermal performance of building materials and products - Determination of thermal resistance by means of guarded hot plate and heat flow meter methods - Dry and moist products of medium and low thermal resistance.
- [122] ASTM C 518:2010. Standard Test Method for Steady-State Thermal Transmission Properties by Means of the Heat Flow Meter Apparatus.
- [123] LaserComp (2001-2005). FOX600 and FOX800 Series Instruments Manual. *LaserComp, Inc.*
- [124] Yüksel N. (2016). The Review of Some Commonly Used Methods and Techniques to Measure the Thermal Conductivity of Insulation Materials, Insulation Materials in Context of Sustainability. *InTech*.
doi: <https://doi.org/10.5772/64157>
- [125] ASTM C 1113:2013. Standard Test Method for Thermal Conductivity of Refractories by Hot Wire (Platinum Resistance Thermometer Technique).
- [126] ISO 8894-1:2010. Refractory materials -- Determination of thermal conductivity -- Part 1: Hot-wire methods (cross-array and resistance thermometer).
- [127] EN 993-15:2005. Methods of test for dense shaped refractory products - Part 15: Determination of thermal conductivity by the hotwire (parallel) method.

- [128] ISO 22007-2:2015. Plastics - Determination of thermal conductivity and thermal diffusivity - Part 2: Transient plane heat source (hot disc) method.
- [129] Antunes, M.; Realinho, V.; Velasco, J.I.; Solórzano, E.; Rodríguez-Pérez, M.A.; De Saja, J.A. (2012). Thermal conductivity anisotropy in polypropylene foams prepared by supercritical CO₂ dissolution. *Materials Chemistry and Physics*, 136(1): 268-276.
doi: <https://doi.org/10.1016/j.matchemphys.2012.07.001>
- [130] ASTM E 1461:2013. Standard Test Method for Thermal Diffusivity by the Flash Method.
- [131] EN 821-1:1995. Advanced technical ceramics - Monolithic ceramics - Thermophysical properties - Part 1: Determination of thermal expansion.
- [132] Hay, B.; Anhalt, K.; Chapman, L.; Boboridis, K.; Hameury, J.; Krenek, S. (2011). High temperature thermophysical properties of advanced materials for nuclear design. *Proceedings of 2nd IMEKO TC 11 International Symposium Metrological Infrastructure*, pages 71-76.
- [133] PHISIBEL. BISCO: computer program to calculate two-dimensional steady state heat transfer in free-form objects. (2012).
- [134] Energy Plus software
url: <https://energyplus.net/>
(last access: 07/02/2017).
- [135] ISO 15256:2007. Thermal performance of buildings - Calculation of energy use for space heating and cooling - General criteria and validation procedures, European Committee for Standardization.
- [136] Energy Plus weather region
url: https://energyplus.net/weather-region/europe_wmo_region_6/
(last access: 07/02/2017).
- [137] D.L. 192/2005, Attuazione della direttiva 2002/91/CE relativa al rendimento energetico nell'edilizia.
- [138] Fantucci, S.; Garbaccio, S.; Lorenzati, A.; Perino, M. (2018). Thermo-economic analysis of building energy retrofits by using VIP - Vacuum Insulation Panels.
Submitted.
- [139] Berardi, U.; Tronchin, L.; Manfren, M.; Nastasi, B. (2018). On the Effects of Variation of Thermal Conductivity in Buildings in the Italian Construction Sector. *Energies*, 11(4): 872.
doi: <https://doi.org/10.3390/en11040872>

- [140] WUFI® Pro manual. *Fraunhofer Institute for Building Physics*.
url: https://wufi.de/download/WUFI_Pro_4_Manual.pdf/
- [141] EN 15026:2007. Assessment of moisture transfer by numerical simulation.
- [142] ASHRAE 160:2016. Criteria for Moisture-Control Design Analysis in Buildings.
- [143] ISO 13788:2012, Hygrothermal performance of building components and building elements - Internal surface temperature to avoid critical surface humidity and interstitial condensation - Calculation methods.
- [144] Fantucci, S.; Capozzoli, A.; Lorenzati, A.; Perino, M.; Quénard, D. (2017). A methodological framework for the analysis of the service life of VIPs based envelope components in buildings. *Proceedings of 13th International Vacuum Insulation Symposium*.
- [145] BIPM - Bureau International des Poids et Mesures (2012). JCGM 200:2012. International vocabulary of metrology - Basic and general concepts and associated terms (VIM).
url: <https://www.bipm.org/en/publications/guides/>
(last access: 07/02/2017).
- [146] Farrance, I.; Frenkel, R. (2012). Uncertainty of Measurement: A Review of the Rules for Calculating Uncertainty Components through Functional Relationships. *The Clinical Biochemist Reviews*, 33(2): 49-75.
url: <https://www.ncbi.nlm.nih.gov/pmc/articles/PMC3387884/>
- [147] ISO 3534-1:2006. Statistics - Vocabulary and symbols - Part 1: General statistical terms and terms used in probability.
- [148] EN 1946-3:1999. Thermal performance of building products and components - Specific criteria for the assessment of laboratories measuring heat transfer properties - Part 3: Measurements by heat flow meter method.
- [149] EN 1946-2:1999. Thermal performance of building products and components - Specific criteria for the assessment of laboratories measuring heat transfer properties - Part 2: Measurements by guarded hot plate method.
- [150] Holm, A.; Sprengard, C. (2018) International Energy Agency, IEA EBC Annex 65: Long-Term Performance of Super-Insulating Materials in Building Components and Systems. Subtask 2: Characterisation of materials & components - Laboratory Scale. *IEA Energy Technology Network*. Under revision.
- [151] Minitab software
<http://www.minitab.com/en-us/>
(last access: 06/03/2017).

- [152] Sprengard, C.; Treml, S.; Engelhardt, M.; Simon, H.; Kagerer, F. (2017) Vakuum-Isolations-Paneele (VIP) in der Bauanwendung: vom Dämmstoff zum Dämmsystem. Verarbeitung, Befestigung, Dauerhaftigkeit. *Fraunhofer IRB Verlag*.
ISBN-13: 978-3738800234
- [153] Kobari, T.; Okajima, J.; Komiya, A.; Maruyama, S. (2015). Development of guarded hot plate apparatus utilizing Peltier module for precise thermal conductivity measurement of insulation materials. *International Journal of Heat and Mass Transfer*, 116: 91: 1157-1166.
doi: <https://doi.org/10.1016/j.ijheatmasstransfer.2015.08.044>
- [154] D.P.R. 207/2010, Codice dei contratti pubblici relativi ai lavori, servizi e forniture in attuazione delle Direttive 2004/17/CE e 2004/18/CE. (2010).
- [155] Vacupor[®]
url: <http://www.bitbau.it/>
(last access: 22/03/2017)
- [156] Cidienne. Isolanti termo acustici polistirene espanso
url: <http://www.cidienne.it/>
(last access: 22/03/2017).
- [157] Eurostat, Prices of natural gas and electricity (2015).
url: <http://ec.europa.eu/eurostat/data/database/>
- [158] Cushman & Wakefield. (2014). Office space across the world. *Cushman & Wakefield Research Publication*.
url: www.cushmanwakefield.com
- [159] European Central Bank. Euro area 10-year Government Benchmark bond.
url: http://sdw.ecb.europa.eu/quickview.do?SERIES_KEY=143.FM.M.U2.EUR.4F.BB.U2_10Y.YLD
(last access: 22/03/2017).
- [160] European Central Bank. Inflation forecasts.
url: https://www.ecb.europa.eu/stats/ecb_surveys/survey_of_professional_forecasters/html/table_hist_hicp.en.html
(last access: 22/03/2017).
- [161] Simmler, H.; Brunner, S. (2005). Ageing and service life of VIP in buildings. *Proceedings of 7th International Vacuum Insulation Symposium*, pages 15-22.

-
- [162] Johansson; P. (2014). Building Retrofit using Vacuum Insulation Panels: Hygrothermal Performance and Durability. (*PhD thesis*), Chalmers University of Technology, Department of Civil and Environmental Engineering.
url: <http://publications.lib.chalmers.se/records/fulltext/193780/193780.pdf>.
- [163] Baetens, R.; Jelle, B.P.; Gustavsen, A.; Roels, S. (2010). Long-term thermal performance of vacuum insulation panels (VIPs) for building applications investigated by dynamic climate simulations with respect to temperature and humidity. *Proceedings of 1st Central European Symposium on Building Physics*.

Appendix A

HFM sensitivity analysis

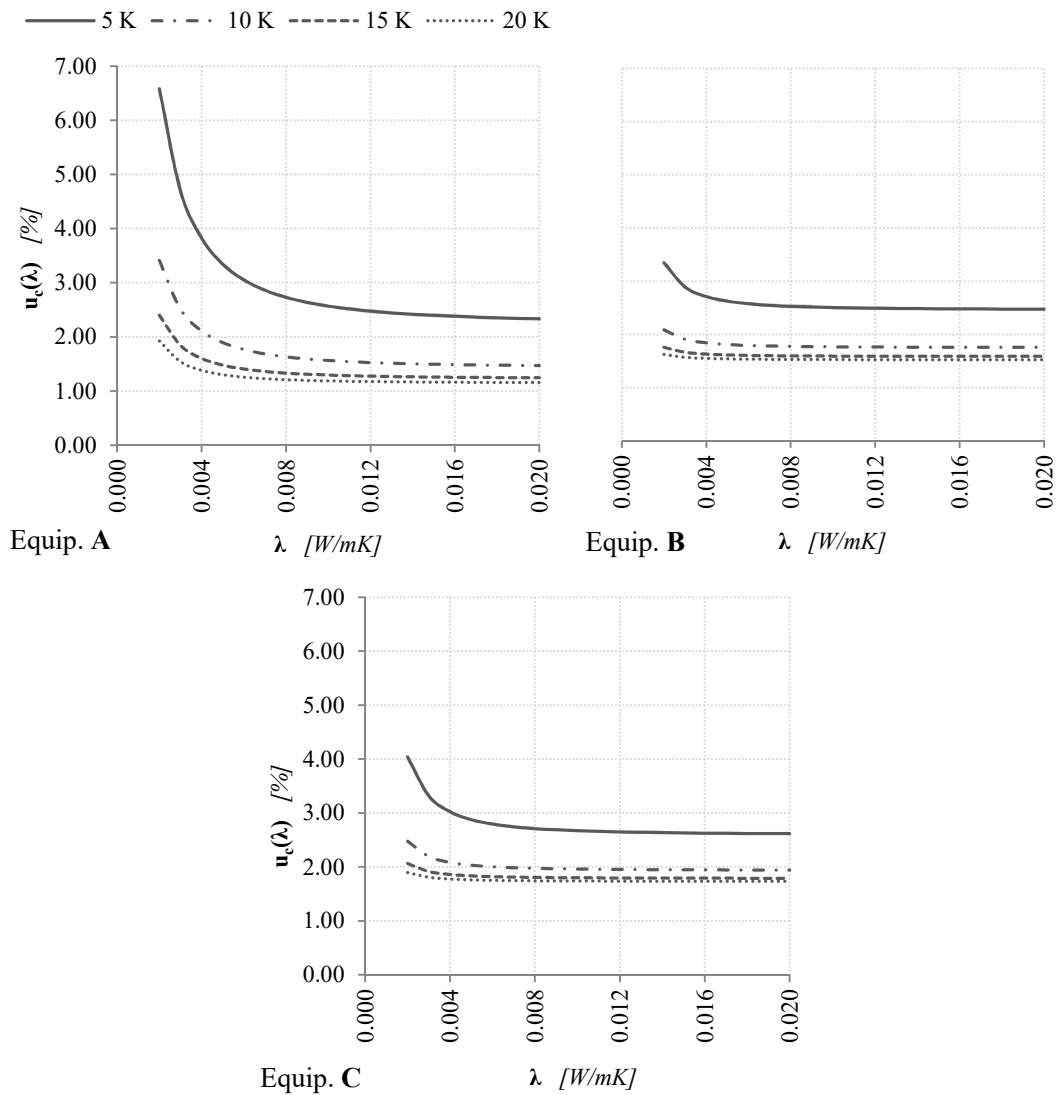


Figure A. 1: HFM - Combined relative uncertainty as a function of thermal conductivity and temperature difference, equipment A, B and C according to EN 1946-3:1999 [148] (sample thickness of 10 mm) [150]

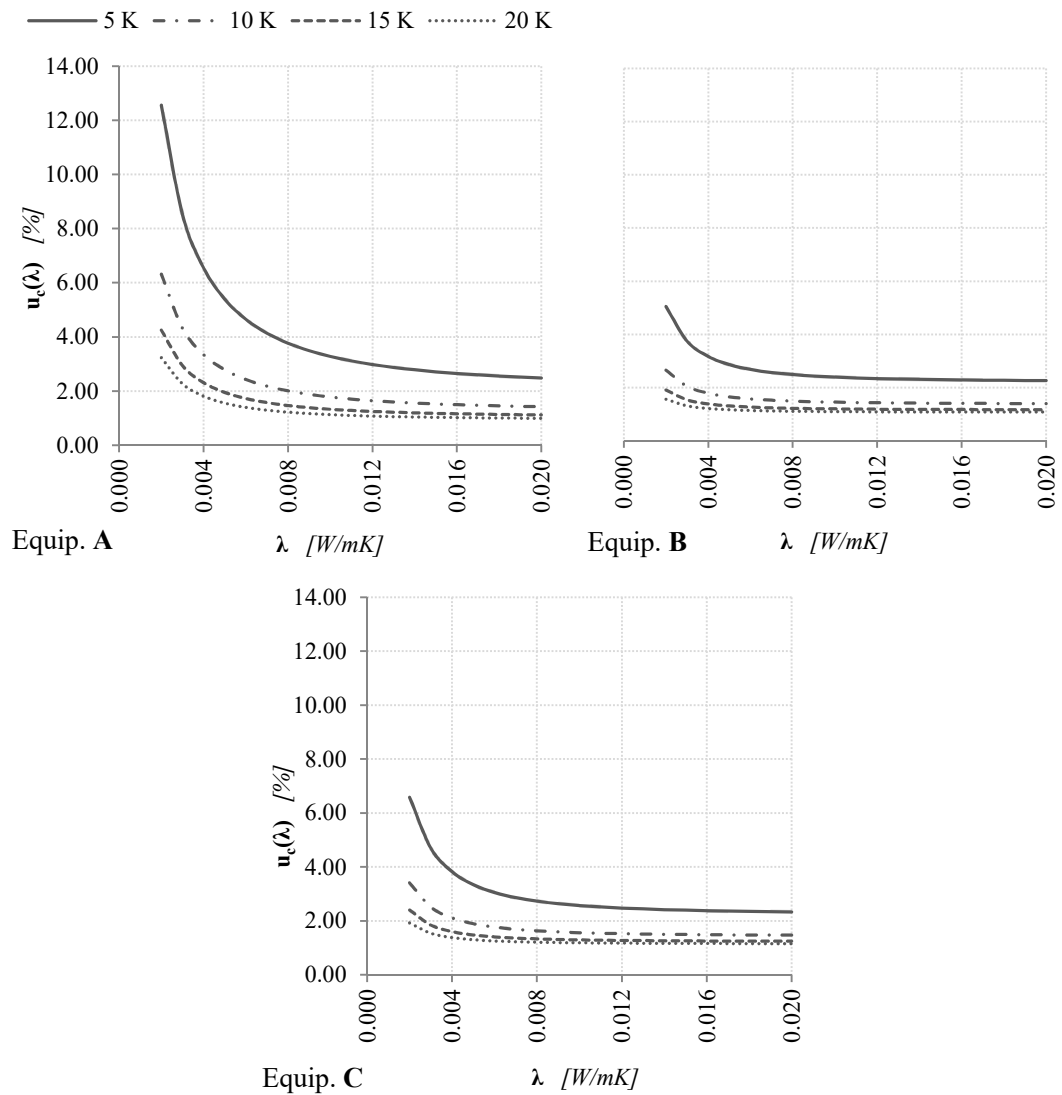


Figure A. 2: HFM - Combined relative uncertainty as a function of thermal conductivity and temperature difference, equipment A, B and C according to EN 1946-3:1999 [148] (sample thickness of 20 mm) [150]

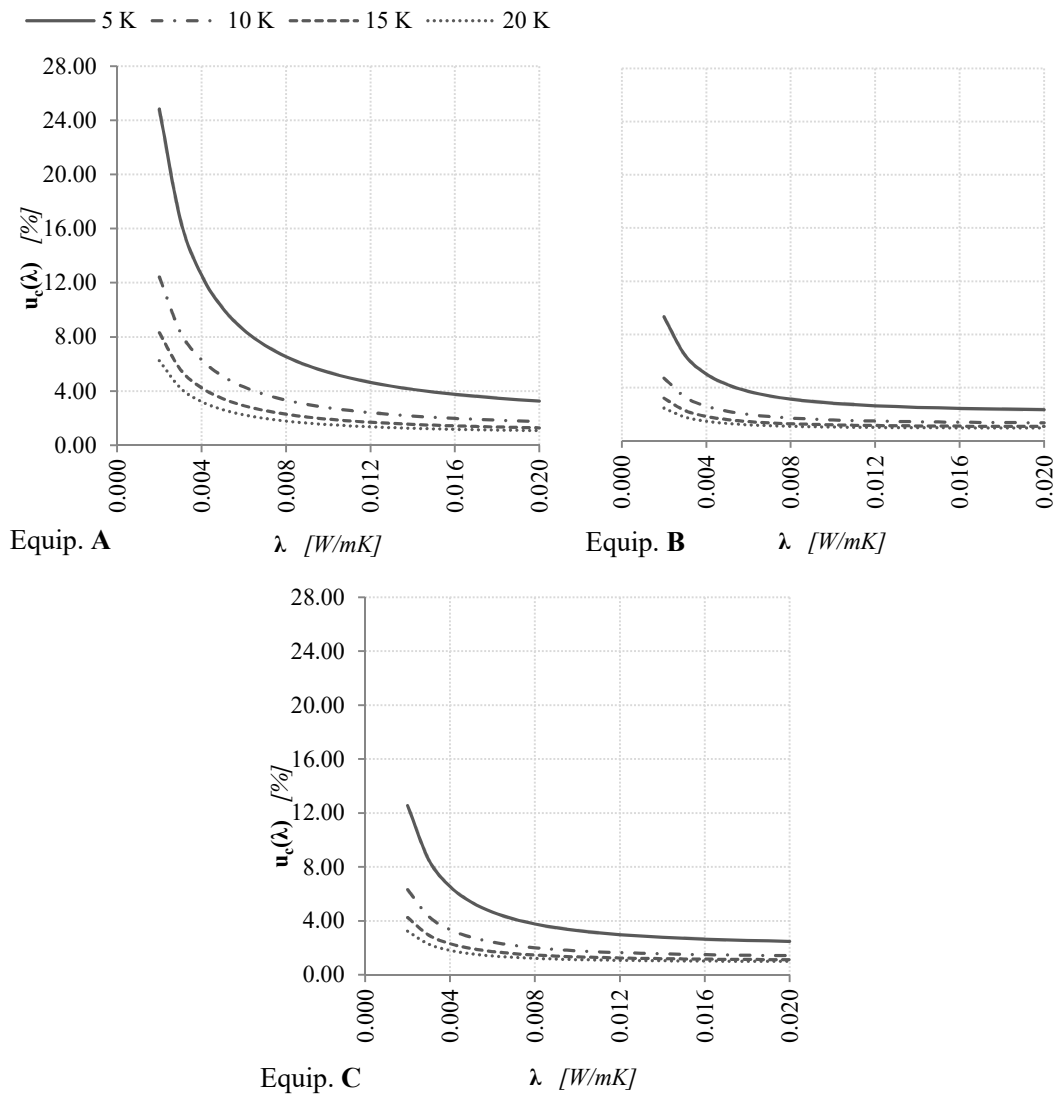


Figure A. 3: HFM - Combined relative uncertainty as a function of thermal conductivity and temperature difference, equipment A, B and C according to EN 1946-3:1999 [148] (sample thickness of 40 mm) [150]

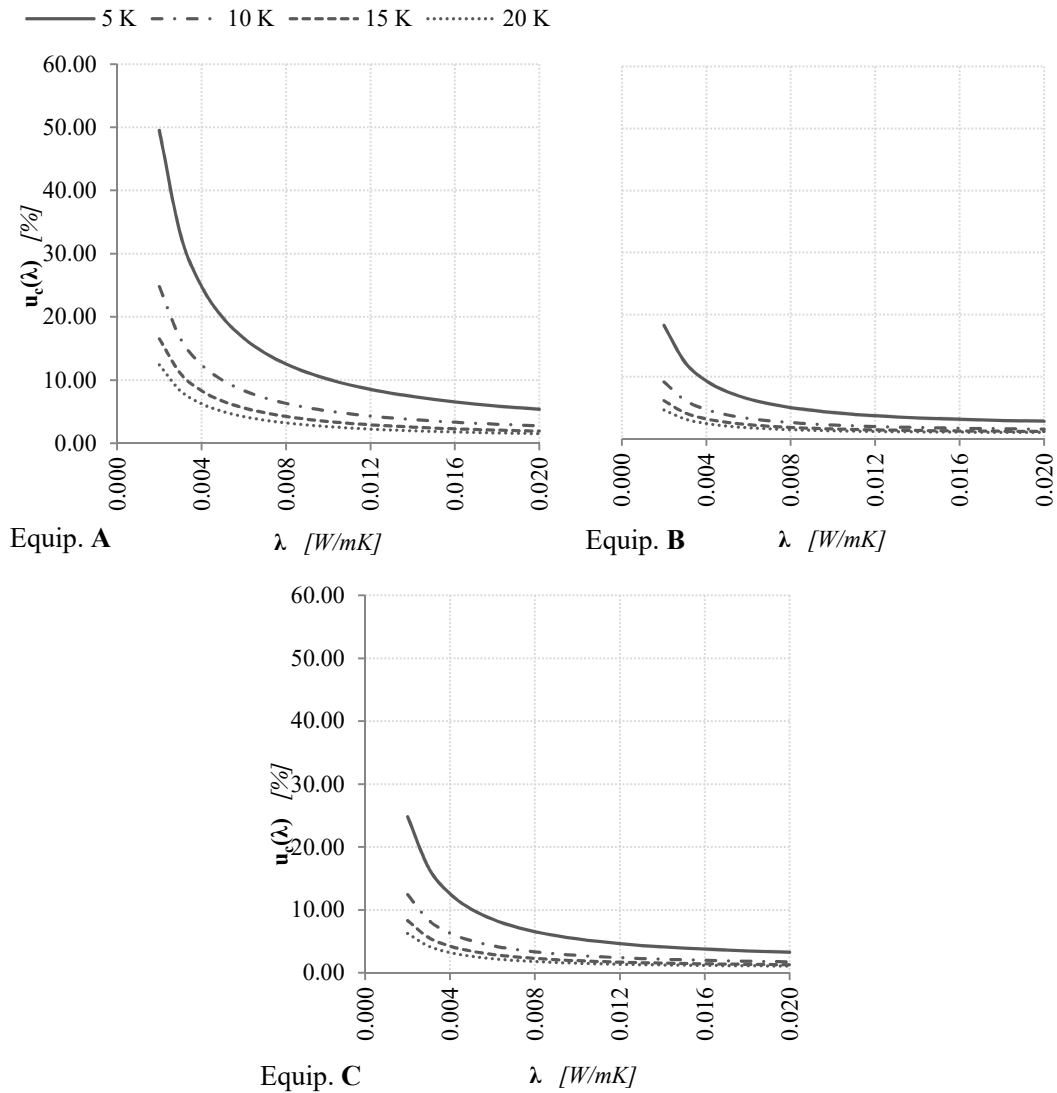


Figure A. 4: HFM - Combined relative uncertainty as a function of thermal conductivity and temperature difference, equipment A, B and C according to EN 1946-3:1999 [148] (sample thickness of 80 mm) [150]

Figure A. 1 to **Figure A. 4** show, for each analysed thickness, the effect of the different temperature difference on $u_c(\lambda)$, and the most relevant results are summarised in **Table 20** to **Table 22**.

Appendix B

Thermal conductivity uncertainty - HFM

An extended version of this appendix is available at the following link:

<http://dx.doi.org/10.17632/v9r5pkwkyg.2#file-05e249b5-ddec-4fc9-a98b-48c9838617cf>

Table B. 1: Type A $u_c(\lambda_{COP})$ assessment, by means of HFM-1 apparatus (Sample: FS based VIP 10 mm thick, $\vartheta_{avg} = 5^\circ\text{C}$, $\Delta\vartheta = 10^\circ\text{C}$)

Test conditions		f_{cal_upper}	f_{cal_lower}	$t_{measured}$	ϑ_{upper}	ϑ_{lower}	Q_{upper}	Q_{lower}	Φ_{upper}	Φ_{lower}	λ_{COP}
10 mm $\vartheta_{avg} = 5^\circ\text{C}$ $\Delta\vartheta = 10^\circ\text{C}$		$[W/m^2 \cdot \mu V]$	$[W/m^2 \cdot \mu V]$	$[mm]$	$[^\circ\text{C}]$	$[^\circ\text{C}]$	$[\mu V]$	$[\mu V]$	$[W/m^2]$	$[W/m^2]$	$[W/mK]$
Mean value	\bar{y}	0.0054	0.0055	10.297	0.015	10.011	-917.0	903.7	4.911	4.972	0.00509
Median		-	-	-	-	-	-916.5	904.0	4.908	4.971	-
Skew		-	-	-	-	-	-0.560	-0.747	0.589	-0.535	-
Standard deviation	s	-	-	-	-	-	4.2	2.7	0.022	0.015	-
Absolute uncertainty	$u(\bar{y})$	0.0001	0.0001	0.005	0.003	0.002	0.5	0.3	0.002	0.002	0.00007
Relative uncertainty	$u(\bar{y})$ [%]	2.00%	2.00%	0.05%	19.25%	0.02%	0.05%	0.03%	0.05%	0.03%	1.42%
Variation coefficient	V [%]	-	-	-	-	-	-0.46%	0.29%	0.45%	0.30%	-
Probability distribution					Triangular	Uniform	Triangular	Normal	Normal	Normal	Normal

Table B. 2: Type A $u_c(\lambda_{COP})$ sensitivity coefficients, by means of HFM-1 apparatus (Sample: FS based VIP 10 mm thick, $\vartheta_{avg} = 5^\circ\text{C}$, $\Delta\vartheta = 10^\circ\text{C}$)

	Sensitivity coefficients			
	$\partial\lambda_{COP}/\partial t$	$\partial\lambda_{COP}/\partial f_{cal}$	$\partial\lambda_{COP}/\partial Q$	$\partial\lambda_{COP}/\partial\Delta\vartheta$
Upper plate	0.491342	944.612745	0.005517	-0.506137
Lower plate	0.497324	930.912255	0.005667	-0.512300

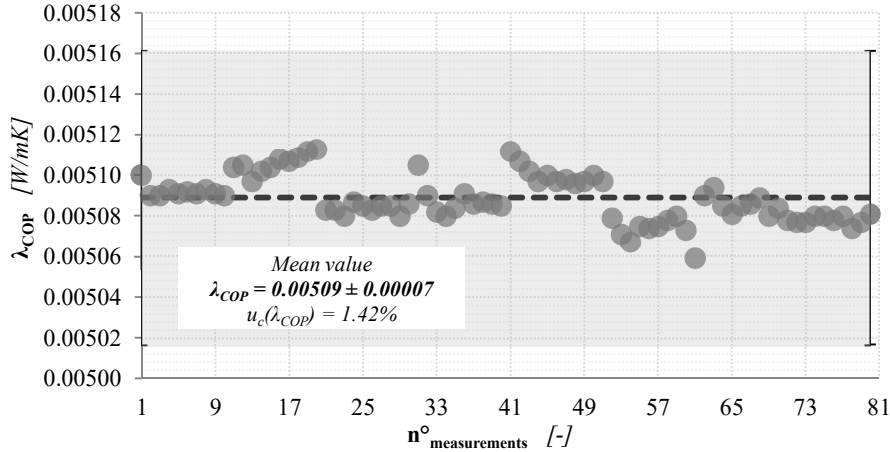


Figure B. 1: λ_{COP} -values assessed by means of HFM-1 apparatus (Sample: FS based VIP 10 mm thick, $\vartheta_{avg} = 5^\circ\text{C}$, $\Delta\vartheta = 10^\circ\text{C}$)

Table B. 3: Type A $u_c(\lambda_{COP})$ assessment, by means of HFM-1 apparatus (Sample: FS based VIP 10 mm thick, $\vartheta_{avg} = 5^\circ\text{C}$, $\Delta\vartheta = 20^\circ\text{C}$)

Test conditions		f_{cal_upper}	f_{cal_lower}	$t_{measured}$	ϑ_{upper}	ϑ_{lower}	Q_{upper}	Q_{lower}	Φ_{upper}	Φ_{lower}	λ_{COP}
10 mm $\vartheta_{avg} = 5^\circ\text{C}$ $\Delta\vartheta = 10^\circ\text{C}$		$[\text{W}/\text{m}^2 \cdot \mu\text{V}]$	$[\text{W}/\text{m}^2 \cdot \mu\text{V}]$	$[\text{mm}]$	$[\text{C}]$	$[\text{C}]$	$[\mu\text{V}]$	$[\mu\text{V}]$	$[\text{W}/\text{m}^2]$	$[\text{W}/\text{m}^2]$	$[\text{W}/\text{mK}]$
Mean value	\bar{y}	0.0054	0.0055	10.298	-4.982	15.013	-1826.2	1807.2	9.883	9.885	0.00509
Median		-	-	-	-	-	-1823.5	1807.0	9.868	9.886	-
Skew		-	-	-	-	-	-0.282	-0.854	0.273	-0.863	-
Standard deviation	s	-	-	-	-	-	7.2	4.2	0.039	0.023	-
Absolute uncertainty	$u(\bar{y})$	0.0001	0.0001	0.007	0.002	0.003	0.8	0.5	0.004	0.003	0.00007
Relative uncertainty	$\frac{u(\bar{y})}{\bar{y}}$ [%]	2.00%	2.00%	0.07%	0.04%	0.02%	0.04%	0.03%	0.04%	0.03%	1.42%
Variation coefficient	$\frac{V}{\bar{y}}$ [%]	-	-	-	-	-	-0.39%	0.23%	0.39%	0.24%	-
Probability distribution				Uniform Triangular Uniform Normal Normal Normal Normal							

Table B. 4: Type A $u_c(\lambda_{COP})$ sensitivity coefficients, by means of HFM-1 apparatus (Sample: FS based VIP 10 mm thick, $\vartheta_{avg} = 5^\circ\text{C}$, $\Delta\vartheta = 20^\circ\text{C}$)

	Sensitivity coefficients			
	$\partial\lambda_{COP}/\partial t$	$\partial\lambda_{COP}/\partial f_{cal}$	$\partial\lambda_{COP}/\partial Q$	$\partial\lambda_{COP}/\partial\Delta\vartheta$
Upper plate	0.494293	940.545516	0.002787	-0.254575
Lower plate	0.494393	930.759970	0.002817	-0.254627

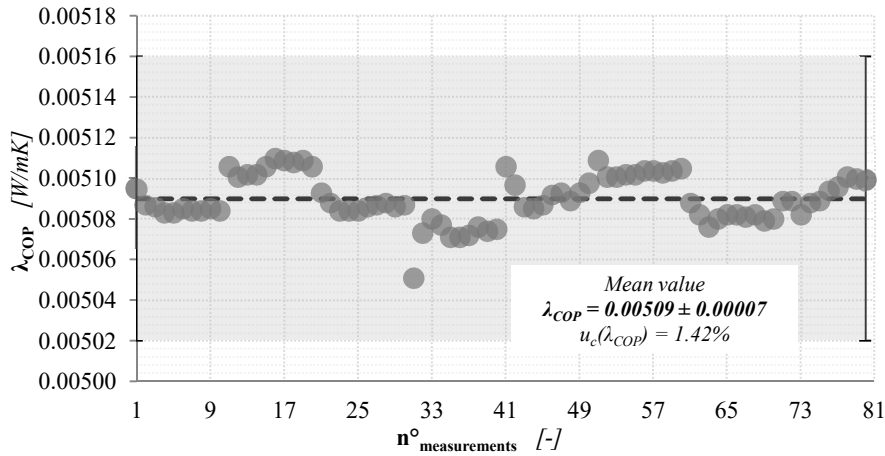
**Figure B. 2:** λ_{COP} -values assessed by means of HFM-1 apparatus (Sample: FS based VIP 10 mm thick, $\vartheta_{avg} = 5^\circ\text{C}$, $\Delta\vartheta = 20^\circ\text{C}$)

Table B. 5: Type A $u_c(\lambda_{COP})$ assessment, by means of HFM-1 apparatus (Sample: FS based VIP 10 mm thick, $\vartheta_{avg} = 5^\circ\text{C}$, $\Delta\vartheta = 30^\circ\text{C}$)

Test conditions		f_{cal_upper}	f_{cal_lower}	$t_{measured}$	ϑ_{upper}	ϑ_{lower}	Q_{upper}	Q_{lower}	Φ_{upper}	Φ_{lower}	λ_{COP}
10 mm $\vartheta_{avg} = 5^\circ\text{C}$ $\Delta\vartheta = 10^\circ\text{C}$		$[W/m^2 \cdot \mu V]$	$[W/m^2 \cdot \mu V]$	$[mm]$	$[^\circ\text{C}]$	$[^\circ\text{C}]$	$[\mu V]$	$[\mu V]$	$[W/m^2]$	$[W/m^2]$	$[W/mK]$
Mean value	\bar{y}	0.0055	0.0054	10.297	-9.962	20.034	-2718	2716.3	14.861	14.773	0.00509
Median		-	-	-	-	-	-2720	2717.5	14.870	14.780	-
Skew		-	-	-	-	-	0.108	-0.580	-0.113	-0.580	-
Standard deviation	s	-	-	-	-	-	10.0	5.9	0.055	0.033	-
Absolute uncertainty	$u(\bar{y})$	0.0001	0.0001	0.005	0.002	0.003	1.1	0.7	0.006	0.004	0.00007
Relative uncertainty	$\frac{u(\bar{y})}{\bar{y}}$ [%]	2.00%	2.00%	0.05%	0.02%	0.01%	0.04%	0.02%	0.04%	0.02%	1.41%
Variation coefficient	$\frac{V}{\bar{y}}$ [%]	-	-	-	-	-	-0.37%	0.22%	0.37%	0.22%	-
Probability distribution		Triangular Triangular Uniform Normal Normal Normal Normal									

Table B. 6: Type A $u_c(\lambda_{COP})$ sensitivity coefficients, by means of HFM-1 apparatus (Sample: FS based VIP 10 mm thick, $\vartheta_{avg} = 5^\circ\text{C}$, $\Delta\vartheta = 30^\circ\text{C}$)

	Sensitivity coefficients			
	$\partial\lambda_{COP}/\partial t$	$\partial\lambda_{COP}/\partial f_{cal}$	$\partial\lambda_{COP}/\partial Q$	$\partial\lambda_{COP}/\partial \Delta\vartheta$
Upper plate	0.495467	933.032604	0.001877	-0.170083
Lower plate	0.492531	932.449030	0.001867	-0.169076

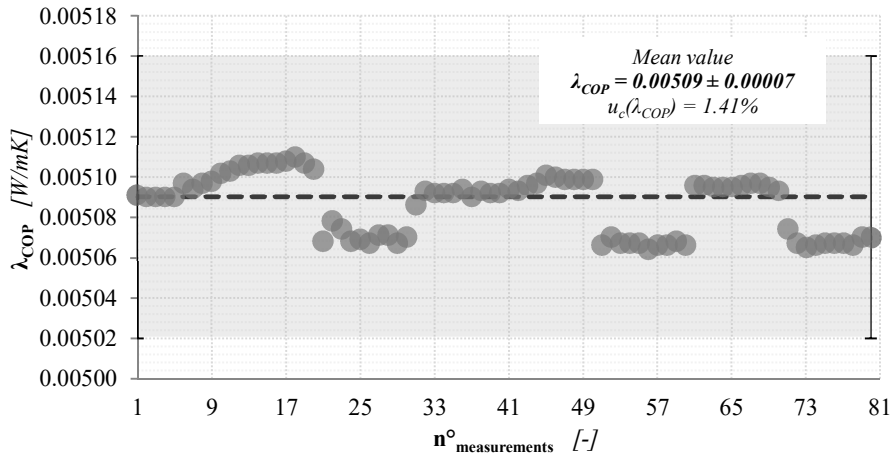


Figure B. 3: λ_{COP} -values assessed by means of HFM-1 apparatus (Sample: FS based VIP 10 mm thick, $\vartheta_{avg} = 5^\circ\text{C}$, $\Delta\vartheta = 30^\circ\text{C}$)

Table B. 7: Type A $u_c(\lambda_{COP})$ assessment, by means of HFM-1 apparatus (Sample: FS based VIP 10 mm thick, $\vartheta_{avg} = 5^\circ\text{C}$, $\Delta\vartheta = 40^\circ\text{C}$)

Test conditions		f_{cal_upper}	f_{cal_lower}	$t_{measured}$	ϑ_{upper}	ϑ_{lower}	Q_{upper}	Q_{lower}	Φ_{upper}	Φ_{lower}	λ_{COP}
10 mm $\vartheta_{avg} = 5^\circ\text{C}$ $\Delta\vartheta = 40^\circ\text{C}$		$[W/m^2 \cdot \mu V]$	$[W/m^2 \cdot \mu V]$	$[mm]$	$[^\circ\text{C}]$	$[^\circ\text{C}]$	$[\mu V]$	$[\mu V]$	$[W/m^2]$	$[W/m^2]$	$[W/mK]$
Mean value	\bar{y}	0.0055	0.0054	10.298	-14.987	25.022	-3584.5	3639.0	19.808	19.679	0.00508
Median		-	-	-	-	-	-3585.5	3639.0	19.810	19.680	-
Skew		-	-	-	-	-	-0.012	-0.823	0.033	-0.807	-
Standard deviation	s	-	-	-	-	-	8.0	4.4	0.045	0.023	-
Absolute uncertainty	$u(\bar{y})$	0.0001	0.0001	0.007	0.003	0.002	0.9	0.5	0.005	0.003	0.00007
Relative uncertainty	$\frac{u(\bar{y})}{\bar{y}}$ [%]	2.00%	2.00%	0.07%	0.02%	0.01%	0.03%	0.01%	0.03%	0.01%	1.42%
Variation coefficient	$\frac{V}{\bar{y}}$ [%]	-	-	-	-	-	-0.22%	0.12%	0.23%	0.12%	-
Probability distribution		Uniform Uniform Triangular Normal Normal Normal Normal									

Table B. 8: Type A $u_c(\lambda_{COP})$ sensitivity coefficients, by means of HFM-1 apparatus (Sample: FS based VIP 10 mm thick, $\vartheta_{avg} = 5^\circ\text{C}$, $\Delta\vartheta = 40^\circ\text{C}$)

	Sensitivity coefficients			
	$\partial\lambda_{COP}/\partial t$	$\partial\lambda_{COP}/\partial f_{cal}$	$\partial\lambda_{COP}/\partial Q$	$\partial\lambda_{COP}/\partial\Delta\vartheta$
Upper plate	0.495087	922.621935	0.001422	-0.127432
Lower plate	0.491882	936.649804	0.001392	-0.126607

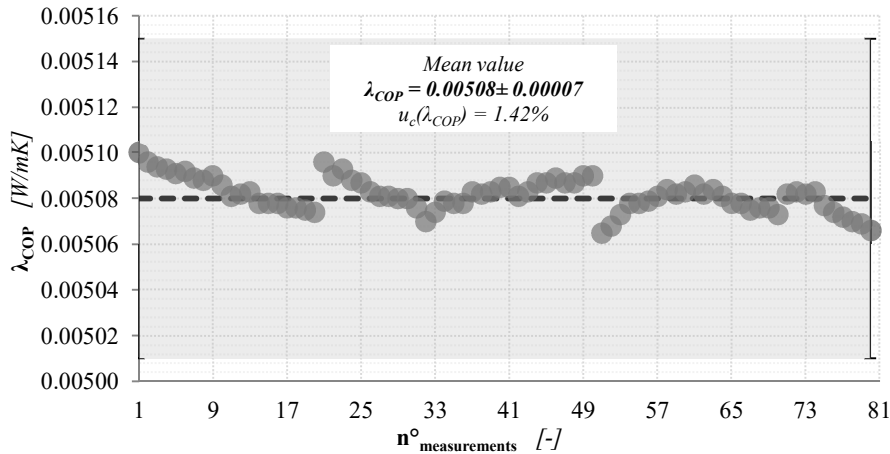
**Figure B. 4:** λ_{COP} -values assessed by means of HFM-1 apparatus (Sample: FS based VIP 10 mm thick, $\vartheta_{avg} = 5^\circ\text{C}$, $\Delta\vartheta = 40^\circ\text{C}$)

Table B. 9: Type A $u_c(\lambda_{COP})$ assessment, by means of HFM-1 apparatus (Sample: FS based VIP 10 mm thick, $\vartheta_{avg} = 10^\circ\text{C}$, $\Delta\vartheta = 10^\circ\text{C}$)

Test conditions		f_{cal_upper}	f_{cal_lower}	$t_{measured}$	ϑ_{upper}	ϑ_{lower}	Q_{upper}	Q_{lower}	Φ_{upper}	Φ_{lower}	λ_{COP}
10 mm $\vartheta_{avg} = 10^\circ\text{C}$ $\Delta\vartheta = 10^\circ\text{C}$		$[W/m^2 \cdot \mu V]$	$[W/m^2 \cdot \mu V]$	$[mm]$	$[^\circ\text{C}]$	$[^\circ\text{C}]$	$[\mu V]$	$[\mu V]$	$[W/m^2]$	$[W/m^2]$	$[W/mK]$
Mean value	\bar{y}	0.0053	0.0055	10.33	5.010	15.014	-937.7	922.6	4.966	5.045	0.00517
Median		-	-	-	-	-	-938.0	922.0	4.969	5.042	-
Skew		-	-	-	-	-	0.319	0.551	-0.295	0.645	-
Standard deviation	s	-	-	-	-	-	2.7	3.2	0.014	0.017	-
Absolute uncertainty	$u(\bar{y})$	0.0001	0.0001	0.03	0.002	0.003	0.3	0.4	0.002	0.002	0.00007
Relative uncertainty	$\frac{u(\bar{y})}{\bar{y}}$ [%]	2.00%	2.00%	0.25%	0.04%	0.02%	0.03%	0.04%	0.03%	0.04%	1.43%
Variation coefficient	$\frac{V}{\bar{y}}$ [%]	-	-	-	-	-	-0.29%	0.35%	0.29%	0.34%	-
Probability distribution				Uniform Triangular Uniform Normal Normal Normal Normal							

Table B. 10: Type A $u_c(\lambda_{COP})$ sensitivity coefficients, by means of HFM-1 apparatus (Sample: FS based VIP 10 mm thick, $\vartheta_{avg} = 10^\circ\text{C}$, $\Delta\vartheta = 10^\circ\text{C}$)

	Sensitivity coefficients			
	$\partial\lambda_{COP}/\partial t$	$\partial\lambda_{COP}/\partial f_{cal}$	$\partial\lambda_{COP}/\partial Q$	$\partial\lambda_{COP}/\partial \Delta\vartheta$
Upper plate	0.496407	968.256797	0.005469	-0.512584
Lower plate	0.504276	952.664734	0.005646	-0.520709

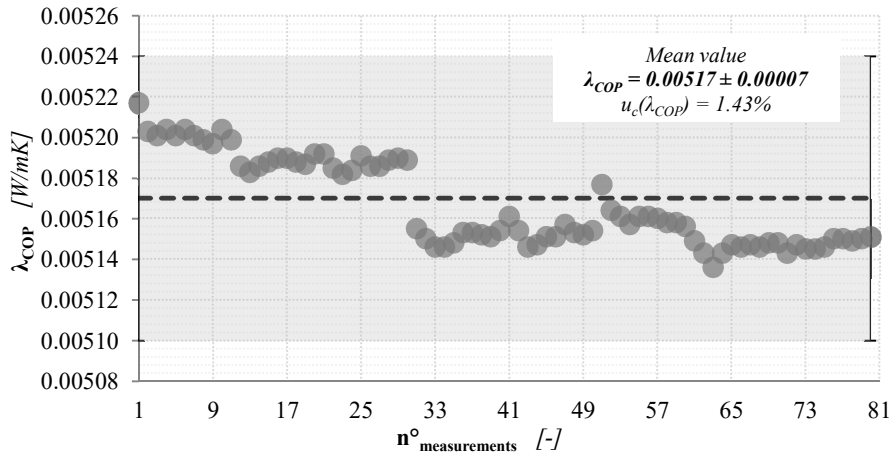


Figure B. 5: λ_{COP} -values assessed by means of HFM-1 apparatus (Sample: FS based VIP 10 mm thick, $\vartheta_{avg} = 10^\circ\text{C}$, $\Delta\vartheta = 10^\circ\text{C}$)

Table B. 11: Type A $u_c(\lambda_{COP})$ assessment, by means of HFM-1 apparatus (Sample: FS based VIP 10 mm thick, $\vartheta_{avg} = 10^\circ\text{C}$, $\Delta\vartheta = 20^\circ\text{C}$)

Test conditions		f_{cal_upper}	f_{cal_lower}	$t_{measured}$	ϑ_{upper}	ϑ_{lower}	Q_{upper}	Q_{lower}	Φ_{upper}	Φ_{lower}	λ_{COP}
10 mm $\vartheta_{avg} = 10^\circ\text{C}$ $\Delta\vartheta = 20^\circ\text{C}$		$[W/m^2 \cdot \mu V]$	$[W/m^2 \cdot \mu V]$	$[mm]$	$[^\circ\text{C}]$	$[^\circ\text{C}]$	$[\mu V]$	$[\mu V]$	$[W/m^2]$	$[W/m^2]$	$[W/mK]$
Mean value	\bar{y}	0.0054	0.0054	10.33	0.014	20.014	-1866.6	1843.4	9.997	10.025	0.00509
Median		-	-	-	-	-	-1867.0	1843.5	9.997	10.025	-
Skew		-	-	-	-	-	-0.612	-2.325	0.591	-2.284	-
Standard deviation	s	-	-	-	-	-	4.0	4.3	0.021	0.024	-
Absolute uncertainty	$u(\bar{y})$	0.0001	0.0001	0.03	0.003	0.003	0.4	0.5	0.002	0.003	0.00007
Relative uncertainty	$\frac{u(\bar{y})}{\bar{y}}$ [%]	2.00%	2.00%	0.25%	20.62%	0.01%	0.02%	0.03%	0.02%	0.03%	1.42%
Variation coefficient	$\frac{V}{\bar{y}}$ [%]	-	-	-	-	-	-0.22%	0.24%	0.21%	0.24%	-
Probability distribution				Uniform Uniform Uniform Normal Normal Normal Normal							

Table B. 12: Type A $u_c(\lambda_{COP})$ sensitivity coefficients, by means of HFM-1 apparatus (Sample: FS based VIP 10 mm thick, $\vartheta_{avg} = 10^\circ\text{C}$, $\Delta\vartheta = 20^\circ\text{C}$)

Sensitivity coefficients				
	$\partial\lambda_{COP}/\partial t$	$\partial\lambda_{COP}/\partial f_{cal}$	$\partial\lambda_{COP}/\partial Q$	$\partial\lambda_{COP}/\partial \Delta\vartheta$
Upper plate	0.499875	964.098900	0.002766	-0.258186
Lower plate	0.501220	952.116100	0.002809	-0.258880

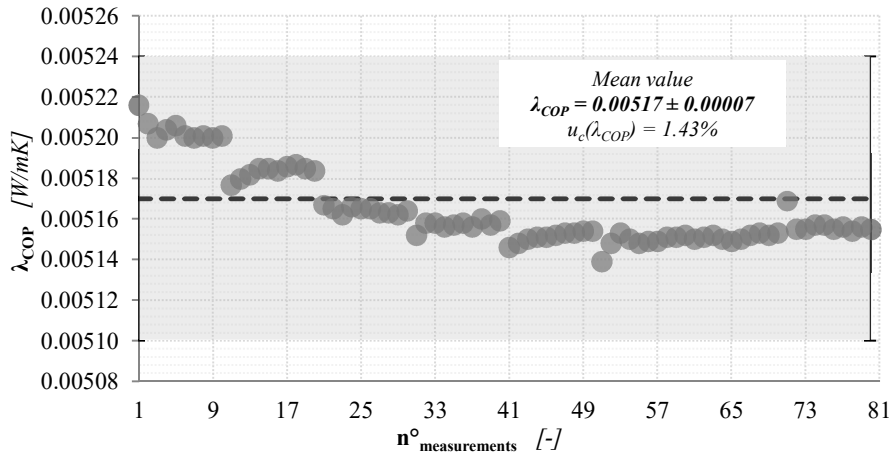


Figure B. 6: λ_{COP} -values assessed by means of HFM-1 apparatus (Sample: FS based VIP 10 mm thick, $\vartheta_{avg} = 10^\circ\text{C}$, $\Delta\vartheta = 20^\circ\text{C}$)

Table B. 13: Type A $u_c(\lambda_{COP})$ assessment, by means of HFM-1 apparatus (Sample: FS based VIP 10 mm thick, $\vartheta_{avg} = 10^\circ\text{C}$, $\Delta\vartheta = 30^\circ\text{C}$)

Test conditions		f_{cal_upper}	f_{cal_lower}	$t_{measured}$	ϑ_{upper}	ϑ_{lower}	Q_{upper}	Q_{lower}	Φ_{upper}	Φ_{lower}	λ_{COP}
10 mm $\vartheta_{avg} = 10^\circ\text{C}$ $\Delta\vartheta = 30^\circ\text{C}$		$[\text{W}/\text{m}^2;\mu\text{V}]$	$[\text{W}/\text{m}^2;\mu\text{V}]$	$[\text{mm}]$	$[\text{C}^\circ]$	$[\text{C}^\circ]$	$[\mu\text{V}]$	$[\mu\text{V}]$	$[\text{W}/\text{m}^2]$	$[\text{W}/\text{m}^2]$	$[\text{W}/\text{mK}]$
Mean value	\bar{y}	0.0054	0.0054	10.32	-4.982	25.020	-2780.4	2777.1	15.067	15.017	0.00517
Median		-	-	-	-	-	-2779.0	2777.0	15.060	15.020	-
Skew		-	-	-	-	-	-1.572	-0.610	1.547	-0.567	-
Standard deviation	s	-	-	-	-	-	8.3	4.7	0.045	0.026	-
Absolute uncertainty	$u(\bar{y})$	0.0001	0.0001	0.02	0.002	0.002	0.9	0.5	0.005	0.003	0.00007
Relative uncertainty	$\frac{u(\bar{y})}{\bar{y}}$ [%]	2.00%	2.00%	0.18%	0.04%	0.01%	0.03%	0.02%	0.03%	0.02%	1.42%
Variation coefficient	$\frac{V}{\bar{y}}$ [%]	-	-	-	-	-	-0.30%	0.17%	0.30%	0.17%	-
Probability distribution		Triangular Triangular Triangular Normal Normal Normal Normal									

Table B. 14: Type A $u_c(\lambda_{COP})$ sensitivity coefficients, by means of HFM-1 apparatus (Sample: FS based VIP 10 mm thick, $\vartheta_{avg} = 10^\circ\text{C}$, $\Delta\vartheta = 30^\circ\text{C}$)

	Sensitivity coefficients			
	$\partial\lambda_{COP}/\partial t$	$\partial\lambda_{COP}/\partial f_{cal}$	$\partial\lambda_{COP}/\partial Q$	$\partial\lambda_{COP}/\partial\Delta\vartheta$
Upper plate	0.502199	956.393840	0.001864	-0.172745
Lower plate	0.500493	955.258716	0.001860	-0.172158

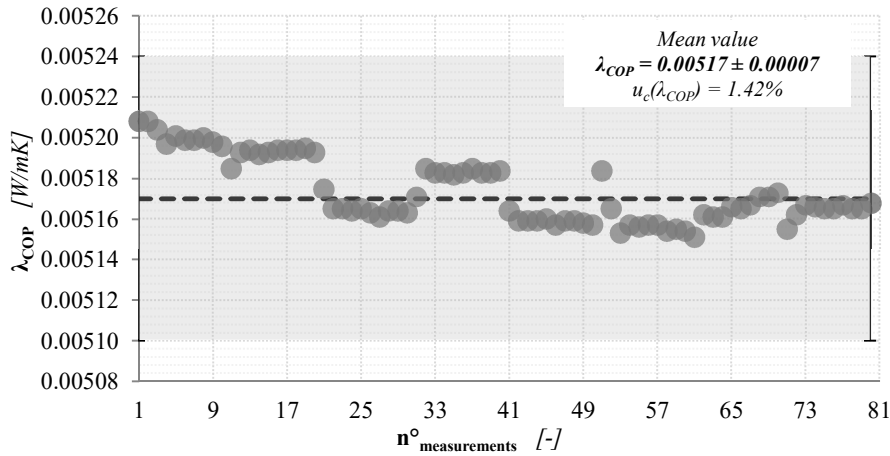


Figure B. 7: λ_{COP} -values assessed by means of HFM-1 apparatus (Sample: FS based VIP 10 mm thick, $\vartheta_{avg} = 10^\circ\text{C}$, $\Delta\vartheta = 30^\circ\text{C}$)

Table B. 15: Type A $u_c(\lambda_{COP})$ assessment, by means of HFM-1 apparatus (Sample: FS based VIP 10 mm thick, $\vartheta_{avg} = 10^\circ\text{C}$, $\Delta\vartheta = 40^\circ\text{C}$)

Test conditions		f_{cal_upper}	f_{cal_lower}	$t_{measured}$	ϑ_{upper}	ϑ_{lower}	Q_{upper}	Q_{lower}	Φ_{upper}	Φ_{lower}	λ_{COP}
10 mm $\vartheta_{avg} = 10^\circ\text{C}$ $\Delta\vartheta = 40^\circ\text{C}$		$[\text{W}/\text{m}^2;\mu\text{V}]$	$[\text{W}/\text{m}^2;\mu\text{V}]$	$[\text{mm}]$	$[\text{C}]$	$[\text{C}]$	$[\mu\text{V}]$	$[\mu\text{V}]$	$[\text{W}/\text{m}^2]$	$[\text{W}/\text{m}^2]$	$[\text{W}/\text{mK}]$
Mean value	\bar{y}	0.0055	0.0054	10.320	-9.962	30.039	-3671.0	3713.3	20.136	19.964	0.00517
Median		-	-	-	-	-	-3667.0	3713.0	20.110	19.960	-
Skew		-	-	-	-	-	-1.288	-0.607	1.268	-0.657	-
Standard deviation	s	-	-	-	-	-	8.4	7.2	0.047	0.039	-
Absolute uncertainty	$u(\bar{y})$	0.0001	0.0001	0.02	0.002	0.002	1.0	0.9	0.006	0.005	0.00007
Relative uncertainty	$\frac{u(\bar{y})}{\bar{y}}$ [%]	2.00%	2.00%	0.18%	0.02%	0.01%	0.03%	0.02%	0.03%	0.02%	1.42%
Variation coefficient	$\frac{V}{\bar{y}}$ [%]	-	-	-	-	-	-0.23%	0.19%	0.23%	0.20%	-
Probability distribution		Triangular Triangular Triangular Normal Normal Normal Normal									

Table B. 16: Type A $u_c(\lambda_{COP})$ sensitivity coefficients, by means of HFM-1 apparatus (Sample: FS based VIP 10 mm thick, $\vartheta_{avg} = 10^\circ\text{C}$, $\Delta\vartheta = 40^\circ\text{C}$)

	Sensitivity coefficients			
	$\partial\lambda_{COP}/\partial t$	$\partial\lambda_{COP}/\partial f_{cal}$	$\partial\lambda_{COP}/\partial Q$	$\partial\lambda_{COP}/\partial\Delta\vartheta$
Upper plate	0.503373	947.094323	0.001415	-0.129867
Lower plate	0.499055	958.007450	0.001387	-0.128753

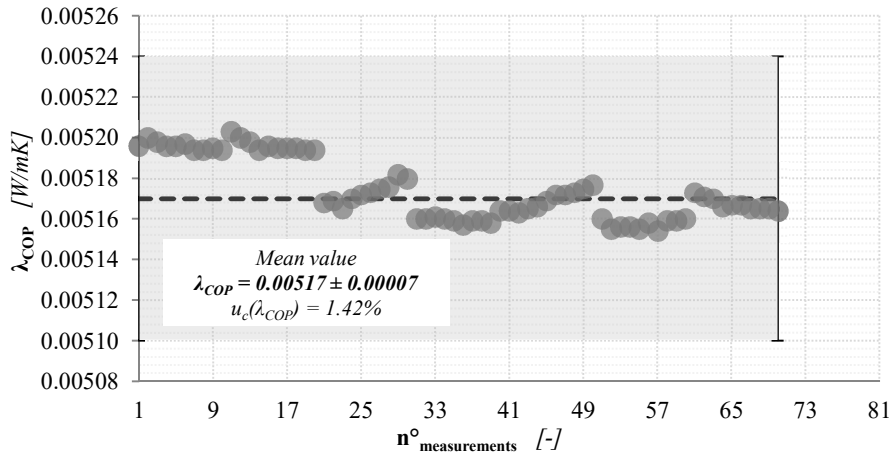
**Figure B. 8:** λ_{COP} -values assessed by means of HFM-1 apparatus (Sample: FS based VIP 10 mm thick, $\vartheta_{avg} = 10^\circ\text{C}$, $\Delta\vartheta = 40^\circ\text{C}$)

Table B. 17: Type A $u_c(\lambda_{COP})$ assessment, by means of HFM-1 apparatus (Sample: FS based VIP 10 mm thick, $\vartheta_{avg} = 23^\circ\text{C}$, $\Delta\vartheta = 10^\circ\text{C}$)

Test conditions		f_{cal_upper}	f_{cal_lower}	$t_{measured}$	ϑ_{upper}	ϑ_{lower}	Q_{upper}	Q_{lower}	Φ_{upper}	Φ_{lower}	λ_{COP}
10 mm $\vartheta_{avg} = 23^\circ\text{C}$ $\Delta\vartheta = 10^\circ\text{C}$		$[W/m^2 \cdot \mu V]$	$[W/m^2 \cdot \mu V]$	$[mm]$	$[^\circ\text{C}]$	$[^\circ\text{C}]$	$[\mu V]$	$[\mu V]$	$[W/m^2]$	$[W/m^2]$	$[W/mK]$
Mean value	\bar{y}	0.0052	0.0054	10.335	18.018	28.014	-1060.9	979.2	5.468	5.277	0.00555
Median		-	-	-	-	-	-1061.0	980.0	5.469	5.279	-
Skew		-	-	-	-	-	-1.301	-2.218	1.206	-2.344	-
Standard deviation	s	-	-	-	-	-	2.9	3.2	0.015	0.018	-
Absolute uncertainty	$u(\bar{y})$	0.0001	0.0001	0.003	0.003	0.003	0.3	0.4	0.002	0.002	0.00008
Relative uncertainty	$\frac{u(\bar{y})}{\bar{y}}$ [%]	2.00%	2.00%	0.03%	0.02%	0.01%	0.03%	0.04%	0.03%	0.04%	1.42%
Variation coefficient	$\frac{V}{\bar{y}}$ [%]	-	-	-	-	-	-0.27%	0.33%	0.27%	0.33%	-
Probability distribution				Triangular Uniform Uniform Normal Normal Normal Normal							

Table B. 18: Type A $u_c(\lambda_{COP})$ sensitivity coefficients, by means of HFM-1 apparatus (Sample: FS based VIP 10 mm thick, $\vartheta_{avg} = 23^\circ\text{C}$, $\Delta\vartheta = 10^\circ\text{C}$)

	Sensitivity coefficients			
	$\partial\lambda_{COP}/\partial t$	$\partial\lambda_{COP}/\partial f_{cal}$	$\partial\lambda_{COP}/\partial Q$	$\partial\lambda_{COP}/\partial\Delta\vartheta$
Upper plate	0.547007	1096.878902	0.005329	-0.565558
Lower plate	0.527902	1012.408163	0.005572	-0.545805

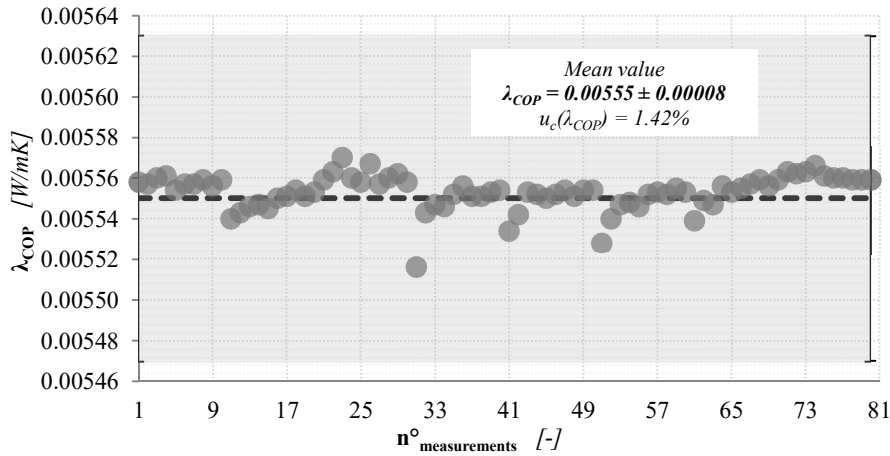


Figure B. 9: λ_{COP} -values assessed by means of HFM-1 apparatus (Sample: FS based VIP 10 mm thick, $\vartheta_{avg} = 23^\circ\text{C}$, $\Delta\vartheta = 10^\circ\text{C}$)

Table B. 19: Type A $u_c(\lambda_{COP})$ assessment, by means of HFM-1 apparatus (Sample: FS based VIP 10 mm thick, $\vartheta_{avg} = 23^\circ\text{C}$, $\Delta\vartheta = 20^\circ\text{C}$)

Test conditions		f_{cal_upper}	f_{cal_lower}	$t_{measured}$	ϑ_{upper}	ϑ_{lower}	Q_{upper}	Q_{lower}	Φ_{upper}	Φ_{lower}	λ_{COP}
10 mm $\vartheta_{avg} = 23^\circ\text{C}$ $\Delta\vartheta = 20^\circ\text{C}$		$[\text{W/m}^2;\mu\text{V}]$	$[\text{W/m}^2;\mu\text{V}]$	$[\text{mm}]$	$[\text{C}^\circ]$	$[\text{C}^\circ]$	$[\mu\text{V}]$	$[\mu\text{V}]$	$[\text{W/m}^2]$	$[\text{W/m}^2]$	$[\text{W/mK}]$
Mean value	\bar{y}	0.0052	0.0054	10.336	13.019	33.019	-2078.5	1985.4	10.821	10.638	0.00509
Median		-	-	-	-	-	-2078.0	1986.0	10.820	10.640	-
Skew		-	-	-	-	-	-2.374	-1.628	2.243	-1.778	-
Standard deviation	s	-	-	-	-	-	2.5	4.6	0.013	0.025	-
Absolute uncertainty	$u(\bar{y})$	0.0001	0.0001	0.003	0.002	0.002	0.3	0.5	0.002	0.003	0.00007
Relative uncertainty	$\frac{u(\bar{y})}{\bar{y}}$ [%]	2.00%	2.00%	0.03%	0.02%	0.01%	0.01%	0.03%	0.01%	0.03%	1.42%
Variation coefficient	$\frac{V}{\bar{y}}$ [%]	-	-	-	-	-	-0.12%	0.23%	0.12%	0.23%	-
Probability distribution				Triangular Triangular Triangular Normal Normal Normal Normal							

Table B. 20: Type A $u_c(\lambda_{COP})$ sensitivity coefficients, by means of HFM-1 apparatus (Sample: FS based VIP 10 mm thick, $\vartheta_{avg} = 23^\circ\text{C}$, $\Delta\vartheta = 20^\circ\text{C}$)

	Sensitivity coefficients			
	$\partial\lambda_{COP}/\partial t$	$\partial\lambda_{COP}/\partial f_{cal}$	$\partial\lambda_{COP}/\partial Q$	$\partial\lambda_{COP}/\partial\Delta\vartheta$
Upper plate	0.541034	1074.168800	0.002690	-0.279606
Lower plate	0.531889	1026.054720	0.002769	-0.274880

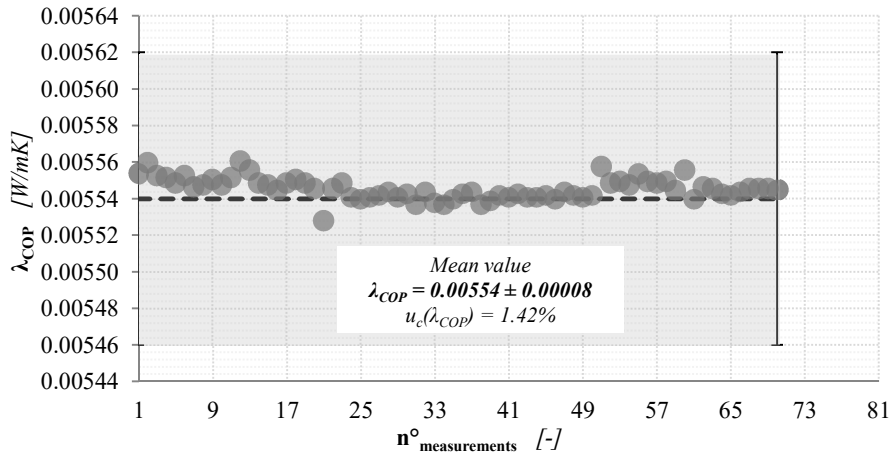


Figure B. 10: λ_{COP} -values assessed by means of HFM-1 apparatus (Sample: FS based VIP 10 mm thick, $\vartheta_{avg} = 23^\circ\text{C}$, $\Delta\vartheta = 20^\circ\text{C}$)

Table B. 21: Type A $u_c(\lambda_{COP})$ assessment, by means of HFM-1 apparatus (Sample: FS based VIP 10 mm thick, $\vartheta_{avg} = 23^\circ\text{C}$, $\Delta\vartheta = 30^\circ\text{C}$)

Test conditions		f_{cal_upper}	f_{cal_lower}	$t_{measured}$	ϑ_{upper}	ϑ_{lower}	Q_{upper}	Q_{lower}	Φ_{upper}	Φ_{lower}	λ_{COP}
10 mm $\vartheta_{avg} = 23^\circ\text{C}$ $\Delta\vartheta = 30^\circ\text{C}$		$[\text{W}/\text{m}^2;\mu\text{V}]$	$[\text{W}/\text{m}^2;\mu\text{V}]$	$[\text{mm}]$	$[\text{C}^\circ]$	$[\text{C}^\circ]$	$[\mu\text{V}]$	$[\mu\text{V}]$	$[\text{W}/\text{m}^2]$	$[\text{W}/\text{m}^2]$	$[\text{W}/\text{mK}]$
Mean value	\bar{y}	0.0053	0.0053	10.336	8.010	38.020	-3073.6	2998.1	16.171	15.971	0.00553
Median		-	-	-	-	-	-3073.0	2998.5	16.170	15.970	-
Skew		-	-	-	-	-	-1.416	-0.103	1.559	-0.238	-
Standard deviation	s	-	-	-	-	-	3.1	4.5	0.016	0.024	-
Absolute uncertainty	$u(\bar{y})$	0.0001	0.0001	0.003	0.002	0.002	0.4	0.5	0.002	0.003	0.00008
Relative uncertainty	$\frac{u(\bar{y})}{\bar{y}}$ [%]	2.00%	2.00%	0.03%	0.03%	0.01%	0.01%	0.02%	0.01%	0.02%	1.41%
Variation coefficient	$\frac{V}{\bar{y}}$ [%]	-	-	-	-	-	-0.10%	0.15%	0.10%	0.15%	-
Probability distribution		Triangular Triangular Triangular Normal Normal Normal Normal									

Table B. 22: Type A $u_c(\lambda_{COP})$ sensitivity coefficients, by means of HFM-1 apparatus (Sample: FS based VIP 10 mm thick, $\vartheta_{avg} = 23^\circ\text{C}$, $\Delta\vartheta = 30^\circ\text{C}$)

Sensitivity coefficients				
	$\partial\lambda_{COP}/\partial t$	$\partial\lambda_{COP}/\partial f_{cal}$	$\partial\lambda_{COP}/\partial Q$	$\partial\lambda_{COP}/\partial\Delta\vartheta$
Upper plate	0.538827	1058.604785	0.001812	-0.185582
Lower plate	0.532185	1032.601186	0.001835	-0.183294

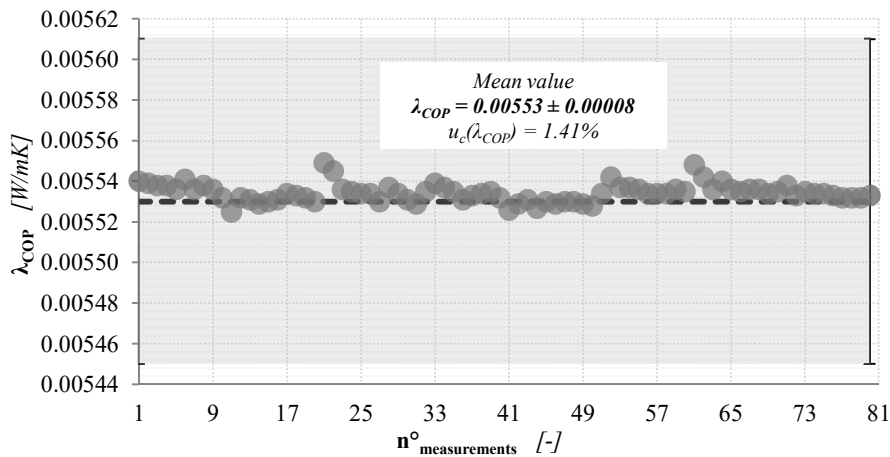


Figure B. 11: λ_{COP} -values assessed by means of HFM-1 apparatus (Sample: FS based VIP 10 mm thick, $\vartheta_{avg} = 23^\circ\text{C}$, $\Delta\vartheta = 30^\circ\text{C}$)

Table B. 23: Type A $u_c(\lambda_{COP})$ assessment, by means of HFM-1 apparatus (Sample: FS based VIP 10 mm thick, $\vartheta_{avg} = 23^\circ\text{C}$, $\Delta\vartheta = 40^\circ\text{C}$)

Test conditions		f_{cal_upper}	f_{cal_lower}	$t_{measured}$	ϑ_{upper}	ϑ_{lower}	Q_{upper}	Q_{lower}	Φ_{upper}	Φ_{lower}	λ_{COP}
10 mm $\vartheta_{avg} = 5^\circ\text{C}$ $\Delta\vartheta = 10^\circ\text{C}$		$[W/m^2 \cdot \mu V]$	$[W/m^2 \cdot \mu V]$	$[mm]$	$[^\circ\text{C}]$	$[^\circ\text{C}]$	$[\mu V]$	$[\mu V]$	$[W/m^2]$	$[W/m^2]$	$[W/mK]$
Mean value	\bar{y}	0.0053	0.0053	10.335	3.010	43.024	-4038.7	4011.3	21.483	21.242	0.00552
Median		-	-	-	-	-	-4038.5	4011.0	21.480	21.240	-
Skew		-	-	-	-	-	-1.401	0.128	1.126	0.113	-
Standard deviation	s	-	-	-	-	-	3.8	4.4	0.021	0.024	-
Absolute uncertainty	$u(\bar{y})$	0.0001	0.0001	0.003	0.002	0.003	0.4	0.5	0.002	0.003	0.00008
Relative uncertainty	$\frac{u(\bar{y})}{\bar{y}}$ [%]	2.00%	2.00%	0.03%	0.07%	0.01%	0.01%	0.01%	0.01%	0.01%	1.41%
Variation coefficient	$\frac{V}{\bar{y}}$ [%]	-	-	-	-	-	-0.09%	0.11%	0.10%	0.11%	-
Probability distribution		Triangular Triangular Uniform Normal Normal Normal Normal									

Table B. 24: Type A $u_c(\lambda_{COP})$ sensitivity coefficients, by means of HFM-1 apparatus (Sample: FS based VIP 10 mm thick, $\vartheta_{avg} = 23^\circ\text{C}$, $\Delta\vartheta = 40^\circ\text{C}$)

	Sensitivity coefficients			
	$\partial\lambda_{COP}/\partial t$	$\partial\lambda_{COP}/\partial f_{cal}$	$\partial\lambda_{COP}/\partial Q$	$\partial\lambda_{COP}/\partial \Delta\vartheta$
Upper plate	0.536858	1043.134016	0.001374	-0.138662
Lower plate	0.530910	1036.057018	0.001368	-0.137126

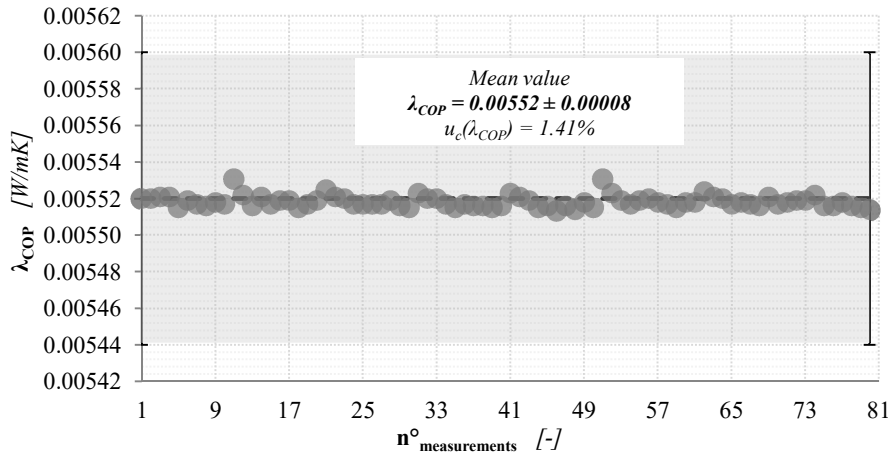
**Figure B. 12:** λ_{COP} -values assessed by means of HFM-1 apparatus (Sample: FS based VIP 10 mm thick, $\vartheta_{avg} = 23^\circ\text{C}$, $\Delta\vartheta = 40^\circ\text{C}$)

Table B. 25: Type A $u_c(\lambda_{COP})$ assessment, by means of HFM-1 apparatus (Sample: FS based VIP 10 mm thick, $\vartheta_{avg} = 40^\circ\text{C}$, $\Delta\vartheta = 10^\circ\text{C}$)

Test conditions		f_{cal_upper}	f_{cal_lower}	$t_{measured}$	ϑ_{upper}	ϑ_{lower}	Q_{upper}	Q_{lower}	Φ_{upper}	Φ_{lower}	λ_{COP}
10 mm $\vartheta_{avg} = 40^\circ\text{C}$ $\Delta\vartheta = 10^\circ\text{C}$		$[\text{W}/\text{m}^2 \cdot \mu\text{V}]$	$[\text{W}/\text{m}^2 \cdot \mu\text{V}]$	$[\text{mm}]$	$[\text{C}^\circ]$	$[\text{C}^\circ]$	$[\mu\text{V}]$	$[\mu\text{V}]$	$[\text{W}/\text{m}^2]$	$[\text{W}/\text{m}^2]$	$[\text{W}/\text{mK}]$
Mean value	\bar{y}	0.0050	0.0053	10.37	35.020	45.021	-1275.9	1117.2	6.383	5.902	0.00637
Median		-	-	-	-	-	-1276.5	1117.0	6.386	5.902	-
Skew		-	-	-	-	-	1.138	-0.376	-1.219	-0.324	-
Standard deviation	s	-	-	-	-	-	3.6	3.2	0.018	0.017	-
Absolute uncertainty	$u(\bar{y})$	0.0001	0.0001	0.02	0.002	0.002	0.4	0.4	0.002	0.002	0.00009
Relative uncertainty	$u(\bar{y})$ [%]	2.00%	2.00%	0.15%	0.01%	0.005%	0.03%	0.03%	0.03%	0.03%	1.42%
Variation coefficient	V [%]	-	-	-	-	-	-0.28%	0.28%	0.28%	0.28%	-
Probability distribution					Triangular	Triangular	Triangular	Normal	Normal	Normal	Normal

Table B. 26: Type A $u_c(\lambda_{COP})$ sensitivity coefficients, by means of HFM-1 apparatus (Sample: FS based VIP 10 mm thick, $\vartheta_{avg} = 40^\circ\text{C}$, $\Delta\vartheta = 10^\circ\text{C}$)

	Sensitivity coefficients			
	$\partial\lambda_{COP}/\partial t$	$\partial\lambda_{COP}/\partial f_{cal}$	$\partial\lambda_{COP}/\partial Q$	$\partial\lambda_{COP}/\partial \Delta\vartheta$
Upper plate	0.638269	1322.976002	0.005188	-0.661819
Lower plate	0.590158	1158.420558	0.005478	-0.611932

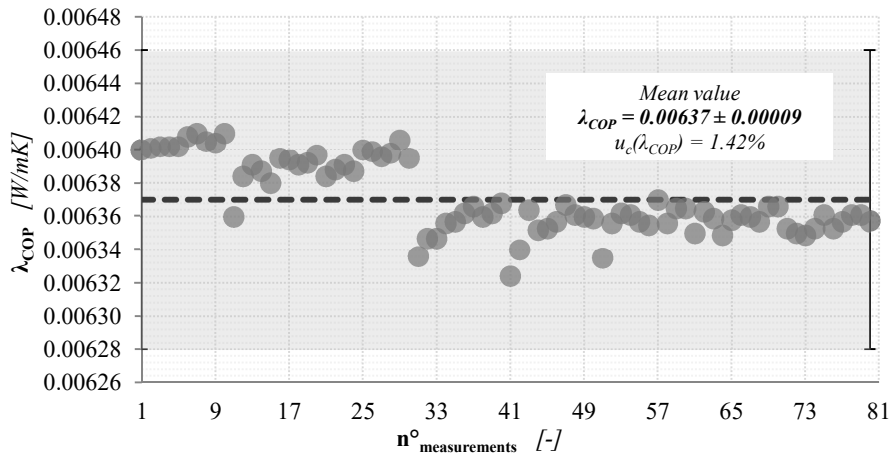


Figure B. 13: λ_{COP} -values assessed by means of HFM-1 apparatus (Sample: FS based VIP 10 mm thick, $\vartheta_{avg} = 40^\circ\text{C}$, $\Delta\vartheta = 10^\circ\text{C}$)

Table B. 27: Type A $u_c(\lambda_{COP})$ assessment, by means of HFM-1 apparatus (Sample: FS based VIP 10 mm thick, $\vartheta_{avg} = 40^\circ\text{C}$, $\Delta\vartheta = 20^\circ\text{C}$)

Test conditions		f_{cal_upper}	f_{cal_lower}	$t_{measured}$	ϑ_{upper}	ϑ_{lower}	Q_{upper}	Q_{lower}	Φ_{upper}	Φ_{lower}	λ_{COP}
10 mm $\vartheta_{avg} = 40^\circ\text{C}$ $\Delta\vartheta = 20^\circ\text{C}$		$[\text{W}/\text{m}^2 \cdot \mu\text{V}]$	$[\text{W}/\text{m}^2 \cdot \mu\text{V}]$	$[\text{mm}]$	$[\text{C}^\circ]$	$[\text{C}^\circ]$	$[\mu\text{V}]$	$[\mu\text{V}]$	$[\text{W}/\text{m}^2]$	$[\text{W}/\text{m}^2]$	$[\text{W}/\text{mK}]$
Mean value	\bar{y}	0.0050	0.0053	10.37	30.020	50.021	-2465.4	2291.9	12.434	12.036	0.00634
Median		-	-	-	-	-	-2466.0	2291.5	12.440	12.030	-
Skew		-	-	-	-	-	0.687	0.419	-0.598	0.427	-
Standard deviation	s	-	-	-	-	-	2.9	5.3	0.015	0.028	-
Absolute uncertainty	$u(\bar{y})$	0.0001	0.0001	0.02	0.002	0.002	0.3	0.6	0.002	0.003	0.00009
Relative uncertainty	$u(\bar{y})$ [%]	2.00%	2.00%	0.15%	0.01%	0.004%	0.01%	0.03%	0.01%	0.03%	1.42%
Variation coefficient	V [%]	-	-	-	-	-	-0.12%	0.23%	0.12%	0.23%	-
Probability distribution					Triangular	Triangular	Triangular	Normal	Normal	Normal	Normal

Table B. 28: Type A $u_c(\lambda_{COP})$ sensitivity coefficients, by means of HFM-1 apparatus (Sample: FS based VIP 10 mm thick, $\vartheta_{avg} = 40^\circ\text{C}$, $\Delta\vartheta = 20^\circ\text{C}$)

	Sensitivity coefficients			
	$\partial\lambda_{COP}/\partial t$	$\partial\lambda_{COP}/\partial f_{cal}$	$\partial\lambda_{COP}/\partial Q$	$\partial\lambda_{COP}/\partial\Delta\vartheta$
Upper plate	0.621620	1278.245988	0.002615	-0.322294
Lower plate	0.601823	1188.290735	0.002723	-0.312030

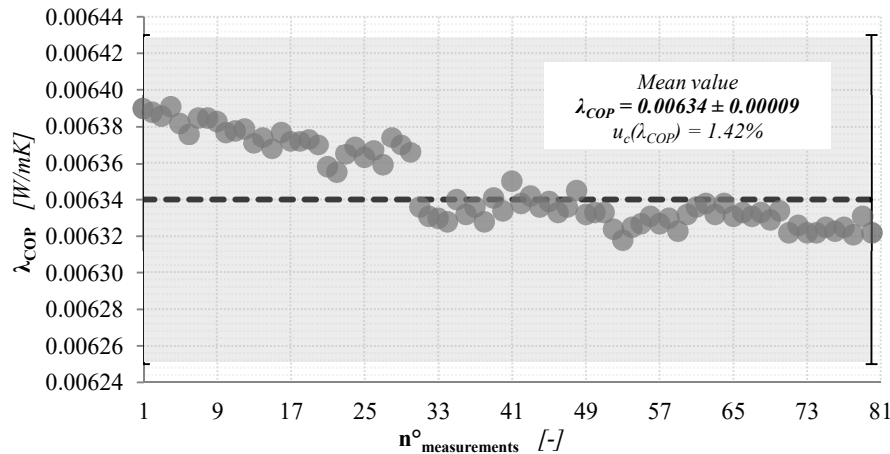
**Figure B. 14:** λ_{COP} -values assessed by means of HFM-1 apparatus (Sample: FS based VIP 10 mm thick, $\vartheta_{avg} = 40^\circ\text{C}$, $\Delta\vartheta = 20^\circ\text{C}$)

Table B. 29: Type A $u_c(\lambda_{COP})$ assessment, by means of HFM-1 apparatus (Sample: FS based VIP 10 mm thick, $\vartheta_{avg} = 40^\circ\text{C}$, $\Delta\vartheta = 30^\circ\text{C}$)

Test conditions		f_{cal_upper}	f_{cal_lower}	$t_{measured}$	ϑ_{upper}	ϑ_{lower}	Q_{upper}	Q_{lower}	Φ_{upper}	Φ_{lower}	λ_{COP}
10 mm $\vartheta_{avg} = 5^\circ\text{C}$ $\Delta\vartheta = 10^\circ\text{C}$		$[\text{W}/\text{m}^2 \cdot \mu\text{V}]$	$[\text{W}/\text{m}^2 \cdot \mu\text{V}]$	$[\text{mm}]$	$[\text{C}^\circ]$	$[\text{C}^\circ]$	$[\mu\text{V}]$	$[\mu\text{V}]$	$[\text{W}/\text{m}^2]$	$[\text{W}/\text{m}^2]$	$[\text{W}/\text{mK}]$
Mean value	\bar{y}	0.0051	0.0052	10.36	25.022	55.021	-3617.6	3459.3	18.403	18.057	0.00630
Median		-	-	-	-	-	-3617.0	3460.0	18.400	18.060	-
Skew		-	-	-	-	-	-0.153	0.071	0.188	0.127	-
Standard deviation	s	-	-	-	-	-	3.2	8.0	0.017	0.042	-
Absolute uncertainty	$u(\bar{y})$	0.0001	0.0001	0.02	0.002	0.004	0.4	0.9	0.002	0.005	0.00009
Relative uncertainty	$u(\bar{y})$ [%]	2.00%	2.00%	0.16%	0.01%	0.01%	0.01%	0.03%	0.01%	0.03%	1.42%
Variation coefficient	V [%]	-	-	-	-	-	-0.09%	0.23%	0.09%	0.23%	-
Probability distribution					Triangular	Triangular	Triangular	Normal	Normal	Normal	Normal

Table B. 30: Type A $u_c(\lambda_{COP})$ sensitivity coefficients, by means of HFM-1 apparatus (Sample: FS based VIP 10 mm thick, $\vartheta_{avg} = 40^\circ\text{C}$, $\Delta\vartheta = 30^\circ\text{C}$)

Sensitivity coefficients				
	$\partial\lambda_{COP}/\partial t$	$\partial\lambda_{COP}/\partial f_{cal}$	$\partial\lambda_{COP}/\partial Q$	$\partial\lambda_{COP}/\partial \Delta\vartheta$
Upper plate	0.613445	1249.319511	0.001757	-0.211850
Lower plate	0.601938	1194.651422	0.001803	-0.207876

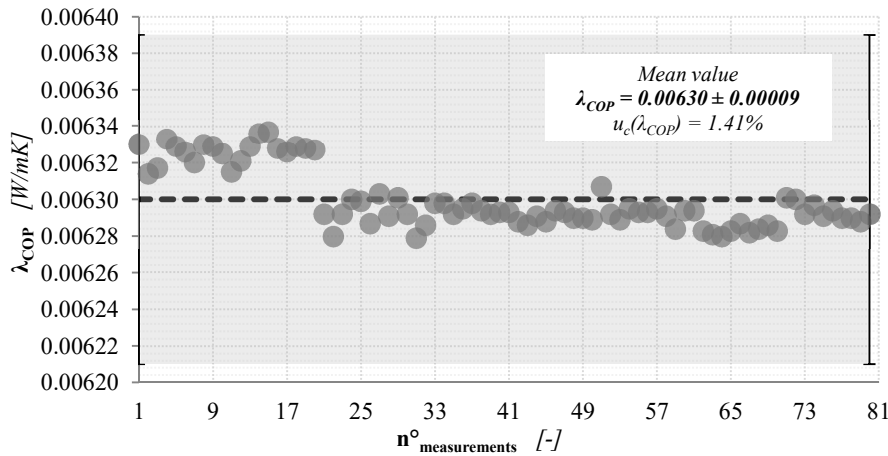


Figure B. 15: λ_{COP} -values assessed by means of HFM-1 apparatus (Sample: FS based VIP 10 mm thick, $\vartheta_{avg} = 40^\circ\text{C}$, $\Delta\vartheta = 30^\circ\text{C}$)

Table B. 31: Type A $u_c(\lambda_{COP})$ assessment, by means of HFM-1 apparatus (Sample: FS based VIP 10 mm thick, $\vartheta_{avg} = 40^\circ\text{C}$, $\Delta\vartheta = 40^\circ\text{C}$)

Test conditions		f_{cal_upper}	f_{cal_lower}	$t_{measured}$	ϑ_{upper}	ϑ_{lower}	Q_{upper}	Q_{lower}	Φ_{upper}	Φ_{lower}	λ_{COP}
10 mm $\vartheta_{avg} = 5^\circ\text{C}$ $\Delta\vartheta = 10^\circ\text{C}$		$[W/m^2 \cdot \mu V]$	$[W/m^2 \cdot \mu V]$	$[mm]$	$[^\circ\text{C}]$	$[^\circ\text{C}]$	$[\mu V]$	$[\mu V]$	$[W/m^2]$	$[W/m^2]$	$[W/mK]$
Mean value	\bar{y}	0.0051	0.0052	10.36	20.015	60.023	-4728.8	4623	24.281	23.984	0.00625
Median		-	-	-	-	-	-4730.0	4620.5	24.290	23.970	-
Skew		-	-	-	-	-	1.089	1.154	-1.018	1.126	-
Standard deviation	s	-	-	-	-	-	5.5	9.9	0.028	0.052	-
Absolute uncertainty	$u(\bar{y})$	0.0001	0.0001	0.02	0.003	0.004	0.6	1.1	0.003	0.006	0.00009
Relative uncertainty	$u(\bar{y})$ [%]	2.00%	2.00%	0.16%	0.01%	0.01%	0.01%	0.02%	0.01%	0.02%	1.42%
Variation coefficient	V [%]	-	-	-	-	-	-0.12%	0.22%	0.12%	0.22%	-
Probability distribution				Triangular	Uniform	Triangular	Normal	Normal	Normal	Normal	

Table B. 32: Type A $u_c(\lambda_{COP})$ sensitivity coefficients, by means of HFM-1 apparatus (Sample: FS based VIP 10 mm thick, $\vartheta_{avg} = 40^\circ\text{C}$, $\Delta\vartheta = 40^\circ\text{C}$)

	Sensitivity coefficients			
	$\partial\lambda_{COP}/\partial t$	$\partial\lambda_{COP}/\partial f_{cal}$	$\partial\lambda_{COP}/\partial Q$	$\partial\lambda_{COP}/\partial\Delta\vartheta$
Upper plate	0.606938	1224.514297	0.001330	-0.157166
Lower plate	0.599483	1197.117576	0.001343	-0.155235

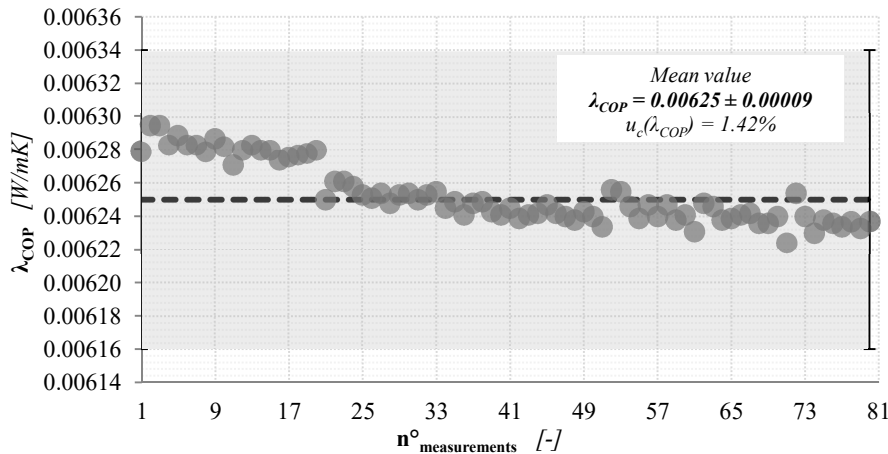
**Figure B. 16:** λ_{COP} -values assessed by means of HFM-1 apparatus (Sample: FS based VIP 10 mm thick, $\vartheta_{avg} = 40^\circ\text{C}$, $\Delta\vartheta = 40^\circ\text{C}$)

Table B. 33: Type A $u_c(\lambda_{COP})$ assessment, by means of HFM-1 apparatus (Sample: FS based VIP 20 mm thick, $\vartheta_{avg} = 5^\circ\text{C}$, $\Delta\vartheta = 10^\circ\text{C}$)

Test conditions		f_{cal_upper}	f_{cal_lower}	$t_{measured}$	ϑ_{upper}	ϑ_{lower}	Q_{upper}	Q_{lower}	Φ_{upper}	Φ_{lower}	λ_{COP}
20 mm $\vartheta_{avg} = 5^\circ\text{C}$ $\Delta\vartheta = 10^\circ\text{C}$		$[\text{W}/\text{m}^2 \cdot \mu\text{V}]$	$[\text{W}/\text{m}^2 \cdot \mu\text{V}]$	$[\text{mm}]$	$[\text{C}^\circ]$	$[\text{C}^\circ]$	$[\mu\text{V}]$	$[\mu\text{V}]$	$[\text{W}/\text{m}^2]$	$[\text{W}/\text{m}^2]$	$[\text{W}/\text{mK}]$
Mean value	\bar{y}	0.0054	0.0055	20.885	0.017	10.010	-283	312	1.516	1.714	0.00338
Median		-	-	-	-	-	-280	312	1.501	1.714	-
Skew		-	-	-	-	-	-1.174	0.330	1.186	0.326	-
Standard deviation	s	-	-	-	-	-	11.8	11.7	0.063	0.064	-
Absolute uncertainty	$u(\bar{y})$	0.0001	0.0001	0.009	0.003	0.002	1.4	1.4	0.008	0.008	0.00005
Relative uncertainty	$u(\bar{y})$ [%]	2.00%	2.00%	0.04%	16.98%	0.02%	0.45%	0.45%	0.50%	0.45%	1.46%
Variation coefficient	V [%]	-	-	-	-	-	-3.78%	3.74%	4.17%	3.74%	-
Probability distribution				Uniform	Uniform	Triangular	Normal	Normal	Normal	Normal	

Table B. 34: Type A $u_c(\lambda_{COP})$ sensitivity coefficients, by means of HFM-1 apparatus (Sample: FS based VIP 20 mm thick, $\vartheta_{avg} = 5^\circ\text{C}$, $\Delta\vartheta = 10^\circ\text{C}$)

	Sensitivity coefficients			
	$\partial\lambda_{COP}/\partial t$	$\partial\lambda_{COP}/\partial f_{cal}$	$\partial\lambda_{COP}/\partial Q$	$\partial\lambda_{COP}/\partial \Delta\vartheta$
Upper plate	0.151735	591.668518	0.011194	-0.317120
Lower plate	0.171751	652.068448	0.011497	-0.358954

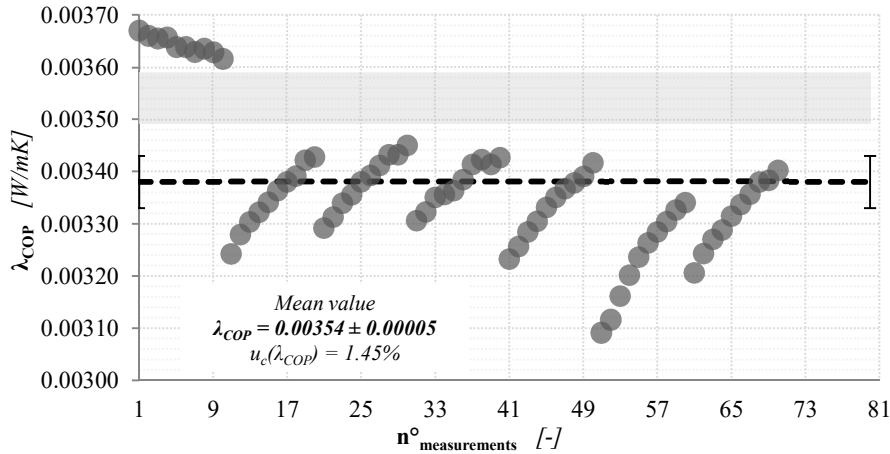


Figure B. 17: λ_{COP} -values assessed by means of HFM-1 apparatus (Sample: FS based VIP 20 mm thick, $\vartheta_{avg} = 5^\circ\text{C}$, $\Delta\vartheta = 10^\circ\text{C}$)

Table B. 35: Type A $u_c(\lambda_{COP})$ assessment, by means of HFM-1 apparatus (Sample: FS based VIP 20 mm thick, $\vartheta_{avg} = 5^\circ\text{C}$, $\Delta\vartheta = 20^\circ\text{C}$)

Test conditions		f_{cal_upper}	f_{cal_lower}	$t_{measured}$	ϑ_{upper}	ϑ_{lower}	Q_{upper}	Q_{lower}	Φ_{upper}	Φ_{lower}	λ_{COP}
20 mm $\vartheta_{avg} = 5^\circ\text{C}$ $\Delta\vartheta = 20^\circ\text{C}$		$[\text{W}/\text{m}^2 \cdot \mu\text{V}]$	$[\text{W}/\text{m}^2 \cdot \mu\text{V}]$	$[\text{mm}]$	$[\text{C}^\circ]$	$[\text{C}^\circ]$	$[\mu\text{V}]$	$[\mu\text{V}]$	$[\text{W}/\text{m}^2]$	$[\text{W}/\text{m}^2]$	$[\text{W}/\text{mK}]$
Mean value	\bar{y}	0.0054	0.0055	20.885	-4.981	15.014	-612	638	3.31	3.49	0.00355
Median		-	-	-	-	-	-600	628	3.25	3.43	-
Skew		-	-	-	-	-	-0.551	0.391	0.550	0.388	-
Standard deviation	s	-	-	-	-	-	21.7	22.8	0.12	0.13	-
Absolute uncertainty	$u(\bar{y})$	0.0001	0.0001	0.009	0.002	0.003	2.4	2.6	0.01	0.01	0.00005
Relative uncertainty	$u(\bar{y})$	2.00%	2.00%	0.04%	0.04%	0.02%	0.40%	0.40%	0.40%	0.40%	1.44%
Variation coefficient	V	-	-	-	-	-	-3.55%	3.58%	3.56%	3.59%	-
Probability distribution					Uniform	Triangular	Uniform	Normal	Normal	Normal	Normal

Table B. 36: Type A $u_c(\lambda_{COP})$ sensitivity coefficients, by means of HFM-1 apparatus (Sample: FS based VIP 20 mm thick, $\vartheta_{avg} = 5^\circ\text{C}$, $\Delta\vartheta = 20^\circ\text{C}$)

	Sensitivity coefficients			
	$\partial\lambda_{COP}/\partial t$	$\partial\lambda_{COP}/\partial f_{cal}$	$\partial\lambda_{COP}/\partial Q$	$\partial\lambda_{COP}/\partial\Delta\vartheta$
Upper plate	0.165649	639.240810	0.005653	-0.173022
Lower plate	0.174537	666.398100	0.005713	-0.182305

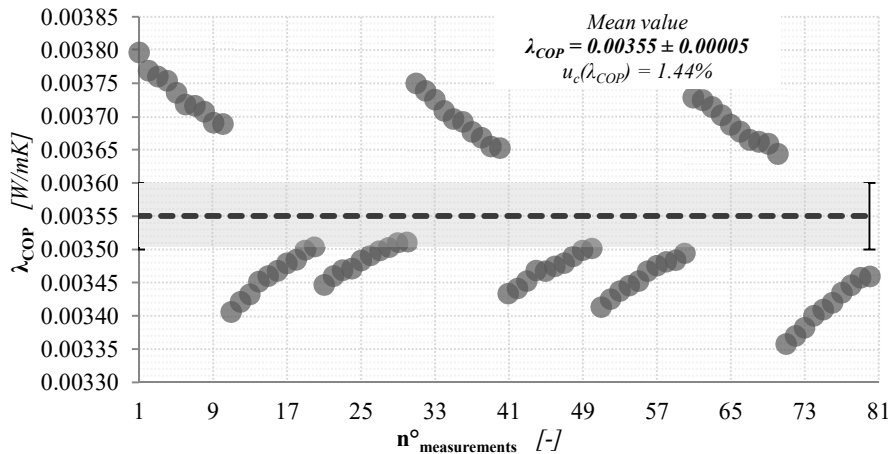
**Figure B. 18:** λ_{COP} -values assessed by means of HFM-1 apparatus (Sample: FS based VIP 20 mm thick, $\vartheta_{avg} = 5^\circ\text{C}$, $\Delta\vartheta = 20^\circ\text{C}$)

Table B. 37: Type A $u_c(\lambda_{COP})$ assessment, by means of HFM-1 apparatus (Sample: FS based VIP 20 mm thick, $\vartheta_{avg} = 5^\circ\text{C}$, $\Delta\vartheta = 30^\circ\text{C}$)

Test conditions		f_{cal_upper}	f_{cal_lower}	$t_{measured}$	ϑ_{upper}	ϑ_{lower}	Q_{upper}	Q_{lower}	Φ_{upper}	Φ_{lower}	λ_{COP}
20 mm $\vartheta_{avg} = 5^\circ\text{C}$ $\Delta\vartheta = 30^\circ\text{C}$		$[\text{W}/\text{m}^2 \cdot \mu\text{V}]$	$[\text{W}/\text{m}^2 \cdot \mu\text{V}]$	$[\text{mm}]$	$[\text{C}^\circ]$	$[\text{C}^\circ]$	$[\mu\text{V}]$	$[\mu\text{V}]$	$[\text{W}/\text{m}^2]$	$[\text{W}/\text{m}^2]$	$[\text{W}/\text{mK}]$
Mean value	\bar{y}	0.0055	0.0054	20.885	-9.984	20.015	-945	973	5.17	5.29	0.00364
Median		-	-	-	-	-	-946	981	5.17	5.34	-
Skew		-	-	-	-	-	-0.588	-0.462	0.580	-0.463	-
Standard deviation	s	-	-	-	-	-	21.1	21.6	0.12	0.12	-
Absolute uncertainty	$u(\bar{y})$	0.0001	0.0001	0.009	0.003	0.003	2.4	2.4	0.01	0.01	0.00005
Relative uncertainty	$u(\bar{y})$ [%]	2.00%	2.00%	0.04%	0.03%	0.01%	0.25%	0.25%	0.25%	0.25%	1.43%
Variation coefficient	V [%]	-	-	-	-	-	-2.24%	2.22%	2.24%	2.23%	-
Probability distribution		Triangular Uniform Triangular Normal Normal Normal Normal									

Table B. 38: Type A $u_c(\lambda_{COP})$ sensitivity coefficients, by means of HFM-1 apparatus (Sample: FS based VIP 20 mm thick, $\vartheta_{avg} = 5^\circ\text{C}$, $\Delta\vartheta = 30^\circ\text{C}$)

	Sensitivity coefficients			
	$\partial\lambda_{COP}/\partial t$	$\partial\lambda_{COP}/\partial f_{cal}$	$\partial\lambda_{COP}/\partial Q$	$\partial\lambda_{COP}/\partial\Delta\vartheta$
Upper plate	0.172248	657.899430	0.003807	-0.119917
Lower plate	0.176411	677.392746	0.003787	-0.122815

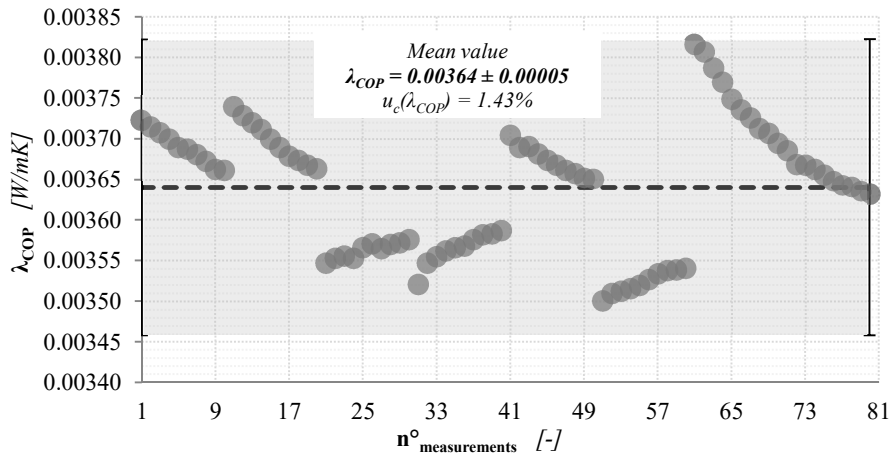


Figure B. 19: λ_{COP} -values assessed by means of HM-1 apparatus (Sample: FS based VIP 20 mm thick, $\vartheta_{avg} = 5^\circ\text{C}$, $\Delta\vartheta = 30^\circ\text{C}$)

Table B. 39: Type A $u_c(\lambda_{COP})$ assessment, by means of HFM-1 apparatus (Sample: FS based VIP 20 mm thick, $\vartheta_{avg} = 5^\circ\text{C}$, $\Delta\vartheta = 40^\circ\text{C}$)

Test conditions		f_{cal_upper}	f_{cal_lower}	$t_{measured}$	ϑ_{upper}	ϑ_{lower}	Q_{upper}	Q_{lower}	Φ_{upper}	Φ_{lower}	λ_{COP}
20 mm $\vartheta_{avg} = 5^\circ\text{C}$ $\Delta\vartheta = 40^\circ\text{C}$		$[\text{W}/\text{m}^2 \cdot \mu\text{V}]$	$[\text{W}/\text{m}^2 \cdot \mu\text{V}]$	$[\text{mm}]$	$[\text{C}^\circ]$	$[\text{C}^\circ]$	$[\mu\text{V}]$	$[\mu\text{V}]$	$[\text{W}/\text{m}^2]$	$[\text{W}/\text{m}^2]$	$[\text{W}/\text{mK}]$
Mean value	\bar{y}	0.0055	0.0054	20.884	-14.990	25.022	-1277	1312.2	7.06	7.096	0.00369
Median		-	-	-	-	-	-1273	1313.0	7.03	7.102	-
Skew		-	-	-	-	-	-1.318	-0.105	1.320	-0.119	-
Standard deviation	s	-	-	-	-	-	20.7	7.4	0.11	0.040	-
Absolute uncertainty	$u(\bar{y})$	0.0001	0.0001	0.006	0.004	0.003	2.3	0.8	0.01	0.004	0.00005
Relative uncertainty	$u(\bar{y})$ [%]	2.00%	2.00%	0.03%	0.03%	0.01%	0.18%	0.06%	0.18%	0.06%	1.42%
Variation coefficient	V [%]	-	-	-	-	-	-1.62%	0.57%	1.63%	0.57%	-
Probability distribution				Triangular	Triangular	Uniform	Normal	Normal	Normal	Normal	

Table B. 40: Type A $u_c(\lambda_{COP})$ sensitivity coefficients, by means of HFM-1 apparatus (Sample: FS based VIP 20 mm thick, $\vartheta_{avg} = 5^\circ\text{C}$, $\Delta\vartheta = 40^\circ\text{C}$)

	Sensitivity coefficients			
	$\partial\lambda_{COP}/\partial t$	$\partial\lambda_{COP}/\partial f_{cal}$	$\partial\lambda_{COP}/\partial Q$	$\partial\lambda_{COP}/\partial \Delta\vartheta$
Upper plate	0.176365	666.521743	0.002884	-0.092052
Lower plate	0.177356	684.894152	0.002823	-0.092570

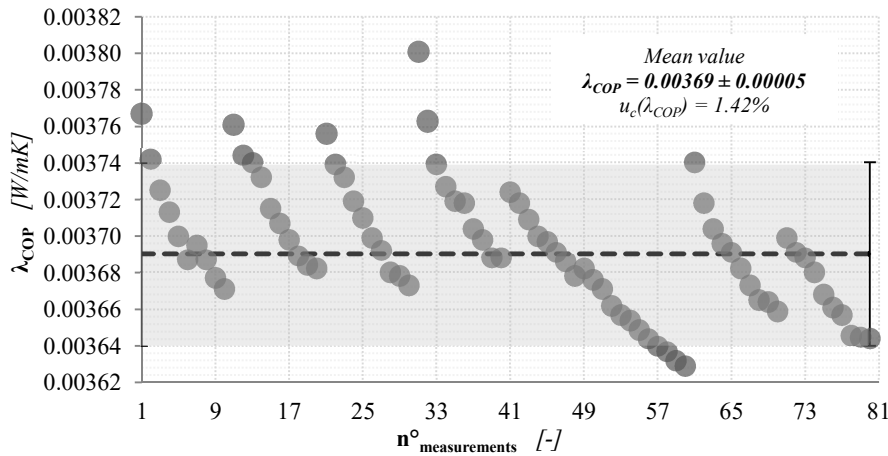


Figure B. 20: λ_{COP} -values assessed by means of HFM-1 apparatus (Sample: FS based VIP 20 mm thick, $\vartheta_{avg} = 5^\circ\text{C}$, $\Delta\vartheta = 40^\circ\text{C}$)

Table B. 41: Type A $u_c(\lambda_{COP})$ assessment, by means of HFM-1 apparatus (Sample: FS based VIP 20 mm thick, $\vartheta_{avg} = 10^\circ\text{C}$, $\Delta\vartheta = 10^\circ\text{C}$)

Test conditions		f_{cal_upper}	f_{cal_lower}	$t_{measured}$	ϑ_{upper}	ϑ_{lower}	Q_{upper}	Q_{lower}	Φ_{upper}	Φ_{lower}	λ_{COP}
20 mm $\vartheta_{avg} = 10^\circ\text{C}$ $\Delta\vartheta = 10^\circ\text{C}$		$[\text{W}/\text{m}^2 \cdot \mu\text{V}]$	$[\text{W}/\text{m}^2 \cdot \mu\text{V}]$	$[\text{mm}]$	$[\text{C}^\circ]$	$[\text{C}^\circ]$	$[\mu\text{V}]$	$[\mu\text{V}]$	$[\text{W}/\text{m}^2]$	$[\text{W}/\text{m}^2]$	$[\text{W}/\text{mK}]$
Mean value	\bar{y}	0.0053	0.0055	20.974	5.010	15.011	-321.8	324.1	1.704	1.772	0.00365
Median		-	-	-	-	-	-320.0	324.0	1.695	1.774	-
Skew		-	-	-	-	-	-1.734	-0.166	1.760	-0.150	-
Standard deviation	s	-	-	-	-	-	8.4	4.6	0.044	0.025	-
Absolute uncertainty	$u(\bar{y})$	0.0001	0.0001	0.003	0.002	0.002	0.9	0.5	0.005	0.003	0.00005
Relative uncertainty	$u(\bar{y})$ [%]	2.00%	2.00%	0.01%	0.04%	0.01%	0.29%	0.16%	0.29%	0.16%	1.42%
Variation coefficient	V [%]	-	-	-	-	-	-2.61%	1.41%	2.58%	1.39%	-
Probability distribution					Triangular	Triangular	Triangular	Normal	Normal	Normal	Normal

Table B. 42: Type A $u_c(\lambda_{COP})$ sensitivity coefficients, by means of HFM-1 apparatus (Sample: FS based VIP 20 mm thick, $\vartheta_{avg} = 10^\circ\text{C}$, $\Delta\vartheta = 10^\circ\text{C}$)

Sensitivity coefficients				
	$\partial\lambda_{COP}/\partial t$	$\partial\lambda_{COP}/\partial f_{cal}$	$\partial\lambda_{COP}/\partial Q$	$\partial\lambda_{COP}/\partial \Delta\vartheta$
Upper plate	0.170408	674.875832	0.011107	-0.357379
Lower plate	0.177200	679.699370	0.011467	-0.371622

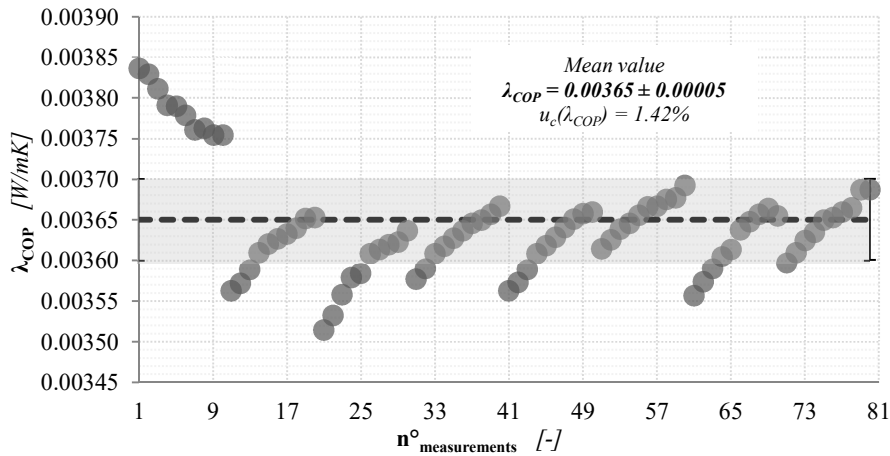


Figure B. 21: λ_{COP} -values assessed by means of HFM-1 apparatus (Sample: FS based VIP 20 mm thick, $\vartheta_{avg} = 10^\circ\text{C}$, $\Delta\vartheta = 10^\circ\text{C}$)

Table B. 43: Type A $u_c(\lambda_{COP})$ assessment, by means of HFM-1 apparatus (Sample: FS based VIP 20 mm thick, $\vartheta_{avg} = 10^\circ\text{C}$, $\Delta\vartheta = 20^\circ\text{C}$)

Test conditions		f_{cal_upper}	f_{cal_lower}	$t_{measured}$	ϑ_{upper}	ϑ_{lower}	Q_{upper}	Q_{lower}	Φ_{upper}	Φ_{lower}	λ_{COP}
20 mm $\vartheta_{avg} = 10^\circ\text{C}$ $\Delta\vartheta = 20^\circ\text{C}$		$[W/m^2 \cdot \mu V]$	$[W/m^2 \cdot \mu V]$	$[mm]$	$[^\circ\text{C}]$	$[^\circ\text{C}]$	$[\mu V]$	$[\mu V]$	$[W/m^2]$	$[W/m^2]$	$[W/mK]$
Mean value	\bar{y}	0.0054	0.0054	20.974	0.017	20.014	-655	650	3.51	3.53	0.00369
Median		-	-	-	-	-	-649	643	3.47	3.50	-
Skew		-	-	-	-	-	-0.855	0.399	0.850	0.391	-
Standard deviation	s	-	-	-	-	-	19.8	22.3	0.106	0.121	-
Absolute uncertainty	$u(\bar{y})$	0.0001	0.0001	0.004	0.003	0.003	2.2	2.5	0.01	0.01	0.00005
Relative uncertainty	$u(\bar{y})$ [%]	2.00%	2.00%	0.02%	16.98%	0.01%	0.34%	0.38%	0.34%	0.38%	1.44%
Variation coefficient	V [%]	-	-	-	-	-	-3.02%	3.43%	3.02%	3.43%	-
Probability distribution				Uniform	Uniform	Uniform	Normal	Normal	Normal	Normal	

Table B. 44: Type A $u_c(\lambda_{COP})$ sensitivity coefficients, by means of HFM-1 apparatus (Sample: FS based VIP 20 mm thick, $\vartheta_{avg} = 10^\circ\text{C}$, $\Delta\vartheta = 20^\circ\text{C}$)

	Sensitivity coefficients			
	$\partial\lambda_{COP}/\partial t$	$\partial\lambda_{COP}/\partial f_{cal}$	$\partial\lambda_{COP}/\partial Q$	$\partial\lambda_{COP}/\partial \Delta\vartheta$
Upper plate	0.175435	687.001550	0.005618	-0.184007
Lower plate	0.176762	681.757264	0.005704	-0.185398

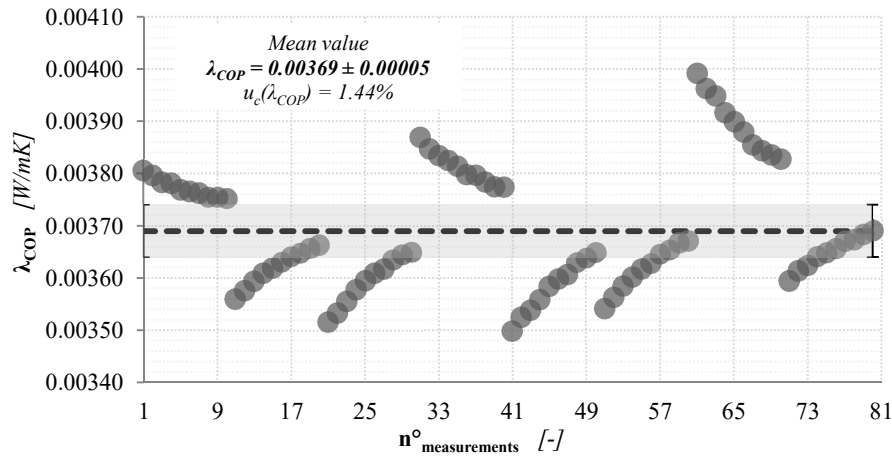
**Figure B. 22:** λ_{COP} -values assessed by means of HFM-1 apparatus (Sample: FS based VIP 20 mm thick, $\vartheta_{avg} = 10^\circ\text{C}$, $\Delta\vartheta = 20^\circ\text{C}$)

Table B. 45: Type A $u_c(\lambda_{COP})$ assessment, by means of HFM-1 apparatus (Sample: FS based VIP 20 mm thick, $\vartheta_{avg} = 10^\circ\text{C}$, $\Delta\vartheta = 30^\circ\text{C}$)

Test conditions		f_{cal_upper}	f_{cal_lower}	$t_{measured}$	ϑ_{upper}	ϑ_{lower}	Q_{upper}	Q_{lower}	Φ_{upper}	Φ_{lower}	λ_{COP}
20 mm $\vartheta_{avg} = 10^\circ\text{C}$ $\Delta\vartheta = 30^\circ\text{C}$		$[\text{W}/\text{m}^2 \cdot \mu\text{V}]$	$[\text{W}/\text{m}^2 \cdot \mu\text{V}]$	$[\text{mm}]$	$[\text{C}^\circ]$	$[\text{C}^\circ]$	$[\mu\text{V}]$	$[\mu\text{V}]$	$[\text{W}/\text{m}^2]$	$[\text{W}/\text{m}^2]$	$[\text{W}/\text{mK}]$
Mean value	\bar{y}	0.0054	0.0054	20.974	-4.983	25.023	-994	997	5.39	5.39	0.00377
Median		-	-	-	-	-	-990	1000	5.36	5.41	-
Skew		-	-	-	-	-	-1.814	0.316	1.820	0.314	-
Standard deviation	s	-	-	-	-	-	21.4	20.5	0.116	0.111	-
Absolute uncertainty	$u(\bar{y})$	0.0001	0.0001	0.004	0.003	0.003	2.4	2.3	0.01	0.01	0.00005
Relative uncertainty	$u(\bar{y})$ [%]	2.00%	2.00%	0.02%	0.06%	0.01%	0.24%	0.23%	0.24%	0.23%	1.42%
Variation coefficient	V [%]	-	-	-	-	-	-2.15%	2.05%	2.15%	2.05%	-
Probability distribution				Uniform	Uniform	Uniform	Normal	Normal	Normal	Normal	

Table B. 46: Type A $u_c(\lambda_{COP})$ sensitivity coefficients, by means of HFM-1 apparatus (Sample: FS based VIP 20 mm thick, $\vartheta_{avg} = 10^\circ\text{C}$, $\Delta\vartheta = 30^\circ\text{C}$)

	Sensitivity coefficients			
	$\partial\lambda_{COP}/\partial t$	$\partial\lambda_{COP}/\partial f_{cal}$	$\partial\lambda_{COP}/\partial Q$	$\partial\lambda_{COP}/\partial\Delta\vartheta$
Upper plate	0.179514	694.799573	0.003788	-0.125479
Lower plate	0.179657	696.896554	0.003779	-0.125579

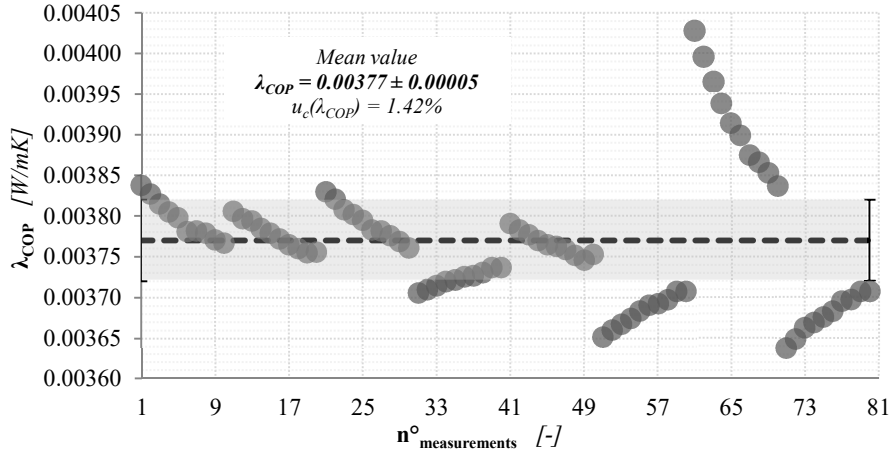


Figure B. 23: λ_{COP} -values assessed by means of HFM-1 apparatus (Sample: FS based VIP 20 mm thick, $\vartheta_{avg} = 10^\circ\text{C}$, $\Delta\vartheta = 30^\circ\text{C}$)

Table B. 47: Type A $u_c(\lambda_{COP})$ assessment, by means of HFM-1 apparatus (Sample: FS based VIP 20 mm thick, $\vartheta_{avg} = 10^\circ\text{C}$, $\Delta\vartheta = 40^\circ\text{C}$)

Test conditions		f_{cal_upper}	f_{cal_lower}	$t_{measured}$	ϑ_{upper}	ϑ_{lower}	Q_{upper}	Q_{lower}	Φ_{upper}	Φ_{lower}	λ_{COP}
20 mm $\vartheta_{avg} = 10^\circ\text{C}$ $\Delta\vartheta = 40^\circ\text{C}$		$[W/m^2 \cdot \mu V]$	$[W/m^2 \cdot \mu V]$	$[mm]$	$[^\circ\text{C}]$	$[^\circ\text{C}]$	$[\mu V]$	$[\mu V]$	$[W/m^2]$	$[W/m^2]$	$[W/mK]$
Mean value	\bar{y}	0.0055	0.0054	20.974	-9.965	30.021	-1344	1354	7.37	7.281	0.00384
Median		-	-	-	-	-	-1335	1353	7.32	7.272	-
Skew		-	-	-	-	-	-1.572	0.850	1.580	0.854	-
Standard deviation	s	-	-	-	-	-	30.2	9.5	0.165	0.051	-
Absolute uncertainty	$u(\bar{y})$	0.0001	0.0001	0.003	0.003	0.002	3.4	1.1	0.02	0.006	0.00005
Relative uncertainty	$u(\bar{y})$ [%]	2.00%	2.00%	0.01%	0.03%	0.01%	0.25%	0.08%	0.25%	0.08%	1.42%
Variation coefficient	V [%]	-	-	-	-	-	-2.25%	0.70%	2.24%	0.70%	-
Probability distribution		Triangular Uniform Triangular Normal Normal Normal Normal									

Table B. 48: Type A $u_c(\lambda_{COP})$ sensitivity coefficients, by means of HFM-1 apparatus (Sample: FS based VIP 20 mm thick, $\vartheta_{avg} = 10^\circ\text{C}$, $\Delta\vartheta = 40^\circ\text{C}$)

	Sensitivity coefficients			
	$\partial\lambda_{COP}/\partial t$	$\partial\lambda_{COP}/\partial f_{cal}$	$\partial\lambda_{COP}/\partial Q$	$\partial\lambda_{COP}/\partial \Delta\vartheta$
Upper plate	0.184361	704.973141	0.002877	-0.096703
Lower plate	0.182075	710.218476	0.002820	-0.095505

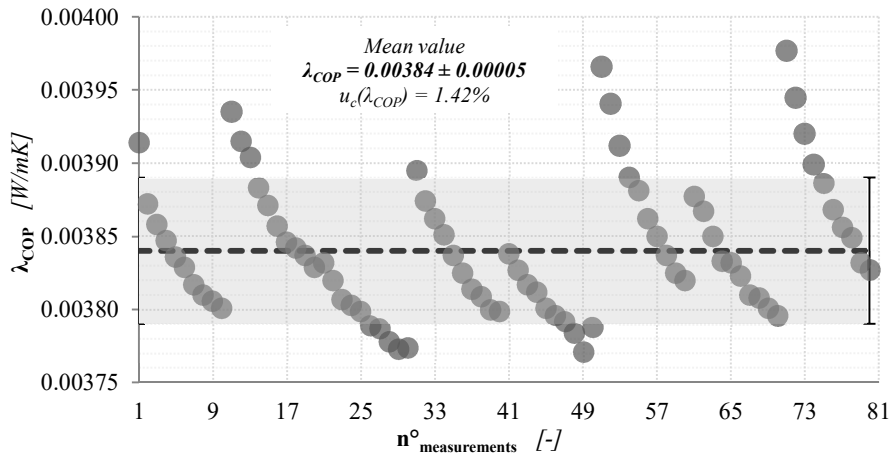


Figure B. 24: λ_{COP} -values assessed by means of HFM-1 apparatus (Sample: FS based VIP 20 mm thick, $\vartheta_{avg} = 10^\circ\text{C}$, $\Delta\vartheta = 40^\circ\text{C}$)

Table B. 49: Type A $u_c(\lambda_{COP})$ assessment, by means of HFM-1 apparatus (Sample: FS based VIP 20 mm thick, $\vartheta_{avg} = 23^\circ\text{C}$, $\Delta\vartheta = 10^\circ\text{C}$)

Test conditions		f_{cal_upper}	f_{cal_lower}	$t_{measured}$	ϑ_{upper}	ϑ_{lower}	Q_{upper}	Q_{lower}	Φ_{upper}	Φ_{lower}	λ_{COP}
20 mm $\vartheta_{avg} = 23^\circ\text{C}$ $\Delta\vartheta = 10^\circ\text{C}$		$[\text{W}/\text{m}^2 \cdot \mu\text{V}]$	$[\text{W}/\text{m}^2 \cdot \mu\text{V}]$	$[\text{mm}]$	$[\text{C}^\circ]$	$[\text{C}^\circ]$	$[\mu\text{V}]$	$[\mu\text{V}]$	$[\text{W}/\text{m}^2]$	$[\text{W}/\text{m}^2]$	$[\text{W}/\text{mK}]$
Mean value	\bar{y}	0.0052	0.0054	20.998	18.019	28.014	-382.0	326	1.969	1.756	0.00391
Median		-	-	-	-	-	-383.0	324	1.976	1.746	-
Skew		-	-	-	-	-	1.582	0.775	-1.540	0.804	-
Standard deviation	s	-	-	-	-	-	4.4	10.3	0.023	0.056	-
Absolute uncertainty	$u(\bar{y})$	0.0001	0.0001	0.008	0.002	0.003	0.5	1.2	0.003	0.006	0.00006
Relative uncertainty	$u(\bar{y})$ [%]	2.00%	2.00%	0.04%	0.01%	0.01%	0.13%	0.35%	0.13%	0.35%	1.43%
Variation coefficient	V [%]	-	-	-	-	-	-1.14%	3.17%	1.16%	3.17%	-
Probability distribution				Triangular	Triangular	Uniform	Normal	Normal	Normal	Normal	

Table B. 50: Type A $u_c(\lambda_{COP})$ sensitivity coefficients, by means of HFM-1 apparatus (Sample: FS based VIP 20 mm thick, $\vartheta_{avg} = 23^\circ\text{C}$, $\Delta\vartheta = 10^\circ\text{C}$)

	Sensitivity coefficients			
	$\partial\lambda_{COP}/\partial t$	$\partial\lambda_{COP}/\partial f_{cal}$	$\partial\lambda_{COP}/\partial Q$	$\partial\lambda_{COP}/\partial\Delta\vartheta$
Upper plate	0.196981	802.524862	0.010828	-0.413828
Lower plate	0.175769	684.877239	0.011321	-0.369265

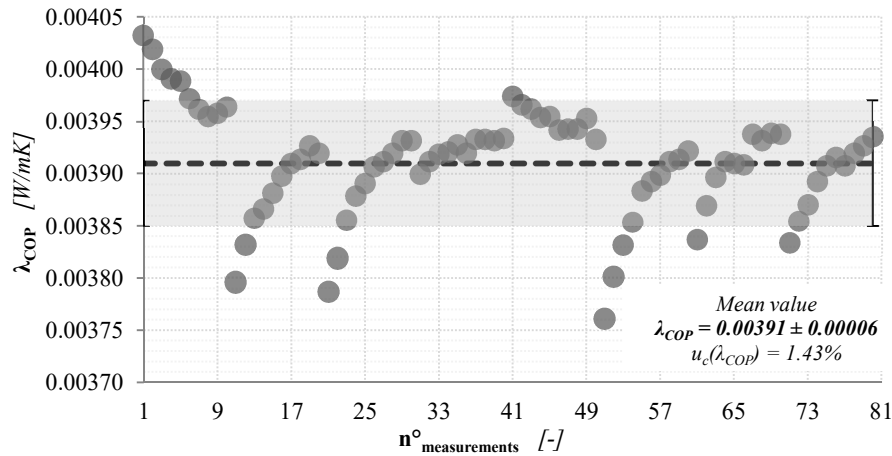


Figure B. 25: λ_{COP} -values assessed by means of HFM-1 apparatus (Sample: FS based VIP 20 mm thick, $\vartheta_{avg} = 23^\circ\text{C}$, $\Delta\vartheta = 10^\circ\text{C}$)

Table B. 51: Type A $u_c(\lambda_{COP})$ assessment, by means of HFM-1 apparatus (Sample: FS based VIP 20 mm thick, $\vartheta_{avg} = 23^\circ\text{C}$, $\Delta\vartheta = 20^\circ\text{C}$)

Test conditions		f_{cal_upper}	f_{cal_lower}	$t_{measured}$	ϑ_{upper}	ϑ_{lower}	Q_{upper}	Q_{lower}	Φ_{upper}	Φ_{lower}	λ_{COP}
20 mm $\vartheta_{avg} = 23^\circ\text{C}$ $\Delta\vartheta = 20^\circ\text{C}$		$[\text{W}/\text{m}^2 \cdot \mu\text{V}]$	$[\text{W}/\text{m}^2 \cdot \mu\text{V}]$	$[\text{mm}]$	$[\text{C}^\circ]$	$[\text{C}^\circ]$	$[\mu\text{V}]$	$[\mu\text{V}]$	$[\text{W}/\text{m}^2]$	$[\text{W}/\text{m}^2]$	$[\text{W}/\text{mK}]$
Mean value	\bar{y}	0.0052	0.0054	20.998	13.020	33.018	-741	675	3.855	3.62	0.00392
Median		-	-	-	-	-	-741	671	3.859	3.60	-
Skew		-	-	-	-	-	-0.608	0.536	0.580	0.54	-
Standard deviation	s	-	-	-	-	-	11.8	22.4	0.061	0.120	-
Absolute uncertainty	$u(\bar{y})$	0.0001	0.0001	0.008	0.002	0.002	1.3	2.5	0.007	0.01	0.00006
Relative uncertainty	$u(\bar{y})$ [%]	2.00%	2.00%	0.04%	0.02%	0.01%	0.18%	0.37%	0.18%	0.37%	1.43%
Variation coefficient	V [%]	-	-	-	-	-	-1.59%	3.32%	1.58%	3.32%	-
Probability distribution		Triangular Traingular Traingular Normal Normal Normal Normal									

Table B. 52: Type A $u_c(\lambda_{COP})$ sensitivity coefficients, by means of HFM-1 apparatus (Sample: FS based VIP 20 mm thick, $\vartheta_{avg} = 23^\circ\text{C}$, $\Delta\vartheta = 20^\circ\text{C}$)

	Sensitivity coefficients			
	$\partial\lambda_{COP}/\partial t$	$\partial\lambda_{COP}/\partial f_{cal}$	$\partial\lambda_{COP}/\partial Q$	$\partial\lambda_{COP}/\partial\Delta\vartheta$
Upper plate	0.192902	778.053705	0.005466	-0.202548
Lower plate	0.180851	708.753375	0.005626	-0.189894

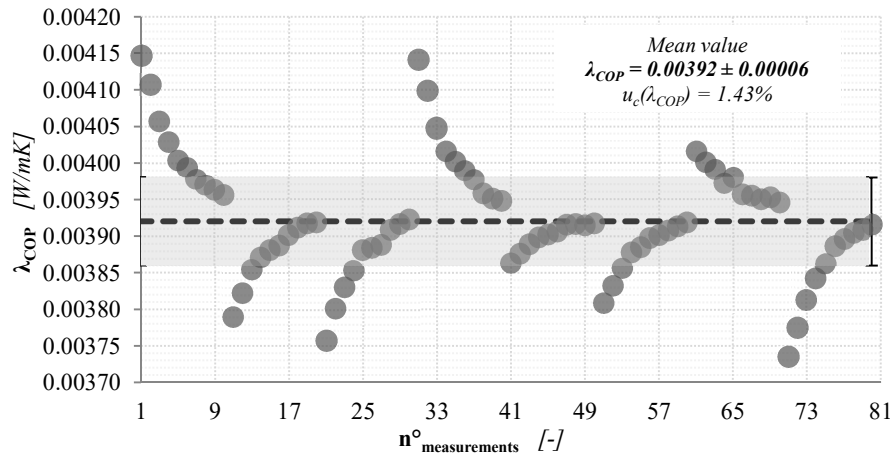
**Figure B. 26:** λ_{COP} -values assessed by means of HFM-1 apparatus (Sample: FS based VIP 20 mm thick, $\vartheta_{avg} = 23^\circ\text{C}$, $\Delta\vartheta = 20^\circ\text{C}$)

Table B. 53: Type A $u_c(\lambda_{COP})$ assessment, by means of HFM-1 apparatus (Sample: FS based VIP 20 mm thick, $\vartheta_{avg} = 23^\circ\text{C}$, $\Delta\vartheta = 30^\circ\text{C}$)

Test conditions		f_{cal_upper}	f_{cal_lower}	$t_{measured}$	ϑ_{upper}	ϑ_{lower}	Q_{upper}	Q_{lower}	Φ_{upper}	Φ_{lower}	λ_{COP}
20 mm $\vartheta_{avg} = 23^\circ\text{C}$ $\Delta\vartheta = 30^\circ\text{C}$		$[\text{W}/\text{m}^2 \cdot \mu\text{V}]$	$[\text{W}/\text{m}^2 \cdot \mu\text{V}]$	$[\text{mm}]$	$[\text{C}^\circ]$	$[\text{C}^\circ]$	$[\mu\text{V}]$	$[\mu\text{V}]$	$[\text{W}/\text{m}^2]$	$[\text{W}/\text{m}^2]$	$[\text{W}/\text{mK}]$
Mean value	\bar{y}	0.0053	0.0053	20.998	8.010	38.023	-1093	1039	5.753	5.54	0.00395
Median		-	-	-	-	-	-1093	1041	5.748	5.54	-
Skew		-	-	-	-	-	-0.783	0.310	0.780	0.31	-
Standard deviation	s	-	-	-	-	-	16.3	28.4	0.086	0.151	-
Absolute uncertainty	$u(\bar{y})$	0.0001	0.0001	0.008	0.002	0.003	1.8	3.2	0.010	0.02	0.00006
Relative uncertainty	$u(\bar{y})$ [%]	2.00%	2.00%	0.04%	0.03%	0.01%	0.17%	0.31%	0.17%	0.31%	1.42%
Variation coefficient	V [%]	-	-	-	-	-	-1.49%	2.73%	1.49%	2.73%	-
Probability distribution				Triangular	Triangular	Uniform	Normal	Normal	Normal	Normal	

Table B. 54: Type A $u_c(\lambda_{COP})$ sensitivity coefficients, by means of HFM-1 apparatus (Sample: FS based VIP 20 mm thick, $\vartheta_{avg} = 23^\circ\text{C}$, $\Delta\vartheta = 30^\circ\text{C}$)

	Sensitivity coefficients			
	$\partial\lambda_{COP}/\partial t$	$\partial\lambda_{COP}/\partial f_{cal}$	$\partial\lambda_{COP}/\partial Q$	$\partial\lambda_{COP}/\partial\Delta\vartheta$
Upper plate	0.191593	764.695765	0.003681	-0.134044
Lower plate	0.184412	726.915737	0.003727	-0.129020

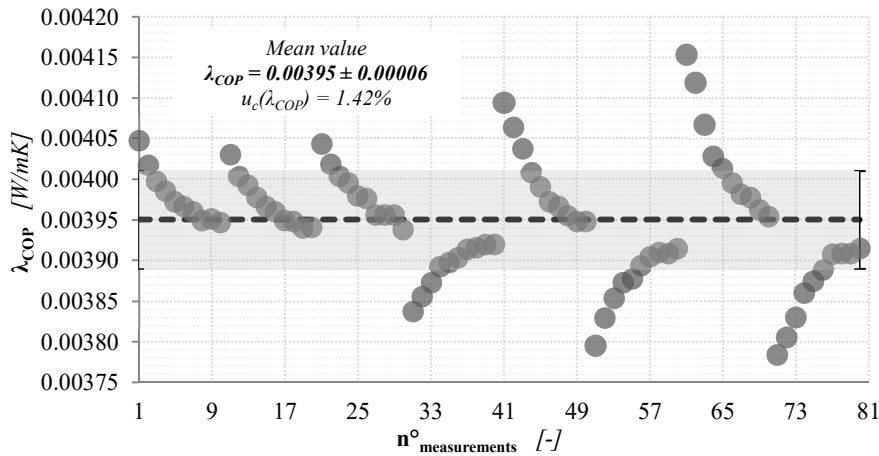


Figure B. 27: λ_{COP} -values assessed by means of HFM-1 apparatus (Sample: FS based VIP 20 mm thick, $\vartheta_{avg} = 23^\circ\text{C}$, $\Delta\vartheta = 30^\circ\text{C}$)

Table B. 55: Type A $u_c(\lambda_{COP})$ assessment, by means of HFM-1 apparatus (Sample: FS based VIP 20 mm thick, $\vartheta_{avg} = 23^\circ\text{C}$, $\Delta\vartheta = 40^\circ\text{C}$)

Test conditions		f_{cal_upper}	f_{cal_lower}	$t_{measured}$	ϑ_{upper}	ϑ_{lower}	Q_{upper}	Q_{lower}	Φ_{upper}	Φ_{lower}	λ_{COP}
20 mm $\vartheta_{avg} = 23^\circ\text{C}$ $\Delta\vartheta = 40^\circ\text{C}$		$[\text{W}/\text{m}^2 \cdot \mu\text{V}]$	$[\text{W}/\text{m}^2 \cdot \mu\text{V}]$	$[\text{mm}]$	$[\text{C}^\circ]$	$[\text{C}^\circ]$	$[\mu\text{V}]$	$[\mu\text{V}]$	$[\text{W}/\text{m}^2]$	$[\text{W}/\text{m}^2]$	$[\text{W}/\text{mK}]$
Mean value	\bar{y}	0.0053	0.0053	20.998	3.009	43.028	-1447	1413	7.695	7.48	0.00398
Median		-	-	-	-	-	-1441	1409	7.666	7.46	-
Skew		-	-	-	-	-	-1.234	0.908	1.240	0.92	-
Standard deviation	s	-	-	-	-	-	13.3	16.2	0.071	0.086	-
Absolute uncertainty	$u(\bar{y})$	0.0001	0.0001	0.008	0.002	0.002	1.5	1.8	0.008	0.01	0.00006
Relative uncertainty	$u(\bar{y})$ [%]	2.00%	2.00%	0.04%	0.07%	0.00%	0.10%	0.13%	0.10%	0.13%	1.42%
Variation coefficient	V [%]	-	-	-	-	-	-0.92%	1.14%	0.92%	1.14%	-
Probability distribution					Triangular	Traingular	Traingular	Normal	Normal	Normal	Normal

Table B. 56: Type A $u_c(\lambda_{COP})$ sensitivity coefficients, by means of HFM-1 apparatus (Sample: FS based VIP 20 mm thick, $\vartheta_{avg} = 23^\circ\text{C}$, $\Delta\vartheta = 40^\circ\text{C}$)

	Sensitivity coefficients			
	$\partial\lambda_{COP}/\partial t$	$\partial\lambda_{COP}/\partial f_{cal}$	$\partial\lambda_{COP}/\partial Q$	$\partial\lambda_{COP}/\partial\Delta\vartheta$
Upper plate	0.192323	759.242010	0.002791	-0.100912
Lower plate	0.186992	741.402184	0.002779	-0.098115

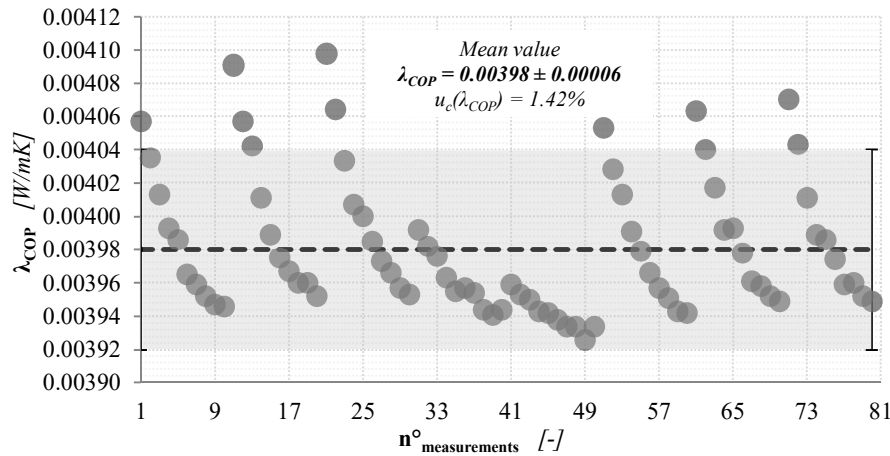
**Figure B. 28:** λ_{COP} -values assessed by means of HFM-1 apparatus (Sample: FS based VIP 20 mm thick, $\vartheta_{avg} = 23^\circ\text{C}$, $\Delta\vartheta = 40^\circ\text{C}$)

Table B. 57: Type A $u_c(\lambda_{COP})$ assessment, by means of HFM-1 apparatus (Sample: FS based VIP 20 mm thick, $\vartheta_{avg} = 40^\circ\text{C}$, $\Delta\vartheta = 10^\circ\text{C}$)

Test conditions		f_{cal_upper}	f_{cal_lower}	$t_{measured}$	ϑ_{upper}	ϑ_{lower}	Q_{upper}	Q_{lower}	Φ_{upper}	Φ_{lower}	λ_{COP}
20 mm $\vartheta_{avg} = 40^\circ\text{C}$ $\Delta\vartheta = 10^\circ\text{C}$		$[\text{W}/\text{m}^2 \cdot \mu\text{V}]$	$[\text{W}/\text{m}^2 \cdot \mu\text{V}]$	$[\text{mm}]$	$[\text{C}^\circ]$	$[\text{C}^\circ]$	$[\mu\text{V}]$	$[\mu\text{V}]$	$[\text{W}/\text{m}^2]$	$[\text{W}/\text{m}^2]$	$[\text{W}/\text{mK}]$
Mean value	\bar{y}	0.0050	0.0053	20.94	35.020	45.021	-470	336	2.350	1.777	0.00432
Median		-	-	-	-	-	-470	337	2.349	1.780	-
Skew		-	-	-	-	-	-0.178	-1.232	0.220	-1.238	-
Standard deviation	s	-	-	-	-	-	2.2	3.4	0.011	0.018	-
Absolute uncertainty	$u(\bar{y})$	0.0001	0.0001	0.01	0.002	0.002	0.2	0.4	0.001	0.002	0.00006
Relative uncertainty	$u(\bar{y})$ [%]	2.00%	2.00%	0.05%	0.01%	0.00%	0.05%	0.11%	0.05%	0.11%	1.43%
Variation coefficient	V [%]	-	-	-	-	-	-0.47%	1.01%	0.46%	0.99%	-
Probability distribution		Triangular Traingular Traingular Normal Normal Normal Normal									

Table B. 58: Type A $u_c(\lambda_{COP})$ sensitivity coefficients, by means of HFM-1 apparatus (Sample: FS based VIP 20 mm thick, $\vartheta_{avg} = 40^\circ\text{C}$, $\Delta\vartheta = 10^\circ\text{C}$)

	Sensitivity coefficients			
	$\partial\lambda_{COP}/\partial t$	$\partial\lambda_{COP}/\partial f_{cal}$	$\partial\lambda_{COP}/\partial Q$	$\partial\lambda_{COP}/\partial \Delta\vartheta$
Upper plate	0.235117	984.081592	0.010475	-0.492287
Lower plate	0.177491	703.513649	0.011061	-0.371629

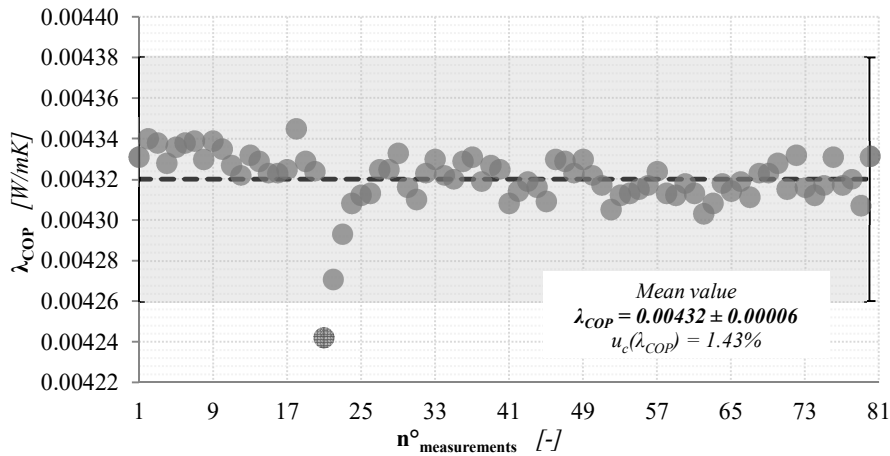


Figure B. 29: λ_{COP} -values assessed by means of HFM-1 apparatus (Sample: FS based VIP 20 mm thick, $\vartheta_{avg} = 40^\circ\text{C}$, $\Delta\vartheta = 10^\circ\text{C}$)

Table B. 59: Type A $u_c(\lambda_{COP})$ assessment, by means of HFM-1 apparatus (Sample: FS based VIP 20 mm thick, $\vartheta_{avg} = 40^\circ\text{C}$, $\Delta\vartheta = 20^\circ\text{C}$)

Test conditions		f_{cal_upper}	f_{cal_lower}	$t_{measured}$	ϑ_{upper}	ϑ_{lower}	Q_{upper}	Q_{lower}	Φ_{upper}	Φ_{lower}	λ_{COP}
20 mm $\vartheta_{avg} = 40^\circ\text{C}$ $\Delta\vartheta = 20^\circ\text{C}$		$[\text{W}/\text{m}^2 \cdot \mu\text{V}]$	$[\text{W}/\text{m}^2 \cdot \mu\text{V}]$	$[\text{mm}]$	$[\text{C}^\circ]$	$[\text{C}^\circ]$	$[\mu\text{V}]$	$[\mu\text{V}]$	$[\text{W}/\text{m}^2]$	$[\text{W}/\text{m}^2]$	$[\text{W}/\text{mK}]$
Mean value	\bar{y}	0.0050	0.0053	20.94	30.020	50.021	-869.2	728	4.384	3.822	0.00430
Median		-	-	-	-	-	-869.0	728	4.382	3.822	-
Skew		-	-	-	-	-	-0.521	0.008	0.510	0.006	-
Standard deviation	s	-	-	-	-	-	2.6	9.7	0.013	0.051	-
Absolute uncertainty	$u(\bar{y})$	0.0001	0.0001	0.01	0.002	0.002	0.3	1.1	0.001	0.006	0.00006
Relative uncertainty	$u(\bar{y})$	2.00%	2.00%	0.07%	0.01%	0.00%	0.03%	0.15%	0.03%	0.15%	1.42%
Variation coefficient	V	-	-	-	-	-	-0.30%	1.33%	0.30%	1.33%	-
Probability distribution					Uniform	Traingular	Traingular	Normal	Normal	Normal	Normal

Table B. 60: Type A $u_c(\lambda_{COP})$ sensitivity coefficients, by means of HFM-1 apparatus (Sample: FS based VIP 20 mm thick, $\vartheta_{avg} = 40^\circ\text{C}$, $\Delta\vartheta = 20^\circ\text{C}$)

	Sensitivity coefficients			
	$\partial\lambda_{COP}/\partial t$	$\partial\lambda_{COP}/\partial f_{cal}$	$\partial\lambda_{COP}/\partial Q$	$\partial\lambda_{COP}/\partial\Delta\vartheta$
Upper plate	0.219158	910.006900	0.005280	-0.229447
Lower plate	0.191163	762.177891	0.005499	-0.200138

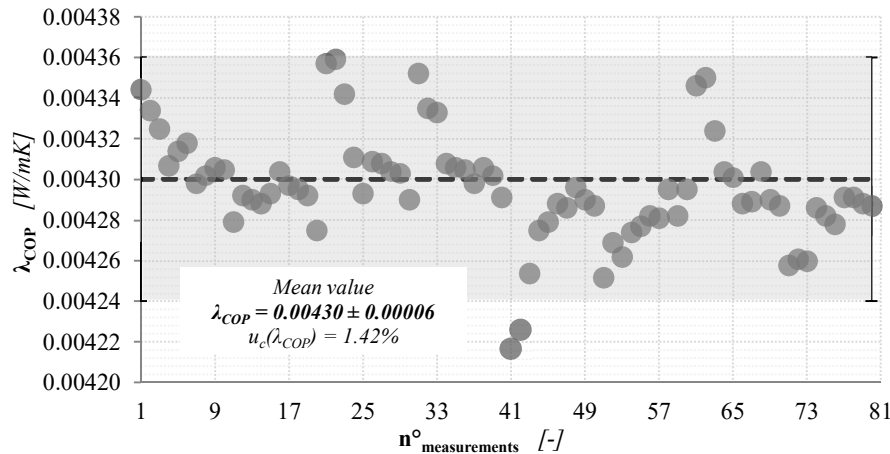
**Figure B. 30:** λ_{COP} -values assessed by means of HFM-1 apparatus (Sample: FS based VIP 20 mm thick, $\vartheta_{avg} = 40^\circ\text{C}$, $\Delta\vartheta = 20^\circ\text{C}$)

Table B. 61: Type A $u_c(\lambda_{COP})$ assessment, by means of HFM-1 apparatus (Sample: FS based VIP 20 mm thick, $\vartheta_{avg} = 40^\circ\text{C}$, $\Delta\vartheta = 30^\circ\text{C}$)

Test conditions		f_{cal_upper}	f_{cal_lower}	$t_{measured}$	ϑ_{upper}	ϑ_{lower}	Q_{upper}	Q_{lower}	Φ_{upper}	Φ_{lower}	λ_{COP}
20 mm $\vartheta_{avg} = 40^\circ\text{C}$ $\Delta\vartheta = 30^\circ\text{C}$		$[\text{W}/\text{m}^2 \cdot \mu\text{V}]$	$[\text{W}/\text{m}^2 \cdot \mu\text{V}]$	$[\text{mm}]$	$[\text{C}^\circ]$	$[\text{C}^\circ]$	$[\mu\text{V}]$	$[\mu\text{V}]$	$[\text{W}/\text{m}^2]$	$[\text{W}/\text{m}^2]$	$[\text{W}/\text{mK}]$
Mean value	\bar{y}	0.0051	0.0052	20.94	25.022	55.021	-1257.5	1123	6.397	5.862	0.00428
Median		-	-	-	-	-	-1258.0	1121	6.400	5.849	-
Skew		-	-	-	-	-	0.645	1.195	-0.630	1.190	-
Standard deviation	s	-	-	-	-	-	3.3	14.2	0.017	0.074	-
Absolute uncertainty	$u(\bar{y})$	0.0001	0.0001	0.01	0.002	0.002	0.4	1.6	0.002	0.008	0.00006
Relative uncertainty	$u(\bar{y})$ [%]	2.00%	2.00%	0.07%	0.01%	0.00%	0.03%	0.14%	0.03%	0.14%	1.42%
Variation coefficient	V [%]	-	-	-	-	-	-0.26%	1.26%	0.26%	1.27%	-
Probability distribution		Uniform		Traingular	Traingular	Normal	Normal	Normal	Normal		

Table B. 62: Type A $u_c(\lambda_{COP})$ sensitivity coefficients, by means of HFM-1 apparatus (Sample: FS based VIP 20 mm thick, $\vartheta_{avg} = 40^\circ\text{C}$, $\Delta\vartheta = 30^\circ\text{C}$)

	Sensitivity coefficients			
	$\partial\lambda_{COP}/\partial t$	$\partial\lambda_{COP}/\partial f_{cal}$	$\partial\lambda_{COP}/\partial Q$	$\partial\lambda_{COP}/\partial \Delta\vartheta$
Upper plate	0.213237	877.764259	0.003551	-0.148845
Lower plate	0.195409	783.880129	0.003644	-0.136400

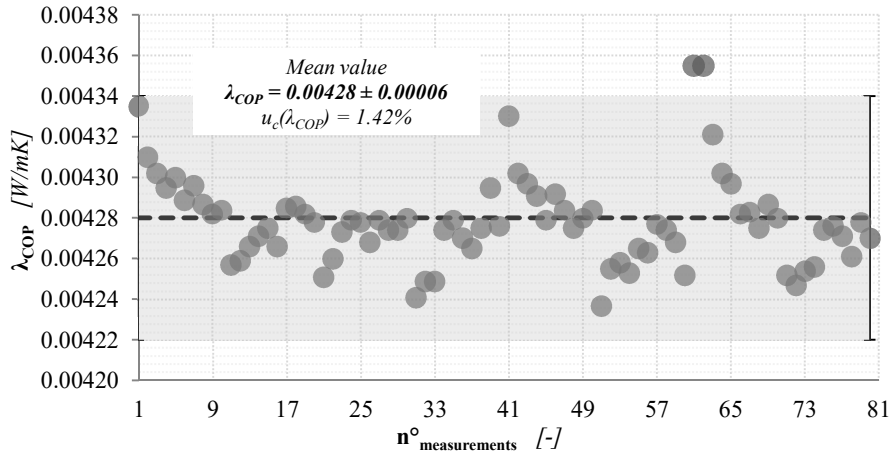


Figure B. 31: λ_{COP} -values assessed by means of HFM-1 apparatus (Sample: FS based VIP 20 mm thick, $\vartheta_{avg} = 40^\circ\text{C}$, $\Delta\vartheta = 30^\circ\text{C}$)

Table B. 63: Type A $u_c(\lambda_{COP})$ assessment, by means of HFM-1 apparatus (Sample: FS based VIP 20 mm thick, $\vartheta_{avg} = 40^\circ\text{C}$, $\Delta\vartheta = 40^\circ\text{C}$)

Test conditions		f_{cal_upper}	f_{cal_lower}	$t_{measured}$	ϑ_{upper}	ϑ_{lower}	Q_{upper}	Q_{lower}	Φ_{upper}	Φ_{lower}	λ_{COP}
20 mm $\vartheta_{avg} = 40^\circ\text{C}$ $\Delta\vartheta = 40^\circ\text{C}$		$[W/m^2 \cdot \mu V]$	$[W/m^2 \cdot \mu V]$	$[mm]$	$[^\circ\text{C}]$	$[^\circ\text{C}]$	$[\mu V]$	$[\mu V]$	$[W/m^2]$	$[W/m^2]$	$[W/mK]$
Mean value	\bar{y}	0.0051	0.0052	20.94	20.018	60.025	-1625	1539	8.343	7.98	0.00426
Median		-	-	-	-	-	-1630	1535	8.370	7.96	-
Skew		-	-	-	-	-	2.136	1.572	-2.130	1.563	-
Standard deviation	s	-	-	-	-	-	13.4	17.6	0.069	0.091	-
Absolute uncertainty	$u(\bar{y})$	0.0001	0.0001	0.01	0.003	0.003	1.5	2.0	0.008	0.01	0.00006
Relative uncertainty	$u(\bar{y})$ [%]	2.00%	2.00%	0.07%	0.01%	0.00%	0.09%	0.13%	0.09%	0.13%	1.42%
Variation coefficient	V [%]	-	-	-	-	-	-0.82%	1.14%	0.82%	1.14%	-
Probability distribution					Uniform	Uniform	Uniform	Normal	Normal	Normal	Normal

Table B. 64: Type A $u_c(\lambda_{COP})$ sensitivity coefficients, by means of HFM-1 apparatus (Sample: FS based VIP 20 mm thick, $\vartheta_{avg} = 40^\circ\text{C}$, $\Delta\vartheta = 40^\circ\text{C}$)

	Sensitivity coefficients			
	$\partial\lambda_{COP}/\partial t$	$\partial\lambda_{COP}/\partial f_{cal}$	$\partial\lambda_{COP}/\partial Q$	$\partial\lambda_{COP}/\partial\Delta\vartheta$
Upper plate	0.208573	850.538656	0.002688	-0.109169
Lower plate	0.199573	805.525533	0.002715	-0.104458

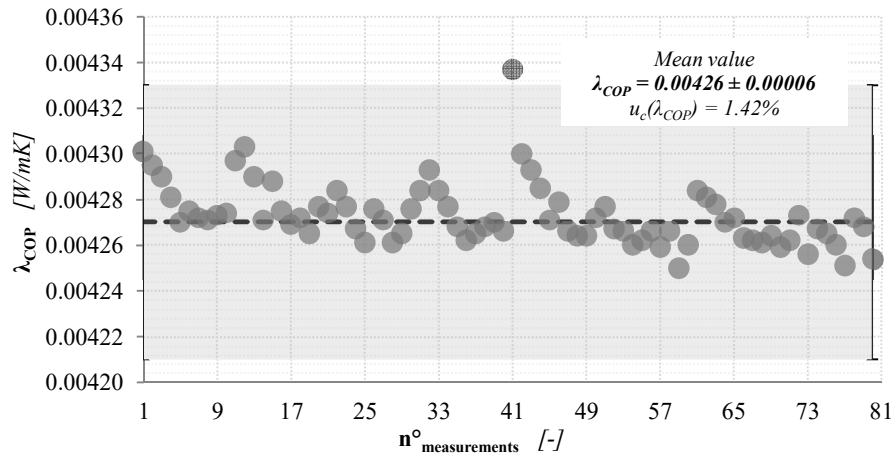
**Figure B. 32:** λ_{COP} -values assessed by means of HFM-1 apparatus (Sample: FS based VIP 20 mm thick, $\vartheta_{avg} = 40^\circ\text{C}$, $\Delta\vartheta = 40^\circ\text{C}$)

Table B. 65: Type A $u_c(\lambda_{COP})$ assessment, by means of HFM-1 apparatus (Sample: FS based VIP 30 mm thick, $\vartheta_{avg} = 5^\circ\text{C}$, $\Delta\vartheta = 10^\circ\text{C}$)

Test conditions		f_{cal_upper}	f_{cal_lower}	$t_{measured}$	ϑ_{upper}	ϑ_{lower}	Q_{upper}	Q_{lower}	Φ_{upper}	Φ_{lower}	λ_{COP}
30 mm $\vartheta_{avg} = 5^\circ\text{C}$ $\Delta\vartheta = 10^\circ\text{C}$		$[\text{W}/\text{m}^2 \cdot \mu\text{V}]$	$[\text{W}/\text{m}^2 \cdot \mu\text{V}]$	$[\text{mm}]$	$[\text{C}^\circ]$	$[\text{C}^\circ]$	$[\mu\text{V}]$	$[\mu\text{V}]$	$[\text{W}/\text{m}^2]$	$[\text{W}/\text{m}^2]$	$[\text{W}/\text{mK}]$
Mean value	\bar{y}	0.0054	0.0055	29.56	0.016	10.010	-287.2	293.5	1.539	1.615	0.00466
Median		-	-	-	-	-	-285.0	295.5	1.529	1.625	-
Skew		-	-	-	-	-	-1.899	-0.583	1.900	-0.586	-
Standard deviation	s	-	-	-	-	-	7.5	7.5	0.040	0.041	-
Absolute uncertainty	$u(\bar{y})$	0.0001	0.0001	0.02	0.003	0.002	0.8	0.8	0.005	0.005	0.00007
Relative uncertainty	$u(\bar{y})$ [%]	2.00%	2.00%	0.08%	18.04%	0.02%	0.29%	0.29%	0.29%	0.29%	1.43%
Variation coefficient	V [%]	-	-	-	-	-	-2.63%	2.57%	2.63%	2.56%	-
Probability distribution		Triangular Uniform Triangular Normal Normal Normal Normal									

Table B. 66: Type A $u_c(\lambda_{COP})$ sensitivity coefficients, by means of HFM-1 apparatus (Sample: FS based VIP 30 mm thick, $\vartheta_{avg} = 5^\circ\text{C}$, $\Delta\vartheta = 10^\circ\text{C}$)

	Sensitivity coefficients			
	$\partial\lambda_{COP}/\partial t$	$\partial\lambda_{COP}/\partial f_{cal}$	$\partial\lambda_{COP}/\partial Q$	$\partial\lambda_{COP}/\partial\Delta\vartheta$
Upper plate	0.153917	849.472884	0.015842	-0.455251
Lower plate	0.161551	868.106864	0.016271	-0.477832

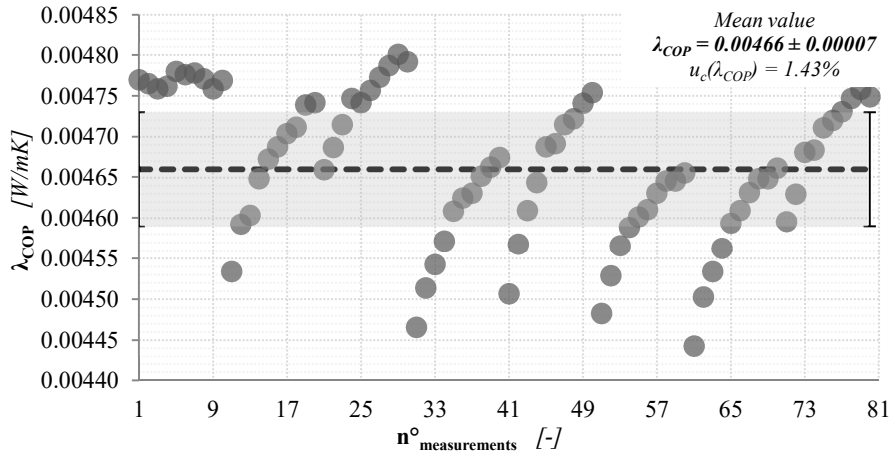


Figure B. 33: λ_{COP} -values assessed by means of HFM-1 apparatus (Sample: FS based VIP 30 mm thick, $\vartheta_{avg} = 5^\circ\text{C}$, $\Delta\vartheta = 10^\circ\text{C}$)

Table B. 67: Type A $u_c(\lambda_{COP})$ assessment, by means of HFM-1 apparatus (Sample: FS based VIP 30 mm thick, $\vartheta_{avg} = 5^\circ\text{C}$, $\Delta\vartheta = 20^\circ\text{C}$)

Test conditions		f_{cal_upper}	f_{cal_lower}	$t_{measured}$	ϑ_{upper}	ϑ_{lower}	Q_{upper}	Q_{lower}	Φ_{upper}	Φ_{lower}	λ_{COP}
30 mm $\vartheta_{avg} = 5^\circ\text{C}$ $\Delta\vartheta = 20^\circ\text{C}$		$[\text{W}/\text{m}^2 \cdot \mu\text{V}]$	$[\text{W}/\text{m}^2 \cdot \mu\text{V}]$	$[\text{mm}]$	$[\text{C}^\circ]$	$[\text{C}^\circ]$	$[\mu\text{V}]$	$[\mu\text{V}]$	$[\text{W}/\text{m}^2]$	$[\text{W}/\text{m}^2]$	$[\text{W}/\text{mK}]$
Mean value	\bar{y}	0.0054	0.0055	29.56	-4.981	15.013	-588.3	595	3.184	3.254	0.00476
Median		-	-	-	-	-	-588.5	593	3.185	3.244	-
Skew		-	-	-	-	-	-0.575	0.052	0.647	0.058	-
Standard deviation	s	-	-	-	-	-	6.4	15.3	0.035	0.084	-
Absolute uncertainty	$u(\bar{y})$	0.0001	0.0001	0.02	0.002	0.003	0.7	1.7	0.004	0.009	0.00007
Relative uncertainty	$u(\bar{y})$	2.00%	2.00%	0.08%	0.04%	0.02%	0.12%	0.29%	0.12%	0.29%	1.42%
Variation coefficient	V	-	-	-	-	-	-1.09%	2.56%	1.09%	2.57%	-
Probability distribution					Triangular	Triangular	Uniform	Normal	Normal	Normal	Normal

Table B. 68: Type A $u_c(\lambda_{COP})$ sensitivity coefficients, by means of HFM-1 apparatus (Sample: FS based VIP 30 mm thick, $\vartheta_{avg} = 5^\circ\text{C}$, $\Delta\vartheta = 20^\circ\text{C}$)

	Sensitivity coefficients			
	$\partial\lambda_{COP}/\partial t$	$\partial\lambda_{COP}/\partial f_{cal}$	$\partial\lambda_{COP}/\partial Q$	$\partial\lambda_{COP}/\partial\Delta\vartheta$
Upper plate	0.159242	869.768330	0.008001	-0.235430
Lower plate	0.162781	879.673902	0.008087	-0.240663

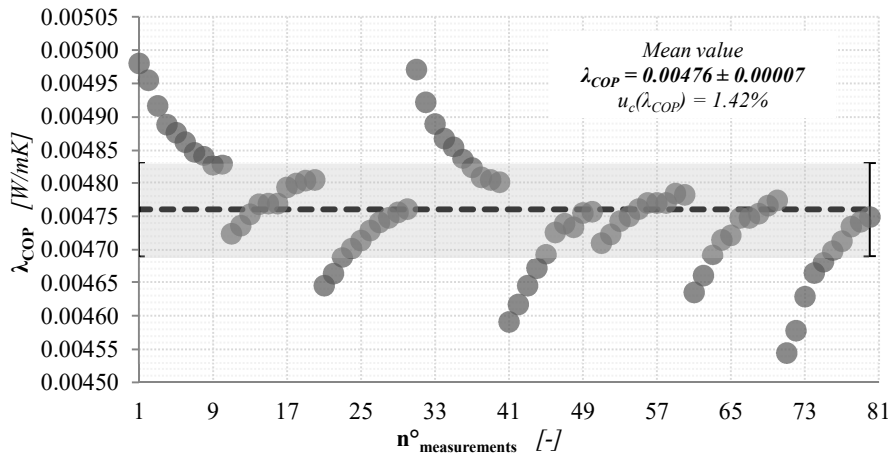
**Figure B. 34:** λ_{COP} -values assessed by means of HFM-1 apparatus (Sample: FS based VIP 30 mm thick, $\vartheta_{avg} = 5^\circ\text{C}$, $\Delta\vartheta = 20^\circ\text{C}$)

Table B. 69: Type A $u_c(\lambda_{COP})$ assessment, by means of HFM-1 apparatus (Sample: FS based VIP 30 mm thick, $\vartheta_{avg} = 5^\circ\text{C}$, $\Delta\vartheta = 30^\circ\text{C}$)

Test conditions		f_{cal_upper}	f_{cal_lower}	$t_{measured}$	ϑ_{upper}	ϑ_{lower}	Q_{upper}	Q_{lower}	Φ_{upper}	Φ_{lower}	λ_{COP}
30 mm $\vartheta_{avg} = 5^\circ\text{C}$ $\Delta\vartheta = 30^\circ\text{C}$		$[\text{W}/\text{m}^2 \cdot \mu\text{V}]$	$[\text{W}/\text{m}^2 \cdot \mu\text{V}]$	$[\text{mm}]$	$[\text{C}^\circ]$	$[\text{C}^\circ]$	$[\mu\text{V}]$	$[\mu\text{V}]$	$[\text{W}/\text{m}^2]$	$[\text{W}/\text{m}^2]$	$[\text{W}/\text{mK}]$
Mean value	\bar{y}	0.0055	0.0054	29.57	-9.982	20.014	-886	902	4.843	4.90	0.00481
Median		-	-	-	-	-	-885	896	4.840	4.87	-
Skew		-	-	-	-	-	-0.005	-0.001	0.001	-0.004	-
Standard deviation	s	-	-	-	-	-	14.3	23.3	0.078	0.13	-
Absolute uncertainty	$u(\bar{y})$	0.0001	0.0001	0.03	0.002	0.003	1.6	2.6	0.009	0.01	0.00007
Relative uncertainty	$u(\bar{y})$ [%]	2.00%	2.00%	0.12%	0.02%	0.01%	0.18%	0.29%	0.18%	0.29%	1.43%
Variation coefficient	V [%]	-	-	-	-	-	-1.61%	2.58%	1.61%	2.58%	-
Probability distribution					Uniform	Triangular	Uniform	Normal	Normal	Normal	Normal

Table B. 70: Type A $u_c(\lambda_{COP})$ sensitivity coefficients, by means of HFM-1 apparatus (Sample: FS based VIP 30 mm thick, $\vartheta_{avg} = 5^\circ\text{C}$, $\Delta\vartheta = 30^\circ\text{C}$)

	Sensitivity coefficients			
	$\partial\lambda_{COP}/\partial t$	$\partial\lambda_{COP}/\partial f_{cal}$	$\partial\lambda_{COP}/\partial Q$	$\partial\lambda_{COP}/\partial \Delta\vartheta$
Upper plate	0.161510	873.417122	0.005390	-0.159216
Lower plate	0.163554	889.189892	0.005362	-0.161232

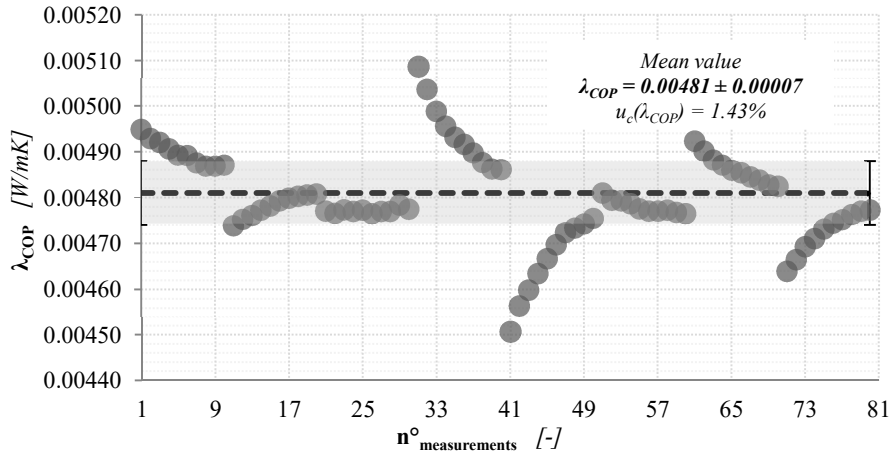


Figure B. 35: λ_{COP} -values assessed by means of HFM-1 apparatus (Sample: FS based VIP 30 mm thick, $\vartheta_{avg} = 5^\circ\text{C}$, $\Delta\vartheta = 30^\circ\text{C}$)

Table B. 71: Type A $u_c(\lambda_{COP})$ assessment, by means of HFM-1 apparatus (Sample: FS based VIP 30 mm thick, $\vartheta_{avg} = 5^\circ\text{C}$, $\Delta\vartheta = 40^\circ\text{C}$)

Test conditions		f_{cal_upper}	f_{cal_lower}	$t_{measured}$	ϑ_{upper}	ϑ_{lower}	Q_{upper}	Q_{lower}	Φ_{upper}	Φ_{lower}	λ_{COP}
30 mm $\vartheta_{avg} = 5^\circ\text{C}$ $\Delta\vartheta = 40^\circ\text{C}$		$[\text{W}/\text{m}^2 \cdot \mu\text{V}]$	$[\text{W}/\text{m}^2 \cdot \mu\text{V}]$	$[\text{mm}]$	$[\text{C}^\circ]$	$[\text{C}^\circ]$	$[\mu\text{V}]$	$[\mu\text{V}]$	$[\text{W}/\text{m}^2]$	$[\text{W}/\text{m}^2]$	$[\text{W}/\text{mK}]$
Mean value	\bar{y}	0.0055	0.0054	29.57	-14.990	25.027	-1195	1240	6.606	6.704	0.00492
Median		-	-	-	-	-	-1190	1237	6.578	6.688	-
Skew		-	-	-	-	-	-1.189	0.792	1.200	0.789	-
Standard deviation	s	-	-	-	-	-	16.8	12.0	0.093	0.065	-
Absolute uncertainty	$u(\bar{y})$	0.0001	0.0001	0.03	0.002	0.003	1.9	1.3	0.010	0.007	0.00007
Relative uncertainty	$u(\bar{y})$ [%]	2.00%	2.00%	0.12%	0.01%	0.01%	0.16%	0.11%	0.16%	0.11%	1.42%
Variation coefficient	V [%]	-	-	-	-	-	-1.41%	0.97%	1.41%	0.97%	-
Probability distribution				Uniform	Triangular	Uniform	Normal	Normal	Normal	Normal	

Table B. 72: Type A $u_c(\lambda_{COP})$ sensitivity coefficients, by means of HFM-1 apparatus (Sample: FS based VIP 30 mm thick, $\vartheta_{avg} = 5^\circ\text{C}$, $\Delta\vartheta = 40^\circ\text{C}$)

	Sensitivity coefficients			
	$\partial\lambda_{COP}/\partial t$	$\partial\lambda_{COP}/\partial f_{cal}$	$\partial\lambda_{COP}/\partial Q$	$\partial\lambda_{COP}/\partial\Delta\vartheta$
Upper plate	0.165019	883.028463	0.004083	-0.121939
Lower plate	0.167577	916.280581	0.003996	-0.123829

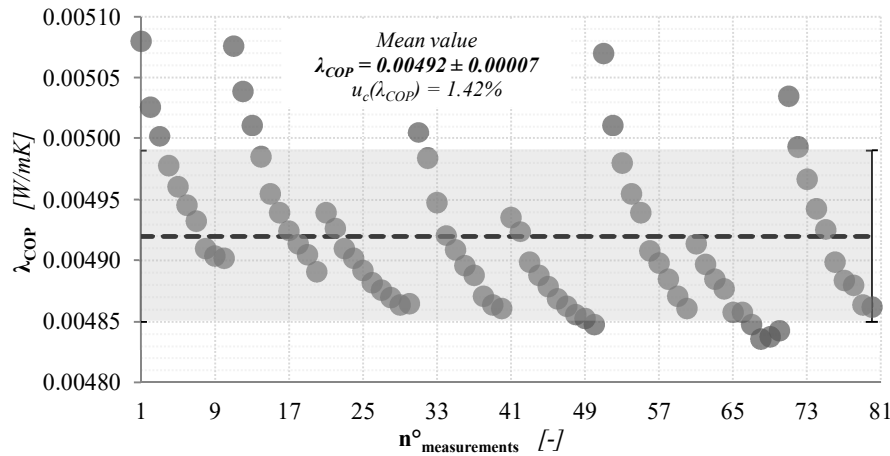
**Figure B. 36:** λ_{COP} -values assessed by means of HFM-1 apparatus (Sample: FS based VIP 30 mm thick, $\vartheta_{avg} = 5^\circ\text{C}$, $\Delta\vartheta = 40^\circ\text{C}$)

Table B. 73: Type A $u_c(\lambda_{COP})$ assessment, by means of HFM-1 apparatus (Sample: FS based VIP 30 mm thick, $\vartheta_{avg} = 10^\circ\text{C}$, $\Delta\vartheta = 10^\circ\text{C}$)

Test conditions		f_{cal_upper}	f_{cal_lower}	$t_{measured}$	ϑ_{upper}	ϑ_{lower}	Q_{upper}	Q_{lower}	Φ_{upper}	Φ_{lower}	λ_{COP}
30 mm $\vartheta_{avg} = 10^\circ\text{C}$ $\Delta\vartheta = 10^\circ\text{C}$		$[\text{W}/\text{m}^2 \cdot \mu\text{V}]$	$[\text{W}/\text{m}^2 \cdot \mu\text{V}]$	$[\text{mm}]$	$[\text{C}^\circ]$	$[\text{C}^\circ]$	$[\mu\text{V}]$	$[\mu\text{V}]$	$[\text{W}/\text{m}^2]$	$[\text{W}/\text{m}^2]$	$[\text{W}/\text{mK}]$
Mean value	\bar{y}	0.0053	0.0055	29.557	5.010	15.011	-305.7	294.6	1.621	1.612	0.00478
Median		-	-	-	-	-	-305.0	296.0	1.619	1.619	-
Skew		-	-	-	-	-	-1.533	-0.934	1.531	-0.956	-
Standard deviation	s	-	-	-	-	-	3.7	5.2	0.019	0.029	-
Absolute uncertainty	$u(\bar{y})$	0.0001	0.0001	0.001	0.002	0.002	0.4	0.6	0.002	0.003	0.00007
Relative uncertainty	$u(\bar{y})$ [%]	2.00%	2.00%	0.004%	0.04%	0.01%	0.13%	0.20%	0.13%	0.20%	1.42%
Variation coefficient	V [%]	-	-	-	-	-	-1.20%	1.78%	1.19%	1.78%	-
Probability distribution		Triangular Triangular Triangular Normal Normal Normal Normal									

Table B. 74: Type A $u_c(\lambda_{COP})$ sensitivity coefficients, by means of HFM-1 apparatus (Sample: FS based VIP 30 mm thick, $\vartheta_{avg} = 10^\circ\text{C}$, $\Delta\vartheta = 10^\circ\text{C}$)

	Sensitivity coefficients			
	$\partial\lambda_{COP}/\partial t$	$\partial\lambda_{COP}/\partial f_{cal}$	$\partial\lambda_{COP}/\partial Q$	$\partial\lambda_{COP}/\partial \Delta\vartheta$
Upper plate	0.162035	903.467143	0.015667	-0.478880
Lower plate	0.161130	870.662154	0.016166	-0.476205

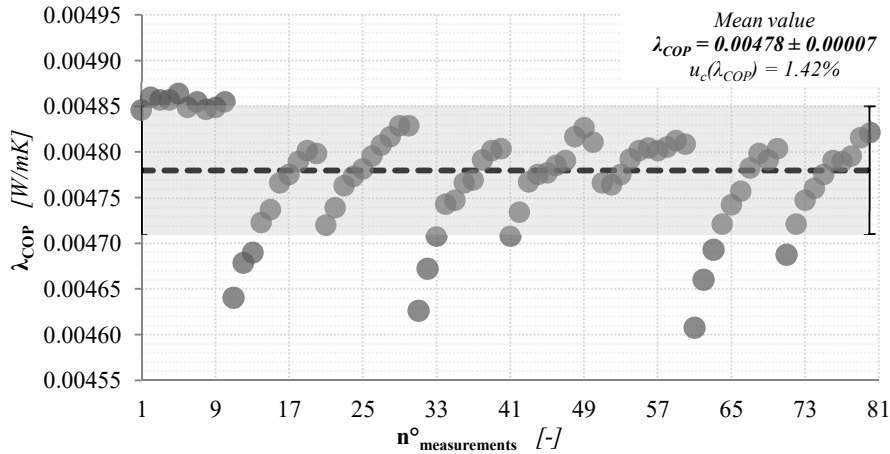


Figure B. 37: λ_{COP} -values assessed by means of HFM-1 apparatus (Sample: FS based VIP 30 mm thick, $\vartheta_{avg} = 10^\circ\text{C}$, $\Delta\vartheta = 10^\circ\text{C}$)

Table B. 75: Type A $u_c(\lambda_{COP})$ assessment, by means of HFM-1 apparatus (Sample: FS based VIP 30 mm thick, $\vartheta_{avg} = 10^\circ\text{C}$, $\Delta\vartheta = 20^\circ\text{C}$)

Test conditions		f_{cal_upper}	f_{cal_lower}	$t_{measured}$	ϑ_{upper}	ϑ_{lower}	Q_{upper}	Q_{lower}	Φ_{upper}	Φ_{lower}	λ_{COP}
30 mm $\vartheta_{avg} = 10^\circ\text{C}$ $\Delta\vartheta = 20^\circ\text{C}$		$[\text{W}/\text{m}^2 \cdot \mu\text{V}]$	$[\text{W}/\text{m}^2 \cdot \mu\text{V}]$	$[\text{mm}]$	$[\text{C}^\circ]$	$[\text{C}^\circ]$	$[\mu\text{V}]$	$[\mu\text{V}]$	$[\text{W}/\text{m}^2]$	$[\text{W}/\text{m}^2]$	$[\text{W}/\text{mK}]$
Mean value	\bar{y}	0.0054	0.0054	29.547	0.015	20.014	-612.4	601	3.280	3.27	0.00484
Median	-	-	-	-	-	-	-611.5	598	3.275	3.25	-
Skew	-	-	-	-	-	-	-1.222	0.151	1.203	0.151	-
Standard deviation	s	-	-	-	-	-	7.1	18.2	0.038	0.10	-
Absolute uncertainty	$u(\bar{y})$	0.0001	0.0001	0.009	0.003	0.003	0.8	2.0	0.004	0.01	0.00007
Relative uncertainty	$u(\bar{y})$ [%]	2.00%	2.00%	0.031%	19.25%	0.01%	0.13%	0.34%	0.13%	0.34%	1.43%
Variation coefficient	V [%]	-	-	-	-	-	-1.17%	3.03%	1.15%	3.03%	-
Probability distribution				Triangular	Uniform	Uniform	Normal	Normal	Normal	Normal	

Table B. 76: Type A $u_c(\lambda_{COP})$ sensitivity coefficients, by means of HFM-1 apparatus (Sample: FS based VIP 30 mm thick, $\vartheta_{avg} = 10^\circ\text{C}$, $\Delta\vartheta = 20^\circ\text{C}$)

	Sensitivity coefficients			
	$\partial\lambda_{COP}/\partial t$	$\partial\lambda_{COP}/\partial f_{cal}$	$\partial\lambda_{COP}/\partial Q$	$\partial\lambda_{COP}/\partial\Delta\vartheta$
Upper plate	0.164009	904.774379	0.007913	-0.242311
Lower plate	0.163450	887.931747	0.008036	-0.241485

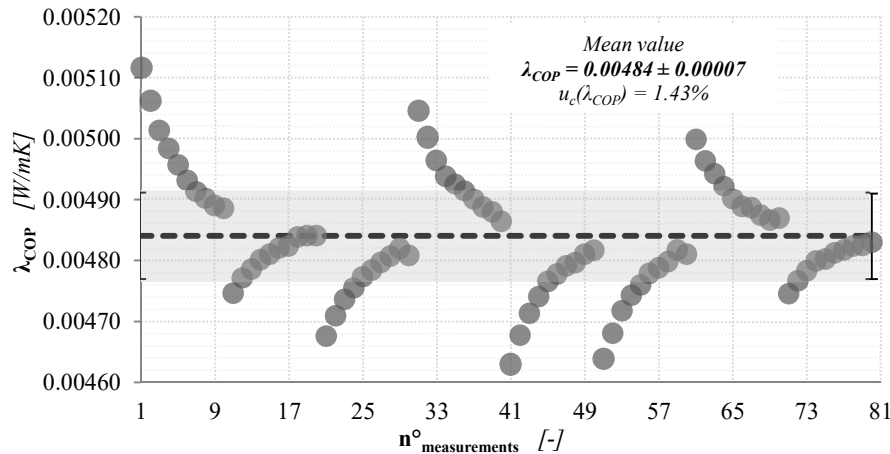
**Figure B. 38:** λ_{COP} -values assessed by means of HFM-1 apparatus (Sample: FS based VIP 30 mm thick, $\vartheta_{avg} = 10^\circ\text{C}$, $\Delta\vartheta = 20^\circ\text{C}$)

Table B. 77: Type A $u_c(\lambda_{COP})$ assessment, by means of HFM-1 apparatus (Sample: FS based VIP 30 mm thick, $\vartheta_{avg} = 10^\circ\text{C}$, $\Delta\vartheta = 30^\circ\text{C}$)

Test conditions		f_{cal_upper}	f_{cal_lower}	$t_{measured}$	ϑ_{upper}	ϑ_{lower}	Q_{upper}	Q_{lower}	Φ_{upper}	Φ_{lower}	λ_{COP}
30 mm $\vartheta_{avg} = 10^\circ\text{C}$ $\Delta\vartheta = 30^\circ\text{C}$		$[\text{W}/\text{m}^2 \cdot \mu\text{V}]$	$[\text{W}/\text{m}^2 \cdot \mu\text{V}]$	$[\text{mm}]$	$[\text{C}^\circ]$	$[\text{C}^\circ]$	$[\mu\text{V}]$	$[\mu\text{V}]$	$[\text{W}/\text{m}^2]$	$[\text{W}/\text{m}^2]$	$[\text{W}/\text{mK}]$
Mean value	\bar{y}	0.0054	0.0054	29.557	-4.985	25.024	-920	922	4.978	4.99	0.00491
Median		-	-	-	-	-	-918	928	4.967	5.01	-
Skew		-	-	-	-	-	0.058	-0.405	-0.057	-0.399	-
Standard deviation	s	-	-	-	-	-	14.8	25.1	0.080	0.14	-
Absolute uncertainty	$u(\bar{y})$	0.0001	0.0001	0.001	0.003	0.003	1.7	2.8	0.009	0.02	0.00007
Relative uncertainty	$u(\bar{y})$ [%]	2.00%	2.00%	0.004%	0.06%	0.01%	0.18%	0.30%	0.18%	0.30%	1.42%
Variation coefficient	V [%]	-	-	-	-	-	-1.61%	2.72%	1.61%	2.72%	-
Probability distribution				Triangular	Uniform	Uniform	Normal	Normal	Normal	Normal	

Table B. 78: Type A $u_c(\lambda_{COP})$ sensitivity coefficients, by means of HFM-1 apparatus (Sample: FS based VIP 30 mm thick, $\vartheta_{avg} = 10^\circ\text{C}$, $\Delta\vartheta = 30^\circ\text{C}$)

	Sensitivity coefficients			
	$\partial\lambda_{COP}/\partial t$	$\partial\lambda_{COP}/\partial f_{cal}$	$\partial\lambda_{COP}/\partial Q$	$\partial\lambda_{COP}/\partial \Delta\vartheta$
Upper plate	0.165918	906.142824	0.005330	-0.163419
Lower plate	0.166156	908.112700	0.005327	-0.163653

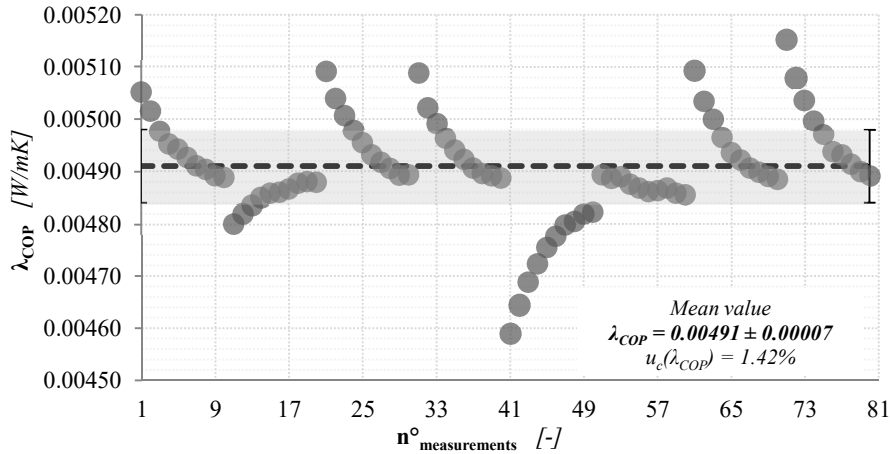


Figure B. 39: λ_{COP} -values assessed by means of HFM-1 apparatus (Sample: FS based VIP 30 mm thick, $\vartheta_{avg} = 10^\circ\text{C}$, $\Delta\vartheta = 30^\circ\text{C}$)

Table B. 79: Type A $u_c(\lambda_{COP})$ assessment, by means of HFM-1 apparatus (Sample: FS based VIP 30 mm thick, $\vartheta_{avg} = 10^\circ\text{C}$, $\Delta\vartheta = 40^\circ\text{C}$)

Test conditions		f_{cal_upper}	f_{cal_lower}	$t_{measured}$	ϑ_{upper}	ϑ_{lower}	Q_{upper}	Q_{lower}	Φ_{upper}	Φ_{lower}	λ_{COP}
30 mm $\vartheta_{avg} = 10^\circ\text{C}$ $\Delta\vartheta = 40^\circ\text{C}$		$[W/m^2 \cdot \mu V]$	$[W/m^2 \cdot \mu V]$	$[mm]$	$[^\circ\text{C}]$	$[^\circ\text{C}]$	$[\mu V]$	$[\mu V]$	$[W/m^2]$	$[W/m^2]$	$[W/mK]$
Mean value	\bar{y}	0.0055	0.0054	29.547	-9.988	30.024	-1233	1256	6.74	6.75	0.00498
Median		-	-	-	-	-	-1227	1256	6.71	6.75	-
Skew		-	-	-	-	-	-1.221	-0.461	1.217	-0.463	-
Standard deviation	s	-	-	-	-	-	21.1	27.3	0.11	0.15	-
Absolute uncertainty	$u(\bar{y})$	0.0001	0.0001	0.009	0.003	0.003	2.4	3.0	0.01	0.02	0.00007
Relative uncertainty	$u(\bar{y})$ [%]	2.00%	2.00%	0.031%	0.03%	0.01%	0.19%	0.24%	0.19%	0.24%	1.42%
Variation coefficient	V [%]	-	-	-	-	-	-1.71%	2.17%	1.71%	2.17%	-
Probability distribution				Triangular	Uniform	Uniform	Normal	Normal	Normal	Normal	

Table B. 80: Type A $u_c(\lambda_{COP})$ sensitivity coefficients, by means of HFM-1 apparatus (Sample: FS based VIP 30 mm thick, $\vartheta_{avg} = 10^\circ\text{C}$, $\Delta\vartheta = 40^\circ\text{C}$)

	Sensitivity coefficients			
	$\partial\lambda_{COP}/\partial t$	$\partial\lambda_{COP}/\partial f_{cal}$	$\partial\lambda_{COP}/\partial Q$	$\partial\lambda_{COP}/\partial\Delta\vartheta$
Upper plate	0.168501	910.513121	0.004038	-0.124430
Lower plate	0.168756	927.497551	0.003970	-0.124618

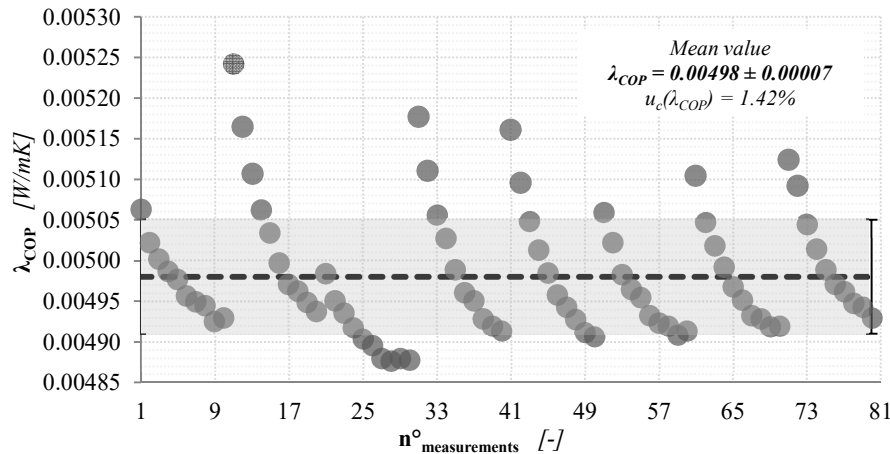
**Figure B. 40:** λ_{COP} -values assessed by means of HFM-1 apparatus (Sample: FS based VIP 30 mm thick, $\vartheta_{avg} = 10^\circ\text{C}$, $\Delta\vartheta = 40^\circ\text{C}$)

Table B. 81: Type A $u_c(\lambda_{COP})$ assessment, by means of HFM-1 apparatus (Sample: FS based VIP 30 mm thick, $\vartheta_{avg} = 23^\circ\text{C}$, $\Delta\vartheta = 10^\circ\text{C}$)

Test conditions		f_{cal_upper}	f_{cal_lower}	$t_{measured}$	ϑ_{upper}	ϑ_{lower}	Q_{upper}	Q_{lower}	Φ_{upper}	Φ_{lower}	λ_{COP}
30 mm $\vartheta_{avg} = 23^\circ\text{C}$ $\Delta\vartheta = 10^\circ\text{C}$		$[\text{W}/\text{m}^2 \cdot \mu\text{V}]$	$[\text{W}/\text{m}^2 \cdot \mu\text{V}]$	$[\text{mm}]$	$[\text{C}^\circ]$	$[\text{C}^\circ]$	$[\mu\text{V}]$	$[\mu\text{V}]$	$[\text{W}/\text{m}^2]$	$[\text{W}/\text{m}^2]$	$[\text{W}/\text{mK}]$
Mean value	\bar{y}	0.0052	0.0054	29.51	18.018	28.013	-362.4	303	1.871	1.634	0.00517
Median		-	-	-	-	-	-363.0	303	1.876	1.633	-
Skew		-	-	-	-	-	1.550	0.536	-1.518	0.534	-
Standard deviation	s	-	-	-	-	-	7.2	9.7	0.037	0.052	-
Absolute uncertainty	$u(\bar{y})$	0.0001	0.0001	0.01	0.003	0.003	0.8	1.1	0.004	0.006	0.00007
Relative uncertainty	$u(\bar{y})$ [%]	2.00%	2.00%	0.04%	0.02%	0.01%	0.22%	0.36%	0.22%	0.36%	1.43%
Variation coefficient	V [%]	-	-	-	-	-	-1.99%	3.21%	1.99%	3.20%	-
Probability distribution				Triangular	Uniform	Uniform	Normal	Normal	Normal	Normal	

Table B. 82: Type A $u_c(\lambda_{COP})$ sensitivity coefficients, by means of HFM-1 apparatus (Sample: FS based VIP 30 mm thick, $\vartheta_{avg} = 23^\circ\text{C}$, $\Delta\vartheta = 10^\circ\text{C}$)

	Sensitivity coefficients			
	$\partial\lambda_{COP}/\partial t$	$\partial\lambda_{COP}/\partial f_{cal}$	$\partial\lambda_{COP}/\partial Q$	$\partial\lambda_{COP}/\partial \Delta\vartheta$
Upper plate	0.187201	1069.977389	0.015244	-0.552706
Lower plate	0.163368	894.600300	0.015911	-0.482341

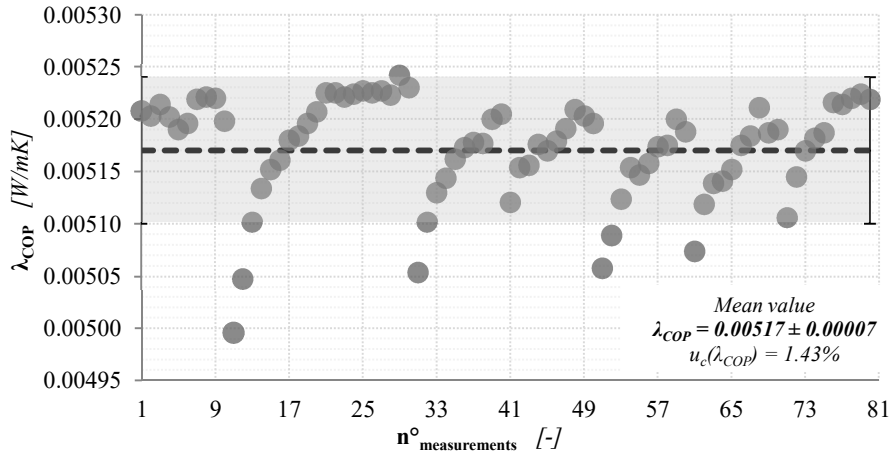


Figure B. 41: λ_{COP} -values assessed by means of HFM-1 apparatus (Sample: FS based VIP 30 mm thick, $\vartheta_{avg} = 23^\circ\text{C}$, $\Delta\vartheta = 10^\circ\text{C}$)

Table B. 83: Type A $u_c(\lambda_{COP})$ assessment, by means of HFM-1 apparatus (Sample: FS based VIP 30 mm thick, $\vartheta_{avg} = 23^\circ\text{C}$, $\Delta\vartheta = 20^\circ\text{C}$)

Test conditions		f_{cal_upper}	f_{cal_lower}	$t_{measured}$	ϑ_{upper}	ϑ_{lower}	Q_{upper}	Q_{lower}	Φ_{upper}	Φ_{lower}	λ_{COP}
30 mm $\vartheta_{avg} = 23^\circ\text{C}$ $\Delta\vartheta = 20^\circ\text{C}$		$[\text{W}/\text{m}^2 \cdot \mu\text{V}]$	$[\text{W}/\text{m}^2 \cdot \mu\text{V}]$	$[\text{mm}]$	$[\text{C}^\circ]$	$[\text{C}^\circ]$	$[\mu\text{V}]$	$[\mu\text{V}]$	$[\text{W}/\text{m}^2]$	$[\text{W}/\text{m}^2]$	$[\text{W}/\text{mK}]$
Mean value	\bar{y}	0.0052	0.0054	29.51	13.020	33.018	-700.9	630	3.656	3.373	0.00519
Median		-	-	-	-	-	-701.0	628	3.657	3.366	-
Skew		-	-	-	-	-	-0.548	0.650	0.580	0.634	-
Standard deviation	s	-	-	-	-	-	6.2	17.5	0.032	0.094	-
Absolute uncertainty	$u(\bar{y})$	0.0001	0.0001	0.01	0.002	0.003	0.7	2.0	0.004	0.010	0.00007
Relative uncertainty	$u(\bar{y})$ [%]	2.00%	2.00%	0.05%	0.02%	0.01%	0.10%	0.31%	0.10%	0.31%	1.42%
Variation coefficient	V [%]	-	-	-	-	-	-0.88%	2.77%	0.87%	2.78%	-
Probability distribution				Uniform	Triangular	Uniform	Normal	Normal	Normal	Normal	

Table B. 84: Type A $u_c(\lambda_{COP})$ sensitivity coefficients, by means of HFM-1 apparatus (Sample: FS based VIP 30 mm thick, $\vartheta_{avg} = 23^\circ\text{C}$, $\Delta\vartheta = 20^\circ\text{C}$)

	Sensitivity coefficients			
	$\partial\lambda_{COP}/\partial t$	$\partial\lambda_{COP}/\partial f_{cal}$	$\partial\lambda_{COP}/\partial Q$	$\partial\lambda_{COP}/\partial \Delta\vartheta$
Upper plate	0.182813	1034.281378	0.007697	-0.269768
Lower plate	0.168794	929.657966	0.007907	-0.249080

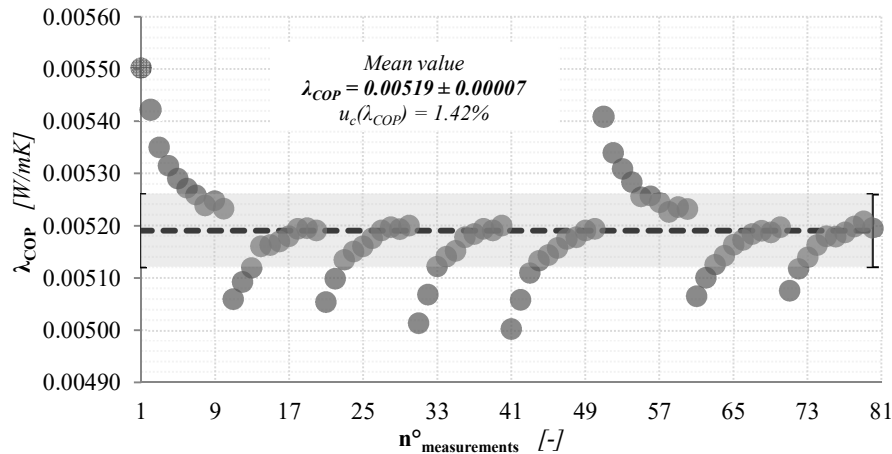
**Figure B. 42:** λ_{COP} -values assessed by means of HFM-1 apparatus (Sample: FS based VIP 30 mm thick, $\vartheta_{avg} = 23^\circ\text{C}$, $\Delta\vartheta = 20^\circ\text{C}$)

Table B. 85: Type A $u_c(\lambda_{COP})$ assessment, by means of HFM-1 apparatus (Sample: FS based VIP 30 mm thick, $\vartheta_{avg} = 23^\circ\text{C}$, $\Delta\vartheta = 30^\circ\text{C}$)

Test conditions		f_{cal_upper}	f_{cal_lower}	$t_{measured}$	ϑ_{upper}	ϑ_{lower}	Q_{upper}	Q_{lower}	Φ_{upper}	Φ_{lower}	λ_{COP}
30 mm $\vartheta_{avg} = 23^\circ\text{C}$ $\Delta\vartheta = 30^\circ\text{C}$		$[\text{W}/\text{m}^2 \cdot \mu\text{V}]$	$[\text{W}/\text{m}^2 \cdot \mu\text{V}]$	$[\text{mm}]$	$[\text{C}^\circ]$	$[\text{C}^\circ]$	$[\mu\text{V}]$	$[\mu\text{V}]$	$[\text{W}/\text{m}^2]$	$[\text{W}/\text{m}^2]$	$[\text{W}/\text{mK}]$
Mean value	\bar{y}	0.0053	0.0053	29.51	8.011	38.023	-1020	988	5.375	5.26	0.00523
Median		-	-	-	-	-	-1024	988	5.392	5.26	-
Skew		-	-	-	-	-	1.039	0.045	-1.032	0.038	-
Standard deviation	s	-	-	-	-	-	17.8	31.4	0.094	0.17	-
Absolute uncertainty	$u(\bar{y})$	0.0001	0.0001	0.01	0.002	0.003	2.0	3.5	0.010	0.02	0.00007
Relative uncertainty	$u(\bar{y})$ [%]	2.00%	2.00%	0.05%	0.03%	0.01%	0.19%	0.36%	0.19%	0.36%	1.43%
Variation coefficient	V [%]	-	-	-	-	-	-1.74%	3.18%	1.74%	3.18%	-
Probability distribution				Uniform	Triangular	Uniform	Normal	Normal	Normal	Normal	

Table B. 86: Type A $u_c(\lambda_{COP})$ sensitivity coefficients, by means of HFM-1 apparatus (Sample: FS based VIP 30 mm thick, $\vartheta_{avg} = 23^\circ\text{C}$, $\Delta\vartheta = 30^\circ\text{C}$)

	Sensitivity coefficients			
	$\partial\lambda_{COP}/\partial t$	$\partial\lambda_{COP}/\partial f_{cal}$	$\partial\lambda_{COP}/\partial Q$	$\partial\lambda_{COP}/\partial \Delta\vartheta$
Upper plate	0.179074	1002.938824	0.005181	-0.176079
Lower plate	0.175333	971.474077	0.005237	-0.172400

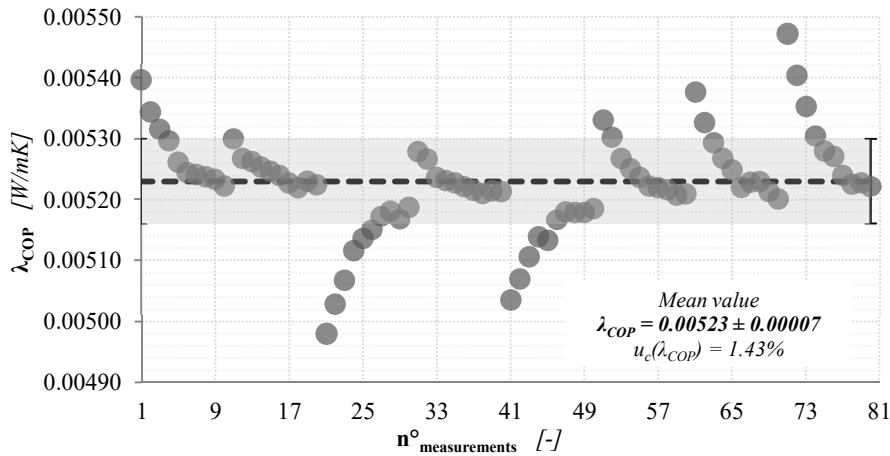


Figure B. 43: λ_{COP} -values assessed by means of HFM-1 apparatus (Sample: FS based VIP 30 mm thick, $\vartheta_{avg} = 23^\circ\text{C}$, $\Delta\vartheta = 30^\circ\text{C}$)

Table B. 87: Type A $u_c(\lambda_{COP})$ assessment, by means of HFM-1 apparatus (Sample: FS based VIP 30 mm thick, $\vartheta_{avg} = 23^\circ\text{C}$, $\Delta\vartheta = 40^\circ\text{C}$)

Test conditions		f_{cal_upper}	f_{cal_lower}	$t_{measured}$	ϑ_{upper}	ϑ_{lower}	Q_{upper}	Q_{lower}	Φ_{upper}	Φ_{lower}	λ_{COP}
30 mm $\vartheta_{avg} = 23^\circ\text{C}$ $\Delta\vartheta = 40^\circ\text{C}$		$[\text{W}/\text{m}^2 \cdot \mu\text{V}]$	$[\text{W}/\text{m}^2 \cdot \mu\text{V}]$	$[\text{mm}]$	$[\text{C}^\circ]$	$[\text{C}^\circ]$	$[\mu\text{V}]$	$[\mu\text{V}]$	$[\text{W}/\text{m}^2]$	$[\text{W}/\text{m}^2]$	$[\text{W}/\text{mK}]$
Mean value	\bar{y}	0.0053	0.0053	29.51	3.010	43.029	-1342	1337	7.143	7.08	0.00524
Median		-	-	-	-	-	-1341	1333	7.139	7.06	-
Skew		-	-	-	-	-	0.746	0.984	-0.733	0.990	-
Standard deviation	s	-	-	-	-	-	16.0	19.2	0.085	0.10	-
Absolute uncertainty	$u(\bar{y})$	0.0001	0.0001	0.01	0.004	0.002	1.8	2.1	0.010	0.01	0.00007
Relative uncertainty	$u(\bar{y})$ [%]	2.00%	2.00%	0.04%	0.14%	0.00%	0.13%	0.16%	0.13%	0.16%	1.42%
Variation coefficient	V [%]	-	-	-	-	-	-1.19%	1.44%	1.19%	1.43%	-
Probability distribution					Triangular	Triangular	Triangular	Normal	Normal	Normal	Normal

Table B. 88: Type A $u_c(\lambda_{COP})$ sensitivity coefficients, by means of HFM-1 apparatus (Sample: FS based VIP 30 mm thick, $\vartheta_{avg} = 23^\circ\text{C}$, $\Delta\vartheta = 40^\circ\text{C}$)

	Sensitivity coefficients			
	$\partial\lambda_{COP}/\partial t$	$\partial\lambda_{COP}/\partial f_{cal}$	$\partial\lambda_{COP}/\partial Q$	$\partial\lambda_{COP}/\partial\Delta\vartheta$
Upper plate	0.178502	989.590445	0.003925	-0.131627
Lower plate	0.176901	985.903446	0.003905	-0.130447

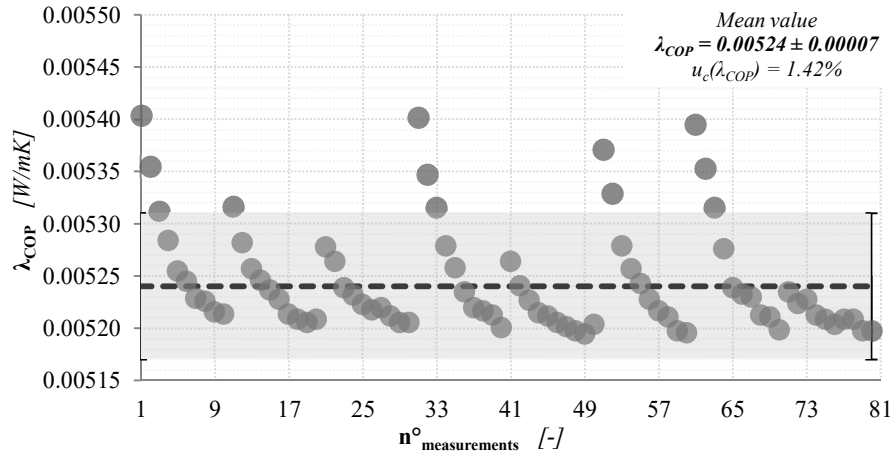
**Figure B. 44:** λ_{COP} -values assessed by means of HFM-1 apparatus (Sample: FS based VIP 30 mm thick, $\vartheta_{avg} = 23^\circ\text{C}$, $\Delta\vartheta = 40^\circ\text{C}$)

Table B. 89: Type A $u_c(\lambda_{COP})$ assessment, by means of HFM-1 apparatus (Sample: FS based VIP 30 mm thick, $\vartheta_{avg} = 40^\circ\text{C}$, $\Delta\vartheta = 10^\circ\text{C}$)

Test conditions		f_{cal_upper}	f_{cal_lower}	$t_{measured}$	ϑ_{upper}	ϑ_{lower}	Q_{upper}	Q_{lower}	Φ_{upper}	Φ_{lower}	λ_{COP}
30 mm $\vartheta_{avg} = 40^\circ\text{C}$ $\Delta\vartheta = 10^\circ\text{C}$		$[\text{W}/\text{m}^2 \cdot \mu\text{V}]$	$[\text{W}/\text{m}^2 \cdot \mu\text{V}]$	$[\text{mm}]$	$[\text{C}^\circ]$	$[\text{C}^\circ]$	$[\mu\text{V}]$	$[\mu\text{V}]$	$[\text{W}/\text{m}^2]$	$[\text{W}/\text{m}^2]$	$[\text{W}/\text{mK}]$
Mean value	\bar{y}	0.0050	0.0053	29.51	35.020	45.021	-459.1	338.2	2.292	1.786	0.00602
Median		-	-	-	-	-	-460.0	337.0	2.295	1.778	-
Skew		-	-	-	-	-	0.661	0.272	-0.670	0.295	-
Standard deviation	s	-	-	-	-	-	4.3	6.6	0.021	0.034	-
Absolute uncertainty	$u(\bar{y})$	0.0001	0.0001	0.01	0.002	0.002	0.5	0.7	0.002	0.004	0.00009
Relative uncertainty	$u(\bar{y})$ [%]	2.00%	2.00%	0.02%	0.01%	0.00%	0.10%	0.22%	0.10%	0.22%	1.43%
Variation coefficient	V [%]	-	-	-	-	-	-0.93%	1.94%	0.91%	1.93%	-
Probability distribution		Uniform Triangular Triangular Normal Normal Normal Normal									

Table B. 90: Type A $u_c(\lambda_{COP})$ sensitivity coefficients, by means of HFM-1 apparatus (Sample: FS based VIP 30 mm thick, $\vartheta_{avg} = 40^\circ\text{C}$, $\Delta\vartheta = 10^\circ\text{C}$)

	Sensitivity coefficients			
	$\partial\lambda_{COP}/\partial t$	$\partial\lambda_{COP}/\partial f_{cal}$	$\partial\lambda_{COP}/\partial Q$	$\partial\lambda_{COP}/\partial \Delta\vartheta$
Upper plate	0.229206	1354.668633	0.014733	-0.676318
Lower plate	0.178619	997.928407	0.015586	-0.527053

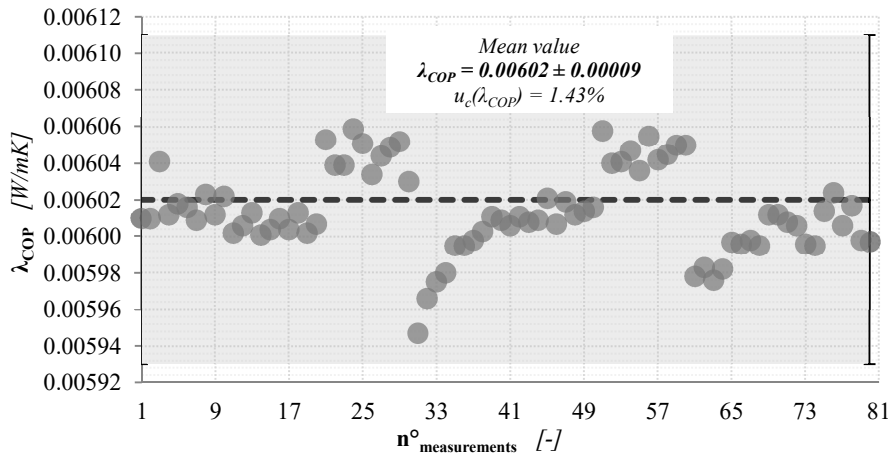


Figure B. 45: λ_{COP} -values assessed by means of HFM-1 apparatus (Sample: FS based VIP 30 mm thick, $\vartheta_{avg} = 40^\circ\text{C}$, $\Delta\vartheta = 10^\circ\text{C}$)

Table B. 91: Type A $u_c(\lambda_{COP})$ assessment, by means of HFM-1 apparatus (Sample: FS based VIP 30 mm thick, $\vartheta_{avg} = 40^\circ\text{C}$, $\Delta\vartheta = 20^\circ\text{C}$)

Test conditions		f_{cal_upper}	f_{cal_lower}	$t_{measured}$	ϑ_{upper}	ϑ_{lower}	Q_{upper}	Q_{lower}	Φ_{upper}	Φ_{lower}	λ_{COP}
30 mm $\vartheta_{avg} = 40^\circ\text{C}$ $\Delta\vartheta = 20^\circ\text{C}$		$[\text{W}/\text{m}^2 \cdot \mu\text{V}]$	$[\text{W}/\text{m}^2 \cdot \mu\text{V}]$	$[\text{mm}]$	$[\text{C}^\circ]$	$[\text{C}^\circ]$	$[\mu\text{V}]$	$[\mu\text{V}]$	$[\text{W}/\text{m}^2]$	$[\text{W}/\text{m}^2]$	$[\text{W}/\text{mK}]$
Mean value	\bar{y}	0.0050	0.0053	29.50	30.021	50.020	-849	728	4.279	3.82	0.00598
Median		-	-	-	-	-	-856	721	4.315	3.79	-
Skew		-	-	-	-	-	1.757	0.649	-1.760	0.642	-
Standard deviation	s	-	-	-	-	-	16.3	24.0	0.082	0.126	-
Absolute uncertainty	$u(\bar{y})$	0.0001	0.0001	0.01	0.002	0.004	1.8	2.7	0.009	0.01	0.00009
Relative uncertainty	$u(\bar{y})$	2.00%	2.00%	0.04%	0.01%	0.01%	0.22%	0.37%	0.22%	0.37%	1.43%
Variation coefficient	V	-	-	-	-	-	-1.93%	3.30%	1.93%	3.30%	-
Probability distribution					Triangular	Triangular	Triangular	Normal	Normal	Normal	Normal

Table B. 92: Type A $u_c(\lambda_{COP})$ sensitivity coefficients, by means of HFM-1 apparatus (Sample: FS based VIP 30 mm thick, $\vartheta_{avg} = 40^\circ\text{C}$, $\Delta\vartheta = 20^\circ\text{C}$)

	Sensitivity coefficients			
	$\partial\lambda_{COP}/\partial t$	$\partial\lambda_{COP}/\partial f_{cal}$	$\partial\lambda_{COP}/\partial Q$	$\partial\lambda_{COP}/\partial\Delta\vartheta$
Upper plate	0.214044	1252.337617	0.007437	-0.315730
Lower plate	0.191146	1073.853693	0.007746	-0.281954

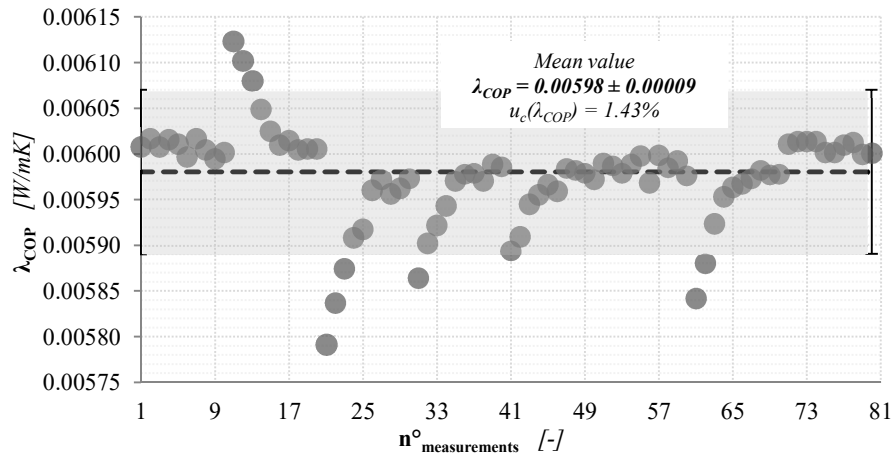
**Figure B. 46:** λ_{COP} -values assessed by means of HFM-1 apparatus (Sample: FS based VIP 30 mm thick, $\vartheta_{avg} = 40^\circ\text{C}$, $\Delta\vartheta = 20^\circ\text{C}$)

Table B. 93: Type A $u_c(\lambda_{COP})$ assessment, by means of HFM-1 apparatus (Sample: FS based VIP 30 mm thick, $\vartheta_{avg} = 40^\circ\text{C}$, $\Delta\vartheta = 30^\circ\text{C}$)

Test conditions		f_{cal_upper}	f_{cal_lower}	$t_{measured}$	ϑ_{upper}	ϑ_{lower}	Q_{upper}	Q_{lower}	Φ_{upper}	Φ_{lower}	λ_{COP}
30 mm $\vartheta_{avg} = 40^\circ\text{C}$ $\Delta\vartheta = 30^\circ\text{C}$		$[\text{W}/\text{m}^2 \cdot \mu\text{V}]$	$[\text{W}/\text{m}^2 \cdot \mu\text{V}]$	$[\text{mm}]$	$[\text{C}^\circ]$	$[\text{C}^\circ]$	$[\mu\text{V}]$	$[\mu\text{V}]$	$[\text{W}/\text{m}^2]$	$[\text{W}/\text{m}^2]$	$[\text{W}/\text{mK}]$
Mean value	\bar{y}	0.0051	0.0052	29.508	25.022	55.022	-1233.0	1127	6.278	5.88	0.00598
Median		-	-	-	-	-	-1232.5	1126	6.276	5.87	-
Skew		-	-	-	-	-	-0.537	-0.110	0.600	-0.103	-
Standard deviation	s	-	-	-	-	-	3.5	18.4	0.018	0.096	-
Absolute uncertainty	$u(\bar{y})$	0.0001	0.0001	0.007	0.002	0.002	0.4	2.1	0.002	0.01	0.00008
Relative uncertainty	$u(\bar{y})$ [%]	2.00%	2.00%	0.02%	0.01%	0.00%	0.03%	0.18%	0.03%	0.18%	1.42%
Variation coefficient	V [%]	-	-	-	-	-	-0.28%	1.63%	0.28%	1.63%	-
Probability distribution					Uniform	Triangular	Triangular	Normal	Normal	Normal	Normal

Table B. 94: Type A $u_c(\lambda_{COP})$ sensitivity coefficients, by means of HFM-1 apparatus (Sample: FS based VIP 30 mm thick, $\vartheta_{avg} = 40^\circ\text{C}$, $\Delta\vartheta = 30^\circ\text{C}$)

	Sensitivity coefficients			
	$\partial\lambda_{COP}/\partial t$	$\partial\lambda_{COP}/\partial f_{cal}$	$\partial\lambda_{COP}/\partial Q$	$\partial\lambda_{COP}/\partial \Delta\vartheta$
Upper plate	0.209281	1212.778800	0.005008	-0.205849
Lower plate	0.196060	1108.517200	0.005133	-0.192845

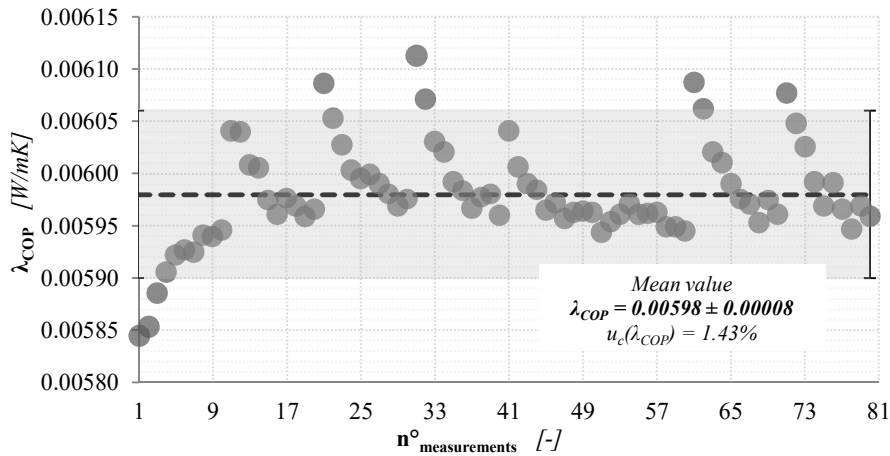


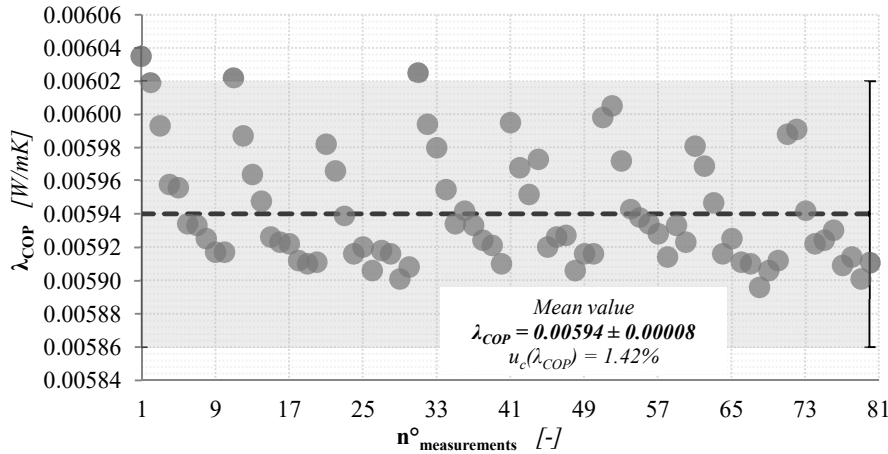
Figure B. 47: λ_{COP} -values assessed by means of HFM-1 apparatus (Sample: FS based VIP 30 mm thick, $\vartheta_{avg} = 40^\circ\text{C}$, $\Delta\vartheta = 30^\circ\text{C}$)

Table B. 95: Type A $u_c(\lambda_{COP})$ assessment, by means of HFM-1 apparatus (Sample: FS based VIP 30 mm thick, $\vartheta_{avg} = 40^\circ\text{C}$, $\Delta\vartheta = 40^\circ\text{C}$)

Test conditions		f_{cal_upper}	f_{cal_lower}	$t_{measured}$	ϑ_{upper}	ϑ_{lower}	Q_{upper}	Q_{lower}	Φ_{upper}	Φ_{lower}	λ_{COP}
30 mm $\vartheta_{avg} = 40^\circ\text{C}$ $\Delta\vartheta = 40^\circ\text{C}$		$[\text{W}/\text{m}^2 \cdot \mu\text{V}]$	$[\text{W}/\text{m}^2 \cdot \mu\text{V}]$	$[\text{mm}]$	$[\text{C}^\circ]$	$[\text{C}^\circ]$	$[\mu\text{V}]$	$[\mu\text{V}]$	$[\text{W}/\text{m}^2]$	$[\text{W}/\text{m}^2]$	$[\text{W}/\text{mK}]$
Mean value	\bar{y}	0.0051	0.0052	29.500	20.015	60.026	-1592.1	1528	8.188	7.93	0.00598
Median		-	-	-	-	-	-1593.0	1523	8.192	7.90	-
Skew		-	-	-	-	-	0.115	0.897	-0.090	0.894	-
Standard deviation	s	-	-	-	-	-	5.8	19.9	0.030	0.103	-
Absolute uncertainty	$u(\bar{y})$	0.0001	0.0001	0.01	0.003	0.006	0.7	2.2	0.003	0.01	0.00008
Relative uncertainty	$u(\bar{y})$	2.00%	2.00%	0.04%	0.01%	0.01%	0.04%	0.15%	0.04%	0.15%	1.42%
Variation coefficient	V	-	-	-	-	-	-0.37%	1.30%	0.37%	1.30%	-
Probability distribution					Uniform	Uniform	Uniform	Normal	Normal	Normal	Normal

Table B. 96: Type A $u_c(\lambda_{COP})$ sensitivity coefficients, by means of HFM-1 apparatus (Sample: FS based VIP 30 mm thick, $\vartheta_{avg} = 40^\circ\text{C}$, $\Delta\vartheta = 40^\circ\text{C}$)

	Sensitivity coefficients			
	$\partial\lambda_{COP}/\partial t$	$\partial\lambda_{COP}/\partial f_{cal}$	$\partial\lambda_{COP}/\partial Q$	$\partial\lambda_{COP}/\partial \Delta\vartheta$
Upper plate	0.204648	1173.850941	0.003792	-0.150886
Lower plate	0.198089	1126.590188	0.003824	-0.146050

**Figure B. 48:** λ_{COP} -values assessed by means of HFM-1 apparatus (Sample: FS based VIP 30 mm thick, $\vartheta_{avg} = 40^\circ\text{C}$, $\Delta\vartheta = 40^\circ\text{C}$)

Appendix C

Thermal conductivity uncertainty - GHP

An extended version of this appendix is available at the following link:

<http://dx.doi.org/10.17632/v9r5pkwkyg.2#file-05e249b5-ddec-4fc9-a98b-48c9838617cf>

Table C. 1: Type A $u_c(\lambda)$ assessment, by means of GHP-1 apparatus (Sample: Aerogel blanket 10 mm thick, $\vartheta_{avg} = 5^\circ\text{C}$, $\Delta\vartheta = 5^\circ\text{C}$)

Test conditions		t_{measured}	ϑ_{cold}	ϑ_{hot}	ϑ_{avg}	$\Delta\vartheta$	U	I	Φ	λ
10 mm $\vartheta_{\text{avg}} = 5^\circ\text{C}$ $\Delta\vartheta = 5^\circ\text{C}$		[mm]	[°C]	[°C]	[°C]	[°C]	[mV]	[A]	[W]	[W/mK]
Mean value	\bar{y}	9.90	2.3559	7.0537	3.1601	4.6978	2.2403	0.08210	0.18392	0.0172
Median	-	-	2.3556	7.0538	-	-	2.2406	0.08211	0.18397	-
Skew	-	-	0.0231	1.1727	-	-	-0.2788	-0.2328	-0.2502	-
Standard deviation	s	-	0.0047	0.0067	-	-	0.0052	0.00019	0.00084	-
Absolute uncertainty	$u(\bar{y})$	0.06	0.0005	0.0007	0.0003	0.0009	0.0006	0.00002	0.00009	0.0002
Relative uncertainty	$\frac{u(\bar{y})}{\bar{y}}$ [%]	0.58%	0.022%	0.011%	0.008%	0.019%	0.026%	0.03%	0.05%	1.16%
Variation coefficient	$\frac{V}{\bar{y}}$ [%]	-	0.20%	0.10%	-	-	0.23%	0.23%	0.46%	-
Probability distribution		Uniform	Normal	Normal			Normal	Normal	Normal	

Table C. 2: Type A $u_c(\lambda)$ sensitivity coefficients, by means of GHP-1 apparatus (Sample: Aerogel blanket 10 mm thick, $\vartheta_{avg} = 5^\circ\text{C}$, $\Delta\vartheta = 5^\circ\text{C}$)

Sensitivity coefficients				
$\partial\lambda/\partial A_m$	$\partial\lambda/\partial t$	$\partial\lambda_{\text{COP}}/\partial I$	$\partial\lambda_{\text{COP}}/\partial U$	$\partial\lambda_{\text{COP}}/\partial\Delta\vartheta$
-382.80085	0.87000	104.91489	3.84457	-1.83342

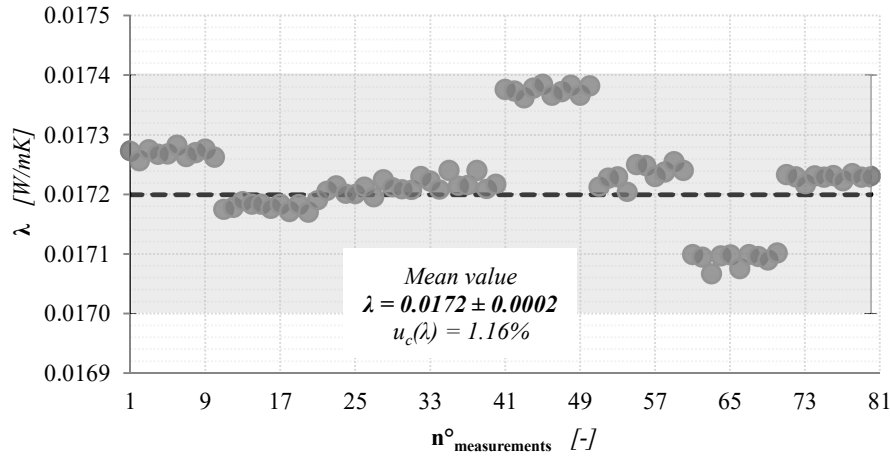


Figure C. 1: λ -values assessed by means of GHP-1 apparatus (Sample: Aerogel blanket 10 mm thick, $\vartheta_{avg} = 5^\circ\text{C}$, $\Delta\vartheta = 5^\circ\text{C}$)

Table C. 3: Type A $u_c(\lambda)$ assessment, by means of GHP-1 apparatus (Sample: Aerogel blanket 10 mm thick, $\vartheta_{avg} = 5^\circ\text{C}$, $\Delta\vartheta = 10^\circ\text{C}$)

Test conditions	t_{measured}	ϑ_{cold}	ϑ_{hot}	ϑ_{avg}	$\Delta\vartheta$	U	I	Φ	λ	
10 mm $\vartheta_{\text{avg}} = 5^\circ\text{C}$ $\Delta\vartheta = 10^\circ\text{C}$	[mm]	[$^\circ\text{C}$]	[$^\circ\text{C}$]	[$^\circ\text{C}$]	[$^\circ\text{C}$]	[mV]	[A]	[W]	[W/mK]	
Mean value	\bar{y}	9.90	-0.2015	9.6065	3.1670	9.8080	3.2162	0.11665	0.3752	0.0168
Median		-	-0.2025	9.6072	-	-	3.2171	0.11671	0.3754	
Skew		-	0.6898	-1.3252	-	-	-0.1519	-0.1742	-0.1657	
Standard deviation	s	-	0.0041	0.0025	-	-	0.0055	0.00020	0.0013	
Absolute uncertainty	$u(\bar{y})$	0.06	0.0005	0.0003	0.0002	0.0005	0.0006	0.00002	0.0001	0.0002
Relative uncertainty	$u(\bar{y})$ [%]	0.58%	0.227%	0.003%	0.007%	0.005%	0.019%	0.02%	0.04%	1.19%
Variation coefficient	$\frac{V}{V}$ [%]	-	2.03%	0.03%	-	-	0.17%	0.17%	0.34%	-
Probability distribution		Uniform	Normal	Normal		Normal	Normal	Normal		

Table C. 4: Type A $u_c(\lambda)$ sensitivity coefficients, by means of GHP-1 apparatus (Sample: Aerogel blanket 10 mm thick, $\vartheta_{avg} = 5^\circ\text{C}$, $\Delta\vartheta = 10^\circ\text{C}$)

Sensitivity coefficients				
$\partial N / \partial A_m$	$\partial N / \partial t$	$\partial \lambda_{\text{COP}} / \partial I$	$\partial \lambda_{\text{COP}} / \partial U$	$\partial \lambda_{\text{COP}} / \partial \Delta\vartheta$
-374.02362	0.85005	72.14125	2.61661	-0.85802

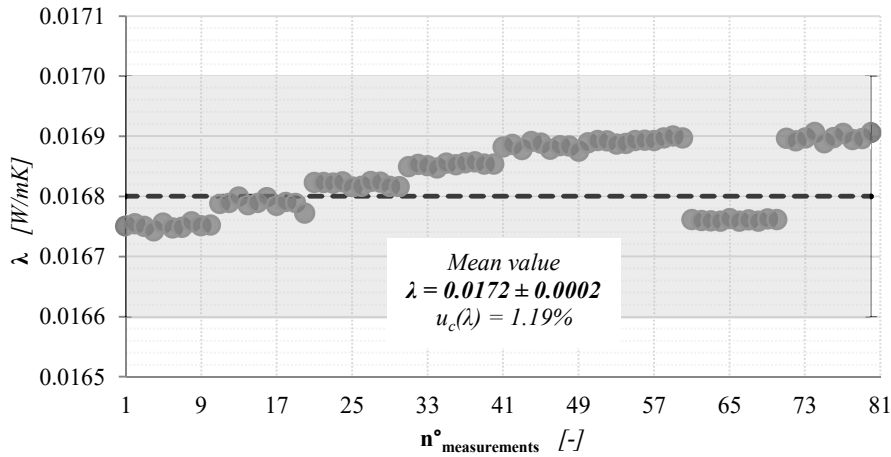
**Figure C. 2:** λ -values assessed by means of GHP-1 apparatus (Sample: Aerogel blanket 10 mm thick, $\vartheta_{avg} = 5^\circ\text{C}$, $\Delta\vartheta = 10^\circ\text{C}$)

Table C. 5: Type A $u_c(\lambda)$ assessment, by means of GHP-1 apparatus (Sample: Aerogel blanket 10 mm thick, $\vartheta_{avg} = 5^\circ\text{C}$, $\Delta\vartheta = 15^\circ\text{C}$)

Test conditions		t_{measured}	ϑ_{cold}	ϑ_{hot}	ϑ_{avg}	$\Delta\vartheta$	U	I	Φ	λ
10 mm $\vartheta_{\text{avg}} = 5^\circ\text{C}$ $\Delta\vartheta = 15^\circ\text{C}$		[mm]	[$^\circ\text{C}$]	[$^\circ\text{C}$]	[$^\circ\text{C}$]	[$^\circ\text{C}$]	[mV]	[A]	[W]	[W/mK]
Mean value	\bar{y}	9.90	-2.7740	12.1556	3.1677	14.9297	4.0979	0.14714	0.6030	0.0178
Median		-	-2.7742	12.1563	-	-	4.0968	0.14709	0.6026	-
Skew		-	0.7491	-1.5035	-	-	0.6667	0.6475	0.6634	-
Standard deviation	s	-	0.0037	0.0028	-	-	0.0064	0.00022	0.0018	-
Absolute uncertainty	$u(\bar{y})$	0.06	0.0004	0.0003	0.0002	0.0005	0.0007	0.00002	0.0002	0.0002
Relative uncertainty	$u(\bar{y})$ [%]	0.58%	0.015%	0.003%	0.006%	0.003%	0.017%	0.02%	0.03%	1.12%
Variation coefficient	$\frac{V}{\bar{y}}$ [%]	-	0.13%	0.02%	-	-	0.16%	0.15%	0.31%	-
Probability distribution		Uniform	Normal	Normal			Normal	Normal	Normal	

Table C. 6: Type A $u_c(\lambda)$ sensitivity coefficients, by means of GHP-1 apparatus (Sample: Aerogel blanket 10 mm thick, $\vartheta_{avg} = 5^\circ\text{C}$, $\Delta\vartheta = 15^\circ\text{C}$)

Sensitivity coefficients				
$\partial\lambda/\partial A_m$	$\partial\lambda/\partial t$	$\partial\lambda_{\text{COP}}/\partial I$	$\partial\lambda_{\text{COP}}/\partial U$	$\partial\lambda_{\text{COP}}/\partial\Delta\vartheta$
-394.91010	0.89752	60.38591	2.16829	-0.59516

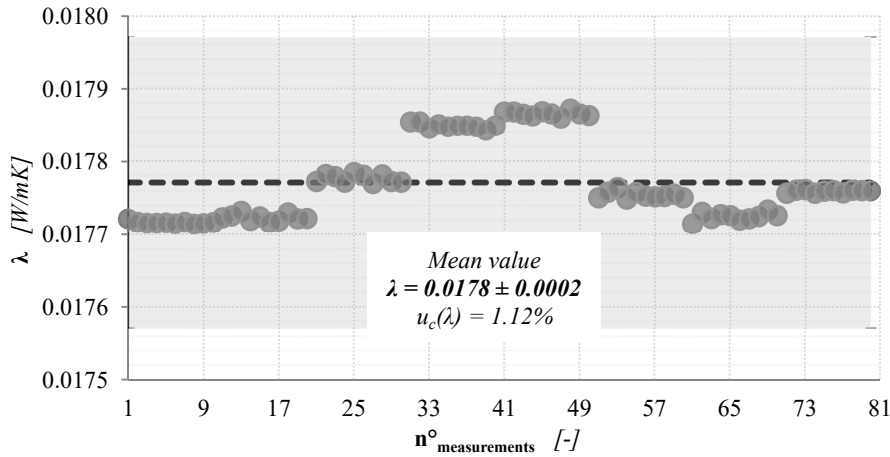


Figure C. 3: λ -values assessed by means of GHP-1 apparatus (Sample: Aerogel blanket 10 mm thick, $\vartheta_{avg} = 5^\circ\text{C}$, $\Delta\vartheta = 15^\circ\text{C}$)

Table C. 7: Type A $u_c(\lambda)$ assessment, by means of GHP-1 apparatus (Sample: Aerogel blanket 10 mm thick, $\vartheta_{avg} = 10^\circ\text{C}$, $\Delta\vartheta = 5^\circ\text{C}$)

Test conditions	t_{measured}	ϑ_{cold}	ϑ_{hot}	ϑ_{avg}	$\Delta\vartheta$	U	I	Φ	λ	
10 mm $\vartheta_{\text{avg}} = 10^\circ\text{C}$ $\Delta\vartheta = 5^\circ\text{C}$	[mm]	[$^\circ\text{C}$]	[$^\circ\text{C}$]	[$^\circ\text{C}$]	[$^\circ\text{C}$]	[mV]	[A]	[W]	[W/mK]	
Mean value	\bar{y}	9.98	7.4557	12.1641	6.5805	4.7083	2.2804	0.08192	0.18680	0.0176
Median	-	-	7.4559	12.1636	-	-	2.2807	0.08192	0.18686	-
Skew	-	-	0.0314	0.3473	-	-	-0.9119	-0.8339	-0.8774	-
Standard deviation	s	-	0.0028	0.0020	-	-	0.0035	0.00012	0.00057	-
Absolute uncertainty	$u(\bar{y})$	0.06	0.0003	0.0002	0.0002	0.0004	0.0004	0.00001	0.00006	0.0002
Relative uncertainty	$u(\bar{y})$ [%]	0.58%	0.004%	0.002%	0.002%	0.008%	0.017%	0.02%	0.03%	1.14%
Variation coefficient	$\frac{V}{V}$ [%]	-	0.04%	0.02%	-	-	0.15%	0.15%	0.30%	-
Probability distribution	Uniform	Normal	Normal			Normal	Normal	Normal		

Table C. 8: Type A $u_c(\lambda)$ sensitivity coefficients, by means of GHP-1 apparatus (Sample: Aerogel blanket 10 mm thick, $\vartheta_{avg} = 10^\circ\text{C}$, $\Delta\vartheta = 5^\circ\text{C}$)

Sensitivity coefficients				
$\partial\lambda/\partial A_m$	$\partial\lambda/\partial t$	$\partial\lambda_{\text{COP}}/\partial I$	$\partial\lambda_{\text{COP}}/\partial U$	$\partial\lambda_{\text{COP}}/\partial\Delta\vartheta$
-390.87246	0.88167	107.35911	3.85667	-1.86789

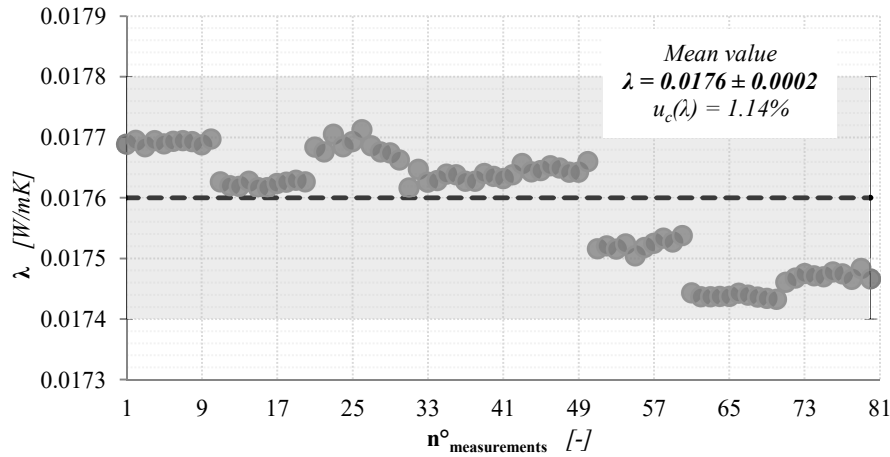
**Figure C. 4:** λ -values assessed by means of GHP-1 apparatus (Sample: Aerogel blanket 10 mm thick, $\vartheta_{avg} = 10^\circ\text{C}$, $\Delta\vartheta = 5^\circ\text{C}$)

Table C. 9: Type A $u_c(\lambda)$ assessment, by means of GHP-1 apparatus (Sample: Aerogel blanket 10 mm thick, $\vartheta_{avg} = 10^\circ\text{C}$, $\Delta\vartheta = 10^\circ\text{C}$)

Test conditions	t_{measured}	ϑ_{cold}	ϑ_{hot}	ϑ_{avg}	$\Delta\vartheta$	U	I	Φ	λ	
10 mm $\vartheta_{\text{avg}} = 10^\circ\text{C}$ $\Delta\vartheta = 10^\circ\text{C}$	[mm]	[$^\circ\text{C}$]	[$^\circ\text{C}$]	[$^\circ\text{C}$]	[$^\circ\text{C}$]	[mV]	[A]	[W]	[W/mK]	
Mean value	\bar{y}	9.98	4.9105	14.7060	6.5878	9.7954	3.2669	0.11618	0.3796	0.0172
Median	-	-	4.9102	14.7041	-	-	3.2670	0.11619	0.3796	-
Skew	-	-	0.4302	0.8618	-	-	0.3805	0.3670	0.3760	-
Standard deviation	s	-	0.0026	0.0064	-	-	0.0042	0.00015	0.0010	-
Absolute uncertainty	$u(\bar{y})$	0.06	0.0003	0.0007	0.0001	0.0008	0.0005	0.00002	0.0001	0.0002
Relative uncertainty	$u(\bar{y})$ [%]	0.58%	0.006%	0.005%	0.002%	0.008%	0.014%	0.01%	0.03%	1.16%
Variation coefficient	$\frac{V}{V}$ [%]	-	0.05%	0.04%	-	-	0.13%	0.13%	0.25%	-
Probability distribution	Uniform	Normal	Normal			Normal	Normal	Normal		

Table C. 10: Type A $u_c(\lambda)$ sensitivity coefficients, by means of GHP-1 apparatus (Sample: Aerogel blanket 10 mm thick, $\vartheta_{avg} = 10^\circ\text{C}$, $\Delta\vartheta = 10^\circ\text{C}$)

Sensitivity coefficients				
$\partial\lambda/\partial A_m$	$\partial\lambda/\partial t$	$\partial\lambda_{\text{COP}}/\partial I$	$\partial\lambda_{\text{COP}}/\partial U$	$\partial\lambda_{\text{COP}}/\partial\Delta\vartheta$
-381.75239	0.86110	73.92938	2.62920	-0.87688

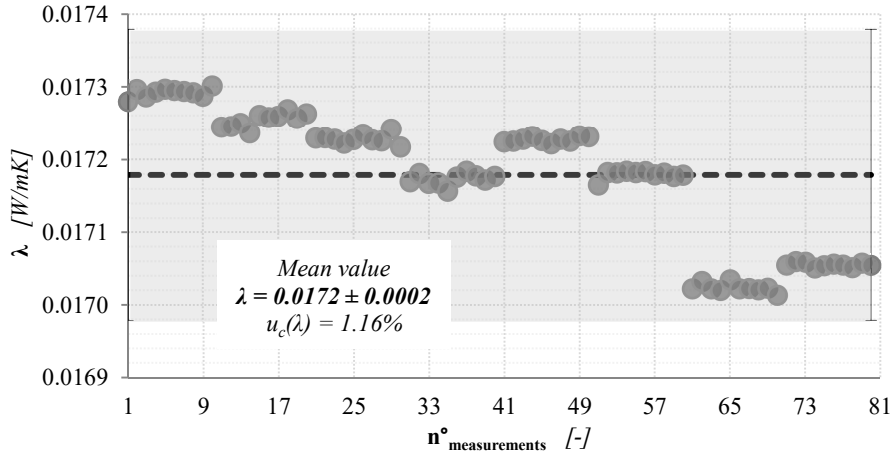


Figure C. 5: λ -values assessed by means of GHP-1 apparatus (Sample: Aerogel blanket 10 mm thick, $\vartheta_{avg} = 10^\circ\text{C}$, $\Delta\vartheta = 10^\circ\text{C}$)

Table C. 11: Type A $u_c(\lambda)$ assessment, by means of GHP-1 apparatus (Sample: Aerogel blanket 10 mm thick, $\vartheta_{avg} = 10^\circ\text{C}$, $\Delta\vartheta = 15^\circ\text{C}$)

Test conditions	t_{measured}	ϑ_{cold}	ϑ_{hot}	ϑ_{avg}	$\Delta\vartheta$	U	I	Φ	λ	
10 mm $\vartheta_{\text{avg}} = 10^\circ\text{C}$ $\Delta\vartheta = 15^\circ\text{C}$	[mm]	[$^\circ\text{C}$]	[$^\circ\text{C}$]	[$^\circ\text{C}$]	[$^\circ\text{C}$]	[mV]	[A]	[W]	[W/mK]	
Mean value	\bar{y}	9.98	2.3649	17.244	6.5939	14.879	4.1449	0.14595	0.6050	0.018
Median	-	-	2.3654	17.241	-	-	4.1442	0.14592	0.6047	-
Skew	-	-	-0.7890	1.9982	-	-	0.2782	0.2522	0.2686	-
Standard deviation	s	-	0.0057	0.0097	-	-	0.0054	0.00018	0.0015	-
Absolute uncertainty	$u(\bar{y})$	0.06	0.0006	0.001	0.0003	0.001	0.0006	0.00002	0.0002	0.0003
Relative uncertainty	$u(\bar{y})$ [%]	0.58%	0.027%	0.006%	0.005%	0.008%	0.015%	0.01%	0.03%	1.67%
Variation coefficient	$\frac{V}{\bar{y}}$ [%]	-	0.24%	0.06%	-	-	0.13%	0.12%	0.25%	-
Probability distribution	Uniform	Normal	Normal			Normal	Normal	Normal		

Table C. 12: Type A $u_c(\lambda)$ sensitivity coefficients, by means of GHP-1 apparatus (Sample: Aerogel blanket 10 mm thick, $\vartheta_{avg} = 10^\circ\text{C}$, $\Delta\vartheta = 15^\circ\text{C}$)

Sensitivity coefficients				
$\partial\lambda/\partial A_m$	$\partial\lambda/\partial t$	$\partial\lambda_{\text{COP}}/\partial I$	$\partial\lambda_{\text{COP}}/\partial U$	$\partial\lambda_{\text{COP}}/\partial\Delta\vartheta$
-400.55582	0.90351	61.74935	2.17435	-0.60570

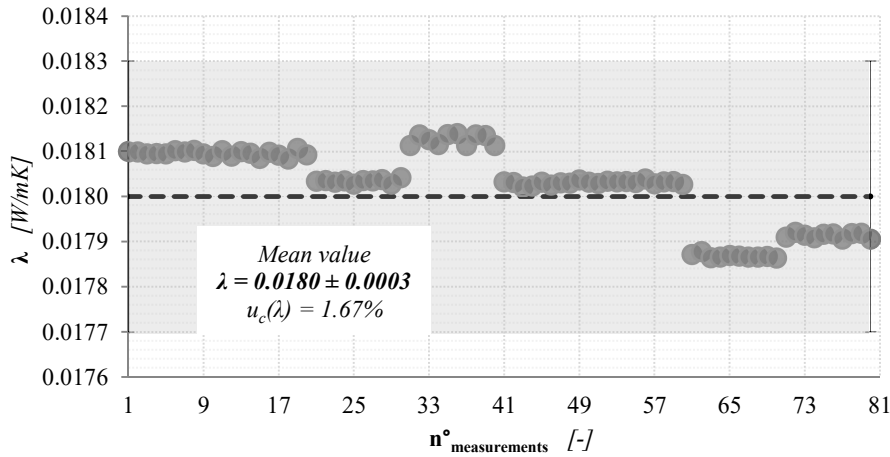
Figure C. 6: λ -values assessed by means of GHP-1 apparatus (Sample: Aerogel blanket 10 mm thick, $\vartheta_{avg} = 10^\circ\text{C}$, $\Delta\vartheta = 15^\circ\text{C}$)

Table C. 13: Type A $u_c(\lambda)$ assessment, by means of GHP-1 apparatus (Sample: Aerogel blanket 10 mm thick, $\vartheta_{avg} = 23^\circ\text{C}$, $\Delta\vartheta = 5^\circ\text{C}$)

Test conditions		t_{measured}	ϑ_{cold}	ϑ_{hot}	ϑ_{avg}	$\Delta\vartheta$	U	I	Φ	λ
10 mm $\vartheta_{\text{avg}} = 23^\circ\text{C}$ $\Delta\vartheta = 5^\circ\text{C}$		[mm]	[°C]	[°C]	[°C]	[°C]	[mV]	[A]	[W]	[W/mK]
Mean value	\bar{y}	9.90	20.5387	25.3608	15.3844	4.8221	2.3932	0.081777	0.19571	0.0179
Median		-	20.5399	25.3618	-	-	2.3931	0.081770	0.19569	-
Skew		-	-1.0399	-0.8198	-	-	0.2916	0.0784	0.1351	-
Standard deviation	s	-	0.0044	0.0023	-	-	0.0013	0.000049	0.00022	-
Absolute uncertainty	$u(\bar{y})$	0.06	0.0005	0.0003	0.0002	0.0006	0.0001	0.000006	0.00002	0.0002
Relative uncertainty	$u(\bar{y})$ [%]	0.58%	0.002%	0.001%	0.002%	0.012%	0.006%	0.01%	0.01%	1.12%
Variation coefficient	$\frac{V}{\bar{y}}$ [%]	-	0.02%	0.01%	-	-	0.05%	0.06%	0.11%	-
Probability distribution		Uniform	Normal	Normal			Normal	Normal	Normal	

Table C. 14: Type A $u_c(\lambda)$ sensitivity coefficients, by means of GHP-1 apparatus (Sample: Aerogel blanket 10 mm thick, $\vartheta_{avg} = 23^\circ\text{C}$, $\Delta\vartheta = 5^\circ\text{C}$)

Sensitivity coefficients				
$\partial\lambda/\partial A_m$	$\partial\lambda/\partial t$	$\partial\lambda_{\text{COP}}/\partial I$	$\partial\lambda_{\text{COP}}/\partial U$	$\partial\lambda_{\text{COP}}/\partial\Delta\vartheta$
-396.83307	0.90189	109.18428	3.73093	-1.85163

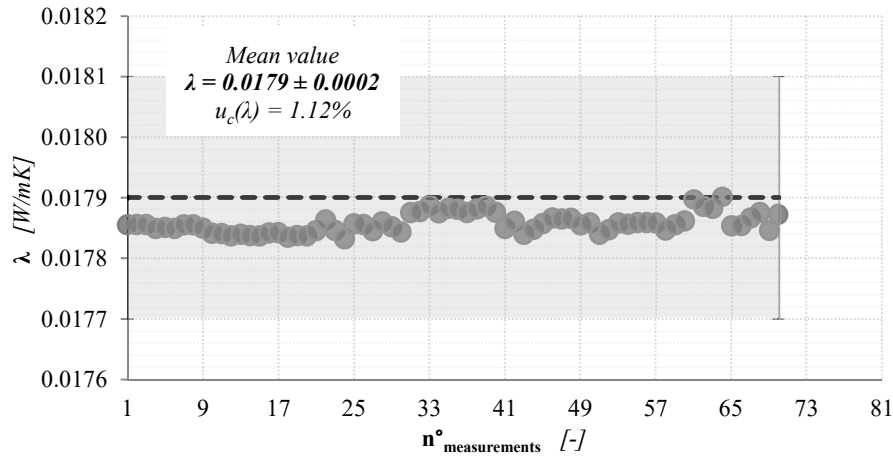


Figure C. 7: λ -values assessed by means of GHP-1 apparatus (Sample: Aerogel blanket 10 mm thick, $\vartheta_{avg} = 23^\circ\text{C}$, $\Delta\vartheta = 5^\circ\text{C}$)

Table C. 15: Type A $u_c(\lambda)$ assessment, by means of GHP-1 apparatus (Sample: Aerogel blanket 10 mm thick, $\vartheta_{avg} = 23^\circ\text{C}$, $\Delta\vartheta = 10^\circ\text{C}$)

Test conditions	t_{measured}	ϑ_{cold}	ϑ_{hot}	ϑ_{avg}	$\Delta\vartheta$	U	I	Φ	λ	
10 mm $\vartheta_{\text{avg}} = 23^\circ\text{C}$ $\Delta\vartheta = 10^\circ\text{C}$	[mm]	[$^\circ\text{C}$]	[$^\circ\text{C}$]	[$^\circ\text{C}$]	[$^\circ\text{C}$]	[mV]	[A]	[W]	[W/mK]	
Mean value	\bar{y}	9.90	18.0289	27.8769	15.3948	9.8480	3.4015	0.115116	0.39156	0.0175
Median	-	-	18.0297	27.8772	-	-	3.4016	0.115124	0.39160	-
Skew	-	-	-0.8486	-0.1483	-	-	0.0662	-0.2635	-0.0658	-
Standard deviation	s	-	0.0034	0.0018	-	-	0.0013	0.000038	0.00027	-
Absolute uncertainty	$u(\bar{y})$	0.06	0.0004	0.0002	0.0002	0.0004	0.0001	0.000004	0.00003	0.0002
Relative uncertainty	$u(\bar{y})$ [%]	0.58%	0.002%	0.001%	0.001%	0.004%	0.004%	0.00%	0.01%	1.14%
Variation coefficient	$\frac{V}{\bar{y}}$ [%]	-	0.02%	0.01%	-	-	0.04%	0.03%	0.07%	-
Probability distribution	Uniform	Normal	Normal			Normal	Normal	Normal		

Table C. 16: Type A $u_c(\lambda)$ sensitivity coefficients, by means of GHP-1 apparatus (Sample: Aerogel blanket 10 mm thick, $\vartheta_{avg} = 23^\circ\text{C}$, $\Delta\vartheta = 10^\circ\text{C}$)

Sensitivity coefficients				
$\partial\lambda/\partial A_m$	$\partial\lambda/\partial t$	$\partial\lambda_{\text{COP}}/\partial I$	$\partial\lambda_{\text{COP}}/\partial U$	$\partial\lambda_{\text{COP}}/\partial\Delta\vartheta$
-388.76987	0.88357	75.98721	2.57164	-0.88824

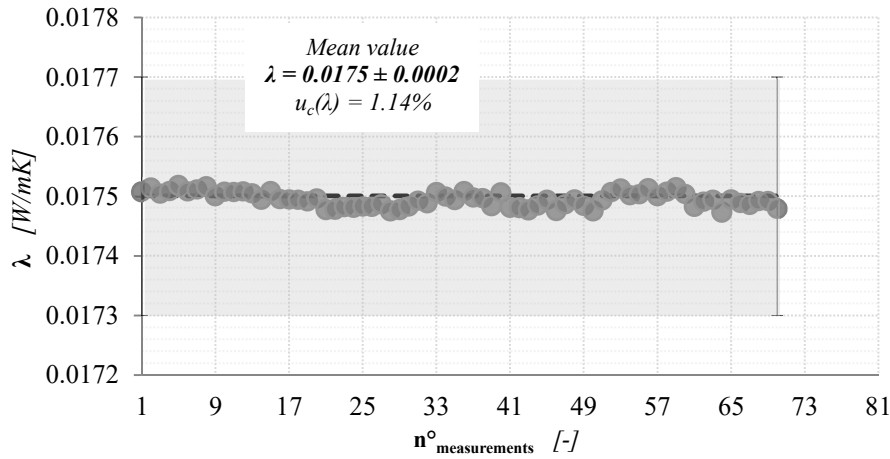
Figure C. 8: λ -values assessed by means of GHP-1 apparatus (Sample: Aerogel blanket 10 mm thick, $\vartheta_{avg} = 23^\circ\text{C}$, $\Delta\vartheta = 10^\circ\text{C}$)

Table C. 17: Type A $u_c(\lambda)$ assessment, by means of GHP-1 apparatus (Sample: Aerogel blanket 10 mm thick, $\vartheta_{avg} = 23^\circ\text{C}$, $\Delta\vartheta = 15^\circ\text{C}$)

Test conditions	t_{measured}	ϑ_{cold}	ϑ_{hot}	ϑ_{avg}	$\Delta\vartheta$	U	I	Φ	λ	
10 mm $\vartheta_{\text{avg}} = 23^\circ\text{C}$ $\Delta\vartheta = 15^\circ\text{C}$	[mm]	[$^\circ\text{C}$]	[$^\circ\text{C}$]	[$^\circ\text{C}$]	[$^\circ\text{C}$]	[mV]	[A]	[W]	[W/mK]	
Mean value	\bar{y}	9.90	15.5175	30.3912	15.4042	14.8736	4.2924	0.14393	0.6178	0.0183
Median	-	-	15.5170	30.3918	-	-	4.2924	0.14391	0.6178	-
Skew	-	-	0.0761	-0.3566	-	-	0.5460	0.6845	0.6281	-
Standard deviation	s	-	0.0034	0.0031	-	-	0.0039	0.00014	0.0011	-
Absolute uncertainty	$u(\bar{y})$	0.06	0.0004	0.0003	0.0002	0.0005	0.0004	0.00002	0.0001	0.0003
Relative uncertainty	$u(\bar{y})$ [%]	0.58%	0.002%	0.001%	0.001%	0.003%	0.010%	0.01%	0.02%	1.64%
Variation coefficient	$\frac{V}{\bar{y}}$ [%]	-	0.02%	0.01%	-	-	0.09%	0.10%	0.18%	-
Probability distribution	Uniform	Normal	Normal			Normal	Normal	Normal		

Table C. 18: Type A $u_c(\lambda)$ sensitivity coefficients, by means of GHP-1 apparatus (Sample: Aerogel blanket 10 mm thick, $\vartheta_{avg} = 23^\circ\text{C}$, $\Delta\vartheta = 15^\circ\text{C}$)

Sensitivity coefficients				
$\partial\lambda/\partial A_m$	$\partial\lambda/\partial t$	$\partial\lambda_{\text{COP}}/\partial I$	$\partial\lambda_{\text{COP}}/\partial U$	$\partial\lambda_{\text{COP}}/\partial\Delta\vartheta$
-406.14790	0.92306	63.49070	2.12893	-0.61440

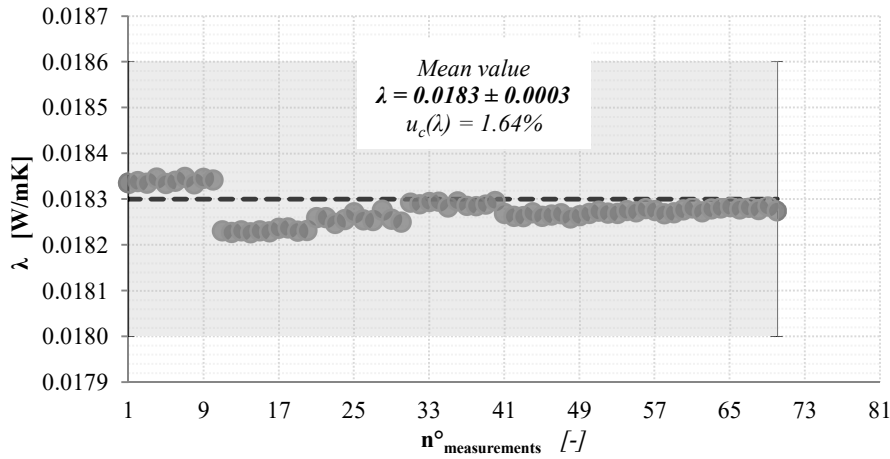


Figure C. 9: λ -values assessed by means of GHP-1 apparatus (Sample: Aerogel blanket 10 mm thick, $\vartheta_{avg} = 23^\circ\text{C}$, $\Delta\vartheta = 15^\circ\text{C}$)

Appendix D

VIP centre of panel thermal characterisation - GHP

An extended version of this appendix is available at the following link:

<http://dx.doi.org/10.17632/v9r5pkwkyg.2#file-05e249b5-ddec-4fc9-a98b-48c9838617cf>

FS based VIPs

Table D. 1: Uncertainty assessment of FS based VIP ($t = 20 \text{ mm}$, $\vartheta_{avg} = 10^\circ\text{C}$)

		<i>FS - 20 mm - 10°C</i>						λ_{COP_avg} [W/mK]	
		A_m [m ²]	t_{VIP_1} [m]	t_{VIP_2} [m]	t_m [m]	I [A]	U [V]		
1 st Side	Hot	0.0401	0.0205	-	0.0206	0.070	3.490	0.00406	
	Cold								
	$u(x_i)$								0.0001
2 nd Side	Hot	0.0401	-	0.0207	0.0003	0.0005	0.0001		
	Cold								
	$u(x_i)$								0.0001
		$\Delta\vartheta_m$ [°C]	C_j [-]	$C_{j,m}$ [-]	$\Delta\lambda_{R,E}$ [-]	$\Delta\lambda_O$ [-]	$\Delta\lambda_S$ [-]		
1 st Side	Hot	15.28	1.013	1.013	1	1	1		0.00007
	Cold								
	$u(x_i)$								
2 nd Side	Hot	0.02	1.013	0.002	1	1	1		
	Cold								
	$u(x_i)$							0.002	
							$u(\lambda_{COP_avg})$ [%]	1.72%	

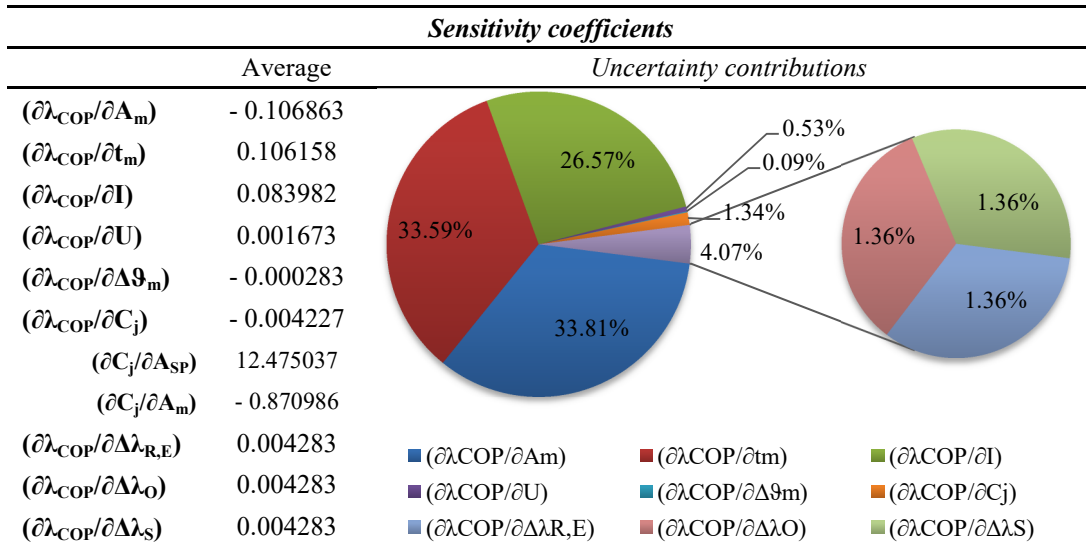
Table D. 2: Sensitivity coefficients and uncertainty contributions of FS based VIP ($t = 20 \text{ mm}$, $\vartheta_{avg} = 10^\circ\text{C}$)

		<i>Sensitivity coefficients</i>		
	Average	<i>Uncertainty contributions</i>		
$(\partial\lambda_{COP}/\partial A_m)$	-0.101181			
$(\partial\lambda_{COP}/\partial t_m)$	0.196861			
$(\partial\lambda_{COP}/\partial I)$	0.057934			
$(\partial\lambda_{COP}/\partial U)$	0.001162			
$(\partial\lambda_{COP}/\partial \Delta\vartheta_m)$	-0.000265			
$(\partial\lambda_{COP}/\partial C_j)$	-0.004002			
$(\partial C_j/\partial A_{SP})$	12.475037			
$(\partial C_j/\partial A_m)$	-0.870986			
$(\partial\lambda_{COP}/\partial \Delta\lambda_{R,E})$	0.004055			
$(\partial\lambda_{COP}/\partial \Delta\lambda_O)$	0.004055			
$(\partial\lambda_{COP}/\partial \Delta\lambda_S)$	0.004055			

Table D. 3: Uncertainty assessment of FS based VIP ($t = 40 \text{ mm}$, $\vartheta_{avg} = 10^\circ\text{C}$)

		<i>FS - 40 mm - 10°C</i>							
		A_m [m ²]	t_{VIP_1} [m]	t_{VIP_2} [m]	t_m [m]	I [A]	U [V]	λ_{COP_avg} [W/mK]	
1 st Side	Hot	0.0401	0.0408	-	0.0404	0.051	2.560	0.00428	
	Cold								
	$u(x_i)$								0.0001
2 nd Side	Hot	0.0401	-	0.0398	0.0004	0.0005	0.0001		
	Cold								
	$u(x_i)$								0.0001
		$\Delta\vartheta_m$ [°C]	C_j [-]	C_{i_m} [-]	$\Delta\lambda_{R,E}$ [-]	$\Delta\lambda_o$ [-]	$\Delta\lambda_s$ [-]		
1 st Side	Hot	15.14	1.013	1.013	1	1	1		0.00006
	Cold								
	$u(x_i)$								
2 nd Side	Hot	0.01	1.013	0.002	1	1	1		
	Cold								
	$u(x_i)$							0.002	
		$u(\lambda_{COP_avg})$ [%]					1.40%		

Table D. 4: Sensitivity coefficients and uncertainty contributions of FS based VIP ($t = 40 \text{ mm}$, $\vartheta_{avg} = 10^\circ\text{C}$)



FG based VIPs

Table D. 5: Uncertainty assessment of FG based VIP ($t = 20$ mm, $\vartheta_{avg} = 10^\circ\text{C}$)

<i>FG - 20 mm - 10°C</i>									
		A_m [m ²]	t_{VIP_1} [m]	t_{VIP_2} [m]	t_m [m]	I [A]	U [V]	λ_{COP_avg} [W/mK]	
1 st Side	Hot	0.0401	0.0216	-	0.0218	0.051	2.540	0.00212	
	Cold								
	$u(x_i)$								0.0001
2 nd Side	Hot	0.0401	-	0.0220	0.0001	0.0005	0.0001		
	Cold								
	$u(x_i)$								0.0001
		$\Delta\vartheta_m$ [°C]	C_j [-]	C_{j_m} [-]	$\Delta\lambda_{R,E}$ [-]	$\Delta\lambda_O$ [-]	$\Delta\lambda_S$ [-]		
1 st Side	Hot	16.40	1.0133	1.0133	1	1	1		0.00002
	Cold								
	$u(x_i)$								
2 nd Side	Hot	0.01	1.0133	0.0008	1	1	1		
	Cold								
	$u(x_i)$							0.01	
							$u(\lambda_{COP_avg})$ [%]	0.95%	

Table D. 6: Sensitivity coefficients and uncertainty contributions of FG based VIP ($t = 20$ mm, $\vartheta_{avg} = 10^\circ\text{C}$)

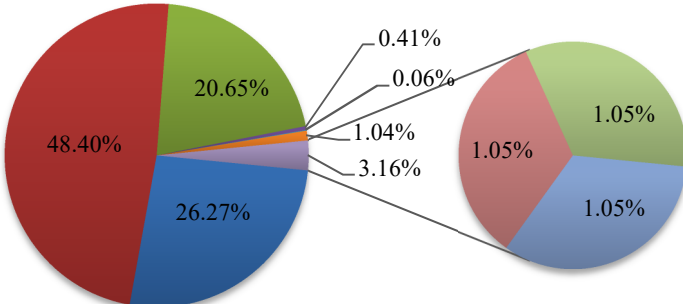
<i>Sensitivity coefficients</i>		<i>Uncertainty contributions</i>	
	Average		
$(\partial\lambda_{COP}/\partial A_m)$	-0.052802		
$(\partial\lambda_{COP}/\partial t_m)$	0.097268		
$(\partial\lambda_{COP}/\partial I)$	0.041496		
$(\partial\lambda_{COP}/\partial U)$	0.000833		
$(\partial\lambda_{COP}/\partial\Delta\vartheta_m)$	-0.000129		
$(\partial\lambda_{COP}/\partial C_j)$	-0.002089		
$(\partial C_j/\partial A_{SP})$	12.475037		
$(\partial C_j/\partial A_m)$	-2.060237		
$(\partial\lambda_{COP}/\partial\Delta\lambda_{R,E})$	0.002116		
$(\partial\lambda_{COP}/\partial\Delta\lambda_O)$	0.002116		
$(\partial\lambda_{COP}/\partial\Delta\lambda_S)$	0.002116		

Table D. 7: Uncertainty assessment of FG based VIP ($t = 20$ mm, $\vartheta_{avg} = 23^\circ\text{C}$)

<i>FG - 20 mm - 23°C</i>									
		A_m [m ²]	t_{VIP_1} [m]	t_{VIP_2} [m]	t_m [m]	I [A]	U [V]	λ_{COP_avg} [W/mK]	
1 st Side	Hot	0.0401	0.0216	-	0.0218	0.058	2.920	0.00230	
	Cold								
	$u(x_i)$								
2 nd Side	Hot	0.0401	-	0.0220	0.0001	0.0005	0.0001		
	Cold								
	$u(x_i)$								
		$\Delta\vartheta_m$ [°C]	C_j [-]	C_{i_m} [-]	$\Delta\lambda_{R,E}$ [-]	$\Delta\lambda_o$ [-]	$\Delta\lambda_s$ [-]		
1 st Side	Hot	19.76	1.0133	1.0133	1	1	1		
	Cold								
	$u(x_i)$								
2 nd Side	Hot	0.02	1.0133	1.0133	1	1	1		
	Cold								
	$u(x_i)$								
							$u(\lambda_{COP_avg})$ [%]	0.87%	

Table D. 8: Sensitivity coefficients and uncertainty contributions of FG based VIP ($t = 20$ mm, $\vartheta_{avg} = 23^\circ\text{C}$)

<i>Sensitivity coefficients</i>			
	Average	Uncertainty contributions	
$(\partial\lambda_{COP}/\partial A_m)$	-0.052802		
$(\partial\lambda_{COP}/\partial t_m)$	0.097268		
$(\partial\lambda_{COP}/\partial I)$	0.041496		
$(\partial\lambda_{COP}/\partial U)$	0.000833		
$(\partial\lambda_{COP}/\partial \Delta\vartheta_m)$	-0.000129		
$(\partial\lambda_{COP}/\partial C_j)$	-0.002089		
$(\partial C_j/\partial A_{SP})$	12.475037		
$(\partial C_j/\partial A_m)$	-2.060237		
$(\partial\lambda_{COP}/\partial \Delta\lambda_{R,E})$	0.002116		
$(\partial\lambda_{COP}/\partial \Delta\lambda_o)$	0.002116		
$(\partial\lambda_{COP}/\partial \Delta\lambda_s)$	0.002116		

Table D. 9: Uncertainty assessment of FG based VIP ($t = 30 \text{ mm}$, $\vartheta_{avg} = 10^\circ\text{C}$)

<i>FG - 30 mm - 10°C</i>									
		A_m [m ²]	t_{VIP_1} [m]	t_{VIP_2} [m]	t_m [m]	I [A]	U [V]	λ_{COP_avg} [W/mK]	
1 st Side	Hot	0.0401	0.0299	-	0.0307	0.042	2.110	0.00216	
	Cold								
	$u(x_i)$								0.0001
2 nd Side	Hot	0.0401	-	0.0316	0.0002	0.0005	0.0001		
	Cold								
	$u(x_i)$								0.0001
		$\Delta\vartheta_m$ [°C]	C_j [-]	C_{i_m} [-]	$\Delta\lambda_{R,E}$ [-]	$\Delta\lambda_o$ [-]	$\Delta\lambda_s$ [-]		
1 st Side	Hot	15.49	1.0133	1.0133	1	1	1		
	Cold								
	$u(x_i)$								0.0008
2 nd Side	Hot	0.01	1.0133	1.0133	1	1	1		
	Cold								
	$u(x_i)$							0.01	0.0008
							$u(\lambda_{COP_avg})$ [%]	1.39%	

Table D. 10: Sensitivity coefficients and uncertainty contributions of FG based VIP ($t = 30 \text{ mm}$, $\vartheta_{avg} = 10^\circ\text{C}$)

<i>Sensitivity coefficients</i>	
Average	Uncertainty contributions
$(\partial\lambda_{COP}/\partial A_m)$	-0.054015
$(\partial\lambda_{COP}/\partial t_m)$	0.070421
$(\partial\lambda_{COP}/\partial I)$	0.051545
$(\partial\lambda_{COP}/\partial U)$	0.001026
$(\partial\lambda_{COP}/\partial\Delta\vartheta_m)$	-0.000140
$(\partial\lambda_{COP}/\partial C_j)$	-0.002136
$(\partial C_j/\partial A_{SP})$	12.475037
$(\partial C_j/\partial A_m)$	-2.060237
$(\partial\lambda_{COP}/\partial\Delta\lambda_{R,E})$	0.002165
$(\partial\lambda_{COP}/\partial\Delta\lambda_o)$	0.002165
$(\partial\lambda_{COP}/\partial\Delta\lambda_s)$	0.002165

■ $(\partial\lambda_{COP}/\partial A_m)$	■ $(\partial\lambda_{COP}/\partial t_m)$	■ $(\partial\lambda_{COP}/\partial I)$
■ $(\partial\lambda_{COP}/\partial U)$	■ $(\partial\lambda_{COP}/\partial\Delta\vartheta_m)$	■ $(\partial\lambda_{COP}/\partial C_j)$
■ $(\partial\lambda_{COP}/\partial\Delta\lambda_{R,E})$	■ $(\partial\lambda_{COP}/\partial\Delta\lambda_o)$	■ $(\partial\lambda_{COP}/\partial\Delta\lambda_s)$

Table D. 11: Uncertainty assessment of FG based VIP ($t = 30 \text{ mm}$, $\vartheta_{avg} = 23^\circ\text{C}$)

<i>FG - 30 mm - 23°C</i>									
		A_m [m ²]	t_{VIP_1} [m]	t_{VIP_2} [m]	t_m [m]	I [A]	U [V]	λ_{COP_avg} [W/mK]	
1 st Side	Hot	0.0401	0.0299	-	0.0307	0.050	2.520	0.00235	
	Cold								
	$u(x_i)$								
2 nd Side	Hot	0.0401	-	0.0316	0.0002	0.0005	0.0001		
	Cold								
	$u(x_i)$								
		$\Delta\vartheta_m$ [°C]	C_j [-]	C_{i_m} [-]	$\Delta\lambda_{R,E}$ [-]	$\Delta\lambda_o$ [-]	$\Delta\lambda_s$ [-]		
1 st Side	Hot	20.26	1.0133	1.0133	1	1	1		
	Cold								
	$u(x_i)$		0.0008		1.2E-05	1.2E-05	2.4E-06		
2 nd Side	Hot	0.01	1.0133	0.0008	1	1	1		
	Cold								
	$u(x_i)$		0.0008		1.2E-05	1.2E-05	2.4E-06		
							$u(\lambda_{COP_avg})$ [%]	1.28%	

Table D. 12: Sensitivity coefficients and uncertainty contributions of FG based VIP ($t = 30 \text{ mm}$, $\vartheta_{avg} = 23^\circ\text{C}$)

<i>Sensitivity coefficients</i>	
Average	Uncertainty contributions
$(\partial\lambda_{COP}/\partial A_m)$	-0.058728
$(\partial\lambda_{COP}/\partial t_m)$	0.076566
$(\partial\lambda_{COP}/\partial I)$	0.047076
$(\partial\lambda_{COP}/\partial U)$	0.000934
$(\partial\lambda_{COP}/\partial \Delta\vartheta_m)$	-0.000116
$(\partial\lambda_{COP}/\partial C_j)$	-0.002323
$(\partial C_j/\partial A_{SP})$	12.475037
$(\partial C_j/\partial A_m)$	-2.060237
$(\partial\lambda_{COP}/\partial \Delta\lambda_{R,E})$	0.002354
$(\partial\lambda_{COP}/\partial \Delta\lambda_o)$	0.002354
$(\partial\lambda_{COP}/\partial \Delta\lambda_s)$	0.002354

■ $(\partial\lambda_{COP}/\partial A_m)$	■ $(\partial\lambda_{COP}/\partial t_m)$	■ $(\partial\lambda_{COP}/\partial I)$
■ $(\partial\lambda_{COP}/\partial U)$	■ $(\partial\lambda_{COP}/\partial \Delta\vartheta_m)$	■ $(\partial\lambda_{COP}/\partial C_j)$
■ $(\partial\lambda_{COP}/\partial \Delta\lambda_{R,E})$	■ $(\partial\lambda_{COP}/\partial \Delta\lambda_o)$	■ $(\partial\lambda_{COP}/\partial \Delta\lambda_s)$

Appendix E

Linear thermal transmittance uncertainty - GHP

An extended version of this appendix is available at the following link:

<http://dx.doi.org/10.17632/v9r5pkwkyg.2#file-05e249b5-ddec-4fc9-a98b-48c9838617cf>

FS based VIPs

Table E. 1: λ_{eq} - Uncertainty assessment of FS based VIPs, Commutated joint
($t = 20$ mm, $\vartheta_{avg} = 10^\circ\text{C}$)

<i>FS - 20 mm - 10°C: COMMUTATED JOINT</i>									
		A_m [m ²]	t_{VIP_1} [m]	t_{VIP_2} [m]	t_m [m]	I [A]	U [V]	λ_{eq_GHP} [W/mK]	
1 st Side	Hot/Cold	0.2483	0.0205	0.02105	0.02058	0.157	10.300		0.00444
	$u(x_j)$	0.0002	0.0003	0.00015					
2 nd Side	Hot/Cold	0.2483	0.02010	0.0207	0.00008	0.0004	0.0004		
	$u(x_j)$	0.0002	0.00001	0.0003					
		$\Delta\vartheta_m$ [°C]	C_j [-]	C_{j_m} [-]	$\Delta\lambda_{R,E}$ [-]	$\Delta\lambda_O$ [-]	$\Delta\lambda_S$ [-]		
1 st Side	Hot/Cold		1.0057		1	1	1		
	$u(x_j)$	14.98	0.0003	1.0057	2.2E-05	2.2E-05	4.4E-06		
2 nd Side	Hot/Cold		1.0057		1	1	1		
	$u(x_j)$	0.24	0.0003	0.0003	2.2E-05	2.2E-05	4.4E-06	0.00008	
							$u(\lambda_{eq_GHP})$ [%]	1.80%	

Table E. 2: λ_{eq} - Sensitivity coefficients and uncertainty contributions of FS based VIPs, Commutated joint ($t = 20$ mm, $\vartheta_{avg} = 10^\circ\text{C}$)

<i>Sensitivity coefficients</i>	
	Average
$(\partial\lambda_{eq_GHP}/\partial A_m)$	- 0.101181
$(\partial\lambda_{eq_GHP}/\partial t_m)$	0.196861
$(\partial\lambda_{eq_GHP}/\partial I)$	0.057934
$(\partial\lambda_{eq_GHP}/\partial U)$	0.001162
$(\partial\lambda_{eq_GHP}/\partial \Delta\vartheta_m)$	- 0.000265
$(\partial\Delta\vartheta_m/\partial A_{COP})$	12.475037
$(\partial\Delta\vartheta_m/\partial \Delta\vartheta_{COP})$	- 0.870986
$(\partial\Delta\vartheta_m/\partial A_{SA})$	12.475037
$(\partial\Delta\vartheta_m/\partial \Delta\vartheta_{SA})$	- 0.870986
$(\partial\Delta\vartheta_m/\partial A_j)$	12.475037
$(\partial\Delta\vartheta_m/\partial \Delta\vartheta_j)$	- 0.870986
$(\partial\lambda_{eq_GHP}/\partial C_j)$	- 0.004002
$(\partial C_j/\partial A_{SP})$	2.013670
$(\partial C_j/\partial A_m)$	- 0.022694
$(\partial\lambda_{eq_GHP}/\partial \Delta\lambda_{R,E})$	0.004055
$(\partial\lambda_{eq_GHP}/\partial \Delta\lambda_O)$	0.004055
$(\partial\lambda_{eq_GHP}/\partial \Delta\lambda_S)$	0.004055

<i>Uncertainty contributions</i>	
$(\partial\lambda_{eq_GHP}/\partial A_m)$	76.98%
$(\partial\lambda_{eq_GHP}/\partial I)$	10.08%
$(\partial\lambda_{eq_GHP}/\partial \Delta\vartheta_m)$	6.37%
$(\partial\lambda_{eq_GHP}/\partial \Delta\lambda_{R,E})$	4.75%
$(\partial\lambda_{eq_GHP}/\partial \Delta\lambda_O)$	1.57%
$(\partial\lambda_{eq_GHP}/\partial \Delta\lambda_S)$	1.58%
$(\partial\lambda_{eq_GHP}/\partial t_m)$	0.15%
$(\partial\lambda_{eq_GHP}/\partial U)$	0.11%
$(\partial\lambda_{eq_GHP}/\partial C_j)$	1.58%

Table E. 3: ψ - Uncertainty assessment of FS based VIPs, Comutated joint
($t = 20 \text{ mm}$, $\vartheta_{avg} = 10^\circ\text{C}$)

		<i>FS - 20 mm - 10°C: COMMUTATED JOINT</i>						
		A_m [m ²]	t_m [m]	I_ψ [m]	I_ψ [m]	λ_{COP_avg} [W/mK]	λ_{eq_GHP} [W/mK]	Ψ_{GHP} [W/mK]
1 st Side	Hot	0.2483	0.0206	0.4983	0.4983	0.00406	0.00444	0.009
	Cold			0.4983				
	$u(x_j)$	0.0002	0.0003	0.0003	0.00007	0.00008		
2 nd Side	Hot	0.2483	0.0001	0.4983	0.0003	0.00007	0.00008	0.002
	Cold			0.4983				
	$u(x_j)$	0.0002	0.0001	0.0003	0.00007	0.00008		
				$u(x_j)$	[%]	1.72%	22.22%	

Table E. 4: $u(\psi)$ - Sensitivity coefficients and uncertainty contributions of FS based VIPs, Commutated joint ($t = 20 \text{ mm}$, $\vartheta_{avg} = 10^\circ\text{C}$)

		<i>Sensitivity coefficients</i>	
		Average	Uncertainty contributions
$(\partial\Psi_{GHP}/\partial A_m)$	0.000000		2.92%
$(\partial\Psi_{GHP}/\partial t_{m,eq})$	0.772399		0.23%
$(\partial\Psi_{GHP}/\partial I_\psi)$	-0.179197		3.45%
$(\partial\Psi_{GHP}/\partial U_{eq_GHP})$	0.010456		3.45%
$(\partial\Psi_{GHP}/\partial I_{eq_GHP})$	0.685984		3.45%
$(\partial\Psi_{GHP}/\partial \Delta\vartheta_{m,eq})$	-0.007189		0.15%
$(\partial\Psi_{GHP}/\partial C_j)$	-0.091187		21.99%
$(\partial\Psi_{GHP}/\partial \Delta\lambda_{R,E,eq})$	0.107700		5.74%
$(\partial\Psi_{GHP}/\partial \Delta\lambda_{O,eq})$	0.107700		0.34%
$(\partial\Psi_{GHP}/\partial \Delta\lambda_{S,eq})$	0.107700		0.00%
$(\partial\Psi_{GHP}/\partial U_{COP_GHP})$	-0.004548		24.76%
$(\partial\Psi_{GHP}/\partial I_{COP_GHP})$	-0.226754		24.70%
$(\partial\Psi_{GHP}/\partial t_{m,COP})$	-0.770524		7.27%
$(\partial\Psi_{GHP}/\partial \Delta\vartheta_{m,COP})$	0.001039		0.03%
$(\partial\Psi_{GHP}/\partial \Delta\lambda_{R,E,COP})$	-0.015873		0.51%
$(\partial\Psi_{GHP}/\partial \Delta\lambda_{O,COP})$	-0.015873		0.51%
$(\partial\Psi_{GHP}/\partial \Delta\lambda_{S,COP})$	-0.015873		0.51%

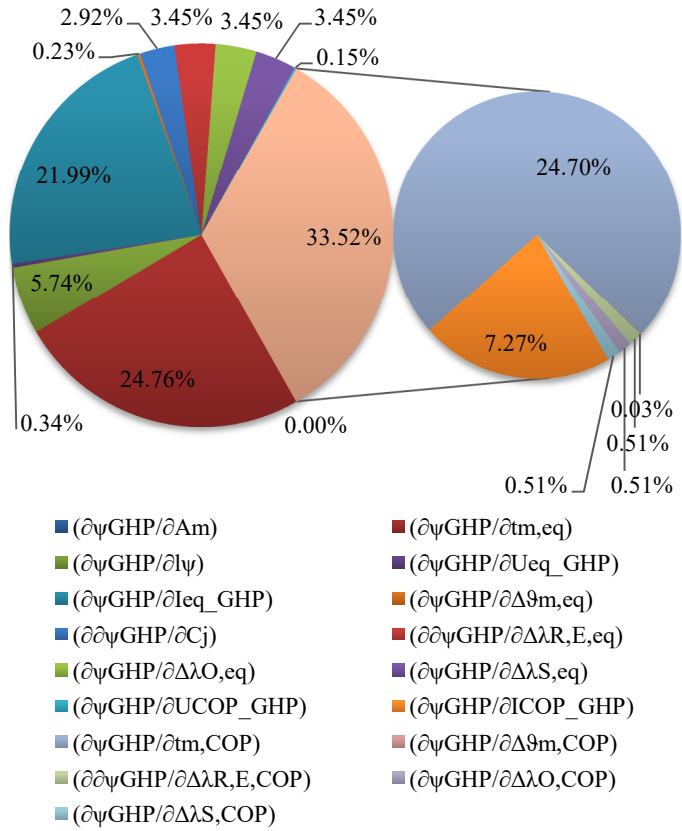


Table E. 5: λ_{eq} - Uncertainty assessment of FS based VIPs, Commutated joint
($t = 40$ mm, $\vartheta_{avg} = 10^\circ\text{C}$)

<i>FS - 40 mm - 10°C: COMMUTATED JOINT</i>								
		A_m [m ²]	t_{VIP_1} [m]	t_{VIP_2} [m]	t_m [m]	I [A]	U [V]	λ_{eq_GHP} [W/mK]
1 st Side	Hot/Cold	0.2483	0.0408	0.04021				0.00471
	$u(x_i)$	0.0002	0.0007	0.00004	0.0405	0.114	7.480	
2 nd Side	Hot/Cold	0.2483	0.04046	0.0399				
	$u(x_i)$	0.0002	0.00007	0.0001	0.0002	0.0004	0.0003	
		$\Delta\vartheta_m$ [°C]	C_j [-]	C_{j_m} [-]	$\Delta\lambda_{R,E}$ [-]	$\Delta\lambda_o$ [-]	$\Delta\lambda_s$ [-]	
1 st Side	Hot/Cold		1.0057		1	1	1	
	$u(x_i)$	14.67	0.0003	1.0057	2.4E-05	2.4E-05	4.7E-06	
2 nd Side	Hot/Cold		1.0057		1	1	1	
	$u(x_i)$	0.24	0.0003	0.0003	2.4E-05	2.4E-05	4.7E-06	
							$u(\lambda_{eq_GHP})$ [%]	

Table E. 6: $u(\lambda_{eq})$ - Sensitivity coefficients and uncertainty contributions of FS based VIPs, Commutated joint ($t = 40$ mm, $\vartheta_{avg} = 10^\circ\text{C}$)

<i>Sensitivity coefficients</i>	
	Average
$(\partial\lambda_{eq_GHP}/\partial A_m)$	- 0.018987
$(\partial\lambda_{eq_GHP}/\partial t_m)$	0.116411
$(\partial\lambda_{eq_GHP}/\partial I)$	0.041356
$(\partial\lambda_{eq_GHP}/\partial U)$	0.000630
$(\partial\lambda_{eq_GHP}/\partial \Delta\vartheta_m)$	- 0.000321
$(\partial\Delta\vartheta_m/\partial A_{COP})$	0.033845
$(\partial\Delta\vartheta_m/\partial \Delta\vartheta_{COP})$	0.967213
$(\partial\Delta\vartheta_m/\partial A_{SA})$	- 0.826811
$(\partial\Delta\vartheta_m/\partial \Delta\vartheta_{SA})$	0.024590
$(\partial\Delta\vartheta_m/\partial A_j)$	- 1.513286
$(\partial\Delta\vartheta_m/\partial \Delta\vartheta_j)$	0.008197
$(\partial\lambda_{eq_GHP}/\partial C_j)$	- 0.004688
$(\partial C_j/\partial A_{SP})$	2.013670
$(\partial C_j/\partial A_m)$	- 0.022694
$(\partial\lambda_{eq_GHP}/\partial \Delta\lambda_{R,E})$	0.004715
$(\partial\lambda_{eq_GHP}/\partial \Delta\lambda_o)$	0.004715
$(\partial\lambda_{eq_GHP}/\partial \Delta\lambda_s)$	0.004715

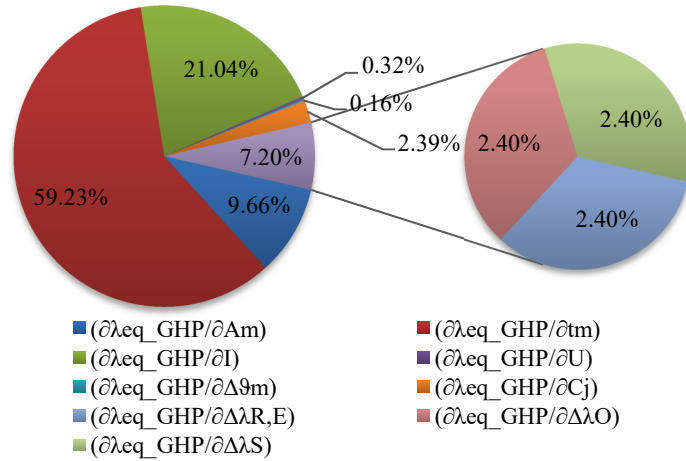


Table E. 7: ψ - Uncertainty assessment of FS based VIPs, Commutated joint ($t = 40 \text{ mm}$, $\vartheta_{avg} = 10^\circ\text{C}$)

		<i>FS - 40 mm - 10°C: COMMUTATED JOINT</i>						
		A_m [m ²]	t_m [m]	I_ψ [m]	I_ψ [m]	λ_{COP_avg} [W/mK]	λ_{eq_GHP} [W/mK]	Ψ_{GHP} [W/mK]
1 st Side	Hot	0.2483	0.0405	0.4983	0.4983	0.00428	0.00471	0.005
	Cold			0.4983				
	$u(x_i)$	0.0002	0.0003	0.0003	0.00006	0.00008	0.0001	
2 nd Side	Hot	0.2483	0.0002	0.4983	0.0003	0.00006	0.00008	0.001
	Cold			0.4983				
	$u(x_i)$	0.0002	0.0003	0.0003	0.00006	0.00008	0.0001	
				$u(x_i)$	[%]	1.75%	20.00%	

Table E. 8: $u(\psi)$ - Sensitivity coefficients and uncertainty contributions of FS based VIPs, Commutated joint ($t = 40 \text{ mm}$, $\vartheta_{avg} = 10^\circ\text{C}$)

Sensitivity coefficients		Uncertainty contributions	
	Average		
$(\partial\Psi_{GHP}/\partial A_m)$	0.000000		
$(\partial\Psi_{GHP}/\partial t_{m,eq})$	0.210043		
$(\partial\Psi_{GHP}/\partial I_\psi)$	- 0.095008		
$(\partial\Psi_{GHP}/\partial U_{eq_GHP})$	0.007755		
$(\partial\Psi_{GHP}/\partial I_{eq_GHP})$	0.508837		
$(\partial\Psi_{GHP}/\partial \Delta\vartheta_{m,eq})$	- 0.003955		
$(\partial\Psi_{GHP}/\partial C_j)$	- 0.049156		
$(\partial\Psi_{GHP}/\partial \Delta\lambda_{R,E,eq})$	0.058007		
$(\partial\Psi_{GHP}/\partial \Delta\lambda_{O,eq})$	0.058007		
$(\partial\Psi_{GHP}/\partial \Delta\lambda_{S,eq})$	0.058007		
$(\partial\Psi_{GHP}/\partial U_{COP_GHP})$	- 0.003323		
$(\partial\Psi_{GHP}/\partial I_{COP_GHP})$	- 0.166795		
$(\partial\Psi_{GHP}/\partial t_{m,COP})$	- 0.210839		
$(\partial\Psi_{GHP}/\partial \Delta\vartheta_{m,COP})$	0.000562		
$(\partial\Psi_{GHP}/\partial \Delta\lambda_{R,E,COP})$	- 0.008507		
$(\partial\Psi_{GHP}/\partial \Delta\lambda_{O,COP})$	- 0.008507		
$(\partial\Psi_{GHP}/\partial \Delta\lambda_{S,COP})$	- 0.008507		

FG based VIPs

Table E. 9: λ_{eq} - Uncertainty assessment of FG based VIPs, Commutated joint
($t = 20$ mm, $\vartheta_{avg} = 10^\circ\text{C}$)

<i>FG - 20 mm - 10°C: COMMUTATED JOINT</i>									
		A_m [m ²]	t_{VIP_1} [m]	t_{VIP_2} [m]	t_m [m]	I [A]	U [V]	λ_{eq_GHP} [W/mK]	
1 st Side	Hot/Cold	0.2483	0.0216	0.0220				0.00715	
	$u(x_j)$	0.0002	0.0001	0.0003	0.0219	0.184	12.810		
2 nd Side	Hot/Cold	0.2483	0.0220	0.0220					
	$u(x_j)$	0.0002	0.0003	0.0002	0.0001	0.0004	0.0005		
		$\Delta\vartheta_m$ [°C]	C_j [-]	C_{j_m} [-]	$\Delta\lambda_{R,E}$ [-]	$\Delta\lambda_O$ [-]	$\Delta\lambda_S$ [-]		
1 st Side	Hot/Cold		1.0057		1	1	1		
	$u(x_j)$	14.42	0.0003	1.0057	3.6E-05	3.6E-05	7.2E-06		
2 nd Side	Hot/Cold		1.00570		1	1	1		
	$u(x_j)$	0.18	0.0003	0.0003	3.6E-05	3.6E-05	7.2E-06		0.00010
							$u(\lambda_{eq_GHP})$ [%]		1.40%

Table E. 10: λ_{eq} - Sensitivity coefficients and uncertainty contributions of FG based VIPs, Commutated joint ($t = 20$ mm, $\vartheta_{avg} = 10^\circ\text{C}$)

<i>Sensitivity coefficients</i>	
	Average
$(\partial\lambda_{eq_GHP}/\partial A_m)$	-0.028806
$(\partial\lambda_{eq_GHP}/\partial t_m)$	0.327331
$(\partial\lambda_{eq_GHP}/\partial I)$	0.038873
$(\partial\lambda_{eq_GHP}/\partial U)$	0.000558
$(\partial\lambda_{eq_GHP}/\partial \Delta\vartheta_m)$	-0.000496
$(\partial\Delta\vartheta_m/\partial A_{COP})$	2.368800
$(\partial\Delta\vartheta_m/\partial \Delta\vartheta_{COP})$	0.680000
$(\partial\Delta\vartheta_m/\partial A_{SA})$	-1.181200
$(\partial\Delta\vartheta_m/\partial \Delta\vartheta_{SA})$	0.240000
$(\partial\Delta\vartheta_m/\partial A_j)$	-16.591200
$(\partial\Delta\vartheta_m/\partial \Delta\vartheta_j)$	0.080000
$(\partial\lambda_{eq_GHP}/\partial C_j)$	-0.007112
$(\partial C_j/\partial A_{SP})$	2.013670
$(\partial C_j/\partial A_m)$	-0.022694
$(\partial\lambda_{eq_GHP}/\partial \Delta\lambda_{R,E})$	0.007153
$(\partial\lambda_{eq_GHP}/\partial \Delta\lambda_O)$	0.007153
$(\partial\lambda_{eq_GHP}/\partial \Delta\lambda_S)$	0.007153

<i>Uncertainty contributions</i>	
$(\partial\lambda_{eq_GHP}/\partial A_m)$	77.09%
$(\partial\lambda_{eq_GHP}/\partial I)$	9.15%
$(\partial\lambda_{eq_GHP}/\partial \Delta\vartheta_m)$	6.78%
$(\partial\lambda_{eq_GHP}/\partial \Delta\lambda_{R,E})$	5.05%
$(\partial\lambda_{eq_GHP}/\partial \Delta\lambda_S)$	1.67%
$(\partial\lambda_{eq_GHP}/\partial t_m)$	0.13%
$(\partial\lambda_{eq_GHP}/\partial U)$	0.12%
$(\partial\lambda_{eq_GHP}/\partial C_j)$	1.68%
$(\partial\lambda_{eq_GHP}/\partial \Delta\lambda_O)$	1.68%

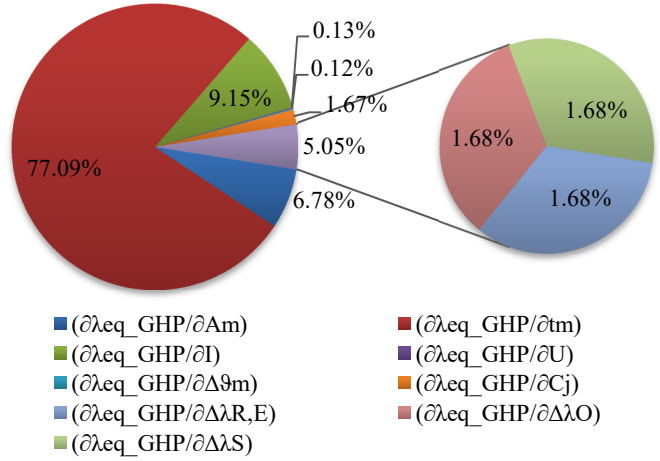


Table E. 11: ψ - Uncertainty assessment of FG based VIPs, Commutated joint ($t = 20 \text{ mm}$, $\vartheta_{avg} = 10^\circ\text{C}$)

		<i>FG - 20 mm - 10°C: COMMUTATED JOINT</i>						
		A_m [m ²]	t_m [m]	l_ψ [m]	l_ψ [m]	λ_{COP_avg} [W/mK]	λ_{eq_GHP} [W/mK]	Ψ_{GHP} [W/mK]
1 st Side	Hot	0.2483	0.0219	0.4983	0.4983	0.00212	0.0072	0.115
	Cold							
	$u(x_i)$	0.0002	0.0003	0.0003	0.00002	0.0001		
2 nd Side	Hot	0.2483	0.0001	0.4983	0.4983	0.00002	0.0001	0.002
	Cold							
	$u(x_i)$	0.0002	0.0003	0.0003	0.00002	0.0001		
				$u(x_i)$	[%]	1.35%	1.74%	

Table E. 12: $u(\psi)$ - Sensitivity coefficients and uncertainty contributions of FG based VIPs, Commutated joint ($t = 20 \text{ mm}$, $\vartheta_{avg} = 10^\circ\text{C}$)

		Sensitivity coefficients	
		Average	Uncertainty contributions
$(\partial\Psi_{GHP}/\partial A_{m,eq})$	- 0.194362		
$(\partial\Psi_{GHP}/\partial d_{m,eq})$	2.208600	1.85%	
$(\partial\Psi_{GHP}/\partial l_\psi)$	- 0.230481	1.86%	
$(\partial\Psi_{GHP}/\partial U_{eq_GHP})$	0.012733	1.86%	
$(\partial\Psi_{GHP}/\partial I_{eq_GHP})$	0.886463	1.86%	
$(\partial\Psi_{GHP}/\partial \Delta\vartheta_{m,eq})$	- 0.011313	1.86%	
$(\partial\Psi_{GHP}/\partial C_{j,eq})$	- 0.162185	0.15%	
$(\partial\Psi_{GHP}/\partial \Delta\lambda_{R,E,eq})$	0.163109	10.78%	
$(\partial\Psi_{GHP}/\partial \Delta\lambda_{O,eq})$	0.163109	25.16%	
$(\partial\Psi_{GHP}/\partial \Delta\lambda_{S,eq})$	0.163109	25.27%	
$(\partial\Psi_{GHP}/\partial U_{COP_GHP})$	- 0.019000	2.63%	
$(\partial\Psi_{GHP}/\partial I_{COP_GHP})$	- 0.946288	2.21%	
$(\partial\Psi_{GHP}/\partial d_{m,COP})$	- 2.218117	0.22%	
$(\partial\Psi_{GHP}/\partial A_{m,COP})$	1.204107	10.10%	
$(\partial\Psi_{GHP}/\partial \Delta\vartheta_{m,COP})$	0.002943	0.13%	
$(\partial\Psi_{GHP}/\partial C_{j,COP})$	0.047627	0.13%	
$(\partial\Psi_{GHP}/\partial \Delta\lambda_{R,E,COP})$	- 0.048261	13.72%	

Table E. 13: λ_{eq} - Uncertainty assessment of FG based VIPs, Commutated joint
($t = 20$ mm, $\vartheta_{avg} = 23^\circ\text{C}$)

<i>FG - 20 mm - 23°C: COMMUTATED JOINT</i>								λ_{eq_GHP} [W/mK]
		A_m [m ²]	t_{VIP_1} [m]	t_{VIP_2} [m]	t_m [m]	I [A]	U [V]	
1 st Side	Hot/Cold	0.2483	0.0216	0.0220				0.00735
	$u(x_i)$	0.0002	0.0001	0.0003	0.0219	0.216	15.170	
2 nd Side	Hot/Cold	0.2483	0.0220	0.0220				
	$u(x_i)$	0.0002	0.0003	0.0002	0.0001	0.0004	0.001	
		$\Delta\vartheta_m$ [°C]	C_j [-]	C_{j_m} [-]	$\Delta\lambda_{R,E}$ [-]	$\Delta\lambda_O$ [-]	$\Delta\lambda_S$ [-]	
1 st Side	Hot/Cold		1.0057		1	1	1	
	$u(x_i)$	19.49	0.0003	1.0057	3.7E-05	3.7E-05	7.4E-06	
2 nd Side	Hot/Cold		1.00570		1	1	1	
	$u(x_i)$	0.18	0.0003	0.0003	3.7E-05	3.7E-05	7.4E-06	
							$u(\lambda_{eq_GHP})$ [%]	

Table E. 14: λ_{eq} - Sensitivity coefficients and uncertainty contributions of FG based VIPs, Commutated joint ($t = 20$ mm, $\vartheta_{avg} = 23^\circ\text{C}$)

<i>Sensitivity coefficients</i>	
	Average
$(\partial\lambda_{eq_GHP}/\partial A_m)$	- 0.029621
$(\partial\lambda_{eq_GHP}/\partial t_m)$	0.336591
$(\partial\lambda_{eq_GHP}/\partial I)$	0.034051
$(\partial\lambda_{eq_GHP}/\partial U)$	0.000485
$(\partial\lambda_{eq_GHP}/\partial \Delta\vartheta_m)$	- 0.000377
$(\partial\Delta\vartheta_m/\partial A_{COP})$	3.252000
$(\partial\Delta\vartheta_m/\partial \Delta\vartheta_{COP})$	0.680000
$(\partial\Delta\vartheta_m/\partial A_{SA})$	- 1.748000
$(\partial\Delta\vartheta_m/\partial \Delta\vartheta_{SA})$	0.240000
$(\partial\Delta\vartheta_m/\partial A_j)$	- 22.398000
$(\partial\Delta\vartheta_m/\partial \Delta\vartheta_j)$	0.080000
$(\partial\lambda_{eq_GHP}/\partial C_j)$	- 0.007313
$(\partial C_j/\partial A_{SP})$	2.013670
$(\partial C_j/\partial A_m)$	- 0.022694
$(\partial\lambda_{eq_GHP}/\partial \Delta\lambda_{R,E})$	0.007355
$(\partial\lambda_{eq_GHP}/\partial \Delta\lambda_O)$	0.007355
$(\partial\lambda_{eq_GHP}/\partial \Delta\lambda_S)$	0.007355

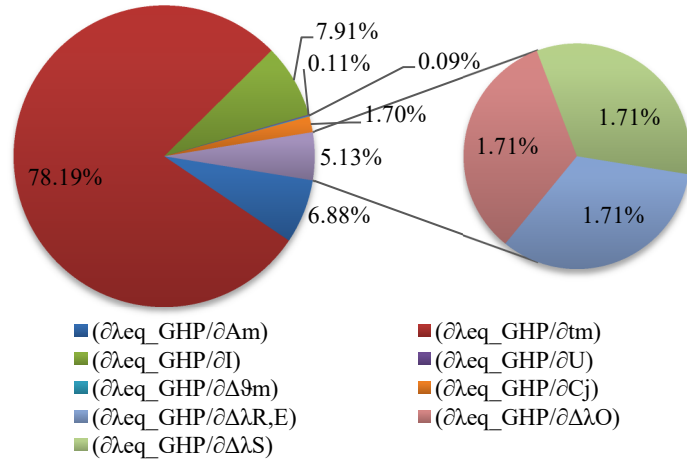


Table E. 15: ψ - Uncertainty assessment of FG based VIPs, Commutated joint ($t = 20 \text{ mm}$, $\vartheta_{avg} = 23^\circ\text{C}$)

		<i>FG - 20 mm - 23°C: COMMUTATED JOINT</i>						
		A_m [m ²]	t_m [m]	l_ψ [m]	l_ψ [m]	λ_{COP_avg} [W/mK]	λ_{eq_GHP} [W/mK]	Ψ_{GHP} [W/mK]
1 st Side	Hot	0.2483	0.0219	0.4983	0.4983	0.00230	0.00735	0.115
	Cold							
	$u(x_i)$	0.0002	0.0003	0.00230	0.00735			
2 nd Side	Hot	0.2483	0.0001	0.4983	0.4983	0.00002	0.00008	0.002
	Cold							
	$u(x_i)$	0.0002	0.0001	0.0003	0.0003	0.00002	0.00008	
				$u(x_i)$	[%]	1.07%	1.74%	

Table E. 16: $u(\psi)$ - Sensitivity coefficients and uncertainty contributions of FG based VIPs, Commutated joint ($t = 20 \text{ mm}$, $\vartheta_{avg} = 23^\circ\text{C}$)

		Sensitivity coefficients	
		Average	Uncertainty contributions
$(\partial\Psi_{GHP}/\partial A_{m,eq})$	- 0.210891		
$(\partial\Psi_{GHP}/\partial d_{m,eq})$	2.396420		
$(\partial\Psi_{GHP}/\partial l_\psi)$	- 0.231504		
$(\partial\Psi_{GHP}/\partial U_{eq_GHP})$	0.011056		
$(\partial\Psi_{GHP}/\partial I_{eq_GHP})$	0.776497		
$(\partial\Psi_{GHP}/\partial \Delta\vartheta_{m,eq})$	- 0.008605		
$(\partial\Psi_{GHP}/\partial C_{j,eq})$	- 0.166773		
$(\partial\Psi_{GHP}/\partial \Delta\lambda_{R,E,eq})$	0.167723		
$(\partial\Psi_{GHP}/\partial \Delta\lambda_{O,eq})$	0.167723		
$(\partial\Psi_{GHP}/\partial \Delta\lambda_{S,eq})$	0.167723		
$(\partial\Psi_{GHP}/\partial U_{COP_GHP})$	- 0.017933		
$(\partial\Psi_{GHP}/\partial I_{COP_GHP})$	- 0.902841		
$(\partial\Psi_{GHP}/\partial d_{m,COP})$	- 2.406746		
$(\partial\Psi_{GHP}/\partial A_{m,COP})$	1.306505		
$(\partial\Psi_{GHP}/\partial \Delta\vartheta_{m,COP})$	0.002651		
$(\partial\Psi_{GHP}/\partial C_{j,COP})$	0.051677		
$(\partial\Psi_{GHP}/\partial \Delta\lambda_{R,E,COP})$	- 0.052365		

Table E. 17: λ_{eq} - Uncertainty assessment of FG based VIPs, Commutated joint
($t = 30$ mm, $\vartheta_{avg} = 10^\circ\text{C}$)

<i>FG - 30 mm - 10°C: COMMUTATED JOINT</i>									
		A_m [m ²]	t_{VIP_1} [m]	t_{VIP_2} [m]	t_m [m]	I [A]	U [V]	λ_{eq_GHP} [W/mK]	
1 st Side	Hot/Cold	0.2483	0.0299	0.0304				0.0076	
	$u(x_i)$	0.0002	0.0004	0.0002	0.0303	0.162	10.670		
2 nd Side	Hot/Cold	0.2483	0.0307	0.0316					
	$u(x_i)$	0.0002	0.0002	0.0002	0.0001	0.0004	0.0004		
		$\Delta\vartheta_m$ [°C]	C_j [-]	C_{j_m} [-]	$\Delta\lambda_{R,E}$ [-]	$\Delta\lambda_o$ [-]	$\Delta\lambda_s$ [-]		
1 st Side	Hot/Cold		1.0057		1	1	1		
	$u(x_i)$	13.79	0.0003	1.0057	3.8E-05	3.8E-05	7.6E-06		
2 nd Side	Hot/Cold		1.0057		1	1	1		
	$u(x_i)$	0.18	0.0003	0.0003	3.8E-05	3.8E-05	7.6E-06		0.0001
							$u(\lambda_{eq_GHP})$ [%]		1.31%

Table E. 18: $u(\lambda_{eq})$ - Sensitivity coefficients and uncertainty contributions of FG based VIPs, Commutated joint ($t = 30$ mm, $\vartheta_{avg} = 10^\circ\text{C}$)

<i>Sensitivity coefficients</i>	
	Average
$(\partial\lambda_{eq_GHP}/\partial A_m)$	- 0.030645
$(\partial\lambda_{eq_GHP}/\partial t_m)$	0.251054
$(\partial\lambda_{eq_GHP}/\partial I)$	0.046970
$(\partial\lambda_{eq_GHP}/\partial U)$	0.000713
$(\partial\lambda_{eq_GHP}/\partial\Delta\vartheta_m)$	- 0.000552
$(\partial\Delta\vartheta_m/\partial A_{COP})$	1.816800
$(\partial\Delta\vartheta_m/\partial\Delta\vartheta_{COP})$	0.680000
$(\partial\Delta\vartheta_m/\partial A_{SA})$	- 1.233200
$(\partial\Delta\vartheta_m/\partial\Delta\vartheta_{SA})$	0.240000
$(\partial\Delta\vartheta_m/\partial A_j)$	- 11.743200
$(\partial\Delta\vartheta_m/\partial\Delta\vartheta_j)$	0.080000
$(\partial\lambda_{eq_GHP}/\partial C_j)$	- 0.007566
$(\partial C_j/\partial A_{SP})$	2.013670
$(\partial C_j/\partial A_m)$	- 0.022694
$(\partial\lambda_{eq_GHP}/\partial\Delta\lambda_{R,E})$	0.007609
$(\partial\lambda_{eq_GHP}/\partial\Delta\lambda_o)$	0.007609
$(\partial\lambda_{eq_GHP}/\partial\Delta\lambda_s)$	0.007609

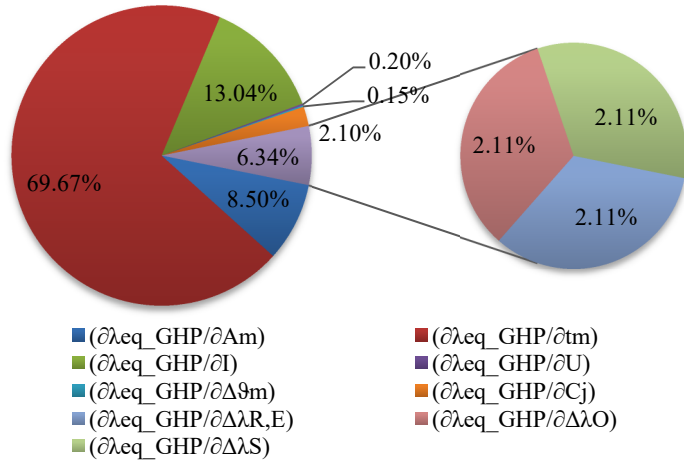


Table E. 19: ψ - Uncertainty assessment of FG based VIPs, Commutated joint ($t = 30 \text{ mm}$, $\vartheta_{avg} = 10^\circ\text{C}$)

		<i>FG - 30 mm - 10°C: COMMUTATED JOINT</i>						
		A_m [m ²]	t_m [m]	l_ψ [m]	l_ψ [m]	λ_{COP_avg} [W/mK]	λ_{eq_GHP} [W/mK]	Ψ_{GHP} [W/mK]
1 st Side	Hot	0.2483	0.0303	0.4983	0.4983	0.00216	0.0076	0.090
	Cold			0.0003				
	$u(x_i)$	0.0002	0.0003	0.0003	0.00003	0.0001	0.002	
2 nd Side	Hot	0.2483	0.0001	0.4983	0.0003	0.00003	0.0001	0.002
	Cold			0.0003				
	$u(x_i)$	0.0002	0.0001	0.0003	0.0003	0.00003	0.0001	
				$u(x_i)$	[%]	1.37%	2.22%	

Table E. 20: $u(\psi)$ - Sensitivity coefficients and uncertainty contributions of FG based VIPs, Commutated joint ($t = 30 \text{ mm}$, $\vartheta_{avg} = 10^\circ\text{C}$)

		Sensitivity coefficients	
		Average	Uncertainty contributions
$(\partial\Psi_{GHP}/\partial A_{m,eq})$	- 0.143344	0.16%	
$(\partial\Psi_{GHP}/\partial d_{m,eq})$	1.174341	2.14%	
$(\partial\Psi_{GHP}/\partial l_\psi)$	- 0.179626	2.14%	
$(\partial\Psi_{GHP}/\partial U_{eq_GHP})$	0.011724	2.13%	
$(\partial\Psi_{GHP}/\partial I_{eq_GHP})$	0.772224	14.50%	
$(\partial\Psi_{GHP}/\partial \Delta\vartheta_{m,eq})$	- 0.009075	0.29%	
$(\partial\Psi_{GHP}/\partial C_{j,eq})$	- 0.124391	3.07%	
$(\partial\Psi_{GHP}/\partial \Delta\lambda_{R,E,eq})$	0.125100	20.09%	
$(\partial\Psi_{GHP}/\partial \Delta\lambda_{O,eq})$	0.125100	0.20%	
$(\partial\Psi_{GHP}/\partial \Delta\lambda_{S,eq})$	0.125100	2.45%	
$(\partial\Psi_{GHP}/\partial U_{COP_GHP})$	- 0.016869	0.07%	
$(\partial\Psi_{GHP}/\partial I_{COP_GHP})$	- 0.847447	0.04%	
$(\partial\Psi_{GHP}/\partial d_{m,COP})$	- 1.157772	0.61%	
$(\partial\Psi_{GHP}/\partial A_{m,COP})$	0.888043	0.61%	
$(\partial\Psi_{GHP}/\partial \Delta\vartheta_{m,COP})$	0.002297	0.61%	
$(\partial\Psi_{GHP}/\partial C_{j,COP})$	0.035126	0.04%	
$(\partial\Psi_{GHP}/\partial \Delta\lambda_{R,E,COP})$	- 0.035593	0.61%	

Table E. 21: λ_{eq} - Uncertainty assessment of FG based VIPs, Commutated joint
($t = 30$ mm, $\vartheta_{avg} = 23^\circ\text{C}$)

<i>FG - 30 mm - 23°C: COMMUTATED JOINT</i>								
		A_m [m ²]	t_{VIP_1} [m]	t_{VIP_2} [m]	t_m [m]	I [A]	U [V]	λ_{eq_GHP} [W/mK]
1 st Side	Hot/Cold	0.2483	0.0299	0.0304				0.00794
	$u(x_i)$	0.0002	0.0004	0.0002	0.0303	0.192	12.640	
2 nd Side	Hot/Cold	0.2483	0.0307	0.0316				
	$u(x_i)$	0.0002	0.0001	0.0002	0.0001	0.0004	0.0005	
		$\Delta\vartheta_m$ [°C]	C_j [-]	C_{j_m} [-]	$\Delta\lambda_{R,E}$ [-]	$\Delta\lambda_O$ [-]	$\Delta\lambda_S$ [-]	
1 st Side	Hot/Cold		1.0057		1	1	1	
	$u(x_i)$	18.56	0.0003	1.0057	4.0E-05	4.0E-05	7.9E-06	
2 nd Side	Hot/Cold		1.0057		1	1	1	
	$u(x_i)$	0.18	0.0003	0.0003	4.0E-05	4.0E-05	7.9E-06	
							$u(\lambda_{eq_GHP})$ [%]	

Table E. 22: $u(\lambda_{eq})$ - Sensitivity coefficients and uncertainty contributions of FG based VIPs, Commutated joint ($t = 30$ mm, $\vartheta_{avg} = 23^\circ\text{C}$)

<i>Sensitivity coefficients</i>	
	Average
$(\partial\lambda_{eq_GHP}/\partial A_m)$	- 0.031958
$(\partial\lambda_{eq_GHP}/\partial t_m)$	0.261815
$(\partial\lambda_{eq_GHP}/\partial I)$	0.041330
$(\partial\lambda_{eq_GHP}/\partial U)$	0.000628
$(\partial\lambda_{eq_GHP}/\partial \Delta\vartheta_m)$	- 0.000428
$(\partial\Delta\vartheta_m/\partial A_{COP})$	2.240800
$(\partial\Delta\vartheta_m/\partial \Delta\vartheta_{COP})$	0.680000
$(\partial\Delta\vartheta_m/\partial A_{SA})$	- 1.219200
$(\partial\Delta\vartheta_m/\partial \Delta\vartheta_{SA})$	0.240000
$(\partial\Delta\vartheta_m/\partial A_j)$	- 15.389200
$(\partial\Delta\vartheta_m/\partial \Delta\vartheta_j)$	0.080000
$(\partial\lambda_{eq_GHP}/\partial C_j)$	- 0.007890
$(\partial C_j/\partial A_{SP})$	2.013670
$(\partial C_j/\partial A_m)$	- 0.022694
$(\partial\lambda_{eq_GHP}/\partial \Delta\lambda_{R,E})$	0.007935
$(\partial\lambda_{eq_GHP}/\partial \Delta\lambda_O)$	0.007935
$(\partial\lambda_{eq_GHP}/\partial \Delta\lambda_S)$	0.007935

Contribution	Percentage
$(\partial\lambda_{eq_GHP}/\partial t_m)$	71.17%
$(\partial\lambda_{eq_GHP}/\partial I)$	11.24%
$(\partial\lambda_{eq_GHP}/\partial U)$	8.69%
$(\partial\lambda_{eq_GHP}/\partial \Delta\lambda_S)$	2.16%
$(\partial\lambda_{eq_GHP}/\partial \Delta\lambda_O)$	2.16%
$(\partial\lambda_{eq_GHP}/\partial \Delta\lambda_{R,E})$	2.14%
$(\partial\lambda_{eq_GHP}/\partial C_j)$	0.17%
$(\partial\lambda_{eq_GHP}/\partial \Delta\lambda_S)$	0.12%

Table E. 23: ψ - Uncertainty assessment of FG based VIPs, Commutated joint
($t = 30 \text{ mm}$, $\vartheta_{avg} = 23^\circ\text{C}$)

		<i>FG - 30 mm - 23°C: COMMUTATED JOINT</i>						
		A_m [m ²]	t_m [m]	l_ψ [m]	l_ψ [m]	λ_{COP_avg} [W/mK]	λ_{eq_GHP} [W/mK]	Ψ_{GHP} [W/mK]
1 st Side	Hot	0.2483	0.0303	0.4983	0.4983	0.00235	0.00794	0.092
	Cold							
	$u(x_j)$	0.0002	0.0003	0.0003	0.0003	0.0003	0.00003	0.00008
2 nd Side	Hot	0.2483	0.0001	0.4983	0.4983	0.00003	0.00008	0.001
	Cold							
	$u(x_j)$	0.0002	0.0001	0.0003	0.0003	0.00003	0.00008	0.001
				$u(x_j)$	[%]	1.06%	1.09%	

Table E. 24: $u(\psi)$ - Sensitivity coefficients and uncertainty contributions of FG based VIPs, Commutated joint ($t = 30 \text{ mm}$, $\vartheta_{avg} = 23^\circ\text{C}$)

		Sensitivity coefficients	
		Average	Uncertainty contributions
$(\partial\Psi_{GHP}/\partial A_{m,eq})$	- 0.155853	2.17%	
$(\partial\Psi_{GHP}/\partial d_{m,eq})$	1.276818	2.17%	
$(\partial\Psi_{GHP}/\partial l_\psi)$	- 0.184154	2.16%	
$(\partial\Psi_{GHP}/\partial U_{eq_GHP})$	0.010321	0.12%	
$(\partial\Psi_{GHP}/\partial I_{eq_GHP})$	0.679492	11.32%	
$(\partial\Psi_{GHP}/\partial \Delta\vartheta_{m,eq})$	- 0.007029	3.07%	
$(\partial\Psi_{GHP}/\partial C_{j,eq})$	-0.129723	0.17%	
$(\partial\Psi_{GHP}/\partial \Delta\lambda_{R,E,eq})$	0.130462	2.60%	
$(\partial\Psi_{GHP}/\partial \Delta\lambda_{O,eq})$	0.130462	2.60%	
$(\partial\Psi_{GHP}/\partial \Delta\lambda_{S,eq})$	0.130462	2.60%	
$(\partial\Psi_{GHP}/\partial U_{COP_GHP})$	- 0.015357	0.17%	
$(\partial\Psi_{GHP}/\partial I_{COP_GHP})$	- 0.773975	2.60%	
$(\partial\Psi_{GHP}/\partial d_{m,COP})$	- 1.258803	2.60%	
$(\partial\Psi_{GHP}/\partial A_{m,COP})$	0.965537	2.60%	
$(\partial\Psi_{GHP}/\partial \Delta\vartheta_{m,COP})$	0.001910	0.17%	
$(\partial\Psi_{GHP}/\partial C_{j,COP})$	0.038191	0.17%	
$(\partial\Psi_{GHP}/\partial \Delta\lambda_{R,E,COP})$	- 0.038699	0.17%	

Appendix F

Linear thermal transmittance uncertainty - HFM

An extended version of this appendix is available at the following link:

<http://dx.doi.org/10.17632/v9r5pkwkyg.2#file-05e249b5-ddec-4fc9-a98b-48c9838617cf>

FS based VIPs

Table F. 1: λ_{eq} - Uncertainty assessment of FS based VIPs, Commutated joint
 ($t = 20$ mm, $\vartheta_{avg} = 10^\circ\text{C}$)

<i>FS - 20 mm - 10°C: COMMUTATED JOINT</i>								
		A_m [m ²]	t_{VIP_1} [m]	t_{VIP_2} [m]	t_m [m]	f_{cal} [W/m ² mV]	λ_{eq_HFM} [W/mK]	
1 st Side	Hot					6.146	0.0043	
	$u(x_j)$	0.2483	0.0205	0.0211	0.0208	0.035		
2 nd Side	Cold					6.727		
	$u(x_j)$	0.0002	0.0003	0.0002	0.0002	0.039		
1 st Side	Hot					7.080		
	$u(x_j)$	0.2483	0.02010	0.0207	0.0204	0.040		
2 nd Side	Cold					7.474		
	$u(x_j)$	0.0002	0.00001	0.0003	0.0001	0.044		
		Q [mV]	$\Delta\vartheta_m$ [°C]	$\Delta\lambda_E$ [-]	$\Delta\lambda_O$ [-]	λ_{eq,i_HFM} [W/mK]		
1 st Side	Hot	0.44816		1	1	0.0040		0.0001
	$u(x_j)$	0.00003	14.47	2.0E-05	4.0E-06	0.0001		
2 nd Side	Cold	0.44745		1	1	0.0043		
	$u(x_j)$	0.00003	0.42	2.2E-05	4.3E-06	0.0001		
1 st Side	Hot	0.38966		1	1	0.0039		
	$u(x_j)$	0.00003	14.58	1.9E-05	3.9E-06	0.0001		
2 nd Side	Cold	0.38462		1	1	0.0040		
	$u(x_j)$	0.00003	0.44	2.0E-05	4.0E-06	0.0001		
						$u(\lambda_{eq_HFM})$ [%]	2.32%	

Table F. 2: λ_{eq} - Sensitivity coefficients and uncertainty contributions of FS based VIPs, Commutated joint ($t = 20 \text{ mm}$, $\vartheta_{avg} = 10^\circ\text{C}$)

<i>Sensitivity coefficients</i>				
	1 st Side Cold	<i>Uncertainty contributions</i>		
$(\partial\lambda_{eq_HFM}/\partial t_m)$	0.208006			
$(\partial\lambda_{eq_HFM}/\partial f_{cal})$	0.000642			
$(\partial\lambda_{eq_HFM}/\partial Q_m)$	0.009658			
$(\partial\lambda_{eq_HFM}/\partial \Delta\vartheta_m)$	- 0.000299			
$(\partial\Delta\vartheta_m/\partial A_{COP})$	823.117049			
$(\partial\Delta\vartheta_m/\partial \Delta\vartheta_{COP})$	0.967213			
$(\partial\Delta\vartheta_m/\partial A_{SA})$	- 1.062094			
$(\partial\Delta\vartheta_m/\partial \Delta\vartheta_{SA})$	0.024590			
$(\partial\Delta\vartheta_m/\partial A_j)$	- 3.339371			
$(\partial\Delta\vartheta_m/\partial \Delta\vartheta_j)$	0.008197			
$(\partial\lambda_{eq_HFM}/\partial \Delta\lambda_E)$	0.004321			
$(\partial\lambda_{eq_HFM}/\partial \Delta\lambda_O)$	0.004321			

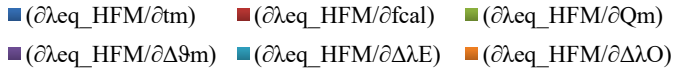


Table F. 3: ψ - Uncertainty assessment of FS based VIPs, Commutated joint
($t = 20 \text{ mm}$, $\vartheta_{avg} = 10^\circ\text{C}$)

		<i>FS - 20 mm - 10°C: COMMUTATED JOINT</i>						
		A_m [m ²]	t_m [m]	l_ψ [m]	l_ψ [m]	λ_{COP_avg} [W/mK]	λ_{eq_HFM} [W/mK]	Ψ_{HFM} [W/mK]
1 st Side	Hot	0.2508	0.0208	0.5008				
	Cold	0.2508	0.0208	0.5008				
	$u(x_i)$	0.0002	0.0002	0.0003	0.5008	0.00406	0.00432	0.006
2 nd Side	Hot	0.2508	0.0204	0.5008				
	Cold	0.2508	0.0204	0.5008				
	$u(x_i)$	0.0002	0.0001	0.0003	0.0003	0.00007	0.00006	0.003
				$u(x_i)$	[%]	3.06%	50.00%	

Table F. 4: $u(\psi)$ - Sensitivity coefficients and uncertainty contributions of FS based VIPs, Commutated joint ($t = 20 \text{ mm}$, $\vartheta_{avg} = 10^\circ\text{C}$)

		<i>Sensitivity coefficients</i>	
		1 st Side Cold	Uncertainty contributions
$(\partial\Psi_{HFM}/\partial A_{m,eq})$	0.006412		
$(\partial\Psi_{HFM}/\partial t_{m,eq})$	4.658685		
$(\partial\Psi_{HFM}/\partial l_\psi)$	-0.012675		
$(\partial\Psi_{HFM}/\partial f_{cal})$	0.015331		
$(\partial\Psi_{HFM}/\partial Q_m)$	0.230486		
$(\partial\Psi_{HFM}/\partial \Delta\vartheta_{m,eq})$	-0.007127		
$(\partial\Psi_{HFM}/\partial \Delta\lambda_E)$	0.103132		
$(\partial\Psi_{HFM}/\partial \Delta\lambda_O)$	0.103132		
$(\partial\Psi_{HFM}/\partial U_{COP})$	-0.027732		
$(\partial\Psi_{HFM}/\partial I_{COP})$	-1.382631		
$(\partial\Psi_{HFM}/\partial t_{m,COP})$	-4.698262		
$(\partial\Psi_{HFM}/\partial A_{m,COP})$	2.414773		
$(\partial\Psi_{HFM}/\partial \Delta\vartheta_{m,COP})$	0.006335		
$(\partial\Psi_{HFM}/\partial C_j)$	0.095514		
$(\partial\Psi_{HFM}/\partial \Delta\lambda_{R,E})$	0.096784		
$(\partial\Psi_{HFM}/\partial \Delta\lambda_O)$	0.096784		
$(\partial\Psi_{HFM}/\partial \Delta\lambda_S)$	0.096784		

Parameter	Contribution (%)
$(\partial\psi_{HFM}/\partial t_{m,eq})$	33.43%
$(\partial\psi_{HFM}/\partial t_{m,COP})$	33.15%
$(\partial\psi_{HFM}/\partial Q_m)$	19.97%
$(\partial\psi_{HFM}/\partial A_{m,COP})$	17.18%
$(\partial\psi_{HFM}/\partial f_{cal})$	9.84%
$(\partial\psi_{HFM}/\partial \Delta\lambda_E)$	0.73%
$(\partial\psi_{HFM}/\partial \Delta\lambda_O)$	1.64%
$(\partial\psi_{HFM}/\partial U_{COP})$	0.09%
$(\partial\psi_{HFM}/\partial I_{COP})$	0.11%
$(\partial\psi_{HFM}/\partial t_{m,COP})$	0.73%
$(\partial\psi_{HFM}/\partial \Delta\vartheta_{m,eq})$	0.05%
$(\partial\psi_{HFM}/\partial \Delta\vartheta_{m,COP})$	0.05%
$(\partial\psi_{HFM}/\partial C_j)$	0.68%
$(\partial\psi_{HFM}/\partial \Delta\lambda_{R,E})$	0.69%
$(\partial\psi_{HFM}/\partial \Delta\lambda_O)$	0.69%
$(\partial\psi_{HFM}/\partial \Delta\lambda_S)$	0.69%

Table F. 5: λ_{eq} , ψ - Uncertainty assessment of FS based VIPs, Commutated joint
($t = 20$ mm, $\vartheta_{avg} = 10^\circ\text{C}$); Type A uncertainty

<i>FS - 20 mm - 10°C: COMMUTATED JOINT (Type A uncertainty)</i>										
		A_m [m ²]	t_{VIP_1} [m]	t_{VIP_2} [m]	t_m [m]	f_{cal} [W/m ² mV]	λ_{eq_HFM} [W/mK]	Ψ_{HFM} [W/mK]		
1 st Side	Hot					6.146	0.00432	0.006		
	$u(x_i)$	0.2483	0.0205	0.0211	0.0208	0.035				
	Cold					6.727				
	$u(x_i)$	0.0002	0.0003	0.0002	0.0002	0.039				
2 nd Side	Hot					7.080				
	$u(x_i)$	0.2483	0.02010	0.0207	0.0204	0.040				
	Cold					7.474				
	$u(x_i)$	0.0002	0.00001	0.0003	0.0001	0.044				
		Q [mV]	$\Delta\vartheta_m$ [°C]	$\Delta\lambda_E$ [-]	$\Delta\lambda_O$ [-]	λ_{eq,i_HFM} [W/mK]				
1 st Side	Hot	0.4482		1	1	0.00395				
	$u(x_i)$	0.0005	14.47	2.0E-05	4.0E-06	0.00006				
	Cold	0.4475		1	1	0.00432				
	$u(x_i)$	0.0001	0.16	2.2E-05	4.3E-06	0.00006				
2 nd Side	Hot	0.3897		1	1	0.00386				
	$u(x_i)$	0.0004	14.58	1.9E-05	3.9E-06	0.00007				
	Cold	0.3846		1	1	0.00402				
	$u(x_i)$	0.0002	0.21	2.0E-05	4.0E-06	0.00007	0.00006	0.002		
				$u(\lambda_{eq_HFM})$	[%]		1.39%	33.33%		

Table F. 6: λ_{eq} - Uncertainty assessment of FS based VIPs, Offset joint
 ($t = 20$ mm, $\vartheta_{avg} = 10^\circ\text{C}$)

<i>FS - 20 mm - 10°C: OFFSET JOINT</i>								
		A_m [m ²]	t_{VIP_1} [m]	t_{VIP_2} [m]	t_m [m]	f_{cal} [W/m ² mV]	λ_{eq_HFM} [W/mK]	
1 st Side	Hot					6.146	0.0043	
	$u(x_j)$	0.2483	0.0205	0.02105	0.0208	0.035		
Cold					6.727			
$u(x_j)$	0.0002	0.0003	0.00001	0.0002	0.039			
2 nd Side	Hot					7.080		
	$u(x_j)$	0.2483	0.02010	0.0207	0.0204	0.040		
Cold					7.474			
$u(x_j)$	0.0002	0.00001	0.0003	0.0001	0.044			
		Q [mV]	$\Delta\vartheta_m$ [°C]	$\Delta\lambda_E$ [-]	$\Delta\lambda_O$ [-]	λ_{eq,i_HFM} [W/mK]		
1 st Side	Hot	0.43830		1	1	0.0039		0.0001
	$u(x_j)$	0.00003	14.42	1.9E-05	3.9E-06	0.0001		
Cold	0.44491		1	1	0.0043			
$u(x_j)$	0.00003	0.42	2.2E-05	4.3E-06	0.0001			
2 nd Side	Hot	0.38624		1	1	0.0038		
	$u(x_j)$	0.00003	14.57	1.9E-05	3.8E-06	0.0001		
Cold	0.38271		1	1	0.0040			
$u(x_j)$	0.00003	0.44	2.0E-05	4.0E-06	0.0001	0.0001		
						$u(\lambda_{eq_HFM})$	[%]	2.32%

Table F. 7: λ_{eq} - Sensitivity coefficients and uncertainty contributions of FS based VIPs, Offset joint ($t = 20 \text{ mm}$, $\vartheta_{avg} = 10^\circ\text{C}$)

<i>Sensitivity coefficients</i>		<i>Uncertainty contributions</i>		
	1 st Side Cold			
$(\partial\lambda_{eq_HFM}/\partial t_m)$	0.207500			
$(\partial\lambda_{eq_HFM}/\partial f_{cal})$	0.000641			
$(\partial\lambda_{eq_HFM}/\partial Q_m)$	0.009689			
$(\partial\lambda_{eq_HFM}/\partial \Delta\vartheta_m)$	- 0.000299			
$(\partial\Delta\vartheta_m/\partial A_{COP})$	839.587080			
$(\partial\Delta\vartheta_m/\partial \Delta\vartheta_{COP})$	0.967213			
$(\partial\Delta\vartheta_m/\partial A_{SA})$	- 0.970369			
$(\partial\Delta\vartheta_m/\partial \Delta\vartheta_{SA})$	0.024590			
$(\partial\Delta\vartheta_m/\partial A_J)$	- 3.745119			
$(\partial\Delta\vartheta_m/\partial \Delta\vartheta_J)$	0.008197			
$(\partial\lambda_{eq_HFM}/\partial \Delta\lambda_E)$	0.004311			
$(\partial\lambda_{eq_HFM}/\partial \Delta\lambda_O)$	0.004311			

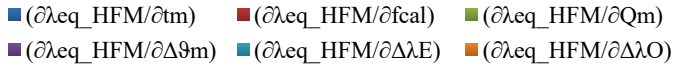


Table F. 8: ψ - Uncertainty assessment of FS based VIPs, Offset joint
($t = 20 \text{ mm}$, $\vartheta_{avg} = 10^\circ\text{C}$)

		<i>FS - 20 mm - 10°C: OFFSET JOINT</i>						
		A_m [m ²]	t_m [m]	I_ψ [m]	I_ψ [m]	λ_{COP_avg} [W/mK]	λ_{eq_HFM} [W/mK]	Ψ_{HFM} [W/mK]
1 st Side	Hot	0.2508	0.0208	0.5008	0.5008	0.00406	0.0043	0.006
	Cold							
	$u(x_i)$							
2 nd Side	Hot	0.2508	0.0204	0.5008	0.0003	0.00007	0.0001	0.003
	Cold							
	$u(x_i)$							
				$u(x_i)$	[%]	3.06%	50.00%	

Table F. 9: $u(\psi)$ - Sensitivity coefficients and uncertainty contributions of FS based VIPs, Offset joint ($t = 20 \text{ mm}$, $\vartheta_{avg} = 10^\circ\text{C}$)

		<i>Sensitivity coefficients</i>	
		1 st Side Cold	Uncertainty contributions
$(\partial\Psi_{HFM}/\partial A_{m,eq})$	0.006158		
$(\partial\Psi_{HFM}/\partial t_{m,eq})$	4.658685	0.20%	
$(\partial\Psi_{HFM}/\partial I_\psi)$	- 0.012174	0.73%	
$(\partial\Psi_{HFM}/\partial f_{cal})$	0.015293		
$(\partial\Psi_{HFM}/\partial Q_m)$	0.231241		
$(\partial\Psi_{HFM}/\partial \Delta\vartheta_{m,eq})$	- 0.007132		
$(\partial\Psi_{HFM}/\partial \Delta\lambda_E)$	0.102881		
$(\partial\Psi_{HFM}/\partial \Delta\lambda_O)$	0.102881	0.05%	
$(\partial\Psi_{HFM}/\partial U_{COP})$	- 0.027732	0.09%	
$(\partial\Psi_{HFM}/\partial I_{COP})$	- 1.382631	0.73%	
$(\partial\Psi_{HFM}/\partial t_{m,COP})$	- 4.698262	1.65%	
$(\partial\Psi_{HFM}/\partial A_{m,COP})$	2.414773	0.11%	
$(\partial\Psi_{HFM}/\partial \Delta\vartheta_{m,COP})$	0.006335		
$(\partial\Psi_{HFM}/\partial C_j)$	0.095514		
$(\partial\Psi_{HFM}/\partial \Delta\lambda_{R,E})$	0.096784		
$(\partial\Psi_{HFM}/\partial \Delta\lambda_O)$	0.096784		
$(\partial\Psi_{HFM}/\partial \Delta\lambda_S)$	0.096784		

Table F. 10: λ_{eq} , ψ - Uncertainty assessment of FS based VIPs, Offset joint
($t = 20$ mm, $\vartheta_{avg} = 10^\circ\text{C}$); Type A uncertainty

<i>FS - 20 mm - 10°C: OFFSET JOINT (Type A uncertainty)</i>										
		A_m [m ²]	t_{VIP_1} [m]	t_{VIP_2} [m]	t_m [m]	f_{cal} [W/m ² mV]	λ_{eq_HFM} [W/mK]	Ψ_{HFM} [W/mK]		
1 st Side	Hot					6.146	0.00431	0.006		
	$u(x_j)$	0.2483	0.0205	0.02105	0.0208	0.035				
	Cold					6.727				
$u(x_j)$	0.0002	0.0003	0.00001	0.0001	0.039					
2 nd Side	Hot					7.080				
	$u(x_j)$	0.2483	0.02010	0.0207	0.0204	0.040				
	Cold					7.474				
$u(x_j)$	0.0002	0.00001	0.0003	0.0001	0.044					
		Q [mV]	$\Delta\vartheta_m$ [°C]	$\Delta\lambda_E$ [-]	$\Delta\lambda_O$ [-]	λ_{eq,i_HFM} [W/mK]				
1 st Side	Hot	0.4383		1	1	0.00388				
	$u(x_j)$	0.0006	14.42	1.9E-05	3.9E-06	0.00006				
	Cold	0.4449		1	1	0.00431				
$u(x_j)$	0.0006	0.17	2.2E-05	4.3E-06	0.00006					
2 nd Side	Hot	0.3862		1	1	0.00383				
	$u(x_j)$	0.0005	14.57	1.9E-05	3.8E-06	0.00006				
	Cold	0.3827		1	1	0.00400				
$u(x_j)$	0.0009	0.20	2.0E-05	4.0E-06	0.00007	0.00006	0.002			
				$u(\lambda_{eq_HFM})$	[%]		1.39%	33.33%		

Table F. 11: λ_{eq} - Uncertainty assessment of FS based VIPs, Gasket strip joint
 ($t = 20$ mm, $\vartheta_{avg} = 10^\circ\text{C}$)

<i>FS - 20 mm - 10°C: GASKET STRIP JOINT</i>								
		A_m [m ²]	t_{VIP_1} [m]	t_{VIP_2} [m]	t_m [m]	f_{cal} [W/m ² mV]	λ_{eq_HFM} [W/mK]	
1 st Side	Hot					6.146	0.0045	
	$u(x_i)$	0.2483	0.0205	0.02105	0.0208	0.035		
Cold						6.727		
	$u(x_i)$	0.0002	0.0003	0.00001	0.0001	0.039		
2 nd Side	Hot					7.080		
	$u(x_i)$	0.2483	0.02010	0.0207	0.0204	0.040		
Cold						7.473		
	$u(x_i)$	0.0002	0.00001	0.0003	0.0001	0.044		
		Q [mV]	$\Delta\vartheta_m$ [°C]	$\Delta\lambda_E$ [-]	$\Delta\lambda_O$ [-]	λ_{eq,i_HFM} [W/mK]		
1 st Side	Hot	0.46006		1	1	0.0041		0.0001
	$u(x_i)$	0.00003	14.41	2.0E-05	4.1E-06	0.0001		
Cold		0.46126		1	1	0.0045		
	$u(x_i)$	0.00003	0.44	2.2E-05	4.5E-06	0.0001		
2 nd Side	Hot	0.40645		1	1	0.0040		
	$u(x_i)$	0.00003	14.57	2.0E-05	4.0E-06	0.0001		
Cold		0.40051		1	1	0.0042		
	$u(x_i)$	0.00003	0.44	2.1E-05	4.2E-06	0.0001	0.0001	
						$u(\lambda_{eq_HFM})$	[%]	2.22%

Table F. 12: λ_{eq} - Sensitivity coefficients and uncertainty contributions of FS based VIPs, Gasket strip joint ($t = 20 \text{ mm}$, $\vartheta_{avg} = 10^\circ\text{C}$)

<i>Sensitivity coefficients</i>		<i>Uncertainty contributions</i>		
	1 st Side Cold			
$(\partial\lambda_{eq_HFM}/\partial t_m)$	0.215269			
$(\partial\lambda_{eq_HFM}/\partial f_{cal})$	0.000665			
$(\partial\lambda_{eq_HFM}/\partial Q_m)$	0.009696			
$(\partial\lambda_{eq_HFM}/\partial \Delta\vartheta_m)$	- 0.000310			
$(\partial\Delta\vartheta_m/\partial A_{COP})$	1076.882645			
$(\partial\Delta\vartheta_m/\partial \Delta\vartheta_{COP})$	0.967213			
$(\partial\Delta\vartheta_m/\partial A_{SA})$	- 1.179751			
$(\partial\Delta\vartheta_m/\partial \Delta\vartheta_{SA})$	0.024590			
$(\partial\Delta\vartheta_m/\partial A_J)$	- 4.998248			
$(\partial\Delta\vartheta_m/\partial \Delta\vartheta_J)$	0.008197			
$(\partial\lambda_{eq_HFM}/\partial \Delta\lambda_E)$	0.004472			
$(\partial\lambda_{eq_HFM}/\partial \Delta\lambda_O)$	0.004472			

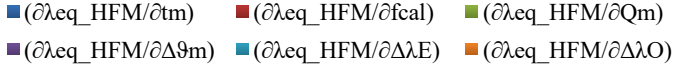


Table F. 13: ψ - Uncertainty assessment of FS based VIPs, Gasket strip joint
($t = 20 \text{ mm}$, $\vartheta_{avg} = 10^\circ\text{C}$)

		<i>FS - 20 mm - 10°C: GASKET STRIP JOINT</i>						
		A_m [m ²]	t_m [m]	l_ψ [m]	l_ψ [m]	λ_{COP_avg} [W/mK]	λ_{eq_HFM} [W/mK]	Ψ_{HFM} [W/mK]
1 st Side	Hot	0.2508	0.02078	0.5008				
	Cold				0.5008	0.00406	0.0045	
	$u(x_i)$	0.0002	0.00014	0.0003				0.010
2 nd Side	Hot	0.2508	0.02040	0.5008				
	Cold				0.0003	0.00007	0.0001	
	$u(x_i)$	0.0002	0.00014	0.0003				0.004
				$u(x_i)$	[%]		3.20%	40.00%

Table F. 14: $u(\psi)$ - Sensitivity coefficients and uncertainty contributions of FS based VIPs, Gasket strip joint ($t = 20 \text{ mm}$, $\vartheta_{avg} = 10^\circ\text{C}$)

		<i>Sensitivity coefficients</i>	
		1 st Side Cold	Uncertainty contributions
$(\partial\Psi_{HFM}/\partial A_{m,eq})$	0.010049	0.20%	
$(\partial\Psi_{HFM}/\partial t_{m,eq})$	4.658685		
$(\partial\Psi_{HFM}/\partial l_\psi)$	- 0.019866		
$(\partial\Psi_{HFM}/\partial f_{cal})$	0.015867		
$(\partial\Psi_{HFM}/\partial Q_m)$	0.231397		
$(\partial\Psi_{HFM}/\partial \Delta\vartheta_{m,eq})$	- 0.007405		
$(\partial\Psi_{HFM}/\partial \Delta\lambda_E)$	0.106733	0.76%	
$(\partial\Psi_{HFM}/\partial \Delta\lambda_O)$	0.106733	0.76%	
$(\partial\Psi_{HFM}/\partial U_{COP})$	- 0.027732	0.05%	
$(\partial\Psi_{HFM}/\partial I_{COP})$	- 1.382631	1.64%	
$(\partial\Psi_{HFM}/\partial t_{m,COP})$	- 4.698262	0.11%	
$(\partial\Psi_{HFM}/\partial A_{m,COP})$	2.414773	0.14%	
$(\partial\Psi_{HFM}/\partial \Delta\vartheta_{m,COP})$	0.006335		
$(\partial\Psi_{HFM}/\partial C_j)$	0.095514		
$(\partial\Psi_{HFM}/\partial \Delta\lambda_{R,E})$	0.096784		
$(\partial\Psi_{HFM}/\partial \Delta\lambda_O)$	0.096784		
$(\partial\Psi_{HFM}/\partial \Delta\lambda_S)$	0.096784		

Table F. 15: λ_{eq} , ψ - Uncertainty assessment of FS based VIPs, Gasket strip joint
($t = 20$ mm, $\vartheta_{avg} = 10^\circ\text{C}$); Type A uncertainty

<i>FS - 20 mm - 10°C: GASKET STRIP JOINT (Type A uncertainty)</i>										
		A_m [m ²]	t_{VIP_1} [m]	t_{VIP_2} [m]	t_m [m]	f_{cal} [W/m ² mV]	λ_{eq_HFM} [W/mK]	Ψ_{HFM} [W/mK]		
1 st Side	Hot					6.146	0.00447	0.010		
	$u(x_j)$	0.2483	0.0205	0.02105	0.0208	0.035				
	Cold					6.727				
$u(x_j)$	0.0002	0.0003	0.00001	0.0001	0.039					
2 nd Side	Hot					7.080				
	$u(x_j)$	0.2483	0.02010	0.0207	0.0204	0.040				
	Cold					7.473				
$u(x_j)$	0.0002	0.00001	0.0003	0.0001	0.044					
		Q [mV]	$\Delta\vartheta_m$ [°C]	$\Delta\lambda_E$ [-]	$\Delta\lambda_O$ [-]	$\lambda_{eq_i_HFM}$ [W/mK]				
1 st Side	Hot	0.4601		1	1	0.00408				
	$u(x_j)$	0.0004	14.41	2.0E-05	4.1E-06	0.00007				
	Cold	0.4613		1	1	0.00447				
$u(x_j)$	0.0002	0.21	2.2E-05	4.5E-06	0.00008					
2 nd Side	Hot	0.4065		1	1	0.00403				
	$u(x_j)$	0.0003	14.57	2.0E-05	4.0E-06	0.00007				
	Cold	0.4005		1	1	0.00419				
$u(x_j)$	0.0003	0.21	2.1E-05	4.2E-06	0.00007	0.00008	0.002			
				$u(\lambda_{eq_HFM})$	[%]		1.79%	20.00%		

Table F. 16: λ_{eq} - Uncertainty assessment of FS based VIPs, Commutated joint
 ($t = 40$ mm, $\vartheta_{avg} = 10^\circ\text{C}$)

<i>FS - 40 mm - 10°C: COMMUTATED JOINT</i>								
		A_m [m ²]	t_{VIP_1} [m]	t_{VIP_2} [m]	t_m [m]	f_{cal} [W/m ² mV]	λ_{eq_HFM} [W/mK]	
1 st Side	Hot					6.146	0.0045	
	$u(x_i)$	0.2483	0.0408	0.04021	0.0405	0.035		
1 st Side	Cold					6.729		
	$u(x_i)$	0.0002	0.0007	0.00004	0.00034	0.039		
2 nd Side	Hot					7.080		
	$u(x_i)$	0.2483	0.04046	0.0399	0.04016	0.040		
2 nd Side	Cold					7.474		
	$u(x_i)$	0.0002	0.00007	0.0001	0.00007	0.044		
		Q [mV]	$\Delta\vartheta_m$ [°C]	$\Delta\lambda_E$ [-]	$\Delta\lambda_O$ [-]	λ_{eq,i_HFM} [W/mK]		
1 st Side	Hot	0.23991		1	1	0.0041		0.0001
	$u(x_i)$	0.00003	14.69	2.0E-05	4.1E-06	0.0001		
1 st Side	Cold	0.24232		1	1	0.0045		
	$u(x_i)$	0.00003	0.40	2.2E-05	4.5E-06	0.0001		
2 nd Side	Hot	0.22007		1	1	0.0042		
	$u(x_i)$	0.00003	14.82	2.1E-05	4.2E-06	0.0001		
2 nd Side	Cold	0.21838		1	1	0.0044		
	$u(x_i)$	0.00003	0.40	2.2E-05	4.4E-06	0.0001		
						$u(\lambda_{eq_HFM})$	2.22%	

Table F. 17: λ_{eq} - Sensitivity coefficients and uncertainty contributions of FS based VIPs, Commutated joint ($t = 40$ mm, $\vartheta_{avg} = 10^\circ\text{C}$)

<i>Sensitivity coefficients</i>			
	1 st Side Cold	<i>Uncertainty contributions</i>	
$(\partial\lambda_{eq_HFM}/\partial t_m)$	0.110977		
$(\partial\lambda_{eq_HFM}/\partial f_{cal})$	0.000668		
$(\partial\lambda_{eq_HFM}/\partial Q_m)$	0.018558		
$(\partial\lambda_{eq_HFM}/\partial\Delta\vartheta_m)$	- 0.000306		
$(\partial\Delta\vartheta_m/\partial A_{COP})$	473.274771		
$(\partial\Delta\vartheta_m/\partial\Delta\vartheta_{COP})$	0.967213		
$(\partial\Delta\vartheta_m/\partial A_{SA})$	-0.593358		
$(\partial\Delta\vartheta_m/\partial\Delta\vartheta_{SA})$	0.024590		
$(\partial\Delta\vartheta_m/\partial A_J)$	-1.972036		
$(\partial\Delta\vartheta_m/\partial\Delta\vartheta_J)$	0.008197		
$(\partial\lambda_{eq_HFM}/\partial\Delta\lambda_E)$	0.004497		
$(\partial\lambda_{eq_HFM}/\partial\Delta\lambda_O)$	0.004497		

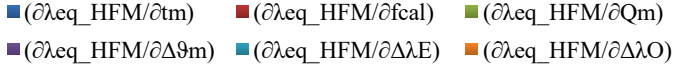


Table F. 18: ψ - Uncertainty assessment of FS based VIPs, Commutated joint
($t = 40 \text{ mm}$, $\vartheta_{avg} = 10^\circ\text{C}$)

		<i>FS - 40 mm - 10°C: COMMUTATED JOINT</i>						
		A_m [m ²]	t_m [m]	I_ψ [m]	I_ψ [m]	λ_{COP_avg} [W/mK]	λ_{eq_HFM} [W/mK]	Ψ_{HFM} [W/mK]
1 st Side	Hot	0.2508	0.0405	0.5008				
	Cold	0.2508	0.0405	0.5008				
	$u(x_i)$	0.0002	0.0004	0.0003	0.5008	0.00428	0.0045	0.003
2 nd Side	Hot	0.2508	0.04016	0.5008				
	Cold	0.2508	0.04016	0.5008				
	$u(x_i)$	0.0002	0.00007	0.0003	0.0003	0.00006	0.0001	0.002
				$u(x_i)$	[%]	2.92%	66.67%	

Table F. 19: $u(\psi)$ - Sensitivity coefficients and uncertainty contributions of FS based VIPs, Commutated joint ($t = 40 \text{ mm}$, $\vartheta_{avg} = 10^\circ\text{C}$)

		<i>Sensitivity coefficients</i>	
		1 st Side Cold	Uncertainty contributions
$(\partial\Psi_{HFM}/\partial A_{m,eq})$	0.002642		
$(\partial\Psi_{HFM}/\partial t_{m,eq})$	1.293345		
$(\partial\Psi_{HFM}/\partial I_\psi)$	- 0.005224		
$(\partial\Psi_{HFM}/\partial f_{cal})$	0.008178		
$(\partial\Psi_{HFM}/\partial Q_m)$	0.227068		
$(\partial\Psi_{HFM}/\partial \Delta\vartheta_{m,eq})$	- 0.003745		
$(\partial\Psi_{HFM}/\partial \Delta\lambda_E)$	0.055024		
$(\partial\Psi_{HFM}/\partial \Delta\lambda_O)$	0.055024		
$(\partial\Psi_{HFM}/\partial U_{COP})$	- 0.020472		
$(\partial\Psi_{HFM}/\partial I_{COP})$	- 1.027607		
$(\partial\Psi_{HFM}/\partial t_{m,COP})$	- 1.298955		
$(\partial\Psi_{HFM}/\partial A_{m,COP})$	1.307582		
$(\partial\Psi_{HFM}/\partial \Delta\vartheta_{m,COP})$	0.003461		
$(\partial\Psi_{HFM}/\partial C_j)$	0.051720		
$(\partial\Psi_{HFM}/\partial \Delta\lambda_{R,E})$	0.052408		
$(\partial\Psi_{HFM}/\partial \Delta\lambda_O)$	0.052408		
$(\partial\Psi_{HFM}/\partial \Delta\lambda_S)$	0.052408		

Parameter	Contribution (%)
$(\partial\Psi_{HFM}/\partial A_{m,COP})$	27.55%
$(\partial\Psi_{HFM}/\partial t_{m,eq})$	23.70%
$(\partial\Psi_{HFM}/\partial Q_m)$	23.54%
$(\partial\Psi_{HFM}/\partial t_{m,COP})$	23.44%
$(\partial\Psi_{HFM}/\partial \Delta\lambda_{R,E})$	18.63%
$(\partial\Psi_{HFM}/\partial \Delta\lambda_O)$	1.00%
$(\partial\Psi_{HFM}/\partial \Delta\lambda_S)$	1.00%
$(\partial\Psi_{HFM}/\partial U_{COP})$	1.00%
$(\partial\Psi_{HFM}/\partial I_{COP})$	0.07%
$(\partial\Psi_{HFM}/\partial t_{m,COP})$	4.12%
$(\partial\Psi_{HFM}/\partial A_{m,eq})$	0.37%
$(\partial\Psi_{HFM}/\partial I_\psi)$	0.09%
$(\partial\Psi_{HFM}/\partial f_{cal})$	0.15%
$(\partial\Psi_{HFM}/\partial \Delta\vartheta_{m,eq})$	0.05%
$(\partial\Psi_{HFM}/\partial \Delta\lambda_E)$	0.05%
$(\partial\Psi_{HFM}/\partial \Delta\vartheta_{m,COP})$	0.95%
$(\partial\Psi_{HFM}/\partial C_j)$	0.95%
$(\partial\Psi_{HFM}/\partial \Delta\lambda_{R,E})$	0.95%
$(\partial\Psi_{HFM}/\partial \Delta\lambda_O)$	0.95%
$(\partial\Psi_{HFM}/\partial \Delta\lambda_S)$	0.94%

Table F. 20: λ_{eq} , ψ - Uncertainty assessment of FS based VIPs, Commutated joint
($t = 40$ mm, $\vartheta_{avg} = 10^\circ\text{C}$); Type A uncertainty

<i>FS - 40 mm - 10°C: COMMUTATED JOINT (Type A uncertainty)</i>										
		A_m [m ²]	t_{VIP_1} [m]	t_{VIP_2} [m]	t_m [m]	f_{cal} [W/m ² mV]	λ_{eq_HFM} [W/mK]	Ψ_{HFM} [W/mK]		
1 st Side	Hot					6.146	0.00450	0.003		
	$u(x_j)$	0.2483	0.0408	0.04021	0.0405	0.035				
	Cold					6.729				
$u(x_j)$	0.0002	0.0007	0.00004	0.0004	0.039					
2 nd Side	Hot					7.080				
	$u(x_j)$	0.2483	0.04046	0.0399	0.04016	0.040				
	Cold					7.474				
$u(x_j)$	0.0002	0.00007	0.0001	0.00007	0.044					
		Q [mV]	$\Delta\vartheta_m$ [°C]	$\Delta\lambda_E$ [-]	$\Delta\lambda_O$ [-]	λ_{eq,i_HFM} [W/mK]				
1 st Side	Hot	0.2399		1	1	0.00407				
	$u(x_j)$	0.0004	14.69	2.0E-05	4.1E-06	0.00005				
	Cold	0.2423		1	1	0.00450				
$u(x_j)$	0.0002	0.09	2.2E-05	4.5E-06	0.00006					
2 nd Side	Hot	0.2201		1	1	0.00422				
	$u(x_j)$	0.0002	14.82	2.1E-05	4.2E-06	0.00004				
	Cold	0.2184		1	1	0.00442				
$u(x_j)$	0.0002	0.10	2.2E-05	4.4E-06	0.00004	0.00006	0.001			
				$u(\lambda_{eq_HFM})$	[%]		1.33%	33.33%		

Table F. 21: λ_{eq} - Uncertainty assessment of FS based VIPs, Offset joint
 ($t = 40$ mm, $\vartheta_{avg} = 10^\circ\text{C}$)

<i>FS - 40 mm - 10°C: OFFSET JOINT</i>								
		A_m [m ²]	t_{VIP_1} [m]	t_{VIP_2} [m]	t_m [m]	f_{cal} [W/m ² mV]	λ_{eq_HFM} [W/mK]	
1 st Side	Hot					6.146	0.0045	
	$u(x_i)$	0.2483	0.0408	0.04021	0.0405	0.035		
2 nd Side	Cold					6.728		
	$u(x_i)$	0.0002	0.0007	0.00004	0.0004	0.039		
1 st Side	Hot					7.080		
	$u(x_i)$	0.2483	0.04046	0.0399	0.04016	0.040		
2 nd Side	Cold					7.473		
	$u(x_i)$	0.0002	0.00007	0.0001	0.00007	0.044		
		Q [mV]	$\Delta\vartheta_m$ [°C]	$\Delta\lambda_E$ [-]	$\Delta\lambda_O$ [-]	λ_{eq,i_HFM} [W/mK]		
1 st Side	Hot	0.23835		1	1	0.0040		0.0001
	$u(x_i)$	0.00003	14.67	2.0E-05	4.0E-06	0.0001		
2 nd Side	Cold	0.24003		1	1	0.0045		
	$u(x_i)$	0.00003	0.40	2.2E-05	4.5E-06	0.0001		
1 st Side	Hot	0.21887		1	1	0.0042		
	$u(x_i)$	0.00003	14.79	2.1E-05	4.2E-06	0.0001		
2 nd Side	Cold	0.21396		1	1	0.0043		
	$u(x_i)$	0.00003	0.40	2.2E-05	4.3E-06	0.0001		
						$u(\lambda_{eq_HFM})$	2.22%	

Table F. 22: λ_{eq} - Sensitivity coefficients and uncertainty contributions of FS based VIPs, Offset joint ($t = 40$ mm, $\vartheta_{avg} = 10^\circ\text{C}$)

<i>Sensitivity coefficients</i>		<i>Uncertainty contributions</i>	
	1 st Side Cold		
$(\partial\lambda_{eq_HFM}/\partial t_m)$	0.110091		
$(\partial\lambda_{eq_HFM}/\partial f_{cal})$	0.000663		
$(\partial\lambda_{eq_HFM}/\partial Q_m)$	0.018585		
$(\partial\lambda_{eq_HFM}/\partial\Delta\vartheta_m)$	- 0.000304		
$(\partial\Delta\vartheta_m/\partial A_{COP})$	502.586468		
$(\partial\Delta\vartheta_m/\partial\Delta\vartheta_{COP})$	0.967213		
$(\partial\Delta\vartheta_m/\partial A_{SA})$	- 0.545213		
$(\partial\Delta\vartheta_m/\partial\Delta\vartheta_{SA})$	0.024590		
$(\partial\Delta\vartheta_m/\partial A_J)$	- 2.348855		
$(\partial\Delta\vartheta_m/\partial\Delta\vartheta_J)$	0.008197		
$(\partial\lambda_{eq_HFM}/\partial\Delta\lambda_E)$	0.004461		
$(\partial\lambda_{eq_HFM}/\partial\Delta\lambda_O)$	0.004461		

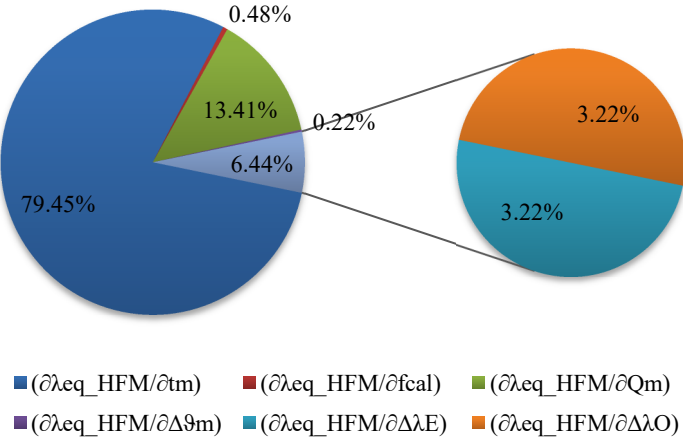


Table F. 23: ψ - Uncertainty assessment of FS based VIPs, Offset joint
($t = 40 \text{ mm}$, $\vartheta_{avg} = 10^\circ\text{C}$)

		<i>FS - 40 mm - 10°C: OFFSET JOINT</i>						
		A_m [m ²]	t_m [m]	I_ψ [m]	I_ψ [m]	λ_{COP_avg} [W/mK]	λ_{eq_HFM} [W/mK]	Ψ_{HFM} [W/mK]
1 st Side	Hot	0.2508	0.0405	0.5008	0.5008	0.00428	0.0045	0.002
	Cold							
	$u(x_i)$							
2 nd Side	Hot	0.2508	0.04016	0.5008	0.0003	0.00006	0.0001	0.002
	Cold							
	$u(x_i)$							
				$u(x_i)$	[%]	2.93%	100.00%	

Table F. 24: $u(\psi)$ - Sensitivity coefficients and uncertainty contributions of FS based VIPs, Offset joint ($t = 40 \text{ mm}$, $\vartheta_{avg} = 10^\circ\text{C}$)

		<i>Sensitivity coefficients</i>	
		1 st Side Cold	Uncertainty contributions
$(\partial\Psi_{HFM}/\partial A_{m,eq})$	0.002199		
$(\partial\Psi_{HFM}/\partial t_{m,eq})$	1.293324		
$(\partial\Psi_{HFM}/\partial I_\psi)$	- 0.004348		
$(\partial\Psi_{HFM}/\partial f_{cal})$	0.008113		
$(\partial\Psi_{HFM}/\partial Q_m)$	0.227404		
$(\partial\Psi_{HFM}/\partial \Delta \vartheta_{m,eq})$	- 0.003721		
$(\partial\Psi_{HFM}/\partial \Delta \lambda_E)$	0.054585		
$(\partial\Psi_{HFM}/\partial \Delta \lambda_O)$	0.054585		
$(\partial\Psi_{HFM}/\partial U_{COP})$	- 0.020472		
$(\partial\Psi_{HFM}/\partial I_{COP})$	- 1.027590		
$(\partial\Psi_{HFM}/\partial t_{m,COP})$	- 1.298933		
$(\partial\Psi_{HFM}/\partial A_{m,COP})$	1.307561		
$(\partial\Psi_{HFM}/\partial \Delta \vartheta_{m,COP})$	0.003461		
$(\partial\Psi_{HFM}/\partial C_j)$	0.051719		
$(\partial\Psi_{HFM}/\partial \Delta \lambda_{R,E})$	0.052407		
$(\partial\Psi_{HFM}/\partial \Delta \lambda_O)$	0.052407		
$(\partial\Psi_{HFM}/\partial \Delta \lambda_S)$	0.052407		

Table F. 25: λ_{eq} , ψ - Uncertainty assessment of FS based VIPs, Offset joint
($t = 40$ mm, $\vartheta_{avg} = 10^\circ\text{C}$); Type A uncertainty

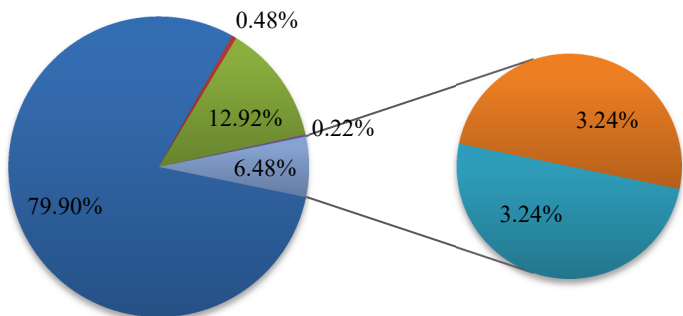
<i>FS - 40 mm - 10°C: OFFSET JOINT (Type A uncertainty)</i>										
		A_m [m ²]	t_{VIP_1} [m]	t_{VIP_2} [m]	t_m [m]	f_{cal} [W/m ² mV]	λ_{eq_HFM} [W/mK]	Ψ_{HFM} [W/mK]		
1 st Side	Hot					6.146	0.00446	0.002		
	$u(x_i)$	0.2483	0.0408	0.04021	0.0405	0.035				
	Cold					6.728				
	$u(x_i)$	0.0002	0.0007	0.00004	0.0004	0.039				
2 nd Side	Hot					7.080				
	$u(x_i)$	0.2483	0.04046	0.0399	0.04016	0.040				
	Cold					7.473				
	$u(x_i)$	0.0002	0.00007	0.0001	0.00007	0.044				
		Q [mV]	$\Delta\vartheta_m$ [°C]	$\Delta\lambda_E$ [-]	$\Delta\lambda_O$ [-]	λ_{eq,i_HFM} [W/mK]				
1 st Side	Hot	0.2384		1	1	0.00405				
	$u(x_i)$	0.0005	14.67	2.0E-05	4.0E-06	0.00005				
	Cold	0.2400		1	1	0.00446				
	$u(x_i)$	0.0007	0.10	2.2E-05	4.5E-06	0.00006				
2 nd Side	Hot	0.2189		1	1	0.00421				
	$u(x_i)$	0.0003	14.79	2.1E-05	4.2E-06	0.00004				
	Cold	0.2140		1	1	0.00434				
	$u(x_i)$	0.0010	0.10	2.2E-05	4.3E-06	0.00004	0.00006	0.001		
				$u(\lambda_{eq_HFM})$	[%]		1.34%	50.00%		

Table F. 26: λ_{eq} - Uncertainty assessment of FS based VIPs, Gasket strip joint
($t = 40$ mm, $\vartheta_{avg} = 10^\circ\text{C}$)

<i>FS - 40 mm - 10°C: GASKET STRIP JOINT</i>								
		A_m [m ²]	t_{VIP_1} [m]	t_{VIP_2} [m]	t_m [m]	f_{cal} [W/m ² mV]	λ_{eq_HFM} [W/mK]	
1 st Side	Hot					6.146	0.0047	
	$u(x_i)$	0.2483	0.0408	0.04021	0.0405	0.035		
2 nd Side	Cold					6.728		
	$u(x_i)$	0.0002	0.0007	0.00004	0.0004	0.039		
1 st Side	Hot					7.080		
	$u(x_i)$	0.2483	0.04046	0.0399	0.04016	0.040		
2 nd Side	Cold					7.474		
	$u(x_i)$	0.0002	0.00007	0.0001	0.00007	0.044		
		Q [mV]	$\Delta\vartheta_m$ [°C]	$\Delta\lambda_E$ [-]	$\Delta\lambda_O$ [-]	λ_{eq,i_HFM} [W/mK]		
1 st Side	Hot	0.24773		1	1	0.0042		0.0001
	$u(x_i)$	0.00003	14.67	2.1E-05	4.2E-06	0.0001		
2 nd Side	Cold	0.25052		1	1	0.0047		
	$u(x_i)$	0.00003	0.40	2.3E-05	4.7E-06	0.0001		
1 st Side	Hot	0.22697		1	1	0.0044		
	$u(x_i)$	0.00003	14.82	2.2E-05	4.4E-06	0.0001		
2 nd Side	Cold	0.23318		1	1	0.0047		
	$u(x_i)$	0.00003	0.40	2.4E-05	4.7E-06	0.0001		
						$u(\lambda_{eq_HFM})$	[%]	2.13%

Table F. 27: λ_{eq} - Sensitivity coefficients and uncertainty contributions of FS based VIPs, Gasket strip joint ($t = 40 \text{ mm}$, $\vartheta_{avg} = 10^\circ\text{C}$)

<i>Sensitivity coefficients</i>	
	1 st Side Cold
$(\partial\lambda_{eq_HFM}/\partial t_m)$	0.114871
$(\partial\lambda_{eq_HFM}/\partial f_{cal})$	0.000692
$(\partial\lambda_{eq_HFM}/\partial Q_m)$	0.018580
$(\partial\lambda_{eq_HFM}/\partial\Delta\vartheta_m)$	- 0.000317
$(\partial\Delta\vartheta_m/\partial A_{COP})$	487.495107
$(\partial\Delta\vartheta_m/\partial\Delta\vartheta_{COP})$	0.967213
$(\partial\Delta\vartheta_m/\partial A_{SA})$	- 0.649778
$(\partial\Delta\vartheta_m/\partial\Delta\vartheta_{SA})$	0.024590
$(\partial\Delta\vartheta_m/\partial A_J)$	- 1.915517
$(\partial\Delta\vartheta_m/\partial\Delta\vartheta_J)$	0.008197
$(\partial\lambda_{eq_HFM}/\partial\Delta\lambda_E)$	0.004655
$(\partial\lambda_{eq_HFM}/\partial\Delta\lambda_O)$	0.004655



■ $(\partial\lambda_{eq_HFM}/\partial t_m)$ ■ $(\partial\lambda_{eq_HFM}/\partial f_{cal})$ ■ $(\partial\lambda_{eq_HFM}/\partial Q_m)$
 ■ $(\partial\lambda_{eq_HFM}/\partial\Delta\vartheta_m)$ ■ $(\partial\lambda_{eq_HFM}/\partial\Delta\lambda_E)$ ■ $(\partial\lambda_{eq_HFM}/\partial\Delta\lambda_O)$

Table F. 28: ψ - Uncertainty assessment of FS based VIPs, Gasket strip joint
($t = 40 \text{ mm}$, $\vartheta_{avg} = 10^\circ\text{C}$)

		<i>FS - 40 mm - 10°C: GASKET STRIP JOINT</i>						
		A_m [m ²]	t_m [m]	l_ψ [m]	l_ψ [m]	λ_{COP_avg} [W/mK]	λ_{eq_HFM} [W/mK]	Ψ_{HFM} [W/mK]
1 st Side	Hot	0.2508	0.0405	0.5008				
	Cold	0.2508	0.0405	0.5008				
	$u(x_i)$	0.0002	0.0004	0.0003	0.5008	0.00428	0.0047	0.005
2 nd Side	Hot	0.2508	0.04016	0.5008				
	Cold	0.2508	0.04016	0.5008				
	$u(x_i)$	0.0002	0.00007	0.0003	0.0003	0.00006	0.0001	0.002
				$u(x_i)$	[%]	2.92%	40.00%	

Table F. 29: $u(\psi)$ - Sensitivity coefficients and uncertainty contributions of FS based VIPs, Gasket strip joint ($t = 40 \text{ mm}$, $\vartheta_{avg} = 10^\circ\text{C}$)

<i>Sensitivity coefficients</i>		<i>Uncertainty contributions</i>	
	1 st Side Cold		
$(\partial\Psi_{HFM}/\partial A_{m,eq})$	0.004593		
$(\partial\Psi_{HFM}/\partial t_{m,eq})$	1.293324		
$(\partial\Psi_{HFM}/\partial l_\psi)$	- 0.009080		
$(\partial\Psi_{HFM}/\partial f_{cal})$	0.008465		
$(\partial\Psi_{HFM}/\partial Q_m)$	0.227341		
$(\partial\Psi_{HFM}/\partial \Delta\theta_{m,eq})$	- 0.003881		
$(\partial\Psi_{HFM}/\partial \Delta\lambda_E)$	0.056954		
$(\partial\Psi_{HFM}/\partial \Delta\lambda_O)$	0.056954		
$(\partial\Psi_{HFM}/\partial U_{COP})$	- 0.020472		
$(\partial\Psi_{HFM}/\partial I_{COP})$	- 1.027590		
$(\partial\Psi_{HFM}/\partial t_{m,COP})$	- 1.298933		
$(\partial\Psi_{HFM}/\partial A_{m,COP})$	1.307561		
$(\partial\Psi_{HFM}/\partial \Delta\theta_{m,COP})$	0.003461		
$(\partial\Psi_{HFM}/\partial C_j)$	0.051719		
$(\partial\Psi_{HFM}/\partial \Delta\lambda_{R,E})$	0.052407		
$(\partial\Psi_{HFM}/\partial \Delta\lambda_O)$	0.052407		
$(\partial\Psi_{HFM}/\partial \Delta\lambda_S)$	0.052407		

Table F. 30: λ_{eq} , ψ - Uncertainty assessment of FS based VIPs, Gasket strip joint
($t = 40$ mm, $\vartheta_{avg} = 10^\circ\text{C}$); Type A uncertainty

<i>FS - 40 mm - 10°C: GASKET STRIP JOINT (Type A uncertainty)</i>										
		A_m [m ²]	t_{VIP_1} [m]	t_{VIP_2} [m]	t_m [m]	f_{cal} [W/m ² mV]	λ_{eq_HFM} [W/mK]	Ψ_{HFM} [W/mK]		
1 st Side	Hot					6.146	0.00465	0.005		
	$u(x_j)$	0.2483	0.0408	0.04021	0.0405	0.035				
	Cold					6.728				
$u(x_j)$	0.0002	0.0007	0.00004	0.0004	0.039					
2 nd Side	Hot					7.080				
	$u(x_j)$	0.2483	0.04046	0.0399	0.04016	0.040				
	Cold					7.474				
$u(x_j)$	0.0002	0.00007	0.0001	0.00007	0.044					
		Q [mV]	$\Delta\vartheta_m$ [°C]	$\Delta\lambda_E$ [-]	$\Delta\lambda_O$ [-]	$\lambda_{eq_i_HFM}$ [W/mK]				
1 st Side	Hot	0.2477		1	1	0.00420				
	$u(x_j)$	0.0005	14.67	2.1E-05	4.2E-06	0.00005				
	Cold	0.2505		1	1	0.00465				
$u(x_j)$	0.0001	0.10	2.3E-05	4.7E-06	0.00006					
2 nd Side	Hot	0.2270		1	1	0.00435				
	$u(x_j)$	0.0003	14.82	2.2E-05	4.4E-06	0.00004				
	Cold	0.2332		1	1	0.00472				
$u(x_j)$	0.0002	0.12	2.4E-05	4.7E-06	0.00005	0.00006	0.001			
				$u(\lambda_{eq_HFM})$	[%]		1.29%	20.00%		

FG based VIPs

Table F. 31: λ_{eq} - Uncertainty assessment of FG based VIPs, Commutated joint
($t = 20$ mm, $\vartheta_{avg} = 10^\circ\text{C}$)

<i>FG - 20 mm - 10°C: COMMUTATED JOINT</i>								
		A_m [m ²]	t_{VIP_1} [m]	t_{VIP_2} [m]	t_m [m]	f_{cal} [W/m ² mV]	λ_{eq_HFM} [W/mK]	
1 st Side	Hot					6.146	0.0061	
	$u(x_j)$	0.2483	0.0216	0.0220	0.0218	0.035		
2 nd Side	Cold					6.723		
	$u(x_j)$	0.0002	0.0001	0.0003	0.0002	0.039		
1 st Side	Hot					7.080		
	$u(x_j)$	0.2483	0.0220	0.0220	0.0220	0.040		
2 nd Side	Cold					7.468		
	$u(x_j)$	0.0002	0.0003	0.0002	0.0002	0.044		
		Q [mV]	$\Delta\vartheta_m$ [°C]	$\Delta\lambda_E$ [-]	$\Delta\lambda_O$ [-]	λ_{eq,i_HFM} [W/mK]		0.0002
1 st Side	Hot	0.59756		1	1	0.0058		
	$u(x_j)$	0.00003	13.68	2.9E-05	5.8E-06	0.0001		
2 nd Side	Cold	0.56987		1	1	0.0061		
	$u(x_j)$	0.00003	0.31	3.0E-05	6.1E-06	0.0002		
1 st Side	Hot	0.49566		1	1	0.0057		
	$u(x_j)$	0.00003	13.62	2.8E-05	5.7E-06	0.0001		
2 nd Side	Cold	0.53276		1	1	0.0064		
	$u(x_j)$	0.00003	0.31	3.2E-05	6.4E-06	0.0002		
						$u(\lambda_{eq_HFM})$ [%]	3.28%	

Table F. 32: λ_{eq} - Sensitivity coefficients and uncertainty contributions of FG based VIPs, Commutated joint ($t = 20$ mm, $\vartheta_{avg} = 10^\circ\text{C}$)

<i>Sensitivity coefficients</i>				
	1 st Side Cold	<i>Uncertainty contributions</i>		
$(\partial\lambda_{eq_HFM}/\partial t_m)$	0.279988			
$(\partial\lambda_{eq_HFM}/\partial f_{cal})$	0.000907			
$(\partial\lambda_{eq_HFM}/\partial Q_m)$	0.010699			
$(\partial\lambda_{eq_HFM}/\partial\Delta\vartheta_m)$	- 0.000446			
$(\partial\Delta\vartheta_m/\partial A_{COP})$	401.675627			
$(\partial\Delta\vartheta_m/\partial\Delta\vartheta_{COP})$	0.680000			
$(\partial\Delta\vartheta_m/\partial A_{SA})$	- 1.104713			
$(\partial\Delta\vartheta_m/\partial\Delta\vartheta_{SA})$	0.240000			
$(\partial\Delta\vartheta_m/\partial A_j)$	- 18.537014			
$(\partial\Delta\vartheta_m/\partial\Delta\vartheta_j)$	0.008197			
$(\partial\lambda_{eq_HFM}/\partial\Delta\lambda_E)$	0.006097			
$(\partial\lambda_{eq_HFM}/\partial\Delta\lambda_O)$	0.006097			

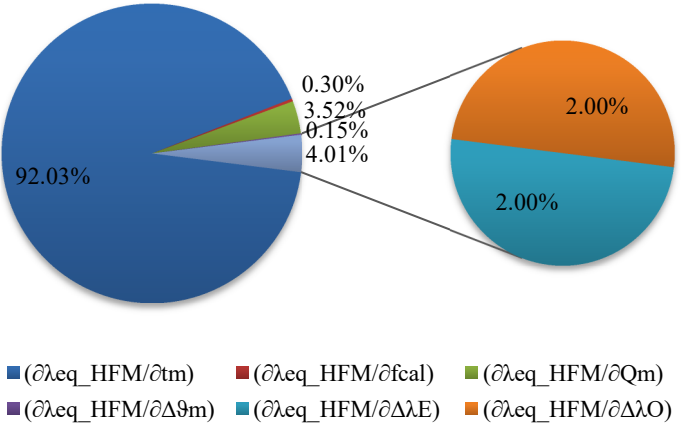


Table F. 33: ψ - Uncertainty assessment of FG based VIPs, Commutated joint
($t = 20 \text{ mm}$, $\vartheta_{avg} = 10^\circ\text{C}$)

		<i>FG - 20 mm - 10°C: COMMUTATED JOINT</i>						
		A_m [m ²]	t_m [m]	l_ψ [m]	l_ψ [m]	λ_{COP_avg} [W/mK]	λ_{eq_HFM} [W/mK]	Ψ_{HFM} [W/mK]
1 st Side	Hot	0.2508	0.0218	0.5008				
	Cold	0.2508	0.0218	0.5008				
	$u(x_i)$	0.0002	0.000	0.0003	0.5008	0.00212	0.0061	0.092
2 nd Side	Hot	0.2508	0.0220	0.5008				
	Cold	0.2508	0.0220	0.5008				
	$u(x_i)$	0.0002	0.0002	0.0003	0.0003	0.00002	0.0002	0.003
				$u(x_i)$	[%]	2.43%	3.26%	

Table F. 34: $u(\psi)$ - Sensitivity coefficients and uncertainty contributions of FG based VIPs, Commutated joint ($t = 20 \text{ mm}$, $\vartheta_{avg} = 10^\circ\text{C}$)

		<i>Sensitivity coefficients</i>	
		1 st Side Cold	Uncertainty contributions
$(\partial\Psi_{HFM}/\partial A_{m,eq})$	0.091549	0.25%	
$(\partial\Psi_{HFM}/\partial t_{m,eq})$	2.212611	1.82%	
$(\partial\Psi_{HFM}/\partial l_\psi)$	- 0.180986	12.41%	
$(\partial\Psi_{HFM}/\partial f_{cal})$	0.020649	0.13%	
$(\partial\Psi_{HFM}/\partial Q_m)$	0.243601	3.20%	
$(\partial\Psi_{HFM}/\partial \Delta\vartheta_{m,eq})$	- 0.010145	0.27%	
$(\partial\Psi_{HFM}/\partial \Delta\lambda_E)$	0.138821	2.38%	
$(\partial\Psi_{HFM}/\partial \Delta\lambda_O)$	0.138821	29.06%	
$(\partial\Psi_{HFM}/\partial U_{COP})$	- 0.018970	1.82%	
$(\partial\Psi_{HFM}/\partial I_{COP})$	- 0.944780	0.62%	
$(\partial\Psi_{HFM}/\partial t_{m,COP})$	- 2.214582	0.04%	
$(\partial\Psi_{HFM}/\partial A_{m,COP})$	1.202188	0.63%	
$(\partial\Psi_{HFM}/\partial \Delta\vartheta_{m,COP})$	0.002939	0.63%	
$(\partial\Psi_{HFM}/\partial C_j)$	0.047551		
$(\partial\Psi_{HFM}/\partial \Delta\lambda_{R,E})$	0.048184		
$(\partial\Psi_{HFM}/\partial \Delta\lambda_O)$	0.048184		
$(\partial\Psi_{HFM}/\partial \Delta\lambda_S)$	0.048184		

Table F. 35: λ_{eq} , ψ - Uncertainty assessment of FG based VIPs, Commutated joint
($t = 20$ mm, $\vartheta_{avg} = 10^\circ\text{C}$); Type A uncertainty

<i>FG - 20 mm - 10°C: COMMUTATED JOINT (Type A uncertainty)</i>										
		A_m [m ²]	t_{VIP_1} [m]	t_{VIP_2} [m]	t_m [m]	f_{cal} [W/m ² mV]	λ_{eq_HFM} [W/mK]	Ψ_{HFM} [W/mK]		
1 st Side	Hot					6.146	0.00610	0.091		
	$u(x_j)$	0.2483	0.0216	0.0220	0.0218	0.035				
	Cold					6.723				
$u(x_j)$	0.0002	0.0001	0.0003	0.0002	0.039					
2 nd Side	Hot					7.080				
	$u(x_j)$	0.2483	0.0220	0.0220	0.0220	0.040				
	Cold					7.468				
$u(x_j)$	0.0002	0.0003	0.0002	0.0002	0.044					
		Q [mV]	$\Delta\vartheta_m$ [°C]	$\Delta\lambda_E$ [-]	$\Delta\lambda_O$ [-]	λ_{eq,i_HFM} [W/mK]				
1 st Side	Hot	0.5976		1	1	0.00584				
	$u(x_j)$	0.0006	13.68	2.9E-05	5.8E-06	0.00006				
	Cold	0.5699		1	1	0.00610				
$u(x_j)$	0.0003	0.07	3.0E-05	6.1E-06	0.00007					
2 nd Side	Hot	0.4957		1	1	0.00566				
	$u(x_j)$	0.0003	13.62	2.8E-05	5.7E-06	0.00006				
	Cold	0.5328		1	1	0.00642				
$u(x_j)$	0.0005	0.07	3.2E-05	6.4E-06	0.00007	0.00007	0.001			
				$u(\lambda_{eq_HFM})$	[%]		1.15%	1.10%		

Table F. 36: λ_{eq} - Uncertainty assessment of FG based VIPs, Commutated joint
 ($t = 20$ mm, $\vartheta_{avg} = 23^\circ\text{C}$)

<i>FG - 20 mm - 23°C: COMMUTATED JOINT</i>								
		A_m [m ²]	t_{VIP_1} [m]	t_{VIP_2} [m]	t_m [m]	f_{cal} [W/m ² mV]	λ_{eq_HFM} [W/mK]	
1 st Side	Hot					6.034	0.0062	
	$u(x_i)$	0.2483	0.0216	0.0220	0.0218	0.035		
Cold						6.585		
	$u(x_i)$	0.0002	0.0001	0.0003	0.0002	0.039		
2 nd Side	Hot					6.927		
	$u(x_i)$	0.2483	0.0220	0.0220	0.0220	0.040		
Cold						7.295		
	$u(x_i)$	0.0002	0.0003	0.0002	0.0002	0.044		
		Q [mV]	$\Delta\vartheta_m$ [°C]	$\Delta\lambda_E$ [-]	$\Delta\lambda_O$ [-]	λ_{eq,i_HFM} [W/mK]		
1 st Side	Hot	0.64979		1	1	0.0060		0.0002
	$u(x_i)$	0.00003	14.16	3.0E-05	6.0E-06	0.0001		
Cold		0.61552		1	1	0.0062		
	$u(x_i)$	0.00003	0.31	3.1E-05	6.2E-06	0.0002		
2 nd Side	Hot	0.54328		1	1	0.0059		
	$u(x_i)$	0.00003	14.14	2.9E-05	5.9E-06	0.0001		
Cold		0.58166		1	1	0.0066		
	$u(x_i)$	0.00003	0.31	3.3E-05	6.6E-06	0.0002		
						$u(\lambda_{eq_HFM})$	3.22%	

Table F. 37: λ_{eq} - Sensitivity coefficients and uncertainty contributions of FG based VIPs, Commutated joint ($t = 20$ mm, $\vartheta_{avg} = 23^\circ\text{C}$)

<i>Sensitivity coefficients</i>			
	1 st Side Cold	<i>Uncertainty contributions</i>	
$(\partial\lambda_{eq_HFM}/\partial t_m)$	0.286277		
$(\partial\lambda_{eq_HFM}/\partial f_{cal})$	0.000947		
$(\partial\lambda_{eq_HFM}/\partial Q_m)$	0.010128		
$(\partial\lambda_{eq_HFM}/\partial\Delta\vartheta_m)$	- 0.000440		
$(\partial\Delta\vartheta_m/\partial A_{COP})$	417.976651		
$(\partial\Delta\vartheta_m/\partial\Delta\vartheta_{COP})$	0.680000		
$(\partial\Delta\vartheta_m/\partial A_{SA})$	- 1.163922		
$(\partial\Delta\vartheta_m/\partial\Delta\vartheta_{SA})$	0.240000		
$(\partial\Delta\vartheta_m/\partial A_j)$	- 19.246164		
$(\partial\Delta\vartheta_m/\partial\Delta\vartheta_j)$	0.008197		
$(\partial\lambda_{eq_HFM}/\partial\Delta\lambda_E)$	0.006234		
$(\partial\lambda_{eq_HFM}/\partial\Delta\lambda_O)$	0.006234		

Table F. 38: ψ - Uncertainty assessment of FG based VIPs, Commutated joint
($t = 20 \text{ mm}$, $\vartheta_{avg} = 23^\circ\text{C}$)

		<i>FG - 20 mm - 23°C: COMMUTATED JOINT</i>						
		A_m [m ²]	t_m [m]	l_ψ [m]	l_ψ [m]	λ_{COP_avg} [W/mK]	λ_{eq_HFM} [W/mK]	Ψ_{HFM} [W/mK]
1 st Side	Hot	0.2508	0.0218	0.5008				
	Cold	0.2508	0.0218	0.5008				
	$u(x_i)$	0.0002	0.0002	0.0003	0.5008	0.00230	0.0062	0.091
2 nd Side	Hot	0.2508	0.0220	0.5008				
	Cold	0.2508	0.0220	0.5008				
	$u(x_i)$	0.0002	0.0002	0.0003	0.0003	0.00002	0.0001	0.003
				$u(x_i)$	[%]	2.37%	3.30%	

Table F. 39: $u(\psi)$ - Sensitivity coefficients and uncertainty contributions of FG based VIPs, Commutated joint ($t = 20 \text{ mm}$, $\vartheta_{avg} = 23^\circ\text{C}$)

		<i>Sensitivity coefficients</i>	
		1 st Side Cold	Uncertainty contributions
$(\partial\Psi_{HFM}/\partial A_{m,eq})$	0.090560	0.22%	
$(\partial\Psi_{HFM}/\partial t_{m,eq})$	2.400772	1.76%	
$(\partial\Psi_{HFM}/\partial l_\psi)$	- 0.179030	0.12%	
$(\partial\Psi_{HFM}/\partial f_{cal})$	0.021556	0.03%	
$(\partial\Psi_{HFM}/\partial Q_m)$	0.230601	1.19%	
$(\partial\Psi_{HFM}/\partial \Delta\vartheta_{m,eq})$	- 0.010026	0.12%	
$(\partial\Psi_{HFM}/\partial \Delta\lambda_E)$	0.141940	1.76%	
$(\partial\Psi_{HFM}/\partial \Delta\lambda_O)$	0.141940	29.83%	
$(\partial\Psi_{HFM}/\partial U_{COP})$	- 0.017905	2.86%	
$(\partial\Psi_{HFM}/\partial I_{COP})$	- 0.901402	0.27%	
$(\partial\Psi_{HFM}/\partial t_{m,COP})$	- 2.402910	2.22%	
$(\partial\Psi_{HFM}/\partial A_{m,COP})$	1.304423	1.12%	
$(\partial\Psi_{HFM}/\partial \Delta\vartheta_{m,COP})$	0.002646	0.03%	
$(\partial\Psi_{HFM}/\partial C_j)$	0.051595	0.65%	
$(\partial\Psi_{HFM}/\partial \Delta\lambda_{R,E})$	0.052281	0.65%	
$(\partial\Psi_{HFM}/\partial \Delta\lambda_O)$	0.052281	29.81%	
$(\partial\Psi_{HFM}/\partial \Delta\lambda_S)$	0.052281	18.82%	

Table F. 40: λ_{eq} , ψ - Uncertainty assessment of FG based VIPs, Commutated joint
($t = 20$ mm, $\vartheta_{avg} = 23^\circ\text{C}$); Type A uncertainty

<i>FG - 20 mm - 23°C: COMMUTATED JOINT (Type A uncertainty)</i>										
		A_m [m ²]	t_{VIP_1} [m]	t_{VIP_2} [m]	t_m [m]	f_{cal} [W/m ² mV]	λ_{eq_HFM} [W/mK]	Ψ_{HFM} [W/mK]		
1 st Side	Hot					6.034	0.00623	0.090		
	$u(x_j)$	0.2483	0.0216	0.0220	0.0218	0.035				
	Cold					6.585				
$u(x_j)$	0.0002	0.0001	0.0003	0.0002	0.039					
2 nd Side	Hot					6.927				
	$u(x_j)$	0.2483	0.0220	0.0220	0.0220	0.040				
	Cold					7.295				
$u(x_j)$	0.0002	0.0003	0.0002	0.0002	0.044					
		Q [mV]	$\Delta\vartheta_m$ [°C]	$\Delta\lambda_E$ [-]	$\Delta\lambda_O$ [-]	λ_{eq,i_HFM} [W/mK]				
1 st Side	Hot	0.6498		1	1	0.00603				
	$u(x_j)$	0.0006	14.16	3.0E-05	6.0E-06	0.00006				
	Cold	0.6155		1	1	0.00623				
$u(x_j)$	0.0002	0.07	3.1E-05	6.2E-06	0.00007					
2 nd Side	Hot	0.5433		1	1	0.00585				
	$u(x_j)$	0.0004	14.14	2.9E-05	5.9E-06	0.00006				
	Cold	0.5817		1	1	0.00660				
$u(x_j)$	0.0002	0.07	3.3E-05	6.6E-06	0.00007	0.00007	0.001			
				$u(\lambda_{eq_HFM})$	[%]		1.12%	1.11%		

Table F. 41: λ_{eq} - Uncertainty assessment of FG based VIPs, Gasket strip joint
 ($t = 20 \text{ mm}$, $\vartheta_{avg} = 10^\circ\text{C}$)

<i>FG - 20 mm - 10°C: GASKET STRIP JOINT</i>								
		A_m [m ²]	t_{VIP_1} [m]	t_{VIP_2} [m]	t_m [m]	f_{cal} [W/m ² mV]	λ_{eq_HFM} [W/mK]	
1 st Side	Hot					6.147	0.0070	
	$u(x_i)$	0.2483	0.0216	0.0220	0.0218	0.035		
Cold						6.724		
	$u(x_i)$	0.0002	0.0001	0.0003	0.0002	0.039		
2 nd Side	Hot					7.081		
	$u(x_i)$	0.2483	0.0220	0.0220	0.0220	0.040		
Cold						7.469		
	$u(x_i)$	0.0002	0.0003	0.0002	0.0002	0.044		
		Q [mV]	$\Delta\vartheta_m$ [°C]	$\Delta\lambda_E$ [-]	$\Delta\lambda_O$ [-]	λ_{eq,i_HFM} [W/mK]		
1 st Side	Hot	0.56450		1	1	0.0055		
	$u(x_i)$	0.00003	13.76	2.7E-05	5.5E-06	0.0001		
Cold		0.66130		1	1	0.0070		
	$u(x_i)$	0.00003	0.30	3.5E-05	7.0E-06	0.0002		
2 nd Side	Hot	1.18787		1	1	0.0143		
	$u(x_i)$	0.00003	12.98	7.1E-05	1.4E-05	0.0004		
Cold		1.15255		1	1	0.0146		
	$u(x_i)$	0.00003	0.31	7.3E-05	1.5E-05	0.0004		
					$u(\lambda_{eq_HFM})$ [%]	2.86%		

Table F. 42: λ_{eq} - Sensitivity coefficients and uncertainty contributions of FG based VIPs, Gasket strip joint ($t = 20$ mm, $\vartheta_{avg} = 10^\circ\text{C}$)

<i>Sensitivity coefficients</i>		<i>Uncertainty contributions</i>		
	1 st Side Cold			
$(\partial\lambda_{eq_HFM}/\partial t_m)$	0.323195			
$(\partial\lambda_{eq_HFM}/\partial f_{cal})$	0.001047			
$(\partial\lambda_{eq_HFM}/\partial Q_m)$	0.010643			
$(\partial\lambda_{eq_HFM}/\partial\Delta\vartheta_m)$	- 0.000512			
$(\partial\Delta\vartheta_m/\partial A_{COP})$	342.497439			
$(\partial\Delta\vartheta_m/\partial\Delta\vartheta_{COP})$	0.680000			
$(\partial\Delta\vartheta_m/\partial A_{SA})$	- 0.684443			
$(\partial\Delta\vartheta_m/\partial\Delta\vartheta_{SA})$	0.240000			
$(\partial\Delta\vartheta_m/\partial A_J)$	- 16.578533			
$(\partial\Delta\vartheta_m/\partial\Delta\vartheta_J)$	0.008197			
$(\partial\lambda_{eq_HFM}/\partial\Delta\lambda_E)$	0.007038			
$(\partial\lambda_{eq_HFM}/\partial\Delta\lambda_O)$	0.007038			

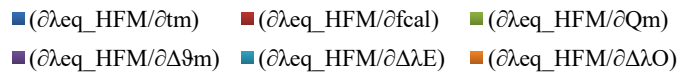
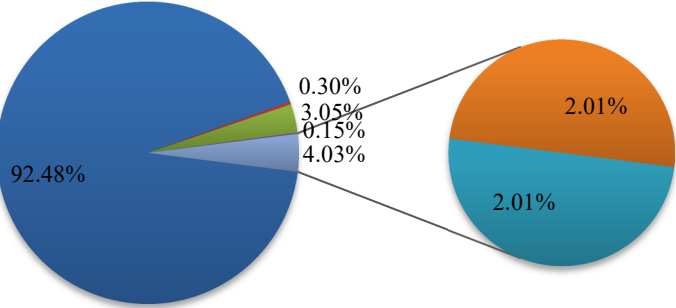


Table F. 43: ψ - Uncertainty assessment of FG based VIPs, Gasket strip joint
($t = 20 \text{ mm}$, $\vartheta_{avg} = 10^\circ\text{C}$)

		<i>FG - 20 mm - 10°C: GASKET STRIP JOINT</i>						
		A_m [m ²]	t_m [m]	l_ψ [m]	l_ψ [m]	λ_{COP_avg} [W/mK]	λ_{eq_HFM} [W/mK]	Ψ_{HFM} [W/mK]
1 st Side	Hot	0.2508	0.0218	0.5008				
	Cold				0.5008	0.00212	0.0070	
	$u(x_i)$	0.0002	0.0002	0.0003				0.113
2 nd Side	Hot	0.2508	0.0220	0.5008				
	Cold				0.0003	0.00002	0.0002	
	$u(x_i)$	0.0002	0.0002	0.0003				0.004
				$u(x_i)$	[%]		2.41%	3.54%

Table F. 44: $u(\psi)$ - Sensitivity coefficients and uncertainty contributions of FG based VIPs, Gasket strip joint ($t = 20 \text{ mm}$, $\vartheta_{avg} = 10^\circ\text{C}$)

		<i>Sensitivity coefficients</i>	
		1 st Side Cold	Uncertainty contributions
$(\partial\Psi_{HFM}/\partial A_{m,eq})$	0.113188		
$(\partial\Psi_{HFM}/\partial t_{m,eq})$	2.212611		
$(\partial\Psi_{HFM}/\partial l_\psi)$	-0.223763		
$(\partial\Psi_{HFM}/\partial f_{cal})$	0.023832		
$(\partial\Psi_{HFM}/\partial Q_m)$	0.242318		
$(\partial\Psi_{HFM}/\partial \Delta\vartheta_{m,eq})$	-0.011647		
$(\partial\Psi_{HFM}/\partial \Delta\lambda_E)$	0.160244		
$(\partial\Psi_{HFM}/\partial \Delta\lambda_O)$	0.160244		
$(\partial\Psi_{HFM}/\partial U_{COP})$	-0.018970		
$(\partial\Psi_{HFM}/\partial I_{COP})$	-0.944780		
$(\partial\Psi_{HFM}/\partial t_{m,COP})$	-2.214582		
$(\partial\Psi_{HFM}/\partial A_{m,COP})$	1.202188		
$(\partial\Psi_{HFM}/\partial \Delta\vartheta_{m,COP})$	0.002939		
$(\partial\Psi_{HFM}/\partial C_j)$	0.047551		
$(\partial\Psi_{HFM}/\partial \Delta\lambda_{R,E})$	0.048184		
$(\partial\Psi_{HFM}/\partial \Delta\lambda_O)$	0.048184		
$(\partial\Psi_{HFM}/\partial \Delta\lambda_S)$	0.048184		

■ $(\partial\Psi_{HFM}/\partial A_{m,eq})$	■ $(\partial\Psi_{HFM}/\partial t_{m,eq})$
■ $(\partial\Psi_{HFM}/\partial l_\psi)$	■ $(\partial\Psi_{HFM}/\partial f_{cal})$
■ $(\partial\Psi_{HFM}/\partial Q_m)$	■ $(\partial\Psi_{HFM}/\partial \Delta\vartheta_{m,eq})$
■ $(\partial\Psi_{HFM}/\partial \Delta\lambda_E)$	■ $(\partial\Psi_{HFM}/\partial \Delta\lambda_O)$
■ $(\partial\Psi_{HFM}/\partial U_{COP})$	■ $(\partial\Psi_{HFM}/\partial I_{COP})$
■ $(\partial\Psi_{HFM}/\partial t_{m,COP})$	■ $(\partial\Psi_{HFM}/\partial A_{m,COP})$
■ $(\partial\Psi_{HFM}/\partial \Delta\vartheta_{m,COP})$	■ $(\partial\Psi_{HFM}/\partial C_j)$
■ $(\partial\Psi_{HFM}/\partial \Delta\lambda_{R,E})$	■ $(\partial\Psi_{HFM}/\partial \Delta\lambda_O)$
■ $(\partial\Psi_{HFM}/\partial \Delta\lambda_S)$	

Table F. 45: λ_{eq} , ψ - Uncertainty assessment of FG based VIPs, Gasket strip joint
($t = 20$ mm, $\vartheta_{avg} = 10^\circ\text{C}$); Type A uncertainty

<i>FG - 20 mm - 10°C: GASKET STRIP JOINT (Type A uncertainty)</i>										
		A_m [m ²]	t_{VIP_1} [m]	t_{VIP_2} [m]	t_m [m]	f_{cal} [W/m ² mV]	λ_{eq_HFM} [W/mK]	Ψ_{HFM} [W/mK]		
1 st Side	Hot					6.147	0.00704	0.113		
	$u(x_j)$	0.2483	0.0216	0.0220	0.0218	0.035				
	Cold					6.724				
$u(x_j)$	0.0002	0.0001	0.0003	0.0002	0.039					
2 nd Side	Hot					7.081				
	$u(x_j)$	0.2483	0.0220	0.0220	0.0220	0.040				
	Cold					7.469				
$u(x_j)$	0.0002	0.0003	0.0002	0.0002	0.044					
		Q [mV]	$\Delta\vartheta_m$ [°C]	$\Delta\lambda_E$ [-]	$\Delta\lambda_O$ [-]	λ_{eq,i_HFM} [W/mK]				
1 st Side	Hot	0.5645		1	1	0.00549				
	$u(x_j)$	0.0002	13.76	2.7E-05	5.5E-06	0.00006				
	Cold	0.6613		1	1	0.00704				
$u(x_j)$	0.0003	0.06	3.5E-05	7.0E-06	0.00007					
2 nd Side	Hot	1.1879		1	1	0.0143				
	$u(x_j)$	0.0001	12.98	7.1E-05	1.4E-05	0.0002				
	Cold	1.1526		1	1	0.0146				
$u(x_j)$	0.0004	0.08	7.3E-05	1.5E-05	0.0002	0.00007	0.001			
				$u(\lambda_{eq_HFM})$	[%]		0.99%	0.88%		

Table F. 46: λ_{eq} - Uncertainty assessment of FG based VIPs, Gasket strip joint
 ($t = 20$ mm, $\vartheta_{avg} = 23^\circ\text{C}$)

<i>FG - 20 mm - 23°C: GASKET STRIP JOINT</i>								
		A_m [m ²]	t_{VIP_1} [m]	t_{VIP_2} [m]	t_m [m]	f_{cal} [W/m ² mV]	λ_{eq_HFM} [W/mK]	
1 st Side	Hot					6.036	0.0072	
	$u(x_i)$	0.2483	0.0216	0.0220	0.0218	0.035		
1 st Side	Cold					6.584		
	$u(x_i)$	0.0002	0.0001	0.0003	0.0002	0.039		
2 nd Side	Hot					6.931		
	$u(x_i)$	0.2483	0.02200	0.0220	0.0220	0.040		
2 nd Side	Cold					7.294		
	$u(x_i)$	0.0002	0.0003	0.0002	0.0002	0.044		
		Q [mV]	$\Delta\vartheta_m$ [°C]	$\Delta\lambda_E$ [-]	$\Delta\lambda_O$ [-]	λ_{eq,i_HFM} [W/mK]		
1 st Side	Hot	0.60008		1	1	0.0057		0.0002
	$u(x_i)$	0.00003	13.96	2.8E-05	5.7E-06	0.0001		
1 st Side	Cold	0.69771		1	1	0.0072		
	$u(x_i)$	0.00003	0.31	3.6E-05	7.2E-06	0.0002		
2 nd Side	Hot	1.27281		1	1	0.0147		
	$u(x_i)$	0.00003	13.22	7.3E-05	1.5E-05	0.0004		
2 nd Side	Cold	1.23176		1	1	0.0150		
	$u(x_i)$	0.00003	0.31	7.5E-05	1.5E-05	0.0004		
						$u(\lambda_{eq_HFM})$ [%]	2.78%	

Table F. 47: λ_{eq} - Sensitivity coefficients and uncertainty contributions of FG based VIPs, Gasket strip joint ($t = 20 \text{ mm}$, $\vartheta_{avg} = 23^\circ\text{C}$)

<i>Sensitivity coefficients</i>			
	1 st Side Cold	<i>Uncertainty contributions</i>	
$(\partial\lambda_{eq_HFM}/\partial t_m)$	0.329114		
$(\partial\lambda_{eq_HFM}/\partial f_{cal})$	0.001088		
$(\partial\lambda_{eq_HFM}/\partial Q_m)$	0.010272		
$(\partial\lambda_{eq_HFM}/\partial\Delta\vartheta_m)$	- 0.000513		
$(\partial\Delta\vartheta_m/\partial A_{COP})$	349.483861		
$(\partial\Delta\vartheta_m/\partial\Delta\vartheta_{COP})$	0.680000		
$(\partial\Delta\vartheta_m/\partial A_{SA})$	- 0.745372		
$(\partial\Delta\vartheta_m/\partial\Delta\vartheta_{SA})$	0.240000		
$(\partial\Delta\vartheta_m/\partial A_j)$	- 16.775807		
$(\partial\Delta\vartheta_m/\partial\Delta\vartheta_j)$	0.080000		
$(\partial\lambda_{eq_HFM}/\partial\Delta\lambda_E)$	0.007167		
$(\partial\lambda_{eq_HFM}/\partial\Delta\lambda_O)$	0.007167		

Table F. 48: ψ - Uncertainty assessment of FG based VIPs, Gasket strip joint
($t = 20 \text{ mm}$, $\vartheta_{avg} = 23^\circ\text{C}$)

		<i>FG - 20 mm - 23°C: GASKET STRIP JOINT</i>						
		A_m [m ²]	t_m [m]	l_ψ [m]	l_ψ [m]	λ_{COP_avg} [W/mK]	λ_{eq_HFM} [W/mK]	Ψ_{HFM} [W/mK]
1 st Side	Hot	0.2508	0.0218	0.5008				
	Cold	0.2508	0.0218	0.5008				
	$u(x_i)$	0.0002	0.0002	0.0003	0.5008	0.00212	0.0072	0.116
2 nd Side	Hot	0.2508	0.0220	0.5008				
	Cold	0.2508	0.0220	0.5008				
	$u(x_i)$	0.0002	0.0002	0.0003	0.0003	0.00002	0.0002	0.004
				$u(x_i)$	[%]	2.38%	3.45%	

Table F. 49: $u(\psi)$ - Sensitivity coefficients and uncertainty contributions of FG based VIPs, Gasket strip joint ($t = 20 \text{ mm}$, $\vartheta_{avg} = 23^\circ\text{C}$)

		<i>Sensitivity coefficients</i>	
		1 st Side Cold	Uncertainty contributions
$(\partial\Psi_{HFM}/\partial A_{m,eq})$	0.116152		
$(\partial\Psi_{HFM}/\partial t_{m,eq})$	2.212611		
$(\partial\Psi_{HFM}/\partial l_\psi)$	-0.229622		
$(\partial\Psi_{HFM}/\partial f_{cal})$	0.024782		
$(\partial\Psi_{HFM}/\partial Q_m)$	0.233879		
$(\partial\Psi_{HFM}/\partial \Delta\vartheta_{m,eq})$	-0.011690		
$(\partial\Psi_{HFM}/\partial \Delta\lambda_E)$	0.163179		
$(\partial\Psi_{HFM}/\partial \Delta\lambda_O)$	0.163179		
$(\partial\Psi_{HFM}/\partial U_{COP})$	-0.018970		
$(\partial\Psi_{HFM}/\partial I_{COP})$	-0.944780		
$(\partial\Psi_{HFM}/\partial t_{m,COP})$	-2.214582		
$(\partial\Psi_{HFM}/\partial A_{m,COP})$	1.202188		
$(\partial\Psi_{HFM}/\partial \Delta\vartheta_{m,COP})$	0.002939		
$(\partial\Psi_{HFM}/\partial C_j)$	0.047551		
$(\partial\Psi_{HFM}/\partial \Delta\lambda_{R,E})$	0.048184		
$(\partial\Psi_{HFM}/\partial \Delta\lambda_O)$	0.048184		
$(\partial\Psi_{HFM}/\partial \Delta\lambda_S)$	0.048184		

Table F. 50: λ_{eq} , ψ - Uncertainty assessment of FG based VIPs, Gasket strip joint
($t = 20$ mm, $\vartheta_{avg} = 23^\circ\text{C}$); Type A uncertainty

<i>FG - 20 mm - 23°C: GASKET STRIP JOINT (Type A uncertainty)</i>										
		A_m [m ²]	t_{VIP_1} [m]	t_{VIP_2} [m]	t_m [m]	f_{cal} [W/m ² mV]	λ_{eq_HFM} [W/mK]	Ψ_{HFM} [W/mK]		
1 st Side	Hot					6.036	0.00717	0.116		
	$u(x_j)$	0.2483	0.0216	0.0220	0.0218	0.035				
	Cold					6.584				
$u(x_j)$	0.0002	0.0001	0.0003	0.0002	0.039					
2 nd Side	Hot					6.931				
	$u(x_j)$	0.2483	0.0220	0.0220	0.0220	0.040				
	Cold					7.294				
$u(x_j)$	0.0002	0.0003	0.0002	0.0002	0.044					
		Q [mV]	$\Delta\vartheta_m$ [°C]	$\Delta\lambda_E$ [-]	$\Delta\lambda_O$ [-]	λ_{eq,i_HFM} [W/mK]				
1 st Side	Hot	0.6001		1	1	0.00565				
	$u(x_j)$	0.0001	13.96	2.8E-05	5.7E-06	0.00006				
	Cold	0.6977		1	1	0.00717				
$u(x_j)$	0.0002	0.06	3.6E-05	7.2E-06	0.00007					
2 nd Side	Hot	1.2728		1	1	0.0147				
	$u(x_j)$	0.0001	13.22	7.3E-05	1.5E-05	0.0002				
	Cold	1.2318		1	1	0.0150				
$u(x_j)$	0.0002	0.08	7.5E-05	1.5E-05	0.0002	0.00007	0.001			
				$u(\lambda_{eq_HFM})$	[%]		0.98%	0.86%		

Table F. 51: λ_{eq} - Uncertainty assessment of FG based VIPs, Commutated joint
 ($t = 30 \text{ mm}$, $\vartheta_{avg} = 10^\circ\text{C}$)

<i>FG - 30 mm - 10°C: COMMUTATED JOINT</i>								
		A_m [m ²]	t_{VIP_1} [m]	t_{VIP_2} [m]	t_m [m]	f_{cal} [W/m ² mV]	λ_{eq_HFM} [W/mK]	
1 st Side	Hot					6.146	0.0069	
	$u(x_i)$	0.2483	0.0299	0.0304	0.0301	0.035		
Cold					6.724			
$u(x_i)$	0.0002	0.0004	0.000	0.0002	0.039			
2 nd Side	Hot					7.080		
	$u(x_i)$	0.2483	0.0307	0.0316	0.0312	0.040		
Cold					7.468			
$u(x_i)$	0.0002	0.0001	0.0002	0.0001	0.044			
		Q [mV]	$\Delta\vartheta_m$ [°C]	$\Delta\lambda_E$ [-]	$\Delta\lambda_O$ [-]	λ_{eq,i_HFM} [W/mK]		
1 st Side	Hot	0.40549		1	1	0.0054		
	$u(x_i)$	0.00003	13.79	2.7E-05	5.4E-06	0.0001		
Cold	0.47130		1	1	0.0069			
$u(x_i)$	0.00003	0.30	3.5E-05	6.9E-06	0.0002			
2 nd Side	Hot	0.39696		1	1	0.0064		
	$u(x_i)$	0.00003	13.70	3.2E-05	6.4E-06	0.0002		
Cold	0.42265		1	1	0.0072			
$u(x_i)$	0.00003	0.31	3.6E-05	7.2E-06	0.0002	0.0002		
				$u(\lambda_{eq_HFM})$	[%]	2.90%		

Table F. 52: λ_{eq} - Sensitivity coefficients and uncertainty contributions of FG based VIPs, Commutated joint ($t = 30$ mm, $\vartheta_{avg} = 10^\circ\text{C}$)

<i>Sensitivity coefficients</i>		<i>Uncertainty contributions</i>	
	1 st Side Cold		
$(\partial\lambda_{eq_HFM}/\partial t_m)$	0.229825		
$(\partial\lambda_{eq_HFM}/\partial f_{cal})$	0.001029		
$(\partial\lambda_{eq_HFM}/\partial Q_m)$	0.014683		
$(\partial\lambda_{eq_HFM}/\partial\Delta\vartheta_m)$	- 0.000502		
$(\partial\Delta\vartheta_m/\partial A_{COP})$	342.166346		
$(\partial\Delta\vartheta_m/\partial\Delta\vartheta_{COP})$	0.680000		
$(\partial\Delta\vartheta_m/\partial A_{SA})$	- 1.079788		
$(\partial\Delta\vartheta_m/\partial\Delta\vartheta_{SA})$	0.240000		
$(\partial\Delta\vartheta_m/\partial A_J)$	- 15.374485		
$(\partial\Delta\vartheta_m/\partial\Delta\vartheta_J)$	0.008197		
$(\partial\lambda_{eq_HFM}/\partial\Delta\lambda_E)$	0.006920		
$(\partial\lambda_{eq_HFM}/\partial\Delta\lambda_O)$	0.006920		

Table F. 53: ψ - Uncertainty assessment of FG based VIPs, Commutated joint
($t = 30 \text{ mm}$, $\vartheta_{avg} = 10^\circ\text{C}$)

		<i>FG - 30 mm - 10°C: COMMUTATED JOINT</i>						
		A_m [m ²]	t_m [m]	l_ψ [m]	l_ψ [m]	λ_{COP_avg} [W/mK]	λ_{eq_HFM} [W/mK]	Ψ_{HFM} [W/mK]
1 st Side	Hot	0.2508	0.0301	0.5008				
	Cold	0.2508	0.0301	0.5008				
	$u(x_i)$	0.0002	0.0002	0.0003	0.5008	0.00216	0.0069	0.079
2 nd Side	Hot	0.2508	0.0312	0.5008				
	Cold	0.2508	0.0312	0.5008				
	$u(x_i)$	0.0002	0.0001	0.0003	0.0003	0.00003	0.0002	0.003
				$u(x_i)$	[%]		2.41%	3.80%

Table F. 54: $u(\psi)$ - Sensitivity coefficients and uncertainty contributions of FG based VIPs, Commutated joint ($t = 30 \text{ mm}$, $\vartheta_{avg} = 10^\circ\text{C}$)

		<i>Sensitivity coefficients</i>	
		1 st Side Cold	Uncertainty contributions
$(\partial\Psi_{HFM}/\partial A_{m,eq})$	0.079090	2.29%	
$(\partial\Psi_{HFM}/\partial t_{m,eq})$	1.183906	0.34%	
$(\partial\Psi_{HFM}/\partial l_\psi)$	- 0.156354	17.07%	
$(\partial\Psi_{HFM}/\partial f_{cal})$	0.016948	0.05%	
$(\partial\Psi_{HFM}/\partial Q_m)$	0.241778	0.71%	
$(\partial\Psi_{HFM}/\partial \Delta\vartheta_{m,eq})$	- 0.008264	0.05%	
$(\partial\Psi_{HFM}/\partial \Delta\lambda_E)$	0.113950	17.88%	
$(\partial\Psi_{HFM}/\partial \Delta\lambda_O)$	0.113950	20.79%	
$(\partial\Psi_{HFM}/\partial U_{COP})$	- 0.016895	0.72%	
$(\partial\Psi_{HFM}/\partial I_{COP})$	- 0.848765	0.72%	
$(\partial\Psi_{HFM}/\partial t_{m,COP})$	- 1.159572	0.72%	
$(\partial\Psi_{HFM}/\partial A_{m,COP})$	0.889424	0.72%	
$(\partial\Psi_{HFM}/\partial \Delta\vartheta_{m,COP})$	0.002301	0.72%	
$(\partial\Psi_{HFM}/\partial C_j)$	0.035180	0.72%	
$(\partial\Psi_{HFM}/\partial \Delta\lambda_{R,E})$	0.035648	0.72%	
$(\partial\Psi_{HFM}/\partial \Delta\lambda_O)$	0.035648	0.72%	
$(\partial\Psi_{HFM}/\partial \Delta\lambda_S)$	0.035648	0.72%	

Table F. 55: λ_{eq} , ψ - Uncertainty assessment of FG based VIPs, Commutated joint
($t = 30$ mm, $\vartheta_{avg} = 10^\circ\text{C}$); Type A uncertainty

<i>FG - 30 mm - 10°C: COMMUTATED JOINT (Type A uncertainty)</i>										
		A_m [m ²]	t_{VIP_1} [m]	t_{VIP_2} [m]	t_m [m]	f_{cal} [W/m ² mV]	λ_{eq_HFM} [W/mK]	Ψ_{HFM} [W/mK]		
1 st Side	Hot					6.146	0.00692	0.079		
	$u(x_j)$	0.2483	0.0299	0.0304	0.0301	0.035				
	Cold					6.724				
$u(x_j)$	0.0002	0.0004	0.0002	0.0002	0.039					
2 nd Side	Hot					7.080				
	$u(x_j)$	0.2483	0.0307	0.0316	0.0312	0.040				
	Cold					7.468				
$u(x_j)$	0.0002	0.0001	0.0002	0.0001	0.044					
		Q [mV]	$\Delta\vartheta_m$ [°C]	$\Delta\lambda_E$ [-]	$\Delta\lambda_O$ [-]	λ_{eq,i_HFM} [W/mK]				
1 st Side	Hot	0.4055		1	1	0.00544				
	$u(x_j)$	0.0004	13.79	2.7E-05	5.4E-06	0.00006				
	Cold	0.4713		1	1	0.00692				
$u(x_j)$	0.0002	0.06	3.5E-05	6.9E-06	0.00007					
2 nd Side	Hot	0.3970		1	1	0.00639				
	$u(x_j)$	0.0003	13.70	3.2E-05	6.4E-06	0.00006				
	Cold	0.4227		1	1	0.00718				
$u(x_j)$	0.0003	0.08	3.6E-05	7.2E-06	0.00006	0.00007	0.001			
				$u(\lambda_{eq_HFM})$	[%]		1.01%	1.27%		

Table F. 56: λ_{eq} - Uncertainty assessment of FG based VIPs, Commutated joint
 ($t = 30$ mm, $\vartheta_{avg} = 23^\circ\text{C}$)

<i>FG - 30 mm - 23°C: COMMUTATED JOINT</i>								
		A_m [m ²]	t_{VIP_1} [m]	t_{VIP_2} [m]	t_m [m]	f_{cal} [W/m ² mV]	λ_{eq_HFM} [W/mK]	
1 st Side	Hot					6.034	0.0070	
	$u(x_i)$	0.2483	0.0299	0.0304	0.0301	0.035		
Cold						6.585		
	$u(x_i)$	0.0002	0.0004	0.0002	0.0002	0.039		
2 nd Side	Hot					6.927		
	$u(x_i)$	0.2483	0.0307	0.0316	0.0312	0.040		
Cold						7.295		
	$u(x_i)$	0.0002	0.0001	0.0002	0.0001	0.044		
		Q [mV]	$\Delta\vartheta_m$ [°C]	$\Delta\lambda_E$ [-]	$\Delta\lambda_O$ [-]	λ_{eq,i_HFM} [W/mK]		
1 st Side	Hot	0.43804		1	1	0.0056		
	$u(x_i)$	0.00003	14.33	2.8E-05	5.6E-06	0.0001		
Cold		0.50917		1	1	0.0070		
	$u(x_i)$	0.00003	0.31	3.5E-05	7.0E-06	0.0002		
2 nd Side	Hot	0.43061		1	1	0.0066		
	$u(x_i)$	0.00003	14.20	3.3E-05	6.5E-06	0.0002		
Cold		0.46058		1	1	0.0074		
	$u(x_i)$	0.00003	0.31	3.7E-05	7.4E-06	0.0002		
				$u(\lambda_{eq_HFM})$	[%]	2.86%		

Table F. 57: λ_{eq} - Sensitivity coefficients and uncertainty contributions of FG based VIPs, Commutated joint ($t = 30 \text{ mm}$, $\vartheta_{avg} = 23^\circ\text{C}$)

<i>Sensitivity coefficients</i>				
	1 st Side Cold	<i>Uncertainty contributions</i>		
$(\partial\lambda_{eq_HFM}/\partial t_m)$	0.233954			
$(\partial\lambda_{eq_HFM}/\partial f_{cal})$	0.001070			
$(\partial\lambda_{eq_HFM}/\partial Q_m)$	0.013835			
$(\partial\lambda_{eq_HFM}/\partial\Delta\vartheta_m)$	- 0.000492			
$(\partial\Delta\vartheta_m/\partial A_{COP})$	374.179801			
$(\partial\Delta\vartheta_m/\partial\Delta\vartheta_{COP})$	0.680000			
$(\partial\Delta\vartheta_m/\partial A_{SA})$	- 1.381846			
$(\partial\Delta\vartheta_m/\partial\Delta\vartheta_{SA})$	0.240000			
$(\partial\Delta\vartheta_m/\partial A_J)$	- 16.209843			
$(\partial\Delta\vartheta_m/\partial\Delta\vartheta_J)$	0.080000			
$(\partial\lambda_{eq_HFM}/\partial\Delta\lambda_E)$	0.007044			
$(\partial\lambda_{eq_HFM}/\partial\Delta\lambda_O)$	0.007044			

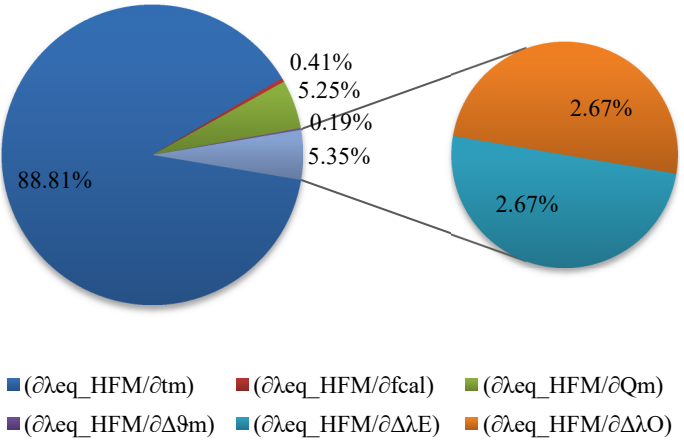


Table F. 58: ψ - Uncertainty assessment of FG based VIPs, Commutated joint
($t = 30 \text{ mm}$, $\vartheta_{avg} = 23^\circ\text{C}$)

		<i>FG - 30 mm - 23°C: COMMUTATED JOINT</i>						
		A_m [m ²]	t_m [m]	l_ψ [m]	l_ψ [m]	λ_{COP_avg} [W/mK]	λ_{eq_HFM} [W/mK]	Ψ_{HFM} [W/mK]
1 st Side	Hot	0.2508	0.0301	0.5008				
	Cold	0.2508	0.0301	0.5008				
	$u(x_i)$	0.0002	0.0002	0.0003	0.5008	0.00235	0.0070	0.078
2 nd Side	Hot	0.2508	0.03116	0.5008				
	Cold	0.2508	0.03116	0.5008				
	$u(x_i)$	0.0002	0.0001	0.0003	0.0003	0.00003	0.0002	0.003
				$u(x_i)$	[%]	2.35%	3.85%	

Table F. 59: $u(\psi)$ - Sensitivity coefficients and uncertainty contributions of FG based VIPs, Commutated joint ($t = 30 \text{ mm}$, $\vartheta_{avg} = 23^\circ\text{C}$)

		<i>Sensitivity coefficients</i>	
		1 st Side Cold	Uncertainty contributions
$(\partial\Psi_{HFM}/\partial A_{m,eq})$	0.078015	2.24%	
$(\partial\Psi_{HFM}/\partial t_{m,eq})$	1.287218	0.30%	
$(\partial\Psi_{HFM}/\partial l_\psi)$	- 0.154230	0.16%	
$(\partial\Psi_{HFM}/\partial f_{cal})$	0.017615	0.34%	
$(\partial\Psi_{HFM}/\partial Q_m)$	0.227815	2.24%	
$(\partial\Psi_{HFM}/\partial \Delta\vartheta_{m,eq})$	- 0.008094	2.24%	
$(\partial\Psi_{HFM}/\partial \Delta\lambda_E)$	0.115997	0.16%	
$(\partial\Psi_{HFM}/\partial \Delta\lambda_O)$	0.115997	0.34%	
$(\partial\Psi_{HFM}/\partial U_{COP})$	- 0.015381	4.40%	
$(\partial\Psi_{HFM}/\partial I_{COP})$	- 0.775179	2.98%	
$(\partial\Psi_{HFM}/\partial t_{m,COP})$	- 1.260761	2.98%	
$(\partial\Psi_{HFM}/\partial A_{m,COP})$	0.967038	2.98%	
$(\partial\Psi_{HFM}/\partial \Delta\vartheta_{m,COP})$	0.001913	2.98%	
$(\partial\Psi_{HFM}/\partial C_j)$	0.038250	2.98%	
$(\partial\Psi_{HFM}/\partial \Delta\lambda_{R,E})$	0.038759	2.98%	
$(\partial\Psi_{HFM}/\partial \Delta\lambda_O)$	0.038759	2.98%	
$(\partial\Psi_{HFM}/\partial \Delta\lambda_S)$	0.038759	2.98%	

Table F. 60: λ_{eq} , ψ - Uncertainty assessment of FG based VIPs, Commutated joint
($t = 30$ mm, $\vartheta_{avg} = 23^\circ\text{C}$); Type A uncertainty

<i>FG - 30 mm - 23°C: COMMUTATED JOINT (Type A uncertainty)</i>										
		A_m [m ²]	t_{VIP_1} [m]	t_{VIP_2} [m]	t_m [m]	f_{cal} [W/m ² mV]	λ_{eq_HFM} [W/mK]	Ψ_{HFM} [W/mK]		
1 st Side	Hot					6.034	0.00704	0.078		
	$u(x_j)$	0.2483	0.0299	0.0304	0.0301	0.035				
	Cold					6.585				
$u(x_j)$	0.0002	0.0004	0.0002	0.0002	0.039					
2 nd Side	Hot					6.927				
	$u(x_j)$	0.2483	0.0307	0.0316	0.0312	0.040				
	Cold					7.295				
$u(x_j)$	0.0002	0.0001	0.0002	0.0001	0.044					
		Q [mV]	$\Delta\vartheta_m$ [°C]	$\Delta\lambda_E$ [-]	$\Delta\lambda_O$ [-]	$\lambda_{eq_i_HFM}$ [W/mK]				
1 st Side	Hot	0.4380		1	1	0.00555				
	$u(x_j)$	0.0006	14.33	2.8E-05	5.6E-06	0.00006				
	Cold	0.5092		1	1	0.00704				
$u(x_j)$	0.0005	0.07	3.5E-05	7.0E-06	0.00008					
2 nd Side	Hot	0.4306		1	1	0.00655				
	$u(x_j)$	0.0004	14.20	3.3E-05	6.5E-06	0.00006				
	Cold	0.4606		1	1	0.00737				
$u(x_j)$	0.0006	0.08	3.7E-05	7.4E-06	0.00007	0.00008	0.001			
				$u(\lambda_{eq_HFM})$	[%]		1.14%	1.28%		

Table F. 61: λ_{eq} - Uncertainty assessment of FG based VIPs, Gasket strip joint
 ($t = 30 \text{ mm}$, $\vartheta_{avg} = 10^\circ\text{C}$)

<i>FG - 30 mm - 10°C: GASKET STRIP JOINT</i>								
		A_m [m ²]	t_{VIP_1} [m]	t_{VIP_2} [m]	t_m [m]	f_{cal} [W/m ² mV]	λ_{eq_HFM} [W/mK]	
1 st Side	Hot					6.036	0.0101	
	$u(x_i)$	0.2483	0.031	0.0304	0.0306	0.035		
Cold						6.584		
	$u(x_i)$	0.0002	0.001	0.0002	0.0006	0.039		
2 nd Side	Hot					6.931		
	$u(x_i)$	0.2483	0.0307	0.0316	0.0312	0.040		
Cold						7.294		
	$u(x_i)$	0.0002	0.0001	0.0002	0.0001	0.044		
		Q [mV]	$\Delta\vartheta_m$ [°C]	$\Delta\lambda_E$ [-]	$\Delta\lambda_O$ [-]	λ_{eq,i_HFM} [W/mK]		
1 st Side	Hot	0.59988		1	1	0.0080		0.0003
	$u(x_i)$	0.00003	13.96	4.0E-05	7.9E-06	0.0002		
Cold		0.69796		1	1	0.0101		
	$u(x_i)$	0.00003	0.31	5.0E-05	1.0E-05	0.0003		
2 nd Side	Hot	1.27250		1	1	0.0208		
	$u(x_i)$	0.00003	13.22	1.0E-04	2.1E-05	0.0005		
Cold		1.23188		1	1	0.0212		
	$u(x_i)$	0.00003	0.31	1.1E-04	2.1E-05	0.0005		
						$u(\lambda_{eq_HFM})$	2.97%	

Table F. 62: λ_{eq} - Sensitivity coefficients and uncertainty contributions of FG based VIPs, Gasket strip joint ($t = 30 \text{ mm}$, $\vartheta_{avg} = 10^\circ\text{C}$)

<i>Sensitivity coefficients</i>		<i>Uncertainty contributions</i>	
	1 st Side Cold		
$(\partial\lambda_{eq_HFM}/\partial t_m)$	0.329287		
$(\partial\lambda_{eq_HFM}/\partial f_{cal})$	0.001531		
$(\partial\lambda_{eq_HFM}/\partial Q_m)$	0.014447		
$(\partial\lambda_{eq_HFM}/\partial\Delta\vartheta_m)$	- 0.000723		
$(\partial\Delta\vartheta_m/\partial A_{COP})$	349.187378		
$(\partial\Delta\vartheta_m/\partial\Delta\vartheta_{COP})$	0.680000		
$(\partial\Delta\vartheta_m/\partial A_{SA})$	- 0.739819		
$(\partial\Delta\vartheta_m/\partial\Delta\vartheta_{SA})$	0.240000		
$(\partial\Delta\vartheta_m/\partial A_J)$	- 16.776338		
$(\partial\Delta\vartheta_m/\partial\Delta\vartheta_J)$	0.008197		
$(\partial\lambda_{eq_HFM}/\partial\Delta\lambda_E)$	0.010084		
$(\partial\lambda_{eq_HFM}/\partial\Delta\lambda_O)$	0.010084		

Table F. 63: ψ - Uncertainty assessment of FG based VIPs, Gasket strip joint
($t = 30 \text{ mm}$, $\vartheta_{avg} = 10^\circ\text{C}$)

		<i>FG - 30 mm - 10°C: GASKET STRIP JOINT</i>						
		A_m [m ²]	t_m [m]	l_ψ [m]	l_ψ [m]	λ_{COP_avg} [W/mK]	λ_{eq_HFM} [W/mK]	Ψ_{HFM} [W/mK]
1 st Side	Hot	0.2508	0.0306	0.5008	0.5008	0.00220	0.0101	0.129
	Cold							
	$u(x_i)$							
2 nd Side	Hot	0.2508	0.0312	0.5008	0.0003	0.00005	0.0003	0.004
	Cold							
	$u(x_i)$							
				$u(x_i)$	[%]	3.05%	3.10%	

Table F. 64: $u(\psi)$ - Sensitivity coefficients and uncertainty contributions of FG based VIPs, Gasket strip joint ($t = 30 \text{ mm}$, $\vartheta_{avg} = 10^\circ\text{C}$)

<i>Sensitivity coefficients</i>		<i>Uncertainty contributions</i>	
	1 st Side Cold		
$(\partial\Psi_{HFM}/\partial A_{m,eq})$	0.128913		
$(\partial\Psi_{HFM}/\partial t_{m,eq})$	1.163716		
$(\partial\Psi_{HFM}/\partial l_\psi)$	-0.254850		
$(\partial\Psi_{HFM}/\partial f_{cal})$	0.024796		
$(\partial\Psi_{HFM}/\partial Q_m)$	0.233916		
$(\partial\Psi_{HFM}/\partial \Delta\vartheta_{m,eq})$	-0.011698		
$(\partial\Psi_{HFM}/\partial \Delta\lambda_E)$	0.163265		
$(\partial\Psi_{HFM}/\partial \Delta\lambda_O)$	0.163265		
$(\partial\Psi_{HFM}/\partial U_{COP})$	-0.016889		
$(\partial\Psi_{HFM}/\partial I_{COP})$	-0.848474		
$(\partial\Psi_{HFM}/\partial t_{m,COP})$	-1.140189		
$(\partial\Psi_{HFM}/\partial A_{m,COP})$	0.889118		
$(\partial\Psi_{HFM}/\partial \Delta\vartheta_{m,COP})$	0.002300		
$(\partial\Psi_{HFM}/\partial C_j)$	0.035168		
$(\partial\Psi_{HFM}/\partial \Delta\lambda_{R,E})$	0.035636		
$(\partial\Psi_{HFM}/\partial \Delta\lambda_O)$	0.035636		
$(\partial\Psi_{HFM}/\partial \Delta\lambda_S)$	0.035636		

Table F. 65: λ_{eq} , ψ - Uncertainty assessment of FG based VIPs, Gasket strip joint
($t = 30$ mm, $\vartheta_{avg} = 10^\circ\text{C}$); Type A uncertainty

<i>FG - 30 mm - 10°C: GASKET STRIP JOINT (Type A uncertainty)</i>										
		A_m [m ²]	t_{VIP_1} [m]	t_{VIP_2} [m]	t_m [m]	f_{cal} [W/m ² mV]	λ_{eq_HFM} [W/mK]	Ψ_{HFM} [W/mK]		
1 st Side	Hot					6.036	0.0101	0.129		
	$u(x_j)$	0.2483	0.031	0.0304	0.0306	0.035				
	Cold					6.584				
$u(x_j)$	0.0002	0.001	0.0002	0.0006	0.039					
2 nd Side	Hot					6.931				
	$u(x_j)$	0.2483	0.0307	0.0316	0.0312	0.040				
	Cold					7.294				
$u(x_j)$	0.0002	0.0001	0.0002	0.0001	0.044					
		Q [mV]	$\Delta\vartheta_m$ [°C]	$\Delta\lambda_E$ [-]	$\Delta\lambda_O$ [-]	λ_{eq,i_HFM} [W/mK]				
1 st Side	Hot	0.5999		1	1	0.0080				
	$u(x_j)$	0.0001	13.96	4.0E-05	7.9E-06	0.0002				
	Cold	0.6980		1	1	0.0101				
$u(x_j)$	0.0002	0.06	5.0E-05	1.0E-05	0.0002					
2 nd Side	Hot	1.2725		1	1	0.0208				
	$u(x_j)$	0.0001	13.22	1.0E-04	2.1E-05	0.0002				
	Cold	1.2319		1	1	0.0212				
$u(x_j)$	0.0002	0.08	1.1E-04	2.1E-05	0.0002	0.0002	0.002			
				$u(\lambda_{eq_HFM})$	[%]		1.98%	1.55%		

Table F. 66: λ_{eq} - Uncertainty assessment of FG based VIPs, Gasket strip joint
 ($t = 30$ mm, $\vartheta_{avg} = 23^\circ\text{C}$)

<i>FG - 30 mm - 23°C: GASKET STRIP JOINT</i>								
		A_m [m ²]	t_{VIP_1} [m]	t_{VIP_2} [m]	t_m [m]	f_{cal} [W/m ² mV]	λ_{eq_HFM} [W/mK]	
1 st Side	Hot					6.036	0.0085	
	$u(x_i)$	0.2483	0.031	0.0304	0.0306	0.035		
Cold						6.585		
	$u(x_i)$	0.0002	0.001	0.0002	0.0006	0.039		
2 nd Side	Hot					6.930		
	$u(x_i)$	0.2483	0.0307	0.0316	0.0312	0.040		
Cold						7.294		
	$u(x_i)$	0.0002	0.0001	0.0002	0.0001	0.044		
		Q [mV]	$\Delta\vartheta_m$ [°C]	$\Delta\lambda_E$ [-]	$\Delta\lambda_O$ [-]	λ_{eq,i_HFM} [W/mK]		
1 st Side	Hot	0.59830		1	1	0.0079		0.0003
	$u(x_i)$	0.00003	14.0959	3.9E-05	7.8E-06	0.0002		
Cold		0.59500		1	1	0.0085		
	$u(x_i)$	0.00003	0.3044	4.3E-05	8.5E-06	0.0003		
2 nd Side	Hot	0.47539		1	1	0.0073		
	$u(x_i)$	0.00003	14.0718	3.6E-05	7.3E-06	0.0002		
Cold		0.45261		1	1	0.0073		
	$u(x_i)$	0.00003	0.3066	3.7E-05	7.3E-06	0.0002		
						$u(\lambda_{eq_HFM})$	3.53%	

Table F. 67: λ_{eq} - Sensitivity coefficients and uncertainty contributions of FG based VIPs, Gasket strip joint ($t = 30 \text{ mm}$, $\vartheta_{avg} = 23^\circ\text{C}$)

<i>Sensitivity coefficients</i>		<i>Uncertainty contributions</i>		
	1 st Side Cold			
$(\partial\lambda_{eq_HFM}/\partial t_m)$	0.277958			
$(\partial\lambda_{eq_HFM}/\partial f_{cal})$	0.001293			
$(\partial\lambda_{eq_HFM}/\partial Q_m)$	0.014305			
$(\partial\lambda_{eq_HFM}/\partial\Delta\vartheta_m)$	- 0.000604			
$(\partial\Delta\vartheta_m/\partial A_{COP})$	329.039977			
$(\partial\Delta\vartheta_m/\partial\Delta\vartheta_{COP})$	0.680000			
$(\partial\Delta\vartheta_m/\partial A_{SA})$	- 1.307662			
$(\partial\Delta\vartheta_m/\partial\Delta\vartheta_{SA})$	0.240000			
$(\partial\Delta\vartheta_m/\partial A_J)$	- 13.976790			
$(\partial\Delta\vartheta_m/\partial\Delta\vartheta_J)$	0.008197			
$(\partial\lambda_{eq_HFM}/\partial\Delta\lambda_E)$	0.008512			
$(\partial\lambda_{eq_HFM}/\partial\Delta\lambda_O)$	0.008512			

Table F. 68: ψ - Uncertainty assessment of FG based VIPs, Gasket strip joint
($t = 30 \text{ mm}$, $\vartheta_{avg} = 23^\circ\text{C}$)

		<i>FG - 30 mm - 23°C: GASKET STRIP JOINT</i>						
		A_m [m ²]	t_m [m]	l_ψ [m]	l_ψ [m]	λ_{COP_avg} [W/mK]	λ_{eq_HFM} [W/mK]	Ψ_{HFM} [W/mK]
1 st Side	Hot	0.2508	0.0306	0.5008				
	Cold	0.2508	0.0306	0.5008				
	$u(x_i)$	0.0002	0.0006	0.0003	0.5008	0.00220	0.0085	0.103
2 nd Side	Hot	0.2508	0.0312	0.5008				
	Cold	0.2508	0.0312	0.5008				
	$u(x_i)$	0.0002	0.0001	0.0003	0.0003	0.00005	0.0003	0.003
				$u(x_i)$	[%]	3.03%	2.91%	

Table F. 69: $u(\psi)$ - Sensitivity coefficients and uncertainty contributions of FG based VIPs, Gasket strip joint ($t = 30 \text{ mm}$, $\vartheta_{avg} = 23^\circ\text{C}$)

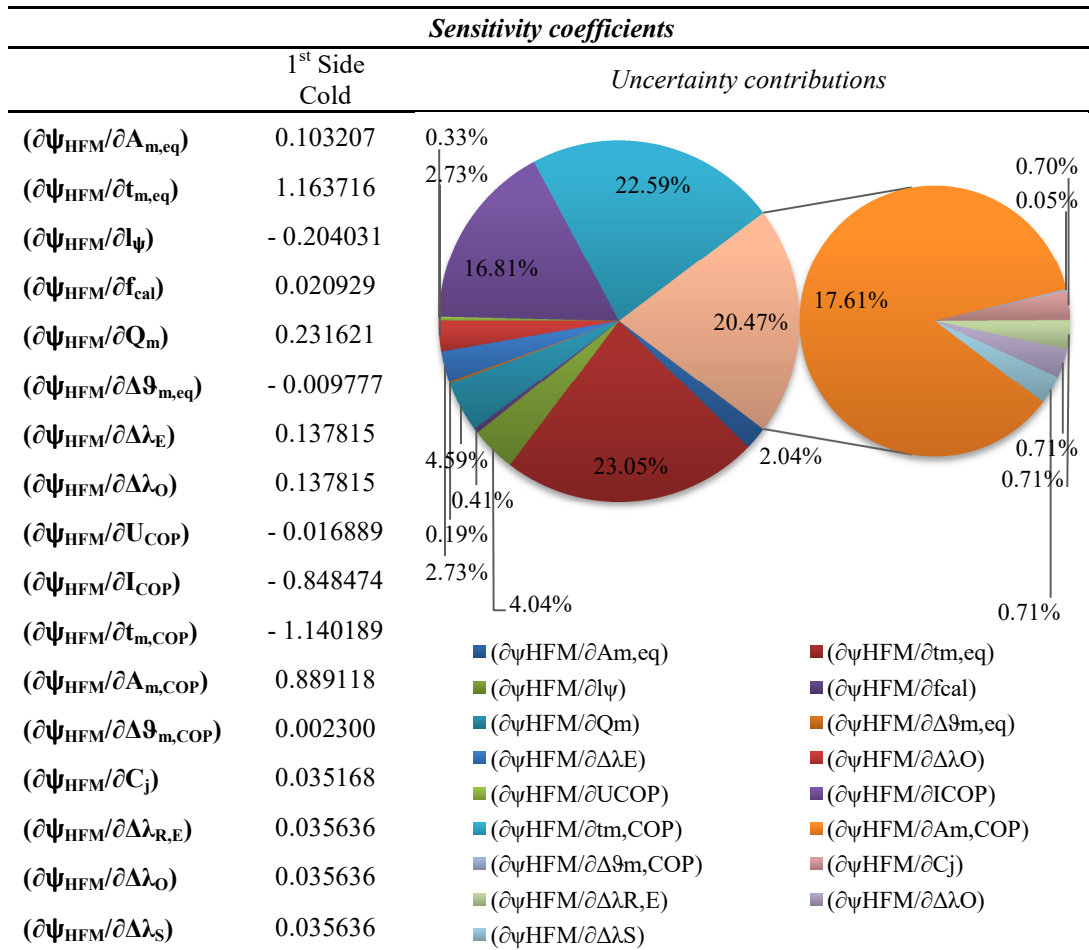


Table F. 70: λ_{eq} , ψ - Uncertainty assessment of FG based VIPs, Gasket strip joint
($t = 30$ mm, $\vartheta_{avg} = 23^\circ\text{C}$); Type A uncertainty

<i>FG - 30 mm - 23°C: GASKET STRIP JOINT (Type A uncertainty)</i>										
		A_m [m ²]	t_{VIP_1} [m]	t_{VIP_2} [m]	t_m [m]	f_{cal} [W/m ² mV]	λ_{eq_HFM} [W/mK]	Ψ_{HFM} [W/mK]		
1 st Side	Hot					6.036	0.0085	0.103		
	$u(x_j)$	0.2483	0.031	0.0304	0.0306	0.035				
	Cold					6.585				
$u(x_j)$	0.0002	0.001	0.0002	0.0006	0.039					
2 nd Side	Hot					6.930				
	$u(x_j)$	0.2483	0.0307	0.0316	0.0314	0.040				
	Cold					7.294				
$u(x_j)$	0.0002	0.0001	0.0004	0.0001	0.044					
		Q [mV]	$\Delta\vartheta_m$ [°C]	$\Delta\lambda_E$ [-]	$\Delta\lambda_O$ [-]	λ_{eq,i_HFM} [W/mK]				
1 st Side	Hot	0.5983		1	1	0.0079				
	$u(x_j)$	0.0001	14.10	3.9E-05	7.8E-06	0.0002				
	Cold	0.5950		1	1	0.0085				
$u(x_j)$	0.0002	0.06	4.3E-05	8.5E-06	0.0002					
2 nd Side	Hot	0.4754		1	1	0.00730				
	$u(x_j)$	0.0001	14.07	3.6E-05	7.3E-06	0.00006				
	Cold	0.4526		1	1	0.00731				
$u(x_j)$	0.0003	0.07	3.7E-05	7.3E-06	0.00006	0.0002	0.001			
				$u(\lambda_{eq_HFM})$	[%]		2.35%	0.97%		

